

Integrated approach for the development across Europe of user oriented climate indicators for GFCS high-priority sectors: Agriculture, disaster risk reduction, energy, health, water and tourism

Work Package 4

Deliverable 4.5

Report on comparison of the ISD with sectorial data



This report arises from the Project INDECIS which is part of ERA4CS, an ERA-NET initiated by JPI Climate, and funded by FORMAS (SE), DLR (DE), BMWFW (AT), IFD (DK), MINECO (ES), ANR (FR), with co-funding by the European Union's Horizon 2020 research and innovation programme

Authors: Sergio M. Vicente-Serrano, Fernando Domínguez-Castro, Dhais Peña-Angulo, Marina Peña-Gallardo, Abel Henriot, Yvan Caballero, Bruno Mougin, Roberto Coscarelli, Loredana Antronico, Fabio Zimbo, Olga Petrucci, Angela Aurora Pasqua, Manuel del Jesus.

In the pursuit of WP4 of INDECIS, we have analysed the relationship between climate indices and sectorial data in different countries of Europe. In general, we have showed a very good correspondence between the variability of climate indices and key impact data with implications for different sectors: crop yields, groundwater, streamflow, landslides, mortality. This reinforces the use of the developed climate indices for the multisectorial monitoring and the assessment of impacts. Here we provide a summary of the obtained results:

- **Streamflow in Spain:** We have used seven climatic drought indices to determine the influence of climatic drought to streamflow droughts in 226 undisturbed river basins in peninsular Spain covering the period 1962-2013. At the same time, we define spatial patterns in the response of streamflow to climatic drought. The study was conducted relating the climatic component represented by three multi-scalar drought indices -the Standardized Precipitation and Evapotranspiration Index (SPEI), the Standardized Precipitation Index (SPI), the Standardized Precipitation Drought Index (SPDI)- and the self-calibrated version of four Palmer's indices (PDSI, PHDI, Z-index and PMDI) with the hydrological-based Standardized Streamflow Index (SSI). Results demonstrated that multi-scalar drought indices outperform the Palmer drought indices (uni-scalars) thanks to their ability of determining climatic anomalies for different cumulative periods. Undisturbed river basins mainly responded at short time-scales of the different climate indices and the precipitation variability is the main driver of streamflow drought severity. Our results also showed that different non-climate factors have a great influence to explain the different times of response of hydrological drought to climate drought characteristics.
- **Vegetation activity in Spain:** We used a high resolution (1.1 km) spatial dataset of the normalized difference vegetation index (NDVI) for the whole of Spain spanning the period from 1981 to 2015, combined with a dataset of the standardized precipitation evapotranspiration index (SPEI) to assess the sensitivity of vegetation types to drought across Spain. Specifically, this study explores the drought timescales at which vegetation activity shows its highest response to drought severity at different moments of the year. Results demonstrate that – over large areas of Spain – vegetation activity is controlled largely by the interannual variability of drought. More than 90% of the land areas exhibited statistically significant positive correlations between the NDVI and the SPEI during dry summers (JJA). Nevertheless, there are some considerable spatio-temporal variations, which can be linked to differences in land cover and aridity conditions. In comparison to other climatic regions across Spain, results indicate that vegetation types located in arid regions showed the strongest response to drought. Importantly, this study stresses that the timescale at which drought is assessed is a dominant factor in understanding the different responses of vegetation activity to drought.
- **Crop yields in Spain and drought indices:** In this study the impacts of drought on two representative rainfed crops in Spain (wheat and barley) were assessed. As the agriculture sector is vulnerable to climate, it is especially important to identify the most appropriate tools for monitoring the impact of the weather on crops, and particularly the impact of drought. Drought indices are the most effective tool for that

purpose. Various drought indices have been used to assess the influence of drought on crop yields in Spain, including the Standardized Precipitation Evapotranspiration Index (SPEI), the Standardized Precipitation Index (SPI), the Palmer drought indices (Palmer Drought Severity Index, PDSI; Palmer Z Index, Z Index; Palmer Hydrological Drought Index, PHDI; Palmer Modified Drought Index, PMDI), and the Standardized Palmer Drought Index (SPDI). Two sets of crop yield data at different spatial scales and temporal periods were used in the analysis. The results showed that drought indices calculated at different timescales (SPI, SPEI) most closely correlated with crop yield. The results also suggested that different patterns of yield response to drought occurred depending on the region, period of the year, and the drought timescale. The differing responses across the country were related to season and the magnitude of various climate variables.

- **Crops in Spain and soil moisture:** In this study, historical droughts are analyzed, not only through SPI and SPEI, but also using SSMI computed with soil moisture time series simulated with the VIC hydrological model. The main objective is to show the importance of considering soil moisture in the study of droughts. Drought occurrence was determined through the impacts of past droughts and not only through the deficit they produce at some point in the water balance process. We conclude that soil moisture is a key factor in the production of cereals and gross grain species but is not relevant for economic impacts.
- **Forests in Spain:** In this study, we assess the response of forest growth and a satellite proxy of the net primary production (NPP) to drought in peninsular Spain and the Balearic Islands, a region characterized by complex climatological, topographical, and environmental characteristics. Herein, we employed three different indicators based on in situ measurements and satellite image-derived vegetation information (i.e., tree-ring width, maximum annual greenness, and an indicator of NPP). We used seven different climate drought indices to assess drought impacts on the tree variables analyzed. The selected drought indices include four versions of the Palmer Drought Severity Index (PDSI, Palmer Hydrological Drought Index (PHDI), Z-index, and Palmer Modified Drought Index (PMDI)) and three multi-scalar indices (Standardized Precipitation Evapotranspiration Index (SPEI), Standardized Precipitation Index (SPI), and Standardized Precipitation Drought Index (SPDI)). Our results suggest that—irrespective of drought index and tree species—tree-ring width shows a stronger response to interannual variability of drought, compared to the greenness and the NPP. In comparison to other drought indices (e.g., PDSI), and our results demonstrate that multi-scalar drought indices (e.g., SPI, SPEI) are more advantageous in monitoring drought impacts on tree-ring growth, maximum greenness, and NPP. This finding suggests that multi-scalar indices are more appropriate.
- **Water sector in Calabria (Italy):** among the 5 springs presented in the Deliverable 4.2, only the “Mezzafiumina” spring has been considered because it presents the longest registration period (1 January 2005 - 31 December 2018). The spring data were compared with the climatic data registered in the San Sosti station (code 1230), which is near this spring. The discharge data averaged in each month have been compared

with the monthly data of some climatic indices, based only on rainfall or rainfall plus precipitation data. The comparisons of the climatic indices values with the discharge data do not seem to show particular correlations. The best matches between the two databases were obtained using the monthly rainfall, the UNEP monthly values and SPEI-3 monthly values. Correlations seem to be clearer comparing the minimum values (on a 12-month timespan) of the average monthly discharge and SPI and SPEI values.

- **Forest fires in Calabria (Italy):** in the ambit of the “disaster risk” sector, data about the burnt areas (monthly data of extension - in hectares - and the number of fires in the period 2008-2018) in each province (Cosenza, Catanzaro, Crotona, Vibo Valentia, and Reggio Calabria) of Calabria, provided by means of the module “Rapid Damage Assessment” (R.D.A.) of E.F.F.I.S. (European Forest Fire Information System) and included in the Deliverable 4.2, have been compared with the Keetch-Byram Drought Index (KBDI). The comparison results show that the peaks of the burnt areas/number of fires almost always correspond with the highest of the KBDI values, but not for all the provinces. A short delay between the peak occurrence of KBDI and the burnt areas/number of fires are present in all the comparisons.
- **Landslides in Calabria (Italy):** the yearly data regarding the occurrences of landslides and floods (from 1990 to 2018), included in the Deliverable 4.2, for the whole territory of Calabria and for each province, have been compared with data of the following climatic indices: RT (RTA, RTM, RTS), R10mm, R20mm, R95TOT, R99TOT, R95%TOT, R99%TOT, RX1day, D50mm, LWP, DR1mm, DR3mm, DR10mm. The comparisons of both the number of landslides and floods with the climatic indices were made considering for each province both the average and the maximum values of the climatic indices calculated for each station belonging to the province. For the best matches, we tried to interpolate the two databases using a linear regression or an exponential curve. Regarding the landslides, the comparisons show clearer agreements with the following climatic indexes: RTA, R10mm, R20mm, R95TOT and D50mm. Regarding the flood events, the comparisons with the climatic indices are weaker than those obtained with landslides, because, given the characteristics of the rivers in Calabria, the occurrence of floods are mostly influenced by extreme hourly rainfall. Nevertheless, comparisons show the best matches with the following climatic indexes: R95TOT, D50mm, R99F.
- **Groundwater monitoring data at the scale of France:** This report presents an attempt to use Artificial Intelligence methods to explore the dependence of the groundwater levels (GWL) to the effective precipitation at the scale of France. A methodological framework has been designed to assess two main parameters of feature engineering: the cumulating depth for effective precipitation rolling sum and the delay between it and GWL time series. Based on a preselected set of 254 piezometers considered to be poorly influenced by pumping, the correlation between effective precipitation (and derived time series) and groundwater level has been explored. Results show that both signals can be rather well correlated (values above 0.6) depending on the way the effective precipitation is cumulated or delayed in time. Even if the goodness of the correlation does not appear to be dependent on one particular parameter, it is now

possible to consider simulating GWL for all piezometers presenting good correlation coefficient values using the effective precipitation grid computed based on E-OBS & INDECIS data at the French scale.

- **Simulating and forecasting groundwater levels in the MétéEAU Nappes website:** The MétéEAU Nappes website offers a large range of services for the monitoring of the current and the future state of French aquifers. This report presents the MétéEAU Nappes tool and how it has been updated in order to use the INDECIS meteorological data for the modelling and forecasting of the groundwater levels time series for some piezometers. The meteorological ECAD point-scale or E-OBS gridded data from the INDECIS project have been used as forcing data to include in the MétéEAU Nappes website, the modelling and seasonal forecasting of groundwater level case studies selected at the European scale. The work performed allow the localisation of the piezometer, the visualisation of the piezometric data time series and the modelling and seasonal forecast of the groundwater levels. Statistical analysis allowed identifying correlations between some of the indices calculated in INDECIS and defining groundwater level thresholds for both dry and wet situations. The public access version of MétéEAU Nappes website will be released in the beginning of 2021, including an Application Programming Interface (API) that will allow interested users to access the interface independently of its implementation.
- **Human mortality in Spain:** This study assessed the spatial and seasonal distributions of mortality rates in mainland Spain and their links to climatic conditions over the period 1979-2016. The analysis was made on a seasonal basis using 79 indices and natural deaths data. Results indicate large spatial variability of natural deaths, which was linked mostly to changes in the percentage of elderly population across the study domain. Spatially, both the highest mortality rates and the largest percentage of elders were distributed in the northwest areas of the study domain. A strong seasonality effect was observed, with the main increasing trend found during wintertime. Also, results suggest strong dependency between climatic indices and natural deaths, albeit with high spatial and season variability.

The following pages provide a detailed assessment of the assessment of climate indices for different applications in different sectors and regions. As some of the studies have been published in open access journals the formatted publication is included.

Response of streamflow to drought indices in Spain

1. Introduction

Among natural extreme hazards, drought entails one of the most difficult to define and characterize due to the complexity of defining the onset and not only the climatic, but also the anthropogenic factors involved in the development of an event (Lloyd-Hughes, 2014; Van Loon et al., 2016; Wilhite and Glantz, 1985). The main cause (but not the unique) of drought is the anomalous reduction of precipitations over a certain period of time, triggering what is known as meteorological drought. Climate anomalies such as precipitation shortages and/or increased atmospheric evaporative demand may propagate to the hydrological cycle by means of soil moisture deficits, streamflow, lake levels, reservoir storages etc., producing a hydrological drought (Barker et al., 2016; Tallaksen and Van Lanen, 2004; Van Loon, 2015; Van Loon and Laaha, 2015).

There are several knowledge gaps on the whole interaction between meteorological droughts and their propagation throughout the entire hydrological system, including streamflow (Haslinger et al., 2014) and groundwater (Lorenzo-Lacruz et al., 2017; Marchant and Bloomfield, 2018). This inherent complexity contribute to the uncertainty of pinpointing the beginning of the event, identifying the trigger mechanisms and constraining factors – naturals or not – and quantifying the impacts caused on water resources (generally linked to socio-economic activities) and the environmental damages associated to a drop in flow regime (e.g. increase of water temperature, changes in aquatic ecosystems, etc.)(Mosley, 2015).

Besides, the different response times of the hydrological system to precipitation deficits vary significantly. Previous studies have shown that the nature of hydrological variables determine different temporalities, for example, lowering in water retained by soils shows up faster than groundwater levels or reservoir storages rates (Barker et al., 2016; Bloomfield et al., 2015; Lorenzo-Lacruz et al., 2010; Peters et al., 2005; Scaini et al., 2015). Catchment physiographical properties also determine different temporal patterns. In a recent study, Peña-Gallardo et al. (2019) analyzed the hydrological response to drought in relatively undisturbed river basins across the U.S. emphasizing the importance of environmental and physical characteristics to explain different modes in the response of hydrological to meteorological droughts. For their part, Van Loon and Laaha, (2015) demonstrated that catchment properties related to climate control are the main explaining factors on streamflow drought duration in Austria. Similarly, many studies (Batalla et al., 2004; López-Moreno et al., 2009; Tjeldeman et al., 2018; Vicente-Serrano et al., 2017) have focus the attention on how the human influence, mainly reflected on water regulation, management and demand, but also land-use/land-cover conditions, biases the hydrological response to meteorological droughts, sometimes mitigating or intensifying the intensity, frequency or duration of these events (Liu et al., 2019; López-Moreno et al., 2009; Vicente-Serrano et al., 2017).

Given the importance of the effects of hydrological droughts, proper management strategies as mitigation plans and early warning systems are necessary in order to assess adequately and effectively drought severity (Huang et al., 2017). There are multiple methods for characterizing the effects of drought (e.g. remote sensing derived information (Ayehu et al., 2019)) but since last century, scientific community have made an effort developing multiple drought indices, commonly used nowadays for operative monitoring purposes. Reviews as the conducted by

Mishra and Singh, (2010) or more recently Mukherjee et al. (2018) provide a comprehensive evaluation of the very diverse drought indices designed to quantitatively analyse drought characteristics (duration, severity and intensity). Particular consideration should be given to Palmer (1965) who proposed for the very first time a drought index, the Palmer Drought Severity Index (PDSI) that allows identifying independent drought periods and objectively determining their severity. For their part, McKee et al. (1993) introduced the time-scale concept with the Standardized Precipitation Index (SPI), recognized by the World Meteorological Organization as the reference drought index (Hayes et al., 2011; WMO, 2012). This novel concept let identifying drought events in any natural system and region under very diverse climatic conditions at different time scales (Vicente-Serrano et al., 2012), in particular the hydrological system response time to climate conditions, which is well known that fluctuate in time and among regions (Barker et al., 2016; López-Moreno et al., 2013; Tetzlaff et al., 2008).

Many studies have assessed the relationship between climatological and hydrological drought and the propagation through different parts of the hydrological system by performing meteorological drought indices and relating them with streamflow discharged data. For example, Lorenzo-Lacruz et al. (2010) evaluated the impact of climatic droughts in a highly regulated basin in the Tagus river (Spain), finding significant correlations between two multi-scalar drought indices and river discharges. Barker et al. (2016) studied the propagation of drought in the 121 near-natural UK catchment identifying significant temporal and spatial differences in the relationship between the SPI and standardized streamflow. For their part, Loukas and Vasiliades, (2004) reported significant and strong correlations between the 2 to-4-month SPI and surface runoff in Greece, whereas soil moisture responded better at 1 to-3-month SPI. Similar results were noticed in the river flows of ten regions in China by Zhai et al. (2010).

The stated drought indices are generally climate-based (precipitation and the AED are the main input variables). Wittingly the non-linear processes associated to climate and natural systems interactions, it is often discussed the appropriateness or not, of applying a single climate-based drought index to characterize a particular drought event (e.g. using a meteorological index to analyse a hydrological drought) (Van Lanen et al., 2013). Integrated systems specifically designed for a risk management also wander incorporating meteorological variables to assess other types of drought (Bachmair et al., 2016) (e.g. European Drought Observatory (EDO), <http://edo.jrc.ec.europa.eu> or the South Asia Drought Monitoring System, <http://dms.iwmi.org>).

Mediterranean region is characterized by a high seasonal and interannual variability of precipitation, being recurrent the long and severe drought events. Climatic characteristics cause that water resources are very limited in Mediterranean river basins. It is therefore necessary the identification of appropriate management tools able to quantify the impact of climatic drought on streamflow.

Previous studies have characterized the connections of drought through the hydrological cycle in Spain (e.g. López-Moreno et al. (2013); Lorenzo-Lacruz et al. (2013), (2017), Vicente-Serrano et al.,(2015), (2017)), however there are no previous studies evaluating the performance of

different climatic drought indices. Moreover, the existing studies focused on a large diversity of basins, several of them affected by large human influences, making impossible to isolate the possible differences in the response of hydrologic to climatic droughts. For these reasons, in this study we analyzed the spatio-temporal response of a hydrological drought index in 226 headwaters basin (avoiding the anthropogenic signal), to climatic drought. To achieve this goal, we provide a performance review for seven of the most well-known multi-scalar (the Standardized Precipitation Index –SPI-, the Standardized Precipitation and Evapotranspiration Index –SPEI-, the Standardized Palmer Drought Index –SPDI-) and uni-scalar (the Palmer Drought Severity Index –PDSI-, the Palmer Drought Hydrological Index –PHDI-, the Palmer Moisture Anomaly Index –Z-Index-, the Palmer Modified Drought Index –PMDI-) drought indices in Peninsular Spain in the period 1962-2013. At the same time, we analysed temporal and spatial patterns of streamflow response to climatic droughts in these basins.

2. Data and methods

2.1. Datasets

2.1.1. Climatic data

Meteorological information (precipitation, maximum and minimum temperature) was obtained from a gridded dataset at 1.1 km resolution available for peninsular Spain and the Balearic Islands at weekly scale for the period 1962-2013. This dataset comprises a larger number of meteorological variables such as relative humidity, wind speed and sunshine duration. The Spanish National Meteorological Agency (AEMET) provided original data. An exhaustive quality control and homogenization of data were conducted before gridding process. More detailed description about the complete procedure of the dataset construction can be found in Vicente-Serrano et al. (2017). The AED was inferred using the available information and following the Penman-Monteith's parametrization recommended by FAO (Allen et al., 1998). Weekly data was transformed to monthly for the different analysis. The water holding capacity information was obtained from the European LUCAS based topsoil data (Ballabio et al., 2016).

2.1.2. Streamflow data

Most of the streamflow series used in this study were provided by the Ministry of Agriculture's CEDEX (<http://ceh-flumen64.cedex.es/general/default.htm>), while the stations located within the autonomous communities of Andalusia (<https://www.agenciamedioambienteyagua.es/>), Basque Country (<http://www.uragentzia.euskadi.eus/u81-0002/es/>) and Catalonia (<http://aca.gencat.cat/ca/inici>) were obtained from the corresponding autonomic agencies websites. A network of 1204 gauging stations in peninsular Spain were collected, however the selection was restricted to those stations with less than the 25% of missing data for the analysed period. In order to work with no missing values in the series, we developed a reconstruction and gap filling procedure based on nearby neighbour and using the whole available stations. Series from 472 gauging stations widespread distributed were filled. Further details about the followed methodology and the statistical validation of the reconstructed series are outlined in Vicente-Serrano et al. (2019, *submitted*). From the final series, we selected a total of 226 stations located in the headwater of major basins, excluding those affected by reservoirs or any other known human regulation activity that may affected the natural signal of streamflow. Figure 1 illustrates the spatial distribution of the selected gauging stations.

2.1.3. Physiographical and land cover information

A digital elevation model (DEM) at 400 m resolution for the entire Iberian Peninsula was obtained from the National Center for Geographic Information (CNIG) (<http://centrodedescargas.cnig.es/CentroDescargas/catalogo.do?Serie=LIDAR>). This DEM served to create drainage and direct flood grids that served to delimitate the drainage basins boundaries associated to each gauging station. For this purpose we used ArcGis watershed tool and the gauging stations were used as the pour points. The resulting drainage basins were used as masks to extract the average climatic and physiographical characteristics in each basin.

The National Geological Map provided by the Spanish Geological Survey (IGME) (<http://info.igme.es/cartografiadigital/geologica/Magna50.aspx?language=en>) was employed to classify the lithological units of Spain. The three major soil classes considered are: chalky, clay and siliceous soils. The land cover map (1980 - 1990) developed by the Spanish Ministry of Agriculture (https://www.mapa.gob.es/es/cartografia-y-sig/publicaciones/agricultura/mac_1980_1990.aspx), originally at the spatial scale of 1:50,000 and later rasterized at 1.1 km resolution was used to a better knowledge of the land classes present in each basins.

2.2. Methodology

2.2.1. Hydrological drought identification

Standardized Streamflow Index (SSI)

Streamflow magnitude and seasonality change considerably depending on the river regime and time, making difficult to compare time series from different regions. To solve this matter, streamflow series are usually standardized letting the comparison among stations not just in space but also in time. Despite streamflow data do not adjust to a unique statistical distribution function, many of the standardized indices in the literature lack of the flexibility to find the most suitable distribution in each time series (Lorenzo-Lacruz et al., 2013). Here, for standardizing the monthly streamflow series we used the Standardized Streamflow Index (SSI) following the methodology described in Vicente-Serrano et al. (2012). Thus, probabilities are obtained by fitting one of the multiple candidate probability functions (e.g. the General Extreme Value, the Pearson type III, the log-logistic, the log-normal, the generalized Pareto or the Weibull distributions). Depending on the robustness found in the adjustment between the L-moments of the sampled station and the L-moments of the specific selected distribution, one or another distribution is fitted. Probabilities are ultimately transformed to z-scores using Abramowitz and Stegun (1970) approximation.

2.2.2. Climatic drought indices

Palmer Drought Severity Indices (PDSIs)

The Palmer Drought Severity Index (PDSI) was enunciated by Palmer, (1965), it is a worldwide known meteorological drought index used for estimating relative dryness. Originally, the PDSI is based on the amount of moisture departure, defined as the 'Climatically Appropriate for

Existing Conditions' (CAFEC), within a two-layered soil moisture simulation for a specific region. Variations of this index include the Palmer hydrological drought index (PHDI), the Palmer moisture anomaly index (Z-index), and the Palmer modified drought index (PMDI). Even though these indices are broadly applied for monitoring purposes and quantification of droughts, they have important limitations to monitor drought conditions (Vicente-Serrano et al., 2011), lacking of multi-scalar features, having a complicated formulation and not being comparable among regions (Alley, 1984; Doesken and Garen, 1991; Guttman, 1998). In this study we used the modified version of PDSIs, the self-calibrated, introduced by Wells et al. (2004), which allows better spatial comparability.

Standardized Precipitation Index (SPI)

Introduced by McKee et al. (1993), the Standardized Precipitation Index (SPI) provides the possibility of identifying either wet and dry conditions at different time scales. This index is worldwide recognized for been a useful tool for monitoring and early warning purposes (WMO, 2012). Among its strengths, it is worth mentioning the less number of variables required in the calculation in comparison to other drought indices. The SPI transforms the sum of monthly precipitation into a probability function fitting a gamma distribution and probability is transformed to standardized units (with mean equal to 0 and variance equal to 1), enabling spatial comparison across regions with different climates characteristics.

Standardized Precipitation Evapotranspiration Index (SPEI)

Vicente-Serrano et al. (2010) developed the Standardized Precipitation Evapotranspiration extending the conceptualization of the SPI considering the AED as another relevant factor that affects drought severity. Previous studies have acknowledged the repercussion of warming on crop productions (Asseng et al., 2014), forests decay (Camarero et al., 2015) and streamflow (Vicente-Serrano et al., 2014) around the world, highlighting the importance of using drought indices that include temperature as principal variable. The SPEI first computes monthly climate balances (D_i) using monthly precipitation and reference evapotranspiration values. Monthly D_i are later aggregated at different time scales and transformed to normal standardized units using a 3-parameter log-logistic distribution.

Standardized Precipitation Drought Index (SPDI)

The standardized precipitation drought index (SPDI) presented by Ma et al. (2014), combines PDSI and SPEI schemes. The SPDI accumulates at various time scales internal water balance anomalies calculated in the PDSI scheme, which are transformed into standardized units fitting a standard normal distribution.

Hereafter, we used the terminology multi-scalar to designate those indices that can be calculated at different time scales - SPEI, SPI, and SPDI – and uni-scalar to the PDSIs.

2.2.3. Statistical analysis

Considering the whole series of streamflow, that is not differentiating between high and low flows periods, we first examined the link between the SSI and the different climatic drought indices and determined which index or indices resulted the most suitable for monitoring streamflow drought conditions. This relationship between the climatic drought indices -

summary of the climatic conditions-, and the standardized streamflow represented by the SSI was conducted calculating Pearson's correlation coefficients. As multi-scalar drought indices were calculated at scales from 1- to 48-months, a total of 576 series (12 months x 48 time-scales) of correlations were obtained for each basins in the case of SSI and multi-scalar indices and 12 series for the SSI and uni-scalar indices.

The time-scale (in the case of multi-scalar indices) at which the strongest correlation occurs between climatic drought indices and SSI is a priori unknown. For this reason, we calculated the correlations at time-scales between 1- and 48-months and for the different monthly series, retaining the maximum r value in each basin independently on the time-scale or month in which it is recorded (only significant correlations $p < 0.05$ were account). A t-test was conducted to investigate possible significant differences or similarities in the correlation coefficients obtained between the SSI and the different climatic drought indices. Once the index with best response to streamflow was determined, we aimed to explain the relationship between the maximum correlations and the climatological characteristics in order to find similarities, or not, in the response to drought of the selected basins with different averaged climatic conditions. At the same time, we extracted the percentage of surface in each basin corresponding to the three basic lithological categories (clay, chalk and siliceous soils) and vegetation cover (irrigated and rain-fed croplands, meadows and shrubs, conifers and deciduous forests).

3. Results

3.1. Relationship between climatic drought indices and the standardized streamflow index

The magnitude of the Pearson's correlation coefficients between the seven climate drought indices and the SSI revealed, in general, that strong and significant relationship exist among the SSI and the climate drought indices in the majority of basins (Figure 2). However, substantial differences were glimpsed between indices. Independently on the month of the year and the drought time-scale, higher correlation coefficients were found considering the different multi-scalar indices (SPI, SPEI and SPDI), with average correlation higher than 0.8 in all of the cases, while correlations tended to be lower with the Palmer indices. The PHDI resulted the drought index with the weakest relation with SSI ($r = 0.52$). The PDSI and the PMDI showed higher median correlation values ($r = 0.57$ and $r = 0.58$ respectively) and almost all the basins recorded significant correlations. Among the Palmer indices, the Z-index showed the strongest correlation with the standardized streamflow, this index was among PDSIs the one that performed very similar to the multi-scalar. The median correlation value was high ($r = 0.78$) but also presented higher dispersion between basins and recorded non-significant correlations. On the other hand, the SPEI, the SPI and the SPDI reached the highest median correlations (SPEI $r = 0.86$, SPI $r = 0.85$, SPDI $r = 0.86$) with little differences among them. Multi-scalar drought indices tended to perform better than the PDSIs, being able to monitor streamflow droughts more effectively.

The spatial distribution of the maximum correlations between the SSI and the different climate indices is illustrated in Figure 3. In the case of the PDSI, the PHDI and the PMDI low to medium correlations values ($r = 0.4 - 0.6$) were found in almost all the territory. The PHDI showed high correlations ($r \geq 0.8$) in the headwater basins located in the Segura, Guadiana and Ebro major basins, these values were recorded by the PDSI and the PMDI in the same basins and a few

others located in the Guadalquivir, Tajo, Duero, Minho and Jucar major basins. The pattern showed by the Z-index varied significantly respecting the other PDSIs. Medium to high ($r = 0.5 - 0.8$) correlations predominated in almost all the basins. Exceptionally, low correlations were registered in the basins of the Segura river, as well as in southwestern regions of Ebro river basin and few basins located in northern Spain. High correlations between the multi-scalar drought indices and the SSI with the strongest correlations coefficients (average $r \geq 0.8$) were found equally distributed in the territory. On the contrary, lower correlations (average $r = 0.5 - 0.6$) were observed, once again, in the basins of the Segura river and northern of the internal basins of Catalonia.

The monthly correlations between the SSI and the seven drought indices are showed in the Figure 4. In general, higher correlations were observed from February to May, especially in the multi-scalar indices (average $r \geq 0.8$) and the Z-index (average $r > 0.6$), but they are also in general high from May to September. The magnitude of the correlations considering the PDSI, the PHDI and the PMDI tended to be low and under significance level in February and March, while the months with lower correlations for the multi-scalar indices and the Z-index were November and December with average correlations below 0.6 and 0.4 respectively. The three multi-scalar drought indices showed little differences in the magnitude of their correlations.

Figure 5 shows the similar magnitudes in the maximum correlations found between the multi-scalar drought indices and the standardized streamflow. Little differences have been observed between the SPEI, the SPI and the SPDI, the level of agreement between pairs of indices is quite notable: the SPEI/SPDI or the SPEI/SPI were $r = 0.98$, while the SPDI/SPI was $r = 0.97$. Comparing the magnitudes of these multi-scalar drought indices with the Z-index, we noticed that the agreement was weaker.

Among the analysed climatic drought indices correlated with the SSI, the multi-scalar drought indices were those that recorded the maximum number of basins where highest correlations were found (Figure 6). Some of the basins, mainly located in the eastern of major river basins, showed stronger agreement with one of the PDSIs, but that percentage ranked for the 12.24% of basins, being the Z-index the most representative (8.30%) and the PDMI the last (0.44%). The SPDI pointed out as the index in which the greatest percentage of basins found the best agreement (41.92%) followed by the SPEI (25.33%) and the SPI (20.52%). Nevertheless, there are not significant differences among the different multi-scalar indices. The results of the t-test performed with the complete correlation matrices (i.e. considering the 48 time steps and months of the year) showed that in less than the 15% of the basins there were significant differences between the correlations recorded between the SPEI and the SPDI, and less than the 30% between the SPEI/SPI and the SPDI/SPI. Next section uses the results based on the SPDI that shows in general a bit higher correlations.

3.2. Seasonal response of the SSI to the different climatic drought indices

Figure 7 displays the spatial distribution of the monthly maximum correlations recorded between the SPDI and the SSI irrespective on the time-scale. In general, high correlations were recorded in most of stations but during summer months, the weakest correlations were

observed. Similar spatial patterns and magnitude of correlations were found with the SPI and the SPEI results.

Table 1 summarized the percentage of basins with the highest correlations between the three climate drought indices and the SSI as a function of the drought time scale at which this correlation is found. More than the 62% of basins presented strongest correlations at short time-scales (1 to-3 months). The 11% of basins correlated more at 1-month, the 14.83% did it at 3-month while more than the 37% found the best agreement with climatic conditions at the 2-month scale.

Maximum monthly correlations between the SPDI and the SSI tended to correspond to short time-scales (1 to-3 months) in more than the 80% of the analysed basins (Figure 8). This percentage varied depending on the observed month. For example, in June approximately the 35% of the basins found the highest correlations at medium to longer time-scales (ranging between 7 and >25 months). It is noteworthy that the majority of the basins, mainly located in Iberian (northeast) and Central System, and Cantabrian range (north) showed, systematically, a stronger dependency to long time-scales (> 10 months). Results for the SPEI/SSI and SPI/SSI. Overall, the differences in the times of response of streamflow droughts to climatic drought suggest the complexity associated to the different mechanisms that determine this link in river basins.

3.3. Physiographical and climatological characteristics

Physiographical characteristics displayed in Figure 9 showed that the average water holding capacity (whc) in most of the basins is estimated in the range of 45-55 mm (Figure 9a). Spatial differences demonstrated that some basins present higher rates of whc, mostly corresponding to those basins that recorded the maximum correlations between the SSI and the climatic drought indices at longer time-scales. These basins also matched with those characterized by high percentages of chalky soils (Figure 9b) mostly located in the north and east of Spain (corresponding with calcareous mountain streams). Probably, chalk aquifers associated to these basins are the responsible to low infiltration dynamics that determine the slow response to drought observed in previous results. Clay soils mainly dominate in basins from the north and northeastern Spain although in the south, also most of the basins from Andalusia Mediterranean basins showed a high percentage of clays (Figure 9c). These basins also presented high to medium rates of whc due to the high retention capacity of these type of permeable soils, tended to response also at medium to longer time-scales. Lastly, most of the basins with major percentage of siliceous soils are located in humid regions of Spain (northwest and central of Spain) and in some tributaries of Guadalquivir river with headwaters located in Sierra Morena) (Figure 9d). Basins from central Spain and Sierra Morena showed the lowest rates of whc but in contrast, the rates recorded by Galician basins were higher.

4. Discussion.

In this study we have performed a dual analysis. On one hand, we provided a comprehensive view of the performance of seven climatic drought indices and their efficacy to detect streamflow response in 226 unregulated basins in peninsular Spain for the period 1962-2013. On the other hand, we tried to identify spatial patterns in the response of streamflow to

climatic drought indices. To this end, we regarded the association of the SPEI, the SPI, the SPDI and the PDSIs with the standardized streamflow (SSI) by calculating Pearson's correlation coefficients. A comparison between the seven drought indices results revealed that the magnitude of the correlation coefficients vary significantly among type of indices. Aware of the shortcomings associated to the PDSIs (Vicente-Serrano et al., 2011), authors noticed that the median magnitude of the maximum correlations achieved by any of the PDSIs was relatively higher than what it was expected. More specifically, the Z-index showed to be more sensitive in reflecting the manifestation of streamflow droughts compared to the rest of the PDSIs. In Iberian Peninsula little references to previous studies performing any of the PDSIs for hydro-climatological purposes were found (Ortega-Gómez et al., 2018; Vicente-Serrano et al., 2012; Von Gunten et al., 2016). In the context of Mediterranean region, Vasiliades and Loukas, (2009) conducted a similar investigation in a basin located in Thessaly (Greece) where they correlated simulated streamflow values with three Palmer drought indices and a modification of the PDSI. The observed correlations ranged between 0.69 and 0.74 in the case of the Z-index, 0.78 and 0.80 for the PDSI and 0.69 and 0.71 for the PHDI. These magnitudes are in line with the ones observed in our study. Even the PHDI, was also found by these authors as the Palmer family index which exhibited the lowest maximum correlations. Contrary to their results that set up the maximum correlations of the PDSIs analysed in December and January, we found May as the month in which any of the four PDSIs registered the highest median maximum correlations. We interpret these high correlations in May as a consequence of the soil moisture conditions of the preceding months, usually corresponding with the rainy season over a large part of the region. The PDSI drought detection ability relates with annual time-scales while the Z-index, as a soil moisture-drought index, is more sensitive to water deficiencies at shorter time-scales (Wang et al., 2015). At this respect and as we will tackle later, the Z-index was found the fourth best-correlated drought index here assessed, displaying a similar performance to the multi-scalar drought indices and depicting an outperformance in comparison with the other PDSIs. Similarly to our observations, Vicente-Serrano et al. (2012) observed by over different river basins at global scale higher magnitudes in the correlations between the Z-index and standardized streamflow than with any other PDSIs. However, contrary to our results concerning the PDSIs performance, Haslinger et al. (2014) observed in their study conducted in Austria a stronger relationship between the self-calibrated version of the PDSI and streamflow than the Z-index, attributing this to the weaker performance of the latter in low flow scenarios. Here we considered the whole period, not distinguishing between low and high flow periods, for this reason we found our results consistent, as we support the initial hypothesis on the response of undisturbed basins to droughts at short time-scales.

Yet, our results demonstrated that the multi-scalar drought indices, calculated at different time-scales (the SPEI, the SPI, the SPDI), presented a superior capability to capture the hydro-climatological associations in comparison to the uni-scalar drought indices (PDSIs). The flexibility and comparability over time and space, independently on the climatological or environmental characteristics these indices provide, is the main reason for their primacy (Liu et al., 2019; Vicente-Serrano et al., 2011). The median magnitude of the correlations recorded with the SSI showed a high agreement during all months of the year, especially from February to May ($r \sim 0.85$). The months of November and December were an exception as the averaged correlations were generally lower in all the indices ($r \sim 0.55$). This is in consistency with previous

comparative studies in different regions where multi-scalar drought indices demonstrated a great efficacy on hydrological drought characterization (Dogan et al., 2012; Lorenzo-Lacruz et al., 2013; Peña-Gallardo et al., 2019; Wang et al., 2015; Zhai et al., 2010). Comparing to prior studies, it was observed that the magnitude of the correlations between the climatic drought indices and the streamflow vary significantly depending on the degree of the anthropogenic impact on river basins. For example, in the analysis conducted by López-Moreno et al. (2013), Lorenzo-Lacruz et al. (2013b) and Zhai et al. (2010) in highly regulated river basins, the association between climatic droughts and streamflow was lower than the observed under near-natural conditions. In these cases, the response of streamflow to drought is not limited to natural mechanisms but to disruptive factors which may mitigate or sharpen the effects of climatic droughts on streamflow (Rangecroft et al., 2018; Tjiedeman et al., 2018).

Precipitation proved to be the major limiting factor that would cause effect on streamflow over the influence role that AED would have. Yang et al. (2018) recently demonstrated the major sensitivity of surface runoff to changes in potential evapotranspiration in comparison to changes in precipitation over past observation and projections for the 21st century globally. However little seasonal variations in the performance of the SPI in comparison to the SPEI/SPDI demonstrated a slightly diminish in the magnitude of the correlations recorded by the SPI and the SSI in August. At this respect, in Iberian Peninsula this task has been already assessed by Vicente-Serrano et al. (2014) under unregulated conditions. These authors found a greater response of the SPEI to the SSI during summer months due to the increase of the AED even when precipitation variability was the main responsible of streamflow's sensitivity to humid/dry conditions. In a comparable setup, the differences in the relationship observed in our study, during summer months among these two indices and the SSI were insignificant.

Overall, we did not find significant general differences among the three multi-scalar drought indices, and the seasonal variations were minor. The median maximum correlation coefficient for the SPI was $r = 0.84$ while for the SPEI and the SPDI was $r = 0.85$. Although the SPDI was found the most correlated index in a greater percentage of basins, the differences in the magnitudes of these correlations are negligible. Consequently, we consider correct the applicability of any of them for analysis of the impact of drought on the streamflow response.

The results also reflected the existence of different times of response of streamflow to climatic drought in peninsular Spain. Thus, we observed that strongest correlations were recorded at short time-scales in a major percentage of basins, especially on a 2-month time-scale with maxima reaching in November, April and July. In line with our results, Vicente-Serrano and López-Moreno, (2005) also found in a closed and unregulated basin located in the central Spanish Pyrenees high correlations in the month of November at short time-scales (1 to-2-month). In contrast, studies performed in regulated river basins found that streamflow drought and climatic droughts were more related at longer time-scales (López-Moreno et al., 2013; Lorenzo-Lacruz et al., 2010, 2013b), mostly due to the multiple practices associated to the regulation of water resources. In keeping with this latter idea, we found out some exceptions indicating a complex heterogeneity response in typically headwater basins not regulated, as already has been reported by Peña-Gallardo et al. (2019) in 289 undisturbed basins in the U.S. and Barker et al. (2016) in 121 near-natural basins in the UK. Thus, no dissimilarities in the

climatic conditions from the 226 basins analysed were observed when comparing with the maximum correlations achieved between the SSI and the climatic drought indices. However, when we attended to the physiographical characteristics of the surface occupied by the basins, we noticed that mostly lithological characteristics in conjunction with the water holding capacity helped to understand the differences observed on the timings of response to drought conditions on streams from basins located in diverse regions of Spain. These results emphasized the basic assumption that many non-climatic local factors also influence the link between climate and streamflow even under unregulated regimens (Van Loon and Laaha, 2015). At this respect, physiographic characteristics were decisive to explain the behavior of these basins. Thus, these basins previously mentioned were located in the main chalky regions. This lithology is characterized by its permeability and high transmissivity and it is associated to chalk aquifers that operate as a reservoir in these regimens thanks to the aquifer recharge any time a precipitation deficit occurs. Our findings were supported by Lorenzo-Lacruz et al. (2013a) who showed similar results to ours in a selection of 58 unregulated basins in Iberian Peninsula (specifically most of these basins are located in Iberian System). At the same time, the elevation, the vegetation cover and the land-use are influential factors that influence the hydrological cycle processes making a substantial difference in the response of basins with diverse characteristics to drought.

5. Conclusions.

- Strong correlations were found between the seven drought indices here assessed and the standardized streamflow. Multi-scalar drought indices excelled as the most suitable tools for hydrological drought purposes. Not having found significant differences in the performance of the SPEI, the SPI or the SPDI, authors suggest the interchangeably use of any of them.
- There is a seasonal component in the response of streamflow to climate that determine the propagation from climatic drought to hydrological drought.
- Undisturbed river basins in peninsular Spain mainly respond to short time-scales, emphasizing the role of precipitation as the major climatic driver in streamflow droughts.
- In line with the latter point, there is a complexity associated to the propagation of climatic drought to streamflow under near-natural conditions. We identified a wide range of temporal responses in peninsular Spain river basins related to local non-climatic characteristics such physiography and vegetation cover.

Authors are aware of the limitations involved in this kind of general analysis and are encouraged to work on further analysis necessary to fully understand the influence of the non-climatic mechanisms controlling the delayed response of streamflow to climatic drought in the basins here assessed.

Tables

Table 1. Percentage of basins per index and time-scale at which the maximum correlations were found. Notice that long time-scales from 13 to 48-month were summarized in two groups (13-24 and >24-month) due the low percentages recorded individually.

	1	2	3	4	5	6	7	8	9	10	11	12	13-24	> 24
SPI	7.93	33.04	14.54	7.93	8.37	3.08	4.41	3.52	0.44	1.32	1.32	1.76	4.41	7.93
SPDI	14.98	42.29	14.10	5.73	3.52	3.08	0.88	1.32	0.88	1.32	0.88	0.88	2.64	7.49
SPEI	10.13	36.12	15.86	8.37	6.61	3.52	0.88	2.20	0.88	1.32	0.44	0.44	4.41	8.81
Averaged (%)	11.01	37.15	14.83	7.34	6.17	3.23	2.06	2.35	0.73	1.32	0.88	1.03	3.82	8.08

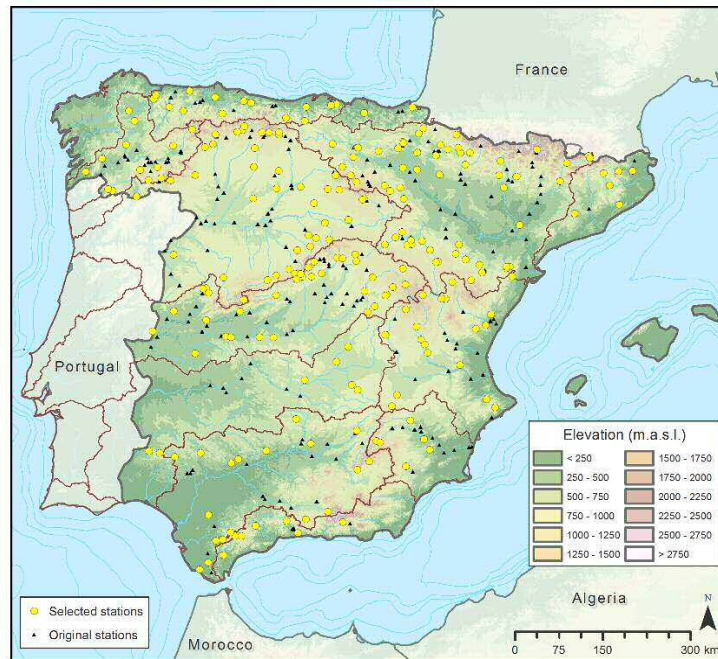


Figure 1. Location of the available (black dots) and selected (yellow dots) streamflow gauging stations.

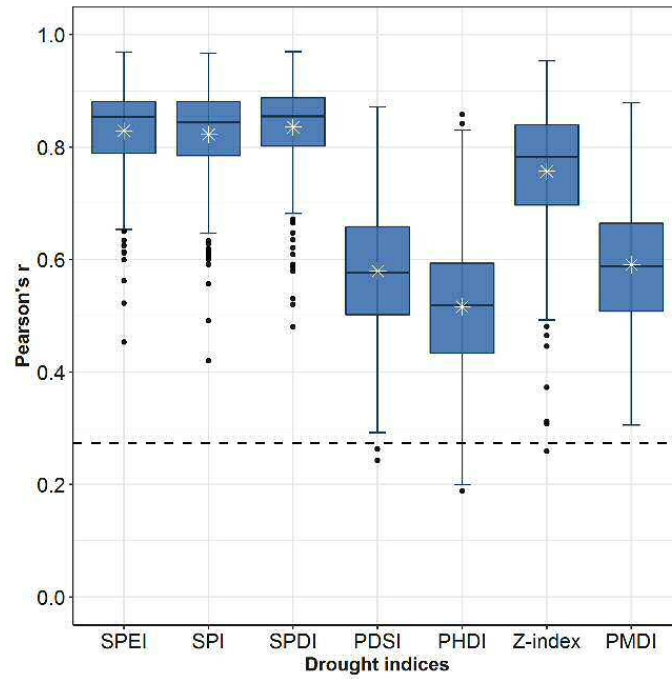


Figure 2. Box plots showing the strongest correlation coefficients found between climatic drought indices and the SSI for the 226 natural basins considered in this study. The solid black line shows the median, the white asterisk shows the mean, and the dashed black line shows the $p < 0.05$ significance level.

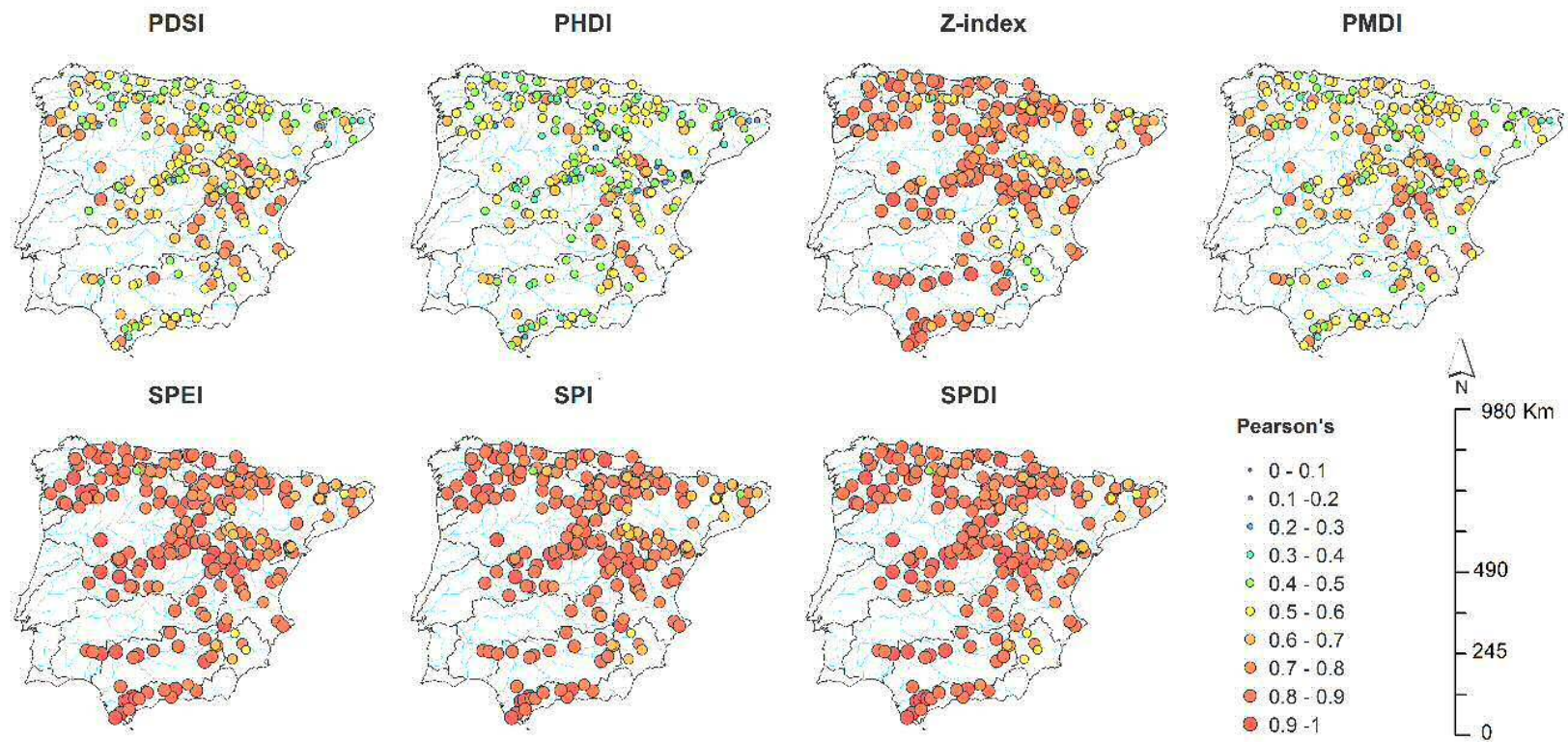


Figure 3. Spatial distribution of the highest correlation coefficients between the climatic drought indices and the SSI independently of the month of the year and drought time-scale.

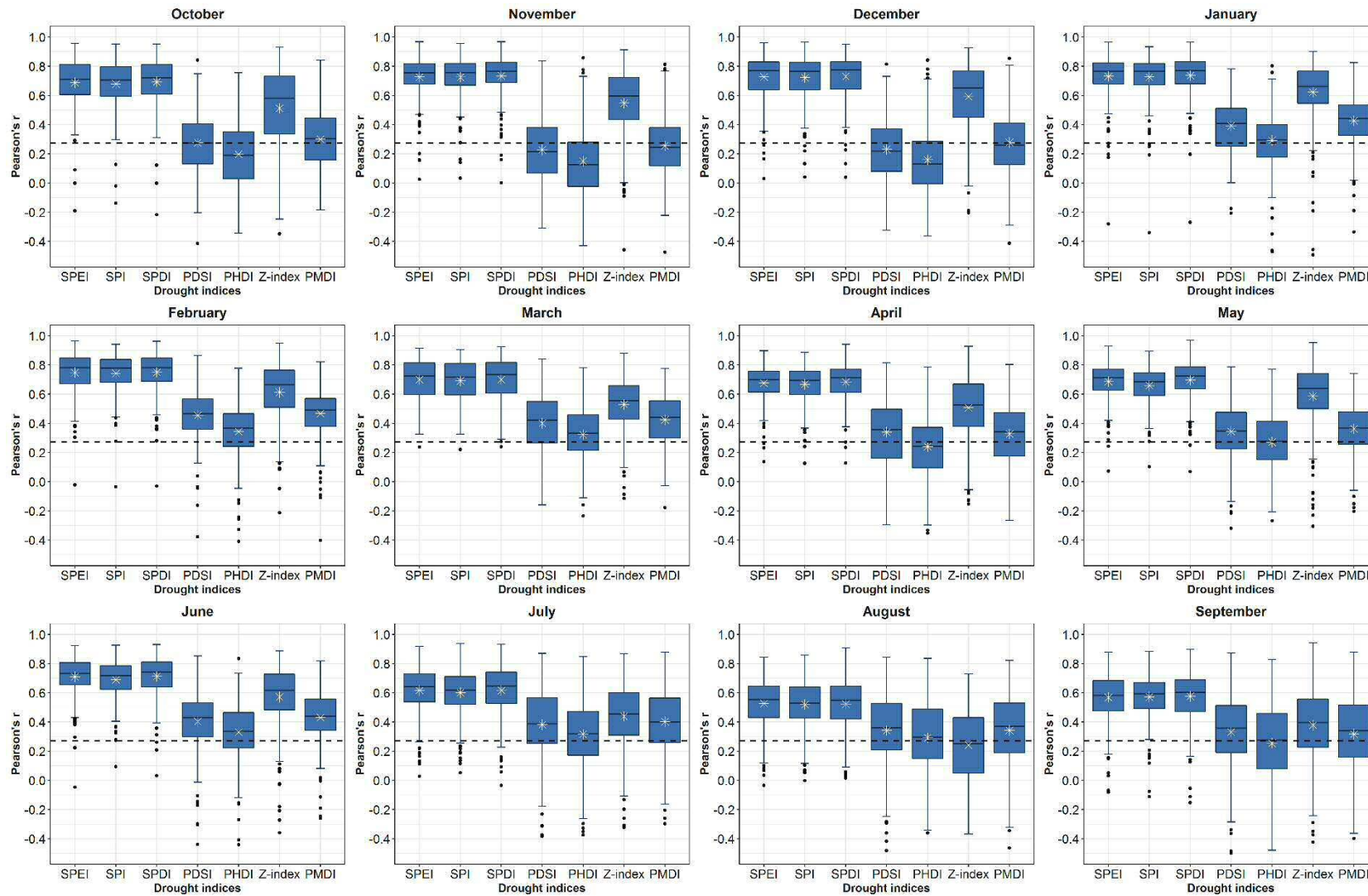


Figure 4. Boxplots showing the monthly Pearson correlation coefficients obtained between series of the SSI and the seven drought indices. The dashed solid black line corresponds to the median, the white asterisk the mean and the dashed black line the $p < 0.05$ significance level.

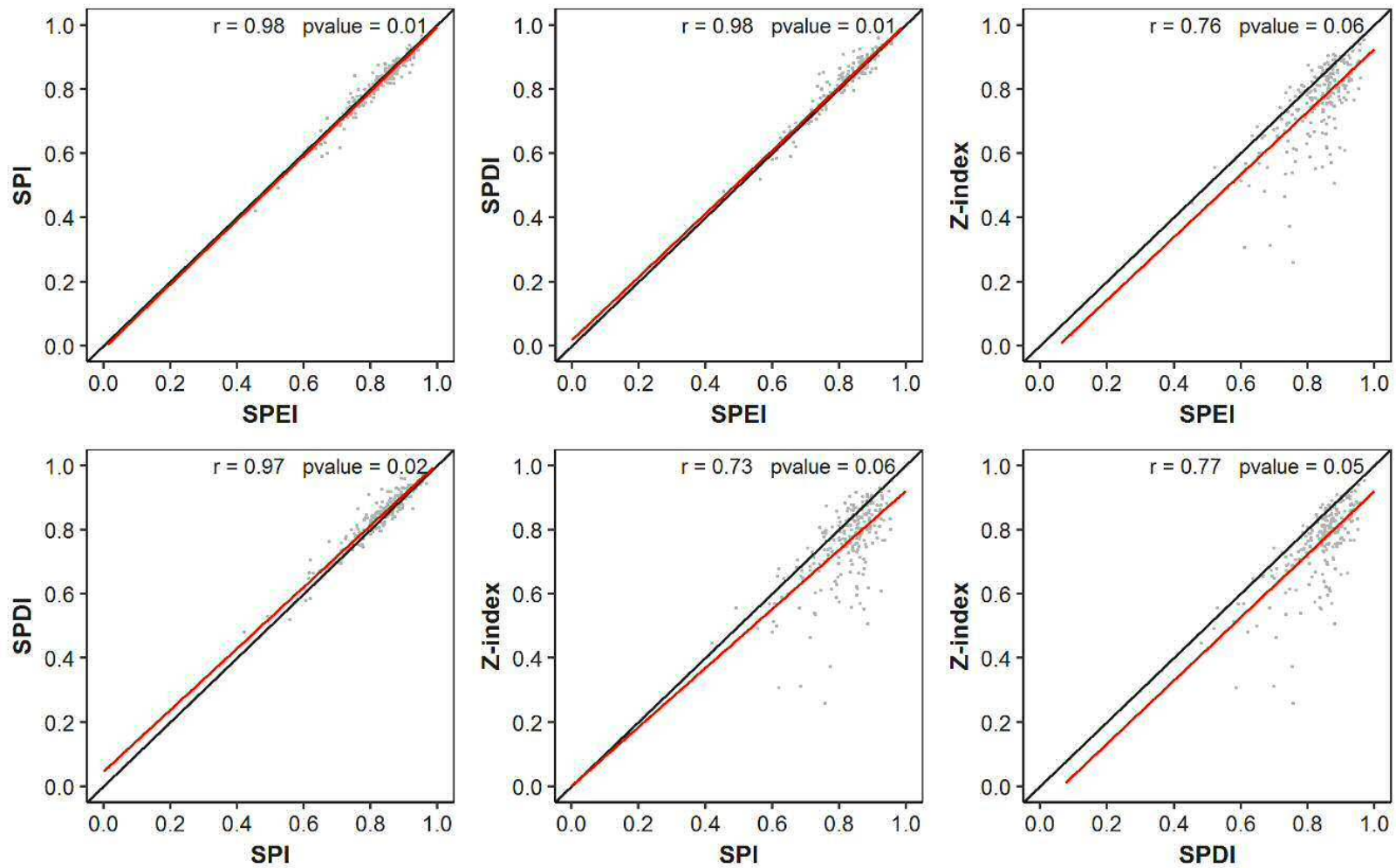


Figure 5. Maximum correlation scatterplots of index pairs (SPEI, SPI, SPDI and Z-index). Each point corresponds to the highest Pearson's correlation coefficient recorded in each basin.

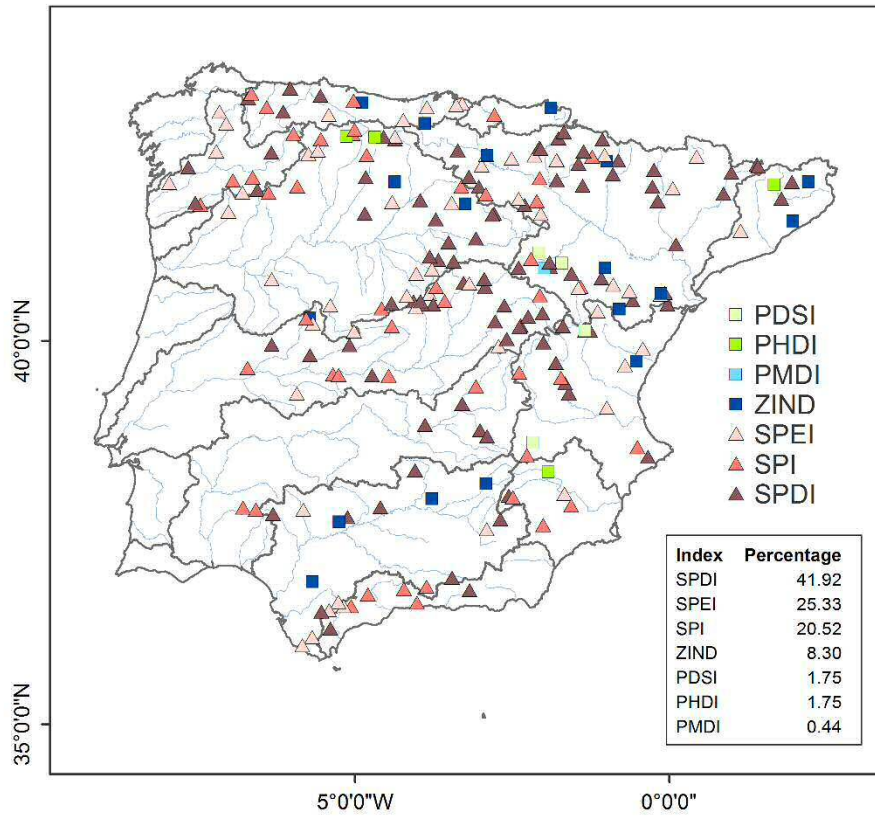


Figure 6. Spatial distribution of the drought indices having the strongest correlations with the SSI and the percentage in each case.

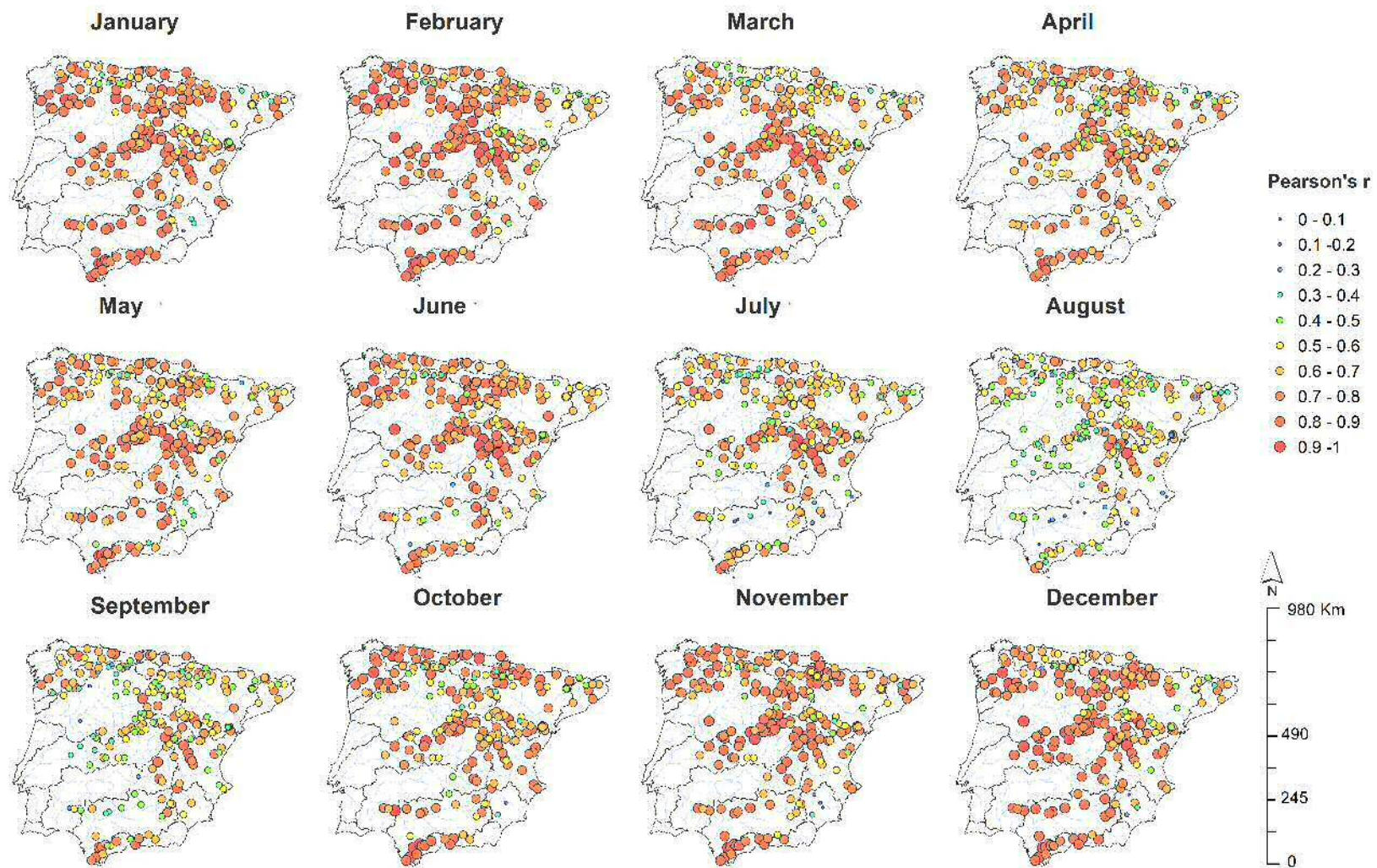


Figure 7. Spatial distribution of the monthly highest correlation coefficients between the SPDI and the SSI independently of the month and time-scale.

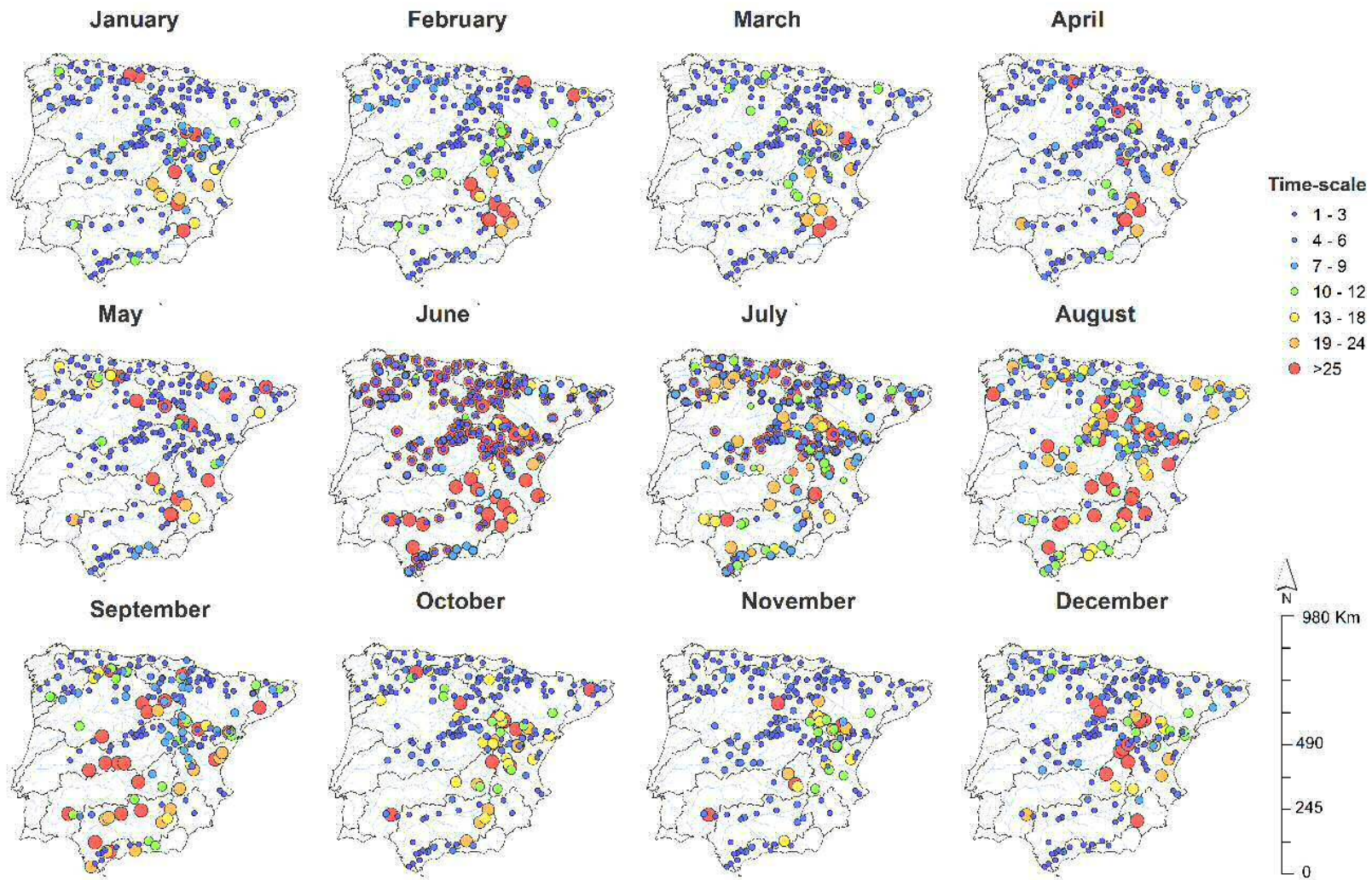


Figure 8. Spatial distribution of the time-scales at which monthly highest correlation coefficients between the SPDI and the SSI were found.

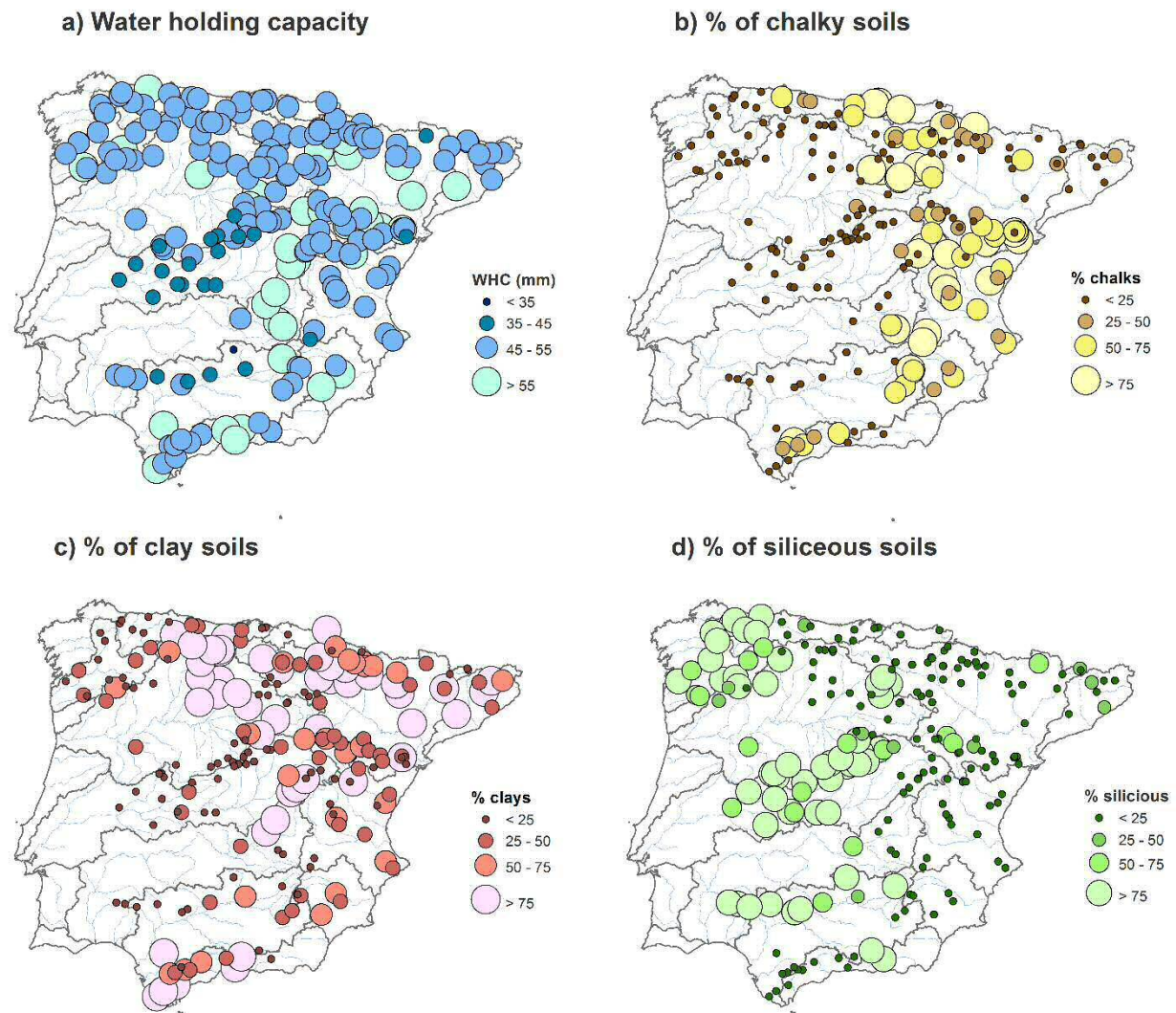


Figure 9. Water holding capacity (a) and percentage of surface characterized by the dominant lithology (b, c, d) of the analysed basins.

References

- Abramowitz, M., Stegun, I.A., 1970. Handbook of mathematical functions : with formulas, graphs, and mathematical tables. Dover Publications.
- Allen, R.G., Pereira, L.S., Raes, D., Smith, M., 1998. Crop Evapotranspiration: Guidelines for Computing Crop Water Requirements.
- Alley, W.M., 1984. The Palmer Drought Severity Index: Limitations and Assumptions. *J. Clim. Appl. Meteorol.* 23, 1100–1109. [https://doi.org/10.1175/1520-0450\(1984\)023<1100:TPDSIL>2.0.CO;2](https://doi.org/10.1175/1520-0450(1984)023<1100:TPDSIL>2.0.CO;2)
- Asseng, S., Ewert, F., Martre, P., Rötter, R.P., Lobell, D.B., Cammarano, D., Kimball, B.A., Ottman, M.J., Wall, G.W., White, J.W., Reynolds, M.P., Alderman, P.D., Prasad, P.V. V., Aggarwal, P.K., Anothai, J., Basso, B., Biernath, C., Challinor, A.J., De Sanctis, G., Doltra, J., Fereres, E., Garcia-Vila, M., Gayler, S., Hoogenboom, G., Hunt, L.A., Izaurralde, R.C., Jabloun, M., Jones, C.D., Kersebaum, K.C., Koehler, A.-K., Müller, C., Naresh Kumar, S., Nendel, C., O’Leary, G., Olesen, J.E., Palosuo, T., Priesack, E., Eyshi Rezaei, E., Ruane, A.C., Semenov, M.A., Shcherbak, I., Stöckle, C., Stratonovitch, P., Streck, T., Supit, I., Tao, F., Thorburn, P.J., Waha, K., Wang, E., Wallach, D., Wolf, J., Zhao, Z., Zhu, Y., 2014. Rising temperatures reduce global wheat production. *Nat. Clim. Chang.* 5, 143–147. <https://doi.org/10.1038/nclimate2470>
- Ayehu, G., Tadesse, T., Gessesse, B., Yigrem, Y., Ayehu, G., Tadesse, T., Gessesse, B., Yigrem, Y., 2019. Soil Moisture Monitoring Using Remote Sensing Data and a Stepwise-Cluster Prediction Model: The Case of Upper Blue Nile Basin, Ethiopia. *Remote Sens.* 11, 125. <https://doi.org/10.3390/rs11020125>
- Bachmair, S., Stahl, K., Collins, K., Hannaford, J., Acreman, M., Svoboda, M., Knutson, C., Smith, K.H., Wall, N., Fuchs, B., Crossman, N.D., Overton, I.C., 2016. Drought indicators revisited: the need for a wider consideration of environment and society. *Wiley Interdiscip. Rev. Water* 3, 516–536. <https://doi.org/10.1002/wat2.1154>
- Ballabio, C., Panagos, P., Monatanarella, L., 2016. Mapping topsoil physical properties at European scale using the LUCAS database. *Geoderma* 261, 110–123. <https://doi.org/10.1016/J.GEODERMA.2015.07.006>
- Barker, L.J., Hannaford, J., Chiverton, A., Svensson, C., 2016. From meteorological to hydrological drought using standardised indicators. *Hydrol. Earth Syst. Sci.* 20, 2483–2505. <https://doi.org/10.5194/hess-20-2483-2016>
- Batalla, R.J., Gómez, C.M., Kondolf, G.M., 2004. Reservoir-induced hydrological changes in the Ebro River basin (NE Spain). *J. Hydrol.* 290, 117–136. <https://doi.org/10.1016/J.JHYDROL.2003.12.002>
- Beguiría, S., López-Moreno, J.I., Lorente, A., Seeger, M., García-Ruiz, J.M., 2003. Assessing the effect of climate oscillations and land-use changes on streamflow in the central Spanish Pyrenees. *Ambio* 32, 283–6.

- Bloomfield, J.P., Marchant, B.P., Bricker, S.H., Morgan, R.B., 2015. Regional analysis of groundwater droughts using hydrograph classification. *Hydrol. Earth Syst. Sci.* 19, 4327–4344. <https://doi.org/10.5194/hess-19-4327-2015>
- Camarero, J.J., Gazol, A., Sangüesa-Barreda, G., Oliva, J., Vicente-Serrano, S.M., 2015. To die or not to die: early warnings of tree dieback in response to a severe drought. *J. Ecol.* 103, 44–57. <https://doi.org/10.1111/1365-2745.12295>
- Doesken, N.J., Garen, D., 1991. Drought monitoring in the Western United States using a surface water supply index. Presented at: 7th Conference on Applied Climatology, Sept. 10-13, 1991 in Salt Lake City, Utah, in: Fort Collins, CO: Colorado State University, D. of A.S. (Ed.), *Development of a Surface Water Supply Index (SWSI) for the Western United States, 1991*. pp. 77–80.
- Dogan, S., Berktaş, A., Singh, V.P., 2012. Comparison of multi-monthly rainfall-based drought severity indices, with application to semi-arid Konya closed basin, Turkey. *J. Hydrol.* 470–471, 255–268. <https://doi.org/10.1016/J.JHYDROL.2012.09.003>
- Guttman, N.B., 1998. Comparing the Palmer Drought Index and the Standardized Precipitation Index. *J. Am. Water Resour. Assoc.* 34, 113–121. <https://doi.org/10.1111/j.1752-1688.1998.tb05964.x>
- Haslinger, K., Koffler, D., Schöner, W., Laaha, G., 2014. Exploring the link between meteorological drought and streamflow: Effects of climate-catchment interaction. *Water Resour. Res.* 50, 2468–2487. <https://doi.org/10.1002/2013WR015051>
- Hayes, M., Svoboda, M., Wall, N., Widhalm, M., 2011. The Lincoln Declaration on Drought Indices Universal Meteorological Drought Index: Recommended Interregional Workshop on Indices and Early Warning Systems for Drought. *Bull. Am. Meteorol. Soc.* 92(4), 485–488. <https://doi.org/10.1175/2010BAMS3103.1>
- Huang, S., Li, P., Huang, Q., Leng, G., Hou, B., Ma, L., 2017. The propagation from meteorological to hydrological drought and its potential influence factors. *J. Hydrol.* 547, 184–195. <https://doi.org/10.1016/J.JHYDROL.2017.01.041>
- Liu, Y., Zhu, Y., Ren, L., Singh, V.P., Yong, B., Jiang, S., Yuan, F., Yang, X., 2019. Understanding the spatiotemporal links between meteorological and hydrological droughts from a three-dimensional perspective. *J. Geophys. Res. Atmos.* 2018JD028947. <https://doi.org/10.1029/2018JD028947>
- Lloyd-Hughes, B., 2014. The impracticality of a universal drought definition. *Theor. Appl. Climatol.* 117, 607–611. <https://doi.org/10.1007/s00704-013-1025-7>
- López-Moreno, J.I., Vicente-Serrano, S.M., Beguería, S., García-Ruiz, J.M., Portela, M.M., Almeida, A.B., 2009. Dam effects on droughts magnitude and duration in a transboundary basin: The Lower River Tagus, Spain and Portugal. *Water Resour. Res.* 45. <https://doi.org/10.1029/2008WR007198>

- López-Moreno, J.I., Vicente-Serrano, S.M., Zabalza, J., Beguería, S., Lorenzo-Lacruz, J., Azorin-Molina, C., Morán-Tejeda, E., 2013. Hydrological response to climate variability at different time scales: A study in the Ebro basin. *J. Hydrol.* 477, 175–188. <https://doi.org/10.1016/J.JHYDROL.2012.11.028>
- Lorenzo-Lacruz, J., Garcia, C., Morán-Tejeda, E., 2017. Groundwater level responses to precipitation variability in Mediterranean insular aquifers. *J. Hydrol.* 552, 516–531. <https://doi.org/10.1016/J.JHYDROL.2017.07.011>
- Lorenzo-Lacruz, J., Morán-Tejeda, E., Vicente-Serrano, S.M., López-Moreno, J.I., 2013a. Streamflow droughts in the Iberian Peninsula between 1945 and 2005: spatial and temporal patterns. *Hydrol. Earth Syst. Sci.* 17, 119–134. <https://doi.org/10.5194/hess-17-119-2013>
- Lorenzo-Lacruz, J., Vicente-Serrano, S., González-Hidalgo, J., López-Moreno, J., Cortesi, N., 2013b. Hydrological drought response to meteorological drought in the Iberian Peninsula. *Clim. Res.* 58, 117–131. <https://doi.org/10.3354/cr01177>
- Lorenzo-Lacruz, J., Vicente-Serrano, S.M., López-Moreno, J.I., Beguería, S., García-Ruiz, J.M., Cuadrat-Prats, J.M., 2010. The impact of droughts and water management on various hydrological systems in the headwaters of the Tagus River (central Spain). *J. Hydrol.* 386, 13–26. <https://doi.org/10.1016/j.jhydrol.2010.01.001>
- Loukas, A., Vasiliades, L., 2004. Probabilistic analysis of drought spatiotemporal characteristics inThessaly region, Greece. *Nat. Hazards Earth Syst. Sci.* 4, 719–731. <https://doi.org/10.5194/nhess-4-719-2004>
- Ma, M., Ren, L., Yuan, F., Jiang, S., Liu, Y., Kong, H., Gong, L., 2014. A new standardized Palmer drought index for hydro-meteorological use. *Hydrol. Process.* 28, 5645–5661. <https://doi.org/10.1002/hyp.10063>
- Marchant, B.P., Bloomfield, J.P., 2018. Spatio-temporal modelling of the status of groundwater droughts. *J. Hydrol.* 564, 397–413. <https://doi.org/https://doi.org/10.1016/j.jhydrol.2018.07.009>
- Mckee, T.B., Doesken, N.J., Kleist, J., 1993. The relationship of drought frequency and duration to time scales. *Eighth Conf. Appl. Climatol.* 17–22.
- Mishra, A.K., Singh, V.P., 2010. A review of drought concepts. *J. Hydrol.* 391, 202–216. <https://doi.org/10.1016/j.jhydrol.2010.07.012>
- Mosley, L.M., 2015. Drought impacts on the water quality of freshwater systems; review and integration. *Earth-Science Rev.* 140, 203–214. <https://doi.org/10.1016/J.EARSCIREV.2014.11.010>
- Mukherjee, S., Mishra, A., Trenberth, K.E., 2018. Climate Change and Drought: a Perspective on Drought Indices. *Curr. Clim. Chang. Reports* 4, 145–163. <https://doi.org/10.1007/s40641-018-0098-x>

Ortega-Gómez, T., Pérez-Martín, M.A., Estrela, T., 2018. Improvement of the drought indicators system in the Júcar River Basin, Spain. *Sci. Total Environ.* 610–611, 276–290. <https://doi.org/10.1016/j.scitotenv.2017.07.250>

Palmer, W.C., 1965. Meteorological Drought. Research Paper No. 45, 1965, 58 p. U.S. Dep. Commer. Weather Bur. Washington, DC. Research P.

Peña-Gallardo, M., Vicente-Serrano, S.M., Hannaford, J., Lorenzo-Lacruz, J., Svoboda, M., Domínguez-Castro, F., Maneta, M., Tomas-Burguera, M., Kenawy, A. El, 2019. Complex influences of meteorological drought time-scales on hydrological droughts in natural basins of the contiguous United States. *J. Hydrol.* 568, 611–625. <https://doi.org/10.1016/j.jhydrol.2018.11.026>

Peters, E., van Lanen, H.A.J., Torfs, P.J.J.F., Bier, G., 2005. Drought in groundwater—drought distribution and performance indicators. *J. Hydrol.* 306, 302–317. <https://doi.org/10.1016/j.jhydrol.2004.09.014>

Rangecroft, S., Van Loon, A.F., Coxon, G., Breña-Naranjo, J.A., Van Ogtrop, F., Van Lanen, H.A.J., 2018. Using paired catchments to quantify the human influence on hydrological droughts. *Hydrol. Earth Syst. Sci. Discuss.* 1–23. <https://doi.org/10.5194/hess-2018-215>

Scaini, A., Sánchez, N., Vicente-Serrano, S.M., Martínez-Fernández, J., 2015. SMOS-derived soil moisture anomalies and drought indices: a comparative analysis using *in situ* measurements. *Hydrol. Process.* 29, 373–383. <https://doi.org/10.1002/hyp.10150>

Tallaksen, L.M., Van Lanen, H.A., 2004. Hydrological drought : processes and estimation methods for streamflow and groundwater, 48th ed, Developments in Water Science. Elsevier Science B.V., Amsterdam, the Netherlands.

Tetzlaff, D., McDonnell, J.J., Uhlenbrook, S., McGuire, K.J., Bogaart, P.W., Naef, F., Baird, A.J., Dunn, S.M., Soulsby, C., 2008. Conceptualizing catchment processes: simply too complex? *Hydrol. Process.* 22, 1727–1730. <https://doi.org/10.1002/hyp.7069>

Tijdeman, E., Hannaford, J., Stahl, K., 2018. Human influences on streamflow drought characteristics in England and Wales. *Hydrol. Earth Syst. Sci.* 22, 1051–1064. <https://doi.org/10.5194/hess-22-1051-2018>

Van Lanen, H.A.J., Wanders, N., Tallaksen, L.M., Van Loon, A.F., 2013. Hydrological drought across the world: impact of climate and physical catchment structure. *Hydrol. Earth Syst. Sci.* 17, 1715–1732. <https://doi.org/10.5194/hess-17-1715-2013>

Van Loon, A.F., 2015. Hydrological drought explained. *Wiley Interdiscip. Rev. Water* 2, 359–392. <https://doi.org/10.1002/wat2.1085>

Van Loon, A.F., Gleeson, T., Clark, J., Van Dijk, A.I.J.M., Stahl, K., Hannaford, J., Di Baldassarre, G., Teuling, A.J., Tallaksen, L.M., Uijlenhoet, R., Hannah, D.M., Sheffield, J., Svoboda, M., Verbeiren, B.,

- Wagener, T., Rangecroft, S., Wanders, N., Van Lanen, H.A.J., 2016. Drought in the Anthropocene. *Nat. Geosci.* 9, 89–91. <https://doi.org/10.1038/ngeo2646>
- Van Loon, A.F., Laaha, G., 2015. Hydrological drought severity explained by climate and catchment characteristics. *J. Hydrol.* 526, 3–14. <https://doi.org/10.1016/j.jhydrol.2014.10.059>
- Vasiliades, L., Loukas, A., 2009. Hydrological response to meteorological drought using the Palmer drought indices in Thessaly, Greece. *Desalination* 237, 3–21. <https://doi.org/10.1016/j.desal.2007.12.019>
- Vicente-Serrano, S.M., Beguería, S., López-Moreno, J.I., 2011. Comment on “Characteristics and trends in various forms of the Palmer Drought Severity Index (PDSI) during 1900–2008” by Aiguo Dai. *J. Geophys. Res.* 116, D19112. <https://doi.org/10.1029/2011JD016410>
- Vicente-Serrano, S.M., Beguería, S., López-Moreno, J.I., Vicente-Serrano, S.M., Beguería, S., López-Moreno, J.I., 2010. A Multiscalar Drought Index Sensitive to Global Warming: The Standardized Precipitation Evapotranspiration Index. *J. Clim.* 23, 1696–1718. <https://doi.org/10.1175/2009JCLI2909.1>
- Vicente-Serrano, S.M., Beguería, S., Lorenzo-Lacruz, J., Camarero, J.J., López-Moreno, J.I., Azorin-Molina, C., Revuelto, J., Morán-Tejeda, E., Sanchez-Lorenzo, A., Vicente-Serrano, S.M., Beguería, S., Lorenzo-Lacruz, J., Camarero, J.J., López-Moreno, J.I., Azorin-Molina, C., Revuelto, J., Morán-Tejeda, E., Sanchez-Lorenzo, A., 2012. Performance of Drought Indices for Ecological, Agricultural, and Hydrological Applications. <http://dx.doi.org/10.1175/2012EI000434.1>. <https://doi.org/10.1175/2012EI000434.1>
- Vicente-Serrano, S.M., Lopez-Moreno, J.-I., Beguería, S., Lorenzo-Lacruz, J., Sanchez-Lorenzo, A., García-Ruiz, J.M., Azorin-Molina, C., Morán-Tejeda, E., Revuelto, J., Trigo, R., Coelho, F., Espejo, F., 2014. Evidence of increasing drought severity caused by temperature rise in southern Europe. *Environ. Res. Lett.* 9, 44001–9. <https://doi.org/10.1088/1748-9326/9/4/044001>
- Vicente-Serrano, S.M., López-Moreno, J.I., 2005. Hydrological response to different time scales of climatological drought: an evaluation of the Standardized Precipitation Index in a mountainous Mediterranean basin. *Hydrol. Earth Syst. Sci.* 9, 523–533. <https://doi.org/10.5194/hess-9-523-2005>
- Vicente-Serrano, S.M., Tomas-Burguera, M., Beguería, S., Reig, F., Latorre, B., Peña-Gallardo, M., Luna, M.Y., Morata, A., González-Hidalgo, J.C., 2017. A High Resolution Dataset of Drought Indices for Spain. *Data* 2, 22. <https://doi.org/10.3390/data2030022>
- Vicente-Serrano, S.M., Zabalza-Martínez, J., Borràs, G., López-Moreno, J.I., Pla, E., Pascual, D., Savé, R., Biel, C., Funes, I., Azorin-Molina, C., Sanchez-Lorenzo, A., Martín-Hernández, N., Peña-Gallardo, M., Alonso-González, E., Tomas-Burguera, M., El Kenawy, A., 2017. Extreme hydrological events and the influence of reservoirs in a highly regulated river basin of northeastern Spain. *J. Hydrol. Reg. Stud.* 12. <https://doi.org/10.1016/j.ejrh.2017.01.004>

Vicente-Serrano, S.M., Zabalza-Martínez, J., Borràs, G., López-Moreno, J.I., Pla, E., Pascual, D., Savé, R., Biel, C., Funes, I., Martín-Hernández, N., Peña-Gallardo, M., Beguería, S., Tomas-Burguera, M., 2015. Effect of reservoirs on streamflow and river regimes in a heavily regulated river basin of Northeast Spain. *Catena*. <https://doi.org/10.1016/j.catena.2016.03.042>

Von Gunten, D., Wöhling, T., Haslauer, C.P., Merchán, D., Causapé, J., Cirpka, O.A., 2016. Using an integrated hydrological model to estimate the usefulness of meteorological drought indices in a changing climate. *Hydrol. Earth Syst. Sci* 20, 4159–4175. <https://doi.org/10.5194/hess-20-4159-2016>

Wang, H., Rogers, J.C., Munroe, D.K., Wang, H., Rogers, J.C., Munroe, D.K., 2015. Commonly Used Drought Indices as Indicators of Soil Moisture in China. *J. Hydrometeorol.* 16, 1397–1408. <https://doi.org/10.1175/JHM-D-14-0076.1>

Wells, N., Goddard, S., Hayes, M.J., Wells, N., Goddard, S., Hayes, M.J., 2004. A Self-Calibrating Palmer Drought Severity Index. *J. Clim.* 17, 2335–2351. [https://doi.org/10.1175/1520-0442\(2004\)017<2335:ASPDSI>2.0.CO;2](https://doi.org/10.1175/1520-0442(2004)017<2335:ASPDSI>2.0.CO;2)

Wilhite, D.A., Glantz, M.H., 1985. Understanding: the Drought Phenomenon: The Role of Definitions. *Water Int.* 10, 111–120. <https://doi.org/10.1080/02508068508686328>

WMO, 2012. Standardized Precipitation Index User Guide. http://www.wamis.org/agm/pubs/SPI/WMO_1090_EN.pdf (Last access, 22 February 2019)

Yang, Y., Zhang, S., McVicar, T.R., Beck, H.E., Zhang, Y., Liu, B., 2018. Disconnection Between Trends of Atmospheric Drying and Continental Runoff. *Water Resour. Res.* 54, 4700–4713. <https://doi.org/10.1029/2018WR022593>

Zargar, A., Sadiq, R., Naser, B., Khan, F.I., 2011. A review of drought indices. *Environ. Rev.* 19, 333–349. <https://doi.org/10.1139/a11-013>

Zhai, J., Su, B., Krysanova, V., Vetter, T., Gao, C., Jiang, T., Zhai, J., Su, B., Krysanova, V., Vetter, T., Gao, C., Jiang, T., 2010. Spatial Variation and Trends in PDSI and SPI Indices and Their Relation to Streamflow in 10 Large Regions of China. *J. Clim.* 23, 649–663. <https://doi.org/10.1175/2009JCLI2968.1>

Human mortality and climate indices in Spain

1. Introduction

Although climate conditions affect human health, physiology, and mortality¹, understanding the impacts of climate change and variability on human health is a challenge. In the context of climate change, a higher frequency of extreme events (e.g. heatwaves, droughts, etc) has been reported in numerous studies at different spatial scales ranging from local to global scales^{2,3,4,5}. Several studies have been conducted to understand the relationships between human mortality and heatwaves^{6,7,8,9}. Most of these studies indicate that heatwaves increase human mortality. A representative example is the 2003 heatwave in which 44,000 excess fatalities in Europe were reported by the World Health Organization (WHO)^{10,11}. However, it is not only heatwaves that can have a high impact on mortality, but cold waves^{12,13} and drought events^{14,15,16,17} can also have a major impact on mortality. Epidemiological evidences indicate that part of the deaths caused by cold waves are due to their infectious nature, while an increase in the number of deaths during heat waves is caused by the direct effects of heat stress on the individual metabolism¹³. Drought, on the other hand, has also significant health impacts, including an increasing risk of morbidity and mortality¹⁴. Also, drought has indirect effects on human health and mortality, as deaths in this case may be caused by the reduction of water resources quantity and quality, crop and food production, or an increased risk of heat-waves and wildfires, among others¹⁸.

The ways in which climate can impact mortality vary considerably, as a function of seasons and dominant climatic conditions^{19,20,21}. Seasonally, the increased mortality during cold months is well-established in relation warm months^{20,22,23}. Causes of death, which are more associated with temperature changes, are circulatory and respiratory diseases¹⁹. Furthermore, it is important to note that seasonal and annual flu epidemics involve a high level of hospitalizations and winter mortality²⁴.

Although mortality is conditioned by climatic conditions, other socio-demographic characteristics, such as age, socioeconomic status, and number of inhabitants, can impact this dependency. There is evidence that climate conditions have a particular impact on elderly population⁷, mainly due to the decreased physiological capacity to regulate body core temperature²⁵. In this regard, the spatial distribution of elderly population allows to define which regions are more sensitive to the impact of climate changes on mortality.

Although most investigations about the relationship between climatic conditions and mortality take into account the effects of temperatures on mortality^{26,27,28}, other important climatic variables that

can affect mortality (e.g. precipitation, wind, radiation, cloud cover, etc.) have received less attention in the literature. For example, precipitation drives droughts; wind conditions influence pollution; and cloudiness affect precipitation. It is therefore important to have a catalog of comprehensive climate indices, which can be used to understand the impacts of different climatic factors on mortality rates. Many efforts have been made to develop climatic indices to understand the evolution and state of climate^{29,30,31,32,33}. These climatic indices have been employed in a number of previous studies to assess the impacts of climate on various sectors, such as the impact of drought on agriculture³⁴ or water resources³⁵, among others. Recently, the database and cartographic viewer “INDECIS dataset” include the highest range of climatic indices (125) for Europe. These indices were published with the aim of serving as a tool to evaluate the impact of climate on different sectors³⁶ (<https://indecis.csic.es/>). This database contains the largest variety of climatic indices, provided at a high spatial resolution and for a continuous and updated period. Also, the “ECTACI database” has been published recently by Peña-Angulo³⁷ (<https://ectaci.csic.es/>), allowing for characterizing climatology, variability and trends of the 125 indices of the INDECIS database.

This study employs the INDECIS climatic dataset to assess the impacts of climate on natural death. The study is carried out in the mainland Spain, which has interesting socio-demographic and climatic characteristics. Specifically, like the whole Spanish territory, the mainland Spain is characterized by high rates of elderly populations and correspondingly a low birth rate^{8,38,39}. Also, Spain is characterized by strong spatial and temporal variability of climate, with several configurations driving this variability (e.g. Atlantic, Mediterranean, sub-tropical, etc.). Specifically, the mainland Spain has witnessed frequent extreme heat events, which can induce high mortality rates. Overall, these demographic and climatic features make the mainland Spain a good base region to assess the spatial and temporal variability of mortality in response to climate change and variability. Overall, this study aims to: i) assess the spatial and seasonal distributions of mortality in mainland Spain; and ii) analyze the relationship between climatic indices and mortality taking into account spatial, seasonal, and inter-index differences.

1. Results

2.1 Spatial and seasonal distribution of natural deaths in mainland Spain

Results indicate large spatial differences in natural deaths, which are linked to the way in which the percentage of elderly population varies across the study domain. Figure 3 depicts the spatial distribution

of the ageing index and the number of natural deaths, compared to the total population in the mainland Spain in 2015. As illustrated, the Northwest territory had a higher ageing index and natural deaths, while the eastern and southern regions had a lower ageing index and natural deaths. As expected, there is a high spatial agreement between provinces exhibiting the largest percentage of elders and those with the highest number of deaths (e.g. Ourense, Lugo, Zamora, Teruel, Soria, Cuenca, Ávila, and Palencia). In contrast, provinces with lower percentages of elders witnessed the lowest number of deaths (e.g. Madrid, Alava, Cadiz, Almeria, Murcia, Sevilla, and Guadalajara).

Spatially, we defined two main patterns summarizing the links between the number of natural deaths and climatic conditions dominating in the study domain. First, the provinces with the highest mortality and aging were located mainly in northwestern provinces characterized by low winter temperatures. Second, younger population and smallest death rates were distributed in southern provinces, with high summer temperatures and moderate temperatures.

Temporarily, results suggest strong seasonal variability of the number of natural deaths. The least mortality rates occurred during summertime, while the largest numbers recorded in winter. Figure 4 shows the regional series of natural deaths, calculated for each season independently. As illustrated, a higher number of deaths was observed in winter, followed by spring. The lowest numbers of death cases were recorded in summer and autumn. Unsurprisingly, a marked peak of natural deaths was noted in summer of 2003, which corresponded to the anomalous heatwave that triggered most of Europe in 2003. On the other hand, winter exhibited higher variability of natural deaths than other seasons.

2.2 Dependency between climatic indices and mortality rates in mainland Spain

Results reveal strong seasonal differences in climate-mortality association. Figure 5 illustrates correlation coefficients computed between regional series of natural deaths and 79 climate indices. Results are presented for each season. As illustrated, correlations were higher and statistically significant in winter and summer. Conversely, Pearson's r coefficients were much lower and mostly non-significant in spring and autumn. In winter, many climate indices exhibited strong negative correlations with natural deaths, while correlations were mostly positive in summer. For cold-day indices (e.g. CFD, CSDI, AT, and WCI), as well as radiation indices (e.g. SND, SSD, and SSP), positive correlation with the number of natural deaths was found during wintertime. Contrarily, negative correlations were found for temperature indices associated with warm days (e.g. XTG, XTN, HI,

and UTCI), cloudiness indices (e.g. CC, FOD), wind indices (e.g. FG, FG6Bft, and FXX), and most precipitation indices (e.g. RTI, PRCPTOT). In summer, natural deaths showed negative correlations for few indices (e.g. DTR and FOD), while the majority of indices were positively correlated with the number of natural deaths. Typically, this was the case for indices related to mean, minimum, and maximum temperatures like CSD, D32, DD17, TN90p, TX90p, VWD, and WSDI.

Overall, results indicated that the frequency of cold days contributed to an increase in mortality rate during wintertime. Rather, high frequency of warm days during winter caused it to decrease. Most climate indices, especially thermal indices, showed positive correlations with the number of natural deaths during summer. Specifically, VDTR, CC, VWD, and WSDI showed the highest correlations with natural deaths. In winter, indices showing highest correlations were CFD, FD, SND, SSD, SSP, CC, and FOD. Notably, in both cases, precipitation indices exhibited remarkably negative correlations with the number of natural deaths, being much stronger in winter than in summer.

Also, the above-described relationships were supported by a spatial analysis that considered these associations, but at the province level (Figure 6). At the province level, it was assured that higher correlations between climate indices and natural deaths were higher in winter and summer, compared to spring and autumn. However, the sign of association and the corresponding spatial distributions were different between these two seasons. Warm indices showed strong correlations with natural deaths, especially for WCI, UTCI, HI, AT, WSDI, TR, TX90p, and TN90p during summer. However, consistent spatial patterns cannot be identified. In the western provinces, precipitation indices showed higher correlations than other provinces.

Figure 7 illustrates the spatial distribution of correlation coefficients calculated between the number of natural deaths and a set of significant temperature (FD, WSDI), precipitation (RTI) and cloud/radiation (CC, SSP) indices. Results are presented for winter and summer. The FD index, defined as the total number of days with minimum temperature lower than 0°C, indicated higher correlations with natural deaths during wintertime, mainly in the western provinces. The WSDI index, which counts periods with at least 6 consecutive days with maximum air temperatures exceeding the 90th percentile of maximum air temperature distribution, correlated significantly and positively with natural deaths during summer. This strong dependency was evident for the whole study domain. On the contrary, correlations were not statistically significant in winter, but with strong differences between maritime and continental provinces. Both RTI (total precipitation) and CC indices (daily mean cloud cover)

revealed consistent seasonal and spatial patterns. Specifically, they showed strong negative correlations with natural deaths during wintertime, especially in the western provinces. In contrast, this dependency was statistically non-significant during summer, with no clear spatial patterns. Similarly, the SSP index (sunshine duration fraction) and CC (daily mean cloud cover) exhibited consistent spatial patterns in their relations with natural deaths, albeit with opposite correlation sign.

2. Discussion

3.1 Spatial and seasonal distribution of natural deaths in mainland Spain

The greatest number of natural deaths with respect to total populations was found mainly in northwestern provinces of the mainland Spain, where elderly populations and colder climate conditions are predominant. Overall, as compared to other European countries, Spain is characterized demographically by a considerable percentage of elders (above 65 years old), with an increasing trend of life expectancy and correspondingly lower birth rates⁴⁰. Indeed, there are important social and economic implications of these demographic characteristics, especially for healthcare services. Furthermore, the spatial distribution of the aging population is strongly heterogeneous, given that more innovative regions (urban areas) attract young people from rural areas. Historically, the differences between urban and rural regions in terms of innovation and aging population have grown rapidly⁴⁰. In Spain, there are higher ageing rates over northern and northwestern regions, while lower ageing population is a characteristic of Madrid and southern regions⁴¹. From a climatic perspective, northern and northwestern portions of the mainland Spain are characterized by colder, but seasonally dependent climate. Several studies have reported that elderly populations are mostly impacted by extreme weather events like heat and cold waves^{8,42,43,44}. This is typically the case in the mainland Spain, where regions of elderly populations are subjected to frequent and more severe extreme events⁴⁵.

Furthermore, the number of natural deaths in relation to climatic conditions was assessed on a seasonal basis. As compared to other seasons, higher and significant number of deaths occurred in winter periods, mainly due to below-normal temperatures. A range of earlier studies have presented similar results^{12,46,47}.

There are several biological processes underlying high and low ambient temperatures. According to Gasparrini⁴⁷, in cold regions, mortality is associated more with cardiovascular and respiratory effects. In contrast, mortality is related to cardiovascular effects in warm regions, as body exceeds its

thermoregulatory threshold. Our study indicates that it is not only heatwaves that should be taken into account. Rather, that cold waves could have a higher risk for populations. In the Spanish case, populations of elderly population are located in the coldest regions, with increased environmental vulnerability to extreme cold⁴⁸.

3.2 Dependency between climatic indices and mortality in mainland Spain

Findings of this study indicate seasonal differences in the response of mortality rates to climatic conditions in the mainland Spain. Natural deaths mostly correspond to summer and winter than to spring and autumn. This is expected because extreme events that affect natural deaths occur both in winter and summer. Nonetheless, climate indices have an opposed relationship with natural deaths in winter and summer. Specifically, climate indices related to high winter temperatures correlate negatively with natural deaths, while they have positive correlations during summertime. In winter, the number of natural fatalities increases when cold waves occur, suggesting that indices related to cold temperatures have major influence on mortality rates during winter. Many studies have indicated that - during summer- heatwaves increase natural deaths^{7,9,11,27,28}, although studies analyzing the effect of cold waves on mortality are limited^{49,50}.

From a spatial perspective, considerable seasonal differences in the relationship between mortality rates and climatic indices can be found. In general, indices of extreme warm temperatures show a significant positive correlation with natural deaths across the entire territory, especially in summer. In winter, indices related to extreme cold temperature events exhibit a significant positive correlation with natural deaths. This was the case in the study domain, especially western provinces of the study domain. On the other hand, precipitation and cloudiness indices showed negative correlations with natural deaths, mainly in winter and in western provinces. In this view, Salvador¹⁷ noted that western portions of the mainland Spain have the highest daily mortality risks associated with drought related conditions. This finding is confirmed in this study, particularly in the western provinces, where there has been an increase in natural deaths during periods of drought, while the natural deaths decrease in wet periods.

Numerous studies have focused on the relationship between temperature and mortality^{28,44,49}. However, few investigations have addressed the association between precipitation and mortality⁵¹.

Most work about precipitation-mortality dependency have indicated that there can be an increase in the number of fatal accidents due to flood or water contamination⁵².

In this study, precipitation indices correlate negatively with natural deaths during winter and summer, albeit with much stronger correlation during wintertime. This relationship can be explained by the notion that – during rainy days- there is an increase in air temperature due to latent heat released when atmospheric water vapor condenses⁵³. The reduction of air pollution levels during wet events is another factor that can explain the decrease of natural deaths in winter^{54,55}. Similar to precipitation indices, cloudiness indices have similar correlations with natural deaths during summer and winter (i.e. negative signal). Rather, radiation indices show an opposite feedback, with positive correlation with mortality rates. In summer more radiation, higher temperature, and a greater number of natural deaths seem to be logical. This situation is completely different during winter, as more radiation implies higher daytime temperatures, and conversely clear-sky nights induce a large radiative deficit and accordingly a strong decline of air temperatures⁵⁶, which has an impact on mortality.

This study provides useful information for health prevention plans in the mainland Spain, given that it indicates that the highest number of natural deaths occur in winter, mainly in the northwestern provinces of the study domain. Elderly populations and colder air temperatures predominate in these regions. Furthermore, climatic indices indicate that cold winter extremes, combined with precipitation deficits, and a reduction of cloudiness can increase mortality.

Our findings demonstrate the utility of employing a large number of climatic indices, based on different climatic variables, to assess the dependency of natural deaths on climatic conditions. This study uses, for the first time, a large database of climate indices for a relatively long period (1979-2016) and for a wide domain (mainland Spain) to assess the possible impacts of climate on mortality rates. This study allowed to define climate indices with major influence on natural deaths. Furthermore, this work enabled us to explore the varying seasonal responses of mortality rates to climatic conditions and to determine which indicators are most relevant during each season. In this regard, this study reveals that a high number of natural deaths are found in winter, suggesting that cold-related mortality is an important aspect of this spatial domain that should be taken into consideration by local planners. While many previous studies have focused on analyzing deaths caused by heatwaves; our findings stress that cold waves should not be underestimated by public health authorities in the mainland Spain¹².

Finally, this study also offers a useful tool for demographic studies to determine areas with the highest mortality rates due to a very aging population. Future studies should, however, aim to improve spatial resolution of the study variables. Indeed, the relationships between climatic conditions and mortality rates can be strengthened by improving the spatial resolution of climatic data. Also, higher temporal resolution can be of particular importance, as it would allow assessing the delay in mortality effects of heat and cold waves.

3. Conclusions

This study analyzes spatial and seasonal distribution of natural death in the mainland Spain and their links to climatic conditions. This dependency was assessed using a newly developed high-resolution climate indices database spanning the period from 1979 to 2017. The key findings of this study can be summarized, as follows:

- The study indicates that, as expected, the number of higher natural deaths in the mainland Spain is located in the northwestern regions of the study domain, where the percentage of the elderly population is the highest and climate is much colder.
- There is a clear seasonality, with more deaths in winter than other seasons.
- In addition to the significant thermal indices, other climatic indices, such as precipitation, cloudiness or radiation indices, are closely associated with the number of natural deaths.
- The increase in the number of natural deaths is mainly linked to thermal indices (e.g. frequency of cold days in winter and very warm days in summer), a both can induce higher mortality rates.
- Precipitation indices also have a remarkably negative correlation with natural deaths, which is stronger in winter than in summer. The same relationship is observed between indices of cloudiness and mortality. Rather, radiation indices show an opposite correlation sign with mortality rates.
- There are large spatial differences in the relation between climatic indices and natural deaths, especially during summer and winter periods. Extreme warm temperature indices show positive correlations with natural deaths throughout the territory, especially in summer. In contrast, indices related to cold extreme temperatures exhibit positive correlations with natural deaths in winter, mainly over western provinces. Similarly, there is a negative correlation between precipitation and cloudiness indices and natural deaths, especially in the western provinces during wintertime.

- The association between climatic conditions and mortality rates is seasonally dependent, with higher correlations found for CFD, FD, SND, SSD, SSP, CC, and FOD indices in winter, and VDTR, CC, VWD, and WSDI indices in summer.

4. Methods

5.1 Data

Mortality was estimated from the daily records of human deaths by natural causes, provided by the Spanish National Statistics Institute (INE). This includes data for 47 provinces in the mainland Spain (Figure 1) for the period 1979-2016. Additionally, the total population of the mainland Spain (Figure 1) and the population distribution by age in each province in 2015 were obtained from the INE.

Regarding climate data, we used seasonal and annual records from 79 climate indices for the mainland Spain spanning the period 1979-2016, at 0.25° spatial resolution. These climate indices were calculated using daily data from different climate variables. Data of these indices are available within the INDECIS project website (<http://www.indecis.eu/>). Further details about the main characteristics of this dataset are documented in Domínguez-Castro³⁶. Principally, climate indices were grouped into eight broad categories: temperature (42), precipitation (21), bioclimatic (21), aridity/continentality (10), cloud/radiation (5), wind (6), and snow (12). A list of these selected indices is given in Figure 2.

5.2 Methods

In this study, data of climatic indices and natural deaths for each province were considered for the period 1979-2016. Data were analyzed on seasonal and annual scales. Seasons were defined as: winter (DJF), spring (MAM), summer (JJA), and autumn (SON). A composite regional series for the mainland Spain was also constructed using an arithmetic average of all province series. To assess trends in the number of deaths at the province and whole region levels, changes were quantified using the ordinary least squares regression method, in which time was considered the independent variable, while the number of deaths was the dependent variable. Importantly, to limit the possible impact of trends presented in population data on calculating trends in the number of deaths, we detrended the series of number of deaths.

In the mainland Spain, we examined the spatial distribution of natural deaths in view of the relationship between natural deaths and the elderly population. The ageing index is the metric used most commonly for the aging process, since it is simply defined as the proportion of the number of people over 65 years old compared with those under 16 years old (INE, 2020). The ageing index was calculated for each province in the mainland Spain in 2015. Also, we estimated the total of natural deaths during the study period with respect to the total population in each province in 2015. Herein, we assumed that the population of each province in 2015 is representative of the population for the whole study period. This assumption was verified using the coefficient of variation (CV) in years with available information through the INE database (<https://www.ine.es/jaxiT3/Tabla.htm?t=2852&L=0>). The CV did not exceed 0.2 in any provinces, indicating that the population is almost homogenous, with low dispersion over time. Finally, we looked at the climate-mortality association using Pearson's r correlation analysis. Correlations were computed between climate indices and seasonal records of natural deaths. The correlation analysis allowed us to define indices with stronger (positive or negative) relationship with natural deaths. Also, the correlation analysis was made at the province level to define spatial variability in the dependency between climate and mortality. For $|r|$ values less than 0.320, a non-significant correlation was defined. Accordingly, significant correlations with p -levels below 0.05 and 0.01 were detected when $|r|$ values exceeding 0.320 and 0.512, respectively.

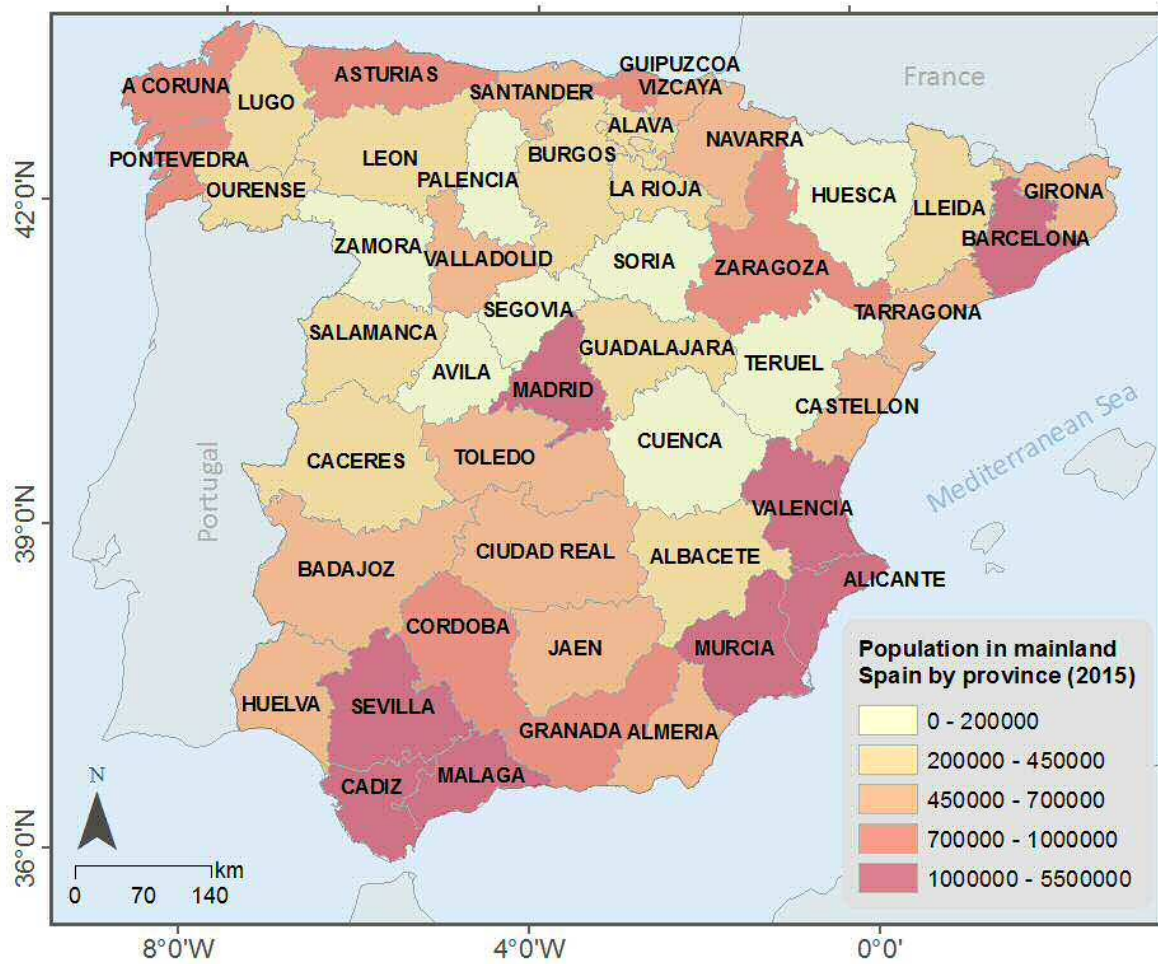


Figure 1. Study area and total population by province in the mainland Spain in 2015.

Temperature	Precipitation	Bioclimatic
CFD Maximum consecutive frost days	CDD Longest dry period	AT Apparent temperature
CSD Maximum number of consecutive summer days	CWD Longest wet period	BIO20 Mean radiation
CSDI Cold spell duration	D50mm Heavy precipitation days	HI Heat index
D32 Days with maximum temperature > 32°C	D95p Very wet days	MI Mould index
DD17 Difference days above/below with TXx 17°C	DD Dry days	UTCI Universal thermal climate index
DTR Diurnal temperature range	DR1mm Wet days 1mm	WCI Wind chill index
ETR Extreme temperature range	DR3mm Wet days 3mm	
FD Frost days	EP Effective precipitation	
GD4 Growing degree days	R10mm Days precipitation ≥ 10mm	
GTG Mean average temperature	R20mm Days precipitation ≥ 20mm	
GTN Mean minimum temperature	R95tot Precipitation fraction very wet days	
GTX Mean maximum temperature	R99tot Precipitation fraction extremely wet days	
HD17 Heating degree days	RTI Total precipitation	
ID Ice days	PRCPTOT Total precipitation wet days	
NTG Minimum mean temperature	RX1day Maximum precipitation	
TNn Minimum minimum temperature	Rx5day Maximum 5 days precipitation	
TXn Minimum maximum temperature	SDII Simple daily intensity index	
OGS6 Onset of growing season 6 days		
OGS10 Onset of growing season 10 days		
SU Summer days		
TN10p Cold nights		
TN90p Warm nights		
TR Tropical nights		
TX10p Cold days		
TX90p Warm days		
VCD Very cold days		
vDTR Mean daily difference DTR		
VWD Very warm days		
WSDI Warm spell duration		
XTG Maximum mean temperature		
TNx Maximum minimum temperature		
TXx Maximum maximum temperature		
ZCD Zero crossing days		

Aridity/Continentality	Cloud/Radiation	Wind
CMD Climatic moisture deficit	ACI Atmospheric Clarity Index	DFx21 Days wind gusts above 21 m/s
ETo Reference evapotranspiration	CC Mean daily cloud cover	FG Mean of daily mean wind strength
UAI UNEP aridity index	FOD Foggy days	FG6Bft Days daily averaged wind above 10.8m/s
	SND Sunny days	fgcalm Calm days
	SSD Sum of sunshine duration	FXx Daily maximum wind gust
	SSp Sunshine duration fraction	

Snow
ASD Average snow depth
FSD Frequency of snow days
HSD Heavy snowy days
MS Maximum snow depth
MSD Mild snowy days
SCD Amount of snow covered days
SD0_10 Snow days depth 1-10
SD10_20 Snow days depth 10-20
SS Snowfall sum

Figure 2. A list of climate indices used in this study, and their definitions.

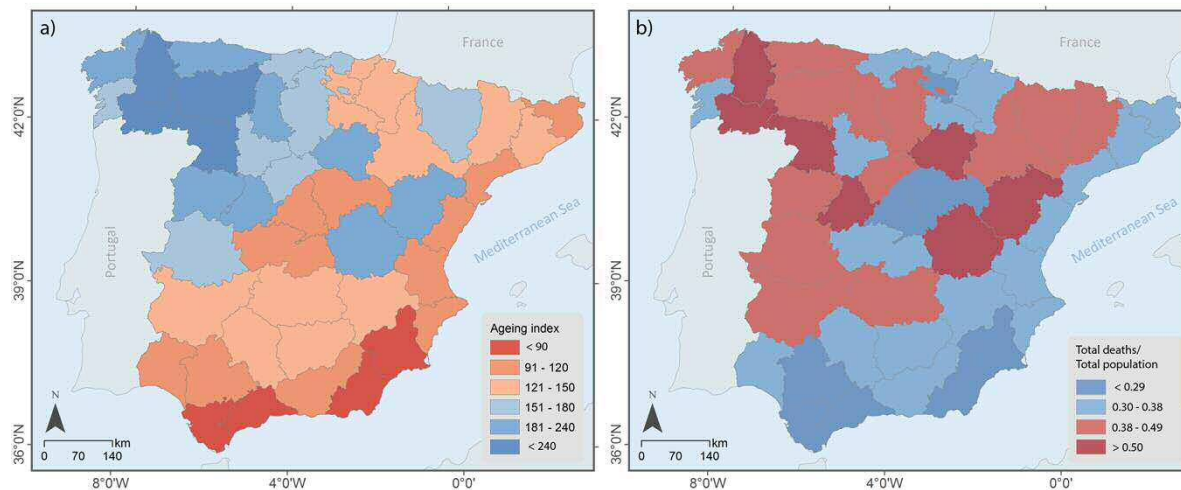


Figure 3. a) Ageing index in 2015. b) The number of natural deaths relative to the total population in 2015. Results are presented for in each province of mainland Spain.

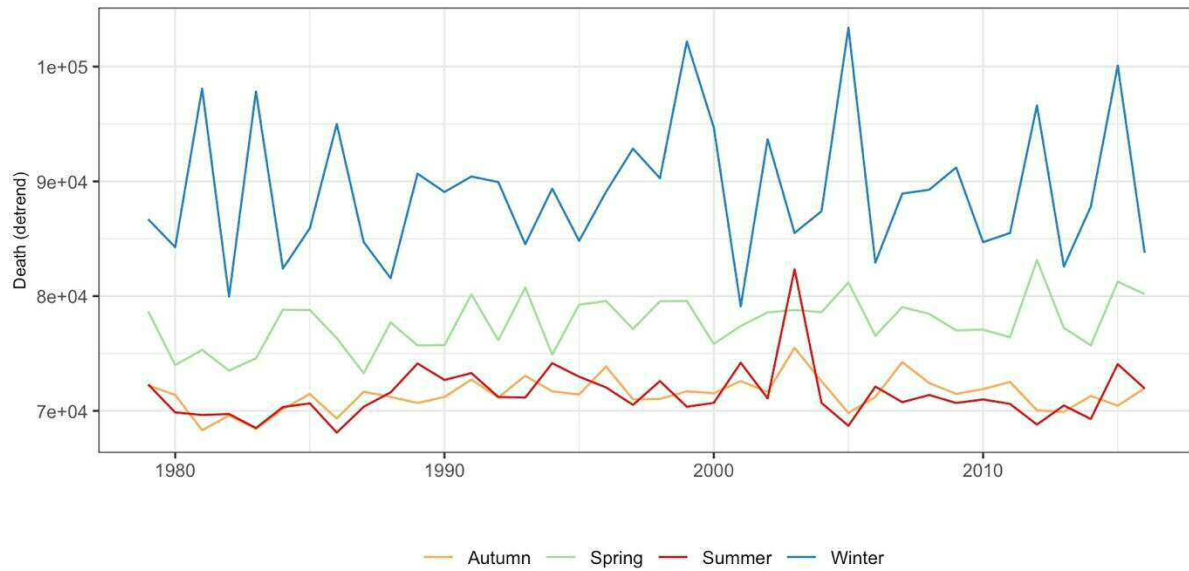


Figure 4. Seasonal number of natural deaths of in the mainland Spain for the period 1979-2016. Results are presented for arithematcally averaged series calculated for the whold domain.

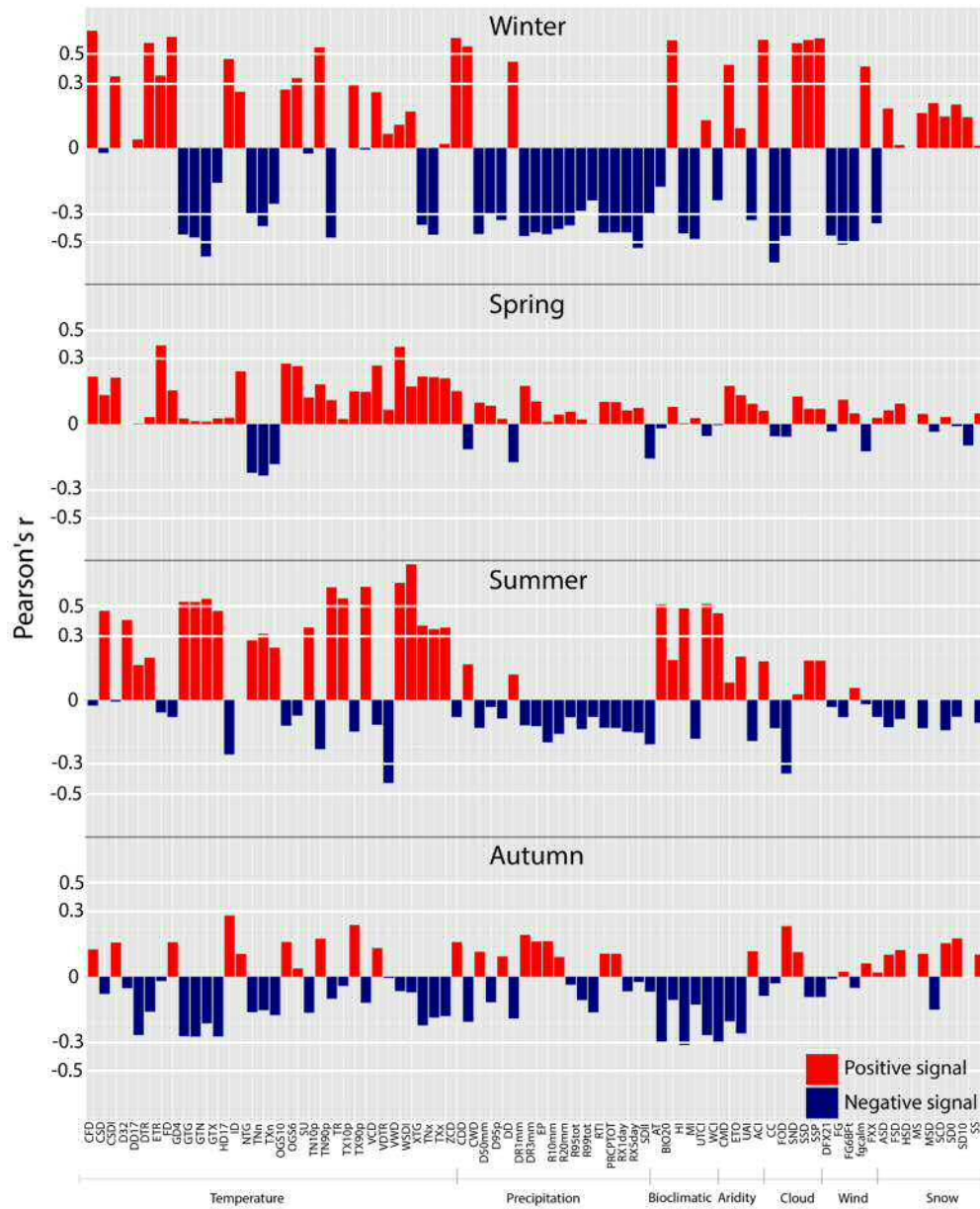


Figure 5. Correlation coefficients between natural deaths and the 79 climate indices for the period 1979-2016 using the arithematically averaged regional series. The horizontal white lines indicate correlation values corresponding to the 95% and 99% significance levels.

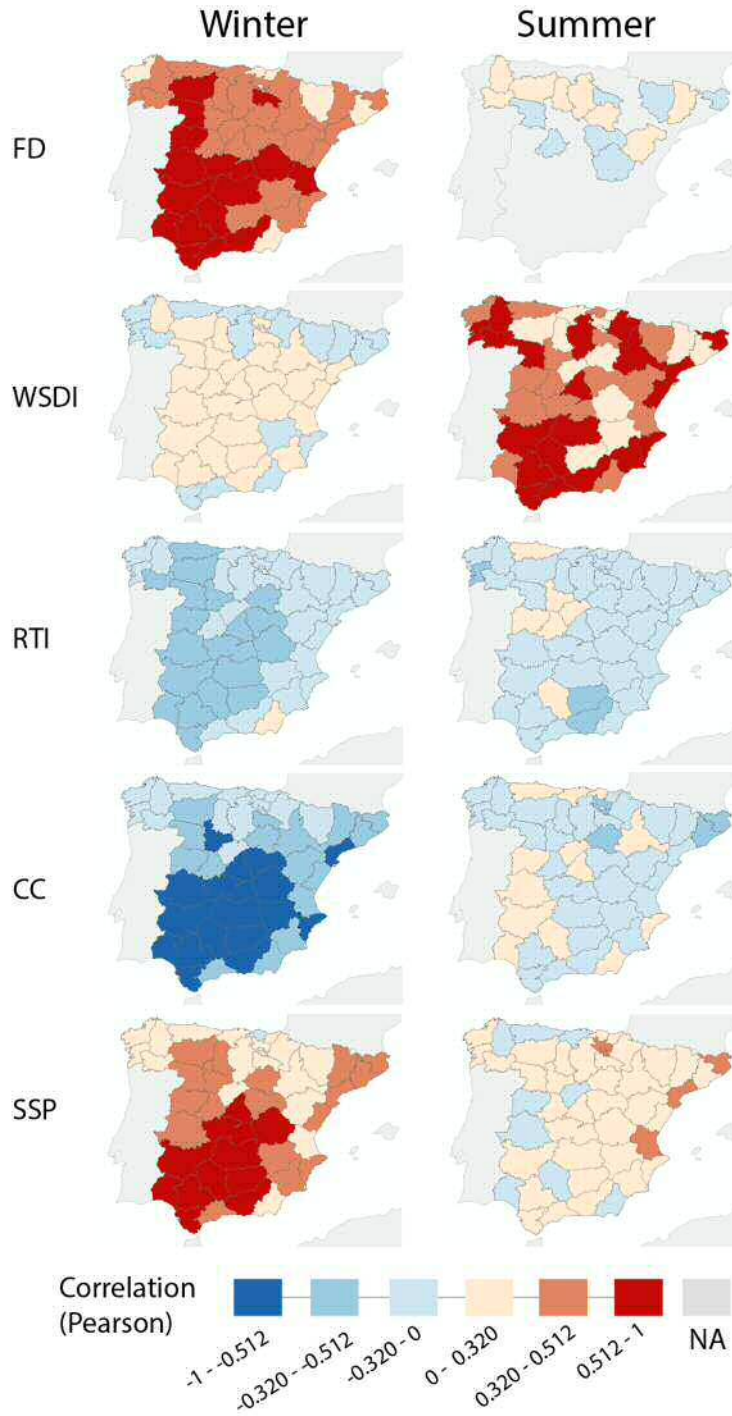


Figure 7. Spatial distribution of correlation coefficients between natural deaths and some significant indices (FD, WSDI, RTI, CC, and SSP) in each province in the mainland Spain during winter (left) and summer (right) for the period 1979-2016.

Reference

1. McMichael, A. J., & Lindgren, E. Climate change: present and future risks to health, and necessary responses. *Journal of internal medicine*, 270(5), 401-413 (2011).
2. Luber, G., & McGeehin, M. Climate change and extreme heat events. *American journal of preventive medicine*, 35(5), 429-435 (2008).
3. Sheffield, J., & Wood, E. F. Projected changes in drought occurrence under future global warming from multi-model, multi-scenario, IPCC AR4 simulations. *Climate Dynamics*, 31(1), 79-105 (2008).
4. IPCC Climate Change 2013: the physical science basis. Contribution of Working Group I to the fifth assessment report of the intergovernmental panel on climate change. (ed. Stocker, T.F. et al.) Cambridge University Press, United Kingdom and New York, NY, USA, 1535 pp (2013).
5. Allan, R., Barlow, M., Byrne, M. P., Cherchi, A., Douville, H., Fowler, H. J., Gan, T. Y., Pendergrass, A. G., Rosenfeld, D., Swann, A. L. S., Wilcox, L. Advances in understanding large-scale responses of the water cycle to climate change. *Annals of the New York Academy of Sciences*, 1472, 49-75 (2020).
6. Basu, R., & Samet, J. M. Relation between elevated ambient temperature and mortality: a review of the epidemiologic evidence. *Epidemiologic reviews*, 24(2), 190-202 (2002).
7. D'Ippoliti, D., Michelozzi, P., Marino, C., De'Donato, F., Menne, B., Katsouyanni, K., ... & Atkinson, R. The impact of heat waves on mortality in 9 European cities: results from the EuroHEAT project. *Environmental Health*, 9(1), 37 (2010).
8. Åström, D. O., Bertil, F., & Joacim, R. Heat wave impact on morbidity and mortality in the elderly population: a review of recent studies. *Maturitas*, 69(2), 99-105 (2011).
9. Yin, P., Chen, R., Wang, L., Liu, C., Niu, Y., Wang, W., ... & You, J. The added effects of heatwaves on cause-specific mortality: A nationwide analysis in 272 Chinese cities. *Environment international*, 121, 898-905 (2018).
10. Trigo, R. M., Ramos, A. M., Nogueira, P. J., Santos, F. D., Garcia-Herrera, R., Gouveia, C., & Santo, F. E. Evaluating the impact of extreme temperature based indices in the 2003 heatwave excessive mortality in Portugal. *environmental science & policy*, 12(7), 844-854 (2009).
11. Tobias, A., Armstrong, B., Zuza, I., Gasparrini, A., Linares, C., & Diaz, J. (2012). Mortality on extreme heat days using official thresholds in Spain: a multi-city time series analysis. *BMC Public Health*, 12(1), 133.

12. Analitis, A., Katsouyanni, K., Biggeri, A., Baccini, M., Forsberg, B., Bisanti, L., ... & Hojs, A. Effects of cold weather on mortality: results from 15 European cities within the PHEWE project. *American journal of epidemiology*, 168(12), 1397-1408 (2008).
13. Montero, J. C., Mirón, I. J., Criado-Álvarez, J. J., Linares, C., & Díaz, J. Mortality from cold waves in castile—La Mancha, Spain. *Science of the total environment*, 408(23), 5768-5774 (2010).
14. Stanke, C.; Kerac, M.; Prudhomme, C.; Medlock, J.; Murray, V. Health Effects of Drought: A Systematic Review of the Evidence. *PLoS Curr.* 5 (2013).
15. Yusa, A.; Berry, P.; Cheng, J.J.; Ogden, N.; Bonsal, B.R.; Stewart, R.E.; Waldick, R. Climate Change, Drought and Human Health in Canada. *Int. J. Environ. Res. Public Health* 12, 8359–8412 (2015).
16. Berman, J.D.; Ebisu, K.; Peng, R.D.; Dominici, F.; Bell, M. Drought and the risk of hospital admissions and mortality in older adults in western USA from 2000 to 2013: A retrospective study. *Lancet Planet. Health* 1, e17–e25 (2017).
17. Salvador, C., Nieto, R., Linares, C., Díaz, J., & Gimeno, L. Quantification of the Effects of Droughts on Daily Mortality in Spain at Different Timescales at Regional and National Levels: A Meta-Analysis. *International Journal of Environmental Research and Public Health*, 17(17), 6114 (2020b).
18. Salvador, C.; Nieto, R.; Linares, C.; Díaz, J.; Gimeno, L. Effects of droughts on health: Diagnosis, repercussion, and adaptation in vulnerable regions under climate change. Challenges for future research. *Sci. Total. Environ.* 703, 134912 (2020a).
19. Ballester-Díez, F., Corella-Piquer, D., Pérez-Hoyos, S., Hervás-Hernandorena, A., & Merino-Egea, C. Variación estacional de la mortalidad en la ciudad de Valencia, España. *Salud pública de México*, 39, 95-101 (1997).
20. Simón, F., Lopez-Abente, G., Ballester, E., & Martínez, F. Mortality in Spain during the heat waves of summer 2003. *Eurosurveillance*, 10(7), 9-10 (2005).
21. López-Perea, N., Méndez, L. S., López-Cuadrado, T., Cámara, A. L., & de Mateo Ontañón, S. Estimación de la mortalidad atribuible a gripe estacional en España. Temporadas 1980-2008. *Boletín epidemiológico semanal*, 19(11), 150-158 (2011).
22. Mackenbach JP, Borst V, Schols JM. Heat-related mortality among nursing-home patients. *Lancet.* 349:1297-8 (1997).
23. Sheridan SC, Kalkstein LS. Progress in heat watch-warning system technology. *Bull Amer Meteor Soc.* 82:1931–41 (2004).

24. Fleming DM. The contribution of influenza to combined acute respiratory infections, hospital admissions, and death in winter. *Communicable Disease and Public Health* 3: 32-38 (2000).
25. Kenney, W. L., & Munce, T. A. (2003). Invited review: aging and human temperature regulation. *Journal of applied physiology*, 95(6), 2598-2603.
26. Díaz, J., Garcia, R., De Castro, F. V., Hernández, E., López, C., & Otero, A. Effects of extremely hot days on people older than 65 years in Seville (Spain) from 1986 to 1997. *International Journal of Biometeorology*, 46(3), 145-149 (2002).
27. Achebak, H., Devolder, D., & Ballester, J. Heat-related mortality trends under recent climate warming in Spain: A 36-year observational study. *PLoS medicine*, 15(7), e1002617 (2018).
28. Rasilla, D., Allende, F., Martilli, A., & Fernández, F. Heat waves and human well-being in Madrid (Spain). *Atmosphere*, 10(5), 288 (2019).
29. Frich, P., Alexander, L. V., Della-Marta, P. M., Gleason, B., Haylock, M., Tank, A. K., & Peterson, T. Observed coherent changes in climatic extremes during the second half of the twentieth century. *Climate Research*, 19(3), 193–212 (2002).
30. Klein Tank, A. M. G., Zwiers, F. W., & Zhang, X. Guidelines on analysis of extremes in a changing climate in support of informed decisions for adaptation, climate data and monitoring WCDMP-No 72, WMO-TD No 1500, p 5 (2009).
31. Alexander, L. V., Zhang, X., Peterson, T. C., Caesar, J., Gleason, B., Tank, A. K., et al. Global observed changes in daily climate extremes of temperature and precipitation. *Journal of Geophysical Research*, 111, D05109 (2006).
32. Moberg, A., & Jones, P. D. Trends in indices for extremes in daily temperature and precipitation in central and western Europe, 1901–99. *International Journal of Climatology: A Journal of the Royal Meteorological Society*, 25(9), 1149–1171 (2005).
33. Klein Tank, A. M. G., & Können, G. P. Trends in indices of daily temperature and precipitation extremes in Europe, 1946–99. *Journal of climate*, 16(22), 3665-3680 (2003).
34. Kuwayama, Y., Thompson, A., Bernknopf, R., Zaitchik, B., & Vail, P. Estimating the impact of drought on agriculture using the US Drought Monitor. *American Journal of Agricultural Economics*, 101(1), 193-210 (2019).
35. Hui-Mean, F., Yusop, Z., & Yusof, F. Drought analysis and water resource availability using standardised precipitation evapotranspiration index. *Atmospheric Research*, 201, 102-115 (2018).

36. Domínguez-Castro, F., Reig, F., Vicente-Serrano, S. M., Aguilar, E., Peña-Angulo, D., Noguera, I., ... & El Kenawy, A. M. A multidecadal assessment of climate indices over Europe. *Scientific Data*, 7(1), 1-7 (2020).
37. Peña-Angulo, D., Reig-Gracia, F., Domínguez-Castro, F., Revuelto, J., Aguilar, E., van der Schrier, G., & Vicente-Serrano, S. M. ECTACI: European Climatology and Trend Atlas of Climate Indices (1979–2017). *Journal of Geophysical Research: Atmospheres*, 125(16), e2020JD032798 (2020).
38. Leasure, J. W. Factors involved in the decline of fertility in Spain 1900–1950. *Population Studies*, 16(3), 271-285 (1963).
39. Pueyo, A., Zuñigo, M., Postigo, R., López, C. L., & Salinas, C. Efectos territoriales del envejecimiento de la población: consecuencias multiescalares del cambio demográfico en los municipios españoles. In *Cambio demográfico y socio territorial en un contexto de crisis: contribuciones* (pp. 29-42). Grupo de Población de la Asociación de Geógrafos Españoles (2014).
40. Gutiérrez Posada, D., Rubiera Morollón, F., & Viñuela, A. Ageing places in an ageing country: The local dynamics of the elderly population in Spain. *Tijdschrift voor economische en sociale geografie*, 109(3), 332-349 (2018).
41. Blasco, B.C. Desigualdades Territoriales en Relación con el Envejecimiento de la Población Española. *Documents d'Anàlisi Geogràfica* 52, pp. 91–110 (2008).
42. Hajat, S., Kovats, R. S., & Lachowycz, K. Heat-related and cold-related deaths in England and Wales: who is at risk? *Occupational and environmental medicine*, 64(2), 93-100 (2007).
43. Abrahamson, V., Wolf, J., Lorenzoni, I., Fenn, B., Kovats, S., Wilkinson, P., ... & Raine, R. Perceptions of heatwave risks to health: interview-based study of older people in London and Norwich, UK. *Journal of public health*, 31(1), 119-126 (2009).
44. Achebak, H., Devolder, D., & Ballester, J. Trends in temperature-related age-specific and sex-specific mortality from cardiovascular diseases in Spain: a national time-series analysis. *The Lancet Planetary Health*, 3(7), e297-e306 (2019).
45. Jiménez, J. J. L. Aproximación a la estructura y distribución espacial del envejecimiento en España (1970-1981). In *Anales de geografía de la Universidad Complutense* (No. 9, pp. 145-168). Servicio de Publicaciones (1989).
46. Carson, C., Hajat, S., Armstrong, B., & Wilkinson, P. Declining vulnerability to temperature-related mortality in London over the 20th century. *American journal of epidemiology*, 164(1), 77-84 (2006).

47. Gasparrini, A., Guo, Y., Hashizume, M., Lavigne, E., Zanobetti, A., Schwartz, J., ... & Leone, M. Mortality risk attributable to high and low ambient temperature: a multicountry observational study. *The Lancet*, 386(9991), 369-375 (2015).
48. Cony, M.; Hernández, E. y Del Teso, T. "Influence of synoptic scale in the generation of extremely cold days in Europe". *Atmósfera*, 21, pp. 389-401 (2008).
49. Díaz, J., García, R., López, C., Linares, C., Tobías, A., & Prieto, L. Mortality impact of extreme winter temperatures. *International Journal of Biometeorology*, 49(3), 179-183 (2005).
50. Carmona, R., Diaz, J., Miron, I. J., Ortíz, C., León, I., & Linares, C. Geographical variation in relative risks associated with cold waves in Spain: The need for a cold wave prevention plan. *Environment international*, 88, 103-111 (2016).
51. Burkart, K., & Kinney, P. Is precipitation a predictor of mortality in Bangladesh? A multi-stratified analysis in a South Asian monsoon climate. *Science of the Total Environment*, 553, 458-465 (2016).
52. Wu J., Yunus M., Streatfield P.K., Emch M. Association of climate variability and childhood diarrhoeal disease in rural Bangladesh, 2000–2006. *Epidemiol. Infect.*, 142, 1859-1868 (2014).
53. Schneider, T., O’Gorman, P. A., & Levine, X. J. Water vapor and the dynamics of climate changes. *Reviews of Geophysics*, 48(3) (2010).
54. Ren C., Williams G.M., Morawska L., Mengersen K., Tong S. Ozone modifies associations between temperature and cardiovascular mortality: analysis of the NMMAPS data. *Occup. Environ. Med.*, 65, pp. 255-260 (2008).
55. Burkart K., Canário P., Breitner S., Schneider A., Scherber K., Andrade H., et al. Interactive short-term effects of equivalent temperature and air pollution on human mortality in Berlin and Lisbon. *Environ. Pollut.*, 183, pp. 54-63 (2013).
56. Cellier, P. An operational model for predicting minimum temperatures near the soil surface under clear sky conditions. *Journal of Applied Meteorology*, 32(5), 871-883 (1993).

Water sector, forest fires and landslides in Calabria

The data collected by CNR-IRPI for the various indices, grouped for sectors, as shown in the Deliverable 4.2, refer to the whole territory of Calabria and/or for the 5 provinces of Calabria (Cosenza, Catanzaro, Crotona, Vibo Valentia, and Reggio Calabria), for specific areas or sites. These data were compared to the climatic indices, listed in the deliverable 4.1. These indices have been evaluated using the ClimIND R software, by means of the climatic data (mainly, daily rainfall, minimum and maximum daily temperature) registered in 93 stations, managed by the Centro Funzionale Multirischi di Regione Calabria (ARPACAL). The same climatic data were made available in the ambit of WP2 and jointly in the European database of ECA&D (Figure 1).

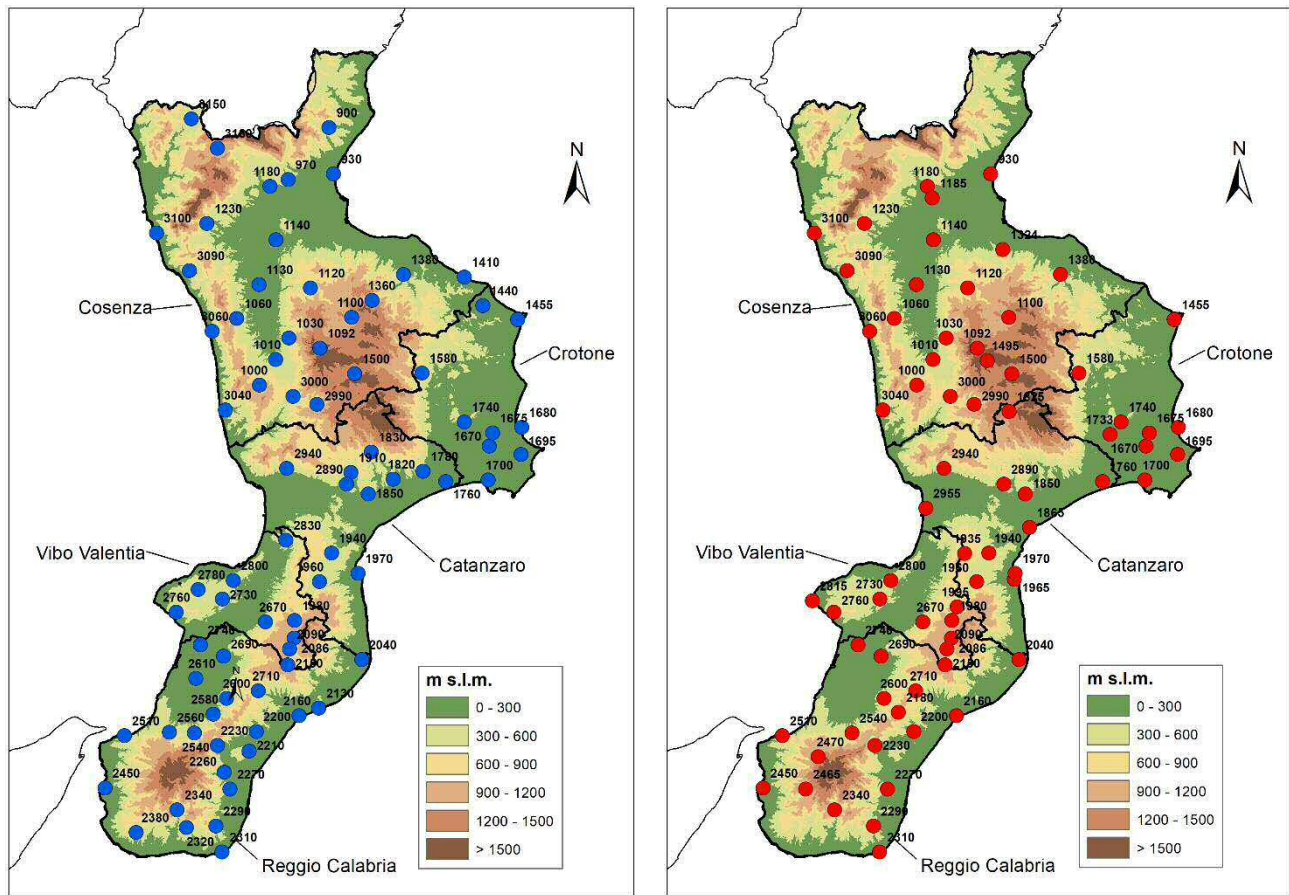


Figure 1. Map of the stations used for the rainfall (left) and temperature (right) data of Calabria, with indication of the 5 provinces.

The comparisons were not carried out for the sector of agriculture, because there are very few data of water consumptions for irrigation, and for the touristic sector, because data needed for the climatic indices were not available for the territory.

In the following, for each sector, first the climatic indices used are indicated and then the results of the comparison are shown.

2. Water

Among the 5 springs presented in the Deliverable 4.2, only the “Mezzafiumina” spring has been considered because it presents the longest registration period. The database contains the average daily discharge registered between 1 January 2005 and 31 December 2018. The spring data were compared with the climatic data registered in the San Sosti station (code 1230), which is near this spring. Figure 2 shows the comparison of the daily mean discharge data and the daily precipitation data in the period above indicated.

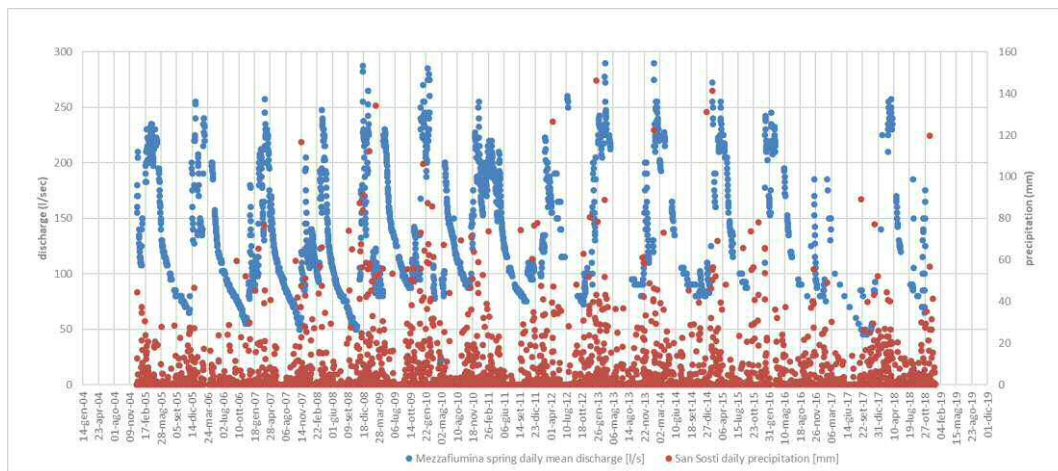


Figure 2. Comparison of the daily mean discharge data of the “Mezzafiumina” spring (l/sec) with the daily rainfall data of the San Sosti station (period 1 January 2005 – 31 December 2018).

The discharge data averaged in each month have been compared with the monthly data of the following climatic indices:

- Monthly rainfall
- U.N.E.P. Aridity Index evaluated on a monthly basis;
- S.P.I. (Standard Precipitation Index) evaluated on 3-6-12-24 months;
- S.P.E.I. (Standard Precipitation Evapotranspiration index) evaluated on 3-6-12-24 months.

Regarding the discharge data, since the database presents several missing daily data, in the evaluation of the monthly data only the months with at least 10 daily data have been considered.

The comparisons of the climatic indices values with the discharge data do not seem to show particular correlations. Figures 3-5 show the best matches between the two databases, considering the monthly rainfall (Figure 3), the UNEP monthly values (Figure 4) and SPEI-3 monthly values (Figure 5).

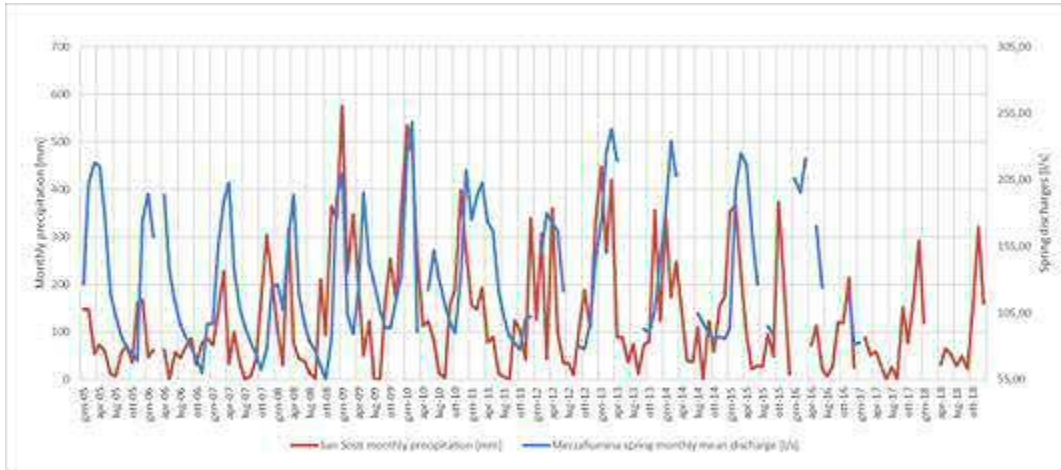


Figure 3. Comparison of the monthly discharge data of the “Mezzafiumina” spring (l/sec) with the San Sosti monthly rainfall (mm).

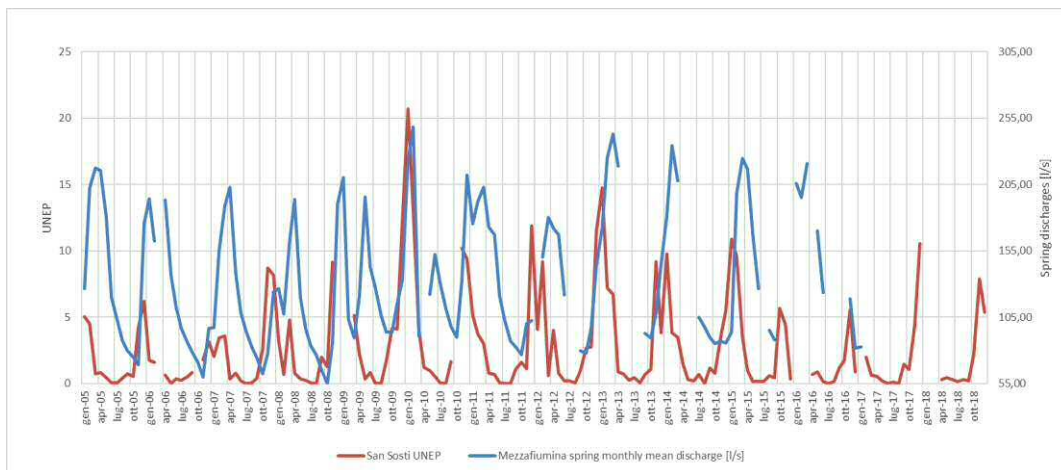


Figure 4. Comparison of the monthly discharge data of the “Mezzafiumina” spring (l/sec) with the San Sosti UNEP monthly values.

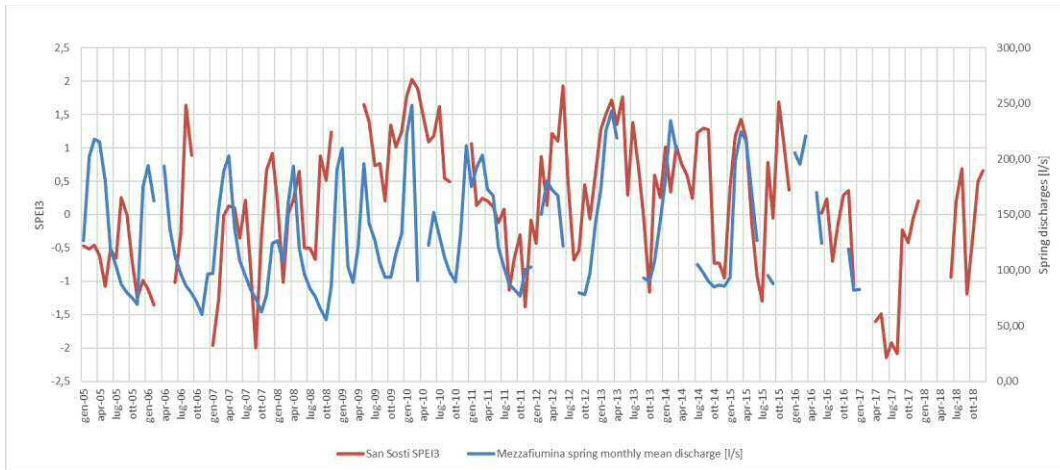


Figure 5. Comparison of the monthly discharge data of the “Mezzafiumina” spring (l/sec) with the San Sosti SPEI-3 values.

Correlations seem to be clearer comparing the minimum values (on a 12-month timespan) of the average monthly discharge and SPI and SPEI values. In particular, Figures 6 and 7 show the comparison of the minimum values of discharge with the SPI-3 and SPI-12 values, respectively.

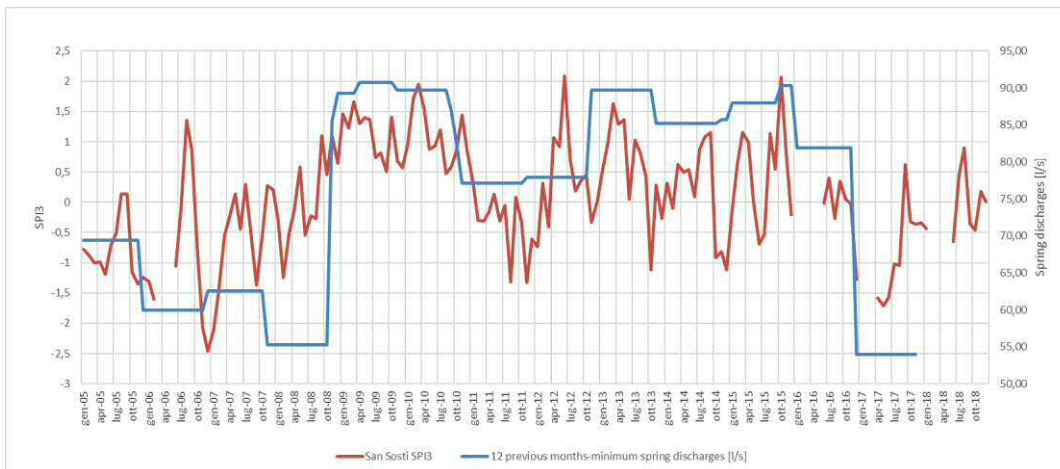


Figure 6. Comparison of the minimum vales (evaluated on 12 previous months) of monthly discharge data of the “Mezzafiumina” spring (l/sec) with the San Sosti SPI3 values.

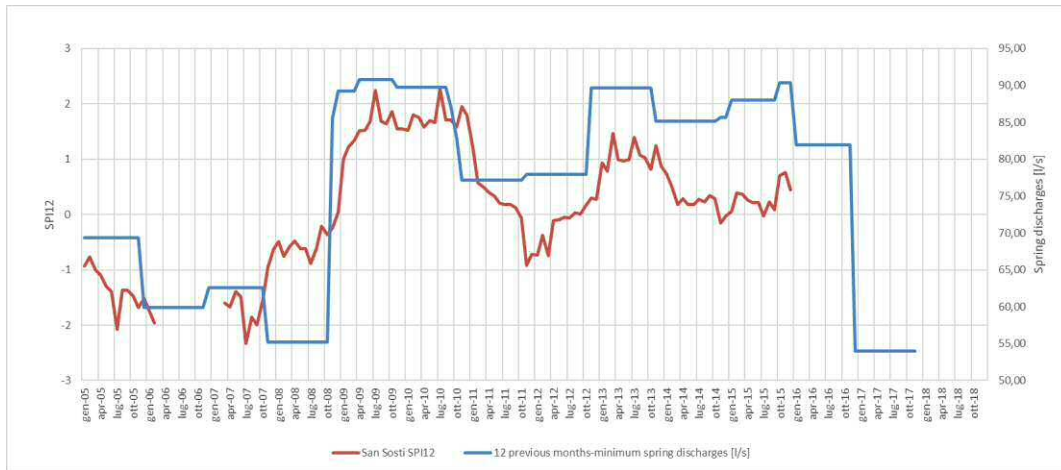


Figure 7. Comparison of the minimum vales (evaluated on 12 previous months) of monthly discharge data of the “Mezzafiumina” spring (l/sec) with the San Sosti SPI12 values.

3. Forest fire

Data about the burnt areas (monthly data of extension - in hectares - and the number of fires in the period 2008-2018), provided by means of the module “Rapid Damage Assessment” (R.D.A.) of E.F.F.I.S. (European Forest Fire Information System) and included in the Deliverable 4.2, have been compared with the Keetch-Byram Drought Index (KBDI). This index, ranging between 0 and 203.2 (extreme dry condition of the soil) is used all over the world for monitoring and forecasting forest fires. The index was calculated with the daily data of all the selected stations and then the monthly mean values were evaluated. The missing data problem was overcome considering only the months with at least 20 daily data. Given that the data of the forest fires are available for each province (summing the data of the municipalities included in each province), the KBDI values were averaged for each province.

The comparison results show that the peaks of the burnt areas almost always correspond with the highest of the KBDI values, but not for all the provinces. Analogous results were obtained considering the number of fires.

Figures 8 and 9 show the results for the provinces of Cosenza and Reggio Calabria, where the agreement seems to be clearer. A short delay between the peak occurrence of KBDI and the burnt areas/number of fires are present in all the comparisons.

Figure 10 shows the results for the whole territory of the Calabria region.

This comparison was also made for the territory of the Sila National Park (study area used for the touristic sector in this Project), whose fire data were included in the Deliverable 4.2. The comparison did not show good results.

Anyhow, it is important to underline that:

- the KBDI monthly mean values is evaluated by means of a database with a variable number of monthly values owing to missing data.
- The number of fires and the extension of burnt areas are influenced not only by climatic conditions but also by anthropic factors.
- The extension of the burnt areas depends on the efficiency of the fire monitoring system and by the rapidity of first response operations.
- The RDA module database of EFFIS is referred to burnt areas with extension greater than 30 hectares (in Europe, these fires are about 75-80% of the total fires) and does not contain differences between natural fires and human-induced fires.

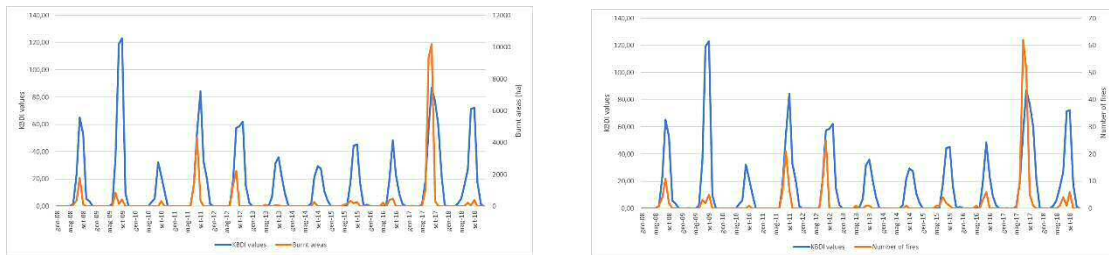


Figure 8 – Comparisons of KBDI monthly mean values with burnt areas (in hectares) (left) or number of fires (right) for the territory of the Cosenza province.

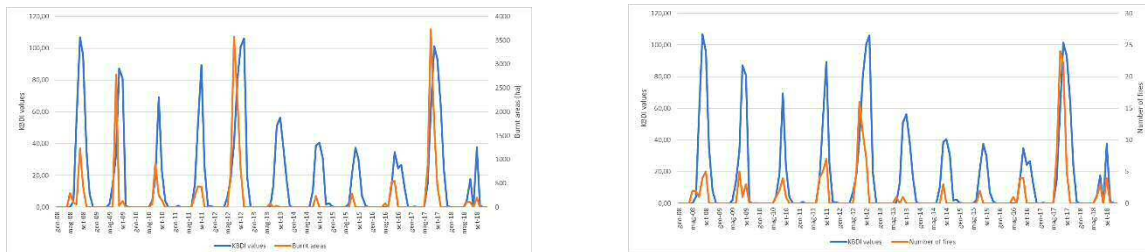


Figure 9 – Comparisons of KBDI monthly mean values with burnt areas (in hectares) (left) or number of fires (right) for the territory of the Reggio Calabria province.

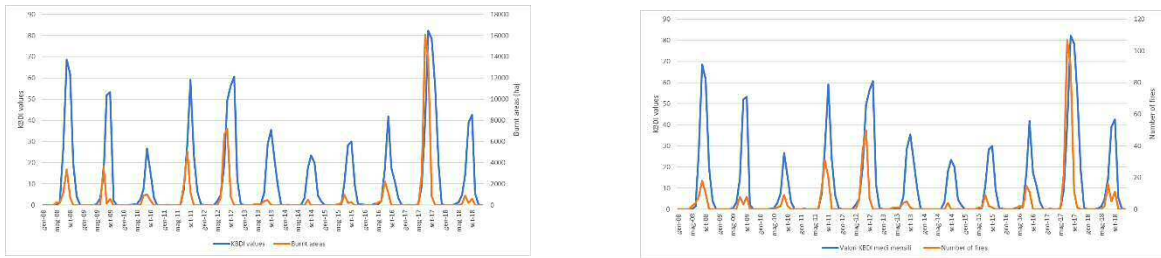


Figure 10 – Comparisons of KBDI monthly mean values with burnt areas (in hectares) (left) or number of fires (right) for the whole territory of the Calabria region.

4. Disaster Risk

The data regarding disasters caused by geo-hydrological events, included in the Deliverable 4.2, show for each year from 1990 to 2018 the number of events, damage and injuries. Data, collected from newspaper articles, technical reports, civil protection reports, etc., were provided for the whole territory of Calabria and for each province (Cosenza, Catanzaro, Crotona, Vibo Valentia, and Reggio Calabria).

In the present deliverable the yearly amounts of landslides and floods (sectorial data) have been compared with data of the following climatic indices:

- **RT**: Total precipitation (mm): annual (**RTA**), monthly (**RTM**), seasonal (**RTS**)
- **R10mm**: Annual count of days when daily precipitation amount ≥ 10 mm
- **R20mm**: Annual count of days when daily precipitation amount ≥ 20 mm
- **R95TOT**: Annual total precipitation when daily rainfall is greater than 95th-percentile
- **R99TOT**: Annual total precipitation when daily rainfall is greater than 99th-percentile
- **R95%TOT**: Precipitation fraction out of the annual total due to very wet days (daily rainfall $> 95^{\text{th}}$ -percentile)
- **R99%TOT**: Precipitation fraction out of the annual total due to extremely wet days (daily rainfall $> 99^{\text{th}}$ -percentile)
- **RX1day**: Monthly maximum 1-day precipitation;
- **RX5day**: Monthly maximum 5-day precipitation;
- **D50mm**: Heavy precipitation days in a year (with daily rainfall ≥ 50 mm);
- **LWP**: Maximum length of consecutive wet days (daily rainfall ≥ 1 mm);

- **RTWD:** Yearly precipitation amount of days with rainfall ≥ 1 mm;
- **DR1mm:** Number of wet days with precipitation ≥ 1 mm;
- **DR3mm:** Number of wet days with precipitation ≥ 3 mm;
- **DR10mm:** Number of wet days with precipitation ≥ 10 mm.

Given the yearly sectorial indices have been provided for each province, the comparisons of both the number of landslides and floods with the climatic indices were made considering for each province both the average and the maximum values of the climatic indices calculated for each station belonging to the province. For the best matches, we tried to interpolate the two databases using a linear regression or an exponential curve. The correlation was tested by means of the Determination Coefficient (R^2) for the linear regression and the Standard Error (SE) for the exponential curve.

Regarding the landslides, the comparisons show clear agreement with the following climatic indexes: RTA, R10mm, R20mm, R95TOT and D50mm. Figures 11-17 show some of these comparisons. Moreover, Figures 18-21 show some interpolations between the data of landslides and climatic indices and the expressions of the interpolation curves.

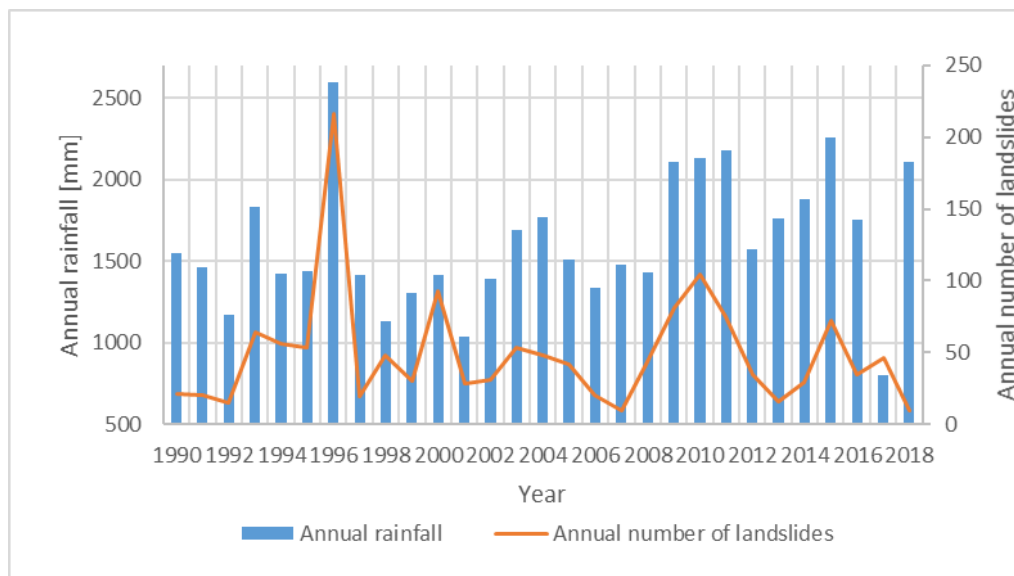


Figure 11 – Comparison of the territorial maximum values of annual rainfall (RTA) with the annual number of landslide in the Reggio Calabria province.

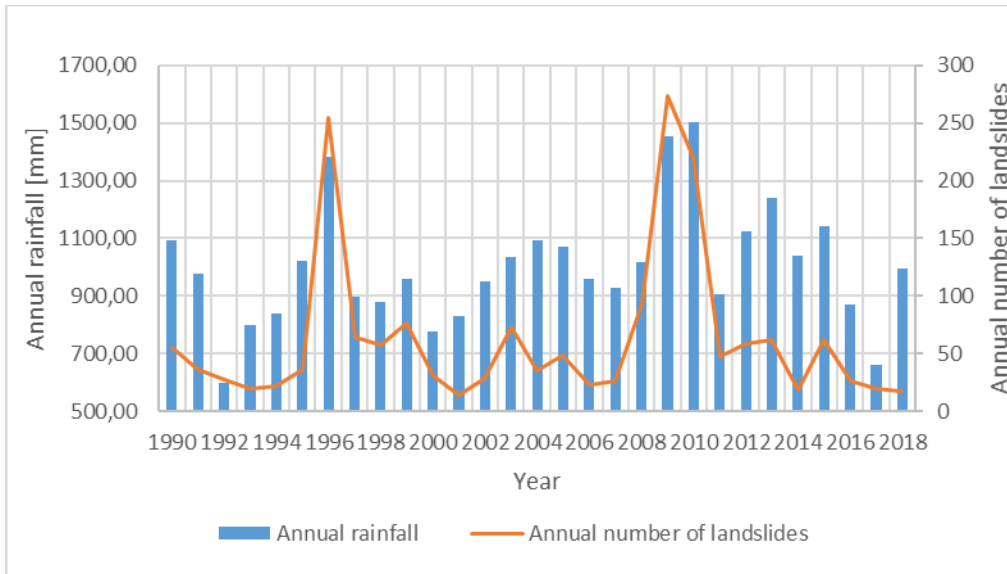


Figure 12 – Comparison of the territorial average values of annual rainfall (RTA) with the annual number of landslides in the Cosenza province.

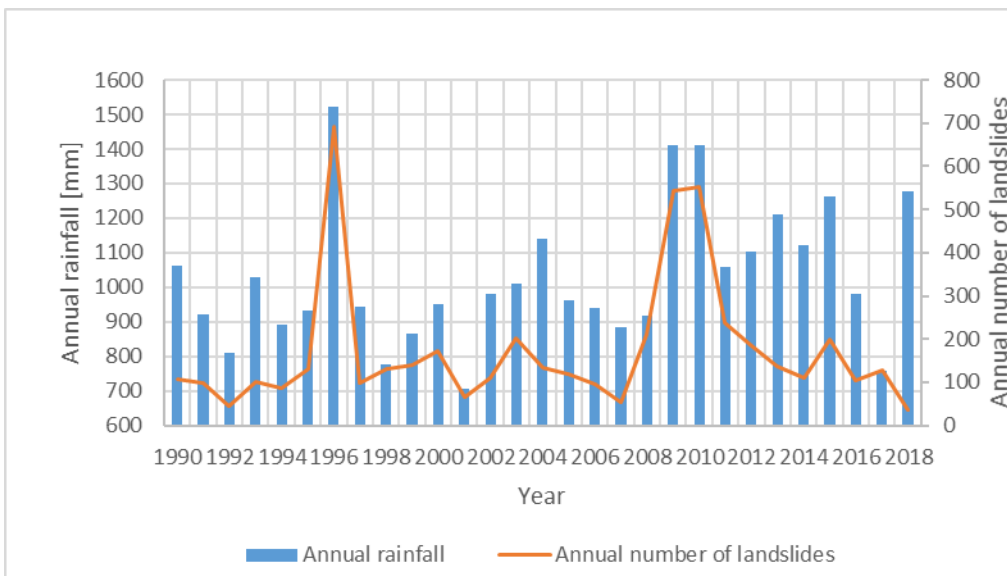


Figure 13 – Comparison of the territorial average values of annual rainfall (RTA) with the annual number of landslides in the whole territory of the Calabria region.

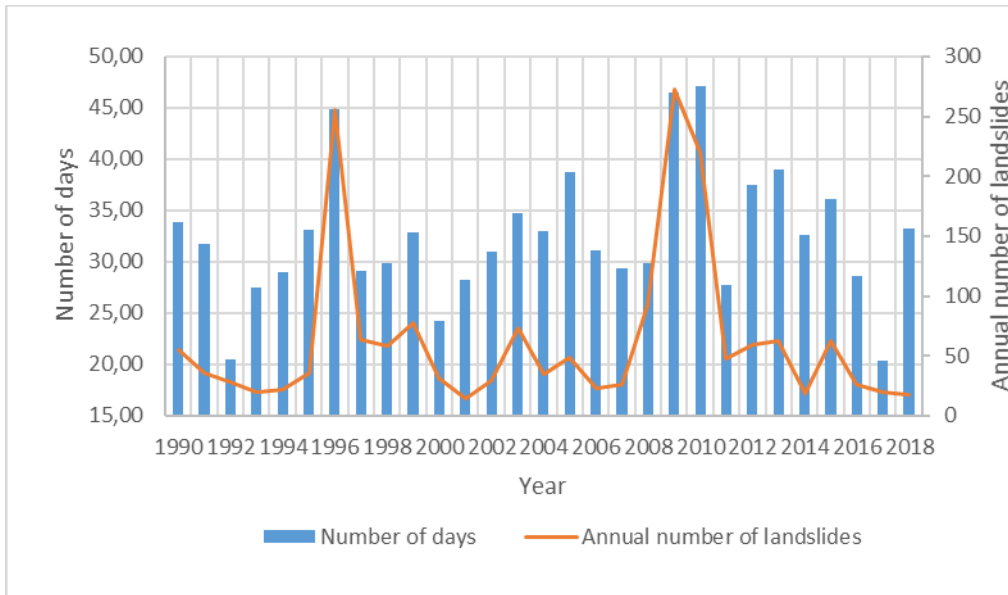


Figure 14 – Comparison of the territorial average values of the annual count of days when daily precipitation amount $\geq 10\text{mm}$ (R10mm) with the annual number of landslides in the Cosenza province.

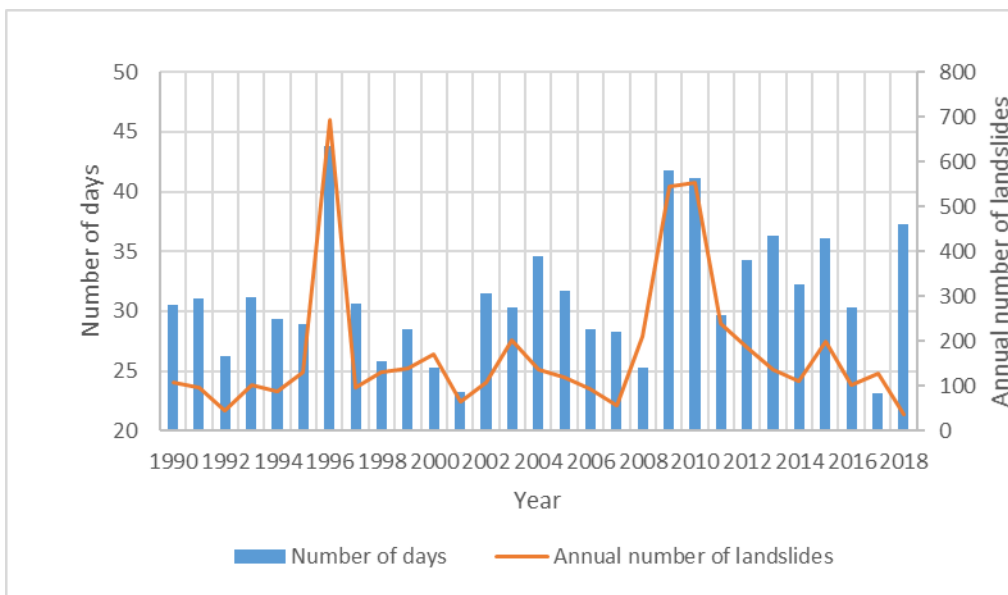


Figure 15 – Comparison of the territorial average values of the annual count of days when daily precipitation amount $\geq 10\text{mm}$ (R10mm) with the annual number of landslides in the whole territory of the Calabria region.

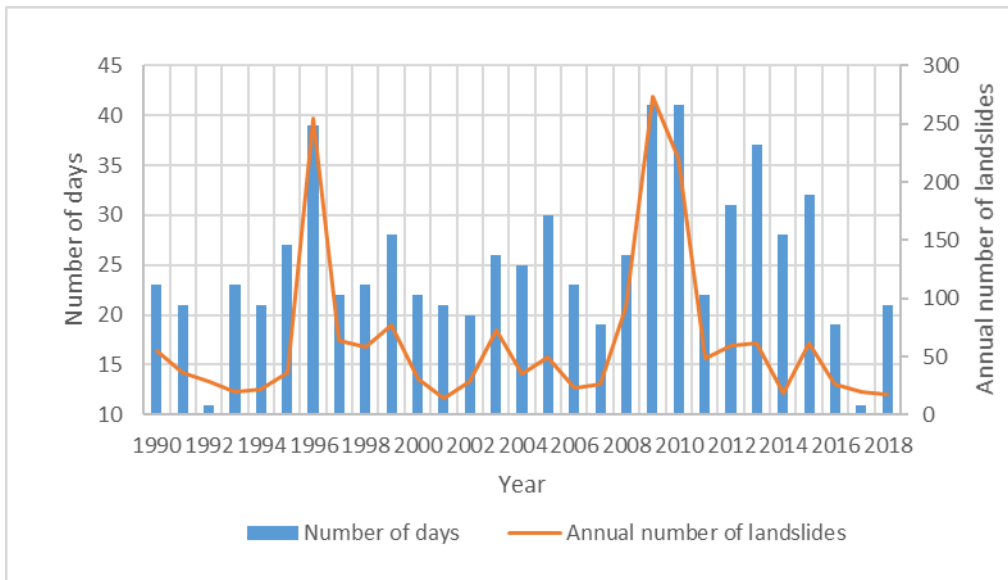


Figure 16 – Comparison of the territorial maximum values of the annual count of days when daily precipitation amount $\geq 20\text{mm}$ (R20mm) with the annual number of landslides in the Cosenza province.

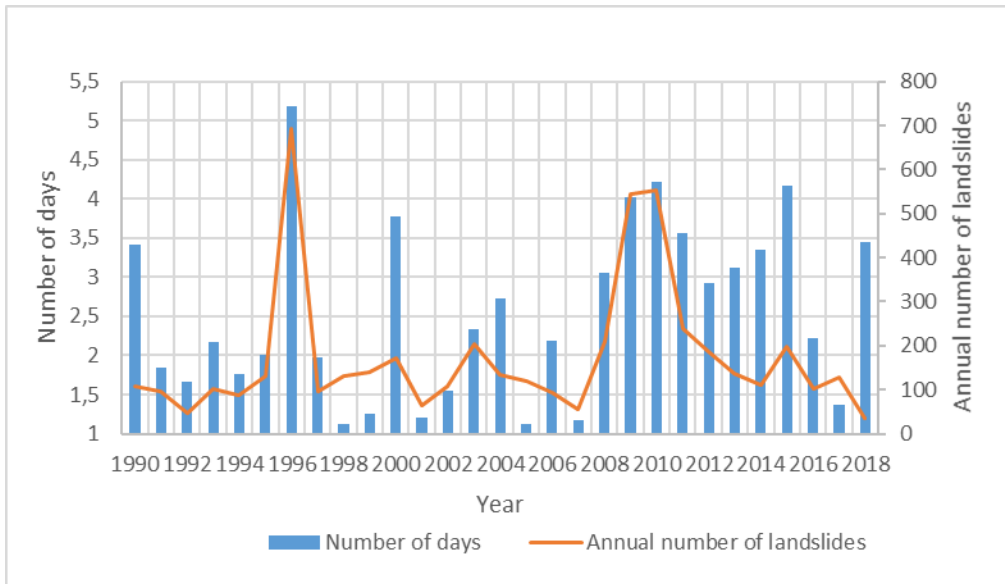


Figure 17 – Comparison of the territorial average values of the heavy precipitation days in a year (with daily rainfall ≥ 50 mm) (D50mm) with the annual landslide amount in the whole territory of the Calabria region.

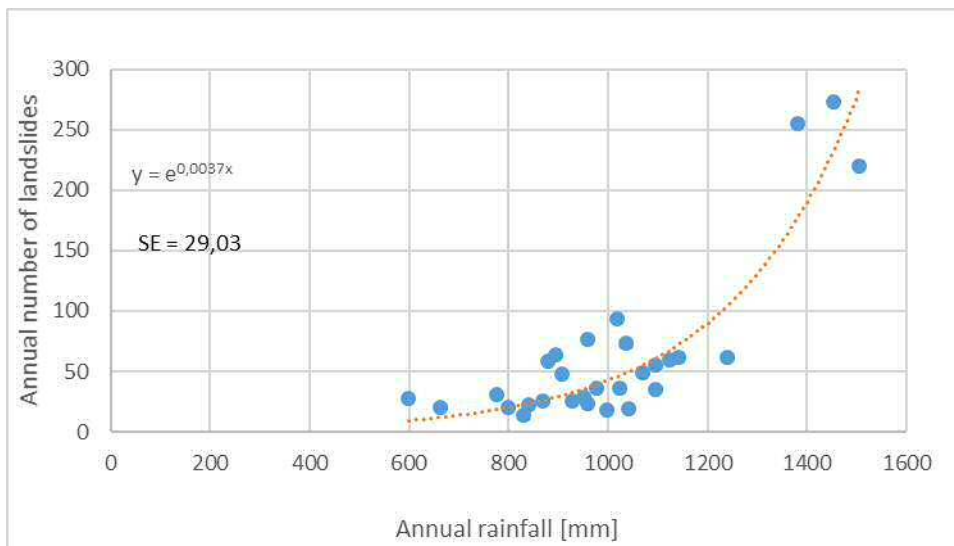


Figure 18 – Interpolation curve between the territorial average values of annual rainfall (RTA) and the annual number of landslides in the Cosenza province.

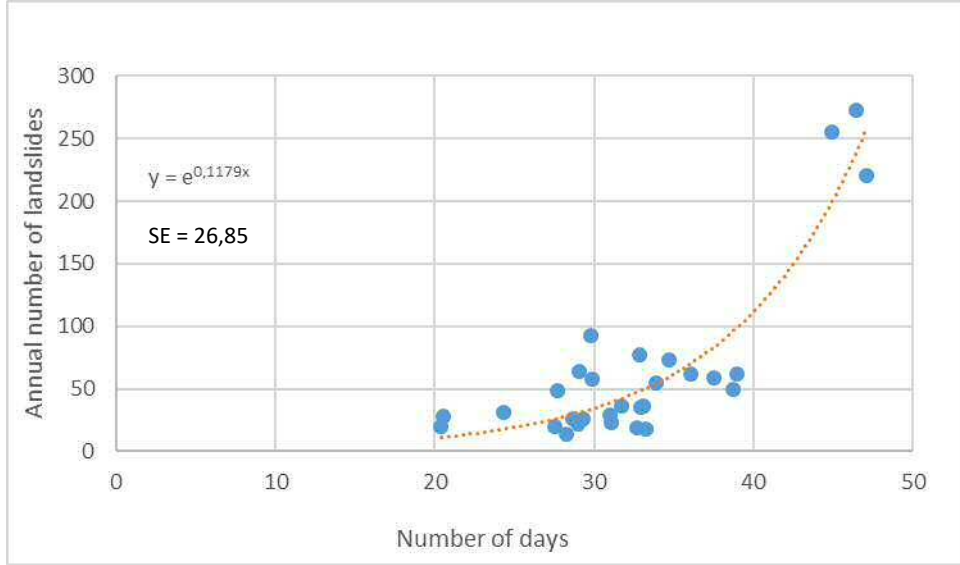


Figure 19 – Interpolation curve between the territorial average values of the annual count of days when daily precipitation amount $\geq 10\text{mm}$ (R10mm) and the annual number of landslides in the Cosenza province.

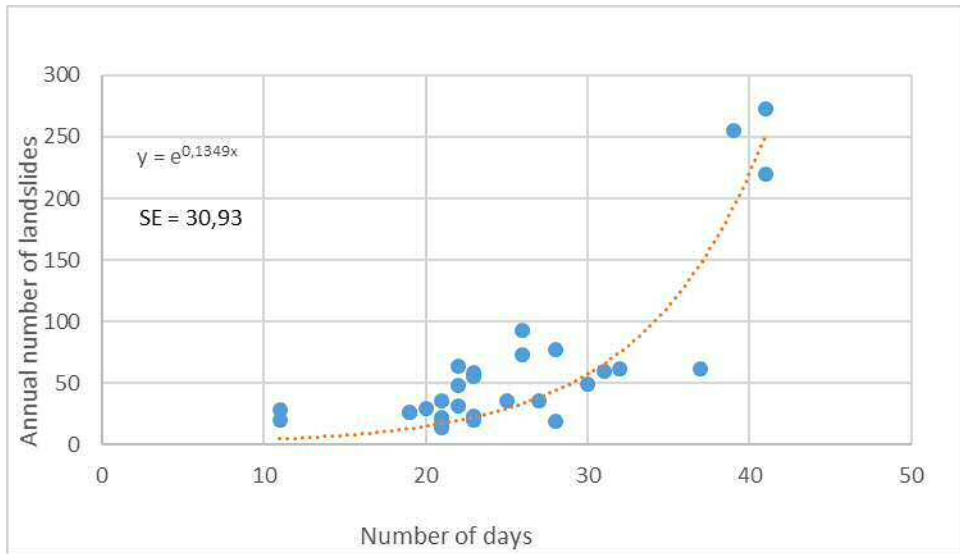


Figure 20 – Interpolation curve between the territorial maximum values of the annual count of days when daily precipitation amount $\geq 20\text{mm}$ (R20mm) and the annual number of landslides in the Cosenza province.

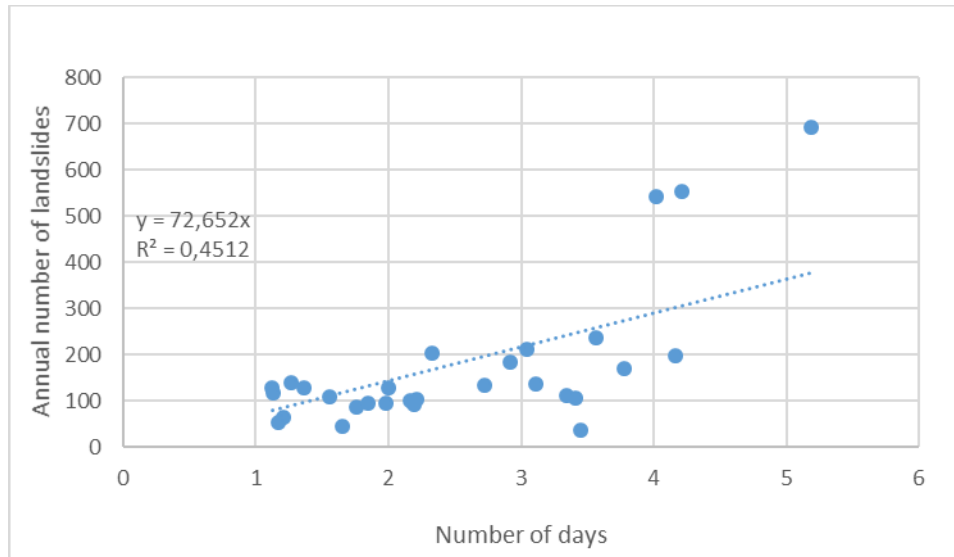


Figure 21 – Interpolation between the territorial average values of the heavy precipitation days in a year (with daily rainfall ≥ 50 mm) (D50mm) and the annual number of landslides in the whole territory of the Calabria region.

Generally, the best agreements were obtained for large province territories (such as Catanzaro, Cosenza, and Reggio Calabria). The results of the other provinces (Vibo Valentia and Crotona) present weak agreements.

Regarding the flood events, the comparisons with the climatic indices are weaker than those obtained with landslides, for the characteristics of the rivers in Calabria. These are often called “fiumare” (small rivers) and are highly irregular: they are very often dry but can become raging torrents after short and heavy rainfall events. This is due to the fact that Calabrian rivers rise in rocky gullies and tumble down steep gradients before reaching gentle valley rivers with pebble beds. In fact, the Time of Concentration of their basins is very low (only very few hours). The rivers with these characteristics can cause floods and consequent damage. For these reasons, the rainfall daily data and, summing them, the monthly and yearly data present low agreements with the number of floods, which are mostly influenced by extreme hourly rainfall.

Nevertheless, comparisons show the best matches with the following climatic indexes: R95TOT, D50mm, R99F. Figures 22-25 show some of these comparisons. Moreover, Figures 26-28 show some interpolations between data of floods and climatic indices values and the expression of the interpolation curves.

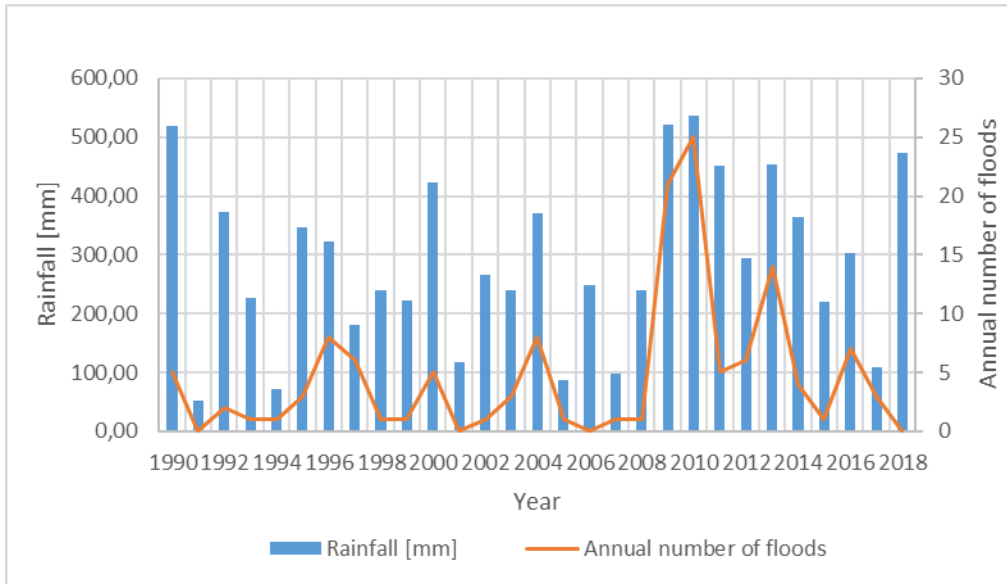


Figure 22 – Comparison of the territorial average values of the annual total precipitation when daily rainfall is greater than 95th-percentile (R95TOT) with the annual number of floods for the Crotona province.

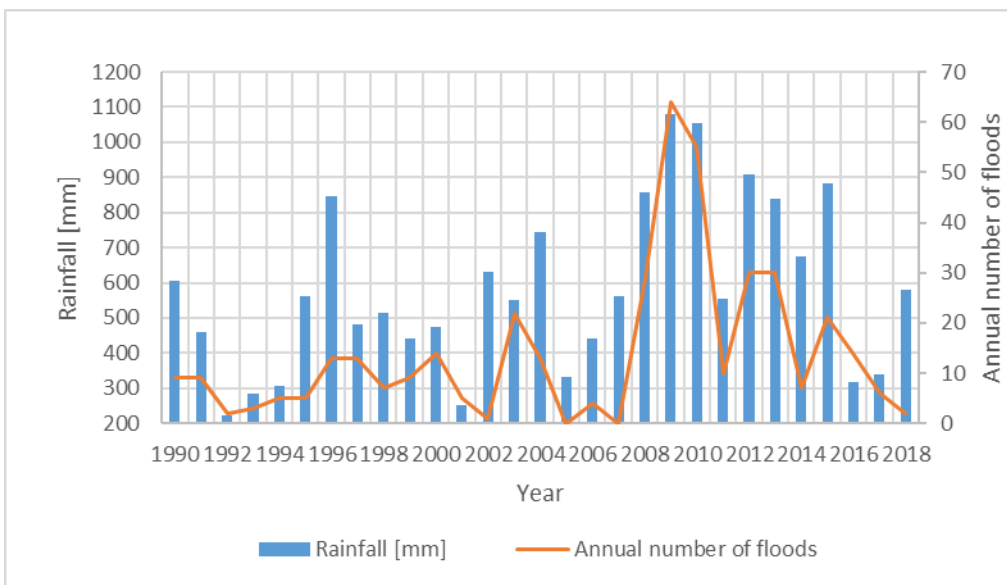


Figure 23 – Comparison of the territorial maximum values of the annual total precipitation when daily rainfall is greater than 95th-percentile (R95TOT) with the annual number of floods for the Cosenza province.

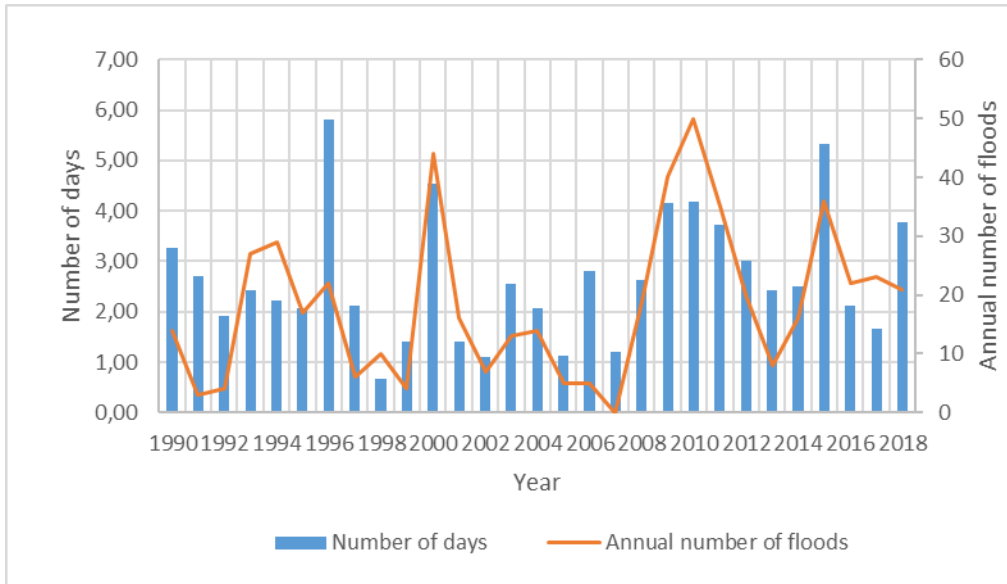


Figure 24 – Comparison of the territorial mean values of the heavy precipitation days in a year (with daily rainfall ≥ 50 mm) (D50mm) with the annual number of floods for the Reggio Calabria province.

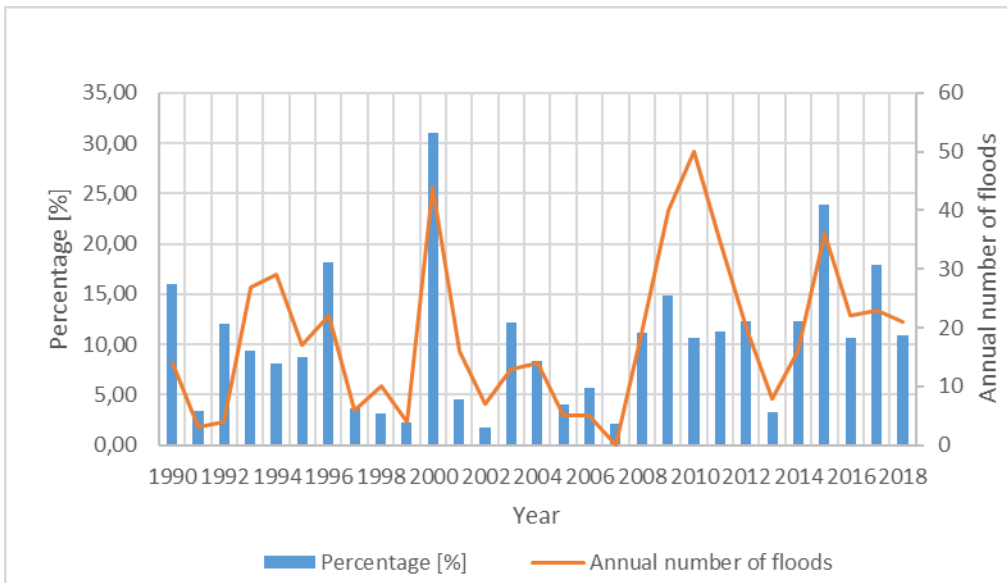


Figure 25 – Comparison of the territorial mean values of the precipitation fraction out of the annual total due to extremely wet days (daily rainfall $> 99^{\text{th}}$ -percentile) - R99%TOT - with the annual number of floods for the Reggio Calabria province.

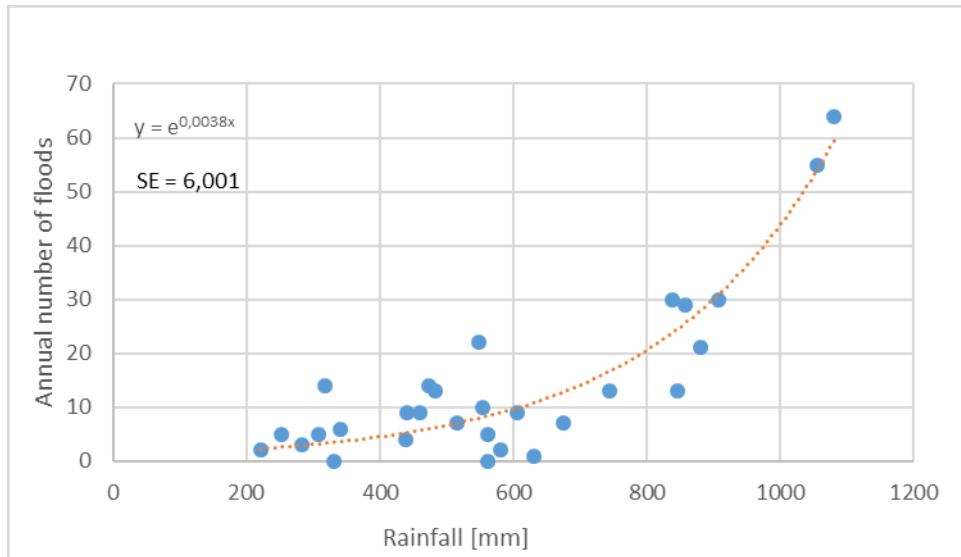


Figure 26 – Interpolation curve between territorial maximum values of the annual total precipitation when daily rainfall is greater than 95th-percentile (R95TOT) and the annual number of floods for the Cosenza province.

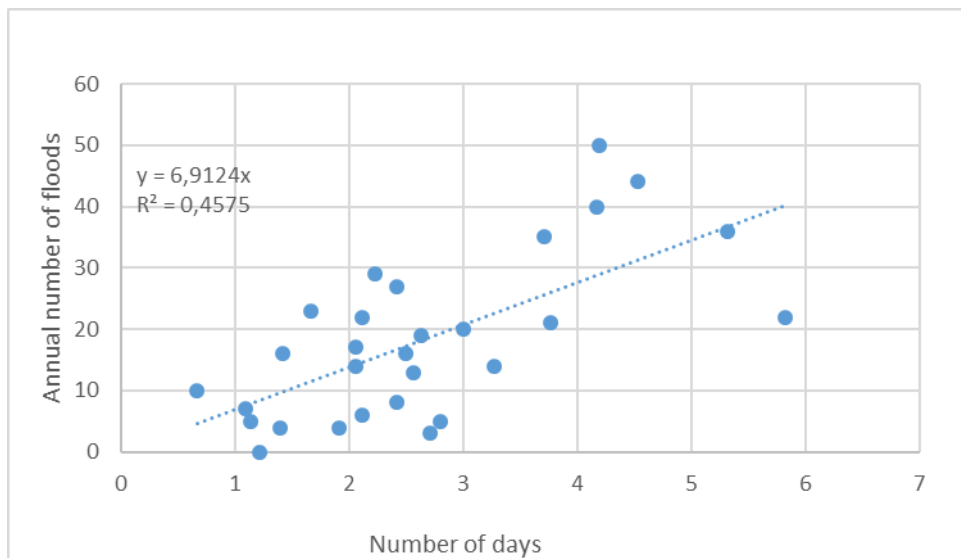


Figure 27 – Interpolation between territorial mean values of the heavy precipitation days in a year (with daily rainfall ≥ 50 mm) (D50mm) with the annual number of floods for the Reggio Calabria province.

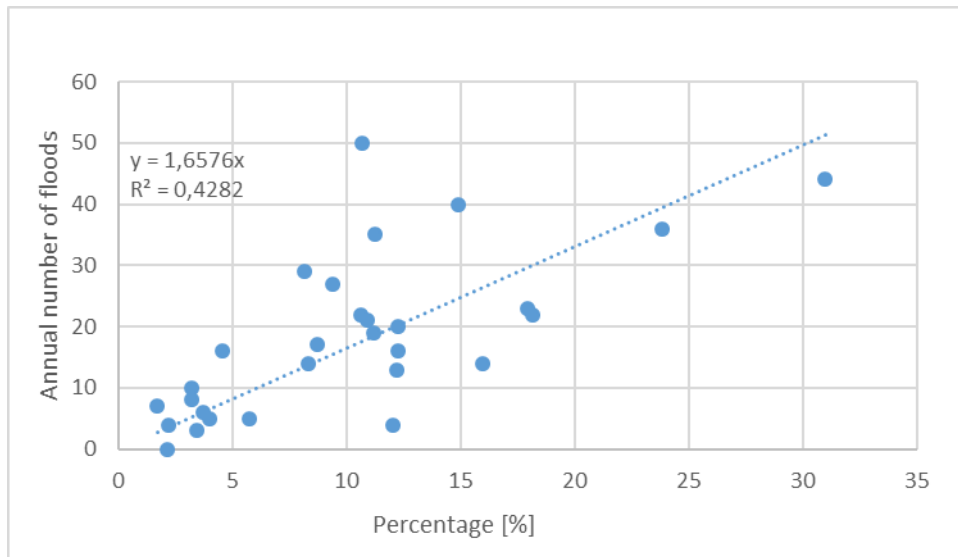


Figure 28 – Interpolation between the territorial mean values of the precipitation fraction out of the annual total due to extremely wet days (daily rainfall > 99th-percentile) - R99%TOT – and the annual number of floods for the Reggio Calabria province.

**Using INDECIS data for simulating and forecasting groundwater
levels in the MétéEAU Nappes website**

1. Context

1.1. Description of *MétéEAU Nappes* website

The *MétéEAU Nappes* web-tool (Mougin et al., 2018; Mougin et al., 2020), developed by BRGM, allows, for some monitored points, to visualize present and future aquifer quantitative state. These data are available on dynamic maps and curves resulting from modelling of groundwater levels for low and high flows conditions (in connection with drought and flood problems). The hydrological global models used (GARDENIA (Thiéry, 1988) and TEMPO (Pinault, 2001)) allow from meteorological, hydrological and piezometric input data (combined with pumping data), the simulation and forecast of groundwater levels. These forecasts, launched over 6 months, are compared with piezometric drought thresholds values taken from current prefectural regulations for water use restriction during drought. Meteorological, hydrological and groundwater data are provided in real time conditions and using an interoperable format over a dozen of case studies in France.

MétéEAU Nappes website offers a large range of services for the monitoring of the current and the future state of French aquifers (and thus, for management aspects, to anticipate possible deficits of water resources). It is a real decision-making tool for water resource management in high-stakes territories (water use conflicts, droughts, river floods, floods by rising groundwater level, climate change...).

Thirty public and private french stakeholders are already accessing and using the current website in its prototype version (DREAL, DDTM, Service de Prévision des Crues, Météo-France, Agence de l'Eau, Régions et Départements, EPCI, Presse, Industriels, Opérateurs numériques...).

1.2. Functions and services

The *MétéEAU Nappes* website offers a large set of services useful for drought and flood problems due to low and high groundwater levels:

- a website with reserved access (address: <https://meteeaunappes.brgm.fr>) and associated Informatics Technology services ;
- an easy-to-use and quickly understandable web interface (real-time maps and curves, dynamic data sheets updated at each connection; i.e. refreshed on the current date) ;
- a historical and real-time display (maps and curves) of meteorological, groundwater, and surface water data available from various French data providers (SCHAPI, Météo-France, BRGM) ;
- a map of the current (including real-time for some sectors) and future aquifers situation (aquifer behaviour forecasts) assessed using the Standard Piezometric Level Index (SPLI - Seguin, 2015, Vergnes et al., 2020) calculation from piezometric data of the French National Data Base ADES portal (<http://www.ades.eaufrance.fr/>, Sharples et al., 2020), according to various climate forecasted scenarios ;
- some curves with overlay of a relevant information set (piezometric levels: formerly measured, real-time data, forecast levels; piezometric drought/flood thresholds values; real-time river flow; real-time rainfall) ;
- some tools associated with maps and curves: tooltips, zoom thresholds, history of chronicles, legend, possibility to display (or not) a point or a curve, printing ;
- using GARDENIA model, an automatic monthly refreshment of projected groundwater levels data with recent weather data (currently those of the previous month) ;

- a provision of metadata associated with exposed predictions (model used, time step, calibration period, correlation coefficient, stations used, whether or not pumping data is taken into account, terrain elevation at the piezometer, bibliographic reference of piezometric thresholds values [prefectural orders, BRGM studies...]) ;
- a dynamic private application programming interface (API); for a selected piezometer: return of the simulated piezometric curves and return of a point associated with the current or future SPLI symbology and color.

The technological devices used to achieve these services are: GPRS technology (today deployed on nearly 1,400 stations of the national piezometric network) to make data available every day, as well as a specific technical architecture based on international standards and recent technologies allowing to cross real-time data from different organisms and the exploitation of models already carried out.

At the beginning of 2021, the BRGM will finalize the creation of *MétéEAU Nappes* API and then propose a new design of *MétéEAU Nappes* website.

2. Objectives of this study

In this context, the objectives of the study performed in the framework of the INDECIS project were :

- to test the climate data available on INDECIS website (<http://www.indecis.eu/data.php>) for groundwater levels simulation in contrasted aquifers, both for France and Europe ;
- based on the built models, launch groundwater levels forecasts ;
- to include the resulting models into the *MétéEAU Nappes* website.

As a result, new models were included into *MétéEAU Nappes* website and the potential for expanding it at the European scale demonstrated.

3. Performed work and results

Results presented in this section will be illustrated for the Aubagne piezometer (10446X0267/PIEZ), located near Marseille in the south-east of France (Figure 1). Results of the 12 other case studies are detailed in Annex A.

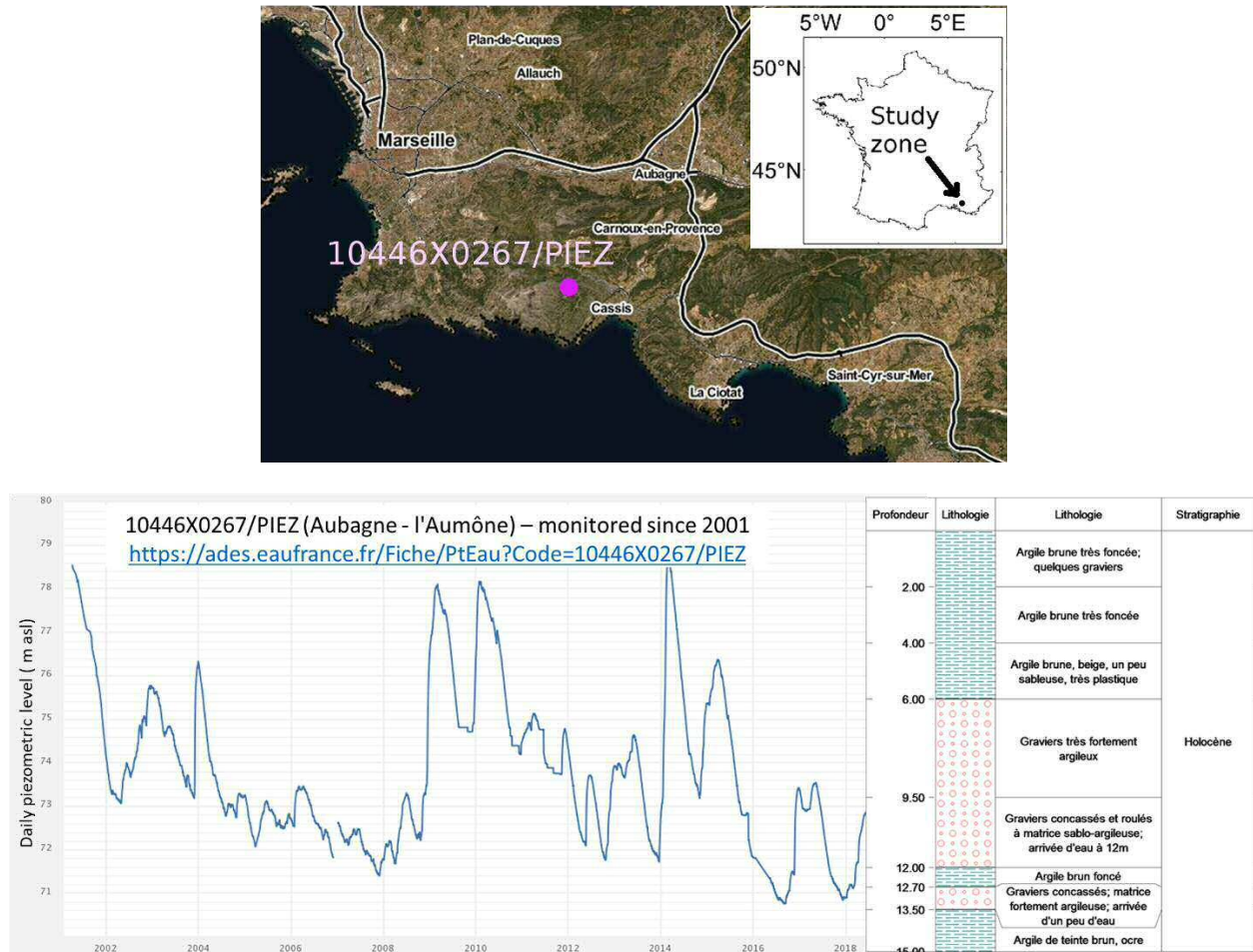


Figure 1 - Location of Aubagne case study near Marseille in France, and historical groundwater levels

3.1. INDECIS climate data

The following data fields have been extracted from the INDECIS website and among the 136 sector-oriented climate indices (http://www.indecis.eu/docs/Deliverables/INDICIS-list_4.2.pdf):

- “Reference evapotranspiration” (Aridity/continentality indices, number 91, ID Eto), - Monthly data were extracted from the grid available on <http://www.indecis.eu/indices.php> (Figure 2);
- “Daily precipitation amount RR”, files downloaded from the website <http://www.indecis.eu/data.php> (Figure 3) - Blended and Non-blended ECA dataset were both used (Download predefined subsets in ASCII);
- “Potential evapotranspiration (PET)” and “6-month Standardized Precipitation Index (SPI6)”, files downloaded from the website <http://www.indecis.eu/data.php> - Monthly data were extracted from Drought Indices data (Download predefined sets of aggregated indices data (ASCII)).

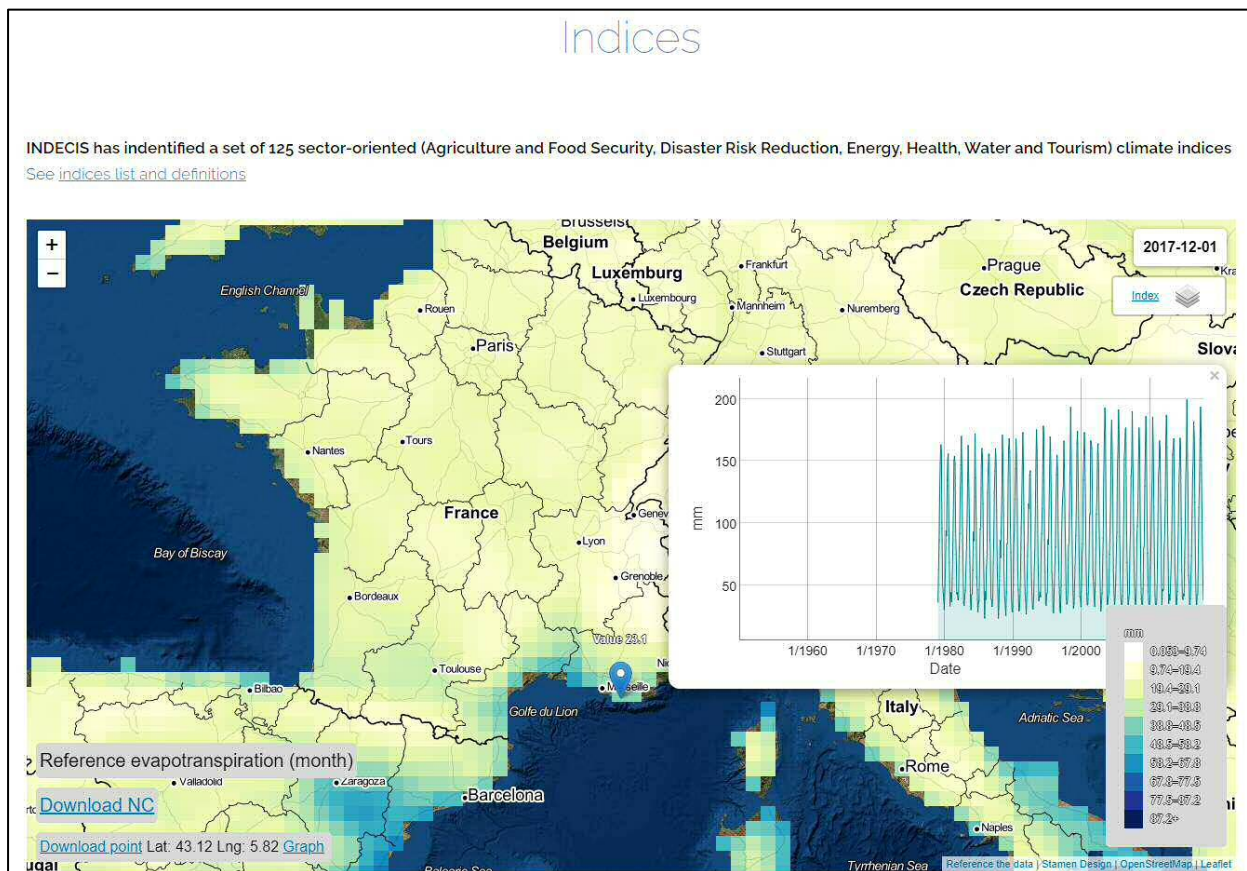


Figure 2 - Extraction of monthly “Reference evapotranspiration” near Marseille (France) on INDECIS website

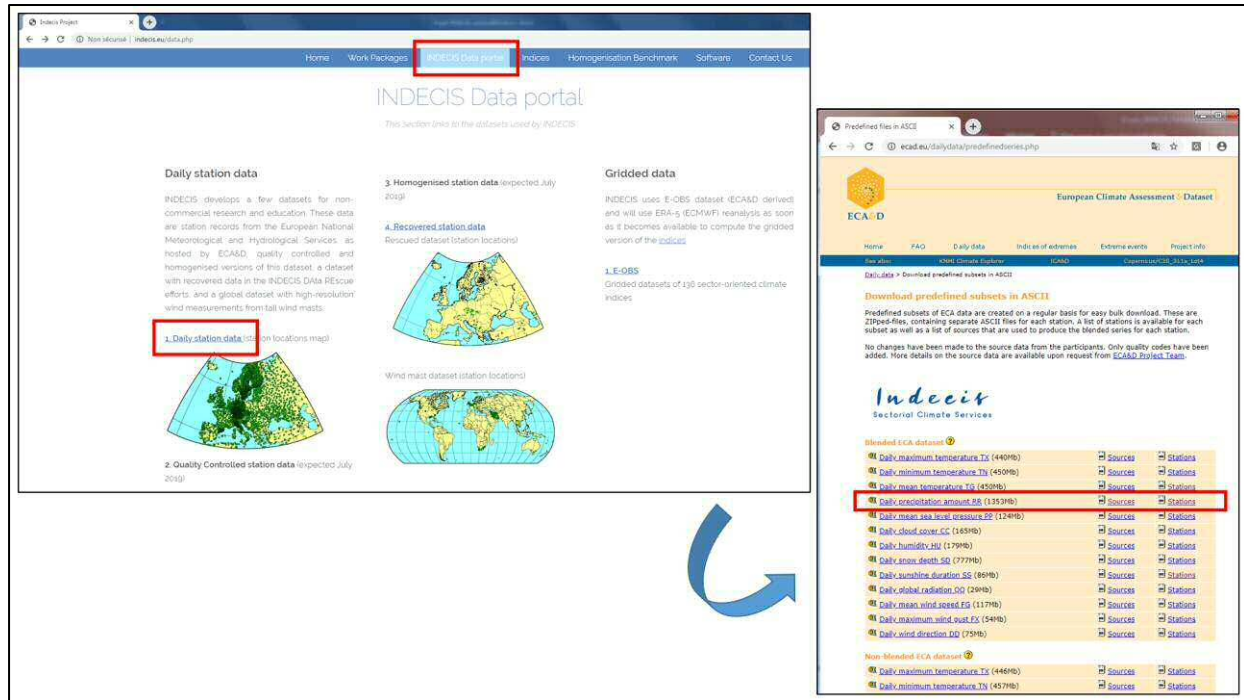


Figure 3 - Daily precipitation data downloaded on INDECIS website

3.2. Case studies and statistical analyses

8 case studies with meteorological stations providing both precipitation and evapotranspiration variables and located near piezometers monitored by the BRGM were selected in France (Figure 4). The selection was based on the following criteria: piezometer included in the French European Water Framework Directive network; piezometers with real-time measurements; time-series length coherent with that of INDECIS meteorological data; diverse hydrogeological contexts and groundwater dynamics (reactive or inertial) and representativeness of a typical groundwater body. Piezometric data from these 8 French case sites were extracted from the national data base ADES.

Based on a review of the web services for groundwater monitoring data available at the European scale (Koreimann et al., 1996), 5 more case studies located in Ireland, Sweden, Denmark, Germany and Spain were added, where piezometric data time series were freely available (Figure 4). The list of reviewed web services is presented in Annex B. The piezometric data for these 5 European sites were downloaded from the websites of the organisations in charge of the monitoring (Umwelt Sachsen in Germany, Gobierno De España in Spain, Environmental Protection Agency in Ireland, SGU Geological Survey of Sweden, GEUS The Geological Survey of Denmark and Greenland).

The characteristics of the final set of 13 case studies for INDECIS are detailed in Figure 5.

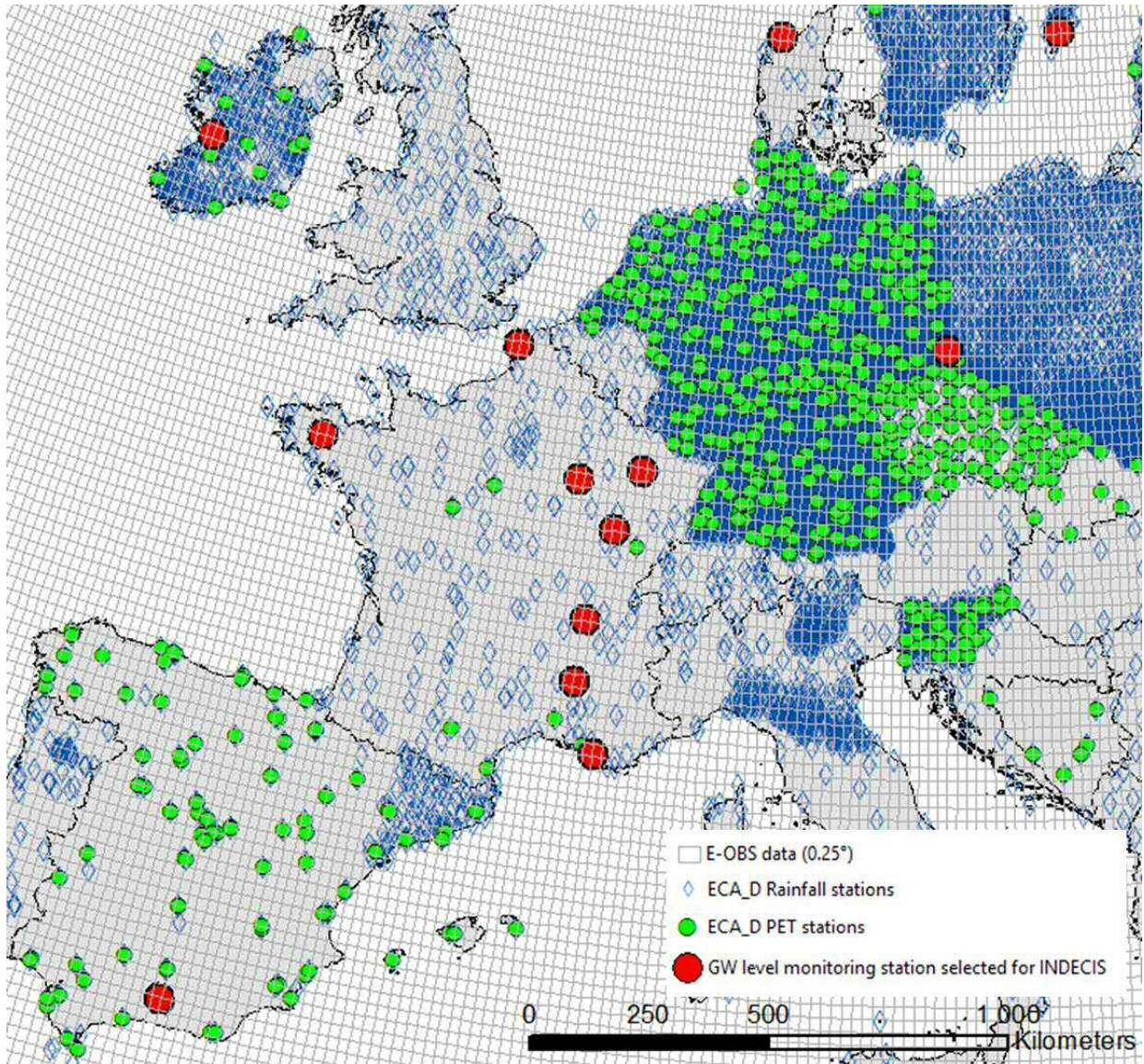


Figure 4 – Location of the 13 case studies considered for INDECIS. Available precipitation and evapotranspiration data from ECA-D and Indices grid were respectively considered depending on the piezometer location.

Country	Region	Precipitation station number	Precipitation station name	PET station number	PET station name	Piezometer code	Piezometer name	Geology	Groundwater dynamics	Modelling period (Gardinia)	Correlation coefficient - calibration (%)	Forecast	
France	BRE	434	Brest-Guipavas	-	Indices Grid	03124X0088/F	Rostrenen	hard-rock	reactive	2005-2019 (5-year initialization)	90%	yes	
France	CHA	11243	Troyes-Barbère	-	Indices Grid	02982X0028/F	Vailly	Turonian shalk and marls	inertial	1980-2019 (5-year initialization)	94%	yes	
France	BOU	745	Dijon-Longvic	-	Indices Grid	04398X0002/SONDAG	Bourberain	Jurassic limestone	reactive	1980-2019 (5-year initialization)	92%	yes	
France	PACA	39	Marignane	39	Marignane	10446X0267/PIEZ	Aubagne - l'Aumône	alluvium	inertial	2001-2019 (6-year initialization)	90%	yes	
France	RHA	37	Lyon - St Exupery	751	Lyon-Bron	06987A0186/S	La Doua (Villeurbanne)	alluvium	reactive	1977-2019 (2-year initialization)	81%	-	
France	RHA	786	Montelimar	786	Montelimar	08662X0408/F	Saint-Marcelles-Sauzet	alluvium	reactive	2006-2019 (1 an initialisation)	76%	-	
France	LOR	11246	Nancy-Ochey	741	Nancy-Essey	02296X0038/P1	Dommartin-Les-Toul	alluvium	reactive	2003-2019 (1 an initialisation)	94%	yes	
France	PIC	736	Abbeville	-	Indices Grid	00104X0054/P1	Puits de la Ferme Delattre (Wirwignes)	Jurassic limestone	reactive	1984-2018 (5-year initialization)	86%	yes	
Ireland	Galway	2139	Shannon	2139	Shannon	IE_WE_G_0002_1200_0013	Killiny	limestone	reactive	2003-2019 (5-year initialization)	94%	yes	
Sweden	Gotland island	5265	Hemse	-	Indices Grid	8_4	Hemse_4	Limestone, sandstone, schists	reactive	1986-2019 (5-year initialization)	84%	yes	
Denmark	North Jutland	107	Vestervig	-	Indices Grid	22.368 Hindingvej 27	Thisted	moraine, limestone, shalk	reactive	1985-2019 (5-year initialization)	86%	yes	
Germany	Dresde	14215	Muecka	484	Gorlitz	46549384	Neudorf, B 384/68	hard-rock	reactive	1991-2019 (5-year initialization)	88%	yes	
Spain	Granada	3932	Granada/Aeropuerto	3932	Granada/Aeropuerto	05.32.008 CHG Romilla - P4	Chauchina	Cretaceous-Jurassic limestones?	inertial	1993-2017 (5-year initialization)	84%	-	

Figure 5 – Table overview of datasets and results for the 13 case studies.

In the *MétéEAU Nappes* website, it is now possible to show the hydrological situation of the groundwater bodies monitored by the corresponding piezometers at a given day (Figure 6). For each monitoring point, the groundwater level (cf. symbol color) and its instantaneous daily tendency (rise / drop / stability – cf. symbol type) relative to their available historical data series are presented.

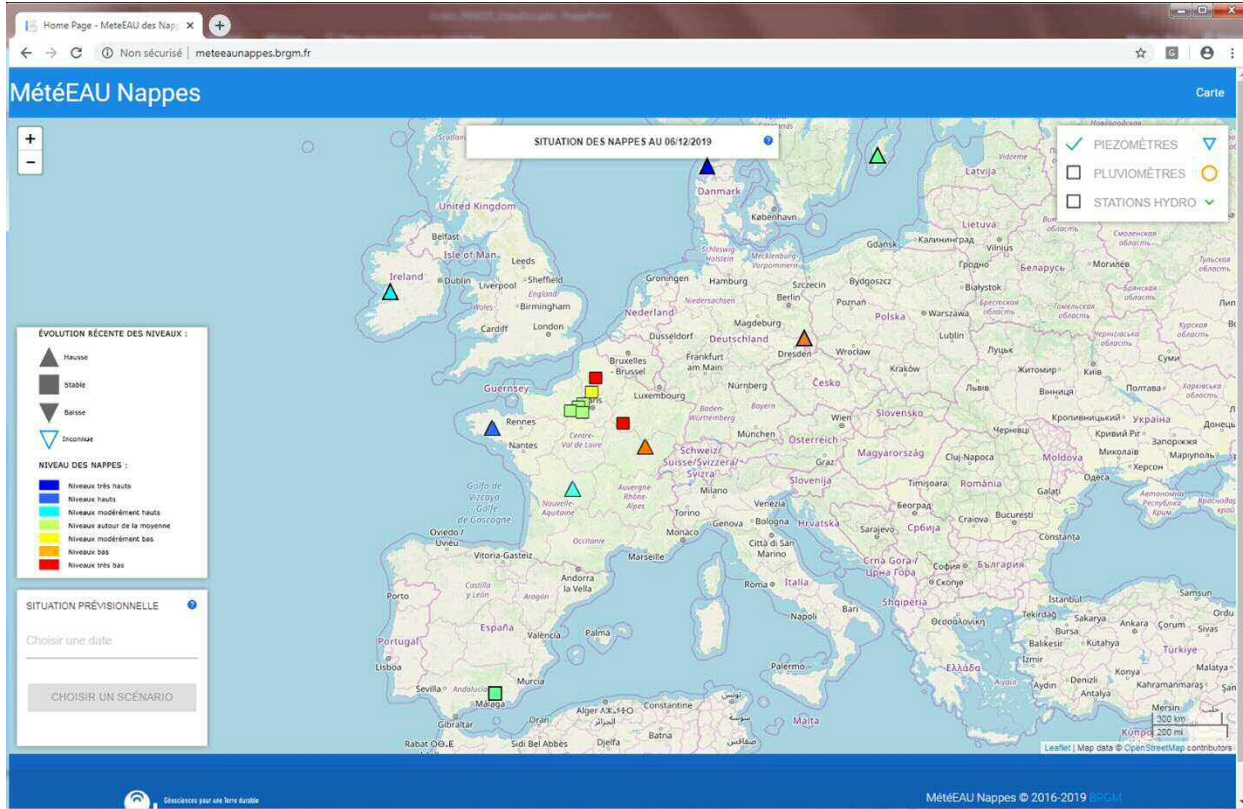


Figure 6 – hydrological situation of the 13 piezometers included in the *MétéEAU Nappes* website for any given day (here 06/12/2019).

Piezometric data of all case studies have been analysed in order to define the main statistical characteristics of the data series using the ESTHER software (Seguin et al., 2018). In the absence of low-flow thresholds values, specific low-flow return period values (20, 10 and 5-year) were calculated based on the fitting of a statistical law on minimum mean monthly groundwater level values time series (Figure 7). Those dry and wet return period values can then be used to inform groundwater managers about the groundwater resource hydrological situation regarding its data history (Figure 8).

For each of the 13 case studies, cross-correlation analysis between the 6-month Standard Precipitation Index (SPI6) and groundwater levels time monthly series were performed. For the sake of consistency, the 6-month Standard Piezometric Level Index (Seguin et al., 2018 ; Vernoux et al., 2012) was computed and used in the cross-correlations (Figure 9). The resulting correlation percentage and time lags are summarized in Figure 5. Figure 9 shows, for example, that the precipitations measured at the MARIIGNANE station (STAIID: 39) and summarized using the SPI6 are relatively well correlated ($R=0.64$) with groundwater levels at Aubagne (10446X0267/PIEZ) considering a time lag between the 2 signals of around 4 months. This shows the potential of the SPI6 for the Aubagne groundwater level forecasting.

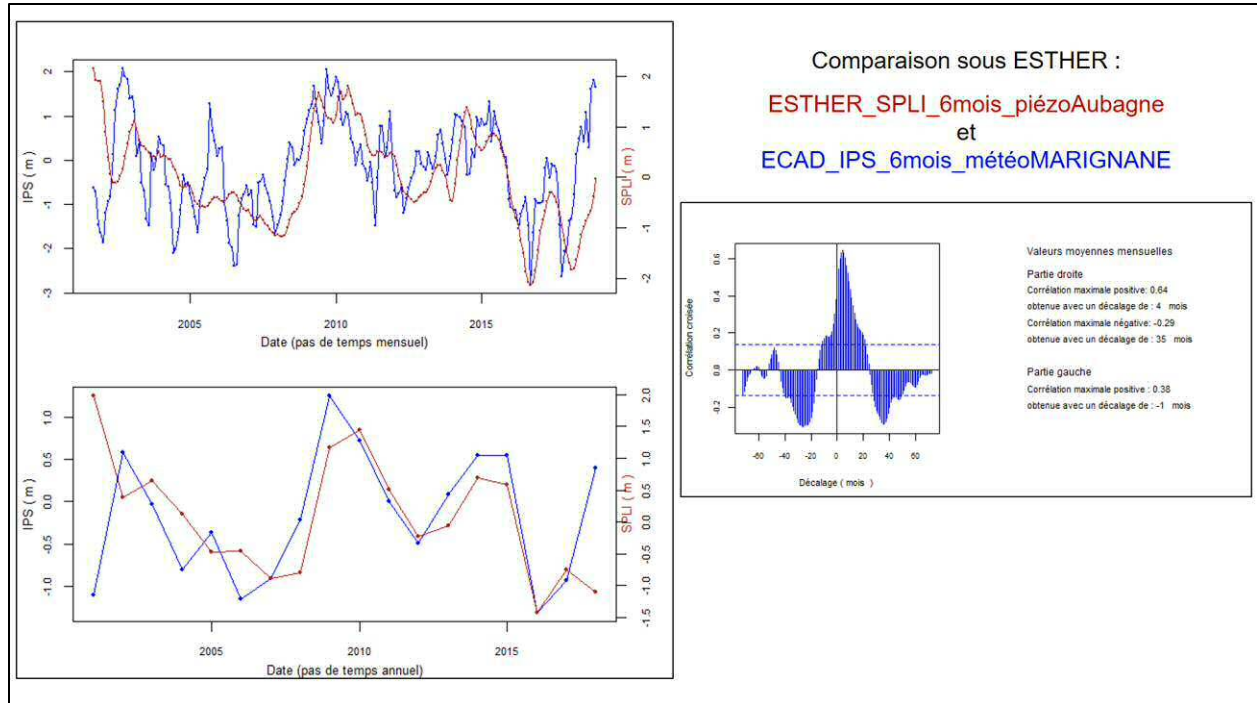


Figure 9 - Comparison between the 6-month Standardized Precipitation Index (here called IPS_6) and the 6-month Standard Piezometric Level Index (here called SPLI_6).

3.3. Rainfall-piezometric level modeling

3.3.1. The GARDENIA lumped hydrological model

GARDENIA is a BRGM modelling tool (Figure 10) developed for rainfall/river flow/groundwater level budget simulation (Nicolle et al., 2014). GARDENIA (acronym for « Modèle Global À Réservoirs pour la simulation de DÉbits et de Niveaux Aquifères » in French) uses meteorological data time series related to a catchment area (precipitation and potential evapotranspiration) as input data to calculate:

- the flow rate at the outlet of a river (or spring);
- and/or the groundwater level at a given location in the underlying unconfined aquifer.

The presence of one or a set of pumping boreholes in the catchment can also be taken into account.

GARDENIA simulates the main water cycle mechanisms in a catchment (rainfall, snowmelt evapotranspiration, infiltration, runoff) by applying simplified physical laws to flow through successive reservoirs. Non-linear transfer functions improve the capability of this schematic representation to simulate a complex system.

The calculations can be made at a daily, weekly, 10-day, or monthly time step. Users can also choose a much shorter time step, e.g. half-hourly or every five minutes.

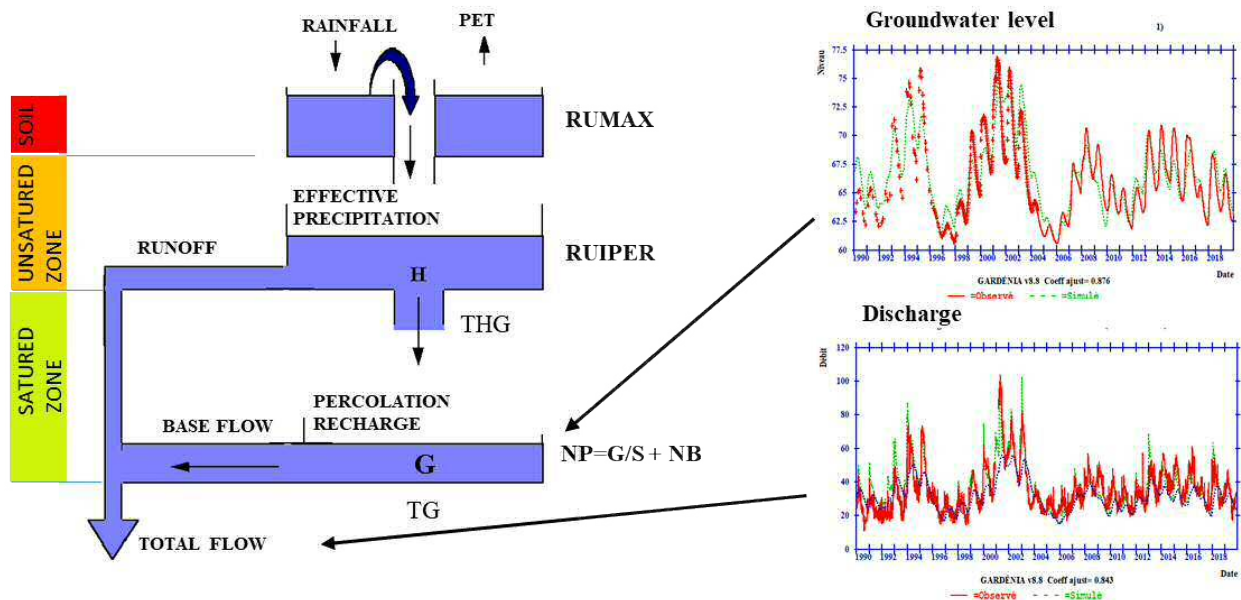


Figure 10 - Principle of GARDENIA global hydrological model for simulating the river discharges and/or piezometric levels.

3.3.2. Modeling piezometric levels for the 13 case studies

The GARDENIA model was used to calculate groundwater levels at the 13 selected piezometers (Figure 5). The calculations were made at a daily time step using the INDECIS climate data: “Daily precipitation amount (RR)” and “Potential evapotranspiration (PET)” (see 3.1.), from meteorological stations or gridded data presented in Figure 5. No pumping withdrawals have been taken into account. The simulation periods

for each of the 13 piezometers are specified in Figure 5. Models calibration performance was assessed using correlation coefficient (R) and Efficiency criteria (Nash (Nash & Sutcliffe, 1970)).

Calibration and validation results for the Aubagne piezometer are shown in Figure 11. Both Aubagne calibration and validation model's correlation and Nash coefficient values are satisfactory. Results for the other case studies are presented in Annex A and their calibration performance detailed in Figure 5. For the 13 case studies, the correlation coefficients range from 76% to 94% with an average of 88%.

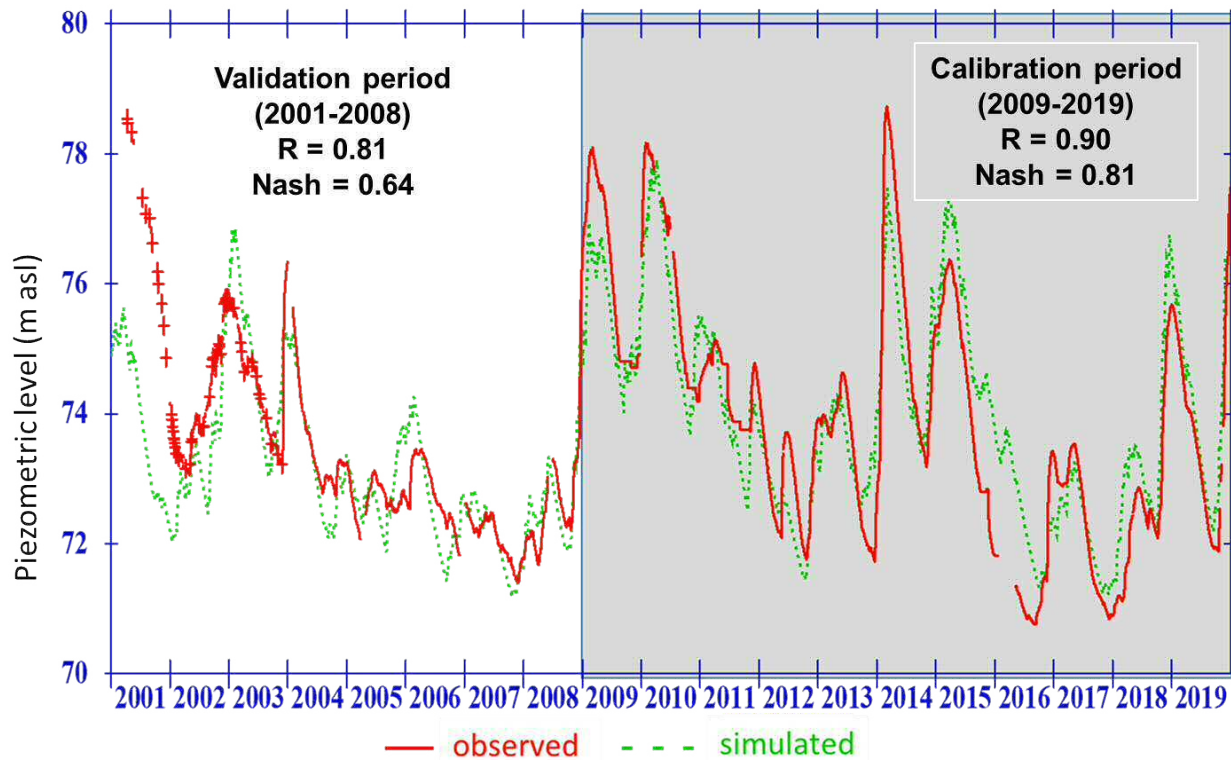


Figure 11 - Results of the groundwater level modelling calibration (2009-2019) and validation (2001-2008) periods for the Aubagne case study.

3.3.3. Forecasting piezometric levels

For well enough calibrated models, groundwater levels forecasting starting at the beginning of summer low-flows period until the end of the year was performed in order to provide information for water managers. Forecasts are also feasible during high-flows conditions if a risk related to flood by rising groundwater level exists in a case study (this was tested for instance on Wirwignes piezometer - 00104X0054/P1, see Annex A).

Forecasting groundwater levels was not possible for 2 out of the 13 case studies, for the following reasons: strong downward trend (La Doua Villeurbanne piezometer - 06987A0186/S) and episodic very low values (Saint-Marcel-les-Sauzet - 08662X0408/F).

Figure 12 presents the resulting groundwater piezometric levels forecasts for the Aubagne piezometer, launched over 6 months, according to different scenarios. Meteorological forecasting scenarios are built based on the probability distribution of the meteorological historical data for each day of the forecasting

period. Low-flows (dry, 0.9 and 0.6), median and high-flows (wet, 0.4 and 0.1) characteristic quantiles are used to generate the rainfall and PET time series for the forecasting period.

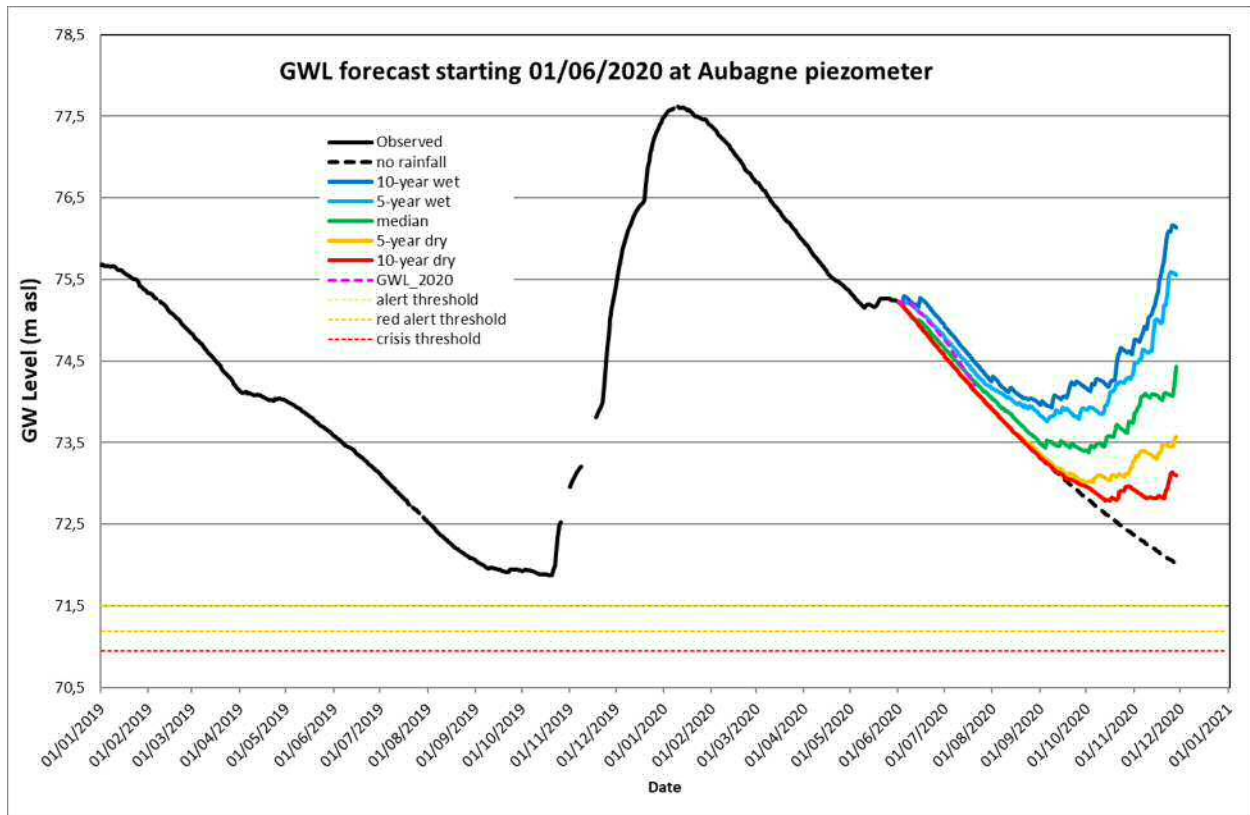


Figure 12 - Results of forecasts for the Aubagne case study model groundwater piezometric levels

For piezometers lacking threshold values fixed by water managers for the water use control during droughts, statistical threshold levels have been defined based on historical piezometric time series analyses (cf. Figure 7 and Figure 8). Forecasts performed with GARDENIA over a 6-month period can then be compared with these thresholds in order to anticipate potential water shortages that may trigger water use restrictions by the end of the year.

In the example of the Aubagne case study, Figure 12 shows that all the forecasted groundwater level scenarios may remain above the drought threshold values for the 2020 low-flow period. We also see that the groundwater level observed during June-July 2020 is within the forecasted curve envelope, fluctuating between 5-year wet precipitation return period and the median precipitation forecasts.

4. Conclusions

Modelling and seasonal forecasting of groundwater level case studies selected at the European scale have been included in the MétéEAU Nappes website, using the INDECIS meteorological point-scale or gridded data. The work performed allow the localisation of the piezometer, the visualisation of the piezometric data time series and the modelling and seasonal forecast of the groundwater levels. Statistical analysis allowed identifying correlations between some of the indices calculated in INDECIS and defining groundwater level thresholds for both dry and wet situations.

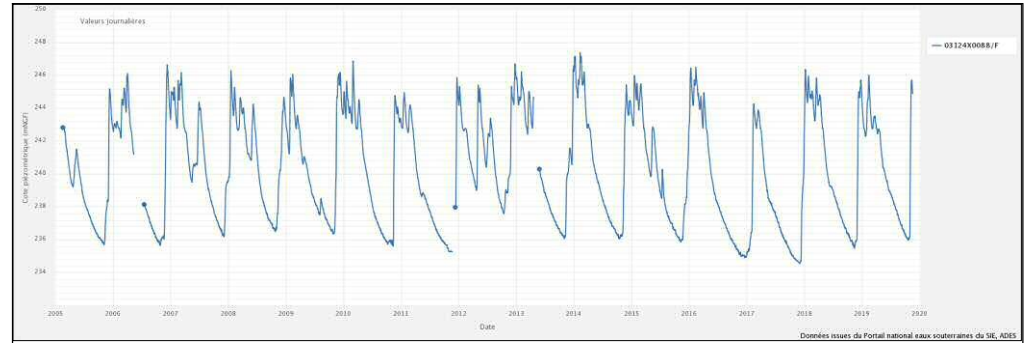
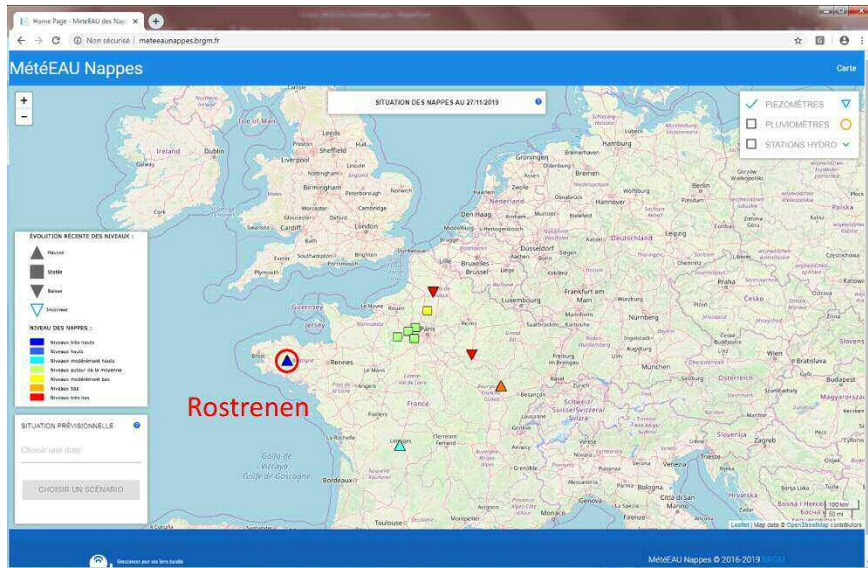
The public access version of MétéEAU Nappes website will be released in the beginning of 2021, including an Application Programming Interface (API) that will allow interested users to access the interface independently of its implementation.

5. References

- Koreimann, C., J. Grath, G. Winkler, W. Nagy and W-R. Vogel (1996) - Groundwater monitoring in Europe - European Topic Centre on Inland Waters - European Environment Agency - Topic Report Number 14
- Mougin B., Nicolas J., Bessiere H., Vigier Y., Loigerot S. (2018). Vers une prévision en temps réel du niveau des nappes françaises ? L’outil d’aide à la décision « MétéEau des nappes ». *Géologues*, 195, 16-21.
- Mougin B., Nicolas J., Vigier Y., Bessière H., Loigerot S. (2020). «MétéEAU Nappes»: a website with useful services for water and drought management. *La Houille Blanche*, 5, 28-36, <https://doi.org/10.1051/lhb/2020045>.
- Nash, J. E. & Sutcliffe, J. V. (1970) River flow forecasting through conceptual models. *Journal of Hydrology*, 10, 282–290.
- Nicolle, P. R. Pushpalatha, C. Perrin, D. François, D. Thiéry, T. Mathevet, M. Le Lay, F. Besson, J.-M. Soubeyroux, C. Viel, F. Regimbeau, V. Andréassian, P. Maugis, B. Augéard, & E. Morice. (2014). Benchmarking hydrological models for low-flow simulation and forecasting on French catchments. *Hydrology and Earth System Sciences*, 18(8), 2829–2857. <https://doi.org/10.5194/hess-18-2829-2014>
- Pinault, J. L., Plagnes, V., Aquilina, L., and Bakalowicz, M. (2001): Inverse modeling of the hydrological and the hydrochemical behavior of hydrosystems: characterization of Karst System Functioning, *Water Resour. Res.*, 37, 2191, doi:10.1029/2001WR900018
- Seguin, J.-J. (2015), Proposition d’un indicateur piézométrique standardisé pour le Bulletin de Situation Hydrologique “Nappes”, Technical report, [BRGM/RP-64147-FR](https://doi.org/10.1029/2001WR900018)
- Seguin J.-J., Allier D., Croiset N., Klinka T., Manceau J.-C. (2018) - ESTHER. Etude de Séries Temporelles en Hydrogéologie avec le logiciel R. Guide d'utilisation. Technical report, [BRGM/RP-67518-FR](https://doi.org/10.1029/2001WR900018)
- Sharples, J. Elisabeth Carrara, Lindsay Preece, Laurence Chery, Benjamin Lopez and Jean Daniel Rinaudo (2020), Information Systems for Sustainable Management of Groundwater Extraction in France and Australia, in « Sustainable Groundwater Management : A comparative Analysis of French and Australian Policies and Implications to Other Countries ». *Global Issues in Water Policy* 24, eds. Jean-Daniel Rinaudo; Cameron Holley; Steve Barnett; Marielle Montginoul, chapter 9, 163-190, ISBN 978-3-030-32765-1, <https://doi.org/10.1007/978-3-030-32766-8>
- Thiéry D. (1988) – Forecast of changes in piezometric levels by a lumped hydrological model. *Journal of Hydrology* 97 (1988), pp. 129-148
- Vergnes, J.-P., Nicolas Roux, Florence Habets, Philippe Ackerer, Nadia Amraoui, et al.. (2020). The AquifR hydrometeorological modelling platform as a tool for improving groundwater resource monitoring over France: evaluation over a 60-year period. *Hydrology and Earth System Sciences*, European Geosciences Union, 24 (2), pp.633-654. <https://doi.org/10.5194/hess-24-633-2020>

Vernoux J.F., Seguin J.J. (2012) - Établissement d'un réseau de référence piézométrique pour le suivi de l'impact du changement climatique sur les eaux souterraines (année 3) et essai de détermination d'un index piézométrique standardisé, Technical report, [BRGM/RP-61807-FR](#)

Annex A: Analyses and modelling results for all considered piezometers (Figure 5)

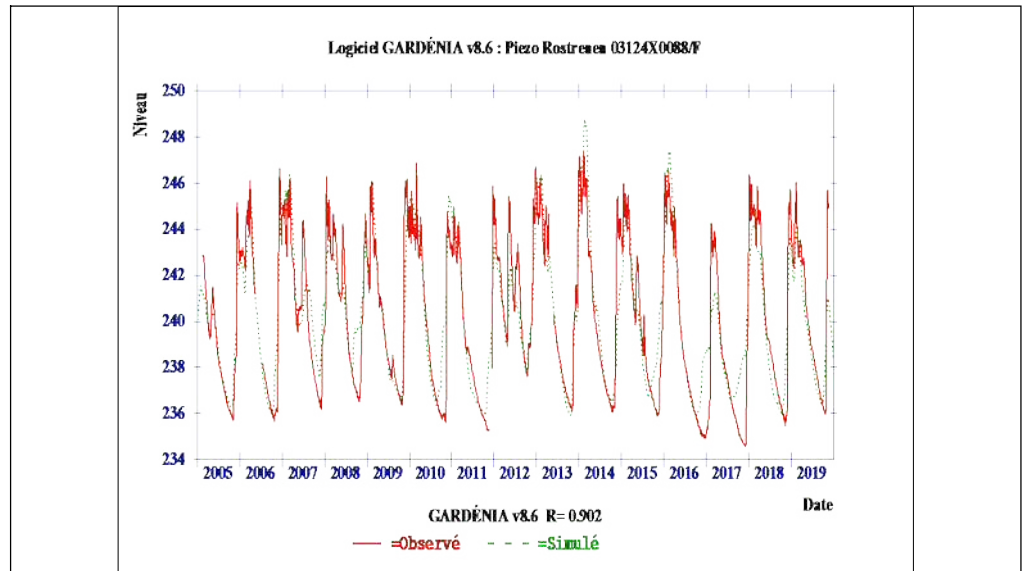
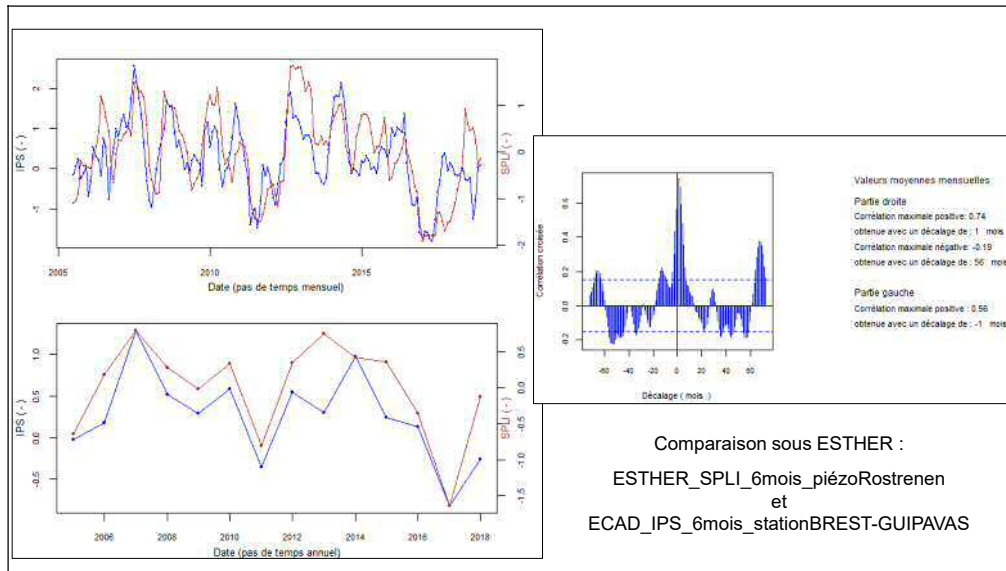


Piezomètre
Profondeur : 28 m

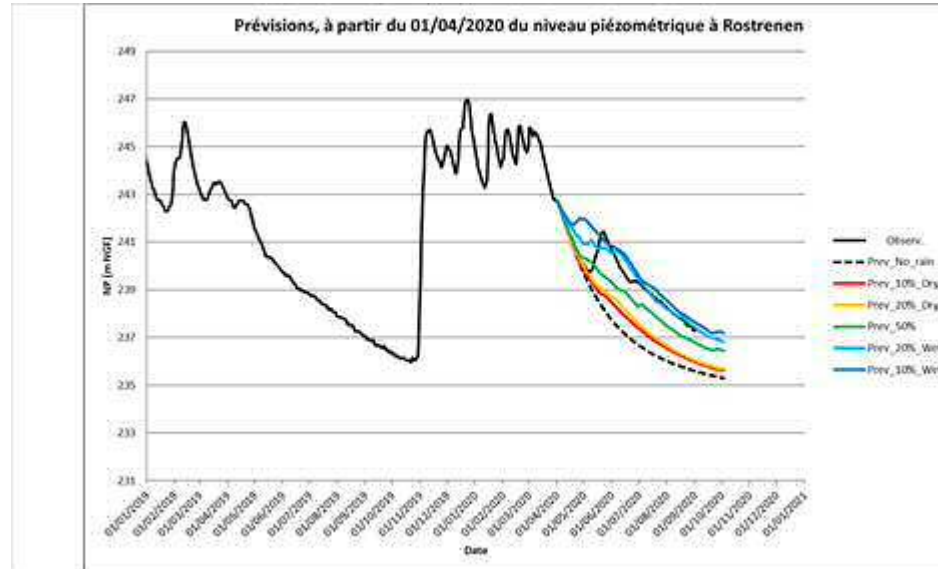
03124X0088/F - Rostrenen - mesures depuis 2005

BDLISA
Socle Plutonique
Dans Le Bassin Versant
Du Canal De Nantes À Brest
Jusqu'au Blavet (Non Inclus) - 195AA03

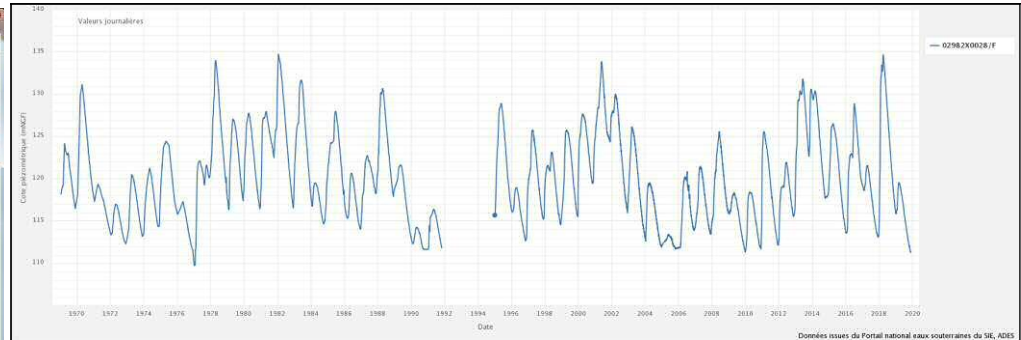
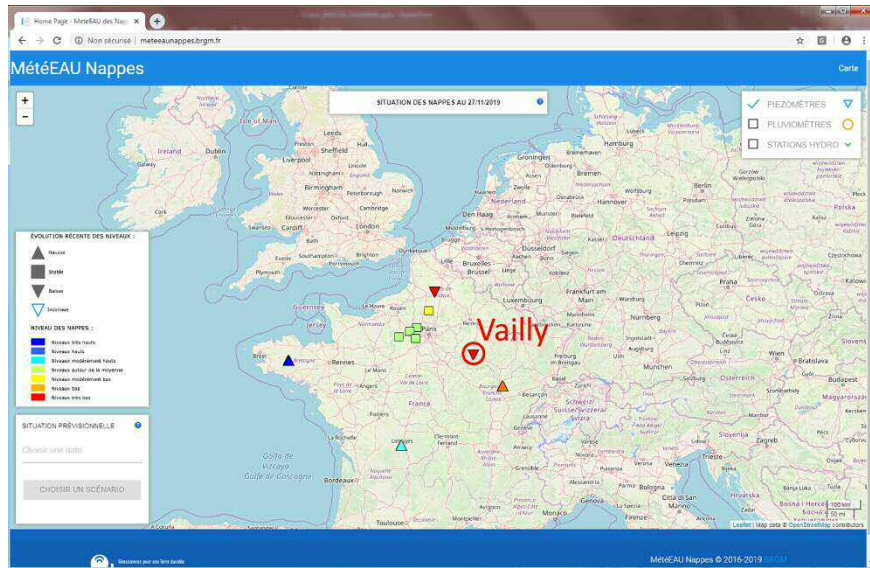
https://ades.eaufrance.fr/Fiche/PtEau?Code=03124X0088/F#mesures_graphiques



Analyses and modelling results for the Rostrenen piezometer



Analyses and modelling results for the Rostrenen piezometer

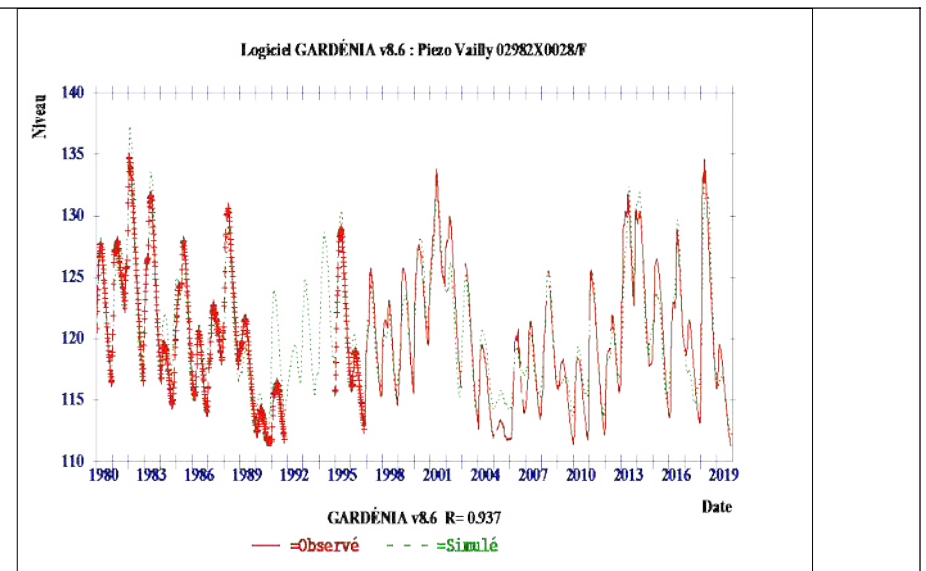
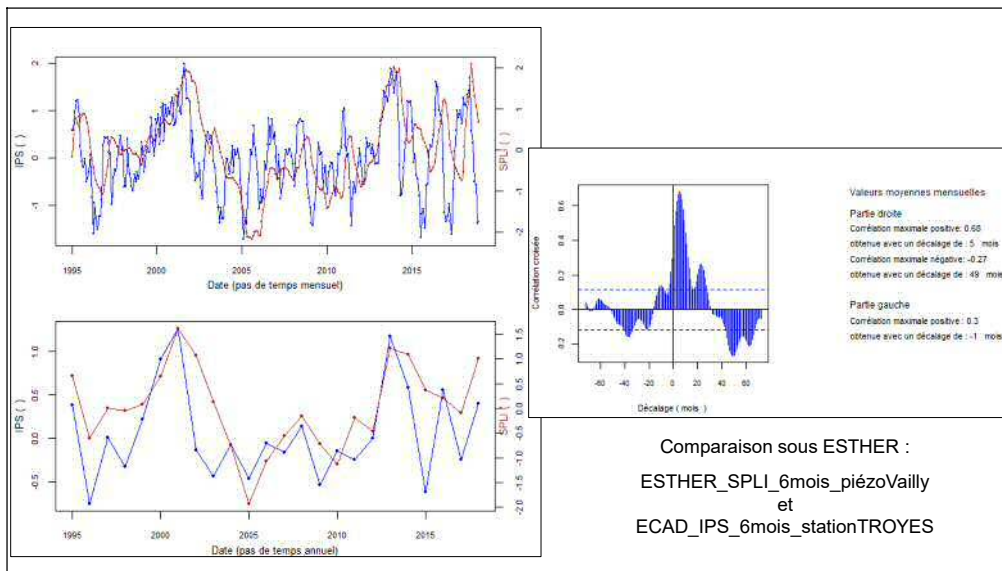


Piezomètre
Profondeur : 36 m

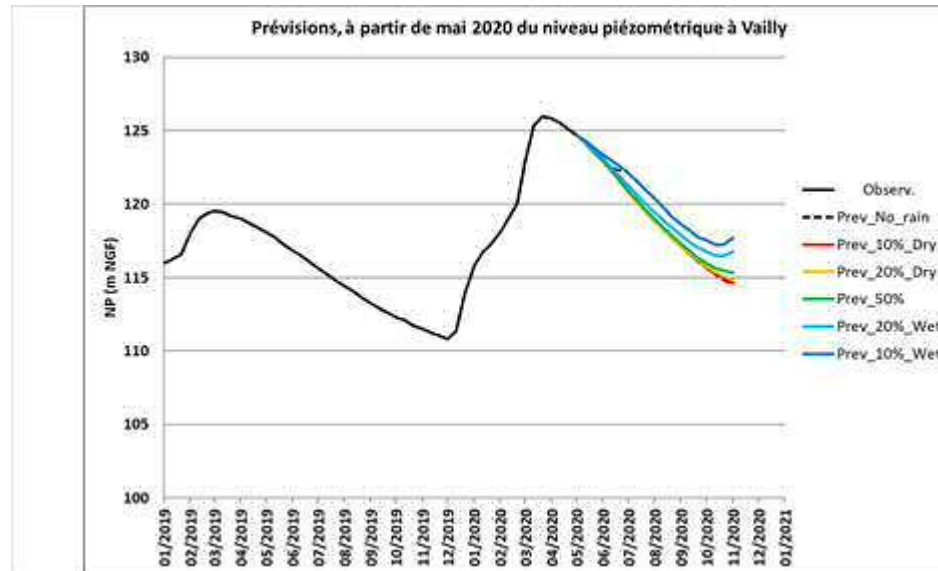
02982X0028/F - Vailly - mesures depuis 1969

BDLisa
Craie Marseuse Et Marnes Du Turonien Inférieur
Du Bassin Versant De L'Aube Et De La Seine
(Bassin Seine-Normandie) - 121A030

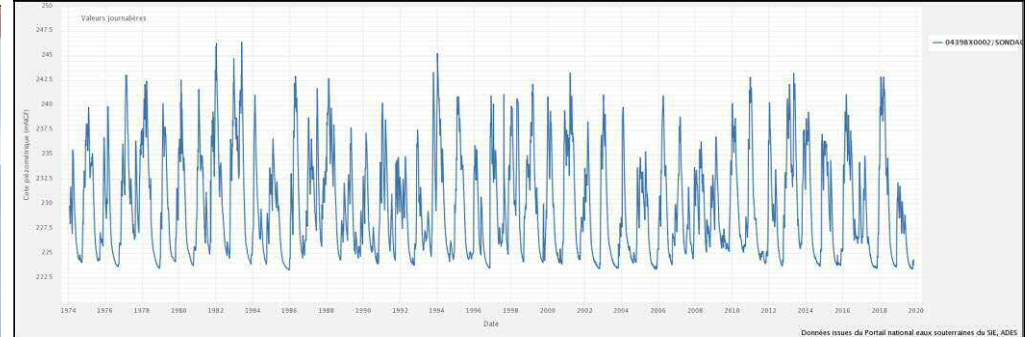
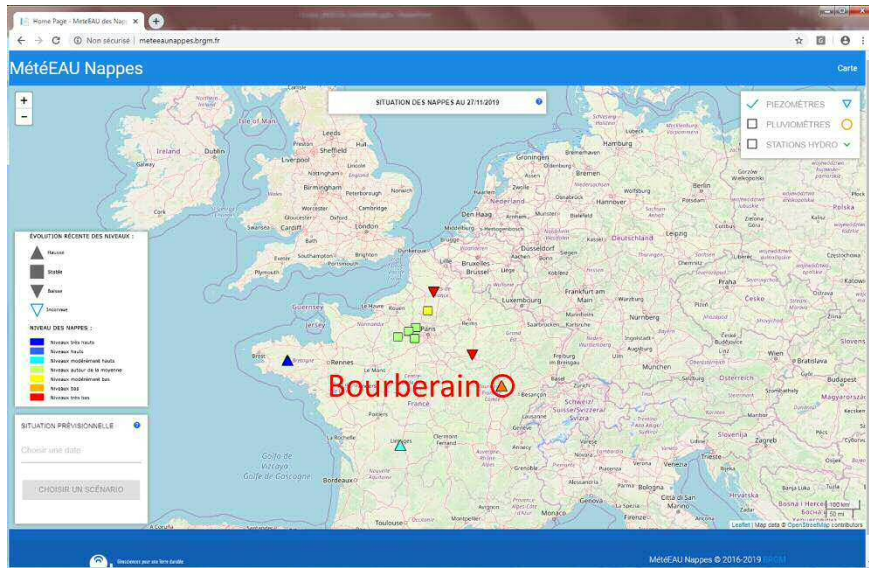
https://ades.eaufrance.fr/Fiche/PtEau?Code=02982X0028/F#mesures_graphiques



Analyses and modelling results for the Vailly piezometer



Analyses and modelling results for the Vailly piezometer

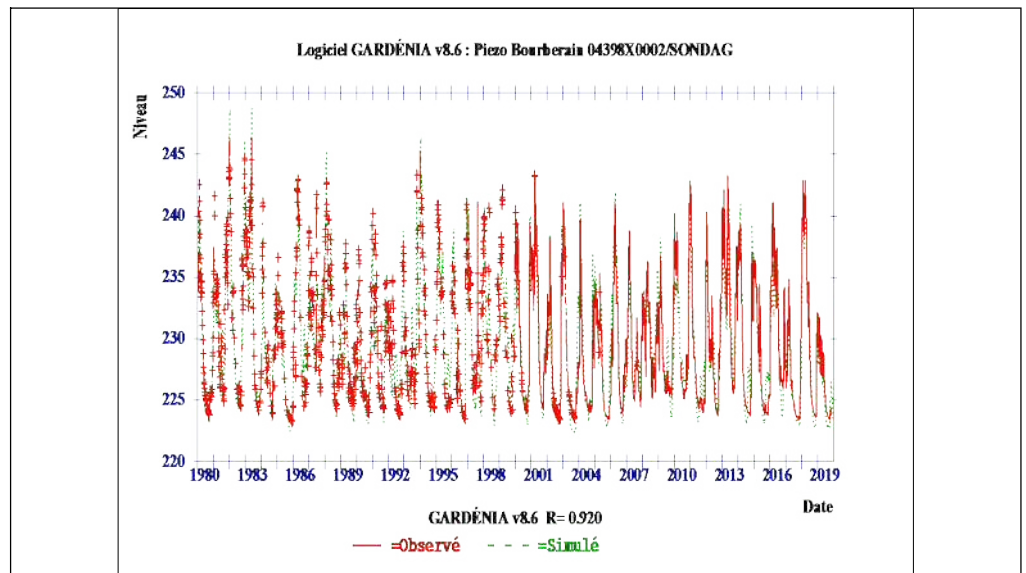
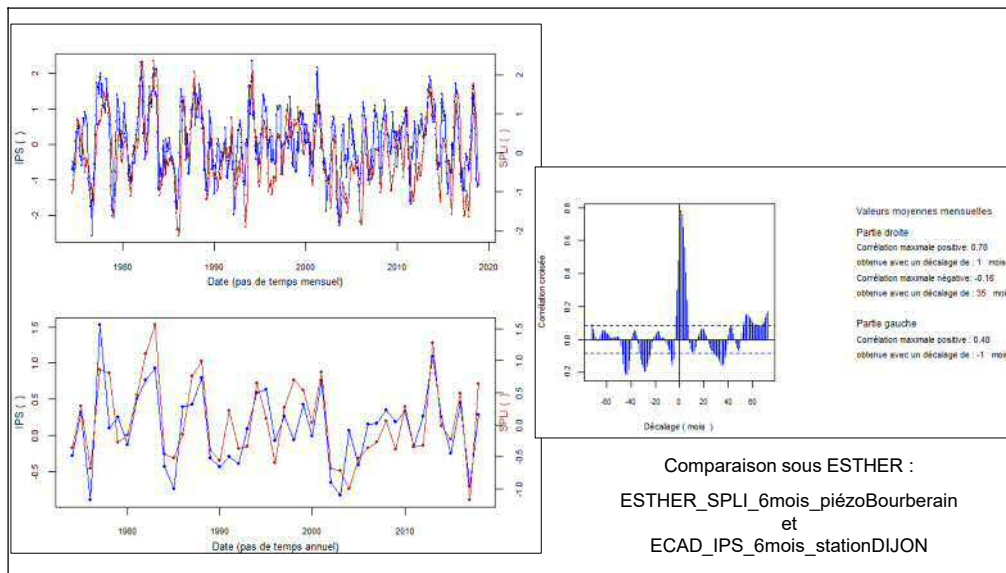


Piezomètre
Profondeur : 54 m

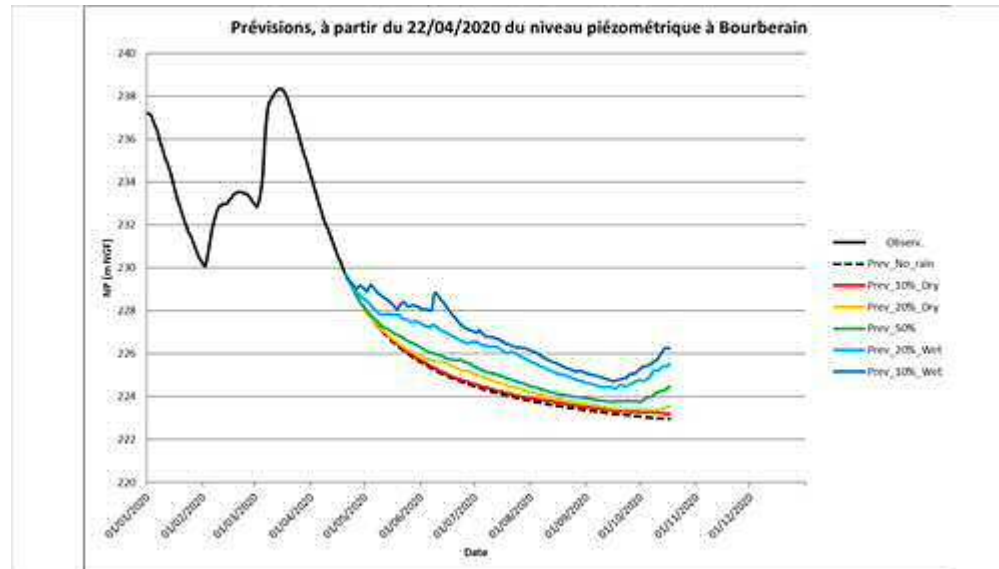
04398X0002/SONDAG - Bourberain - mesures depuis 1974

https://ades.eaufrance.fr/Fiche/PtEau?Code=04398X0002/SONDAG#mesures_graphiques

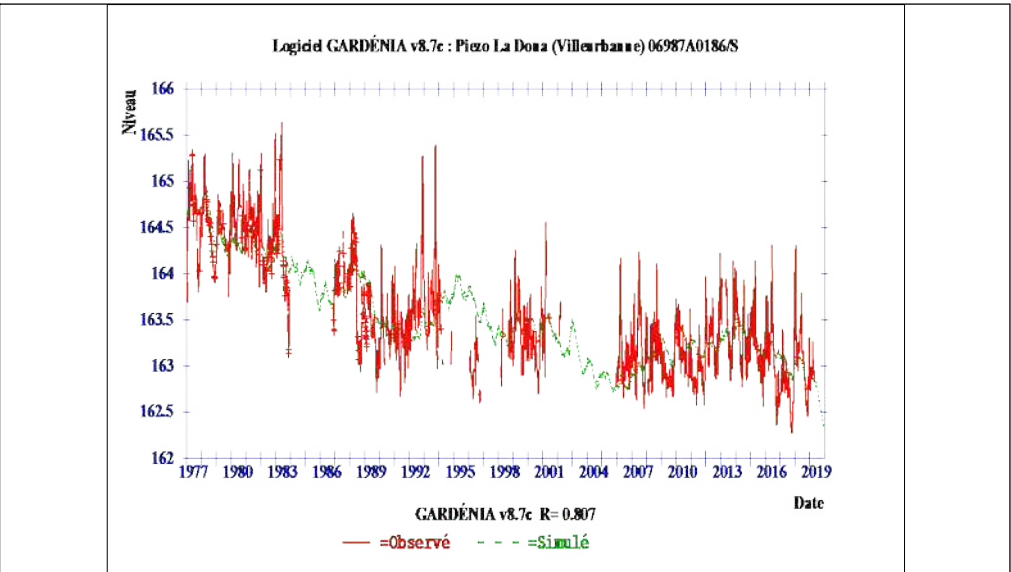
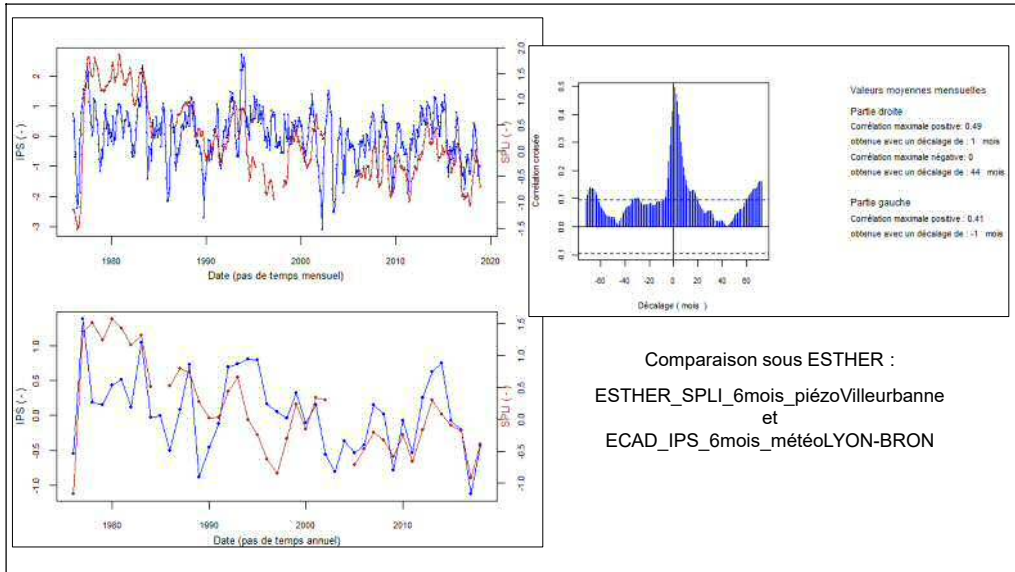
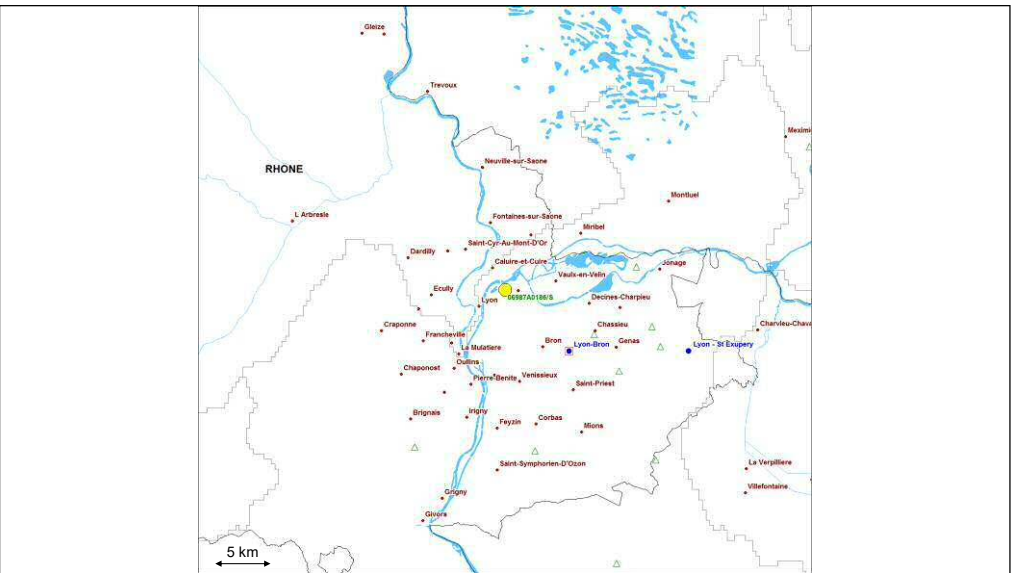
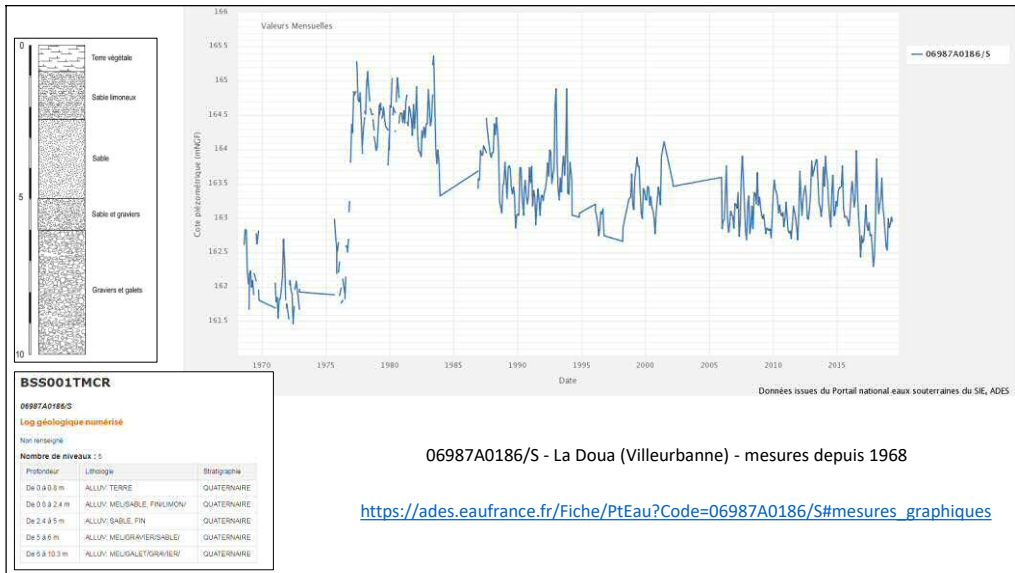
BDLisa
Calcaires Jurassiques
Entre Ouche Et Vingeanne - 139A005



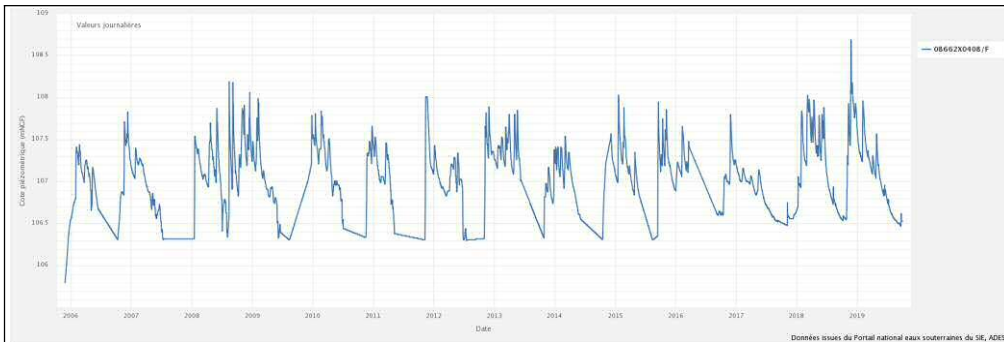
Analyses and modelling results for the Bourberain piezometer



Analyses and modelling results for the Bourberain piezometer



Analyses and modelling results for the La Doua piezometer

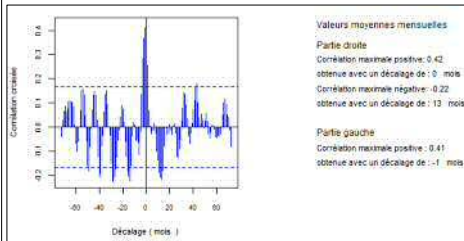
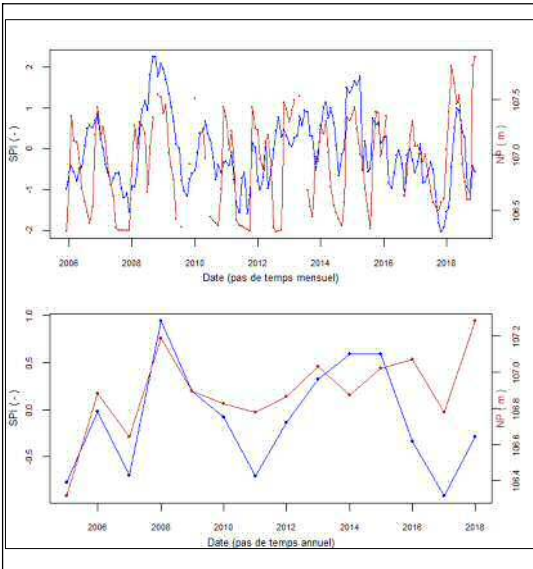
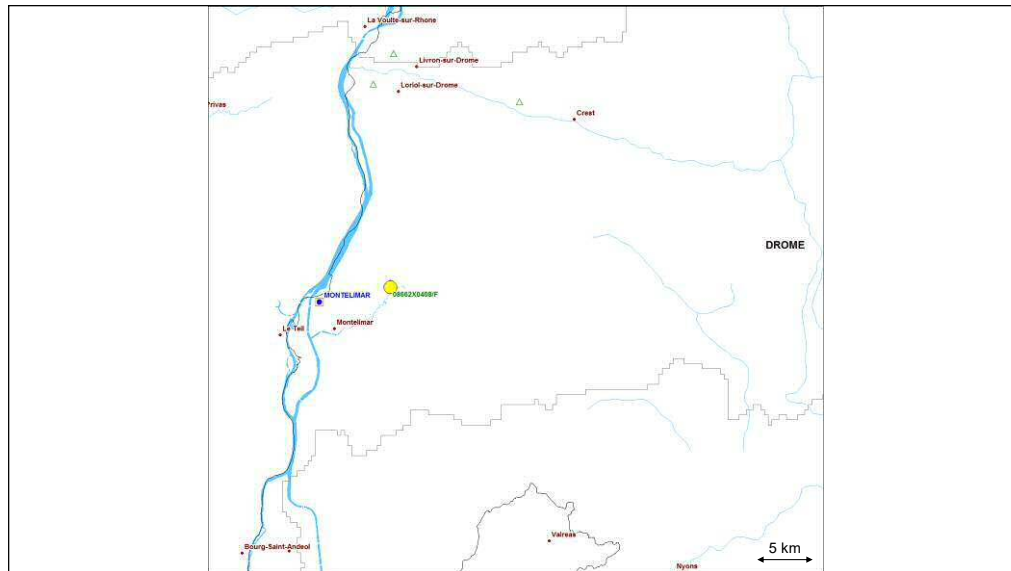


Aucune coupe disponible

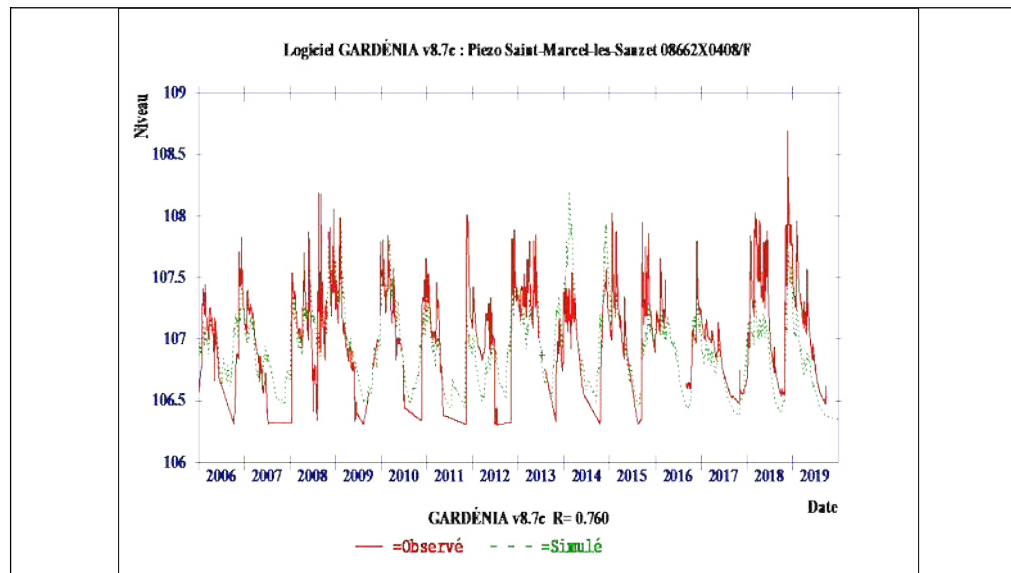
BDLisa
Alluvions Du Roubion Et Du Jabron
712BE24

08662X0408/F - Fin de Route(Saint-Marcel-les-Sauzet) - mesures depuis 2005

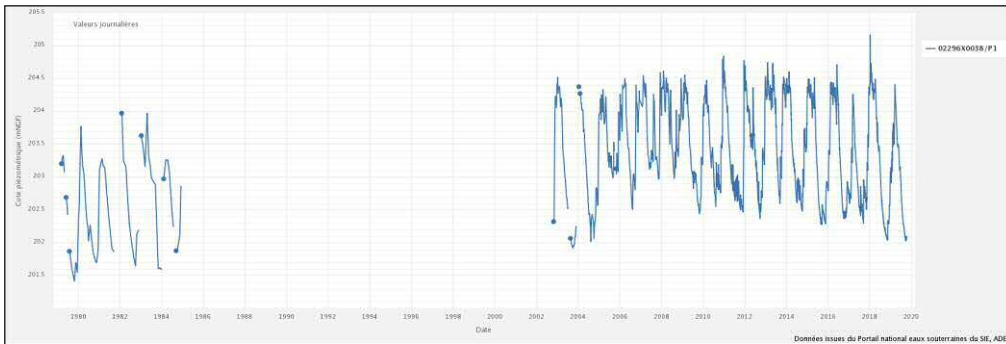
https://ades.eaufrance.fr/Fiche/PtEau?Code=08662X0408/F#mesures_graphiques



Comparaison sous ESTHER :
Saint-Marcel-les-Sauzet_08662X0408_mois
et
ECAD_IPS_6mois_stationMONTELMAR



Analyses and modelling results for the Saint-Marcel piezometer



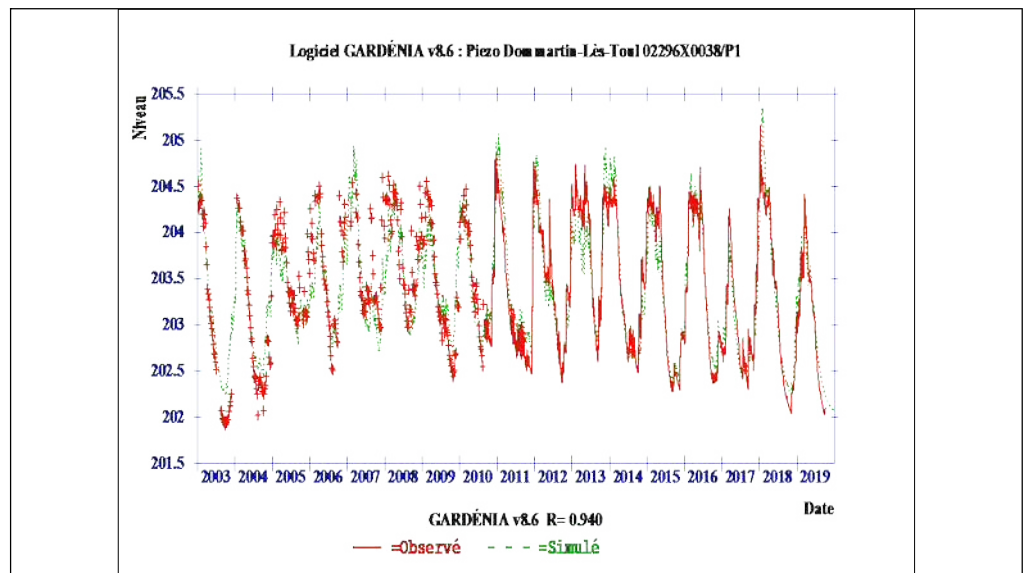
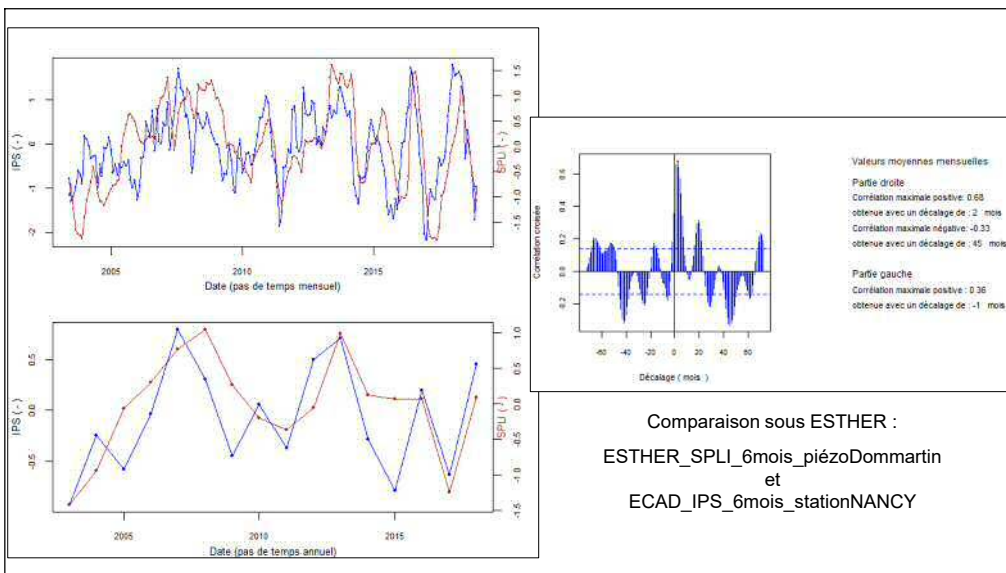
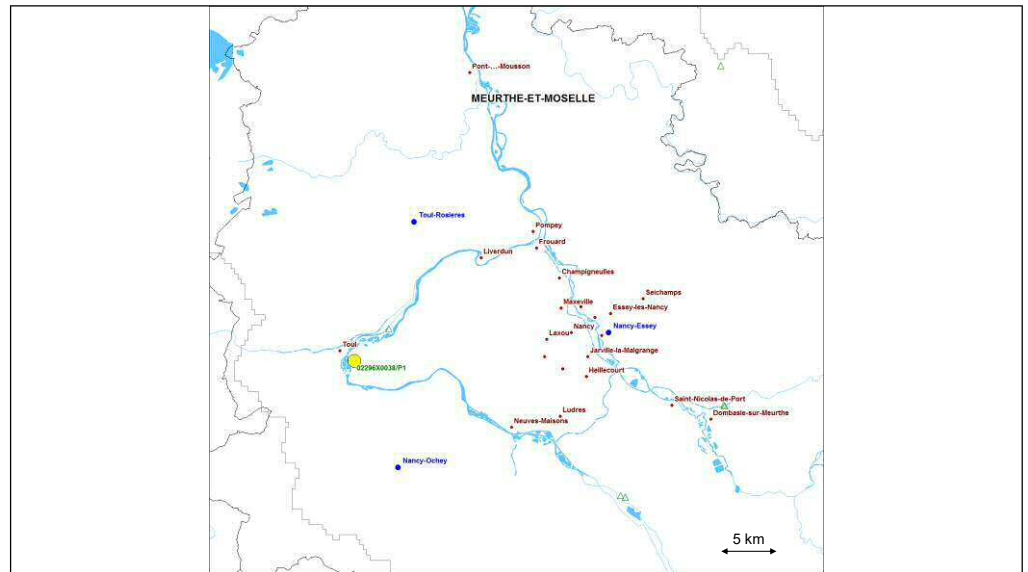
PUITS FILTRANT 1- ANCIENNE AEP
Profondeur atteinte : 8.3 m

Aucune coupe disponible

BDLisa
Alluvions actuelles à anciennes
de la Moselle sur calcaire du Dogger
952AC17

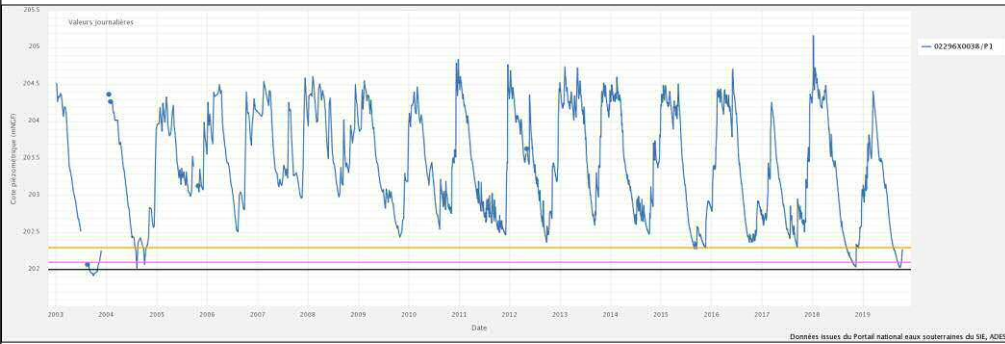
02296X0038/P1 - DOMMARTIN-LES-TOUL - mesures depuis 2002

https://ades.eaufrance.fr/Fiche/PtEau?Code=02296X0038/P1#mesures_graphiques



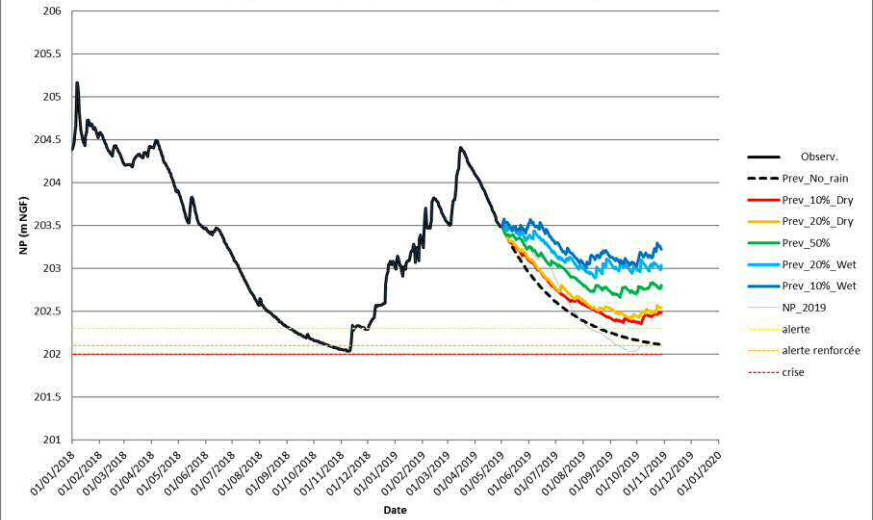
Analyses and modelling results for the Dommartin piezometer

02296X0038/P1 - DOMMARTIN-LES-TOUL
ADES et idée de seuils sécheresse définis avec ESTHER

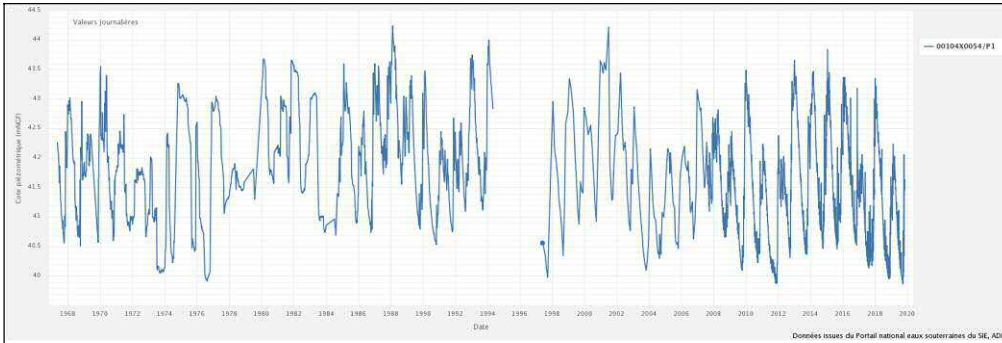


Données issues du Portail national eaux souterraines du SIÉ, ADES

Prévisions, à partir du 01/05/2019 du niveau piézométrique à Dommartin



Analyses and modelling results for the Dommartin piezometer

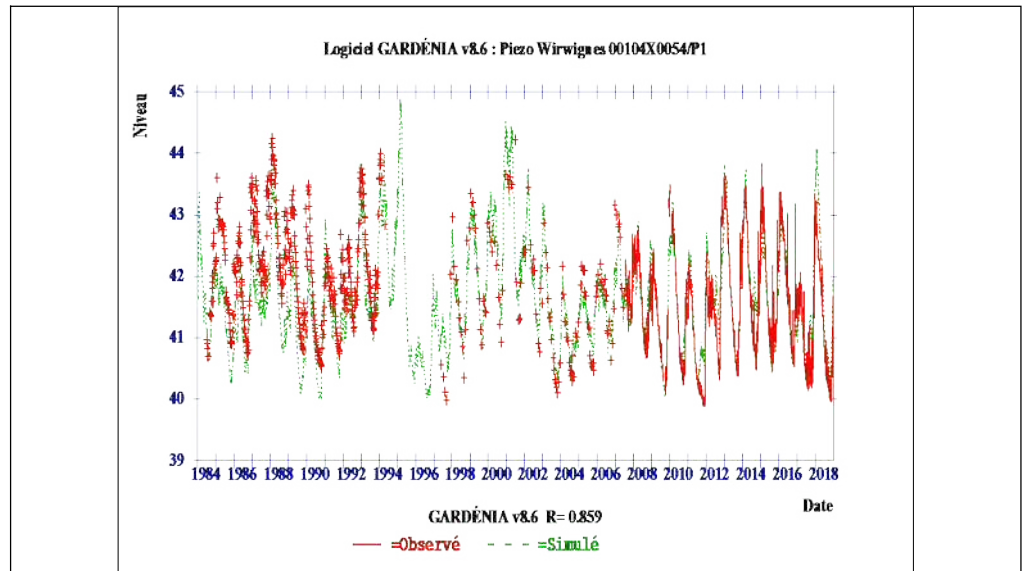
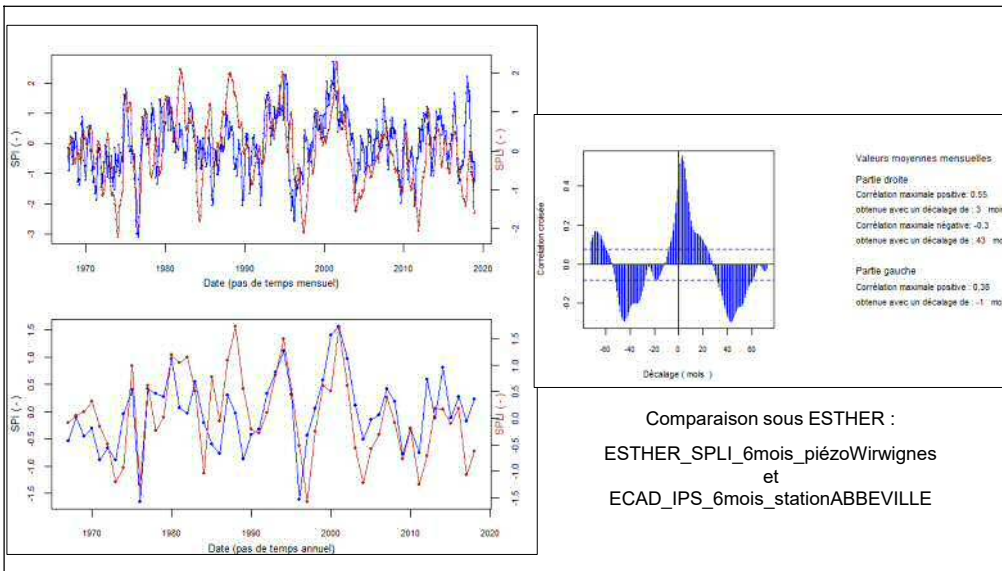
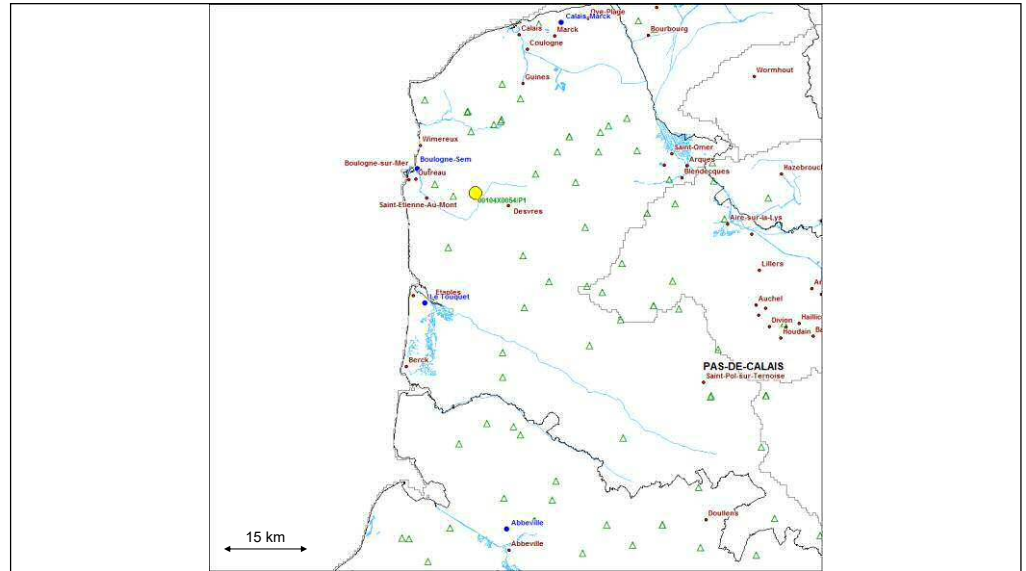


PUITS
 Profondeur atteinte : 7.75 m
 Aucune coupe disponible

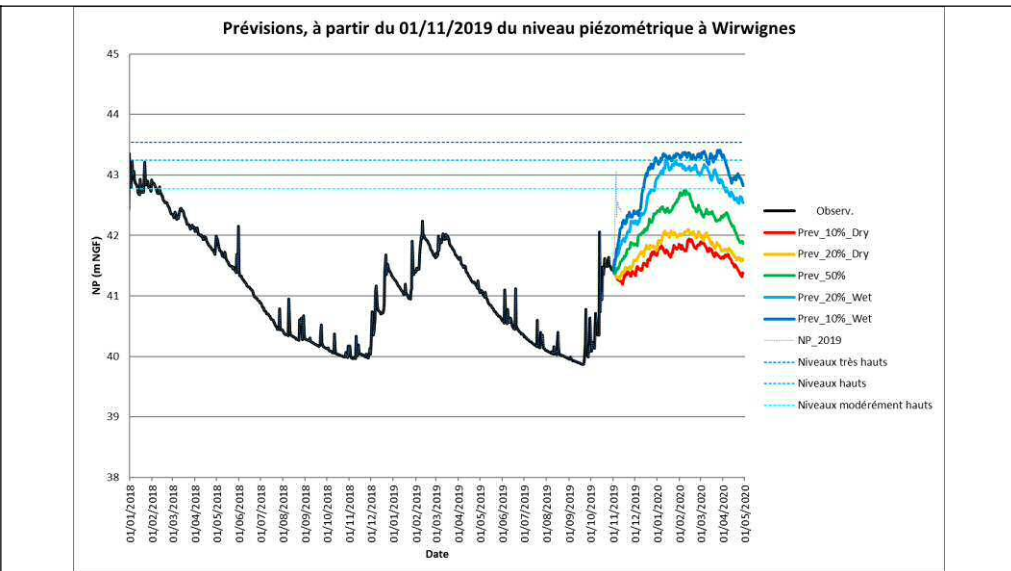
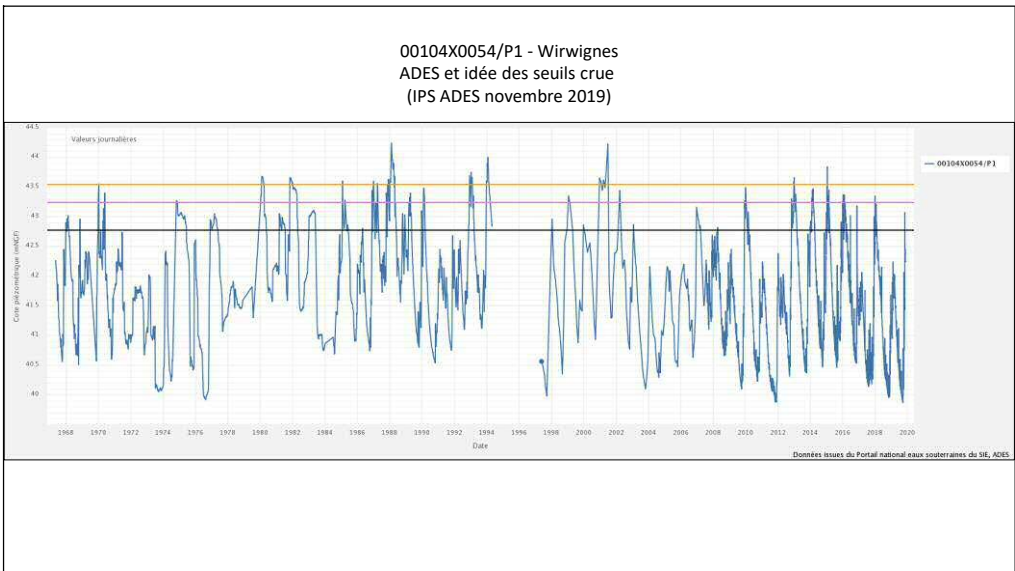
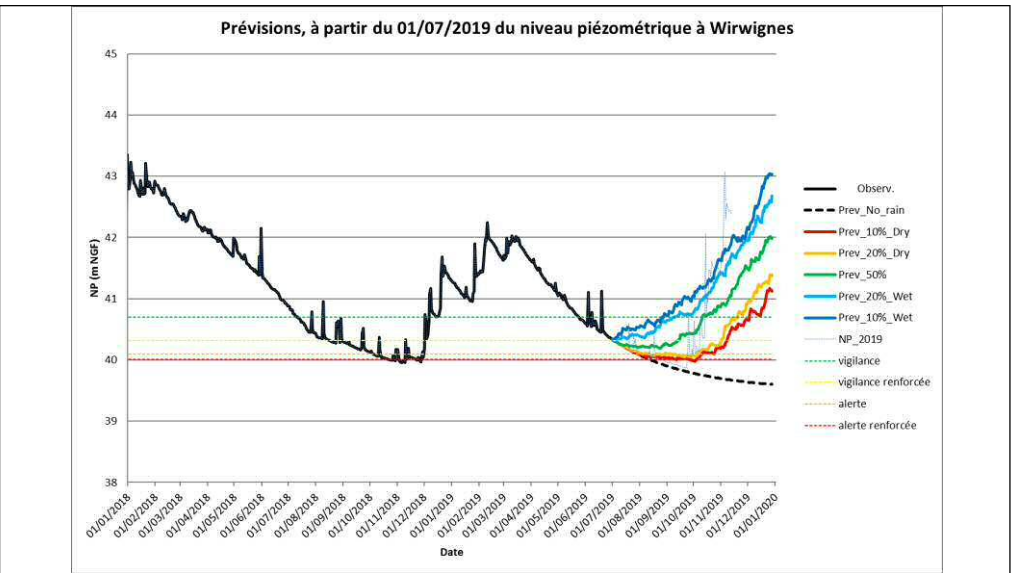
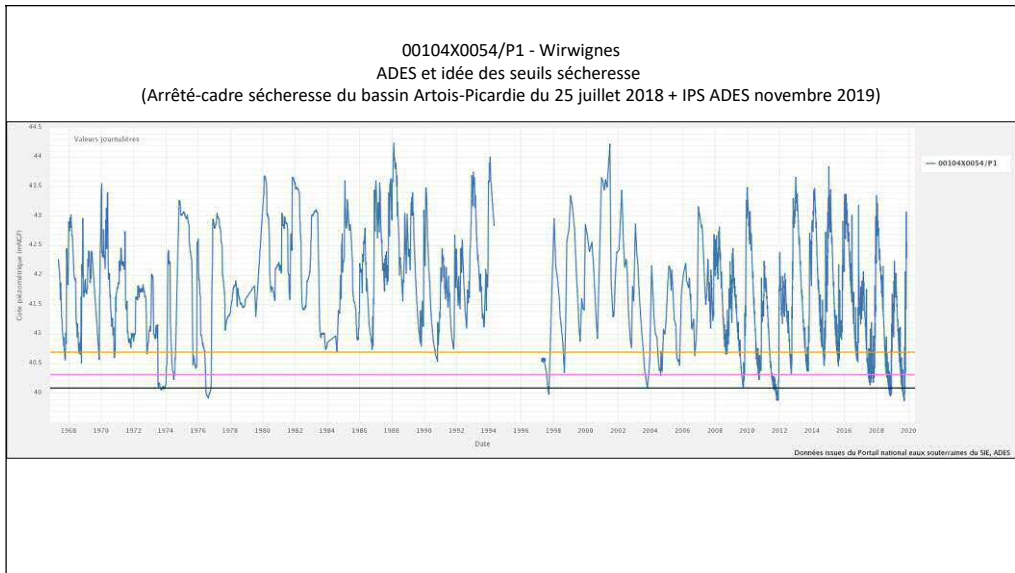
00104X0054/P1 - Puits de la Ferme Delattre (Wirwignes) - mesures depuis 1967
https://ades.eaufrance.fr/Fiche/PtEau?Code=00104X0054/P1#mesures_graphiques

BSH : nappe du calcaire Oolithe à Wirwignes, secteur du Boulonnais, Jurassique supérieur

BDLisa - 135AA15
 Calcaire De Brecquerecque, Caillasses D'Hesdigneul, Oolithe D'Hesdin-L'Abbé,
 Grès De Brunembert Du Boulonnais Dans Le Bassin Artois-Picardie

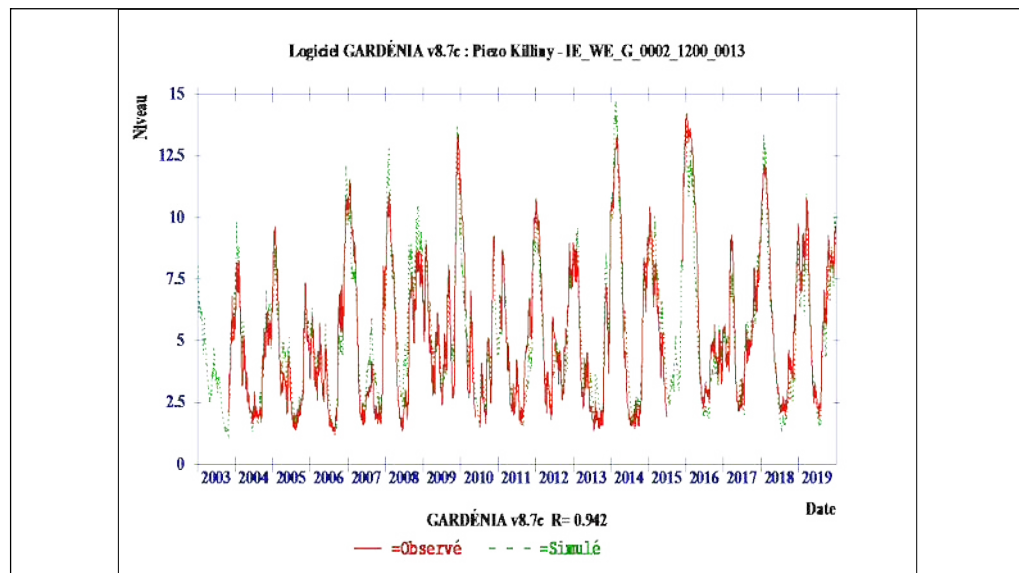
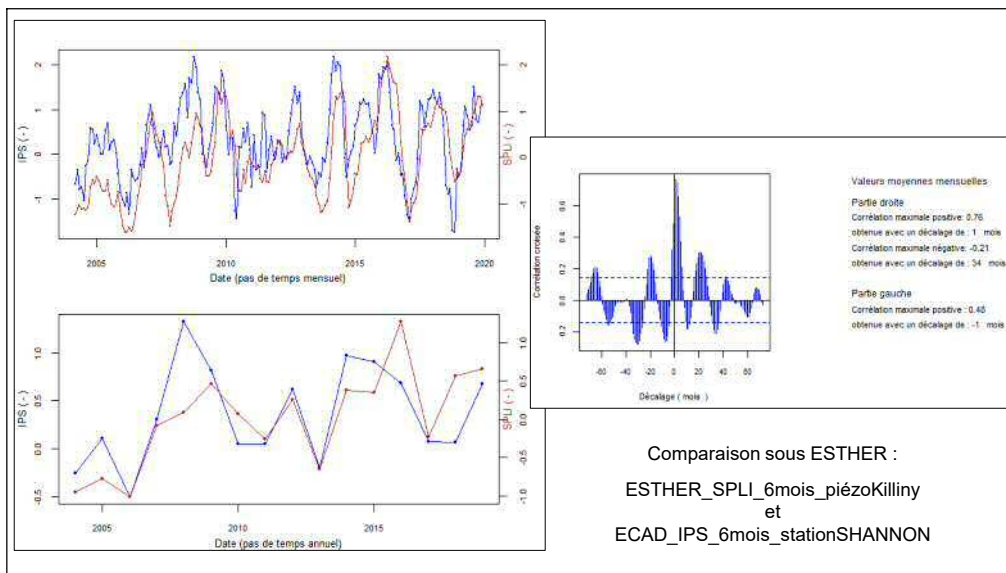
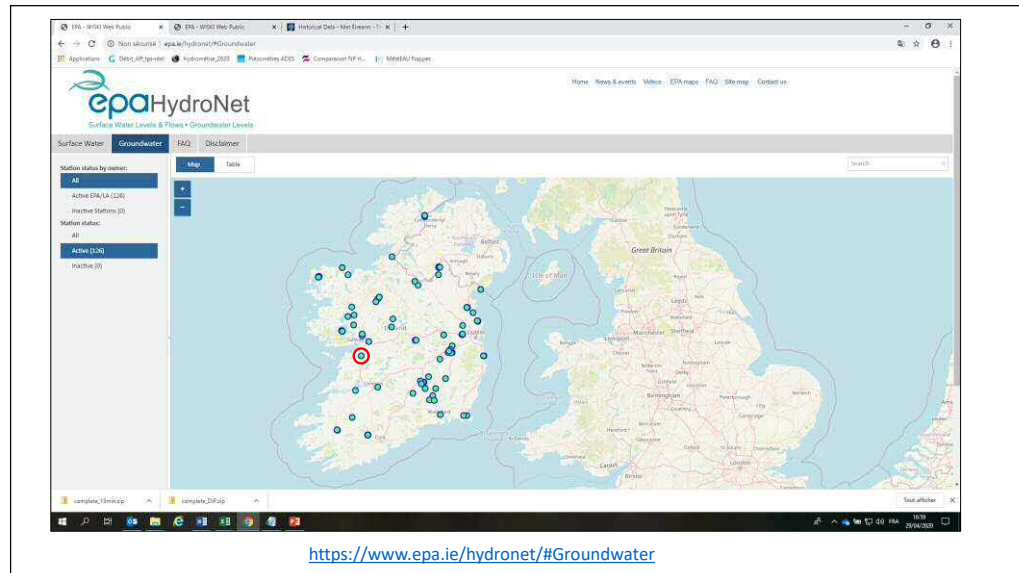
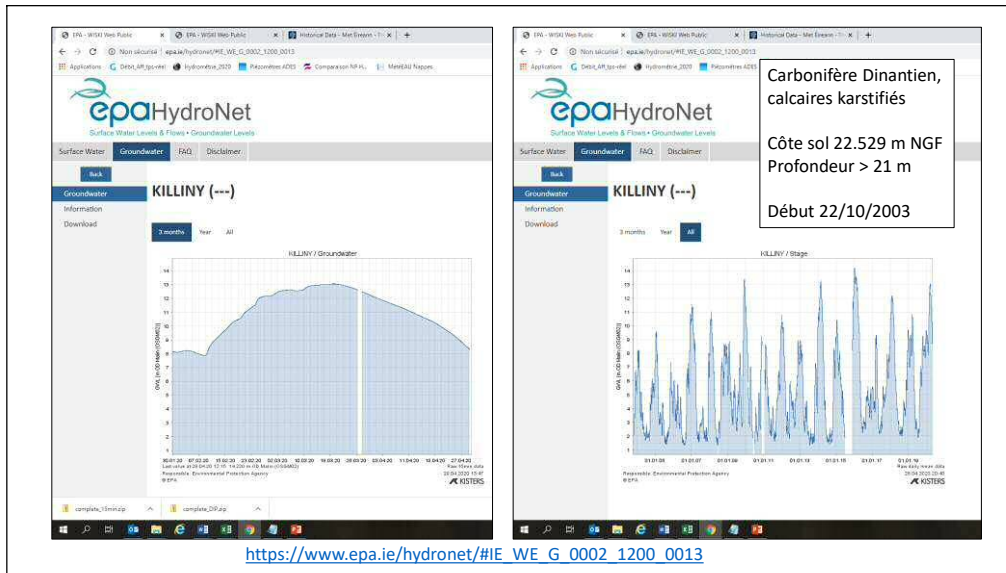


Analyses and modelling results for the Wirwignes piezometer



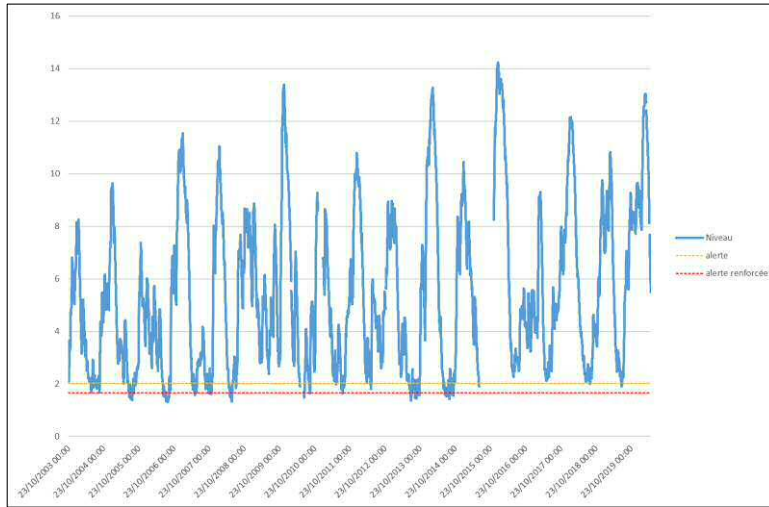
Analyses and modelling results for the Wirwignes piezometer

(High flows are also forecasted as groundwater may influence flood processes for that case study)

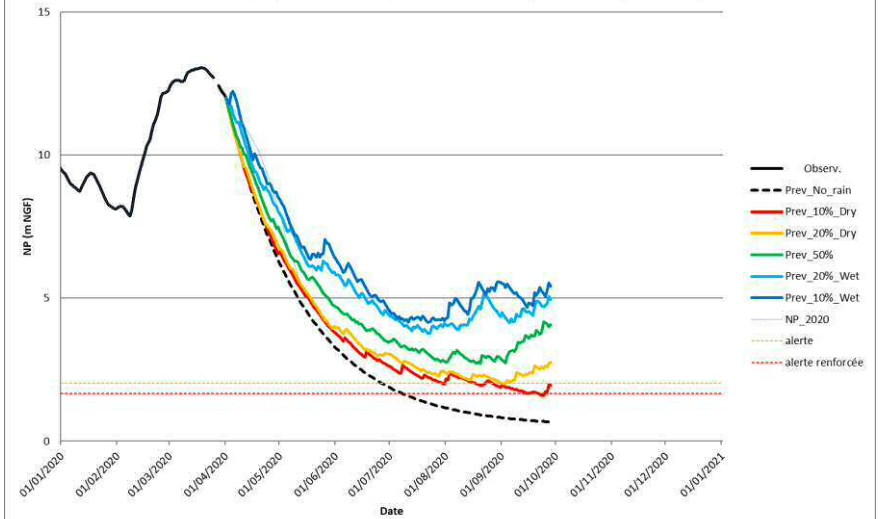


Analyses and modelling results for the Killiny piezometer

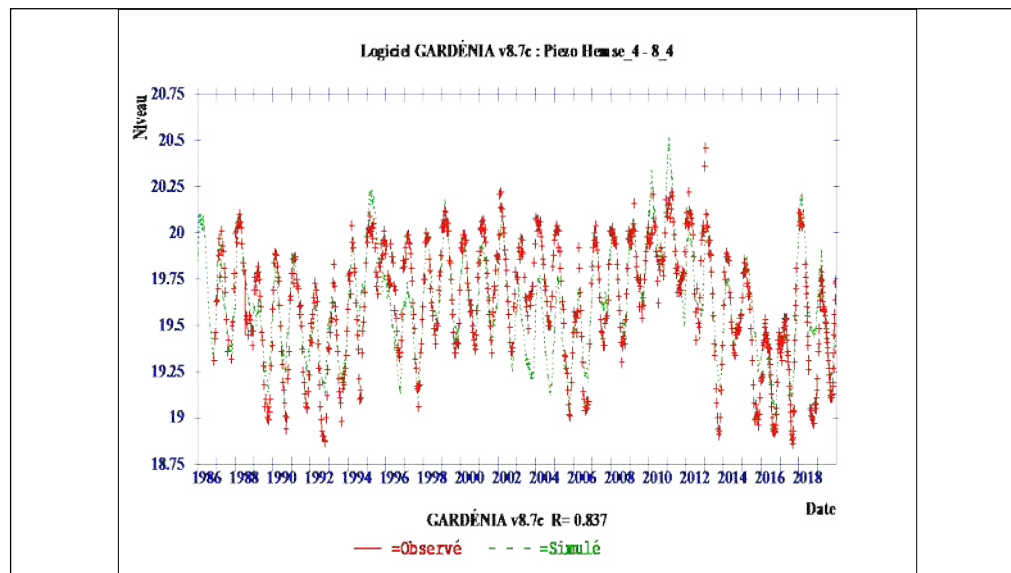
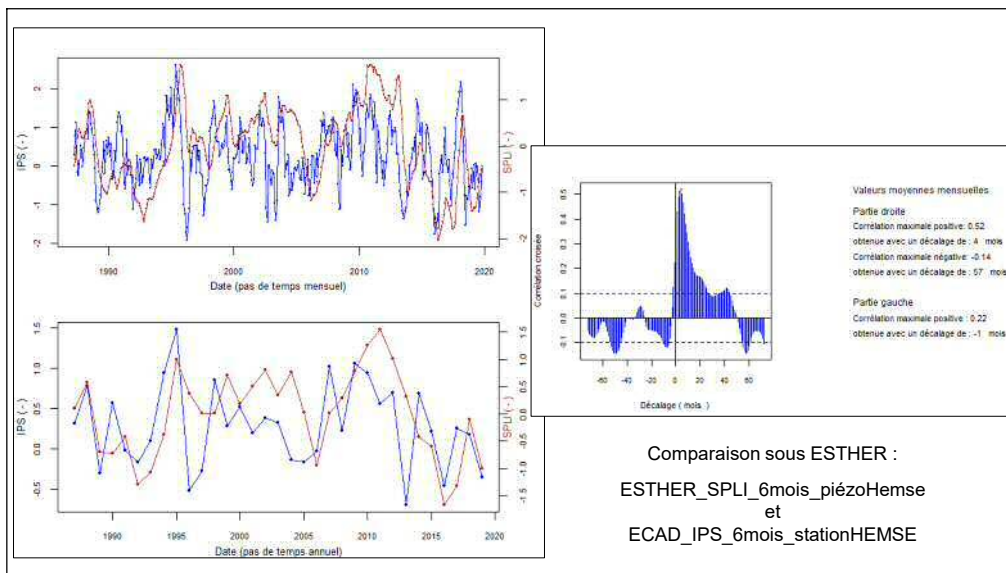
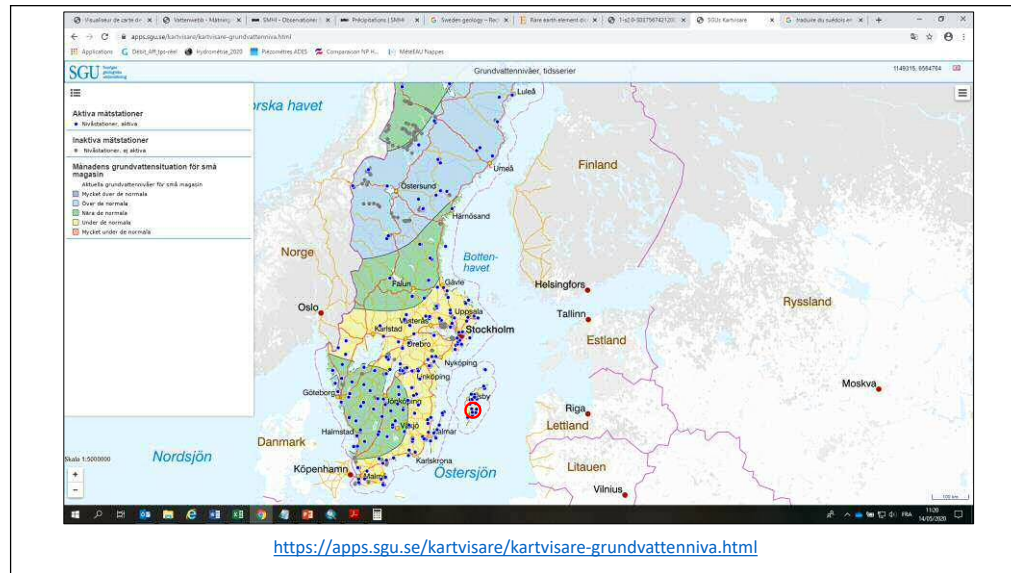
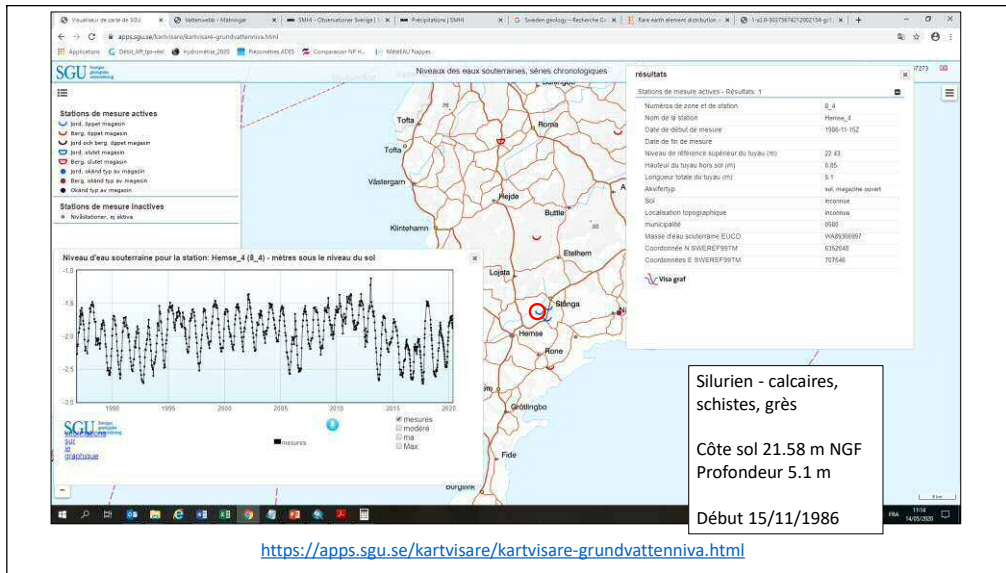
IE_WE_G_0002_1200_0013 - KILLINY
piézométrie et idée de seuils sécheresse définis avec ESTHER



Prévisions, à partir du 01/04/2020 du niveau piézométrique à Killiny

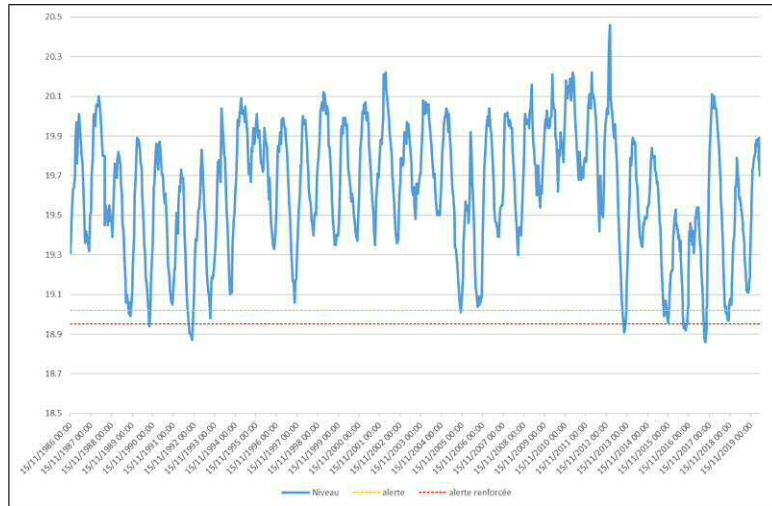


Analyses and modelling results for the Killiny piezometer

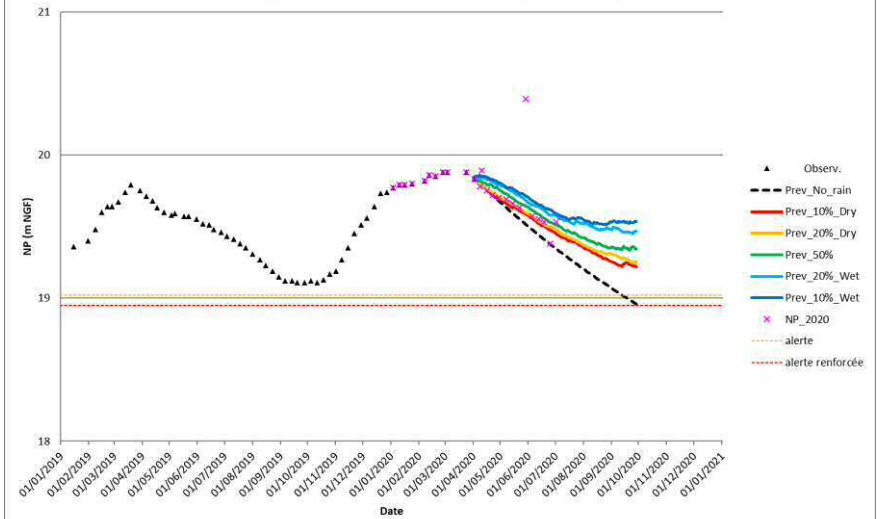


Analyses and modelling results for the Hemse piezometer

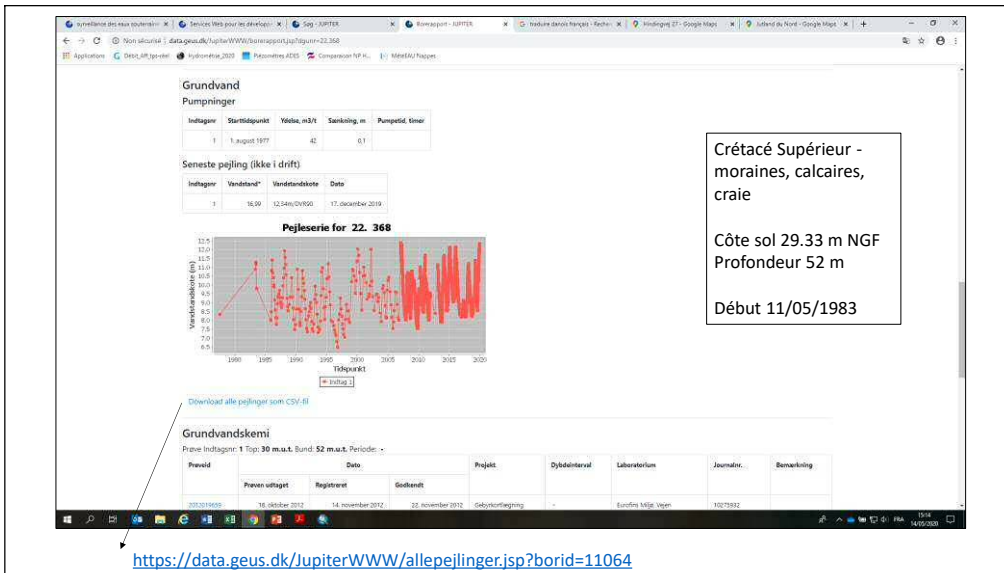
8_4 - Hemse_4
piézométrie et idée de seuils sécheresse définis avec ESTHER



Prévisions, à partir du 01/04/2020 du niveau piézométrique à Hemse



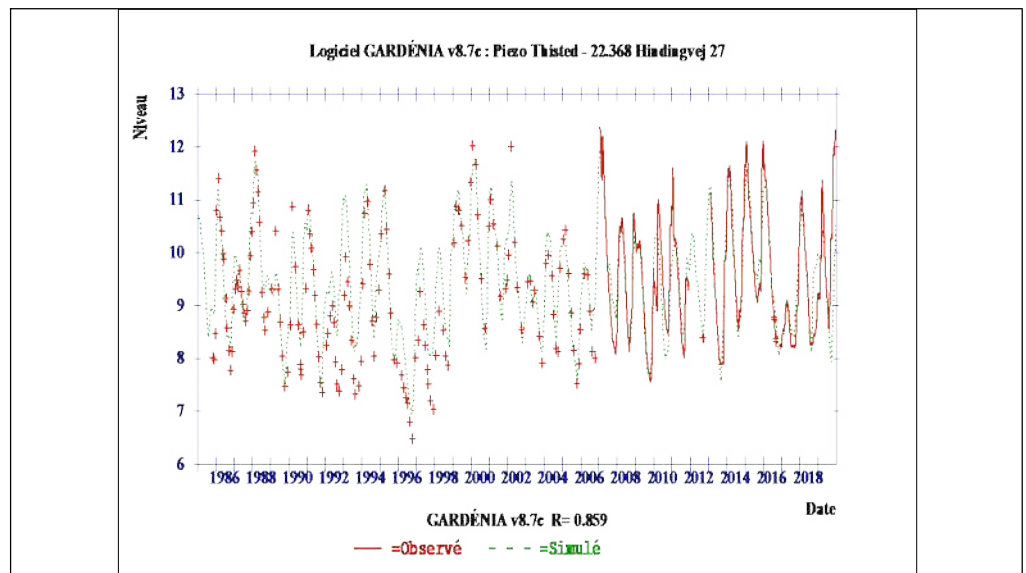
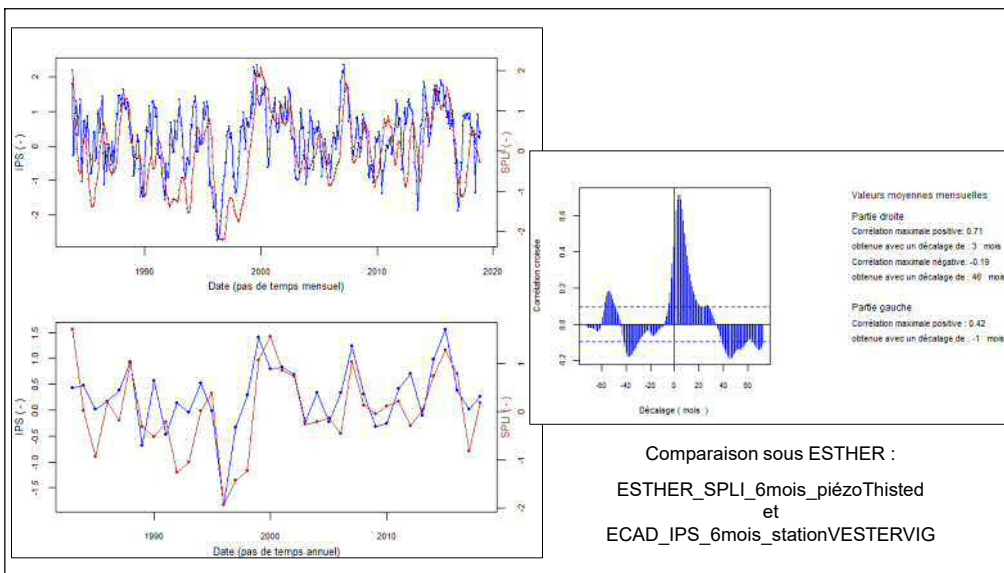
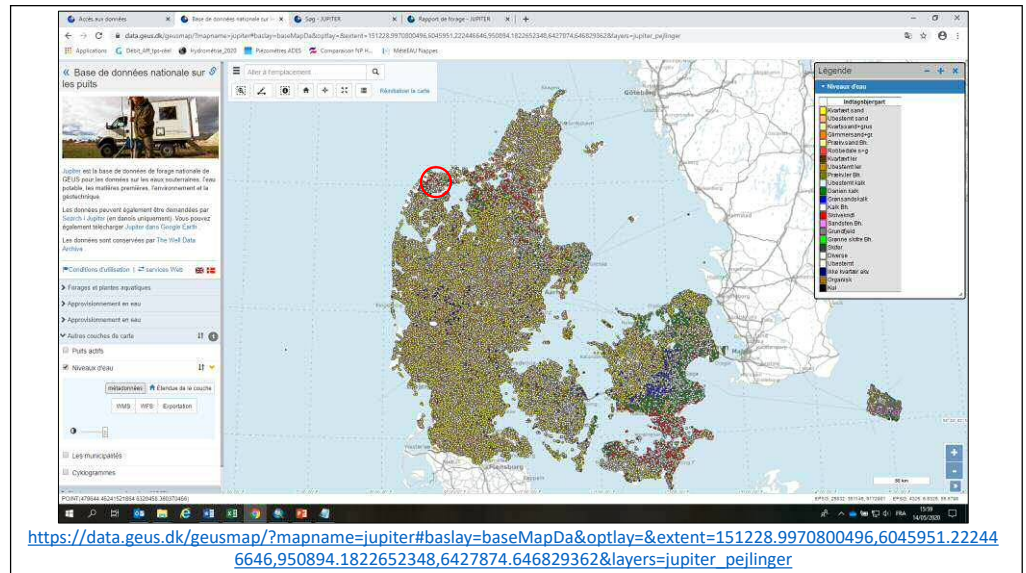
Analyses and modelling results for the Hemse piezometer



Crétacé Supérieur -
moraines, calcaires,
craie

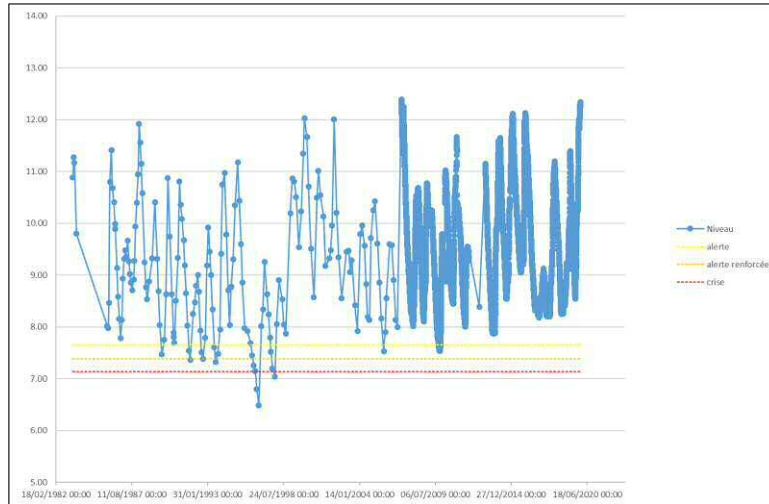
Côte sol 29.33 m NGF
Profondeur 52 m

Début 11/05/1983

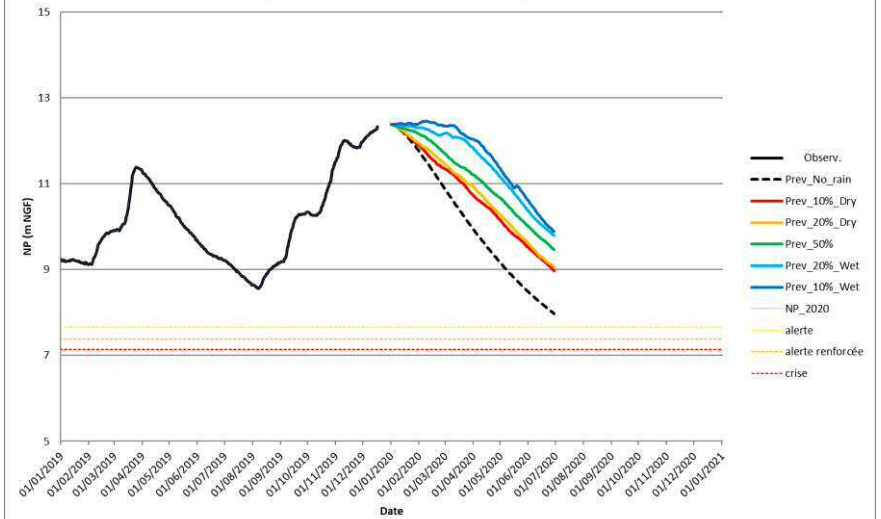


Analyses and modelling results for the Thisted piezometer

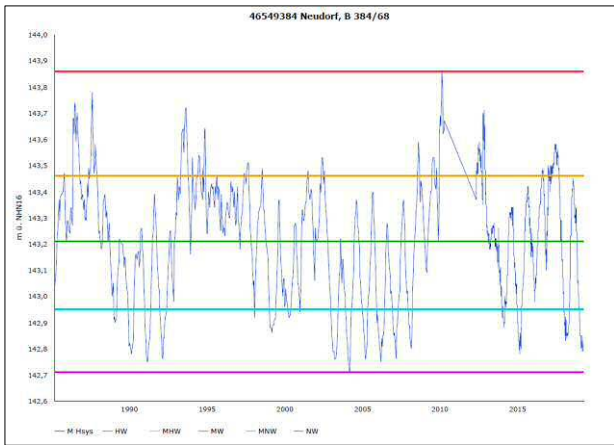
22.368 Hindingvej 27 - Thisted
piézométrie et idée de seuils sécheresse définis avec ESTHER



Prévisions, à partir du 01/01/2020 du niveau piézométrique à Thisted



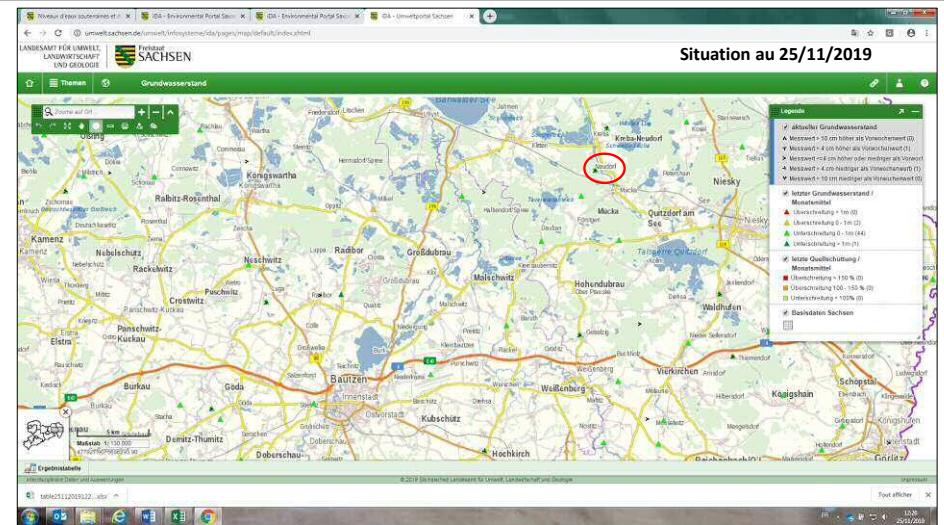
Analyses and modelling results for the Thisted piezometer



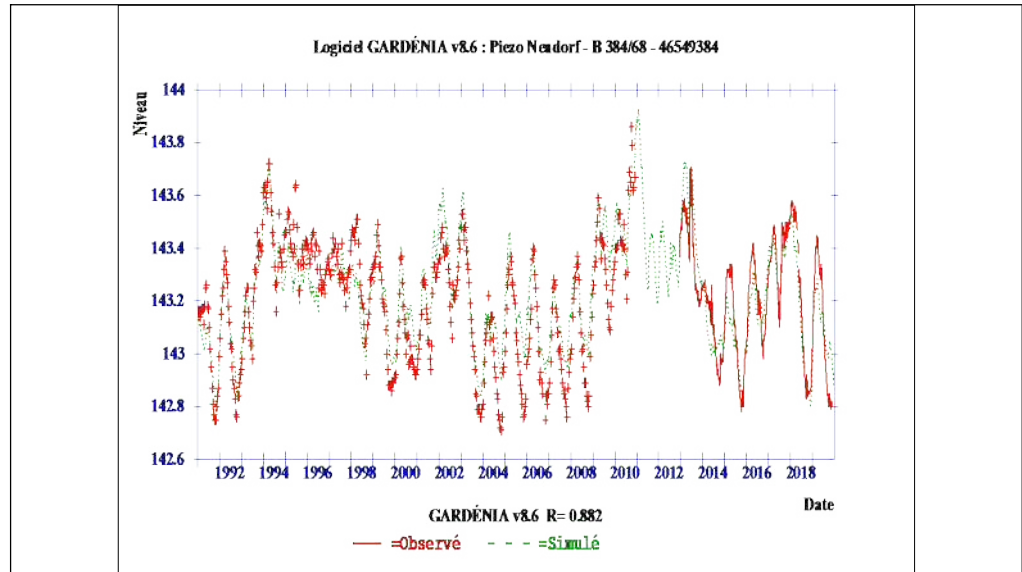
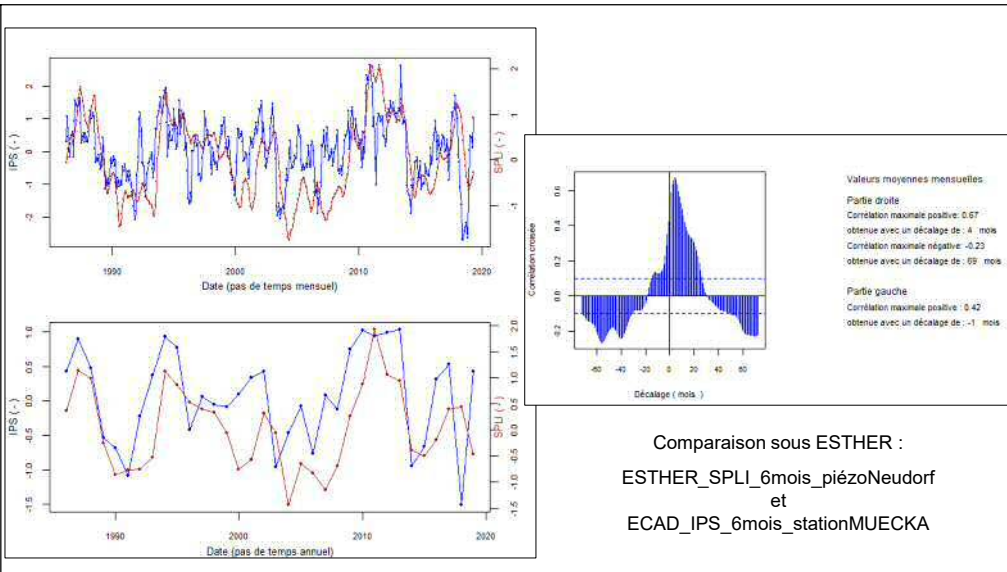
Paléozoïque-Précambrien, roches métamorphiques
Côte sol 145.76 m NGF Profondeur 8 m

http://www.umwelt.sachsen.de/umwelt/infosysteme/ida/p/diagramm_w?mkz=46549384

MKZ	Messstellenname	Messstellenart	Ostwert	Nordwert	Messpunkt	Wert	Einheit	Wert in cm unter Gelände	Höhensystem	HW	MHW	MW	MNW	NW	Abflussjahr
46549384	Neudorf, B 384/68	Grundwasserbeobachtung	477894	5686503	01.11.1985	143.04	m	Höhensystem	272	NHN16	143.86	143.46	143.21	142.95	1986

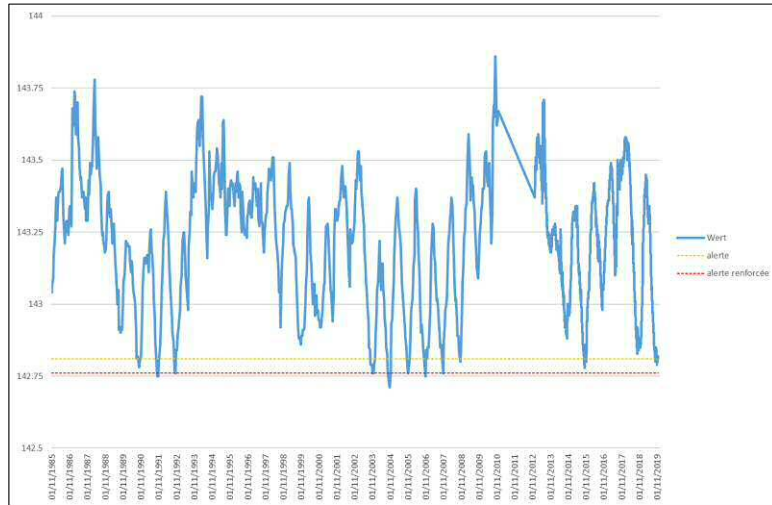


<https://www.umwelt.sachsen.de/umwelt/infosysteme/ida/pages/map/default/index.xhtml>

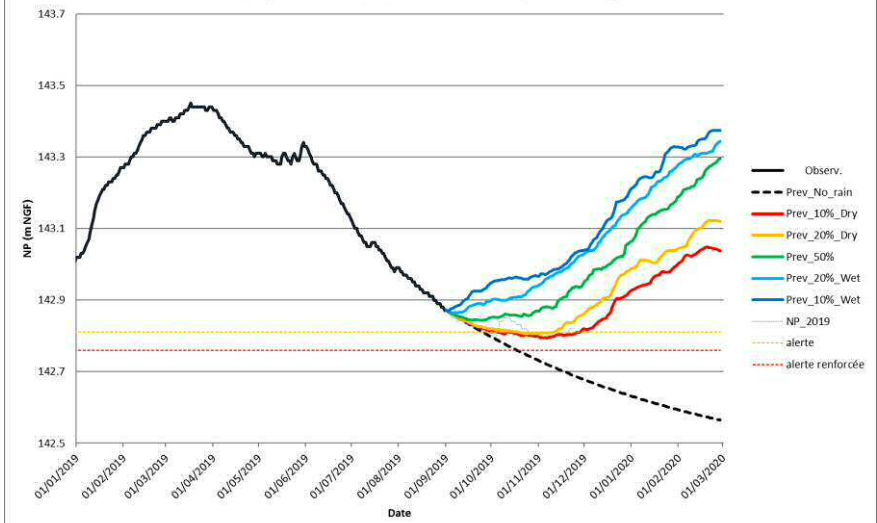


Analyses and modelling results for the Neudorf piezometer

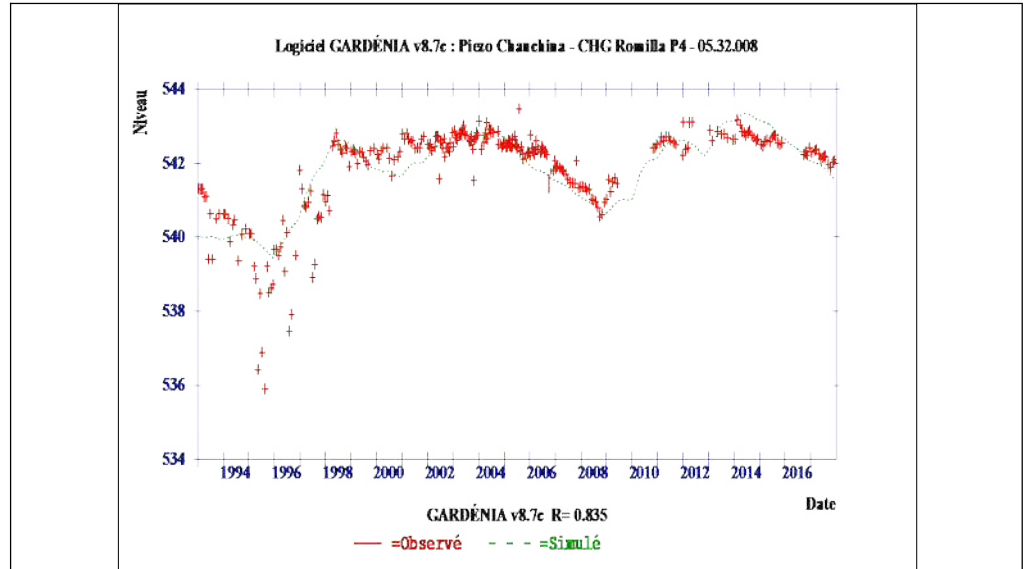
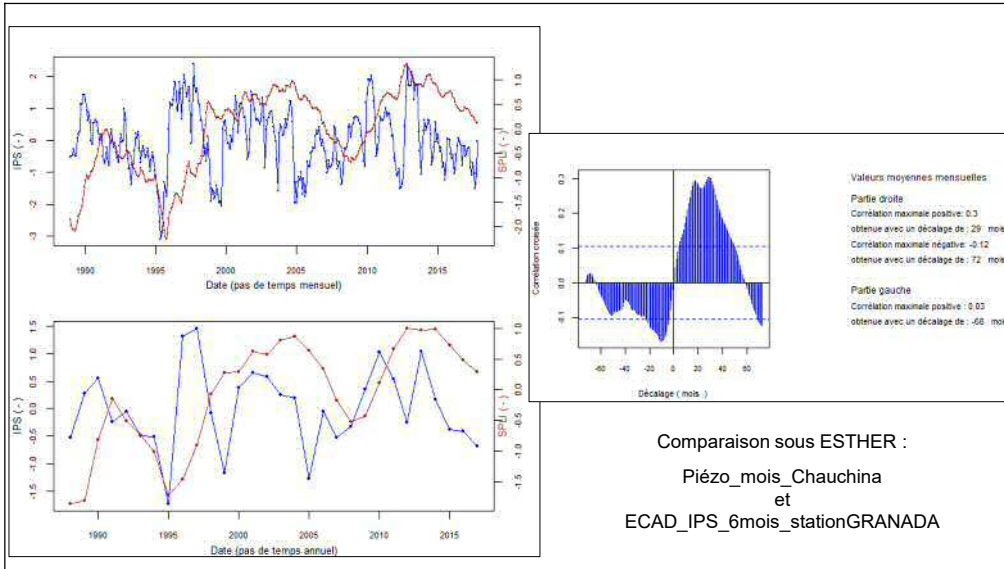
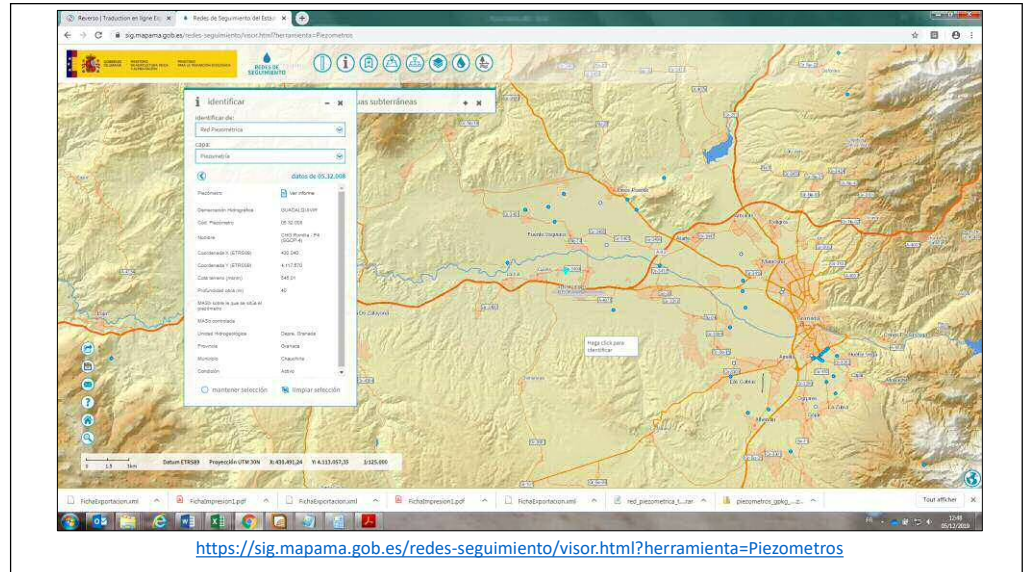
46549384 - NEUDORF, B 384/68
piézométrie et idée de seuils sécheresse définis avec ESTHER



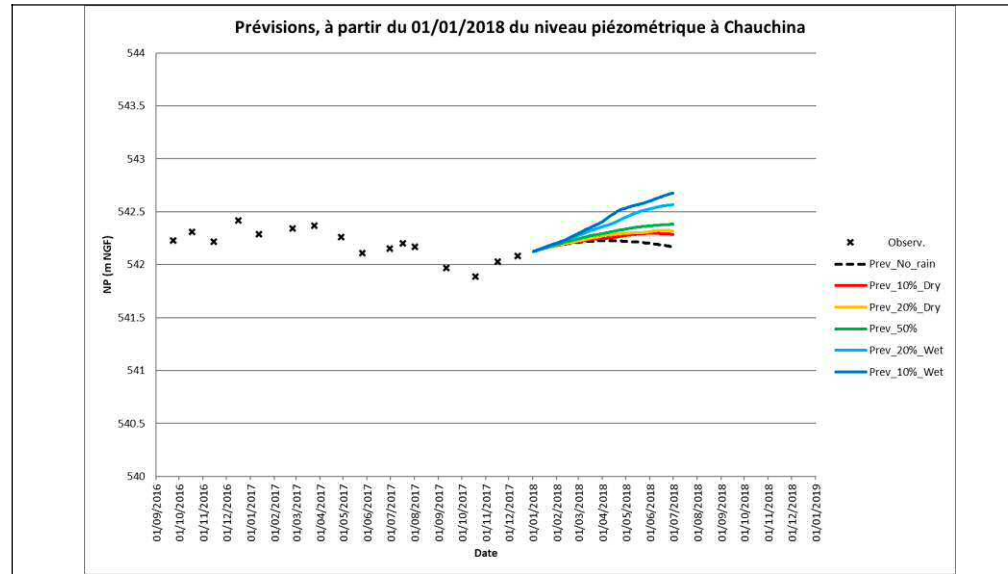
Prévisions, à partir du 01/09/2019 du niveau piézométrique à Neudorf



Analyses and modelling results for the Neudorf piezometer



Analyses and modelling results for the Chauchina piezometer



Analyses and modelling results for the Chauchina piezometer

Annex B: List of reviewed web services providing access to monitored piezometric data (last accessed – 30 june 2020)

Belgium

<https://iwaponline.com/jh/article-pdf/10/4/317/386301/317.pdf>

Danemark

<https://www.geus.dk/produkter-ydelser-og-faciliteter/data-og-kort/national-boringsdatabase-jupiter/>

<https://data.geus.dk/geusmap/ows/help/?mapname=jupiter&epsg=25832>

<https://www.geus.dk/vandressourcer/overvaagningsprogrammer/grundvandsovervaagning/>

<https://www.geus.dk/produkter-ydelser-og-faciliteter/data-og-kort/national-boringsdatabase-jupiter/adgang-til-data/>

<https://www.geus.dk/produkter-ydelser-og-faciliteter/data-og-kort/national-boringsdatabase-jupiter/webservices-for-udviklere/>

<https://data.geus.dk/JupiterWWW/index.jsp#dgunr=&kommunenr=&minpostal=&maxpostal=®ion=&sted=&anvendelseskoder=M&formaalskoder=&order=5&ascend=false>

<https://data.geus.dk/JupiterWWW/borerapport.jsp?dgunr=34.1706>

<https://data.geus.dk/JupiterWWW/borerapport.jsp?dgunr=5.939>

Finland

<http://v-web002.deltares.nl/fewsprojectviewer/projectviewer/>

France

<http://hubeau.eaufrance.fr/page/api-piezometrie>

Germany

<http://www.hochwasser-rlp.de/karte/einzelpegel/flussgebiet/rhein/teilgebiet/oberrhein/pegel/WORMS>

<https://www.noe.gv.at/wasserstand/#/de/Messstellen>

<https://www.noe.gv.at/wasserstand/#/en/Static/links/0>

<https://www.noe.gv.at/wasserstand/#/en/Static/erlauterungen/4>

<http://www.umwelt.sachsen.de/umwelt/wasser/6103.htm>

http://www.umwelt.sachsen.de/umwelt/infosysteme/ida/p/diagramm_w?mkz=51480001

http://www.umwelt.sachsen.de/umwelt/infosysteme/ida/p/diagramm_w?mkz=46549384

<https://www.umwelt.sachsen.de/umwelt/infosysteme/ida/pages/map/default/index.xhtml>

<http://www.wasserdaten.niedersachsen.de/cadenza/>

<http://www.wasserdaten.niedersachsen.de/cadenza/pages/selector/index.xhtml>

<http://www.wasserdaten.niedersachsen.de/cadenza/pages/selector/index.xhtml>

Ireland

<http://www.epa.ie/water/wm/groundwater/level/>

<https://www.epa.ie/hydronet/#Groundwater>

https://www.epa.ie/hydronet/#IE_SH_G_0039_2500_0002
<https://www.epa.ie/hydronet/#Flow>
<https://www.met.ie/climate/available-data/historical-data>

Italy

https://www.arpae.it/dettaglio_generale.asp?id=679&idlivello=247
https://geo.regione.emilia-romagna.it/cartografia_sgss/user/viewer.jsp?service=ewater
<http://geo.regione.emilia-romagna.it/eWaterDataDistributionSgss/EwaterDetailForm?dataType=well&id=MO03-01&lang=it>

Luxembourg

https://eau.public.lu/eaux_souterraines/reseau_surveillance/index.html

Norway

<https://www.ngu.no/en/topic/api-and-wms-services>
http://geo.ngu.no/kart/granada_mobil/

Spain

<https://www.miteco.gob.es/es/cartografia-y-sig/ide/descargas/agua/red-piezometrica.aspx>
<https://sig.mapama.gob.es/redes-seguimiento/index.html?herramienta=Piezometros>
https://sig.mapama.gob.es/93/ClienteWS/redes-seguimiento/Default.aspx?nombre=PIEZOMETROS&claves=DGAGUA.PIEZOMETROS.PIE_NUMPIE&valores=1671

Sweden

<http://resource.sgu.se/service/wms/130/brunnar>
http://resource.sgu.se/service/wms/130/miljoovervakning_grundvatten
<https://apps.sgu.se/kartvisare/kartvisare-grundvattenniva.html>
<http://vattenweb.smhi.se/station/>
<https://www.smhi.se/en/weather/sweden-weather/observations#ws=wpt-a,proxy=wpt-a,tab=vader,param=t>
https://www.smhi.se/en/weather/sweden-weather/observations#ws=wpt-a,proxy=wpt-a,tab=vader,param=p_day

The Netherlands

<https://www.dinoloket.nl/en/nieuws/dive-dutch-groundwater-our-interactive-tools>
<https://www.dinoloket.nl/en/subsurface-data>
<https://www.dinoloket.nl/aanleveren-grondwatermonitoring-gegevens>
<https://www.dinoloket.nl/sites/default/files/2019-01/Voorbeeldbestand.txt>
https://www.dinoloket.nl/sites/default/files/file/dinoloket_nitg_formaat_20161220.pdf

United Kingdom

<http://www.hydoutuk.net/>
<http://www.hydoutuk.net/archive/2019/february-2019/further-information-february-2019/>
http://v-web002.deltares.nl/fewsprojectviewer/projectviewer/projectdata/1460448322-NGMS-folder_concept3.pdf
<https://www.bgs.ac.uk/discoverymetadata/13480430.html>
https://www.bgs.ac.uk/research/groundwater/datainfo/levels/levels_data.html
<https://www.bgs.ac.uk/research/groundwater/datainfo/levels/home.html>
<http://mapapps.bgs.ac.uk/groundwatertimeline/home.html#>

**Linking INDECIS meteorological data with groundwater
monitoring data at the scale of France**

Introduction

The groundwater level (GWL), defined as the altitude of the water table into an aquifer reservoir, roughly results from the budget of different fluxes. Provided there is no infiltration from rivers or surface water bodies or underground inflow from neighboring aquifers, the input term is the infiltration of part of the effective precipitation (the fraction of snow and/or rain not consumed by vegetation, neither stored in the soil). The output term of the budget is the drainage through springs and rivers, and uptakes from wells and boreholes. The stock variation dynamic is a function depending both on the ratio between input and output, and on the aquifer properties (reservoir size, porosity, etc.). This dynamic is usually well reproduced using lumped models, stochastic models, or deterministic numerical models.

Nevertheless, there is an increased interest for using artificial intelligence (AI), and especially machine learning approaches, as a new way for the modelling of GWL (particularly when data on aquifer properties is scarce). For AI modelling implementation, two key steps must be completed: i) the selection of contributing variables to the target signal (here GWL), by assessing how strong is the dependence of the target to an individual input signal, and ii) the feature engineering i.e. the transformation of an observed signal (e.g. rain) into a more significant signal for the target to simulate (e.g. : daily rain, anomaly of rain compared to the normal, etc...).

In the framework of the INDECIS project, meteorological data sets and indices have been computed. Building on this data, gridded effective precipitation daily time series have been computed at the France scale on a regular grid of $0.25^{\circ} \times 0.25^{\circ}$ (see INDECIS Deliverable 6.4).

In France, GWL is actively monitored in springs, wells and boreholes at about 6k different places, and 16k additional datasets are available, with at least one measurement of the GW depth, spread over the entire territory, and at different depths. This monitoring has been designed to include the different types of existing aquifers, exploited or not for the supply of different sectors (drinking water, agriculture, industrial uses). This monitoring is then heterogeneous in quality and resolution depending on the importance of the groundwater resource for the water users. Aquifers used for drinking water supply are usually monitored with a high resolution and quality. At the opposite, wells used for irrigation are usually found with approximate location, poor temporal resolution, and short time series lengths.

Baulon et. al. (2021), showed that, at the scale of France, only 254 GWL time series out of the total monitored wells and boreholes, are longer than 30 years. These data present an almost continuous signal (few proportion of 'no data'), and temporal variations exhibiting contrasted behaviors (annual variation, seasonal variation, interannual variation, wide/narrow amplitude, etc.).

Combining the two datasets is of interest to better understand the contribution of rain to the GWL time evolution. The implementation, calibration, validation and analysis of the results of lumped, stochastic or deterministic models may be computationally costly at the national scale. AI-like models represent an interesting alternative in that matter. This work reports the progress done in that direction, exploring the two first steps described above: variable selection and feature engineering.

In order to explore the dependence of the GWL to the effective precipitation at the vertical of the boreholes, and in the close vicinity, a methodological framework has been designed to assess two main

parameters of feature engineering: the cumulating depth, and the delay. First applied using effective precipitation, the framework can easily be adapted to other climate-based indices available in the Indecis data portal (such as SPI3-6-12, SPEI3-6-12).

Material and methods

This section describes the data that were used and the methodology associated to the study

Data

Effective precipitation

The effective precipitation computed in the INDECIS WP6 is a gridded dataset, available over Europe. This dataset provide time series of effective precipitation from 1950 to 2019 at cell 0.25°x0.25° grid cells at a daily time step. The data used for the effective precipitation modelling was downloaded from E-OBS web portal (<https://www.ecad.eu/download/ensembles/download.php>) for precipitation and temperature data and from the Indices INDECIS web portal (<http://www.indecis.eu/indices.php>) for Potential Evapotranspiration. More information on the data and computing method can be found in the WP6 D6.4 report.

Groundwater levels observations

In France, GWL data are freely available through the Hub'eau API (<https://hubeau.eaufrance.fr/>). Two different operators were downloaded:

- the stations description: https://hubeau.eaufrance.fr/api/v1/niveaux_nappes/stations
- the data measurements: https://hubeau.eaufrance.fr/api/v1/niveaux_nappes/chroniques

These operators are mirroring the data stored in the French national database ADES (www.ades.eaufrance.fr), with no prior treatment or modifications.

254 time series have been selected on the basis of criteria such as: continuity of the signal, no to little gaps and different variation in time. Details on this process can be found in Baulon et al. (2021).

Methods

GWL interpolation, normalization

Nowadays, the temporal resolution of the GWL data is daily but, for earlier periods, the frequency was frequently weekly and even monthly. Nevertheless, the selected time series show regular variations since at least 20 years, with no to very little effect of pumping or other man-based influence.

Interpolation has been carried to fill potential gaps, based on the implementation of the 'time interpolation method' of the python library pandas¹, which is designed for time-index time series,

¹ <https://github.com/pandas-dev/pandas/blob/v1.1.5/pandas/core/generic.py#L6602-L6894>

possibly unevenly sampled. A second transformation was performed in order to normalize the time series. The normalization is made using equation 1.

Equation 1

With :

$Y_{t,norm}$: normalized value at time t

Y_t : bulk value at time t

\bar{Y} : arithmetic mean of the time series

Y_{max}, Y_{min} : maximum and minimum value of the time series.

Effective precipitation

Effective precipitation has been considered using three different formulations:

- as daily data ;
- as cumulated data ;
- as delayed signal (both for daily data and cumulated data).

The three different time series have been normalized using Equation 1 before further computing.

The selection of the effective precipitation cell corresponding to a given GWL time series location was based on the following coordinates comparison:

$$X_{cmin} < X_{GWL} < X_{cmax} \text{ and } Y_{cmin} < Y_{GWL} < Y_{cmax}$$

Where X_{GWL}, Y_{GWL} are the coordinates of the piezometer and $X_{cmin}, X_{cmax}, Y_{cmin}, Y_{cmax}$ are the coordinates of the corresponding effective precipitation cell. Once the latter located, the 8 cells to it are also selected.

Cumulated effective precipitation

The cumulated effective precipitation is performed using a rolling sum over the whole time series, with a given depth for the period over which the sum is computed (equation 2). The rolling sum calculated at time t with the given depth i is attributed to the time index t .

Equation 2

The period depth (i in Equation 2, in days) for the sum can vary in an interval given by the user. After several trial and errors, the interval for the period depth parameter of the rolling sum has been set to [5-545] days, with a time increment step of 15 days, i.e. 36 different depths, the longest depth extending over about a year and a half.

Delayed effective precipitation

Taken the two formulations described above (daily effective precipitation, cumulated effective precipitation), a variable time delay has been applied. This parameter will be used to assess the potential percolation delay of infiltrated effective precipitation to reach the groundwater table. The delayed time series were calculated with respect to equation 3, where i represents the delay value chosen by the user.

Equation 3

Values for the delay have been set up as a function of the depth parameter for the cumulated effective precipitation computation. The maximum delay value is three times greater the depth value, from which intermediate delay values are computed (every 1/6 of the maximum delay). For example, if the cumulated effective precipitation have been calculated over 30 days, new time series have been set up, for cumulated efficient precipitation delayed by 15, 30, 45, 60, 75, 90 days (Illustration 1).

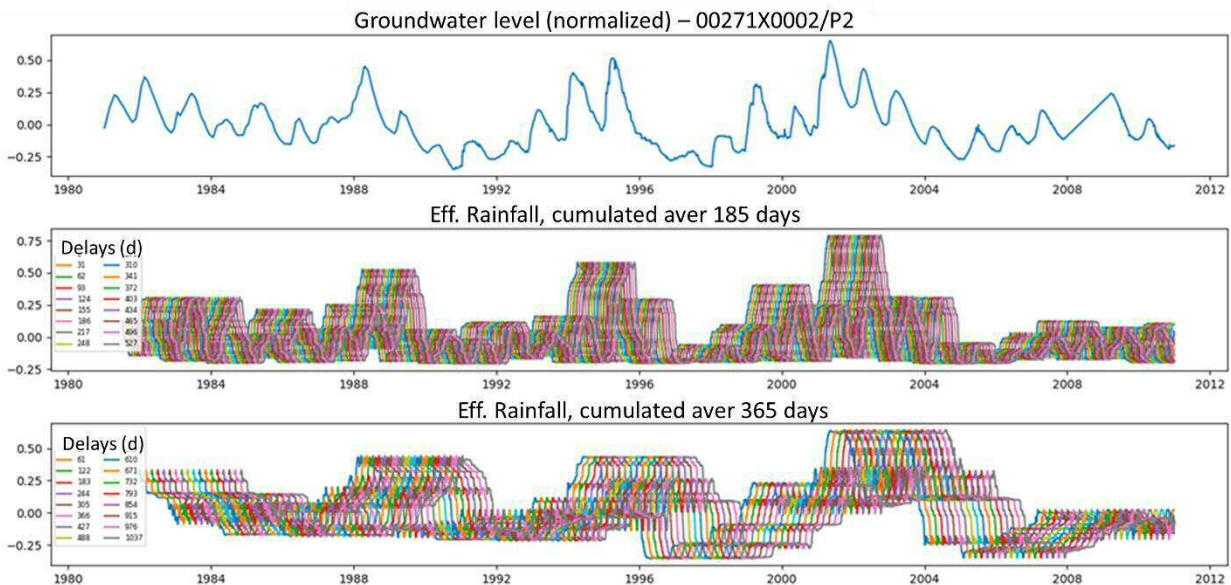


Illustration 1: Example of the time series used to assess the transfer dynamic between effective precipitation and groundwater levels. From top to bottom: groundwater level at piezometer 00271X0002/P2 ; effective precipitation cumulated over 185 days and delayed using variable time periods (0,31,62,...,527 days), effective precipitation cumulated over 365 days and delayed by 0,61,122,...,1037 days.

Comparison of the GWL and effective precipitation signal

To provide an overview on the parameters one should use to find the best link between effective precipitation and GWL, the Pearson correlation coefficient² which “measures the linear relationship between two datasets was computed. Like other correlation coefficients, this one varies between -1 and +1 with 0 implying no correlation. Correlations of -1 or +1 imply an exact linear relationship. Positive correlations imply that as x increases, so does y. Negative correlations imply that as x increases, y decreases”.

² <https://docs.scipy.org/doc/scipy/reference/generated/scipy.stats.pearsonr.html>

The correlation has been calculated for all the 6165 pairs of GWL and effective precipitation related signal (illustration 2).

	At corresponding effective precipitation cell			For each adjacent cell		
	Raw data	Cumulative sum	Cumulative sum + delay	Raw data	Cumulative sum	Cumulative sum + delay
GWL	1	36	36x18=648	1	36	36x18=648

Illustration 2: Detail of the number of paired dataset for which the correlation has been computed, for each piezometer

The parameters (depth of the rolling sum, delay and the position of the cell (vertical to the piezometer or in the vicinity)) corresponding to the best correlation among the 6165 calculated Pearson coefficients is stored for further processing.

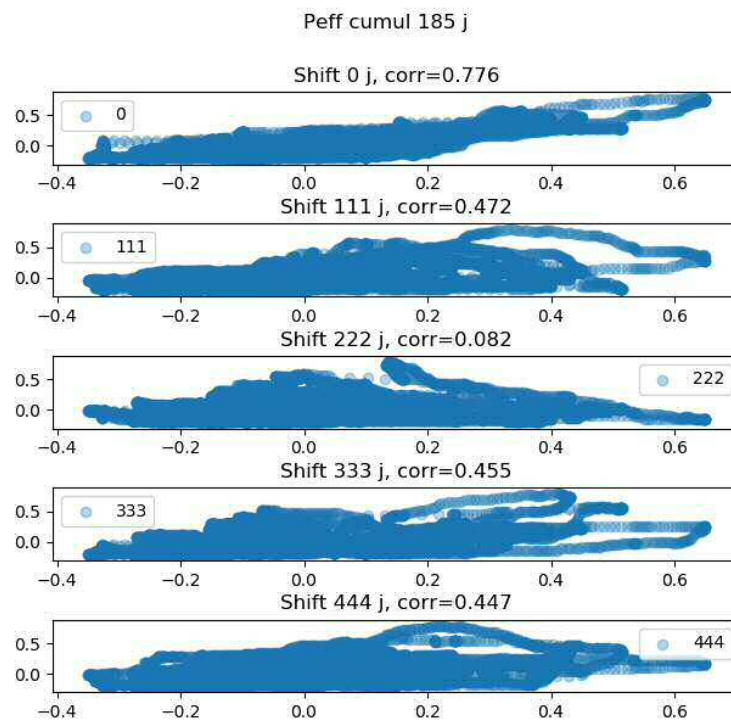


Illustration 3: Example of comparison between effective precipitation (Y axis, normalized, here cumulated over 185 days), delayed effective precipitation (here delays varies from 111 days to 444 days) and GWL (normalized, Y axis). Shift represent the amount of days the Y signal is delayed, 'corr' represent the pearson coefficient.

Illustration 3 gives an example of the effect of the delay (named 'shift' in the figure) on the Pearson correlation coefficient calculated for an effective precipitation cumulated over 185 days and a GWL time series. In that particular case, best coefficient is found at delay= 0 day, with a value of 0.776. Iterating over the proposed range of depth for the cumulated depth, will lead to obtain, for each value of depth, the delay at which the correlation is maximum.

The same procedure is applied for each of the 8 adjacent cells of the effective precipitation grid, and stored for further processing.

Results

The search for best fit between GWL and a signal based on effective precipitation has been carried out for the 254 selected piezometers and selected parameters (depth of rolling sum and delay). Information related to best correlation coefficient value and corresponding parameters is stored so as to be attributed either to the piezometer or to corresponding effective precipitation grid cell. Computation time is about 2.5 hours.

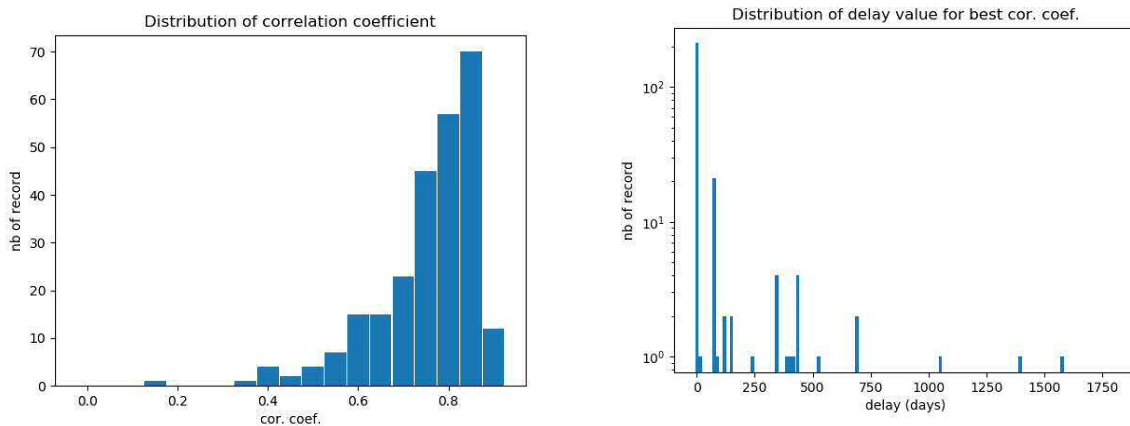


Illustration 4: Distribution of correlation coefficient (left) and delay values (right, Y axis in log scale) for the best correlation coefficient found.

Correlation coefficient values found at the end of the fitting procedure are generally high (illustration 4), with a majority of values above 0.7. There are very few values below 0.5, which represents a threshold under which no correlation is expected. The coefficient are always positive as only the maximum coefficient have been stored (a negative relationship between effective precipitation and GWL would not be physically explainable). Illustration 4 (right) shows that the most frequent situation is the best correlation is found with a 0 delay (no delay). The rest of the delay values are gathered around half a year (60-150 days) and then around a year (350-400 days). Few cases present delays greater than 1 year.

The distribution of the depth of rolling sum parameter associated with the best correlation coefficient (illustration 5) shows that most depth values range between 10 and 200 days. Few cases fall into the 250-450 interval, the remaining cases showing depth values higher than 450 days peak of cases for the maximum parameter value. This last peak should be interpreted as the fact that the best correlation coefficient falls outside the chosen interval (i.e. for depth of rolling sum greater than 545 days) but increases with increasing depth of rolling sum. Under this assumption, the greater is the depth parameter, the greater is the correlation coefficient, even if the maximum coefficient has not been found. It has been found costly in computation time to extend the interval. This cases could be interpreted as the need to compute a rolling sum on a large amount of time (more than a year and a half) to explain the link to the hydraulic heads and concerns particularly aquifers with great inertia.

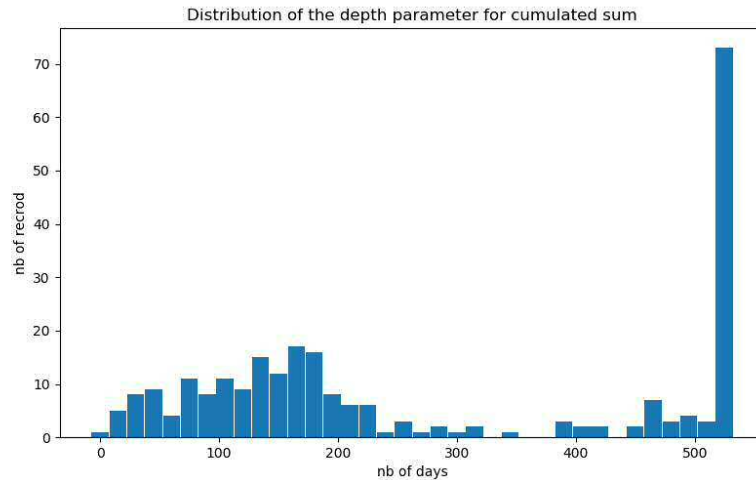


Illustration 5: Distribution of the depth parameter for effective precipitation rolling sum.

Illustration 9 shows that the correlation coefficient values fitted not seem to strongly depend neither on the depth nor on the delay parameters. This is explained by the wide distribution of climate, soils, land use and aquifers characteristics included in the set of 254 selected piezometers across the French territory for this experiment. It is in turn possible to characterize this diversity by combining the proposed parameters in order to obtain a good enough correlation between effective precipitation and GWL, for most of the studied piezometers.

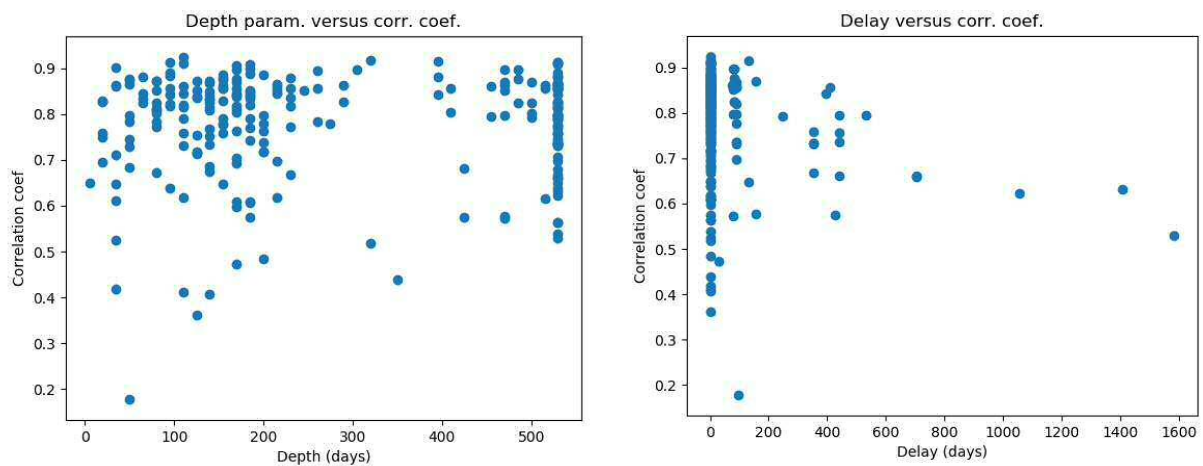


Illustration 6: Dependence of the correlation coefficient to the depth for rolling sum (left) or the delay (right) parameters.

When plotting those parameter along the French territory, no spatial pattern is found for the value of correlation coefficient (illustration 6).

The spatial distribution of the depth parameter for cumulated effective precipitation seems to present more consistency in some regions (**Erreur ! Source du renvoi introuvable.**), particularly for depths inferior to 6 months (west, east and south) and superior to a year (north, Seine basin).

The spatial distribution of the delay parameter (illustration 8) show values below one month all over the studied area, higher values being grouped in the north, in the Seine basin, same as for depth parameter (**Erreur ! Source du renvoi introuvable.**).

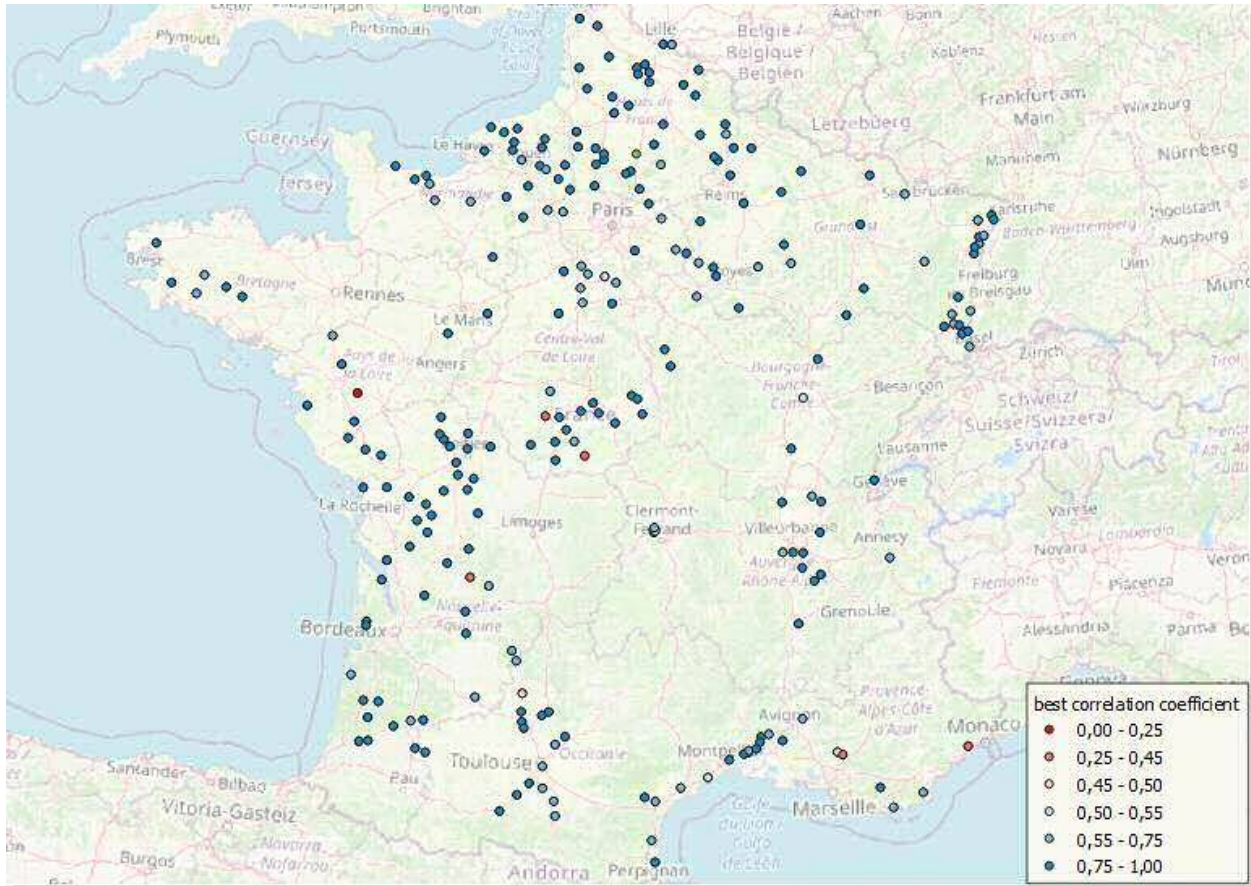


Illustration 7: Representation of the best correlation coefficient fitted for the 254 piezometers.

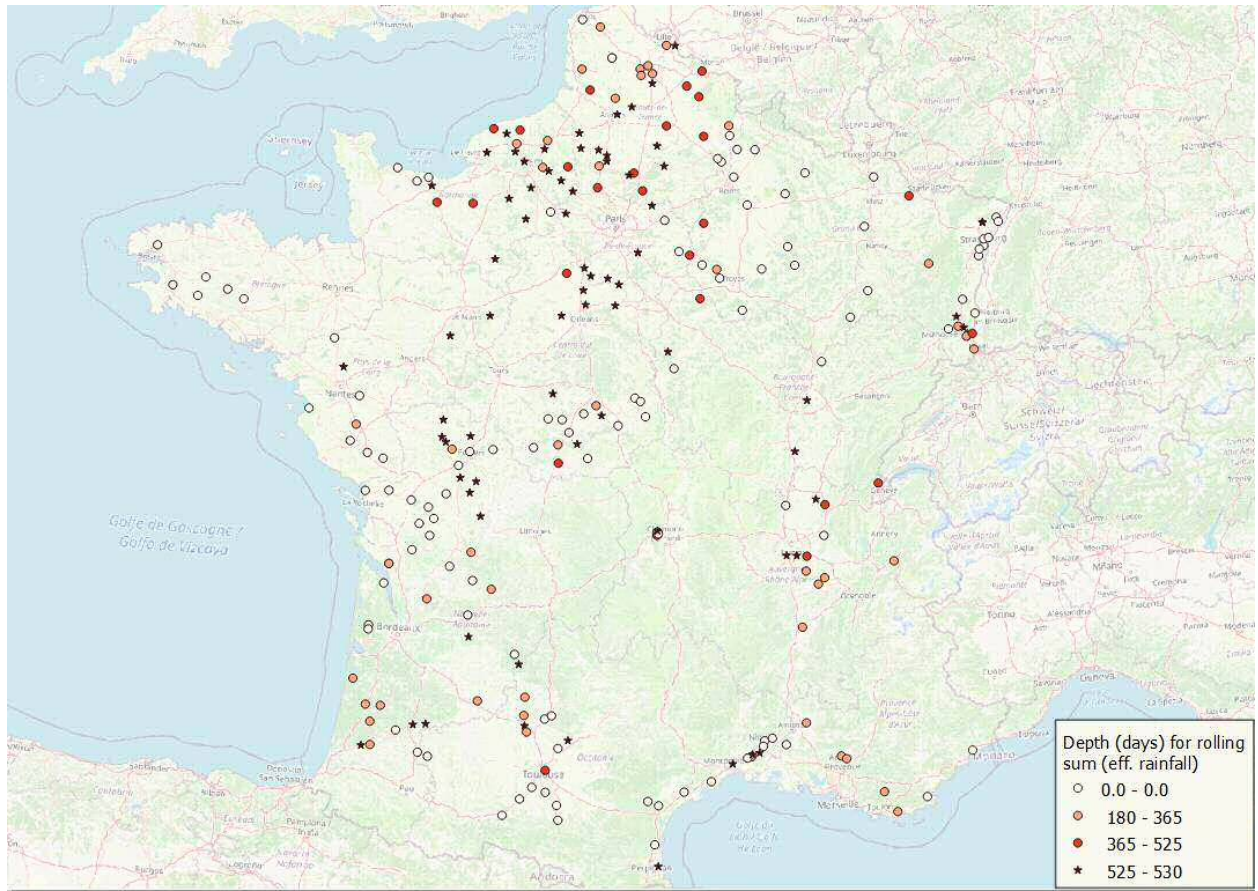


Illustration 8: Values of the depth parameter for rolling sum (effective precipitation).

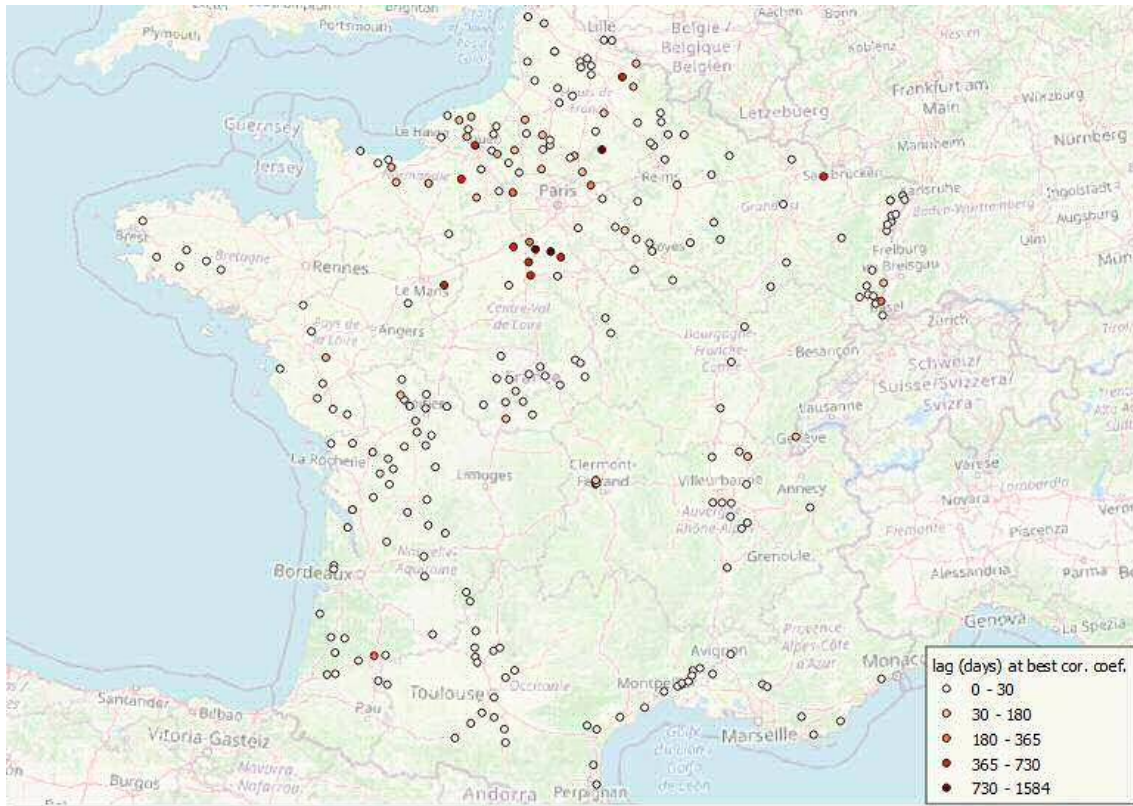


Illustration 9: Delay parameter values over France.

The best correlation coefficient does not seem to be found for a particular cell over the considered piezometer (illustration 10). Cells centered on the piezometer are not the most frequent as cells located east, north-east, north-west, south-east and south-west can be more frequently selected for the best correlation (30 cases or more). Cells located to the south and west seem to be less frequent.

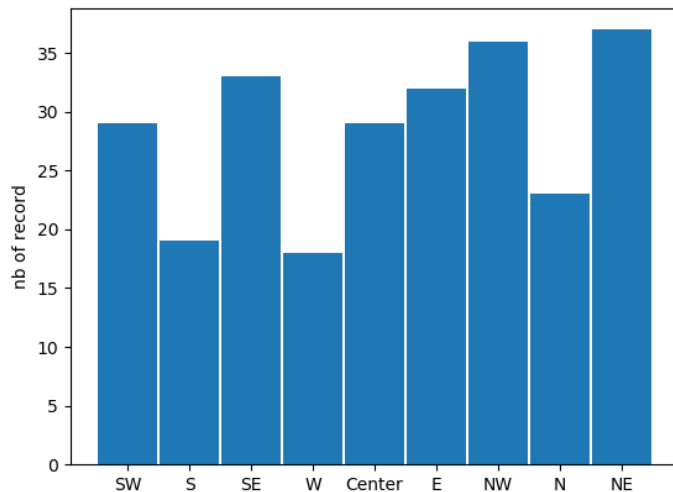


Illustration 10: Distribution of the geographical position of the cell for which the best correlation coefficient has been found between effective precipitation and GWL.

4. Conclusions

Based on a preselected set of 254 piezometers considered to be poorly influenced by pumping, the correlation between effective precipitation (and derived time series) and groundwater level has been explored over France. Results show that both signals can be rather well correlated (values above 0.6) depending on the way the effective precipitation is cumulated or delayed in time.

To obtain good relation between those two signals, a preprocessing of the effective precipitation has been carried out. Several parameters related to effective precipitation have been explored to maximize the correlation: the value of the depth for the rolling sum of effective precipitation, the value of the considered delay between effective precipitation and the GWL time series and the location of the cell of the effective precipitation grid compared to the considered piezometer position.

The goodness of the correlation does not appear to be dependent on one particular parameter and rather good correlation values have been found all over France. The depth parameter to compute the rolling sum for effective precipitation seems to be consistent across some regions and more clustered. The delay parameter appears to follow a similar behavior to that of the depth parameter. The highest values for both parameters are observed in the north of France (Seine basin). No particular importance seems to be linked to the considered effective precipitation cell location.

A main result of this study is the new parameter set associated to the 254 piezometers: it is now possible to consider simulating GWL rather well of those piezometers presenting good correlation coefficient values using the effective precipitation grid computed based on E-OBS & INDECIS data. For each piezometer are provided, the effective precipitation grid cell coordinates, the depth of the rolling sum and the delay to consider in order to obtain a first acceptable simulation using machine-learning algorithms for GWL simulation at the French scale.

5. References

Baulon, L., Allier, D., Massei, N., Bessiere, H., Fournier, M., Bault, V. (2021). Influence de la variabilité basse-fréquence sur l'occurrence et l'amplitude des extrêmes piézométriques. *Revue Géologues* n°207.

**Analysis of historical droughts through their induced impacts
in Spain**

Análisis de sequías históricas a través de los impactos derivados

Analysis of historical droughts through their induced impacts

Sainz de la Maza, M. ^{a1}, del Jesus, M. ^{a2}

^aInstituto de Hidráulica Ambiental, Universidad de Cantabria - Calle Isabel Torres nº15, Parque Científico y Tecnológico de Cantabria, 39011, Santander, España.

E-mail: ^{a2}manuel.deljesus@unican.es.

Recibido: 05/08/2019

Aceptado: 08/07/2020

Publicado: 31/07/2020

Citar como: Sainz de la Maza, M., del Jesus, M. 2020. Analysis of historical droughts through their induced impacts. *Ingeniería del agua*, 24(3), 141-156. <https://doi.org/10.4995/la.2020.12182>

RESUMEN

A pesar de que hoy en día la identificación y caracterización de sequías sigue siendo un proceso no estandarizado, lo más habitual es utilizar índices como el SPI o el SPEI entre otros. En este estudio se han analizado sequías históricas, no solo a través de los índices SPI y SPEI, sino también a través del índice SSMI, con series de humedad de suelo simuladas con el modelo hidrológico *Variable Infiltration Capacity* (VIC). El objetivo es mostrar la importancia de considerar la humedad del suelo en estudios de sequías. La ocurrencia de las sequías se ha determinado a través de los impactos económicos y agrícolas generados, y no únicamente a través del déficit hídrico. Se puede concluir que la humedad del suelo es un factor determinante en el estudio del impacto de la sequía en la producción de cereales y especies de grano grueso, pero no en las pérdidas económicas inducidas.

Palabras clave | sequía; España; SPI; SPEI; SSMI; VIC; humedad del suelo; impactos económicos; producción agrícola.

ABSTRACT

Nowadays, the identification and characterization of droughts is not yet a standardized process, in most cases, indices such as SPI or SPEI are used for this task. In this study, historical droughts are analyzed, not only through SPI and SPEI, but also using SSMI computed with soil moisture time series simulated with the VIC hydrological model. The main objective is to show the importance of considering soil moisture in the study of droughts. Drought occurrence was determined through the impacts of past droughts and not only through the deficit they produce at some point in the water balance process. We conclude that soil moisture is a key factor in the production of cereals and gross grain species but is not relevant for economic impacts.

Key words | drought; Spain; SPI; SPEI; SSMI; VIC; soil moisture; economic impacts; agricultural production.

INTRODUCCIÓN

Las sequías se caracterizan por un déficit hídrico, inicialmente desencadenado por la falta de precipitación. Es por ello que muchos estudios de sequías se han centrado en identificar y caracterizar estos eventos únicamente a través del déficit de precipitación o del balance de agua en el suelo (Vicente-Serrano et al., 2010). Sin embargo, la sequía es un proceso muy complejo en el que no solo la precipitación tiene importancia. El aumento de la temperatura del aire y el consecuente aumento de la evapotranspiración (King et al., 2015), los descensos en la humedad del suelo o los cambios en los usos del suelo tienen también mucha importancia y se han de tener en cuenta a la hora de realizar estudios de sequías (Van Loon et al., 2016).

Los estudios de sequías suelen realizarse haciendo uso del llamado método de umbrales, a través del cual se pueden obtener propiedades de esta como son la intensidad, la severidad, la frecuencia y la duración de un determinado evento. Dada una serie temporal de una variable de interés (precipitación, escorrentía, caudal), estas características se derivan del establecimiento de un umbral por debajo del cual se considera que se produce un déficit de la variable de estudio. Sin embargo, análisis de este tipo presentan varios problemas. Por un lado, el establecimiento de ese umbral sigue siendo una cuestión arbitraria, o al menos subjetiva, y depende del objetivo del estudio que se esté realizando (Fleig et al., 2006; Beyene et al., 2014). El umbral se define a través de un percentil, que suele variar entre un 70 y un 95. Es importante destacar que una mala elección del umbral puede llevar a una mala identificación y caracterización de los eventos producidos en un intervalo de tiempo (Van Loon et al., 2010; Sheffield y Wood, 2011). Por otro lado, incorporar la dimensión espacial a los estudios de sequías no es una tarea sencilla y pese a ello es un aspecto crítico a la hora de definir correctamente una situación de sequía (Mishra y Singh, 2011).

Existen más de 150 índices en la literatura y cada uno de ellos es adecuado para representar uno o dos tipos de sequía –meteorológica, hidrológica, agrícola o socioeconómica–. Los índices son, en principio, dependientes de la zona de estudio. Por ejemplo, se ha visto que con el Índice Estandarizado de Precipitación-Evapotranspiración (SPEI – *Standardized Precipitation-Evapotranspiration Index*) (Vicente-Serrano et al., 2010) se obtienen buenos resultados en la península ibérica entre otras zonas (Beguiría et al., 2014). No obstante, hay ciertos índices que son muy utilizados globalmente. Por ejemplo, el Índice de Precipitación Estandarizado (SPI – *Standardized Precipitation Index*) (McKee et al., 1993) o el Índice de Severidad de Palmer (PDSI – *Palmer Drought Severity Index*) (Palmer, 1965) reproducen relativamente bien situaciones de sequía en diferentes partes del mundo encontrando, sin embargo, diferencias en los resultados obtenidos con unos y otros índices (Vicente-Serrano et al., 2012; Homdee et al., 2016; Liu, et al., 2018).

Una ventaja del estudio de sequías a través de índices es que permite cuantificar la severidad de las sequías. Tradicionalmente, sequías muy severas han producido grandes pérdidas de producción agrícola, tanto de regadío como de secano, que se han traducido en grandes pérdidas económicas (Lopez-Nicolas et al., 2017). La predicción estacional permite reducir el impacto de sequías menos severas mediante adaptaciones de los cultivos por parte de los agricultores. En el estudio realizado por Kim et al., 2019, queda reflejada la importante pérdida de rendimiento que generan las sequías en los cuatro productos más relevantes a nivel mundial: arroz, maíz, soja y trigo. De estas cuatro especies, únicamente dos son relevantes en España: el maíz y el trigo. En el año 2018, en España se regó un 22% de la superficie total cultivada; en el caso del maíz, solo un 8.65%. En el caso del trigo este valor desciende a un 0.77% (ESYRCE, 2018). Estos datos reflejan la importancia que aún tiene el cultivo de secano en los principales cultivos en España y, por tanto, la sensibilidad frente a la sequía que tiene la producción agrícola.

A pesar del conocido impacto económico que generan las sequías, en España no se comenzó a asegurar la producción contra la sequía hasta el año 1980, lo que limita la duración de las series que podemos analizar. Además, es un riesgo muy complicado de asegurar, y cuantificar, debido a que no es un riesgo delimitado en tiempo y en espacio, haciendo que no se pueda establecer de forma precisa el inicio y final de los daños que esta provoca. En la actualidad, se aseguran cultivos extensivos de secano de tipo herbáceo (cebada, trigo, avena, arroz...), uva de vinificación, olivar, frutos secos, maíz y remolacha (Ollero Lara et al., 2018) y la cobertura del riesgo de sequía se considera junto con otras adversidades climáticas como heladas o granizo. Es importante destacar que las otras adversidades climáticas aseguradas provocan daños mucho más fácilmente delimitables en espacio y tiempo.

En este trabajo analizamos sequías históricas en la España peninsular utilizando los índices SPI, SPEI y SSMI (*Standardized Soil Moisture Index*) (Carrão et al., 2016), tanto a nivel agregado como distribuido en el espacio. Las sequías históricas se determinan a través de los impactos que estas generaron a nivel económico, estudiando la capacidad de cada índice de predecirlas. Se comparan

los resultados de los tres índices para identificar la sensibilidad de las sequías a la precipitación, temperatura y humedad del suelo. Para el estudio del SSMI, la humedad del suelo se obtuvo a través del modelo *Variable Infiltration Capacity* (VIC). Además, se ha estudiado la correlación entre los índices y las series temporales, con los impactos económicos y agrícolas generados por los eventos históricos identificados. En términos agrícolas, se ha estudiado el impacto de las sequías en los principales grupos de especies de cultivo en España.

Con este estudio se pretende establecer una metodología que ayude a la correcta definición y caracterización de las grandes sequías, a través del impacto real que generan en la producción agrícola y la economía de España, utilizando índices clásicos como medios de predicción. No se consideran las dinámicas agrícolas de adaptación de cultivo a las condiciones estacionales predichas -cambiando el cultivo típico por uno mejor adaptado a las condiciones climáticas predichas-, interesándonos únicamente por aquellas sequías no mitigables.

CASO DE ESTUDIO

Zona de estudio

El estudio se centra en la España peninsular. La precipitación en la península ibérica es muy variable en espacio y tiempo, debido a su diversidad climática y a su configuración orográfica. La precipitación decrece de norte a sur. En el norte, la precipitación media anual en el período de referencia 1981-2010 es de 1300 mm, mientras que en el centro y en el sur este valor se sitúa en unos 550 mm. Además, España tiene una fuerte variación estacional de la precipitación media. En los meses de invierno, la precipitación media histórica ha sido de unos 75 mm al mes mientras que en verano estos valores descienden hasta los 20 mm. En cuanto a la temperatura, la distribución de las isotermas medias anuales reproduce bastante bien el mapa hipsométrico, con temperaturas medias más bajas en las zonas con mayor altitud. Además, también se observa una fuerte variación estacional en la temperatura, alcanzando los valores medios máximos en verano. Esta climatología lleva a que los períodos más secos correspondan a los meses de julio y agosto mientras que los más húmedos sean los correspondientes al período de noviembre a febrero. En la Figura 1.a y la Figura 1.b. se muestran los ciclos medios anuales en el período histórico de las variables usadas en este estudio: precipitación, temperatura, evapotranspiración potencial y humedad del suelo. Se puede observar que la humedad del suelo y la precipitación media del período histórico tienen una forma similar, pero con un retraso de 1 mes.

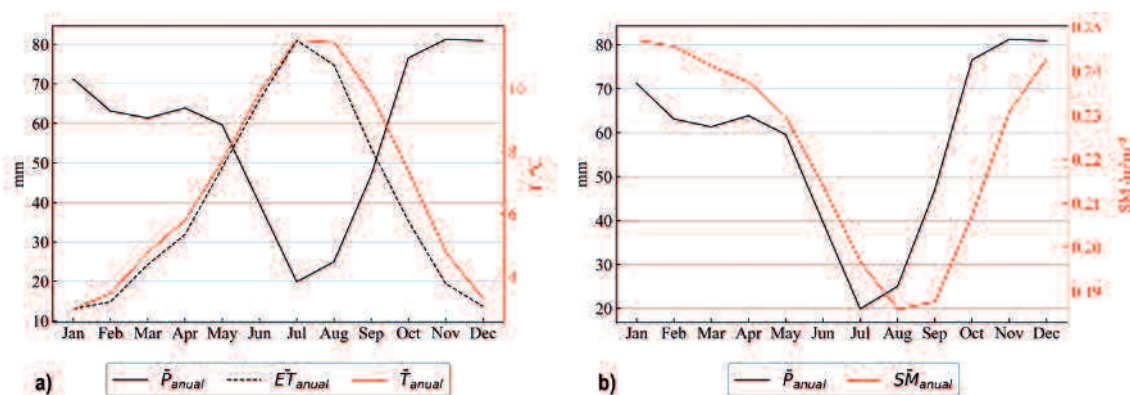


Figura 1 | Ciclos anuales medios de las variables climáticas de estudio en el período histórico de estudio.

Datos

En este estudio se han utilizado las series temporales de las variables climáticas observadas precipitación y temperatura de la base de datos Spain02 versión v5 (Herrera et al., 2012; Herrera et al., 2016). Estas series corresponden a datos a escala diaria en

un mallado de resolución espacial de 0.1 grados para el mallado regular y 0.11 grados para el mallado rotado. Para este estudio, se ha tomado la malla regular. Tanto la precipitación como la temperatura tienen una cobertura temporal desde 1951 hasta 2015.

Para forzar el modelo VIC se necesitan, además, otras variables climáticas adicionales como la radiación, cobertura de nieve y viento entre otras. Éstas han sido obtenidas del *Research Data Archive* que gestiona el National Center for Atmospheric Research (NCAR), que proporciona series temporales de reanálisis (CFSR – *Climate Forecast System Reanalysis*) de muchas variables climáticas. Estas series son series continuas de 32 años de duración cubriendo el período 1971 - 2011 y están disponibles a varias resoluciones espaciales. Para este estudio se ha utilizado la resolución espacial más fina disponible. Por otro lado, se necesita información litológica y edafológica, obtenida de la base de datos *Global Soil Dataset for Earth system modeling* (GSDE); datos de cobertura y usos del suelo, obtenidos a partir del *Corine Land Cover* (CLC) con resolución de 500 m; LAI (*Leaf Area Index*), procedente del *Copernicus Global Land Service* (CGLS) disponible a resolución temporal mensual y espacial de 0.01 grados; y albedo, obtenido de la base de datos *Global Land Cover Facility*, disponible a la misma escala espacio-temporal que el LAI. Todas las bases de datos han sido interpoladas a una resolución de 0.042° (~5 km), que es a la que se ha ejecutado el modelo VIC.

Con el objetivo de verificar la bondad de las series de humedad del suelo simuladas, se han empleado datos de humedad de suelo de satélite, concretamente, la versión 04.4 de la Iniciativa de Cambio Climático (CCI) de la Agencia Espacial Europea (ESA). Esta base de datos está basada en la versión 03.3 y está compuesta de tres productos: activo (a partir de datos de sensor radiométrico), pasivo (a partir de datos de radar) y combinado. La principal diferencia respecto a versiones anteriores es que el producto combinado se crea a partir de los datos de nivel 2 disponibles (humedad de suelo medida por sensores radar y humedad del suelo de radiómetro) y no como combinación de la parte activa y pasiva. Se proporcionan en una malla regular de 0.25°, cobertura global y período de 1978 hasta la actualidad. Está disponible a resolución diaria, 10-diaria y mensual. Además, la base de datos está compuesta por varios datos como son el porcentaje de humedad del suelo (%), la humedad del suelo volumétrica ($\text{m}^3 \text{m}^{-3}$) y la incertidumbre, en una capa de 2 a 5 cm de profundidad. En este estudio se ha utilizado el producto combinado a resolución temporal mensual. No se han considerado los productos activo y pasivo dado que el producto combinado representa adecuadamente los datos de humedad de suelo observada en ciertas áreas de la zona de estudio (González-Zamora et al., 2019).

Tabla 1 | Sequías históricas producidas en la España peninsular.

Inicio	Final	Datos agrícolas	Datos económicos
1953	1954	No	No
1964	1964	Sí	No
1973	1974	Sí	No
1980	1984	Sí	No
1990	1995	Sí	Sí
2005	2005	Sí	Sí
2012	2012	Sí	Sí

Para la identificación de sequías históricas se han utilizado principalmente dos fuentes de datos. Por un lado, se ha utilizado la base de datos *Emergency Event Database* (EM-DAT), que recoge información de distintas fuentes de datos (organizaciones no gubernamentales -ONG-, centros de investigación, aseguradoras, etc). Esta base de datos es global y aunque identifica algunas de las fuertes sequías que ha habido en España, la información es escasa. Por otro lado, se ha utilizado un estudio realizado por la Entidad Estatal de Seguros Agrarios (ENESA) (Ollero Lara et al., 2018) en el que se recoge información de secuencias de sequías históricas en España, así como períodos de sequía en la zona norte de la Península y lluviosos en el sur y viceversa. En la Tabla 1 se muestran los eventos de sequía identificados en el período y la zona de estudio.

Además, en este estudio se recogen datos de parámetros económicos del Consorcio de Compensación de Seguros desde el año 1980. El Consorcio de Compensación de Seguros es un reasegurador obligatorio de carácter público al que todas las pólizas deben contribuir mediante un recargo como aportación a la reserva de estabilización del Consorcio. La reserva se crea con el objetivo de compensar las desviaciones desfavorables de la siniestralidad en cada año, en caso de que las haya. En la Figura 2 se muestran

las series temporales de las primas recibidas e indemnizaciones realizadas. En los años en los que las indemnizaciones superan las primas recibidas, se considera que ha habido una desviación de la siniestralidad desfavorable. En el estudio, se identifican los años 1986, 1992, 1995, 1999, 2005 y 2012 como años con elevados daños por sequía coincidiendo con la existencia de picos sobre el comportamiento medio de la serie.

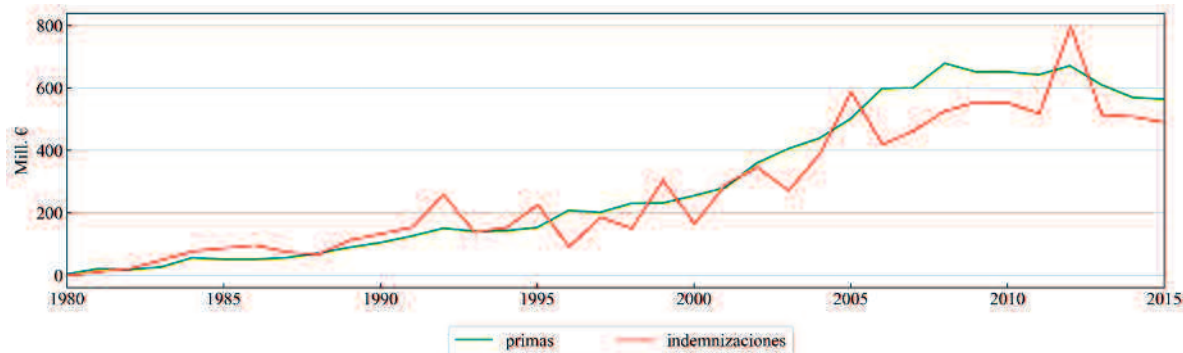


Figura 2 | Primas e indemnizaciones frente a daños agrícolas realizadas por el Consorcio de Compensación de Seguros (Fuente: ENESA).

Estos datos han sido utilizados para correlacionar el impacto económico producido por las sequías mostradas en la Tabla 1 con los índices de sequía SPI, SPEI y SSMI. Asimismo, se ha estudiado la correlación entre los daños económicos producidos en los años de sequía con la producción agrícola en esos años. Los datos de producción agrícola han sido descargados de la Organización de las Naciones Unidas para la Alimentación y la Agricultura (FAOSTAT). Esta base de datos está formada por tres series de datos: producción agrícola (toneladas), área sembrada (hectáreas) y rendimiento (toneladas por hectárea) por tipo de especie y agregada a cada país desde 1961 a 2017. Además, ofrece la posibilidad de descargarse varias especies agrupadas. En este estudio, se ha hecho uso de la modalidad de bases de datos agrupadas en series temporales desde 1961 hasta 2015, límite impuesto por la base de datos de precipitación y temperatura.

METODOLOGÍA

Modelo hidrológico

El modelo hidrológico VIC es actualmente uno de los más aplicados a predicción de clima y cambios en la cobertura del suelo (Gayathri et al., 2015). Es un modelo semi-distribuido que se puede utilizar en dos modos, balance de agua y balance de energía. Utiliza precipitación, temperatura diaria y velocidad del viento entre otras variables, y permite la definición de muchos tipos de cobertura suelo. Es un modelo híbrido entre físico y conceptual ya que la infiltración, escorrentía, etc. están basadas en ecuaciones empíricas. A pesar de deficiencias tales como no reproducir interacciones entre el agua del subsuelo y la superficie, o no tener un mecanismo explícito para producir exceso de infiltración, el VIC es un modelo muy utilizado en estudios de sequías (Trambauer et al., 2014).

En este estudio, el modelo VIC se ha utilizado en su modalidad de balance de agua. Para ello, el modelo VIC resuelve la ecuación de continuidad de la masa en cada paso de tiempo entre los inputs (precipitación) y los outputs (evaporación, escorrentía y flujo base). La evaporación se calcula como suma de la evaporación del agua desde tres sistemas: cubierta vegetal, transpiración y suelo desnudo. Para el cálculo de la evapotranspiración potencial utiliza la fórmula de Penman-Monteith.

Las simulaciones se han realizado a escala diaria y a resolución espacial de ~ 0.05 grados (aproximadamente 5 km). La calibración del modelo VIC se suele realizar variando 6 parámetros, entre los que está la profundidad del suelo. En este caso, se ha asumido una profundidad constante en todas las celdas, sin realizar ninguna calibración para, posteriormente, realizar una corrección de las series obtenidas. A pesar de que la humedad de suelo de satélite mide la cantidad de agua en una profundidad de 5 a 10 cm, en este estudio se han simulado todas las celdas con una profundidad de la primera capa de 1 m. Se ha realizado así

debido a que la simulación con una capa superficial de 10 cm generaba mucho ruido sobre el comportamiento medio de las series simuladas. Con una profundidad de 1 m se ha conseguido simular ese comportamiento medio más suavizado y que se ha observado que reproduce mejor las condiciones medidas con satélite.

Índices de sequía

En el presente estudio se han utilizado los índices SPI, SPEI y SSMI a agregaciones espaciales de 1, 3, 6, 9 y 12 meses. Los tres índices poseen el mismo método de cálculo, el cual se basa en calcular cuánto se desvía cierta variable respecto de la media histórica. En el caso del SPI la variable usada es la precipitación (P), en el caso del SPEI es la diferencia entre la precipitación y la evapotranspiración potencial ($P - ET_0$) y para el caso del SSMI se hace uso de la humedad del suelo (SM). El cálculo se realiza ajustando una función de densidad de probabilidad (FDP) a la serie histórica para después transformarla en una distribución normal de media cero y desviación uno, que es la que proporciona el valor de los índices. En el caso de los índices SPI y SSMI los autores recomiendan ajustar una FDP de tipo gamma (McKee et al., 1993; Carrão et al., 2016), mientras que en el caso del SPEI la función más adecuada es una log-logística (Vicente-Serrano et al., 2010). En el presente estudio se han realizado los cálculos siguiendo dichas recomendaciones.

Los tres índices de sequía se han calculado a partir de datos mensuales, es decir, se han obtenido 12 funciones de densidad de probabilidad, una por mes. Las variables precipitación y temperatura se proporcionan directamente como valores mensuales mientras que la humedad del suelo media mensual ha sido obtenida a partir de simulaciones diarias del modelo hidrológico VIC. Para verificar la bondad de las series de humedad de suelo obtenidas, se han comparado con las series de humedad del suelo de satélite a través del coeficiente de correlación r de Pearson.

Puesto que el comportamiento hidrológico en España no es uniforme en todo el territorio, habiendo zonas más susceptibles de sufrir sequía, como es la zona sureste de la Península, la evaluación realizada está basada en un análisis distribuido de los índices SPI, SPEI y SSMI. Para el estudio comparativo entre los tres índices, se han calculado los valores medios mensuales para todo el período de estudio píxel a píxel y en cinco períodos de agregación a 1, 3, 6, 9 y 12 meses. Así, se han obtenido 15 índices por píxel de la malla de VIC cuya correlación se ha estudiado nuevamente a través del coeficiente de correlación r de Pearson. Este análisis se ha realizado tanto para toda la serie histórica como agrupada por meses, dando lugar a matrices de correlación de dimensión 15×15 . El estudio distribuido permite, además, identificar qué áreas de la zona de estudio son más sensibles a cada variable (precipitación, temperatura y humedad del suelo) y a cada período de agregación.

Los datos económicos y agrícolas se tienen agregados espacialmente y en series anuales. Por tanto, este estudio permite identificar y cuantificar el impacto de las grandes sequías sufridas en todo el territorio español y no de sequías locales. Para poder cruzar los datos de índices con los económicos y agrícolas, se han calculado series anuales para las agregaciones de 1, 3, 6, 9 y 12 meses para cada uno de los índices. Se parte, entonces, de series mensuales de los índices que se han de convertir en series anuales. Para cada año, se tienen 12 valores de cada índice (uno por mes) pero finalmente se han creado un total de 20 series temporales por año. Éstas, corresponden a los 12 valores de cada mes y a los estadísticos correspondientes a la media anual, mediana anual, máximo y mínimo anuales, y la media aritmética de 3 meses consecutivos (EFM, AMJ, JAS, OND) para ver posibles correlaciones estacionales. Se ha seguido esta metodología de cálculo para determinar si hay algún mes más relevante que el resto o si, por el contrario, el comportamiento económico y agrícola responde mejor a un comportamiento medio (media, mediana, estacional) o extremo (máximo o mínimo) de los índices. Todas las series agregadas han sido calculadas como la media aritmética de los valores en cada píxel y teniendo, en total, $20 \text{ series} \times 5 \text{ agregaciones} \times 3 \text{ índices}$ (300 series temporales) para toda la península ibérica.

Análisis de impactos

Para cada una de las 20×5 series temporales de cada índice, se ha estudiado qué serie correlaciona mejor con la producción agrícola y los impactos económicos reportados. Esta correlación se ha obtenido a través del coeficiente r de Spearman, que mide la interdependencia de dos variables aleatorias cuya relación es monótona pero no necesariamente lineal. Cuando la relación es lineal, el coeficiente r de Spearman corresponde al coeficiente r de Pearson.

Para realizar la correlación de los índices con datos económicos, se ha trabajado con las indemnizaciones porque estas representan el pago por cobertura del impacto directo de la sequía. Como la sequía es un riesgo que se asegura junto con otras inclemencias meteorológicas mucho más fácilmente delimitables en espacio y tiempo, se ha considerado que el comportamiento medio de la serie de indemnizaciones es un riesgo fácilmente predecible. Por tanto, la serie original ha sido tratada para obtener las desviaciones sobre el comportamiento medio eliminando, además, la tendencia creciente que se observa en la Figura 2. Así, la serie original ha sido estandarizada según la Ecuación (1),

$$I_s = \frac{y_d - \mu}{\sigma} \quad (1)$$

donde I_s se refiere a la indemnización estandarizada, y_d son las desviaciones sobre el riesgo efectivo una vez eliminada la tendencia, μ es la media de las desviaciones y σ es la desviación estándar de las desviaciones. Esta estandarización lleva los términos económicos a valores en la misma escala que los índices de sequía.

Las series temporales de producción agrícola se tienen desde el año 1961, por tanto, se ha realizado un análisis semejante al económico, pero más extenso, con cada uno de los grupos de especies de producción agrícola. Es importante destacar que las series temporales de producción agrícola también poseen una tendencia positiva, en la mayor parte de los casos creciente, tal y como se observa en la Figura 3, donde se muestra un ejemplo para todos los grupos de especies.

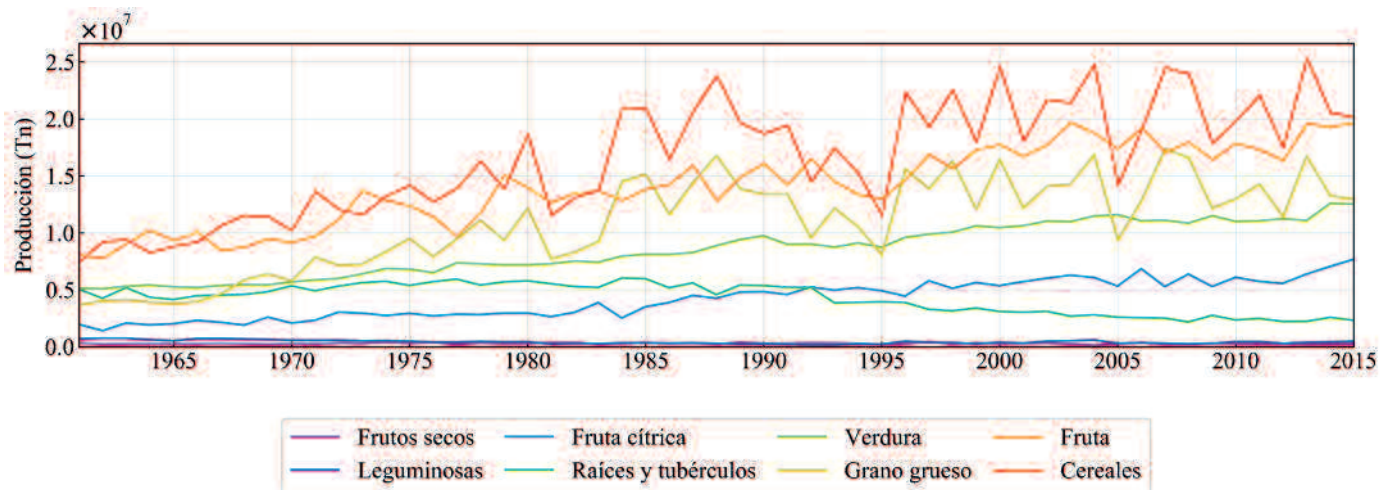


Figura 3 | Evolución temporal de la producción agrícola en España desde 1961 hasta 2015.

Esta tendencia se ha considerado de índole no climática, debido a la innovación tecnológica producida en la agricultura. Los datos de producción se han comparado por un lado con los datos de desviaciones económicas, y con los índices de sequía por otro. A la hora de comparar la producción agrícola con los datos económicos, lo que permite saber qué especies provocan mayores pérdidas económicas, se han comparado las series originales únicamente extrayendo su tendencia. Sin embargo, a la hora de comparar con índices climáticos se ha utilizado el rendimiento de la producción, transformando también las series de rendimiento en series estandarizadas a través de la Ecuación (1). Para este caso, es el valor residual de producción una vez eliminada la tendencia, es la media de los valores residuales de producción y es la desviación estándar del valor residual de producción. Con esta estandarización, es posible comparar la producción entre diversas especies o grupos de especies.

La relación entre cada índice y las series de producción estandarizadas se ha evaluado también a través del coeficiente r de Spearman, dada la no linealidad en la relación entre índices de sequía y producción agrícola. Por último, para cada evento histórico, se ha observado qué valor de desviación económica y de producción hubo en esos años, estudiando el comportamiento de los índices en eventos de sequía.

RESULTADOS

Índices de sequía

Correlación de índices de sequía

Las simulaciones realizadas con el modelo VIC están a una resolución de 0.05° mientras que la humedad del suelo de satélite se encuentra a 0.25° . Para poder realizar una comparativa entre las series obtenidas y las de satélite, se ha agregado la humedad de suelo simulada a la resolución de satélite calculando la media aritmética de los valores de humedad de suelo de las celdas de simulación integradas en cada celda de satélite. En la Figura 4 se muestran los mapas de correlación y sesgo de las series de humedad de suelo simuladas respecto a las observadas. Se muestran correlaciones r de Pearson positivas significativas con $p < 0.01$. Se puede observar cómo las series tienen una alta correlación en la mayoría de la península ibérica ($r > 0.6$ en más del 70% del área de estudio) a excepción de la zona centro-este ($r < 0.4$ en aproximadamente un 7% de las celdas). En cuanto al sesgo que poseen las series simuladas, se puede observar cómo en varias zonas de la Península las series poseen un sesgo no despreciable.

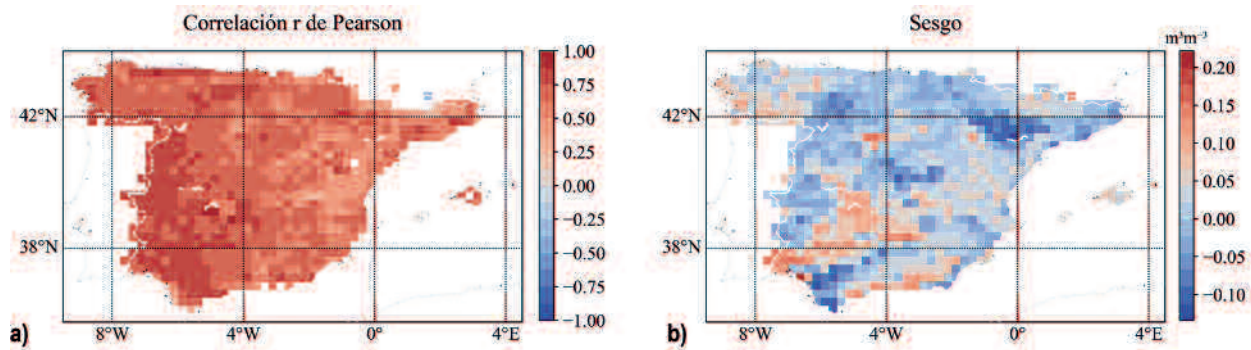


Figura 4 | Mapas de a) correlación y b) sesgo de las series de humedad del suelo simuladas frente a las de satélite.

Como ya se ha comentado, la profundidad a la que está medida la humedad del suelo de satélite es diferente a la de las series simuladas. Por tanto, se ha aplicado una corrección de sesgo a las series simuladas de tipo lineal según la Ecuación (2):

$$SM_{sc} = (SM_s - a) b + c \quad (2)$$

Donde SM_s es la humedad del suelo simulada, SM_{sc} es la humedad del suelo corregida y a , b y c son factores correctores del sesgo y amplitud de la señal. Los coeficientes se ajustan minimizando el error medio cuadrático entre la serie observada y la corregida mediante un algoritmo genético. En la Figura 5 se muestra un ejemplo de una serie de humedad del suelo antes y después de ser corregidas en una celda al suroeste de la Península, donde encontramos los mayores valores de sesgo.

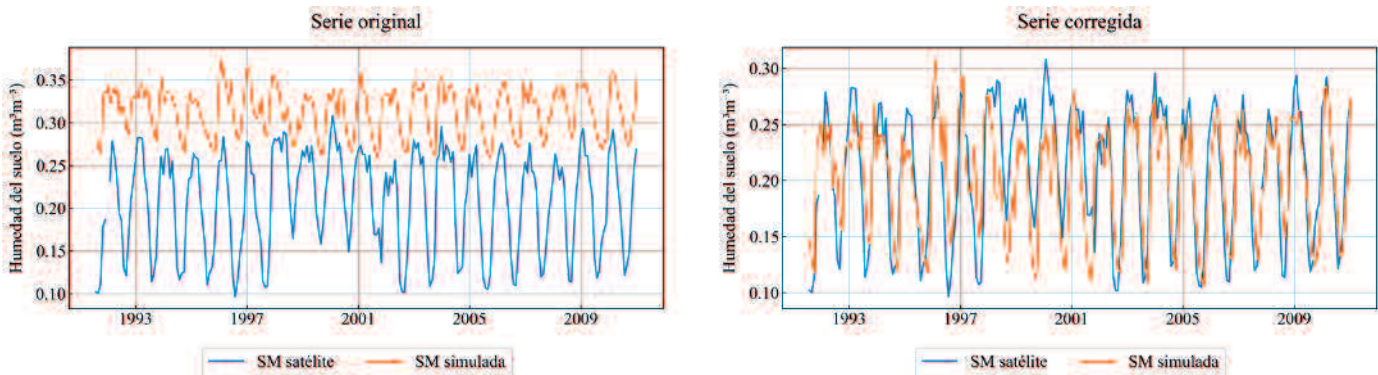


Figura 5 | Ejemplo de una serie de humedad de suelo de satélite vs. Simulada antes (izquierda) y después (derecha) de aplicar la corrección.

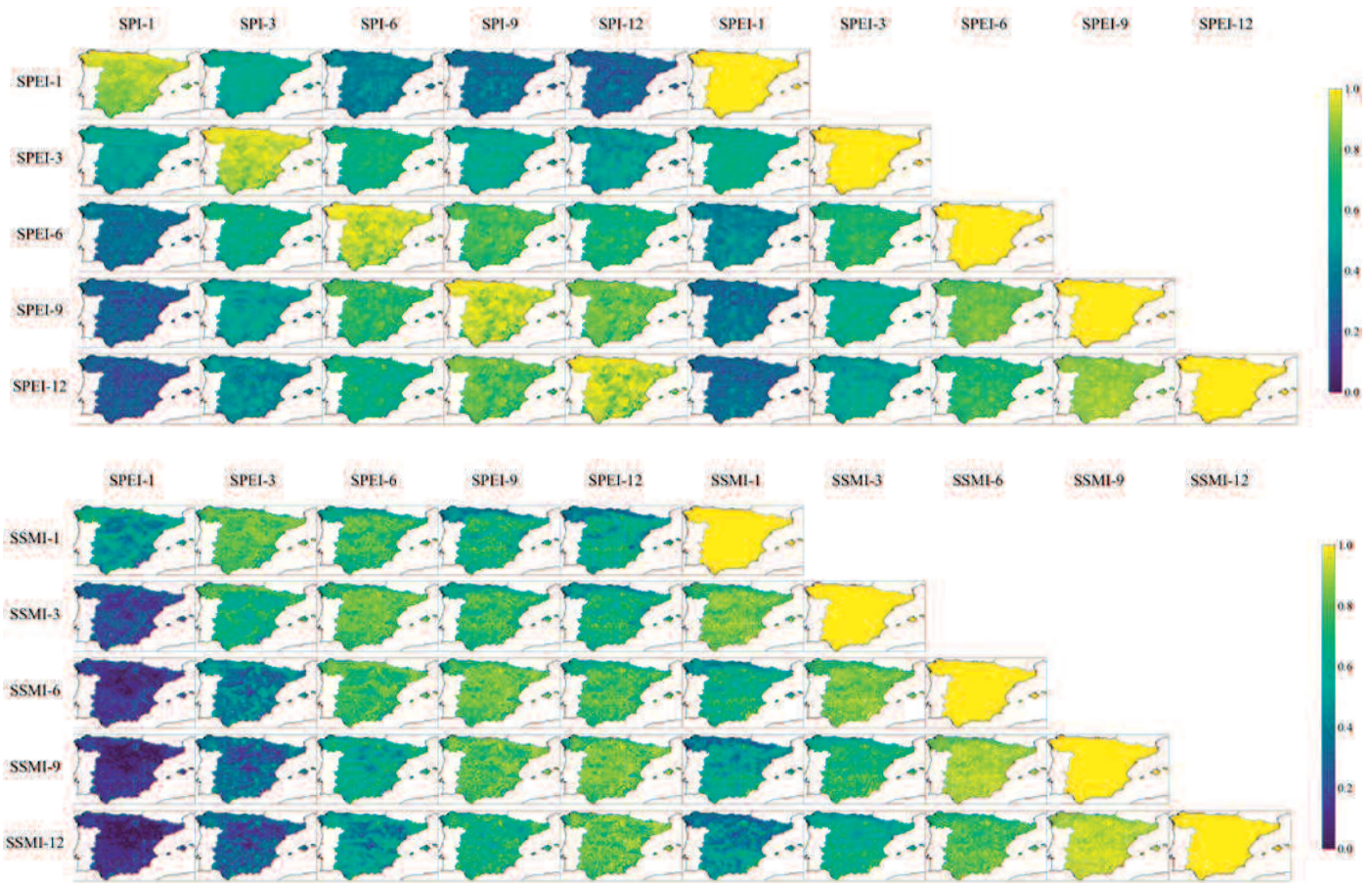


Figura 6 | Matrices de correlación de los índices SPI con SPEI (panel a) y SPEI con SSMI (panel b).

En la Figura 6 se muestran los mapas de correlación para los índices SPI con SPEI y SPEI con SSMI. No se muestran los mapas de correlación de SPI con SSMI porque son muy similares a los obtenidos entre SPEI y SSMI, dada la alta correlación entre los índices SPI y SPEI. La escala gráfica de presentación es de 0 a 1, para observar las diferencias de forma más clara dada la alta correlación existente entre alguna pareja de índices. En concreto, se puede observar la alta correlación de los índices SPI y SPEI cuando están agregados la misma escala temporal (Panel a). La correlación es total en prácticamente toda la franja norte. Esto puede ser debido al elevado volumen de lluvias, haciendo que sea una zona donde la evaporación carece de importancia respecto a la precipitación. Esta correlación va disminuyendo a medida que se avanza hacia el sur de la Península y reflejando, por tanto, la importancia de la temperatura frente a la precipitación. También se observa una correlación alta entre diferentes escalas temporales de los mismos índices (Paneles a y b). Así, la correlación entre el SPI-9 con SPI-12 y SPEI-9 con SPEI-12 es superior a 0.8 en prácticamente toda la Península. Esta situación sugiere que el comportamiento de estos índices a escala temporal de 9 meses no se ve muy modificado por lo que ocurre los 3 meses siguientes, pudiendo así determinar el comportamiento medio de un año a través de los anteriores 9 meses.

En general, se observa una mejor correlación en toda la zona peninsular para escalas de agregación con 3 meses de diferencia, es decir, SSMI-1 con SPI-3 y SPEI-3, SSMI-3 con SPI-6 y SPEI-6, etc. Esto indica que, en general, la humedad del suelo de cierto mes está condicionada por lo que llovió los 3 meses anteriores, la humedad del suelo agregada a 3 meses está relacionada con lo que llovió en los 6 meses anteriores, etc. Para ciertas localizaciones en la zona centro y sur de España, la humedad del suelo también se ve condicionada por la temperatura que hubo. Además, es notable la baja correlación existente entre el índice SPEI-1 con las agregaciones 3, 6, 9 y 12 del índice SSMI, indicativo de que la información de precipitación y temperatura de un mes no determina la humedad del suelo de los 3, 6, 9 o 12 meses anteriores. No obstante, para la misma escala

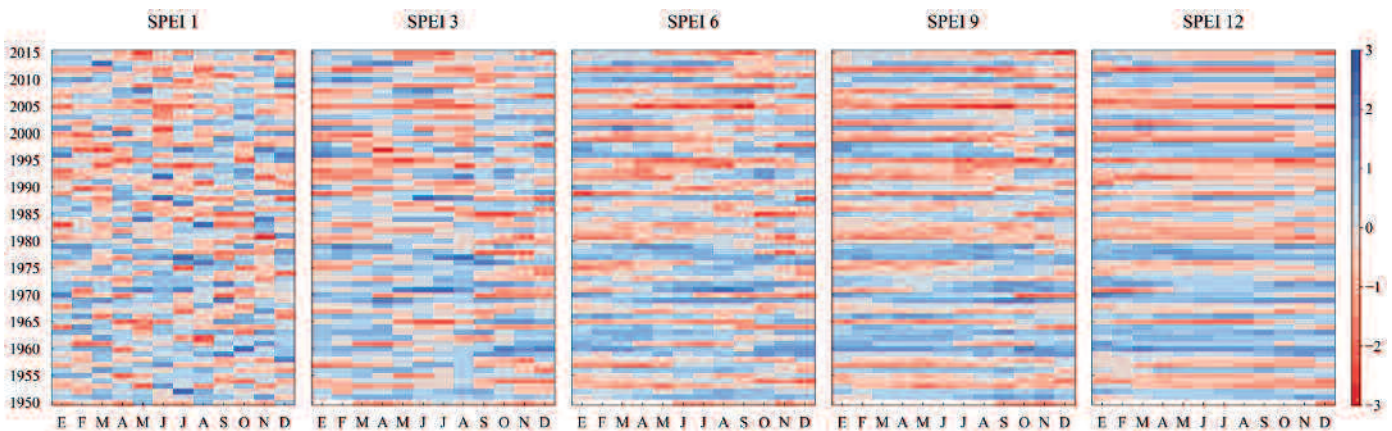
de agregación temporal, la correlación entre los índices SSMI con SPI y SPEI es progresivamente creciente cuanto mayor es la agregación temporal.

Por último, cabe destacar la alta correlación entre el índice SSMI a diferentes agregaciones temporales. Encontramos una fuerte correlación entre los índices SSMI-6 con SSMI-9 y SSMI-9 con SSMI-12, derivando de ella que la humedad media de una ventana temporal de 6 y 9 meses no se va a ver muy modificada por los 3 meses siguientes, pudiendo determinar la humedad media del suelo de un año completo a partir de los 9 meses anteriores. De hecho, se puede apreciar cómo los mapas de SPEI-12 correlacionan de forma prácticamente igual con los mapas de SSMI-9 y SSMI-12. Una excepción a este comportamiento se puede encontrar en la zona norte, donde se observa que la correlación es más baja que en la zona centro o sur de España. Se encuentra que esta situación es la contraria a lo que ocurriría con los mapas de correlación de los índices SPI con SPEI indicando que, en este caso, la humedad del suelo en la zona norte adquiere importancia respecto a las variables precipitación y temperatura.

Agregación espacial

En la Figura 7 se muestran 12 de las 20 series temporales estudiadas para los índices SPEI y SSMI. Nuevamente el índice SPI no se muestra porque, como era de esperar tras observar la alta correlación de los índices SPI y SPEI en su forma distribuida, en su forma agregada son muy similares con ligeros cambios en la intensidad de los índices. Para cada índice, se tiene una serie histórica anual (eje de ordenadas) correspondiente a la agregación de cada índice en cada uno de los meses (eje de abscisas), generándose estas 12 series anuales de enero, febrero, marzo, etc. Se puede observar cómo, a medida que la escala de agregación aumenta, se van reconociendo fácilmente qué años fueron secos y qué años fueron húmedos. Además, para años secos, como por ejemplo el año 2005, se observa ese retraso de 3 meses del SSMI respecto a los índices SPI y SPEI, fundamentalmente para agregaciones a partir de 6 meses.

a)



b)

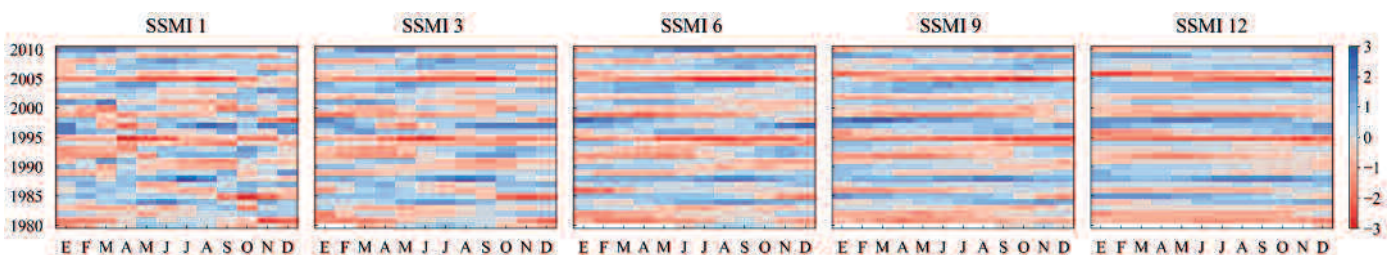


Figura 7 | Series de los índices de sequía SPEI (panel a) y SSMI (panel b) agregados espacialmente a toda la península ibérica.

Para el panel de desviaciones económicas, las mejores correlaciones se obtienen para los índices SPI y SPEI a una agregación temporal de 9 meses para la serie de mayo. En el caso del SSMI, la mejor correlación se obtiene para una agregación de 6 meses y para la serie anual de junio. Estos resultados agregados son consistentes con todo lo comentado en el análisis desagregado con relación a la agregación temporal de 3 meses de diferencia que marcaba la mejor correlación entre los índices SPI y SPEI con el SSMI. A pesar de la alta correlación entre los índices SPI y SPEI, en general se obtienen valores de correlación más bajos para SPEI cuando se cruzan con datos económicos. Esta correlación es aún más baja en la mayoría de las agregaciones del índice SSMI, mejorando únicamente su correlación para una agregación de 1 mes. Además, se puede observar como a medida que aumenta el período de agregación la correlación mejora en la mayoría de las series. Esto indica que las desviaciones económicas no están influenciadas por lo que pueda ocurrir climáticamente un mes del año (de hecho, las correlaciones a agregación de 1 mes son muy bajas), sino que es el conjunto del clima de 9 y de 12 meses lo que marca la desviación económica de cierto año. En cualquier caso, se deduce de estos resultados que es el clima de septiembre a mayo el que mejor correlaciona con las desviaciones económicas de cierto año, sin tanta relevancia para la humedad del suelo. Ese resultado parece tener sentido si se relaciona con los calendarios de siembra de las especies aseguradas. Tanto en uno como en otro tipo, hay de invierno y de primavera. La variedad de invierno se siembra en otoño, entre el 1 de octubre y el 15 de noviembre mientras que la variedad de primavera se siembra del 15 de febrero al 1 de abril. El período crítico para la economía de las desviaciones del riesgo asegurado se produce exactamente en el período de siembra de ambas especies. Además, para la variedad de invierno también abarca su período de recolección.

Para el panel de rendimiento estandarizado de cereales, la mejor correlación se obtiene para el índice SSMI a una agregación temporal de 1 mes para la serie de mayo. En el caso de los índices SPI y SPEI se obtiene una correlación muy similar, siendo la mayor obtenida para la agregación de 3 meses y los meses de mayo. Nuevamente se observa la consistencia con los resultados obtenidos en el análisis desagregado. No obstante, destaca la alta correlación del índice SSMI, con un valor de r de Spearman de 0.92. Esto refleja la importancia que tiene la humedad del suelo en el mes de mayo en la producción de ese año. Este valor va descendiendo para los meses de verano y drásticamente para los meses de otoño e invierno, con resultados que no presentan apenas correlación con el rendimiento de la producción. Si se observa la Figura 1, donde se presentaban los ciclos de precipitación, temperatura y humedad del suelo de la serie histórica, se puede ver que, durante el período de siembra de las variedades de invierno, la precipitación adquiere valores máximos y la temperatura mínimos. Por tanto, es una variedad sembrada en época húmeda y cuyo crecimiento también se produce en una época húmeda. Sin embargo, la variedad de primavera se siembra cuando la precipitación comienza a descender y la temperatura a aumentar, con un crecimiento de la plantación que se va a producir en los meses de mayo y junio, meses en los que las precipitaciones comienzan a descender y la temperatura a ascender. Es, por tanto, un momento mucho más crítico para la producción que el momento en el que se plantan las variedades de invierno. De hecho, se observan también correlaciones altas para el SSMI-3 en estos meses calificados como críticos para la producción.

Por último, en el panel de rendimiento estandarizado de grano grueso, como se ha comentado, se obtiene una situación similar a la descrita en el párrafo anterior. La mayor correlación se obtiene nuevamente para el índice SSMI agregado a 1 mes para la serie formada por los mayo históricos. En general, los valores son algo más bajos que en el caso anterior, sin ser algo notable, pero que puede indicar mayor sensibilidad a la sequía de las especies englobadas en el grupo cereales que las englobadas en el grupo de grano grueso.

Con el objetivo de visualizar de forma gráfica las mejores correlaciones obtenidas, se ha representado en la Figura 10 las diferencias de las desviaciones en el riesgo (arriba), el rendimiento de cereales (centro) y rendimiento de grano grueso (abajo) con las series temporales de SPI, SPEI y SSMI que mejor correlacionan en cada uno de los 3 casos de estudio. Se puede observar el parecido entre las dos series de diferencias referidas a producción. Se puede observar una gran desviación en las series de desviaciones del riesgo de los tres índices en algunos años, como el año 2000. Si se observa la Figura 2, en ese año no solo no existe un pico, sino que parece una desviación favorable y, no obstante, los tres índices estudiados adquieren valores cercanos a -1. Esta situación representa una situación clara en la que el método de umbrales no habría resultado válido, indicando que es un año seco cuando en realidad no ha generado impacto en la economía. Esta situación se repite, aunque menos acentuada, en el caso del rendimiento de producción.

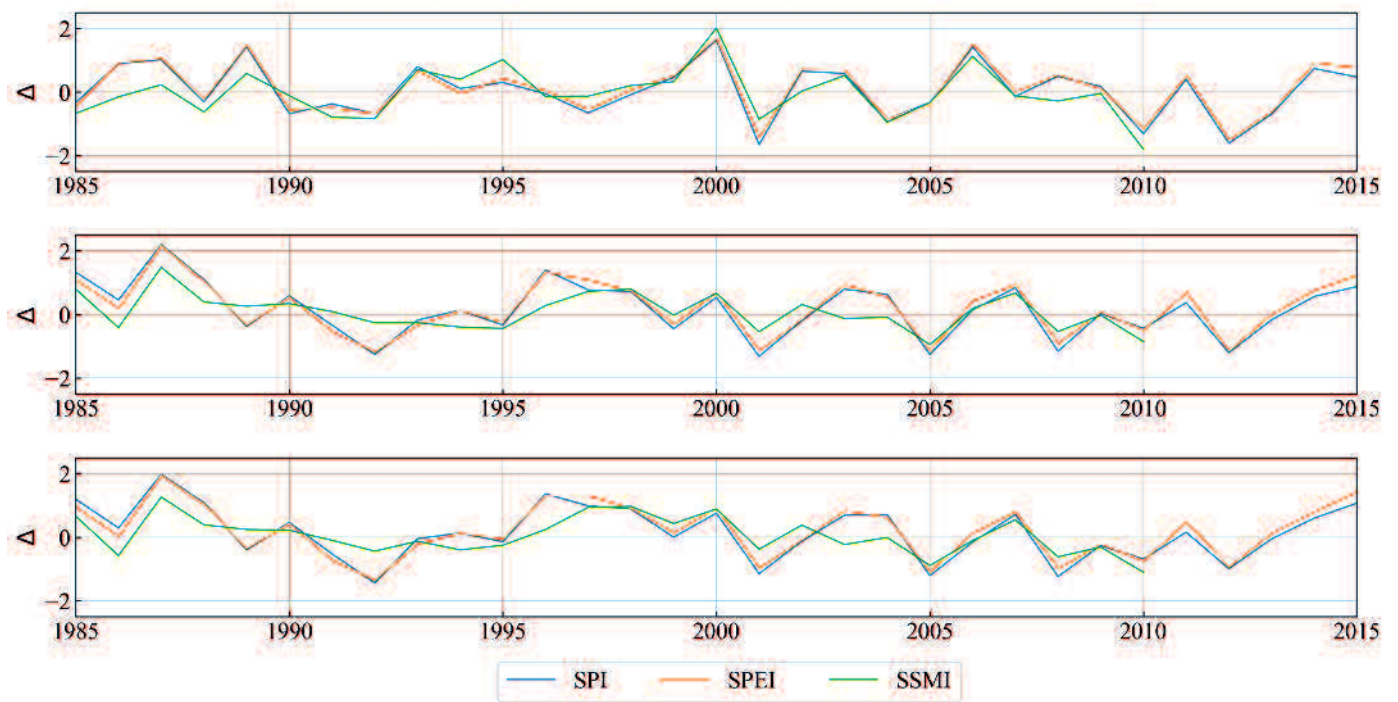


Figura 10 | Desviaciones en el riesgo (arriba), el rendimiento de cereales (centro) y rendimiento de grano grueso (abajo) con las series temporales de SPI, SPEI y SSMI que mejor correlacionan en cada uno de los 3 casos de estudio.

DISCUSIÓN Y CONCLUSIONES

El estudio realizado ha permitido evaluar las grandes sequías históricas ocurridas en España desde el punto de vista de los impactos generados por estos eventos. Se ha comprobado cómo los 3 índices utilizados (SPI, SPEI y SSMI) tienen una estrecha relación con los valores de anomalías económicas y producción agrícola. La escala global del estudio realizado está condicionada por los datos económicos de partida, ya que pertenecen a reaseguradoras y éstas realizan indemnizaciones en situaciones extremadamente adversas. Por tanto, este estudio ha permitido identificar y cuantificar el impacto de las sequías sufridas en todo el territorio español y no de sequías locales.

Se ha observado cómo se produce un mismo comportamiento de los índices cuando estos están agregados espacialmente que en su forma desagregada. Así, las principales conclusiones obtenidas del estudio píxel a píxel son:

- un período de agregación de 9 meses es suficiente para representar el comportamiento anual de los 3 índices,
- los índices SPI y SPEI muestran correlaciones muy altas para los mismos períodos de agregación, siendo la temperatura una variable que afecta principalmente a la zona sur de España,
- el índice SSMI presenta correlaciones muy altas con los índices SPI y SPEI a períodos de agregación de 3 meses de diferencia, concluyendo de ello que, para la humedad del suelo, es más relevante la precipitación y temperatura de los 3 meses previos que del mes en curso o de épocas anteriores a 3 meses.

Para el cálculo del SSMI se han utilizado valores de humedad de suelo simulados y se ha comprobado su bondad con datos de satélite. Se ha visto que, en parte de las celdas de estudio, el valor de correlación es pobre. Esto puede ser debido a que los datos de satélite son incompletos y, en muchas de las celdas de estudio, hay huecos de más de un año de datos. No obstante, el comportamiento en la mayor parte de las celdas (más de un 70%) es bueno.

Del análisis de la relación de los impactos con los índices de sequía, se ha observado que los períodos de agregación que presentan más correlación con las desviaciones de riesgo estandarizadas son diferentes a los períodos de agregación que mejor se correlacionan con el rendimiento estandarizado de la producción. Por ello, identificar sequías a través de los impactos derivados requiere de un estudio específico del período de agregación que mejor lo representa.

En el caso económico, se ha obtenido la mejor correlación para períodos de agregación de 9 meses para el SPI y SPEI y de 6 meses para el SSMI, mostrando esa diferencia de 3 meses entre ambas agregaciones. No obstante, la humedad del suelo parece no ser determinante en la determinación del impacto económico derivado, puesto que su correlación y su coeficiente de determinación han mostrado valores muy pobres. Contrariamente, la precipitación y la temperatura sí parecen ser factores más importantes.

En el caso de la producción, la agregación que presenta mejor correlación es de 3 meses para SPI y SPEI y de 1 mes para SSMI, nuevamente con una diferencia de 3 meses, para los dos grupos de especies estudiados. De esta información se deriva la importancia que tiene la humedad del suelo en el mes de mayo para determinar la producción agrícola anual. Además, la correlación para el caso del SSMI resulta tener valores muy elevados, con lo que se concluye que la humedad del suelo es un parámetro muy importante que considerar en el análisis de sequías cuando se quiere evaluar los impactos reales que éstas generan en la producción de las especies más importantes de España.

De los 3 casos de estudio (económico, producción de cereales y producción de grano grueso), se observa que el SSMI es el índice que mejor se correlaciona de entre todas las relaciones estudiadas, ya que los valores obtenidos de correlación r y r^2 de SPI y SPEI con datos económicos son mucho menores que aquellos obtenidos con el SSMI y datos de producción. Por tanto, queda patente la importancia de la humedad del suelo en el estudio de sequías.

AGRADECIMIENTOS

Los autores agradecen al proyecto INDECIS, que forma parte de la iniciativa ERA 4CS, ERA-NET desarrollada por JPI Climate, y financiada por FORMAS (SE), DLR (DE), BMFWF (AT), IFD (DK), MINECO (ES), ANR (FR) y cofinanciada por la European Union (Grant 690462).

REFERENCIAS

- AEMET. 2012. *Escenarios-PNAC*. http://www.aemet.es/es/serviciosclimaticos/cambio_climat/datos_mensuales/ayuda; <http://www.meteo.unican.es/escenarios-pnacc>.
- Beguiría, S., Vicente-Serrano, S.M., Latorre Fergus Reig, B. 2014. Standardized precipitation evapotranspiration index (SPEI) revisited: parameter fitting, evapotranspiration models, tools, datasets and drought monitoring. *International Journal of Climatology* 34(10), 3001-3023. <https://doi.org/10.1002/joc.3887>
- Beyene, B.S., Van Loon, A.F., Van Lanen, H.A.J., Torfs, P.J.J.F. 2014. Investigation of variable threshold level approaches for hydrological drought identification. *Hydrology and Earth System Sciences Discussions*, 11, 12765-12797. <https://doi.org/10.5194/hessd-11-12765-2014>
- Carrão, H., Russo, S., Sepulcre-Canto, G., Barbosa, P. 2016. An empirical standardized soil moisture index for agricultural drought assessment from remotely sensed data. *International Journal of Applied Earth Observation and Geoinformation*, 48, 74-84. <https://doi.org/10.1016/j.jag.2015.06.011>
- ESYRCE. 2018. *Encuesta sobre Superficies y rendimientos*. Ministerio de Agricultura, Pesca y Alimentación.
- Fleig, A.K., Tallaksen, L.M., Hisdal, H., Demuth, S. 2006. «A global evaluation of streamflow drought characteristics.» *Hydrology and Earth System Sciences*. <https://doi.org/10.5194/hess-10-535-2006>

- Gayathri, K.D., Ganasri, B.P., Dwarakish, G.S. 2015. A Review on Hydrological Models. *Aquatic Procedia*, 4, 1001-1007. <https://doi.org/10.1016/j.aqpro.2015.02.126>
- Global Land Cover Facility*. 2018. <http://www.landcover.org/data/lai/>.
- González-Zamora, Á., Sánchez, N., Pablos, M., Martínez-Fernández, J. 2019. CCI soil moisture assessment with SMOS soil moisture and *in situ* data under different environmental conditions and spatial scales in Spain. *Elsevier*, 225, 469-482. <https://doi.org/10.1016/j.rse.2018.02.010>
- Herrera, S., Fernández, J., Gutiérrez, J.M. 2016. Update of the Spain02 Gridded Observational Dataset for Euro-CORDEX evaluation: Assessing the Effect of the Interpolation Methodology. *International Journal of Climatology*, 36, 900-908. <https://doi.org/10.1002/joc.4391>
- Herrera, S., Gutiérrez, J.M., Ancell, R., Pons, M.R., Frías, M.D., Fernández J. 2012. Development and Analysis of a 50 year high-resolution daily gridded precipitation dataset over Spain (Spain02). *International Journal of Climatology*, 35, 74-85. <https://doi.org/10.1002/joc.2256>
- Homdee, T., Pongput, K., Kanae, S. 2016. A comparative performance analysis of three standardized climatic drought indices in the Chi River basin, Thailand. *Agriculture and Natural Resources*, 50(3), 211-219. <https://doi.org/10.1016/j.anres.2016.02.002>
- Kim, W., Iizumi, T., Nishimori, M. 2019. Global Patterns of Crop Production Losses Associated with Droughts from 1983 to 2009. *Journal of Applied Meteorology and Climatology*, 58(6), 1233-1244. <https://doi.org/10.1175/JAMC-D-18-0174.1>
- King, D.A., Bachelet, D.M., Symstad, A.J., Ferschweiler, K., Hobbins, M. 2015. Estimation of potential evapotranspiration from extraterrestrial radiation, air temperature and humidity to assess future climate change effects on the vegetation of the Northern Great Plains, USA. *Ecological Modelling*, 297, 86-97. <https://doi.org/10.1016/j.ecolmodel.2014.10.037>
- Liu, X., Zhu, X., Pan, Y., Bai, J., Li, S. 2018. Performance of different drought indices for agriculture drought in the North China Plain. *Journal of Arid Land*, 10, 507-516. <https://doi.org/10.1007/s40333-018-0005-2>
- Lopez-Nicolas, A., Pulido-Velazquez, M., Macian-Sorribes, H. 2017. Economic risk assessment of drought impacts on irrigated agriculture. *Journal of Hydrology*, 550, 580-589. <https://doi.org/10.1016/j.jhydrol.2017.05.004>
- Martín Vide, J., Ocina Cantos, J. 2001. *Climas y tiempos de España*. Madrid: Alianza Editorial.
- Martínez, E. 2010. Evaluación del impacto producido por el cambio climático sobre los recursos hídricos de varias cuencas piloto catalanas y navarras. *Tecniberia*, 26, 49-51.
- McKee, T.B., Doesken, N.J., Kleist, J. 1993. *The relationship of drought frequency and duration of time scales*. Anaheim, California: American Meteorological Society, Boston.
- Mishra, A.K., Singh, V.P. 2011. Drought modeling – A review. *Journal of Hydrology*, 403(1-2), 157-175. <https://doi.org/10.1016/j.jhydrol.2011.03.049>
- Ollero Lara, A., Crespo Vergara, S.I., Pérez Cimas, M. 2018. *Las sequías y España. La respuesta del seguro agrario a un problema intermitente*. Madrid: CONAMA.
- Palmer, W.C. 1965. *Meteorological Drought*. Research Paper No. 45, 58. US Weather Bureau, Washington, DC.
- Samper, J., Álvares, D. 2005. *Evaluación de los impactos del cambio climático en los recursos hídricos del río Ebro*. Oficina de Planificación Hidrológica de la Confederación Hidrográfica del Ebro, Dirección General del Agua, Ministerio de Agricultura y Pesca, Alimentación y Medio Ambiente.
- Sheffield, J., Wood, E.F. 2011. *Drought: past problems and future scenarios*. London: Routledge. <https://doi.org/10.4324/9781849775250>
- Trambauer, P., Werner, M., Winsemius, H., Maskey, S., Dutra, E., Uhlenbrook, S. 2014. Hydrological drought forecasting and skill assessment for the Limpopo river basin, Southern Africa. *Hydrology and Earth System Sciences Discussions*, 19, 1695-1711. <https://doi.org/10.5194/hess-19-1695-2015>

Van Loon, A.F., Van Lanen, H.A., Tallaksen, H., Hisdal, L.M., Fendeková, M., Oosterwijk, J., Horvát, O., Machlica, A. 2010. Understanding hydrological winter drought in Europe. Morocco: *Proc. of the Sixth World FRIEND conference*.

Van Loon, A.F., Gleeson, T., Clark, J., Van Dijk, A.I.J.M., Stahl, K., Hannaford, J., Di Baldassarre, G., ... Van Lanen, H.A.J. 2016. Drought in the Anthropocene. *Nature Geoscience*, 9, 89-91. <https://doi.org/10.1038/ngeo2646>

Vicente Serrano, S.M., Beguería, S., Lorenzo-Lacruz, J., Camarero, J.J., López-Moreno, J.I., Azorín-Molina, C., Revuelto, J., Morán-Tejeda, E., Sánchez-Lorenzo, A. 2012. *Análisis comparativo de diferentes índices de sequía para aplicaciones ecológicas, agrícolas e hidrológicas*. Salamanca: Asociación Española de Climatología.

Vicente-Serrano, S.M., Beguería, S., López-Moreno, J.I. 2010. A Multiscalar Drought Index Sensitive to Global Warming: The Standardized Precipitation Evapotranspiration Index. *Journal of climate*, 23, 1696-1718. <https://doi.org/10.1175/2009JCLI2909.1>

Vicente-Serrano, S.M., Lopez-Moreno, J.I., Beguería, S., Sanchez-Lorenzo, A., García-Ruiz, J.M., Azorin-Molina, C., Morán-Tejeda, E., ... Espejo, F. 2014. Evidence of increasing drought severity caused by temperature rise in southern Europe. *Environmental Research Letters*, 9(4). <https://doi.org/10.1088/1748-9326/9/4/044001>

Drought Sensitiveness on Forest Growth in Peninsular Spain and the Balearic Islands

Article

Drought Sensitiveness on Forest Growth in Peninsular Spain and the Balearic Islands

Marina Peña-Gallardo ^{1,*}, Sergio M. Vicente-Serrano ¹, J. Julio Camarero ¹ , Antonio Gazol ¹ , Raúl Sánchez-Salguero ², Fernando Domínguez-Castro ¹ , Ahmed El Kenawy ^{1,3}, Santiago Beguería-Portugés ⁴, Emilia Gutiérrez ⁵, Martín de Luis ⁶ , Gabriel Sangüesa-Barreda ¹ , Klemen Novak ^{6,7}, Vicente Rozas ⁸, Pedro A. Tíscar ⁹, Juan C. Linares ² , Edurne Martínez del Castillo ⁶ , Montserrat Ribas Matamoros ⁵, Ignacio García-González ¹⁰ , Fernando Silla ¹¹ , Álvaro Camisón ¹², Mar Génova ¹³ , José M. Olano ⁸ , Luis A. Longares ⁶, Andrea Hevia ¹⁴ and J. Diego Galván ¹⁵

¹ Instituto Pirenaico de Ecología (IPE-CSIC), 50192 Zaragoza, Spain; svicen@ipe.csic.es (S.M.V.-S.); jjcamarero@ipe.csic.es (J.J.C.); agazol@ipe.csic.es (A.G.); f.dominguez@ipe.csic.es (F.D.-C.); kenawy@ipe.csic.es (A.E.K.); gsanguesa@ipe.csic.es (G.S.-B.)

² Departamento de Sistemas Físicos, Químicos y Naturales, Universidad de Pablo de Olavide, 41013 Sevilla, Spain; rsanchez@upo.es (R.S.-S.); jclincal@upo.es (J.C.L.)

³ Department of Geography, Mansoura University, 35516 Mansoura, Egypt

⁴ Estación Experimental Aula Dei, Consejo Superior de Investigaciones Científicas (EEAD-CSIC), 50192 Zaragoza, Spain; santiago.begueria@csic.es

⁵ Department of Evolutionary Biology, Ecology and Environmental Sciences, Barcelona University, 08028 Barcelona, Spain; emgutierrez@ub.edu (E.G.); mrribas@porthos.bio.ub.es (M.R.M.)

⁶ Departamento de Geografía y Ordenación del Territorio—IUCA, Universidad de Zaragoza, 50009 Zaragoza, Spain; mdla@unizar.es (M.d.L.); kn4@alu.ua.es (K.N.); edurne@unizar.es (E.M.d.C.); lalongar@unizar.es (L.A.L.)

⁷ Departamento de Ecología, Universidad de Alicante, Carretera San Vicente del Raspeig s/n, 03080 Alicante, Spain

⁸ Departamento de Ciencias Agroforestales, EU de Ingenierías Agrarias, iuFOR—Universidad de Valladolid, 42004 Soria, Spain; vicentefernando.rozas@uva.es (V.R.); josemiguel.olano@uva.es (J.M.O.)

⁹ Centro de Capacitación y Experimentación Forestal. C/. Vadillo-Castril, 23470 Cazorla, Spain; pedroa.tiscar@juntadeandalucia.es

¹⁰ Departamento de Botánica, Escola Politécnica Superior de Enxeñaría Campus Terra, Universidade de Santiago de Compostela, 27002 Lugo, Spain; ignacio.garcia@usc.es

¹¹ Departamento de Biología Animal, Parasitología, Ecología, Edafología y Química Agrícola, Universidad de Salamanca, 37071 Salamanca, Spain; fsilla@usal.es

¹² Ingeniería Forestal y del Medio Natural, Universidad de Extremadura, 10600 Plasencia, Spain; alvarocc@unex.es

¹³ Departamento de Sistemas y Recursos Naturales, Universidad de Politécnica de Madrid, 28040 Madrid, Spain; mar.genova@upm.es

¹⁴ Forest and Wood Technology Research Centre (CETEMAS), 33936 Asturias, Spain; ahevia@cetemas.es

¹⁵ Ionplus AG. Lerzenstrasse 12, 8953 Dietikon, Switzerland; galvan@ionplus.ch

* Correspondence: marinapgallardo@ipe.csic.es

Received: 23 July 2018; Accepted: 27 August 2018; Published: 30 August 2018



Abstract: Drought is one of the key natural hazards impacting net primary production and tree growth in forest ecosystems. Nonetheless, tree species show different responses to drought events, which make it difficult to adopt fixed tools for monitoring drought impacts under contrasting environmental and climatic conditions. In this study, we assess the response of forest growth and a satellite proxy of the net primary production (NPP) to drought in peninsular Spain and the Balearic Islands, a region characterized by complex climatological, topographical, and environmental characteristics. Herein, we employed three different indicators based on

in situ measurements and satellite image-derived vegetation information (i.e., tree-ring width, maximum annual greenness, and an indicator of NPP). We used seven different climate drought indices to assess drought impacts on the tree variables analyzed. The selected drought indices include four versions of the Palmer Drought Severity Index (PDSI, Palmer Hydrological Drought Index (PHDI), Z-index, and Palmer Modified Drought Index (PMDI)) and three multi-scalar indices (Standardized Precipitation Evapotranspiration Index (SPEI), Standardized Precipitation Index (SPI), and Standardized Precipitation Drought Index (SPDI)). Our results suggest that—irrespective of drought index and tree species—tree-ring width shows a stronger response to interannual variability of drought, compared to the greenness and the NPP. In comparison to other drought indices (e.g., PDSI), and our results demonstrate that multi-scalar drought indices (e.g., SPI, SPEI) are more advantageous in monitoring drought impacts on tree-ring growth, maximum greenness, and NPP. This finding suggests that multi-scalar indices are more appropriate for monitoring and modelling forest drought in peninsular Spain and the Balearic Islands.

Keywords: normalized difference vegetation index; tree-rings; drought indices; forest productivity; Spain

1. Introduction

Drought is a major hydroclimatic hazard that is difficult to quantify, analyze, monitor and, thus, mitigate [1]. This is because drought has a complex nature, given that it is the result of the synergy among a wide range of variables (e.g., precipitation, temperature, land use, human activities, etc.). Additionally, assessing the impacts of drought on natural and human environments can vary among regions and systems depending on their response and vulnerability. Furthermore, it is difficult to prevent droughts, due to their slow and less evident onset compared to other natural hazards (e.g., floods, landslides, volcanic eruptions), on one hand, and their serious and adverse socioeconomic and environmental impacts, on the other hand [2,3].

Droughts may trigger forest decay and mortality episodes [4,5], which have increased over the last decades in many regions worldwide [6,7]. The Mediterranean region has witnessed frequent and severe drought episodes, inducing important impacts to forests [8,9] given that both primary and secondary growth are constrained by water availability [10]. Some tree species and phenotypes are more sensitive to drought-triggered growth decline and damage [11,12]. Local environmental and climatic conditions can complicate further the response of forests to drought [13,14]. However, assessing forest response to drought is a challenging task, as species [15], and even individuals [16], differ in their sensitivity to this phenomenon. Moreover, spatial variability in climatic and topographic conditions adds a finer grain to drought pattern predictions.

The Iberian Peninsula (IP) is characterized by a great heterogeneity of climate types, ranging from a humid Atlantic climate in the northwest and north to semi-arid Mediterranean conditions in the east and southeast [17]. As such, the response of forests to drought incidence vary markedly over space. In this context, changing climatic conditions (e.g., abnormal low precipitation, temperature rise), mostly during the previous winter of the growing season, cause a reduction in Net Primary Production (NPP), growth decline, as well as forest die-off in some extreme cases [5,18–20]. In Mediterranean forests, radial growth sensitivity to drought intensity varies depending on soil moisture and precipitation, both factors being highly variable in space and time in the region. In particular, while tree growth responses at short time scales are more associated with consecutive periods of dryness and moisture conditions, responses at longer time scales are linked to less frequent, but more intense, drought events [10]. Some Mediterranean species experience a higher recovery to pre-drought growth level at short-term than at long-term timescale, either for declining or non-declining individuals [18]. Nonetheless, a general increase of crown defoliation trend has

been observed in the IP over the last decades, especially in drier areas, where tree mortality is also related to dynamic changes at the trophic level as a consequence of drought impacts related to climate warming [21].

Forests are an important component of the terrestrial ecosystems dynamics, given its capital role in the hydrological and carbon cycles [22,23]. Furthermore, forests are sources for minerals, agricultural products, recreation and other benefits to mankind [4]. In this respect, Zhao et al. [24] found that drought is the leading cause of global NPP depletion. The eco-physiological impacts drought causes in vegetation are diverse [25], with some plant responses to drought stress related to stomata regulation, osmotic adjustment, and anti-oxidative defense [26]. However, reduction of photosynthesis is the ultimate impact of drought. Dramatic changes in primary metabolism lead to a decline in leaf net carbon uptake as a consequence of a decrease in water availability [27]. A prolonged reduced photosynthetic activity may lead to the decrease of molecular oxygen and the increase of reactive oxygen species inducing important damage to the photosynthetic apparatus [28]. Accordingly, the response of forests to drought has been a matter of interest in the scientific community [29–31]. In this context, a comprehensive assessment of the links between drought, NPP, and secondary growth among different forest ecosystems is still lacking.

Dendrochronological techniques have quantified secondary growth over time in a wealth of tree species [10,11,32,33]. Tree-rings provide short- to long-term information about annual radial growth, a proxy of carbon uptake and NPP [34]. Tree-ring width data have been used to identify the effects of drought on forest growth and vitality [20,35]. However, few dendrochronological studies have related tree-ring width data with surrogates of primary growth and NPP at consistent temporal (long) and spatial (broad coverage) scales [36]. Vegetation indices derived from satellite remote-sensing data, have proven valuable to monitor forests from local [37–39] to global scales [40]. The Normalized Difference Vegetation Index (NDVI) is commonly used to quantify the photosynthetic activity, which is closely related to the total biomass production and the vegetation NPP [41,42]. In the same context, a wide range of drought indices have been developed over the last decades [43,44]. These indices are well-recognized as useful tools for assessing drought under different hydrological and agricultural conditions [3,45–47].

The aims of this work are two-fold. First, it aims at comparing and assessing the performance of a range of drought indices for monitoring the response of vegetation activity, as summarized by tree-ring width, maximum annual greenness, and a surrogate of the NPP, to drought impacts. Second, it assesses and contrasts the response of tree-ring width and NDVI to drought conditions for different species. To accomplish this task, we linked seven widely used drought indices: Standardized Precipitation Evapotranspiration Index (SPEI), Standardized Precipitation Index (SPI), Standardized Palmer Drought Severity Index (SPDSI), and four Palmer-related drought indices (Palmer Drought Severity Index (PDSI), Palmer Hydrological Drought Index (PHDI), Palmer Z-Index (Z), and Palmer Modified Drought Index (PMDI)) with climatic, NDVI, and dendrochronological data for the IP and the Balearic Islands for the period 1981–2015. As a result we should be able to assess the validity of these drought indices to assessing and monitor the impacts of drought on forest growth and vitality [48–50].

2. Data and Methods

2.1. Datasets Description

We employed a daily dataset of meteorological variables (precipitation, maximum and minimum air temperatures, wind speed, sunshine duration and relative humidity) provided by the Spanish National Meteorological Agency (AEMET). The original dataset was subjected to a rigorous procedure to ensure data quality and homogeneity. Daily records were aggregated to weekly data and gridded at a 1.1 km resolution. Further details about data development are outlined in Vicente-Serrano et al. [51]. Based on the available input variables, we also calculated reference evapotranspiration (ET_o) using

the Penman-Monteith equation recommended by the FAO [52]. For this analysis, we aggregated the weekly gridded data at monthly scale for the period 1981–2015.

2.2. NDVI Data

The Normalized Difference Vegetation Index (NDVI) is widely-used to assess vegetation activity, with a good agreement with the photosynthetically-active radiation absorbed by vegetation [41,53]. Here, we employed NDVI data at 1.1 km resolution for the period 1981 to 2015 at a monthly time scale aggregation [54]. The original data were obtained from the National Oceanic and Atmospheric Administration (NOAA) polar orbiting satellites that used the Advanced Very High Resolution Radiometer (AVHRR) sensors to provide daily satellite images. Our selection allowed to characterize vegetation activity with more detailed spatial coverage and finer temporal resolution than other publicly available data sets such as the Global Inventory Monitoring and Mapping Studies (GIMMS) and the Moderate-Resolution Imaging Spectroradiometer (MODIS) [41,51,52]. In order to obtain the final NDVI product, the original data were subjected to a series of data processing, including radiometric calibration [55,56], geometric and topographic corrections [57,58], cloud cover removal [59] to obtain semi-monthly composite images by maximum NDVI value (two images per month) [60]. A comprehensive explanation of this procedure is found in Vicente-Serrano et al. [54].

2.3. Tree-Ring Width Data

We compiled annual tree-ring width chronologies of 568 forest stands covering the majority of forest areas across the IP and the Balearic Islands from 1981 to 2015 (Figure 1). Chronologies were obtained using the basic dendrochronological protocol [34]. At least 10 dominant or codominant trees located in undisturbed stands were selected and cored at 1.3 m using increment borers to obtain 2–3 cores per tree in each forest. The selected study sites represent a wide sample of conifers and hardwood species subjected to different climatic and edaphic conditions along the Spanish territory. Latitude, longitude, and mean elevation were recorded at each sample. Wood samples were air-dried and sanded until rings were clearly visible and then visually cross-dated. Tree-ring width was measured to at least the nearest 0.01 mm using binocular microscopes and measuring device systems (Lintab, RinnTech, Heidelberg, Germany; Velmex Inc., Bloomfield, NY, USA). In order to check the accuracy of visual cross-dating and measurements, we used the COFECHA program, based on moving correlations between each individual tree-ring series and the mean site series [61]. Additionally, to remove the trends in tree-ring width due to tree aging and the enlargement of the stem, we used traditional dendrochronological protocols [34]. Specifically, we detrended each individual tree-ring width series by fitting negative exponential curves and then obtained the residuals through dividing the observed values by the fitted ones. Then, we averaged the detrended series of tree-ring width indices (hereafter TRWi) for each forest by computing bi-weight robust means. The mean site-level chronology represents the average growth series of a variable number of trees of the same species growing at the same forest stand. Since no autoregressive modelling was performed, we removed the low- to mid-frequency variability, while keeping the high-frequency variability and the first-order autocorrelation. The procedure of chronology building was implemented using the ‘dplR’ package within the R platform [62]. Table 1 summarizes the main characteristics of the tree species used in this study.

Table 1. List of tree species, abbreviations, and number of the sampled forests stands; including the average mean annual temperature and precipitation of each species location.

Gymnosperms					Angiosperms		
Tree Species	Abbreviation	Number of Sampled Forests Stands	Mean Annual Temperature (°C)	Annual Precipitation (mm)	Tree Species	Abbreviation	Number of Sampled Forests Stands
<i>Abies alba</i>	ABAL	48	13.10	1439.98	<i>Fagus sylvatica</i>	FASY	51
<i>Abies pinsapo</i>	ABPN	15	17.53	1467.33	<i>Quercus pyrenaica</i>	QUPY	34
<i>Pinus halepensis</i>	PIHA	119	19.93	599.87	<i>Quercus robur</i>	QURO	34
<i>Pinus sylvestris</i>	PISY	76	14.80	958.32	<i>Quercus faginea</i>	QUEFA	19
<i>Pinus nigra</i>	PINI	66	17.05	754.00	<i>Quercus ilex</i>	QUIL	5
<i>Pinus uncinata</i>	PIUN	39	10.11	1442.68	<i>Quercus petraea</i>	QUPE	7
<i>Pinus pinaster</i>	PIPI	20	18.52	705.30	<i>Castanea sativa</i>	CASA	10
<i>Pinus pinea</i>	PIPIN	9	19.98	550.89			
<i>Juniperus thurifera</i>	JUTH	16	17.22	690.59			

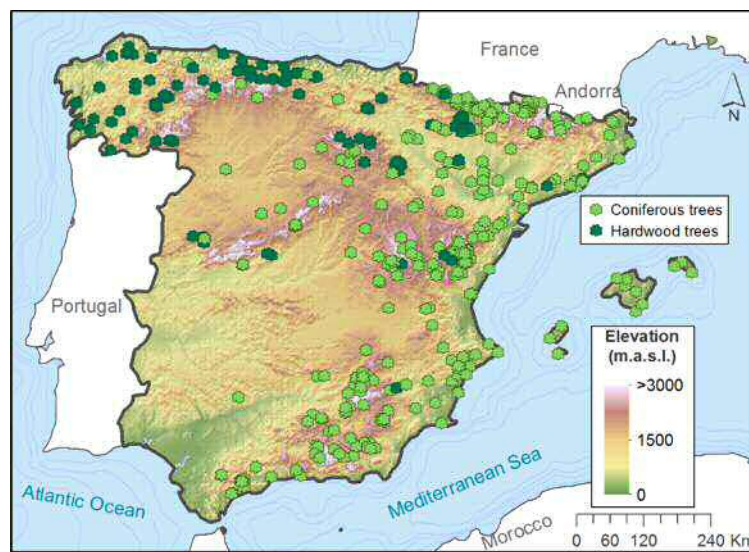


Figure 1. Location of the sampled forest stands in the study domain. Note that the conifer forests ($n = 408$ sites) dominate in the driest regions (Mediterranean climate) of Eastern and Southeastern Spain, and also in mountainous terrain, while hardwood forests prevail in the wettest and temperate regions (Atlantic climate) in Northwestern and Northern Spain ($n = 160$ sites).

2.4. Drought Indices

We computed the seven drought indices based on the monthly climate data for each location to each sampled forest stand as the time of response to drought indices is not known beforehand, described as follows.

2.4.1. Palmer Drought Severity Indices (PDSIs)

The Palmer Drought Severity Index (PDSI) is a well-known meteorological drought index proposed by Palmer [63] along with the Palmer Hydrological Drought Index (PHDI), the Palmer Moisture Anomaly Index (Z-index), and the Palmer Modified Drought Index (PMDI). While Palmer indices account for supply-demand relationship of soil moisture using precipitation and air temperature data, our preference was to use a modification of the original methodology to limit the possible impact of lack of comparability between differentiated regions [64–66]. This issue was solved by Wells et al. [62] who employed the self-calibrated Palmer indices algorithm, which automatically determines the appropriate and spatially-comparable regional coefficients. Hereafter, we will use the original acronyms to refer to the self-calibrated versions of Palmer drought indices. As opposed to multiscale drought indices (e.g., SPI, SPEI, SPDI), PDSIs are uni-scalar.

2.4.2. Standardized Precipitation Index (SPI)

The Standardized Precipitation Index (SPI) was developed by McKee et al. [67]. The SPI introduced for the very first time a new functional definition of drought based on the standardized precipitation and time scales to quantify precipitation shortages along time. The index is based on the conversion of the precipitation series using an incomplete Gamma distribution to a standard normal variable with the mean equal to zero and variance equal to one. The SPI is the universal reference meteorological index according to the World Meteorological Organization [68].

2.4.3. Standardized Precipitation Evapotranspiration Index (SPEI)

The Standardized Precipitation Evapotranspiration Index (SPEI) was proposed by Vicente-Serrano et al. [69], accounting for the possible impact of reference evapotranspiration

on drought. In particular, the SPEI is based on the computation of monthly climate water balances (precipitation minus reference evapotranspiration) accumulated at different timescales. The resulting values are later transformed to a normal standardized variable using a three-parameter log-logistic distribution, allowing for direct comparison over space. The SPEI has been widely used in multiple drought-related studies, with a main focus on evaluation of drought impacts, recurrence, variability, or reconstruction.

2.4.4. Standardized Precipitation Drought Index (SPDI)

The Standardized Precipitation Drought Index (SPDI) was introduced by Ma et al. [70]. It is defined as a combination of the PDSI and SPI. It also implements the timescale concept and the statistical nature of the SPI and SPEI [71] as well as the water balance concept defined by Palmer [64]. For its calculation, the SPDI-accumulated values are transformed to a standard normal variable using a generalized extreme value distribution.

Herein, the multi-scalar indices (i.e., SPEI, SPI and SPDI) were calculated at 1- to 12-, 18-, and 24-timescale. It is noteworthy emphasizing that the monthly drought indices, for each sampled tree, were detrended by fitting a linear regression with the time series. This procedure removes any possible trend that can disturb the comparison among drought and tree-ring growth, given that tree-ring series were already detrended. Finally, the residual of each series was obtained from linear models, and summed to the average of the period to obtain the detrended drought indices.

2.5. Statistical Methods

We assessed the response of vegetation activity to the interannual variations of drought for the common period of time 1981–2015. To achieve the mentioned purpose, three indicators were considered: TRWi, maximum annual NDVI value (NDVI max) and annual integrated NDVI. The NDVI max was obtained from the biweekly series of the NDVI, providing information on the maximum potential vegetation activity in each sampled forest stand. As such, it is considered a reliable indicator of the annual vegetation growth [72]. In this work, the annual cumulative NDVI (NDVI annual) is used as a surrogate of NPP. This is simply because the NPP, defined as the net carbon accumulated by plants per unit and time [73], is closely related to the amount of photosynthetically active radiation (PAR) captured by green foliage. Thus, the NPP depends on the fraction of photosynthetically active radiation (FPAR) absorbed by the canopy [74].

We computed the Pearson correlation coefficient between the TRWi, NDVI max, and NDVI annual and each drought index for the common period 1981–2015. To keep consistency among all variables, we also detrended the NDVI variables. Since the response of vegetation to drought is expected to vary at different time scales [40], and the month when the vegetation is most susceptible to drought is not known a priori, we correlated the 12 monthly series of each drought index with the annual series of TRWi, NDVI max, and NDVI annual and kept the maximum correlation value for analyzing spatial and temporal responses of tree variables to drought and the relationship between vegetation variables and drought by species. We calculated the indices at 1- to 12-, 18-, and 24-month time-scales for the multi-scalar indices (SPEI, SPI, and SPDI). This procedure resulted in 168 correlation values (12 correlations for each time-scale) for the multi-scalar indices and 12 correlations for the uni-scalar indices. We also calculated the climatic water balance as the difference between precipitation and evapotranspiration ($P-ET_o$) at each sampled forest stand.

3. Results

3.1. Spatial and Temporal Responses of Tree Variables to Drought

The magnitude of maximum Pearson correlations found between each of the selected drought indices and the three tree variables (TRWi, NDVI max, and NDVI annual) varied considerably between the two main groups of drought indices: multi-scalar vs. uni-scalar (Figure 2). In general,

multi-scalar indices had higher correlations than for uni-scalar indices. Remarkably, TRWi had higher correlations with drought indices than NDVI max and NDVI annual. This pattern was evident for all drought indices (Figure 2). Correlation values averaged 0.60 for TRWi, and 0.45 and 0.40 for NDVI annual and NDVI max, respectively. Among the uni-scalar drought indices, the Z-index showed the highest correlations, particularly with TRWi, although a high percentage of correlations for the four Palmer indices was statistically non-significant. Among multiscalar indices, SPEI showed the highest correlations with TRWi and NDVI max, while the SPI correlated better with the NDVI annual (Table 2).

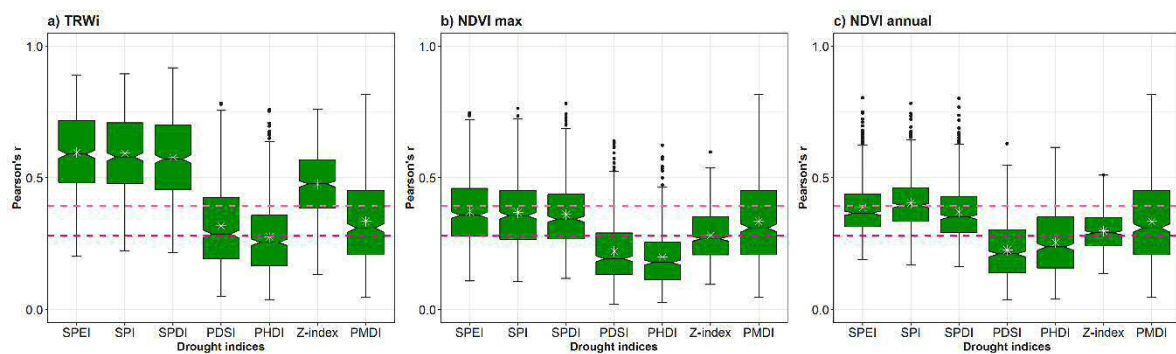


Figure 2. Box plots showing the Pearson correlation coefficients computed between the seven drought indices and ring-width indices, including (a) TRWi, (b) NDVI max, and (c) NDVI annual. The solid black line corresponds to the median, the white asterisks denote the mean and dashed lines show the significant level at $p < 0.05$ (light pink) and $p < 0.01$ (dark pink).

Table 2. Percentage of the sampled forest stands, with the maximum Pearson correlation coefficients found for each forest variable and with each drought index.

	TRWi	NDVI Max	NDVI Annual
SPEI	38.97	43.25	33.50
SPI	35.73	32.48	53.16
SPDI	25.30	24.27	13.33

The spatial distribution of maximum Pearson correlations between the seven drought indices and vegetation variables in each sampled forest stand is shown in Figure 3. The three multi-scalar drought indices showed similar spatial patterns, with higher values ($r = 0.6–1.0$) in forests located mostly in dry areas of Eastern Spain and the Balearic Islands (Figure 3). In contrast, correlations were lower in Northern Spain, where wet conditions prevail and hardwood forests dominate. The highest correlation values for the Palmer drought indices showed spatial patterns similar to those of the multi-scalar indices, albeit with lower magnitudes of correlation. Among the uni-scalar indices, Z-index and TRWi showed the highest correlations followed by PMDI and TRWi, with values ranging between 0.4 and 0.6. In contrast, PDSI and PHDI had the lowest correlations. The differences between PMDI–Z-index and PDSI–PHDI results were less evident for other variables (i.e., NDVI max and NDVI annual), with low ($r = 0.2–0.4$) and spatially homogeneous correlations. Similar results are found for the magnitude and the distribution of the maximum correlations for the NDVI max and NDVI annual. Regarding the SPI, higher correlations ($r = 0.4–0.6$) are found in Northwestern Spain for NDVI annual. The correlations between the SPEI/SPDI and NDVI annual tend to be higher in Southeast Spain than for NDVI max. Additionally, we noted that there are no clear spatial differences in the correlations found between the Palmer drought indices and NDVI max and NDVI annual.

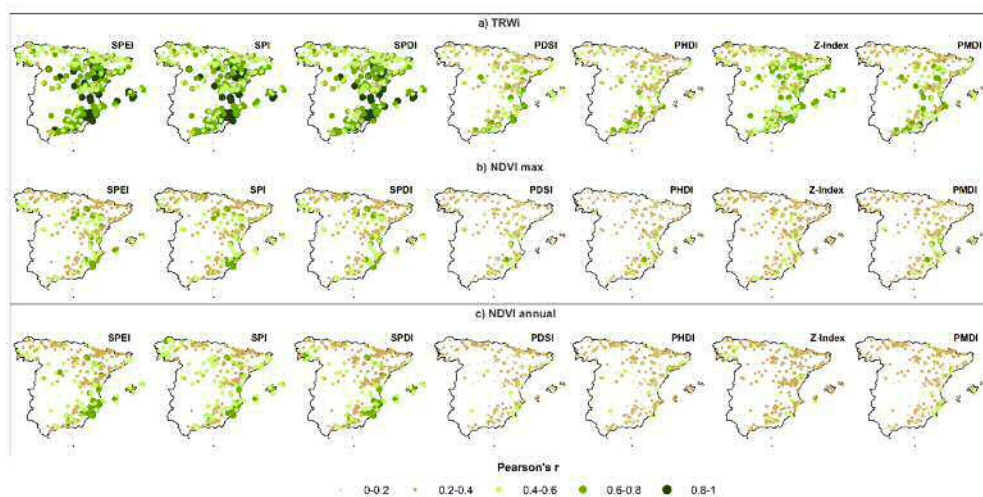


Figure 3. Spatial distribution of the maximum Pearson correlation coefficients computed between the seven drought indices and ring-width indices TRWi (a), NDVI max (b), and integrated annual NDVI (c).

In general, it is evident that TRWi shows a higher response to the interannual variability of drought than the NDVI max and NDVI annual. Figure 4 shows the relationship between the maximum correlations obtained relating TRWi and drought indices and those obtained for the NDVI annual and NDVI max. It can be noted that maximum correlations are much higher considering TRWi than NDVI metrics. Moreover, there are no clear relationships between the spatial patterns of the correlations. In particular, the highest correlations between drought indices and TRWi did not imply the highest correlations with NDVi metrics. The highest percentages of maximum correlations between TRWi and multi-scalar drought indices were in July (43.08%) and August (40.69%) (Table S1). SPEI correlated better with TRWi in July (17.09%), while the SPI and SPDI showed better association with TRWi in August (15.9% and 12.65%, respectively). In contrast, NDVI max showed highest percentage of maximum correlations in April (63.16%) and May (32.99%); the three drought indices also correlated most in April, with very similar percentages (SPEI: 21.28%, SPI: 21.11% and SPDI: 20.77%). For NDVI annual, the majority of forests showed their best correlations in May (90.94%), particularly for the SPEI (37.61%), the SPI (32.48%), and the SPDI (20.85%). Thus, two distinct temporal patterns could be observed depending on the analyzed parameter, whereas secondary growth response to drought severity reached a maximum in July and August, annual vegetation growth (NDVI max) and NPP (NDVI annual) showed a much earlier response to drought in springtime (April and May).

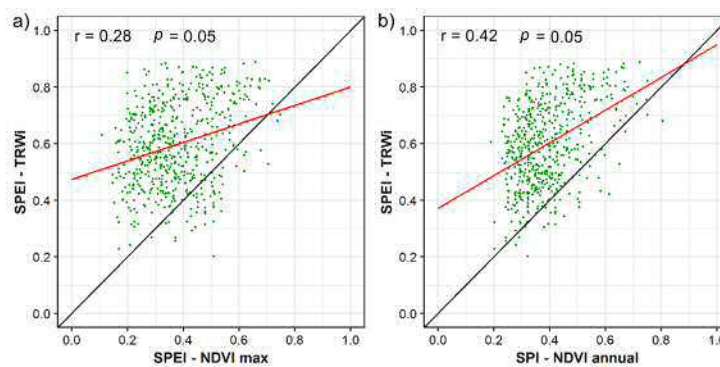


Figure 4. Scatterplots showing maximum Pearson correlation coefficients found for SPEI-TRWi and SPI-NDVianual (a) and SPEI-TRWi and SPEI-NDVImax (b). The solid red line corresponds to the fitted linear regression model and black line, 1:1.

3.2. Relationship between Vegetation Variables and Drought by Species

Among tree species, there are no clear differences in the correlations between the multi-scalar drought indices and NDVI annual and NDVI max (Figure 5). In contrast, the correlations with TRWi show higher variability amongst tree species. Generally, the NDVI metrics suggest that species characteristics of moist and cold regions (e.g., *Abies alba* and *Pinus uncinata*) tend to show lower correlations than species of semi-arid climates (e.g., *Pinus halepensis*).

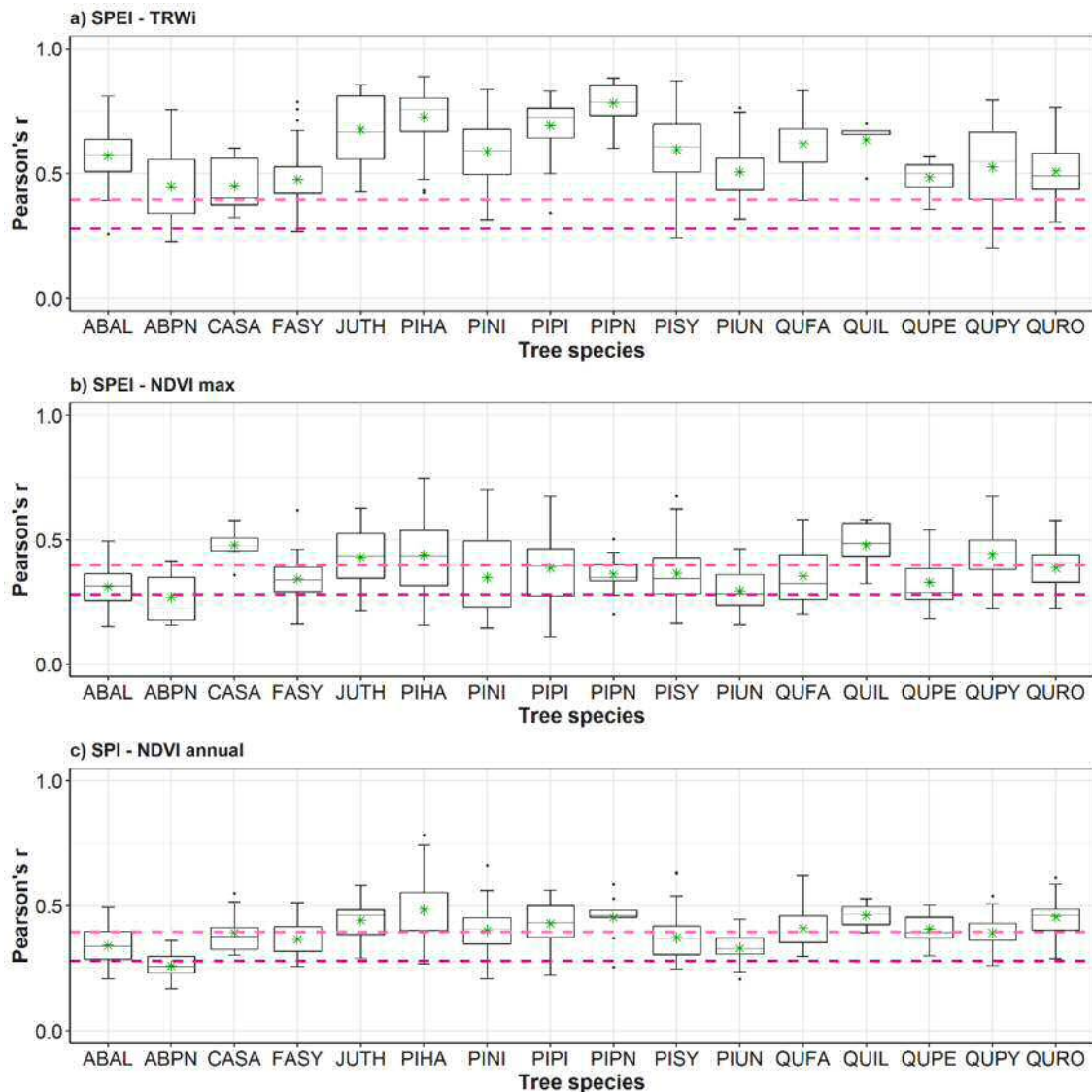


Figure 5. Box plots showing maximum Pearson correlation coefficients computed between ring-width indices (TRWi, (a)), NDVI max (b), NDVI annual (c), and the most correlated drought index for each tree species. The solid black line corresponds to the median, green asterisks mark the mean and dashed lines show the significance level at $p < 0.05$ (light pink) and $p < 0.01$ (dark pink). Species' codes correspond to those listed in Table 1.

Conifers from dry regions (*Pinus halepensis*, *Pinus pinaster*, and *Juniperus thurifera*) recorded the highest correlation coefficients in the case of TRWi ($r = 0.70$); on the contrary, conifers (*Abies pinsapo*) and hardwood species (*Castanea sativa* and *Fagus sylvatica*) from wet and temperate regions recorded lower correlations ($r = 0.45$). The response of the species to NDVI max—SPEI relationship was more evident for two species dominant in dry areas: *Pinus halepensis* and *Quercus ilex* ($r = 0.5$). In Figures S1 and S2

are displayed the maximum correlations (S1) and Pearson's partial correlations (S2) for the rest of the indices and variables considered in the analysis for each tree species respectively.

According to Figure 6, the response to medium (4–6 months) to long (>6 months) drought time-scales are frequently observed. Several tree species (e.g., *Quercus ilex*, *Quercus faginea*, *Pinus pinaster*, *Pinus pinea*, *Pinus halepensis*, and *Castanea sativa*) exhibited similar long time-scale responses in the three forest variables. It seems that the response of the interannual variability of tree metrics to drought was not only driven by the differences among species, but also by the general hydro-climatic conditions. Figure S3 illustrates the most correlated time-scale found for the rest of the multi-scalar drought indices and variables considered in the analysis for each tree species respectively.

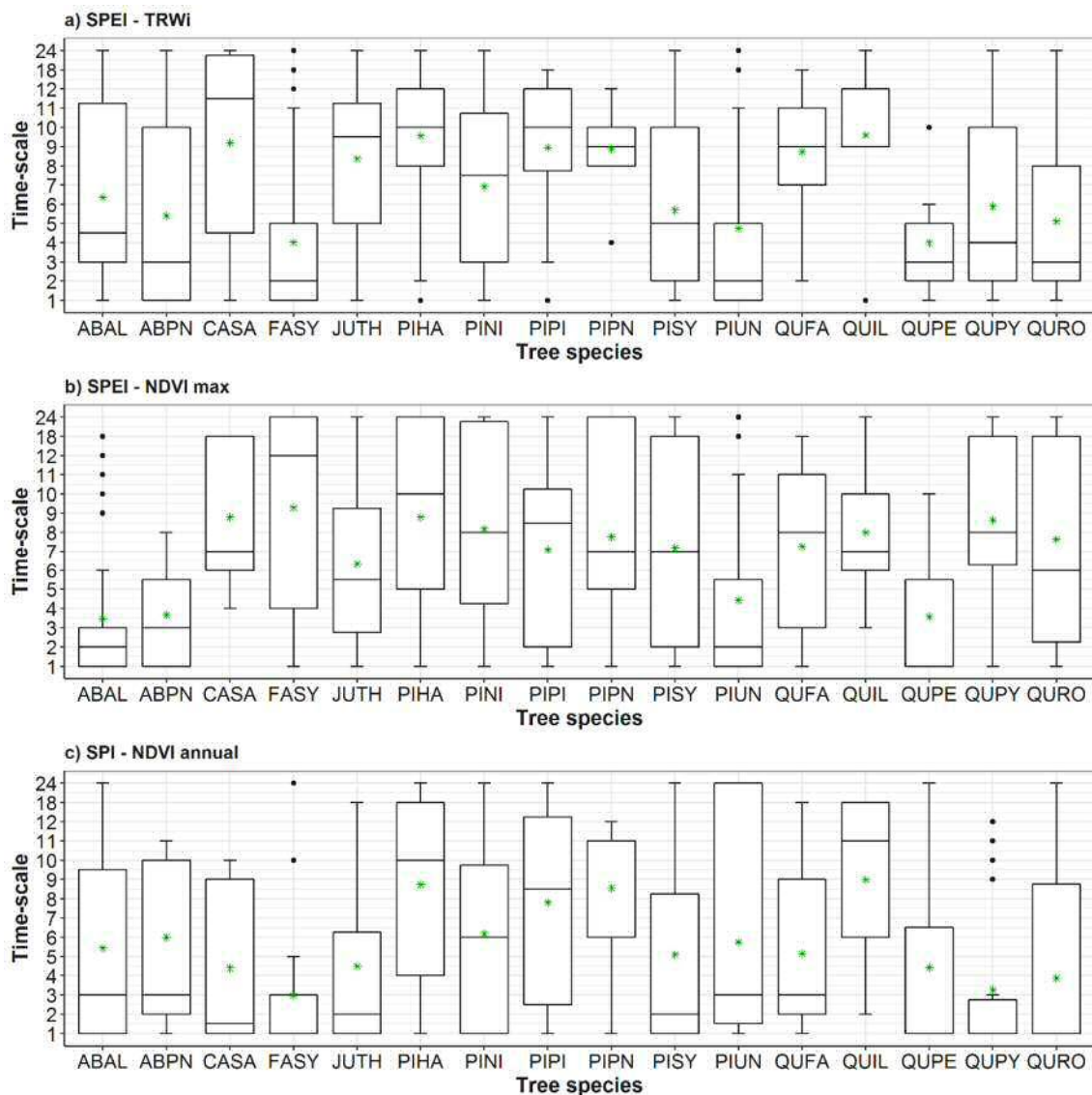


Figure 6. Box plots showing the most correlated timescale found for ring-width indices (TRWi, (a)), NDVI max (b), NDVI annual (c), and the most correlated drought index. The solid black line corresponds to the median, green asterisks mark the means. Species' codes correspond to those listed in Table 1.

Figure 7 illustrates the relationship between the average annual hydro-climatic balance for hardwoods and coniferous species and the correlation found between the most correlated drought index and each of the three variables. As depicted, most conifer forests were characterized by negative

annual hydro-climatic balances, while half of hardwood forests, mainly those located in humid and mountainous regions, showed a positive hydro-climatic balance. Figures S6–S8 summarize this relationship for each species and variable.

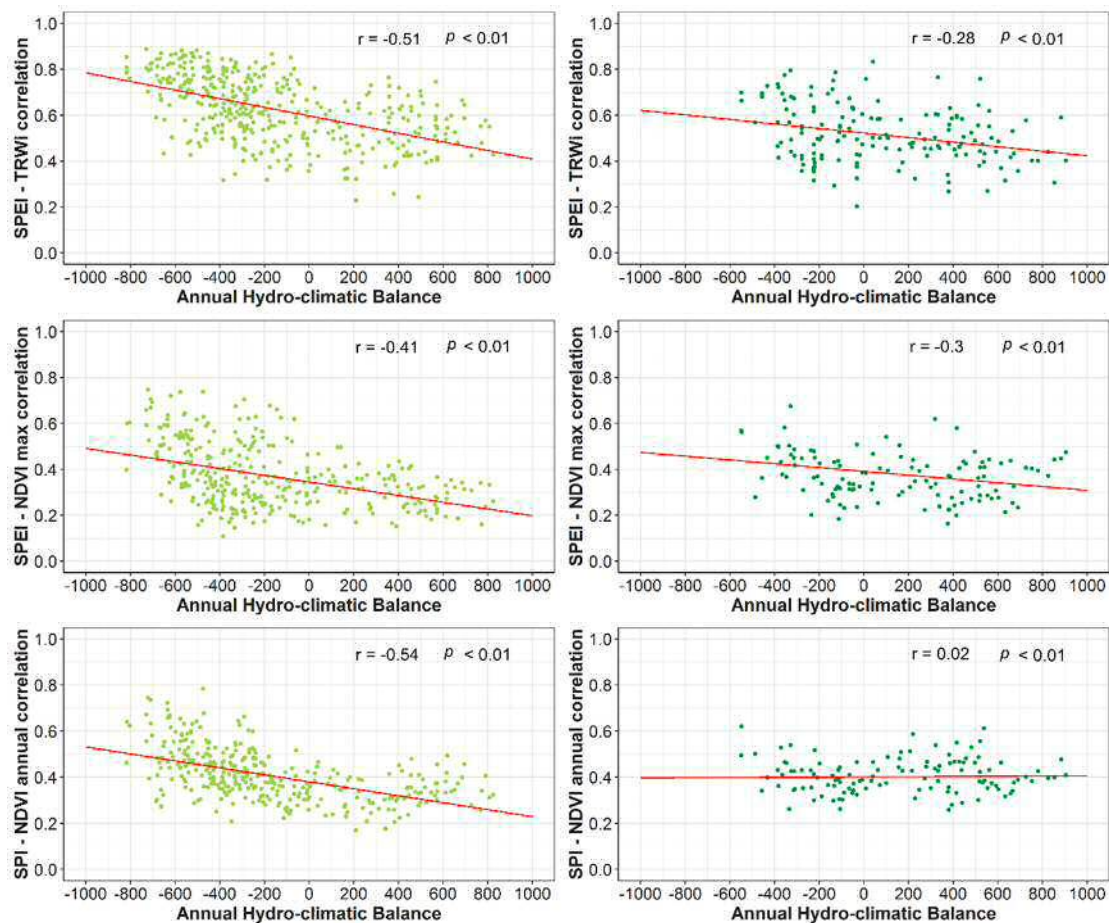


Figure 7. Scatter plots showing the relationship between maximum Pearson correlations found for SPEI-TRWi, SPEI-NDVImax, SPI-NDVIannual, and the average annual water balance of hardwood species (**right**, dark green) and conifers (**left**, light green). Solid red line corresponds to the fitted lines of regression models.

4. Discussion

This study addressed the sensitivity of several drought indices to record responses of NDVI metrics and tree growth to water shortage. In general, we found that multi-scalar drought indices (e.g., SPI, SPEI) outperform uni-scalar drought indices (PDSIs) in terms of capturing the impacts of water shortage on forest growth and NDVI metrics. Likewise, this study assesses the performance of different drought indices to adequately monitor the impact of drought on forests under different climatic and geographical conditions, and taxonomic origins. Our analysis is based on two promising datasets covering the IP and the Balearic Islands. The first comprises tree-ring width data from a dense network of 568 forests for 16 tree species [75]. The second includes a 1.1 km spatial resolution NDVI dataset that allows for detecting the growth and NDVI signal in each forest stand, reducing the interferences associated with the non-related vegetation cover [54]. Changes in vegetation due to adverse environmental conditions have been addressed in the scientific literature from different methodological perspectives. Tardieu et al. [76] proposed a probabilistic approach based on the genetic variability to study the adaptive mechanisms of vegetation to uncertain climatic conditions as drought to contribute to the tolerance of major crops to deal with them. For its part, Almeida et al. [77]

developed a systematic methodology to study the spectral differences of vegetation, discriminate between vegetation assemblages, and assess the phenology of plants applying a principal component analysis to band ratios. They found significant differences in comparison to most traditional approaches such as the NDVI. Previous studies also examined the links between vegetation activity and drought events assessing the response of NDVI to drought using drought indices for finding links between vegetation activity and drought events [78]. Some studies also quantified the impacts of drought on forest growth using dendrochronological methods and multi-scalar drought indices [10], while others assessed the relationship between NDVI and tree-ring width data [32,38,79].

However, very few studies have assessed the varying response of vegetation to various drought indices [48,80,81], considering NDVI and tree-ring width data for different tree species, taxonomic groups and biogeographical regions.

This study demonstrates that TRWi and NDVI metrics show different responses to multi-scalar drought indices (Figures S4 and S5), highlighting the different relationship between wood production and canopy greenness or activity (NPP) with drought. TRWi was more responsive to drought severity than the NDVI metrics. Similar results have been observed by Gazol et al. [75] for Spain, as they noted that tree growth is more sensitive to extreme climate events than the above-ground photosynthetic biomass. They attributed this pattern to: (1) the dependence of leaf and wood formation processes on water availability, (2) the distortion of NDVI signal as a consequence of the spatial resolution, and (3) the effect of nearby vegetation. A similar finding was also observed by Aaltonen et al. [82] who indicated that drought led to a decline in the growth of Scots pine seedlings due to stress. In contrast, the photosynthetic rates did not decrease due to drought, confirming the physiological adaptations (e.g., larger root network) to deal with water scarcity. Similarly, McDowell et al. [83] described different mechanisms to explain mortality caused by drought and water stress. These mechanisms include biotic stressors, hydraulic failure, and carbon starvation. Additionally, numerous studies confirmed that—under soil moisture deficit scenarios—forests can maintain their photosynthetic capacity [84], while dehydration associated with long periods of xylem conductivity loss inevitably can induce tree dieback [85,86]. Thus, it is acceptable that sensitivity of secondary growth to drought is greater than that of the photosynthetic activity. It is also important to consider that, albeit with the high dependence of spectral measurements on the amount of leafy biomass and primary production [41], remotely-sensed vegetation indices (e.g., NDVI) are limited, given that saturation problems can occur, especially in regions with high biomass and strong chlorophyll absorption in the red and near-infrared bands [87,88]. This feature may add further uncertainty to the obtained results, particularly at regional scales.

Our findings on the performance of the different drought indices stress the superiority of multi-scalar indices over the uni-scalar indices. This is clearly evident for the three vegetation indicators considered in this study. In this context, Bhuyan et al. [80] employed a range of drought indices to evaluate the connection between drought and tree growth of nine tree species across Europe. In their comparison of multi-scalar drought indices (i.e., SPI and SPEI) and the self-calibrated PDSI, they found a good agreement for *F. sylvatica* forests between the correlation values found for the Palmer index and the SPEI-SPI at long time scales (>12 months). On the other hand, the SPEI and SPI captured drought signals in the growth series of all tree species, especially in temperate and cold forests. Our results suggest that the Z-Index and the PMDI show more significant and higher correlations with TRWi compared with the PDSI. In this regard, Karl [89] stated that, for some agricultural and forest fires applications, the Z-Index outperforms PDSI given its competence to respond to short-term moisture variances. In our case, the highest correlations of the Z-Index were found for TRWi. In their global assessment, Vicente-Serrano et al. [48] indicated that growth-drought correlations were stronger for the SPI and SPEI indices than for the PDSI and the Z-Index. They also found that a higher percentage of forests from different biomes across the world correlated better with the SPEI than with the SPI. For its part, Bachmair et al. [50] assessed the relationship between meteorological indicators and forests in Europe, suggesting slight differences between the SPEI and SPI. Nonetheless, they noted

that—at shorter time scales—the SPEI shows a stronger response in the forests of southern Europe, a result that is in agreement with the findings of our study.

Our findings also demonstrate that the strength of correlations and timing response to drought vary spatially depending on the species and climatic conditions. Specifically, hardwood species under moist climate in Northern Spain are less correlated with drought indices than the remaining species. The deciduous species (e.g., *Fagus sylvatica*, *Quercus petraea*, *Quercus pyrenaica*, and *Quercus robur*) were, however, more sensitive to drought at short (1–3 months) and medium time scales than most of evergreen coniferous trees, particularly in the dry eastern IP under Mediterranean climate that responded to longer time scales (e.g., *Pinus halepensis*). This entails the resilience capacity of the species to endure with droughts. Gazol et al. [75] found that the same pine species inhabiting southern and eastern dry regions in the IP showed a low resistance to drought and a high post-drought recovery capacity. In semiarid areas, soil water availability is the main constraint for forest growth [72]. This dependence on moisture deficit at medium to longer temporal scales was also found by Rimkus et al. [78] for the Baltic region and Quiring and Ganesh [90] for Texas (USA).

Overall, species growing under humid climate conditions present a weaker correlation with drought indices. Nonetheless, these species are most sensitive to extreme or prolonged drought events, due to the absence of resilience mechanisms to reduce the damage caused by severe water shortage [91], although they can show high resistance to drought in terms of growth loss [75]. In these humid regions, precipitation seems to be the main limiting factor, given the stronger response of SPI to NDVI cumulative annual series (NDVI annual), compared to drought indices that account for precipitation as well as atmospheric evaporative demand (i.e., SPEI) [40]. Furthermore, vegetation from humid regions may respond in a different manner to mild droughts, as suggest by Zhang et al. [92]. This behavior can be interpreted within a context where temperature rise and low cloudiness could increase the incoming photosynthetically-active radiation simultaneously with increased evapotranspiration.

Interestingly, the response of species to drought differs among species belonging of the same genus, and also between sites in the same species, indicating the relevance of local site climatic and soil conditions. Thus, some species dominating in cold and continental mountainous areas (e.g., *Pinus sylvestris* and *Pinus uncinata*) tend to respond to shorter temporal scales because of their higher dependence on water availability [93]. In contrast, *Pinus halepensis* and *Pinus nigra*, which are dominant in dry regions, are less sensitive to moisture deficit, especially during prolonged droughts [94].

In addition, the response of forests to drought indices shows a strong seasonality. For tree-ring growth, moisture conditions during summer, especially in July and August, are determinant of wood formation. On the other hand, for the NDVI (max and annual), late spring months (April and May) are more relevant. The higher sensitivity of wood formation to summer water availability is probably related to phenological patterns of each species [95]. A similar pattern was observed over arid and semi-arid regions of Mongolia and China [92]. Even if spring droughts may lead to severe impacts, these impacts may be lagged to subsequent months, leading to photosynthesis reduction as well as accelerated respiration rates in summer. All these factors together reduced the annual net carbon uptake and, thus, wood formation [96].

5. Conclusions

To sum up, our study reflects some key findings:

1. The multi-scalar drought indices (e.g., SPEI, SPI, and SPDI) perform better than uni-scalar indices (e.g., PDSI) to identify drought impacts on forests for different species.
2. Among the multi-scalar indices, SPEI and SPI correlate better with TRWi and NDVI than the SPDI for most species.
3. Albeit with the few differences in the magnitude of correlations between the SPEI and SPI, our results suggest a major role of the atmospheric evaporative demand in drought severity across forests located in dry Mediterranean areas.

4. Droughts are more prone to impact forest secondary growth (TRWi) during summertime, and annual production and greenness (NDVI) during springtime.
5. The response of the forests to drought is mainly driven by short time scales (1–3 months) in humid-temperate hardwood forests, compared to long to medium (>4 months) time scales in warm-dry conifer forests.
6. Tree-ring growth seems a more reliable indicator of the response of forests to drought, due to its higher association with drought indices.

Supplementary Materials: The following are available online at <http://www.mdpi.com/1999-4907/9/9/524/s1>, Figure S1. Box plots showing the maximum Pearson correlation coefficients computed between NDVI annual (a,f), ring-width indices (TRWi (b,d), and NDVImax (c,e), and the multi-scalar drought indices (SPEI, SPI, and SPDI), Figure S2. Box plots showing the maximum partial Pearson correlation coefficients found between TRWi (b,d), NDVI max (c,e), NDVI annual (a,f), and the multi-scalar drought indices. Figure S3. Box plots showing the most correlated time-scale found for TRWi (b,d), NDVI max (c,e), NDVI annual (a,f), and the multi-scalar drought indices. Figure S4. Scatterplots showing the maximum Pearson correlation coefficients found for SPEI-TRWi and SPI-NDVI annual by species. Figure S5. Scatterplots showing the maximum Pearson correlation coefficients found for SPEI-TRWi and SPEI-NDVI max by species. Figure S6. Scatterplots showing the maximum Pearson correlation coefficients found for SPEI-TRWi and the average annual hydro-climatic balance by species. Figure S7. Same as Figure S6, but for SPEI-NDVI max. Figure S8. Same as Figure S6, but for SPEI-NDVI annual. Table S1. Percentage of sampled forests per drought index and time-scale (number of months) in which the maximum correlation value was found with ring-width indices (TRWi, a), NDVI max (b), and NDVI annual (c).

Author Contributions: Conceptualization, S.M.V.-S.; Data curation, S.M.V.-S., J.J.C., A.G., R.S.-S., E.G., M.d.L., G.S.-B., K.N., V.R., P.A.T., J.C.L., E.M.d.C., M.R.M., I.G.-G., F.S., A.C., M.G., J.M.O., L.A.L., A.H. and J.D.G.; Formal analysis, M.P.-G.; Methodology, M.P.-G. and S.M.V.-S.; Supervision, S.M.V.-S., J.J.C.; Visualization, M.P.-G.; Writing—original draft, M.P.-G.; Writing—review & editing, S.M.V.-S., J.J.C., F.D.-C., A.E.K., S.B.-P., G.S.-B., J.M.O. and A.H.

Funding: This study was financially supported by the Spanish Ministry of Economy projects: CGL2015-69186-C2-1-R (Fundiver), CGL2015-69985-R (CLIMED), CGL2013-48843-C2-1-R (CoMo-ReAdapt), AGL2014-53822-C2-1-R (SATIVA), XIRONO (BFU2010-21451), CGL2014-52135-C03-01, PCIN-2015-220, and CGL2016-81706-REDT (Ecometas Network), 1560/2015 (ECOHIPRO). The study was also funded by IMDROFLOOD (Water Works 2014, EC) and INDECIS (European Research Areas for Climate Services) projects. This work also benefited from funding from Xunta de Galicia (PGIDIT06PXIB502262PR, GRC GI-1809, ROCLIGAL-10MDS291009PR), INIA (RTA200600117), and Interreg V-A POCTEFA (CANOPEE, 2014-2020-FEDER funds) projects. Marina Peña-Gallardo was granted by the Spanish Ministry of Economy and Competitiveness. Raúl Sánchez-Salguero and Antonio Gazol were supported by postdoctoral grants (IJCI-2015-25845 and MINECO-FPDI 2013-16600; FEDER funds).

Conflicts of Interest: The authors declare no conflict of interest.

References

1. Wilhite, D.A.; Pulwarty, R.S. *Drought and Water Crises: Integrating Science, Management, and Policy*; CRC Press: Boca Raton, FL, USA, 2017; ISBN 9781138035645.
2. Bachmair, S.; Kohn, I.; Stahl, K. Exploring the link between drought indicators and impacts. *Nat. Hazards Earth Syst. Sci.* **2015**, *15*, 1381–1397. [[CrossRef](#)]
3. Wilhite, D.A.; Svoboda, M.D.; Hayes, M.J. Understanding the complex impacts of drought: A key to enhancing drought mitigation and preparedness. *Water Resour. Manag.* **2007**, *21*, 763–774. [[CrossRef](#)]
4. Allen, C.D.; Macalady, A.K.; Chenchouni, H.; Bachelet, D.; McDowell, N.; Vennetier, M.; Kitzeberger, T.; Rigling, A.; Breshears, D.D.; Hogg, E.H.; et al. A global overview of drought and heat-induced tree mortality reveals emerging climate change risks for forests. *For. Ecol. Manag.* **2010**, *259*, 660–684. [[CrossRef](#)]
5. Zhang, Q.; Shao, M.; Jia, X.; Wei, X. Relationship of Climatic and Forest Factors to Drought- and Heat-Induced Tree Mortality. *PLoS ONE* **2017**, *12*, e0169770. [[CrossRef](#)] [[PubMed](#)]
6. Young, D.J.N.; Stevens, J.T.; Earles, J.M.; Moore, J.; Ellis, A.; Jirka, A.L.; Latimer, A.M. Long-term climate and competition explain forest mortality patterns under extreme drought. *Ecol. Lett.* **2017**, *20*, 78–86. [[CrossRef](#)] [[PubMed](#)]
7. Greenwood, S.; Ruiz-Benito, P.; Martínez-Vilalta, J.; Lloret, F.; Kitzeberger, T.; Allen, C.D.; Fensham, R.; Laughlin, D.C.; Kattge, J.; Bönisch, G.; et al. Tree mortality across biomes is promoted by drought intensity, lower wood density and higher specific leaf area. *Ecol. Lett.* **2017**, *20*, 539–553. [[CrossRef](#)] [[PubMed](#)]

8. Vicente-Serrano, S.M.; Lopez-Moreno, J.-I.; Beguería, S.; Lorenzo-Lacruz, J.; Sanchez-Lorenzo, A.; García-Ruiz, J.M.; Azorin-Molina, C.; Morán-Tejeda, E.; Revuelto, J.; Trigo, R.; et al. Evidence of increasing drought severity caused by temperature rise in southern Europe. *Environ. Res. Lett.* **2014**, *9*, 44001–44009. [[CrossRef](#)]
9. Dai, A. Increasing drought under global warming in observations and models. *Nat. Clim. Chang.* **2013**, *3*, 52–58. [[CrossRef](#)]
10. Pasho, E.; Camarero, J.J.; de Luis, M.; Vicente-Serrano, S.M. Impacts of drought at different time scales on forest growth across a wide climatic gradient in north-eastern Spain. *Agric. For. Meteorol.* **2011**, *151*, 1800–1811. [[CrossRef](#)]
11. Gazol, A.; Camarero, J.J.; Anderegg, W.R.L.; Vicente-Serrano, S.M. Impacts of droughts on the growth resilience of Northern Hemisphere forests. *Glob. Ecol. Biogeogr.* **2017**, *26*, 166–176. [[CrossRef](#)]
12. Sánchez-Salguero, R.; Navarro-Cerrillo, R.M.; Camarero, J.J.; Fernández-Cancio, Á. Selective drought-induced decline of pine species in southeastern Spain. *Clim. Chang.* **2012**, *113*, 767–785. [[CrossRef](#)]
13. Arzac, A.; Rozas, V.; Rozenberg, P.; Olano, J.M. Water availability controls *Pinus pinaster* xylem growth and density: A multi-proxy approach along its environmental range. *Agric. For. Meteorol.* **2018**, *250–251*, 171–180. [[CrossRef](#)]
14. Arzac, A.; García-Cervigón, A.I.; Vicente-Serrano, S.M.; Loidi, J.; Olano, J.M. Phenological shifts in climatic response of secondary growth allow *Juniperus sabinus* L. to cope with altitudinal and temporal climate variability. *Agric. For. Meteorol.* **2016**, *217*, 35–45. [[CrossRef](#)]
15. Forner, A.; Valladares, F.; Bonal, D.; Granier, A.; Grossiord, C.; Aranda, I. Extreme droughts affecting Mediterranean tree species' growth and water-use efficiency: The importance of timing. *Tree Physiol.* **2018**. [[CrossRef](#)] [[PubMed](#)]
16. Peguero-Pina, J.J.; Sancho-Knapik, D.; Cochard, H.; Barredo, G.; Villarroya, D.; Gil-Pelegrin, E. Hydraulic traits are associated with the distribution range of two closely related Mediterranean firs, *Abies alba* Mill. and *Abies pinsapo* Boiss. *Tree Physiol.* **2011**, *31*, 1067–1075. [[CrossRef](#)] [[PubMed](#)]
17. Martín Vide, J.; Olcina Cantos, J. *Climas y Tiempos de España*; Alianza Editorial: Madrid, Spain, 2001; ISBN 8420657778.
18. Camarero, J.J.; Gazol, A.; Sangüesa-Barreda, G.; Cantero, A.; Sánchez-Salguero, R.; Sánchez-Miranda, A.; Granda, E.; Serra-Maluquer, X.; Ibáñez, R. Forest Growth Responses to Drought at Short- and Long-Term Scales in Spain: Squeezing the Stress Memory from Tree Rings. *Front. Ecol. Evol.* **2018**, *6*, 9. [[CrossRef](#)]
19. Neumann, M.; Mues, V.; Moreno, A.; Hasenauer, H.; Seidl, R. Climate variability drives recent tree mortality in Europe. *Glob. Chang. Biol.* **2017**, *23*, 4788–4797. [[CrossRef](#)] [[PubMed](#)]
20. Camarero, J.J.; Gazol, A.; Sangüesa-Barreda, G.; Oliva, J.; Vicente-Serrano, S.M. To die or not to die: Early warnings of tree dieback in response to a severe drought. *J. Ecol.* **2015**, *103*, 44–57. [[CrossRef](#)]
21. Carnicer, J.; Coll, M.; Ninyerola, M.; Pons, X.; Sánchez, G.; Peñuelas, J. Widespread crown condition decline, food web disruption, and amplified tree mortality with increased climate change-type drought. *Proc. Natl. Acad. Sci. USA* **2011**, *108*, 1474–1478. [[CrossRef](#)] [[PubMed](#)]
22. Bonan, G.B. Forests and climate change: Forcings, feedbacks, and the climate benefits of forests. *Science* **2008**, *320*, 1444–1449. [[CrossRef](#)] [[PubMed](#)]
23. Frank, D.C.; Poulter, B.; Saurer, M.; Esper, J.; Huntingford, C.; Helle, G.; Treydte, K.; Zimmermann, N.E.; Schleser, G.H.; Ahlström, A.; et al. Water-use efficiency and transpiration across European forests during the Anthropocene. *Nat. Clim. Chang.* **2015**, *5*, 579–583. [[CrossRef](#)]
24. Zhao, M.; Running, S.W. Drought-Induced Reduction in Global Terrestrial Net Primary Production from 2000 Through 2009. *Science* **2010**, *329*, 940–943. [[CrossRef](#)] [[PubMed](#)]
25. Gursoy, M.; Balkan, A.; Ulukan, H. Ecophysiological Responses to Stresses in Plants: A General Approach. *Pak. J. Biol. Sci.* **2012**, *15*, 506–516. [[CrossRef](#)] [[PubMed](#)]
26. Li, J.; Cang, Z.; Jiao, F.; Bai, X.; Zhang, D.; Zhai, R. Influence of drought stress on photosynthetic characteristics and protective enzymes of potato at seedling stage. *J. Saudi Soc. Agric. Sci.* **2017**, *16*, 82–88. [[CrossRef](#)]
27. Pinheiro, C.; Chaves, M.M. Photosynthesis and drought: can we make metabolic connections from available data? *J. Exp. Bot.* **2011**, *62*, 869–882. [[CrossRef](#)] [[PubMed](#)]
28. Basu, S.; Ramegowda, V.; Kumar, A.; Pereira, A. Plant adaptation to drought stress. *F1000Research* **2016**, *5*. [[CrossRef](#)] [[PubMed](#)]

29. Granda, E.; Escudero, A.; Valladares, F. More than just drought: Complexity of recruitment patterns in Mediterranean forests. *Oecologia* **2014**, *176*, 997–1007. [[CrossRef](#)] [[PubMed](#)]
30. Lloret, F.; Escudero, A.; Iriondo, J.M.; Martínez-Vilalta, J.; Valladares, F. Extreme climatic events and vegetation: The role of stabilizing processes. *Glob. Chang. Biol.* **2012**, *18*, 797–805. [[CrossRef](#)]
31. Vidal-Macua, J.J.; Ninyerola, M.; Zabala, A.; Domingo-Marimon, C.; Pons, X. Factors affecting forest dynamics in the Iberian Peninsula from 1987 to 2012. The role of topography and drought. *For. Ecol. Manag.* **2017**, *406*, 290–306. [[CrossRef](#)]
32. Vicente-Serrano, S.M.; Camarero, J.J.; Olano, J.M.; Martín-Hernández, N.; Peña-Gallardo, M.; Tomás-Burguera, M.; Gazol, A.; Azorin-Molina, C.; Bhuyan, U.; El Kenawy, A. Diverse relationships between forest growth and the Normalized Difference Vegetation Index at a global scale. *Remote Sens. Environ.* **2016**, *187*, 14–29. [[CrossRef](#)]
33. Babst, F.; Poulter, B.; Trouet, V.; Tan, K.; Neuwirth, B.; Wilson, R.; Carrer, M.; Grabner, M.; Tegel, W.; Levanic, T.; et al. Site- and species-specific responses of forest growth to climate across the European continent. *Glob. Ecol. Biogeogr.* **2013**, *22*, 706–717. [[CrossRef](#)]
34. Fritts, H.C. *Tree Rings and Climate*; Academic Press: Cambridge, MA, USA, 1976; ISBN 9780122684500.
35. Gazol, A.; Sangüesa-Barreda, G.; Granda, E.; Camarero, J.J. Tracking the impact of drought on functionally different woody plants in a Mediterranean scrubland ecosystem. *Plant Ecol.* **2017**, *218*, 1009–1020. [[CrossRef](#)]
36. Vicente-Serrano, S.M.; Martín-Hernández, N.; Camarero, J.J.; Gazol, A.; Sánchez-Salguero, R.; Peña-Gallardo, M.; El Kenawy, A.; Domínguez-Castro, F.; Tomas-Burguera, M.; Gutiérrez, E.; et al. Spatial, temporal and climatic determinants of the responses of tree-ring growth to satellite-derived primary growth in multiple forest biomes. *Sci. Total Environ.* **2018**. under review.
37. Poulter, B.; Pederson, N.; Liu, H.; Zhu, Z.; D'Arrigo, R.; Ciais, P.; Davi, N.; Frank, D.; Leland, C.; Myneni, R.; Piao, S.; Wang, T. Recent trends in Inner Asian forest dynamics to temperature and precipitation indicate high sensitivity to climate change. *Agric. For. Meteorol.* **2013**, *178–179*, 31–45. [[CrossRef](#)]
38. Wang, J.; Rich, P.M.; Price, K.P.; Kettle, W.D. Relations between NDVI and tree productivity in the central Great Plains. *Int. J. Remote Sens.* **2004**, *25*, 3127–3138. [[CrossRef](#)]
39. Bochenek, Z.; Ziolkowski, D.; Bartold, M.; Orłowska, K.; Ochtyra, A. Monitoring forest biodiversity and the impact of climate on forest environment using high-resolution satellite images. *Eur. J. Remote Sens.* **2018**, *51*, 166–181. [[CrossRef](#)]
40. Vicente-Serrano, S.M.; Gouveia, C.; Camarero, J.J.; Beguería, S.; Trigo, R.; López-Moreno, J.I.; Azorín-Molina, C.; Pasho, E.; Lorenzo-Lacruz, J.; Revuelto, J.; et al. Response of vegetation to drought time-scales across global land biomes. *Proc. Natl. Acad. Sci. USA* **2013**, *110*, 52–57. [[CrossRef](#)] [[PubMed](#)]
41. Tucker, C.J. Red and photographic infrared linear combinations for monitoring vegetation. *Remote Sens. Environ.* **1979**, *8*, 127–150. [[CrossRef](#)]
42. Tucker, C.J.; Sellers, P.J. Satellite remote sensing of primary production. *Int. J. Remote Sens.* **1986**, *7*, 1395–1416. [[CrossRef](#)]
43. Keyantash, J.; Dracup, J.A.; Keyantash, J.; Dracup, J.A. The Quantification of Drought: An Evaluation of Drought Indices. *Bull. Am. Meteorol. Soc.* **2002**, *83*, 1167–1180. [[CrossRef](#)]
44. Zargar, A.; Sadiq, R.; Naser, B.; Khan, F.I. A review of drought indices. *Environ. Rev.* **2011**, *19*, 333–349. [[CrossRef](#)]
45. Shukla, S.; Steinemann, A.C.; Lettenmaier, D.P.; Shukla, S.; Steinemann, A.C.; Lettenmaier, D.P. Drought Monitoring for Washington State: Indicators and Applications. *J. Hydrometeorol.* **2011**, *12*, 66–83. [[CrossRef](#)]
46. Lorenzo-Lacruz, J.; Vicente-Serrano, S.M.; López-Moreno, J.I.; Beguería, S.; García-Ruiz, J.M.; Cuadrat, J.M. The impact of droughts and water management on various hydrological systems in the headwaters of the Tagus River (central Spain). *J. Hydrol.* **2010**, *386*, 13–26. [[CrossRef](#)]
47. Peña-Gallardo, M.; Vicente-Serrano, S.M.; Domínguez-Castro, F.; Quiring, S.M.; Svoboda, M.D.; Beguería-Portugués, S.; Hannaford, J. Effectiveness of drought indices in identifying impacts on major crops over the USA. *Clim. Res.* **2018**, in press. [[CrossRef](#)]
48. Vicente-Serrano, S.M.; Beguería, S.; Lorenzo-Lacruz, J.; Camarero, J.J.; López-Moreno, J.I.; Azorin-Molina, C.; Revuelto, J.; Morán-Tejeda, E.; Sanchez-Lorenzo, A.; Vicente-Serrano, S.M.; et al. Performance of Drought Indices for Ecological, Agricultural, and Hydrological Applications. *Earth Int.* **2012**. [[CrossRef](#)]

49. Kempes, C.P.; Myers, O.B.; Breshears, D.D.; Ebersole, J.J. Comparing response of *Pinus edulis* tree-ring growth to five alternate moisture indices using historic meteorological data. *J. Arid Environ.* **2008**, *72*, 350–357. [[CrossRef](#)]
50. Bachmair, S.; Tanguy, M.; Hannaford, J.; Stahl, K. How well do meteorological indicators represent agricultural and forest drought across Europe? *Environ. Res. Lett.* **2018**, *13*, 034042. [[CrossRef](#)]
51. Vicente-Serrano, S.M.; Tomas-Burguera, M.; Beguería, S.; Reig, F.; Latorre, B.; Peña-Gallardo, M.; Luna, M.Y.; Morata, A.; González-Hidalgo, J.C. A High Resolution Dataset of Drought Indices for Spain. *Data* **2017**, *2*, 22. [[CrossRef](#)]
52. Allen, R.G.; Rick, G. Food and Agriculture Organization of the United Nations. In *Crop Evapotranspiration: Guidelines for Computing Crop Water Requirements*; Allen, R.G., Pereira, L.S., Raes, D., Smith, M., Eds.; Food and Agriculture Organization of the United Nations: Rome, Italy, 1998; ISBN 9251042195.
53. Pettorelli, N.; Vik, J.O.; Mysterud, A.; Gaillard, J.-M.; Tucker, C.J.; Stenseth, N.C. Using the satellite-derived NDVI to assess ecological responses to environmental change. *Trends Ecol. Evol.* **2005**, *20*, 503–510. [[CrossRef](#)] [[PubMed](#)]
54. Vicente-Serrano, M.; Martín-Hernández, N.; Camarero, J.J.; Gazol, A.; Sánchez-Salguero, R.; Peña-Gallardo, M.; El Kenawy, A.; Domínguez-Castro, F.; Tomás-Burquera, M.; Gutiérrez, E.; et al. Linking tree-ring growth and satellite-derived gross primary growth in multiple forest biomes. Temporal-scale matters. *Sci. Total Environ.* **2018**. under review.
55. Nagaraja Rao, C.R.; Zhang, N.; Sullivan, J.T. Inter-calibration of meteorological satellite sensors in the visible and near-infrared. *Adv. Space Res.* **2001**, *28*, 3–10. [[CrossRef](#)]
56. Robel, J. NOAA KLM User's Guide—Satellite and Data Description of NOAA's Polar-Orbiting Satellites from NOAA-15 and Later. 2009. Available online: <https://www1.ncdc.noaa.gov/pub/data/satellite/publications/podguides/N-15%20thru%20N-19/pdf/0.0%20NOAA%20KLM%20Users%20Guide.pdf> (accessed on 28 August 2018).
57. Riano, D.; Chuvieco, E.; Salas, J.; Aguado, I. Assessment of different topographic corrections in landsat-TM data for mapping vegetation types (2003). *IEEE Trans. Geosci. Remote Sens.* **2003**, *41*, 1056–1061. [[CrossRef](#)]
58. Baena-Calatrava, R. *Georreferenciación Automática de Imágenes NOAA-AVHRR*; University of Jaén: Jaén, Spain, 2002.
59. Azorin-Molina, C.; Baena-Calatrava, R.; Echave-Calvo, I.; Connell, B.H.; Vicente-Serrano, S.M.; López-Moreno, J.I. A daytime over land algorithm for computing AVHRR convective cloud climatologies for the Iberian Peninsula and the Balearic Islands. *Int. J. Climatol.* **2013**, *33*, 2113–2128. [[CrossRef](#)]
60. Holben, B.N. Characteristics of maximum-value composite images from temporal AVHRR data. *Int. J. Remote Sens.* **1986**, *7*, 1417–1434. [[CrossRef](#)]
61. Holmes, R.L. Computer-assisted quality control in tree-ring dating and measurements. *Tree-Ring Bull.* **1983**, *43*, 69–78.
62. Bunn, A.G. A dendrochronology program library in R (dplR). *Dendrochronologia* **2008**, *26*, 115–124. [[CrossRef](#)]
63. Palmer, W.C. *Meteorological Drought*; U.S. Department of Commerce: Washington, DC, USA, 1965.
64. Alley, W.M. The Palmer Drought Severity Index: Limitations and Assumptions. *J. Clim. Appl. Meteorol.* **1984**, *23*, 1100–1109. [[CrossRef](#)]
65. Doesken, N.J.; Garen, D. Drought monitoring in the Western United States using a surface water supply index. In Proceedings of the 7th Conference on Applied Climatology, Salt Lake City, UT, USA, 10–13 September 1991; Doesken, N.J., Mckee, T.B., Kleist, J., Eds.; Colorado State University: Fort Collins, CO, USA, 1991.
66. Heim, R.R. A Review of Twentieth-Century Drought Indices Used in the United States. *Bull. Am. Meteorol. Soc.* **2002**, *83*, 1149–1165. [[CrossRef](#)]
67. Mckee, T.B.; Doesken, N.J.; Kleist, J. The Relationship of Drought Frequency and Duration to Time Scales. In Proceedings of the 8th Conference on Applied Climatology, Anaheim, CA, USA, 17–22 January 1993.
68. Svoboda, M.; Hayes, M.; Wood, D. *Standardized Precipitation Index User Guide*; World Meteorological Organization: Geneva, Switzerland, 2012.
69. Vicente-Serrano, S.M.; Beguería, S.; López-Moreno, J.I.; Vicente-Serrano, S.M.; Beguería, S.; López-Moreno, J.I. A Multiscalar Drought Index Sensitive to Global Warming: The Standardized Precipitation Evapotranspiration Index. *J. Clim.* **2010**, *23*, 1696–1718. [[CrossRef](#)]
70. Ma, M.; Ren, L.; Yuan, F.; Jiang, S.; Liu, Y.; Kong, H.; Gong, L. A new standardized Palmer drought index for hydro-meteorological use. *Hydrol. Process.* **2014**, *28*, 5645–5661. [[CrossRef](#)]

71. Vicente-Serrano, S.M.; Van der Schrier, G.; Beguería, S.; Azorin-Molina, C.; Lopez-Moreno, J.-I. Contribution of precipitation and reference evapotranspiration to drought indices under different climates. *J. Hydrol.* **2015**, *526*, 42–54. [[CrossRef](#)]
72. Vicente-Serrano, S.; Cabello, D.; Tomás-Burguera, M.; Martín-Hernández, N.; Beguería, S.; Azorin-Molina, C.; Kenawy, A. Drought Variability and Land Degradation in Semiarid Regions: Assessment Using Remote Sensing Data and Drought Indices (1982–2011). *Remote Sens.* **2015**, *7*, 4391–4423. [[CrossRef](#)]
73. Bian, J.; Li, A.; Deng, W. Estimation and analysis of net primary Productivity of Ruoergai wetland in China for the recent 10 years based on remote sensing. *Procedia Environ. Sci.* **2010**, *2*, 288–301. [[CrossRef](#)]
74. Kuenzer, C.; Dech, S.W.; Wagner, W. *Remote Sensing Time Series: Revealing Land Surface Dynamics*; Springer: Berlin, Germany, 2015; ISBN 9783319159676.
75. Gazol, A.; Camarero, J.J.; Vicente-Serrano, S.M.; Sánchez-Salguero, R.; Gutiérrez, E.; de Luis, M.; Sangüesa-Barreda, G.; Novak, K.; Rozas, V.; Tiscar, P.A.; Linares, J.C.; et al. Forest resilience to drought varies across biomes. *Glob. Chang. Biol.* **2018**, *24*, 2143–2158. [[CrossRef](#)] [[PubMed](#)]
76. Tardieu, F.; Simonneau, T.; Muller, B. The Physiological Basis of Drought Tolerance in Crop Plants: A Scenario-Dependent Probabilistic Approach. *Annu. Rev. Plant Biol.* **2018**, *69*, 733–759. [[CrossRef](#)] [[PubMed](#)]
77. Almeida, T.I.R.; Filho, D.S. Principal component analysis applied to feature-oriented band ratios of hyperspectral data: A tool for vegetation studies. *Int. J. Remote Sens.* **2004**, *25*, 5005–5023. [[CrossRef](#)]
78. Rimkus, E.; Stonevicius, E.; Kilpys, J.; Maciulyte, V.; Valiukas, D. Drought identification in the eastern Baltic region using NDVI. *Earth Syst. Dyn.* **2017**, *85194*, 627–637. [[CrossRef](#)]
79. He, J.; Shao, X. Relationships between tree-ring width index and NDVI of grassland in Delingha. *Chin. Sci. Bull.* **2006**, *51*, 1106–1114. [[CrossRef](#)]
80. Bhuyan, U.; Zang, C.; Menzel, A. Different responses of multispecies tree ring growth to various drought indices across Europe. *Dendrochronologia* **2017**, *44*, 1–8. [[CrossRef](#)]
81. Vilhar, U. Comparison of drought stress indices in beech forests: A modelling study. *iForest* **2016**, *9*, 635. [[CrossRef](#)]
82. Aaltonen, H.; Lindén, A.; Heinonsalo, J.; Biasi, C.; Pumpanen, J. Effects of prolonged drought stress on Scots pine seedling carbon allocation. *Tree Physiol.* **2016**, *37*, 418–427. [[CrossRef](#)] [[PubMed](#)]
83. McDowell, N.; Allen, C.D.; Anderson-Teixeira, K.; Brando, P.; Brienen, R.; Chambers, J.; Christoffersen, B.; Davies, S.; Doughty, C.; Duque, A.; et al. Drivers and mechanisms of tree mortality in moist tropical forests. *New Phytol.* **2018**. [[CrossRef](#)] [[PubMed](#)]
84. Rowland, L.; Lobo-do-Vale, R.L.; Christoffersen, B.O.; Melém, E.A.; Kruijt, B.; Vasconcelos, S.S.; Domingues, T.; Binks, O.J.; Oliveira, A.A.R.; Metcalfe, D.; et al. After more than a decade of soil moisture deficit, tropical rainforest trees maintain photosynthetic capacity, despite increased leaf respiration. *Glob. Chang. Biol.* **2015**, *21*, 4662–4672. [[CrossRef](#)] [[PubMed](#)]
85. McDowell, N.G.; Fisher, R.A.; Xu, C.; Domec, J.C.; Hölttä, T.; Mackay, D.S.; Sperry, J.S.; Boutz, A.; Dickman, L.; Gehres, N.; et al. Evaluating theories of drought-induced vegetation mortality using a multimodel-experiment framework. *New Phytol.* **2013**, *200*, 304–321. [[CrossRef](#)] [[PubMed](#)]
86. Rowland, L.; da Costa, A.C.L.; Galbraith, D.R.; Oliveira, R.S.; Binks, O.J.; Oliveira, A.A.R.; Pullen, A.M.; Doughty, C.E.; Metcalfe, D.B.; Vasconcelos, S.S.; et al. Death from drought in tropical forests is triggered by hydraulics not carbon starvation. *Nature* **2015**, *528*, 119. [[CrossRef](#)] [[PubMed](#)]
87. Wang, Q.; Adiku, S.; Tenhunen, J.; Granier, A. On the relationship of NDVI with leaf area index in a deciduous forest site. *Remote Sens. Environ.* **2005**, *94*, 244–255. [[CrossRef](#)]
88. Mutanga, O.; Skidmore, A.K. Narrow band vegetation indices overcome the saturation problem in biomass estimation. *Int. J. Remote Sens.* **2004**, *25*, 3999–4014. [[CrossRef](#)]
89. Karl, T.R. The Sensitivity of the Palmer Drought Severity Index and Palmer’s Z-Index to their Calibration Coefficients Including Potential Evapotranspiration. *J. Clim. Appl. Meteorol.* **1986**, *25*, 77–86. [[CrossRef](#)]
90. Quiring, S.M.; Ganesh, S. Evaluating the utility of the Vegetation Condition Index (VCI) for monitoring meteorological drought in Texas. *Agric. For. Meteorol.* **2010**, *150*, 330–339. [[CrossRef](#)]
91. Jump, A.S.; Ruiz-Benito, P.; Greenwood, S.; Allen, C.D.; Kitzberger, T.; Fensham, R.; Martínez-Vilalta, J.; Lloret, F. Structural overshoot of tree growth with climate variability and the global spectrum of drought-induced forest dieback. *Glob. Chang. Biol.* **2017**, *23*, 3742–3757. [[CrossRef](#)] [[PubMed](#)]

92. Zhang, L.; Xiao, J.; Zhou, Y.; Zheng, Y.; Li, J.; Xiao, H. Drought events and their effects on vegetation productivity in China. *Ecosphere* **2016**, *7*, e01591. [[CrossRef](#)]
93. Irvine, J.; Perks, M.P.; Magnani, F.; Grace, J. The response of *Pinus sylvestris* to drought: stomatal control of transpiration and hydraulic conductance. *Tree Physiol.* **1998**, *18*, 393–402. [[CrossRef](#)] [[PubMed](#)]
94. Klein, T.; Cohen, S.; Yakir, D. Hydraulic adjustments underlying drought resistance of *Pinus halepensis*. *Tree Physiol.* **2011**, *31*, 637–648. [[CrossRef](#)] [[PubMed](#)]
95. Camarero, J.J.; Olano, J.M.; Parras, A. Plastic bimodal xylogenesis in conifers from continental Mediterranean climates. *New Phytol.* **2010**, *185*, 471–480. [[CrossRef](#)] [[PubMed](#)]
96. Noormets, A.; McNulty, S.G.; DeForest, J.L.; Sun, G.; Li, Q.; Chen, J. Drought during canopy development has lasting effect on annual carbon balance in a deciduous temperate forest. *New Phytol.* **2008**, *179*, 818–828. [[CrossRef](#)] [[PubMed](#)]



© 2018 by the authors. Licensee MDPI, Basel, Switzerland. This article is an open access article distributed under the terms and conditions of the Creative Commons Attribution (CC BY) license (<http://creativecommons.org/licenses/by/4.0/>).

A high-resolution spatial assessment of the impacts of drought variability on vegetation activity in Spain from 1981 to 2015



A high-resolution spatial assessment of the impacts of drought variability on vegetation activity in Spain from 1981 to 2015

Sergio M. Vicente-Serrano¹, Cesar Azorin-Molina², Marina Peña-Gallardo¹, Miquel Tomas-Burguera³, Fernando Domínguez-Castro¹, Natalia Martín-Hernández¹, Santiago Beguería³, Ahmed El Kenawy⁴, Iván Noguera¹, and Mónica García⁵

¹Instituto Pirenaico de Ecología, Spanish National Research Council (IPE-CSIC), Campus de Aula Dei, P.O. Box 13034, 50059 Saragossa, Spain

²Department of Earth Sciences, Regional Climate Group, University of Gothenburg, Gothenburg, Sweden

³Estación Experimental de Aula Dei, Spanish National Research Council (EEAD-CSIC), Saragossa, Spain

⁴Department of Geography, Mansoura University, 35516, Mansoura, Egypt

⁵Department of Environmental Engineering, Technical University of Denmark, Lyngby, Denmark

Correspondence: Sergio M. Vicente-Serrano (svicen@ipe.csic.es)

Received: 26 November 2018 – Discussion started: 27 November 2018

Revised: 6 May 2019 – Accepted: 7 May 2019 – Published: 17 June 2019

Abstract. Drought is a major driver of vegetation activity in Spain, with significant impacts on crop yield, forest growth, and the occurrence of forest fires. Nonetheless, the sensitivity of vegetation to drought conditions differs largely amongst vegetation types and climates. We used a high-resolution (1.1 km) spatial dataset of the normalized difference vegetation index (NDVI) for the whole of Spain spanning the period from 1981 to 2015, combined with a dataset of the standardized precipitation evapotranspiration index (SPEI) to assess the sensitivity of vegetation types to drought across Spain. Specifically, this study explores the drought timescales at which vegetation activity shows its highest response to drought severity at different moments of the year. Results demonstrate that – over large areas of Spain – vegetation activity is controlled largely by the interannual variability of drought. More than 90 % of the land areas exhibited statistically significant positive correlations between the NDVI and the SPEI during dry summers (JJA). Nevertheless, there are some considerable spatio-temporal variations, which can be linked to differences in land cover and aridity conditions. In comparison to other climatic regions across Spain, results indicate that vegetation types located in arid regions showed the strongest response to drought. Importantly, this study stresses that the timescale at which drought is assessed is a dominant factor in understanding the different responses of vegetation activity to drought.

1 Introduction

Drought is one of the major hydroclimatic hazards impacting land surface fluxes (Baldocchi et al., 2004; Fischer et al., 2007; Hirschi et al., 2011), vegetation respiration (Ciais et al., 2005), net primary production (Reichstein et al., 2007; Zhao and Running, 2010), primary and secondary forest growth (Allen et al., 2015), and crop yield (Lobell et al., 2015; Asseng et al., 2015). Recently, numerous studies suggested an accelerated impact of drought on vegetation activity and forest mortality under different environmental conditions (Allen et al., 2010, 2015; Breshears et al., 2005) with a reduction in vegetation activity and higher rates of tree decay (e.g. Carnicer et al., 2011; Restaino et al., 2016). Nevertheless, a comprehensive assessment of the impacts of drought on vegetation activity is a challenging task. This is particularly because data on forest conditions and growth are partial, spatially sparse, and restricted to a small number of sampled forests (Grissino-Mayer and Fritts, 1997). Furthermore, the temporal resolution of forest data is insufficient to provide deep insights into the impacts of drought on vegetation activity (e.g. the official forest inventories; Jenkins et al., 2003). In addition to these challenges, the spatial and temporal data on crops are often limited, as they are mostly aggregated to administrative levels and provided at the annual scale, with minor information on vegetation activity across the different periods of the year (FAO, 2018). To handle these limitations,

numerous studies have alternatively employed the available remotely sensed data to assess the impacts of drought on vegetation activity (e.g. Ji and Peters, 2003; Wan et al., 2004; Rhee et al., 2010; Zhao et al., 2017).

Several space-based products allow for quantifying vegetation conditions, given that active vegetation responds dissimilarly to the electromagnetic radiation received in the visible and near-infrared parts of the vegetation spectrum (Knippling, 1970). As such, with the available spectral information recorded by sensors on board satellite platforms, it is possible to calculate vegetation indices and accordingly assess vegetation activity (Tucker, 1979). In this context, several studies have already employed vegetation indices not only to develop drought-related metrics (e.g. Kogan, 1997; Mu et al., 2013), but to determine the impacts of drought on vegetation conditions as well (García et al., 2010; Vicente-Serrano et al., 2013; Zhang et al., 2017). An inspection of these studies reveals that drought impacts can be characterized using vegetation indices, albeit with a different response of vegetation dynamics as a function of a wide-range of factors, including – among others – vegetation type, bioclimatic conditions, and drought severity (Bhuiyan et al., 2006; Vicente-Serrano, 2007; Quiring and Ganesh, 2010; Ivits et al., 2014).

Given the high interannual variability of precipitation, combined with the prevailing semi-arid conditions across vast areas of the territory, Spain has suffered from frequent, intense, and severe drought episodes during the past decades (Vicente-Serrano, 2006). Nonetheless, in the era of temperature rise, the observed increase in atmospheric evaporative demand (AED) during the last decades has accelerated the severity of droughts (Vicente-Serrano et al., 2014c), in comparison to the severity caused only by precipitation deficits (Vicente-Serrano et al., 2014b; González-Hidalgo et al., 2018). Over Spain, the hydrological and socio-economic impacts of droughts are well-documented. Hydrologically, droughts are often associated with a decrease in streamflow and reservoir storages (Lorenzo-Lacruz et al., 2010, 2013). The impacts of drought can extend further to crops, leading to crop failure due to deficit in irrigation water (Iglesias et al., 2003), and even in arable unirrigated lands (Austin et al., 1998; Páscoa et al., 2017). Over Spain, numerous investigations also highlighted the adverse impacts of drought on forest growth (e.g. Camarero et al., 2015; Gazol et al., 2018; Peña-Gallardo et al., 2018a) and forest fires (Hill et al., 2008; Lasanta et al., 2017; Pausas, 2004; Pausas and Fernández-Muñoz, 2012).

Albeit with these adverse drought-driven impacts, there is a lack of comprehensive studies that assess the impacts of drought on vegetation activity over the entire Spanish territory, with a satisfactorily temporal coverage. While numerous studies employed remotely sensed imagery and vegetation indices to analyse spatial and temporal variability and trends in vegetation activity over Spain (e.g. del Barrio et al., 2010; Julien et al., 2011; Stellmes et al., 2013), few attempts have been made to link the temporal dy-

namics of satellite-derived vegetation activity with climate variability and drought evolution (e.g. Vicente-Serrano et al., 2006; Udelhoven et al., 2009; Gouveia et al., 2012; Mühlbauer et al., 2016). An example is González-Alonso and Casanova (1997), who analysed the spatial distribution of droughts in 1994 and 1995 over Spain, concluding that the most affected areas are semi-arid regions. In their comparison of the MODIS normalized difference vegetation index (NDVI) data and the standardized precipitation index (SPI) over Spain, García-Haro et al. (2014) indicated that the response of vegetation dynamics to climate variability is highly variable, according to the regional climate conditions, vegetation community, and growth stages. A similar finding was also confirmed by Vicente-Serrano (2007) and Contreras and Hunink (2015) in their assessment of the response of NDVI to drought in semi-arid regions of northeast and southeast Spain, respectively. With these comprehensive efforts, a detailed spatial assessment of the links between droughts and vegetation activity, which covers a long time period (decades), is highly desired for Spain to explore the differences in the response of vegetation activity to drought under different environments with various land cover and vegetation types.

The overriding objectives of this study are (i) to determine the possible differences in the response of vegetation activity to drought over Spain, as a function of the different land cover types and climatic conditions, and (ii) to explore the drought timescales at which vegetation activity highly responds to drought severity. An innovative aspect of this study is that it provides – for the first time – a comprehensive assessment of the response of vegetation activity to drought using a multidecadal (1981–2015) high-spatial-resolution (1.1 km) NDVI dataset over the study region.

2 Data and methods

2.1 Datasets

2.1.1 NDVI data

Globally, there are several NDVI datasets, which have been widely used to analyse NDVI variability and trends (e.g. Slayback et al., 2003; Herrmann et al., 2005; Anyamba and Tucker, 2005) and to assess the links between NDVI and climate variability and drought (e.g. Dardel et al., 2014; Vicente-Serrano et al., 2015; Gouveia et al., 2016). Amongst these global datasets, the most widely used are those derived from the Advanced Very High Resolution Radiometer (AVHRR) sensor on board the NOAA satellites and those retrieved from the Moderate Resolution Imaging Spectroradiometer (MODIS) data. Both products have been widely employed to evaluate the possible influence of drought on vegetation dynamics in different regions worldwide (e.g. Tucker et al., 2005; Gu et al., 2007; Sona et al., 2012; Pin-

zon and Tucker, 2014; Ma et al., 2015). While the Global Inventory Modeling and Mapping Studies (GIMMS) dataset from NOAA AVHRR is available at a semi-monthly temporal resolution for the period from 1981 onwards (Tucker et al., 2005; Pinzon and Tucker, 2014), its spatial resolution is quite low (64 km^2), which makes it difficult to capture the high spatial variability of vegetation cover over Spain. However, the NDVI dataset derived from MODIS dates back only to 2001 (Huete et al., 2002), which is insufficient to give insights into the long-term response of vegetation activity to drought. To overcome these spatial and temporal limitations, our decision was made to employ a recently developed high-resolution spatial NDVI dataset (Sp_1Km_NDVI), which is available at grid intervals of 1.1 km, spanning the period from 1981 onwards. In accordance with the GIMMS dataset, Sp_1Km_NDVI is available at a semi-monthly temporal resolution. This dataset has already been validated (Vicente-Serrano et al., 2018), showing high performance in comparison to other available NDVI datasets. As such, it can be used – with confidence – to provide a multidecadal assessment of NDVI variability at high spatial resolution, especially in areas of highly variable vegetation. Herein, it is noteworthy to indicate that the data from the Sp_1Km_NDVI dataset was standardized (sNDVI), so that each series has an average equal to zero and a standard deviation equal to 1. This procedure is motivated by the strong seasonality and spatial differences of vegetation activity over Spain. Following this procedure, the magnitudes of all NDVI time series are comparable over space and time. To accomplish this task, the data were fitted to a log-logistic distribution, which shows better skill in standardizing environmental variables, in comparison to other statistical distributions (Vicente-Serrano and Beguería, 2016).

In order to limit the possible impact of changes in land cover on the dependency between drought and vegetation cover, we assumed that strong changes in NDVI can be seen as an indicator of changes in land cover. As such, those pixels with strong changes in NDVI during the study period were excluded from the analysis. These pixels were defined after an exploratory analysis in which we tested different thresholds. Specifically, we excluded those pixels that exhibited a decrease in the annual NDVI higher than 0.05 units or an increase higher than 0.15 units between 1981 and 2015. The spatial distribution of these pixels (not shown here) concurs well with the areas identified in earlier studies over Spain in which there was an abrupt modification of the land cover type: creation of new irrigated lands (Lasanta and Vicente-Serrano, 2012; Lecina et al., 2010; Stellmes et al., 2013; Vicente-Serrano et al., 2018), urban expansion (Gallardo and Martínez-Vega, 2016; Palazón et al., 2016; Serra et al., 2008), agricultural abandonment (Lasanta et al., 2017), deforestation (Camarero et al., 2015; Carnicer et al., 2011), reforestation (Ortigosa et al., 1990), etc. Furthermore, to avoid the possible influence of spatial autocorrelation, which can occur in areas with dominant positive changes in NDVI due to ex-

cessive rural exodus and natural revegetation processes (Hill et al., 2008; Vicente-Serrano et al., 2018), we detrended the standardized NDVI series by means of a linear model. We then add the residuals of the linear trend to the average of NDVI magnitude over the study period. A similar approach has been adopted in several environmental studies (Olsen et al., 2013; Xulu et al., 2018; Zhang et al., 2016). Correlations with the drought dataset were based on the sNDVI.

2.1.2 Drought dataset

Due to its complicated physiological strategies to cope with water stress, vegetation can show specific and even individual resistance and vulnerability to drought (Chaves et al., 2003; Gazol et al., 2017, 2018). As such, it is quite difficult to directly assess the impacts of drought on vegetation activity and forest growth. Alternatively, drought indices can be an appropriate tool to make this assessment, particularly with their calculation at multiple timescales. These timescales summarize the accumulated climatic conditions over different periods, which make drought indices closely related to impact studies. Overall, to calculate drought indices, we employed data for a set of meteorological variables (i.e. precipitation, maximum and minimum air temperature, relative humidity, sunshine duration, and wind speed) from a recently developed gridded climatic dataset (Vicente-Serrano et al., 2017). This gridded dataset was developed using a dense network of quality-controlled and homogenized meteorological records. Data are available for the whole Spanish territory at a spatial resolution of 1.1 km, which is consistent with the resolution of the NDVI dataset (Sect. 2.1.1). Based on this gridded dataset, we computed the atmospheric evaporative demand (AED) and the standardized precipitation evapotranspiration index (SPEI). We used the reference evapotranspiration (ET_o) as the most reliable way of estimating the AED. ET_o was calculated using the physically based FAO-56 Penman–Monteith equation (Allen et al., 1998). Conversely, the SPEI was computed using precipitation and ET_o data (Vicente-Serrano et al., 2010). The SPEI is one of the most widely used drought indices and has thus been employed to quantify drought in a number of agricultural (e.g. Peña-Gallardo et al., 2018b), environmental (e.g. Vicente-Serrano et al., 2012; Bachmair et al., 2018), and socio-economic applications (e.g. Bachmair et al., 2015; Stagge et al., 2015). The SPEI is advantageous compared to the Palmer Drought Severity Index (PDSI), as it is calculated at different timescales. In comparison to the standardized precipitation index (SPI) (McKee et al., 1993), the SPEI does not account only for precipitation, but it also considers the contribution of ET_o in drought evolution.

In this work, the SPEI was calculated for the common 1- to 24-month timescales, but here, given the semi-monthly availability of the data, we calculated the corresponding 1- to 48-semi-monthly timescales. The preference to use various timescales is motivated by our intention to characterize

the response of different hydrological and environmental systems to drought. It is well-recognized that natural systems can show different responses to the timescales of drought (Vicente-Serrano et al., 2011, 2013). The timescale refers to the period in which antecedent climate conditions are accumulated and it allows adaptation of the drought index to the drought impacts since different hydrological and environmental systems show different response sensitivities to the timescales of climate variability. This has been shown for hydrological systems (López-Moreno et al., 2013; Barker et al., 2016), but ecological and agricultural systems also show strong differences in the response to different timescales of climatic droughts (Pasho et al., 2011; Peña-Gallardo et al., 2018b) given different biophysical conditions and the different strategies of vegetation types to cope with water stress (Chaves et al., 2003; McDowell et al., 2008), which are strongly variable in complex Mediterranean ecosystems. For instance, drought indices can be calculated on flexible timescales since it is not known a priori the most suitable period at which the NDVI responds. Herein, we also detrended and standardized the semi-monthly SPEI data to be comparable with the de-trended sNDVI.

Finally, we used the CORINE Land Cover for 2000 (<https://land.copernicus.eu/pan-european/corine-land-cover>, last access: 21 May 2019) to determine how land cover can impact the response of NDVI to drought severity. This map is representative of the main classes of land cover in the study domain over the period of investigation.

2.2 Statistical analysis

We used the Pearson's r correlation coefficient to assess the relationship between the interannual variability of the sNDVI and SPEI. This association was evaluated independently for each semi-monthly period of the year. Specifically, we calculated the correlation between the sNDVI for each semi-monthly period and SPEI recorded in the same period, at 1- and 48-semi-monthly timescales. Significant correlations were set at $p < 0.05$. Importantly, as the data of the sNDVI and SPEI were de-trended, the possible impact of serial correlation on the correlation between sNDVI and SPEI is minimized, with no spurious correlation effects that can be expected from the co-occurrence of the trends. Similarly, as the data were analysed for each semi-monthly period independently, our results are free from any seasonality effect. Given that it is not possible to know a priori the best cumulative period to explain the response of the vegetation activity to drought variability, we retained for further analysis the maximum correlation, independently of the timescale at which this is obtained.

Based on the correlation coefficients between the sNDVI and SPEI in the study domain, we determined the semi-monthly period of the year and the SPEI timescale at which the maximum correlation is found. This information was then used to determine the spatial and seasonal variations accord-

ing to the different land cover categories. Finally, the average climate conditions over the study domain, including aridity (precipitation minus ETo) and average temperature, were related to the timescales at which the maximum correlation between the sNDVI and SPEI was found.

3 Results

3.1 General influence of drought on the sNDVI

Figure 1 shows an example of the spatial distribution of the Pearson's r correlation coefficients calculated between the sNDVI and the SPEI at the timescales of 1, 3, 6, and 12 months (2, 6, 12 and 24 semi-monthly periods). Results are shown only for the second semi-monthly period of each month between April and July. The differential response of the NDVI to the different timescales of the SPEI is illustrated. As depicted, the 6-month timescale was more relevant to vegetation activity in large areas of southwestern and southeastern Spain during the second half of April. Conversely, vegetation activity was more determined by the 12-month SPEI across the Ebro basin in northeastern Spain. This stresses the need to consider different drought timescales to know the climate cumulative period that mostly affects vegetation activity. The 6-month and 12-month SPEIs produced similar results during the second period of May, while the 12-month timescale is more related to vegetation activity in June and July.

Figure 2 summarizes the maximum correlation between the sNDVI and the SPEI, providing insights into the differential response of the NDVI to drought. It can be noted that there are clear seasonal and spatial differences in the response of sNDVI to the SPEI. The sNDVI is more related to the SPEI during the warm season (MJJA). In contrast, the response of the sNDVI to drought is less pronounced from September to April, albeit with some exceptions. One example is the response of vegetation to drought alongside the southeastern Mediterranean coastland, where the correlation between sNDVI and SPEI is almost high all year. Table 1 summarizes the percentage of the total area exhibiting significant or non-significant correlations over Spain during the different semi-monthly periods. Positive (lower sNDVI with drought) and statistically significant correlations are dominant across the entire territory, but with a seasonal component. In particular, a higher percentage of the territory shows positive and significant correlations during the warm season (MJJA). From the middle of May to middle of September, more than 80 % of the study domain shows positive and significant correlations between the sNDVI and the SPEI. A similar finding is also found between the middle of June and the beginning of August. Figure 3 summarizes the average correlations between the SPEI and sNDVI. As illustrated, there is a gradual increase in the response of the sNDVI to the SPEI from the beginning of May to the end of July, when

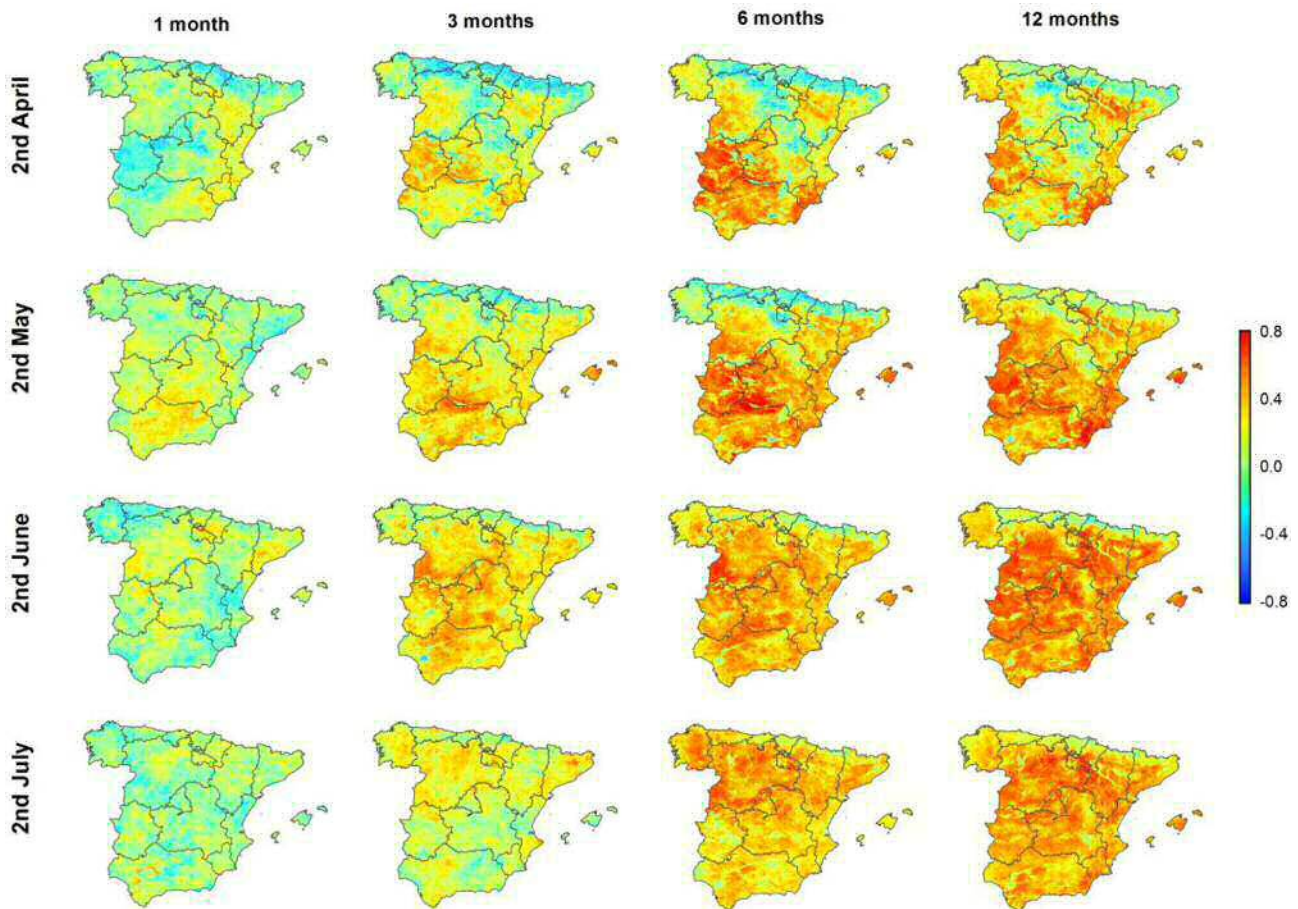


Figure 1. Spatial distribution of the Pearson's r correlation coefficient calculated between the sNDVI and different SPEI timescales for different semi-monthly periods.

the maximum average correlation is recorded. In contrast, the correlations between the SPEI and sNDVI decrease progressively from August to December.

The response of the sNDVI to different timescales of the SPEI and seasons is quite complex. Figure 4 shows the spatial distribution of the SPEI timescale at which the maximum correlation was found for each one of the 24 semi-monthly periods of the year. It can be noted that there are considerable seasonal and spatial differences. Nonetheless, these differences are masked with the estimated average values of the SPEI timescale recorded for the semi-monthly periods (Fig. 5), which are less variable (oscillating between 18 and 22 semi-monthly periods – 9–11 months) throughout the year. In general, the areas and periods with higher correlations are recorded at 7- and 24-semi-monthly timescales (3–12 months).

3.2 Land cover differences

There are differences in the magnitude and seasonality of the Pearson's r correlation coefficients among all land cover types. Figure 6 shows the average and standard error of the

mean of the maximum Pearson's r coefficients between the sNDVI and SPEI for the different land cover types and the 24 semi-monthly periods. The magnitudes of correlation vary considerably, as a function of land cover type, as well as the period of the year in which the highest correlations are recorded. The unirrigated arable lands show a peak of significant correlation between April and June. However, this correlation decreases towards the end of the year. The majority of this land cover shows positive and significant correlations between May and September (Supplement Table S1), with percentages almost close to 100%. Conversely, irrigated lands do not show such a strong response to drought during the warm season. Even with the presence of a seasonal pattern, it is less pronounced than the one observed for unirrigated arable lands. Overall, irrigated areas are characterized by positive and significant correlations between sNDVI and SPEI during summertime (Table S2). Similarly, vineyards show a clear seasonal pattern, albeit with a peak of maximum correlations during the late summer (July to August) and early autumn (September to October) (Table S3). Conversely, olive groves show the highest correlation between

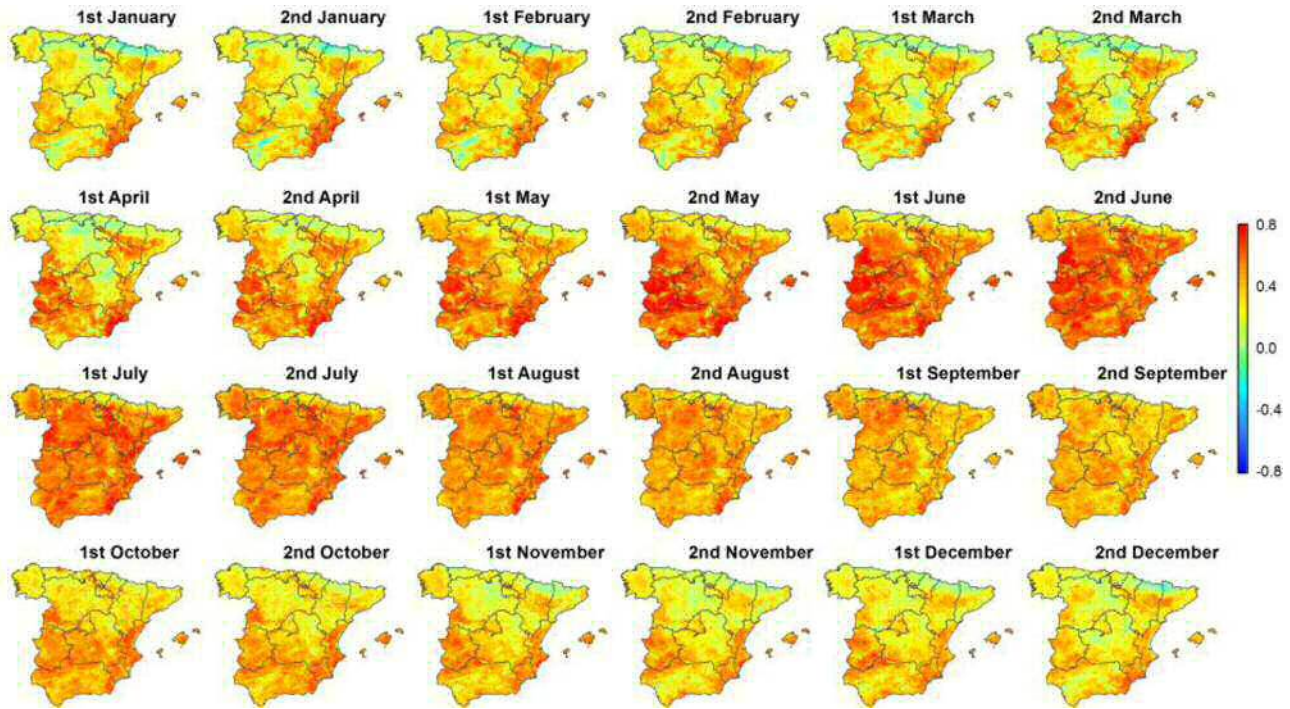


Figure 2. Spatial distribution of the maximum correlation between the sNDVI and the SPEI during the different semi-monthly periods.

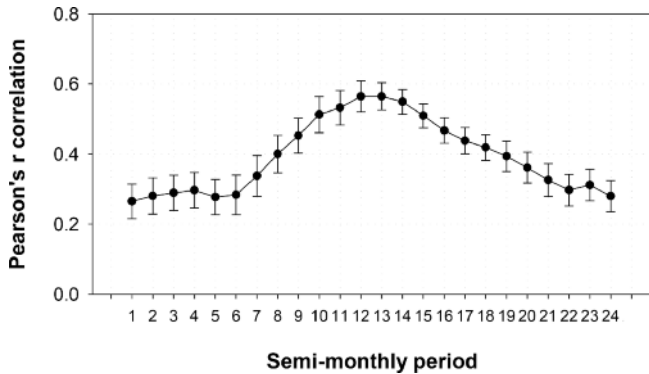


Figure 3. Spatial average and standard error of the Pearson's *r* correlation coefficient between the sNDVI and SPEI time series.

the sNDVI and SPEI during the second half of May and in October, suggesting a quasi-bimodal response of the NDVI to drought. This pattern is also revealed in the percentage of the surface area with significant correlations (Table S4). In the same context, the areas of natural vegetation exhibit their maximum correlation between the sNDVI and SPEI during summer months. The highest correlations are found in July and August for the forest types, compared to earlier June for the natural grasslands and the areas of sclerophyllous vegetation. Conversely, the mixed forests tend to show lower correlations than broad-leaved and coniferous forests. A quick inspection of all these types of land cover indicates that the cor-

relations between the sNDVI and SPEI are generally positive and significant during summer months (Tables S5 to S11).

Large differences across vegetation types were found for the SPEI timescales at which maximum correlations between sNDVI and the SPEI are found (Fig. 7). For example, for unirrigated arable lands, the maximum correlation between SPEI and sNDVI is found for timescales between 11 and 21 semi-monthly periods. This indicates that crops in May–June (the period in which higher correlations are recorded) respond mostly to the climate conditions recorded between June and December of the preceding year. Irrigated lands show a clear seasonal pattern, as maximum correlations are recorded at timescales between 12 and 18 semi-monthly periods (i.e. 6 to 9 months), mainly between November and May. Conversely, the maximum correlations between sNDVI and SPEI during summer are found for timescales between 25 and 28 semi-monthly periods. Similar to irrigated lands, vineyards show a strong seasonality, responding to longer timescales at the end of summertime. In contrast, natural vegetation areas show a less seasonal response to SPEI timescales, which mostly impact the interannual variability of sNDVI. The SPEI timescales, at which the maximum correlation is found between sNDVI and SPEI, vary from 20 semi-monthly periods during the warm season (MJJAS) to 30 semi-monthly periods during the cold season (ONDJFMA). This finding is evident for all forest types and areas of sclerophyllous vegetation and mixed wood–scrub. The only exception corresponds to natural grasslands, which show a re-

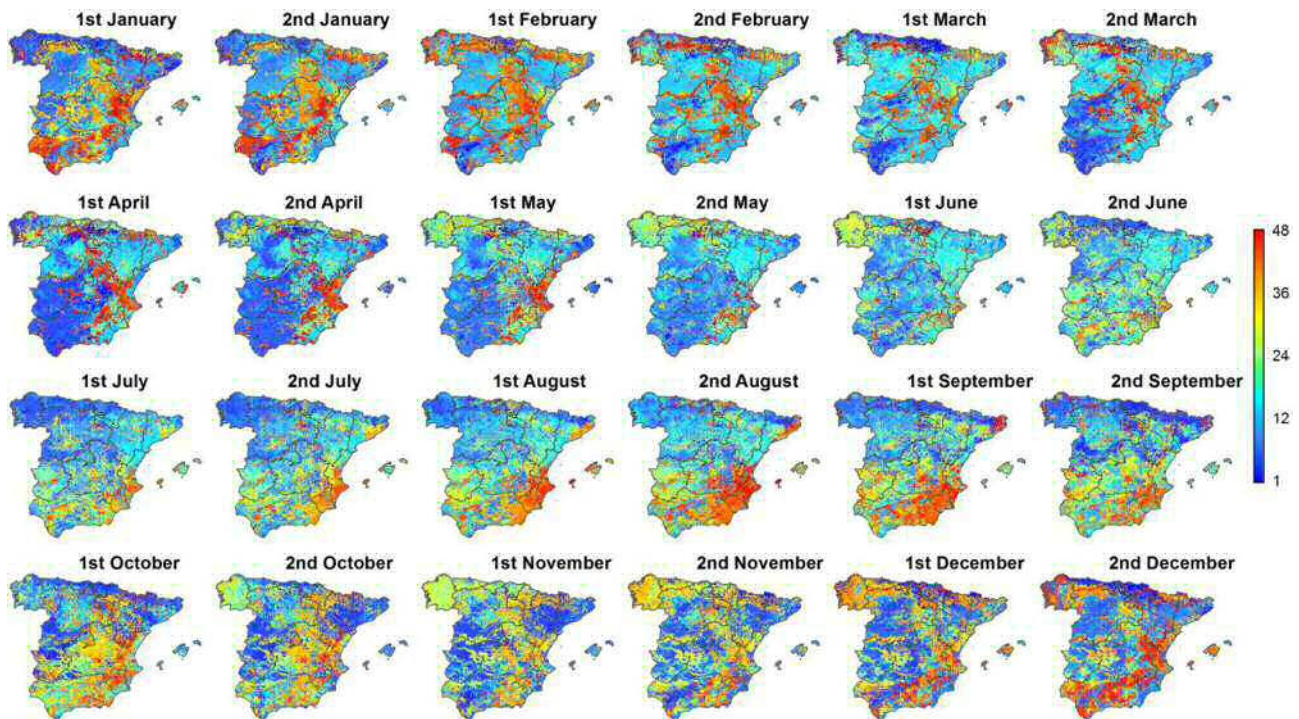


Figure 4. Spatial distribution of the SPEI timescales at which the maximum correlation between the sNDVI and SPEI is found for each one of the semi-monthly periods.

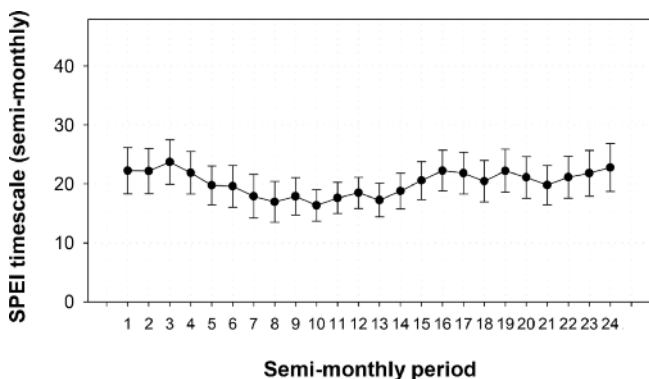


Figure 5. Average and standard error of the SPEI timescale at which the maximum Pearson's r correlation coefficient between the sNDVI and SPEI is found.

response to shorter SPEI timescales (i.e. 20 semi-monthly periods in winter and 15 in spring and early summer).

3.3 Influence of average climatic conditions

In addition to the impact of the timescale at which drought is quantified, the response of vegetation activity to drought can also be closely related to the prevailing climatic conditions. Figure 8 summarizes the spatial correlation between aridity (P-ET₀) and the maximum correlation between the sNDVI and SPEI. For most of the semi-monthly periods of

the year aridity is negatively correlated with the maximum correlation between sNDVI and SPEI, indicating that vegetation activity at arid sites is more responsive to drought variability. This correlation is more pronounced for the period between December and June. In contrast, this negative association becomes weaker and statistically non-significant during warmer months (July to August). Figure 9 illustrates the spatial correlation between mean air temperature and the maximum correlation between the sNDVI and SPEI. Results demonstrate similar results to those found for aridity, with a general positive and significant correlation from March to June, followed by a non-significant and weak correlation during summer months.

Nonetheless, these general patterns vary largely as a function of land cover type (Supplement Figs. S1 to S11). For example, in unirrigated arable lands, there is strong negative correlation between aridity and the sNDVI–SPEI maximum correlation from March to May: a period that witnesses the peak of vegetation activity in this land cover type. This also coincides with the period of the highest average correlations between the sNDVI and SPEI. Taken together, this demonstrates that unirrigated arable lands located in the most arid areas are more sensitive to drought variability than those located in humid regions. As opposed to unirrigated arable lands, the correlations with aridity are found to be statistically non-significant in all periods of the year for irrigated lands, vineyards, and olive groves. Nev-

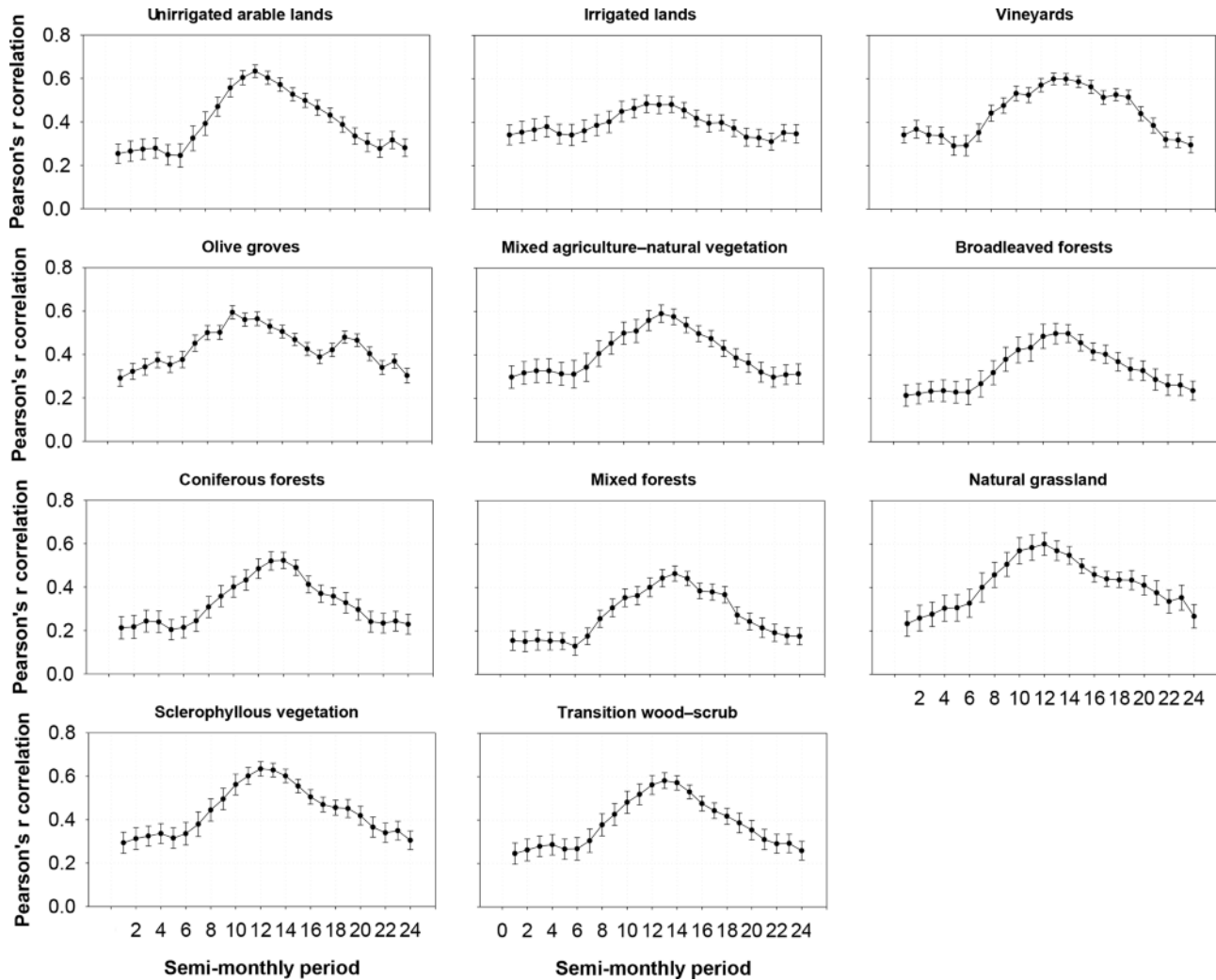


Figure 6. Average and standard error of the Pearson's r correlation coefficient between the sNDVI and SPEI for the different land cover types.

ertheless, for the different natural vegetation categories, the correlations are negative and statistically significant during large periods. The mixed agricultural–natural vegetation areas show a significant correlation between October and July, with stronger association at the beginning of the summer season. Broadleaved and coniferous forests, scrub, and pasturelands also show a negative relationship between the spatial patterns of the sNDVI–SPEI correlations and aridity.

As depicted in Fig. 9, the relationship between the sNDVI–SPEI correlation and air temperature shows that the response of vegetation activity to drought is modulated by air temperature during springtime. This implies that warmer areas are those in which the sNDVI is more controlled by drought. A contradictory pattern is found during warmer months, in which the role of air temperature in modulating the impact of drought on vegetation activity is minimized. The relationships between air temperature and the NDVI–SPEI correla-

tion vary among the different land cover types (Figs. S12 to S22). For example, in unirrigated arable lands, the positive and statistically significant correlation is found in the period from March to May, indicating that the response of the sNDVI to SPEI tends to coincide spatially with areas of warmer conditions. As observed for aridity, the relationship between the sNDVI and SPEI in irrigated lands is less associated with the spatial patterns of air temperature. A similar pattern is recorded for vineyards and olive groves. Nevertheless, the areas of natural vegetation show a clear relationship between air temperature and the sNDVI–SPEI correlations. In the mixed agriculture and natural vegetation areas, we found a statistically significant positive association between the sNDVI and SPEI from October to May. Conversely, this association is less evident during summer months. This general association during springtime, combined with the lack of association during summertime, can also be seen for other

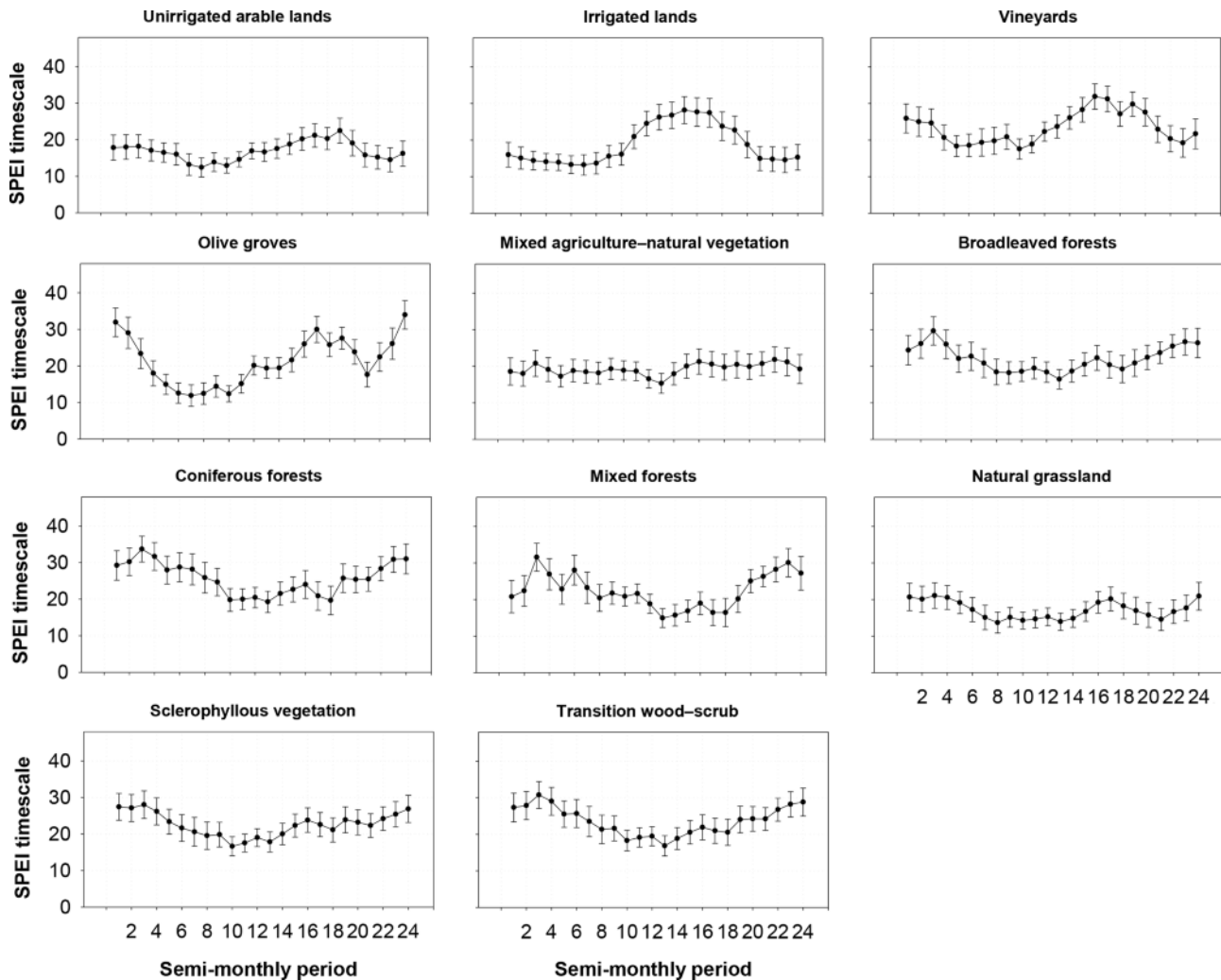


Figure 7. Average and standard error of the SPEI timescale at which the maximum Pearson's r correlation coefficient was found between the sNDVI and SPEI for the different land cover types.

natural vegetation types such as broad-leaved and coniferous forests, natural grasslands, sclerophyllous vegetation, and mixed wood-scrub.

We also analysed the dependency between climatic conditions (i.e. aridity and air temperature) and the SPEI timescale(s) at which the maximum correlation between the sNDVI and SPEI is recorded. Figure 10 shows the values of aridity corresponding to SPEI timescales at which the maximum correlation between the sNDVI and SPEI is found for each semi-monthly period. The different box plots indicate complex patterns, which are quite difficult to interpret. Overall, less arid areas show stronger correlations at longer timescales (25–42 semi-monthly periods) during springtime. In the same context, the regions with maximum correlations at short timescales (1–6 months) tend to be located in less arid regions that record their maximum correlations at timescales between 7 and 24 semi-monthly periods. This suggests that the most arid areas mostly respond to the SPEI

timescales between 6 and 12 months, compared to short (1–3 months) or long (> 12 months) SPEI timescales in more humid regions. In contrast, during the summer season, the interannual variability of the sNDVI in the arid areas is mostly determined by the SPEI recorded at timescales higher than 6 months (12 semi-monthly periods), while responding to short SPEI timescales (< 3 months) over the most humid regions.

Also, we found links between the spatial distribution of air temperature and the SPEI timescales at which maximum correlation between the sNDVI and SPEI is recorded (Fig. 11). In early spring, short SPEI timescales dominate in warmer areas, compared to long SPEI timescales in colder regions. A contradictory pattern is observed from June to September, with a dominance of shorter SPEI timescales in colder areas and longer SPEI timescales in warmer regions.

The spatial distribution of all land cover types, after excluding irrigated lands in which the anthropogenic factors

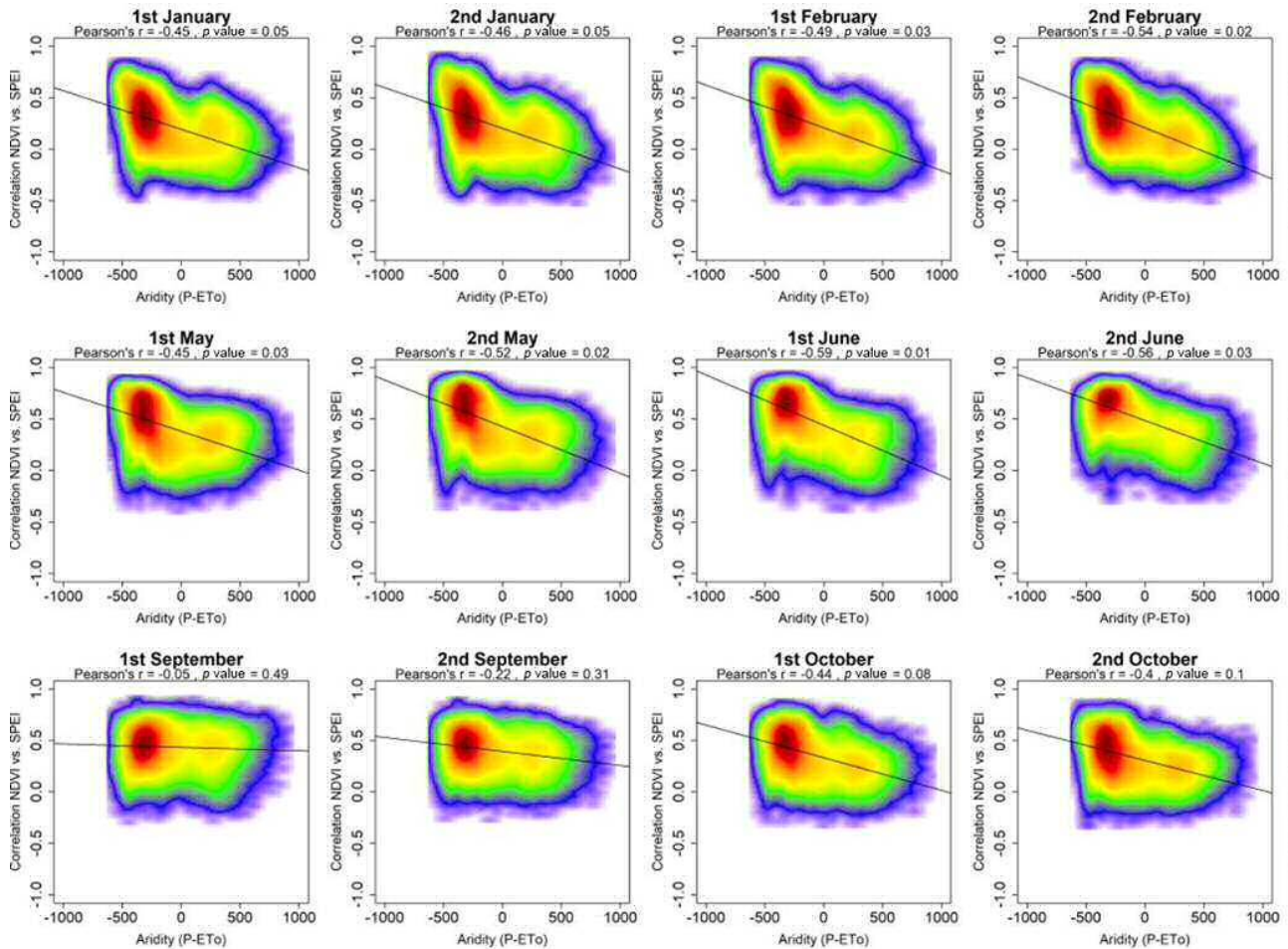


Figure 8.

dominate, is illustrated in Fig. 12. Mixed forests are located in the most humid areas, while vineyards, olive groves, unirrigated arable lands, and the sclerophyllous natural vegetation are distributed at the most arid sites. Nevertheless, there is a gradient of these land cover types in terms of their response to drought, as those types located under more arid conditions show a stronger response of vegetation activity to drought than those located in humid environments. For example, the mixed forests show lower correlations than crop types and other vegetation areas. This pattern is more evident during the different semi-monthly periods, albeit with more differences during spring and autumn. In summer, these differences are much smaller between land cover categories, irrespective of aridity conditions.

There are also differences in the average SPEI timescale at which the maximum sNDVI–SPEI correlation is obtained (Fig. 13). However, these differences are complex, with noticeable seasonal differences in terms of the relationship between climate aridity and land cover types. In spring and late autumn, land cover types located in more arid conditions tend to respond to shorter SPEI timescales than those located in

more humid areas. This pattern can be seen in late summer and early autumn, in which the most arid land cover types (e.g. vineyards and olive groves) tend to respond at longer SPEI timescales, compared to forest types (mostly the mixed forests), which are usually located under more humid conditions.

4 Discussion

This study assesses the response of vegetation activity to drought in Spain using a high-resolution (1.1 km) spatial NDVI dataset that dates back to 1981 (Vicente-Serrano et al., 2018). Based on another high-resolution semi-monthly gridded climatic dataset, drought was quantified using the standardized precipitation evapotranspiration index (SPEI) at different timescales (Vicente-Serrano et al., 2017).

Results demonstrate that vegetation activity over large parts of Spain is closely related to the interannual variability of drought. In summer more than 90 % of the study domain shows statistically significant positive correlations be-

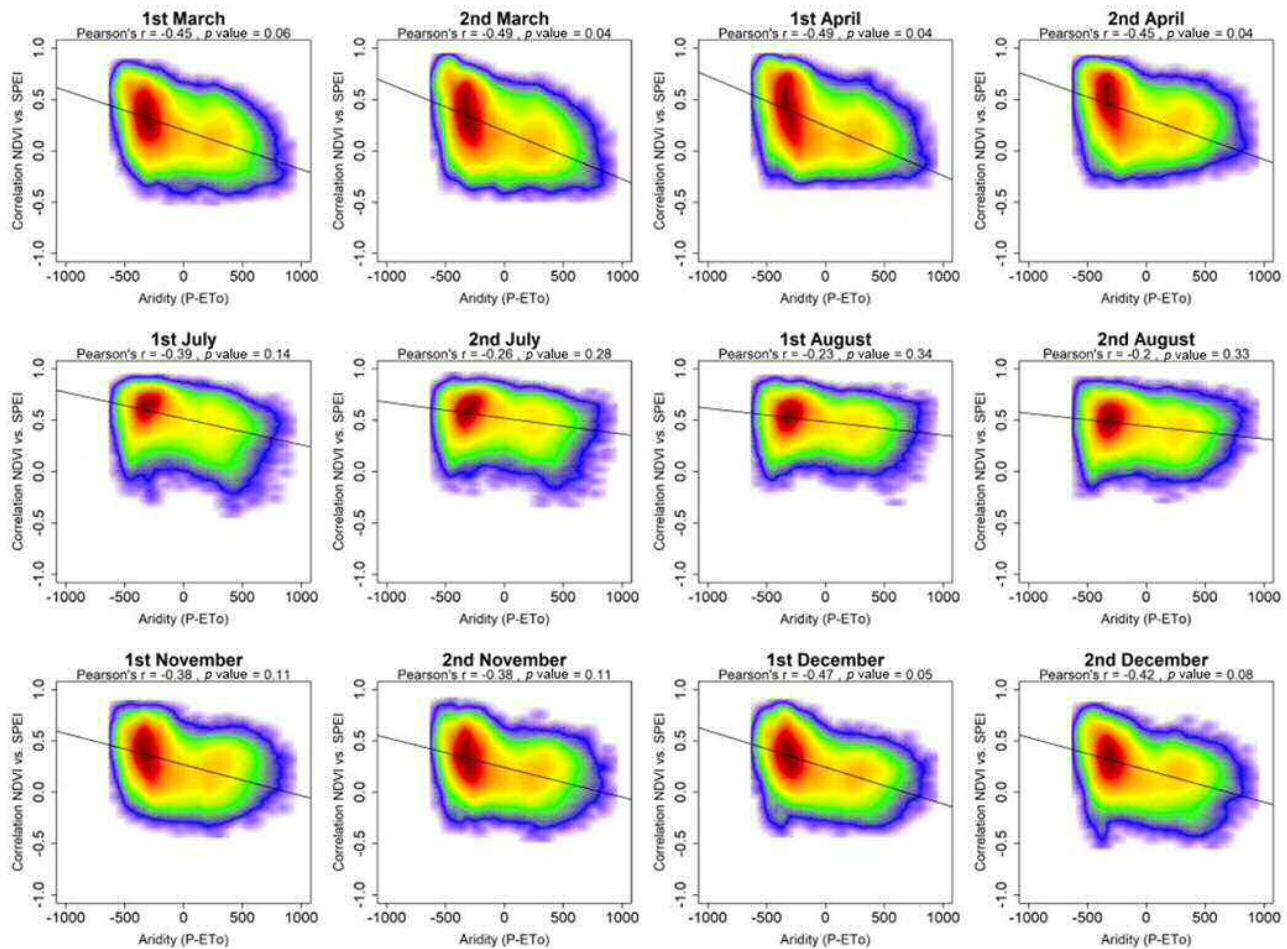


Figure 8. Scatterplots showing the relationships between the maximum correlation obtained between the sNDVI and the SPEI and the climate aridity (precipitation minus ETo). Given the high number of data, the significance of the correlation was obtained using a bootstrap method. A total of 1000 random samples of 30 data points each were extracted, from which correlations and p values were obtained. The final significance was assessed by means of the average of the obtained correlation coefficients and p values, which are indicated in the figure.

tween the NDVI and SPEI. A similar response of the NDVI to drought is confirmed in earlier studies in different semi-arid and subhumid regions worldwide, including northeastern Brazil (e.g. Barbosa et al., 2006), the Sahel (e.g. Herrmann et al., 2005), central Asia (e.g. Gessner et al., 2013), Australia (e.g. De Keersmaecker et al., 2017), and California (e.g. Okin et al., 2018). Albeit with this generalized response, our results also show noticeable spatial and seasonal differences in this response. These differences can be linked to the timescale at which the drought is quantified, in addition to the impact of other dominant climatic conditions (e.g. air temperature and aridity).

4.1 The response of vegetation activity to drought variability

This study stresses that the response of vegetation activity to drought is more pronounced during the warm season (MJ-

JAS), in which vast areas of the Spanish territory show statistically significant positive correlation between the sNDVI and SPEI. This seasonal pattern can be attributed to the phenology of vegetation under different land cover types. In the cold season, some areas, such as pastures and non-permanent broadleaf forests, do not have any vegetation activity. Other areas, with coniferous forests, shrubs, and cereal crops, show a low vegetation activity. As such, irrespective of the recorded drought conditions, the response of vegetation to drought would be low during wintertime. This behaviour is also enhanced by the atmospheric evaporative demand (AED), which is generally low in winter in Spain (Vicente-Serrano et al., 2014d), with a lower water demand of vegetation and accordingly low sensitivity to soil water availability. Austin et al. (1998) indicated that soil water recharge occurs mostly during winter months, given the low water consumption by vegetation. However, in spring, vegetation becomes

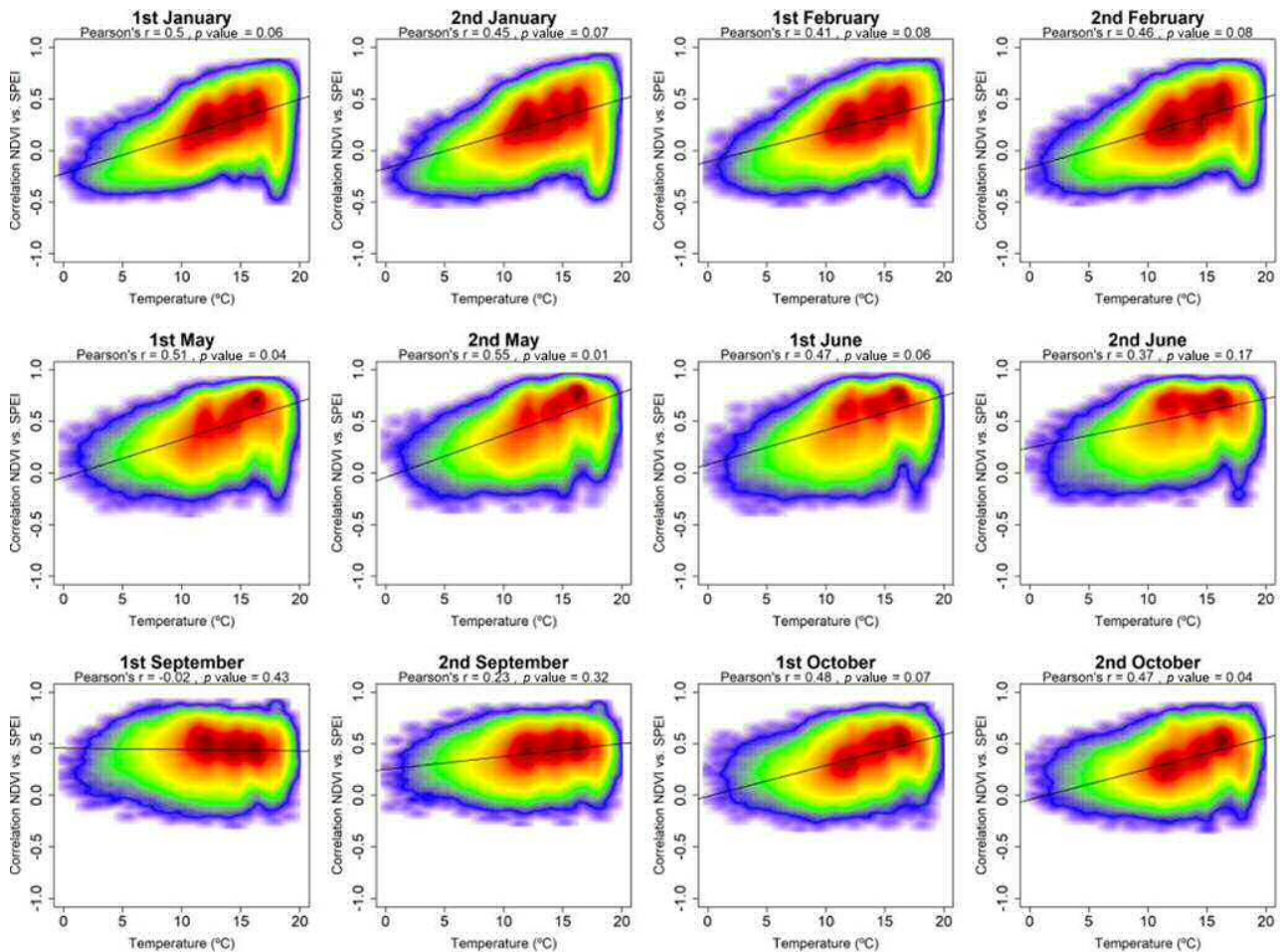


Figure 9.

more sensitive to drought due to temperature rise. Accordingly, the photosynthetic activity, which determines NDVI, is highly controlled by soil water availability (Myneni et al., 1995). In this study, the positive spatial relationship found between air temperature and the sNDVI–SPEI correlation reinforces this explanation. In spring, we found low correlations between the NDVI and SPEI, even in cold areas. In contrast, summer warm temperatures reinforce vegetation activity, but with some exceptions such as cereal cultivations, dry pastures, and shrubs. This would explain why the response of vegetation activity to the SPEI is stronger during summer in vast areas of Spain.

Also, this study suggests clear seasonal differences in the response of the NDVI to drought, and in the magnitude of the correlation between the NDVI and the SPEI, as a function of the dominant land cover. These differences are confirmed at different spatial scales, ranging from regional and local (e.g. Ivits et al., 2014; Zhao et al., 2015; Gouveia et al., 2017; Yang et al., 2018) to global (e.g. Vicente-Serrano et al., 2013). Over Spain, the unirrigated arable lands, natural grasslands, and sclerophyllous vegetation show an earlier

response to drought, mainly in late spring and early summer. This response is mainly linked to the vegetation phenology dominating in these land covers, which usually reach their maximum activity in late spring to avoid dryness and temperature rise during summer months. The root systems of herbaceous species are not very deep, so they depend on the water storage in the most superficial soil layers (Milich and Weiss, 1997), and they could not survive during the long and dry summer in which the surface soil layers are mostly depleted (Martínez-Fernández and Ceballos, 2003). This would explain an earlier and stronger sensitivity to drought also shown in other semi-arid regions (Liu et al., 2017; Yang et al., 2018; Bailing et al., 2018). Conversely, maximum correlations between the NDVI and the SPEI are recorded during summer months in the forests but also in wood cultivations like vineyards and olive groves. In this case, the maximum sensitivity to drought coincides with the maximum air temperature and atmospheric evaporative demand (Vicente-Serrano et al., 2014d). This pattern would be indicative of a different adaptation strategy of trees in comparison to herbaceous vegetation, since whilst herbaceous cover would adapt

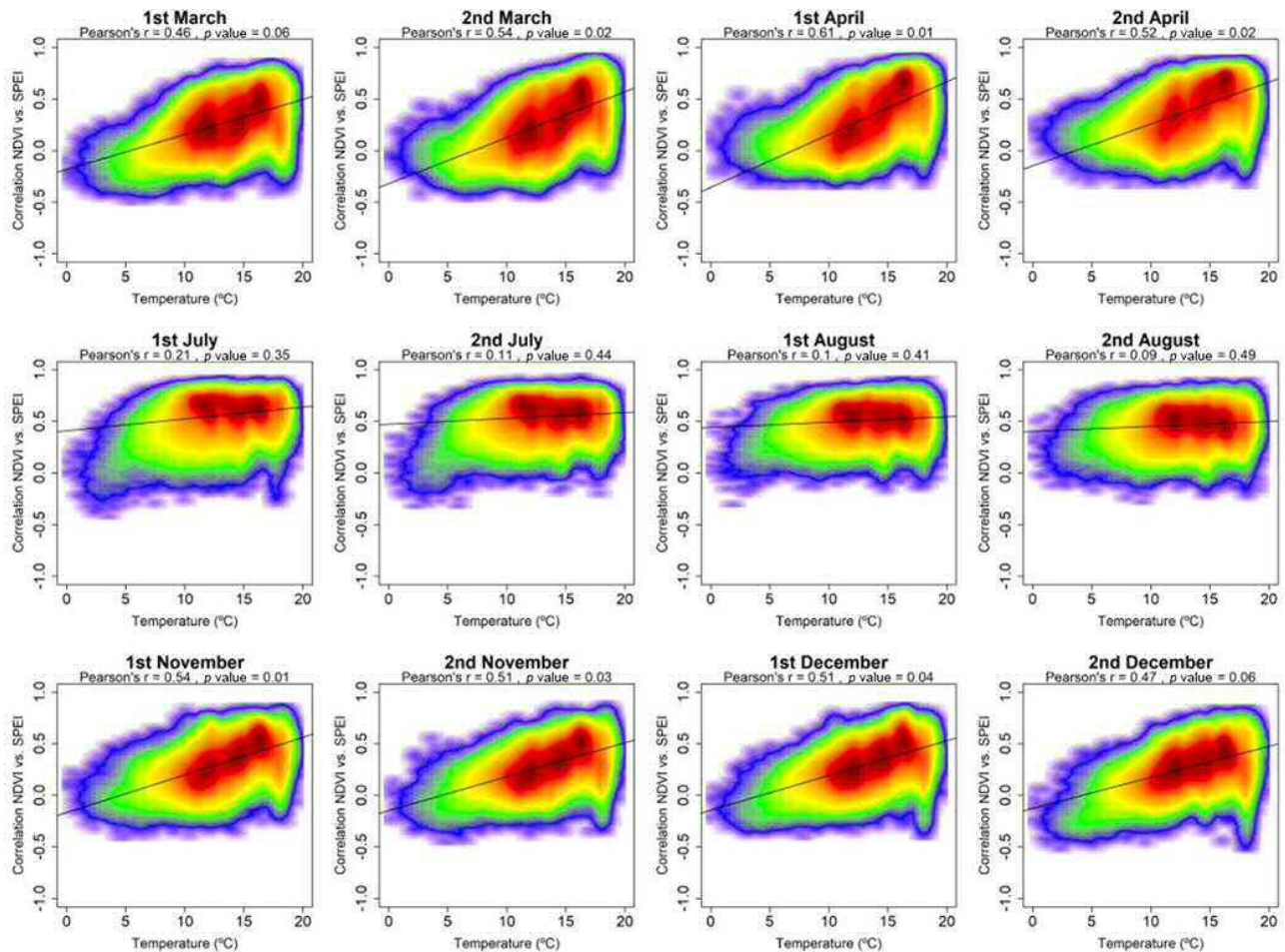


Figure 9. Scatterplots showing the relationships between the maximum correlation obtained between the sNDVI and the SPEI and the average air temperature. Given the high number of points, the significance of correlation was obtained by means of 1000 random samples of 30 cases from which correlations and p values were obtained. The final significance was assessed by means of the average of the obtained p values.

to the summer dryness generating the seed bank before the summer (Peco et al., 1998; Russi et al., 1992), the trees and shrubs would base their adaptation on deeper root systems, translating the drought sensitivity to the period of highest water demand and water limitation.

In addition to the seasonal differences among land cover types, we have shown that in Spain herbaceous crops show a higher correlation between the NDVI and the SPEI than most natural vegetation types (with the exception of the sclerophyllous vegetation). This behaviour could be explained by three different factors: (i) a higher adaptation of natural vegetation to the characteristic climate of the region where drought is a frequent phenomenon (Vicente-Serrano, 2006), (ii) the deeper root systems that allow shrubs and trees to obtain water from the deep soil, and (iii) cultivated lands that tend to be typically located in drier areas than natural vegetation. Different studies showed that the vegetation of dry environments tends to have a more intense response to

drought than subhumid and humid vegetation (Schultz and Halpert, 1995; Abrams et al., 1990; Nicholson et al., 1990; Herrmann et al., 2016). Vicente-Serrano et al. (2013) analysed the sensitivity of the NDVI in the different biomes at a global scale and found a spatial gradient in the sensitivity to drought, which was more important in arid and semi-arid regions.

4.2 Response to the average climatology

In this study we have shown a control in the response of the NDVI to drought severity by the climatic aridity. Thus, there is a significant correlation between the spatial distribution of the climatic aridity and the sensitivity of the NDVI to drought, mostly in spring and autumn. This could be explained because in more humid environments the main limitation to vegetation growth is temperature and radiation rather than water, so not all the water available would be used by vegetation reflected in a water surplus as surface

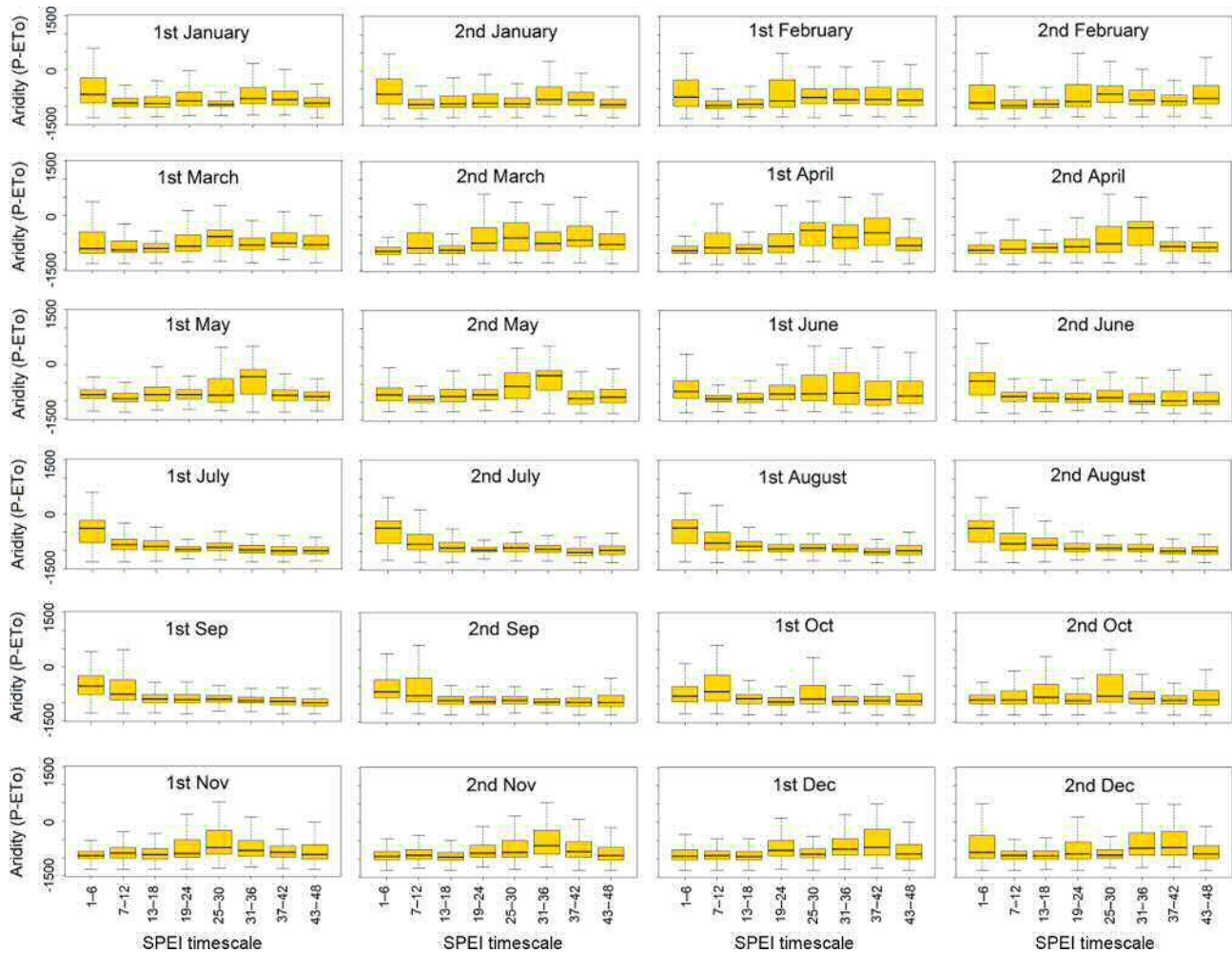


Figure 10. Box plots showing the climate aridity values, as a function of the SPEI timescales at which the maximum correlation between the sNDVI and SPEI is recorded.

runoff. This characteristic would make the vegetation less sensitive to drought in the cold season. Drought indices are relative metrics in comparison to the long-term climate with the purpose of making drought severity conditions comparable between areas of very different climate characteristics (Mukherjee et al., 2018). This means that in humid areas the corresponding absolute precipitation can be sufficient to cover the vegetation water needs although drought indices provide information on below-average conditions. Conversely, in arid regions a low value of a drought index is always representative of limited water availability, which would explain the closer relationship between the NDVI and the SPEI.

Here we also explored if the general pattern observed in humid and semi-arid regions is also affected by the land cover, and found that the behaviour in the unirrigated arable lands is the main reason for the global pattern. Herbaceous crops show that aridity levels have a clear control of the response of the NDVI to drought during the period of vegeta-

tion activity. Nevertheless, after the common harvest period (June) this control by aridity mostly disappears. This is also observed in the grasslands and in the sclerophyllous vegetation, and it could be explained by the low vegetation activity of the herbaceous and shrub species during the summer, given the phenological strategies to cope with water stress with the formation of the seeds before the period of dryness (Chaves et al., 2003). The limiting aridity conditions that characterize the regions in which these vegetation types grow would also contribute to explaining this phenomenon. Conversely, the forests, both broadleaved and coniferous, also show a control by aridity in the relationship between the NDVI and the SPEI during the summer months since these land cover types show the peak of the vegetation activity during this season.

In any case, it is also remarkable that the spatial pattern of the NDVI sensitivity to drought in forests is less controlled by aridity during the summer season, curiously the season in which there are more limiting conditions. This could be

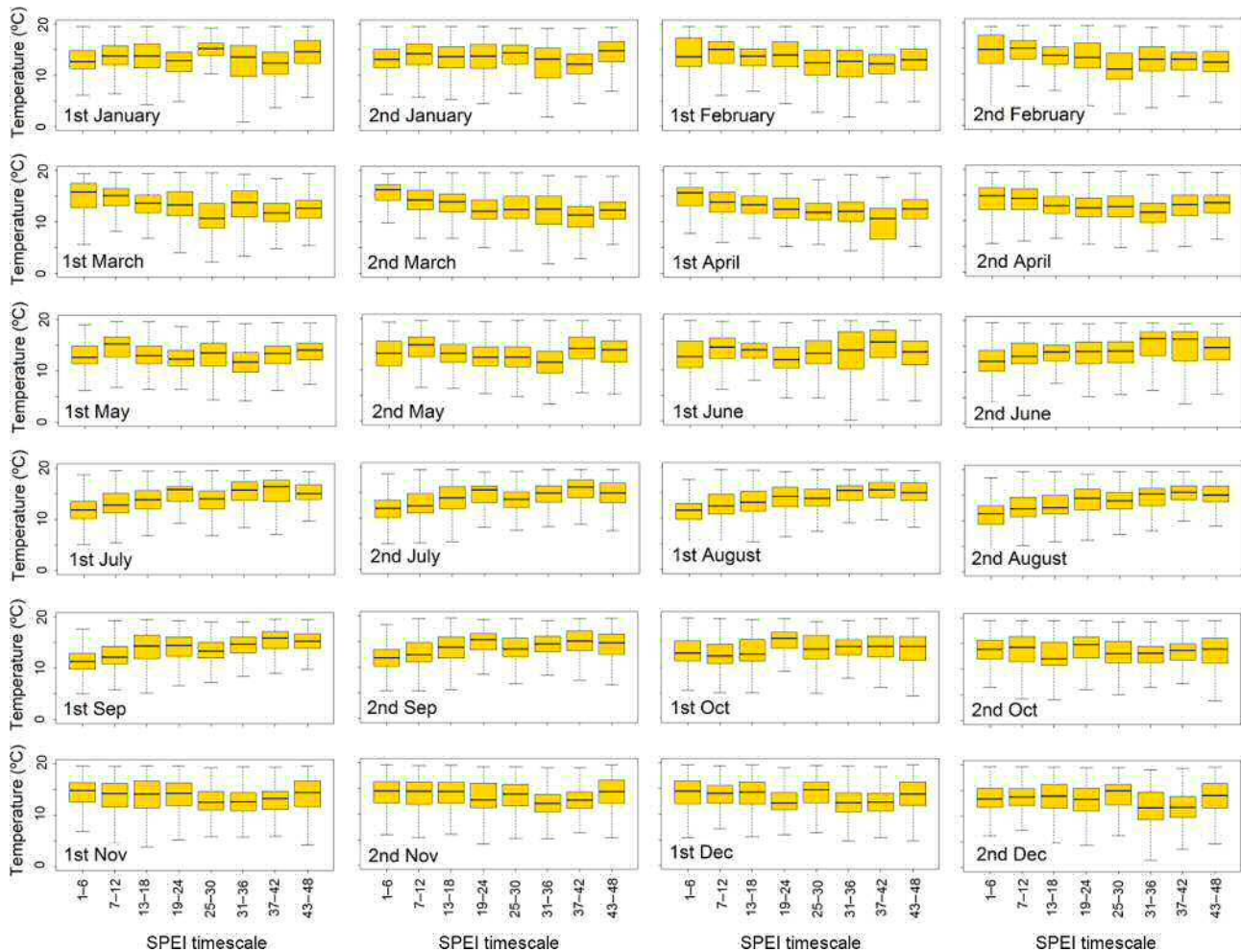


Figure 11. Box plots showing air temperature values, as a function of the SPEI timescales at which the maximum correlation between the sNDVI and SPEI is recorded.

explained by the NDVI saturation under high levels of leaf area index (Carlson and Ripley, 1997) since once the tree tops are completely foliated the electromagnetic signal is not sensitive to additional leaf growth. This could explain the less sensitive response of the forests to drought in comparison to land cover types characterized by lower leaf area (e.g. shrubs or grasslands). Nevertheless, we do not think that this phenomenon can totally explain the decreased sensitivity to drought with aridity in summer since the dominant coniferous and broadleaved forests in Spain are usually not characterized by a 100% leaf coverage (Castro-Díez et al., 1997; Molina and del Campo, 2012), so large signal saturation problems are not expected. Conversely, the ecophysiological strategies of forests to cope with drought may help explain the observed lower relationship between aridity during the summer months. Experimental studies suggested that the interannual variability of the secondary growth could be more sensitive to drought than the sensitivity observed by the photosynthetic activity and the leaf area (Newberry, 2010).

This could be a strategy to optimize the storage of carbohydrates, suggesting that forests in dry years would prioritize the development of an adequate foliar area in relation to the wood formation in order to maintain respiration and photosynthetic processes. Recent studies by Gazol et al. (2018) and Peña-Gallardo et al. (2018b) confirmed that, irrespective of forest species, there is a higher sensitivity of tree-ring growth to drought, compared to the sensitivity of the NDVI. The different spatial and seasonal responses of vegetation activity to drought in our study domain can also be linked to the dominant forest species and species richness, which have been evident in numerous studies (e.g. Lloret et al., 2007). Moreover, this might also be attributed to the ecosystem physiological processes, given that vegetation tends to maintain the same water use efficiency under water stress conditions, regardless of vegetation types and environmental conditions (Huxman et al., 2004). This would explain that – independently of the aridity conditions – the response of the NDVI to drought would be similar. Here, we demonstrated that the

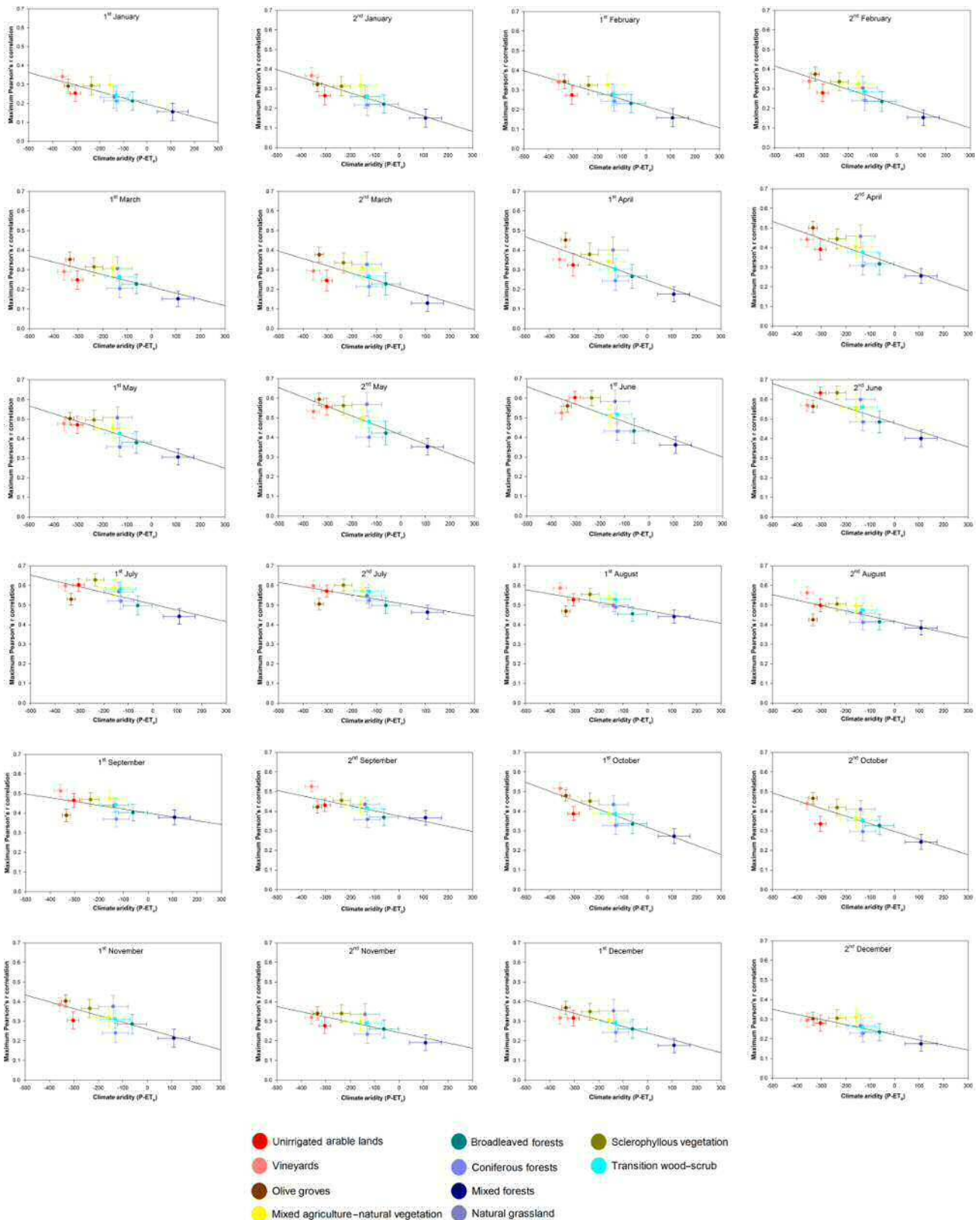


Figure 12. Scatterplots showing the relationship between the mean annual aridity and the maximum correlation found between the sNDVI and the SPEI in the different land cover types analysed in this study. Vertical and horizontal bars represent one-fourth the standard deviation around the mean values.

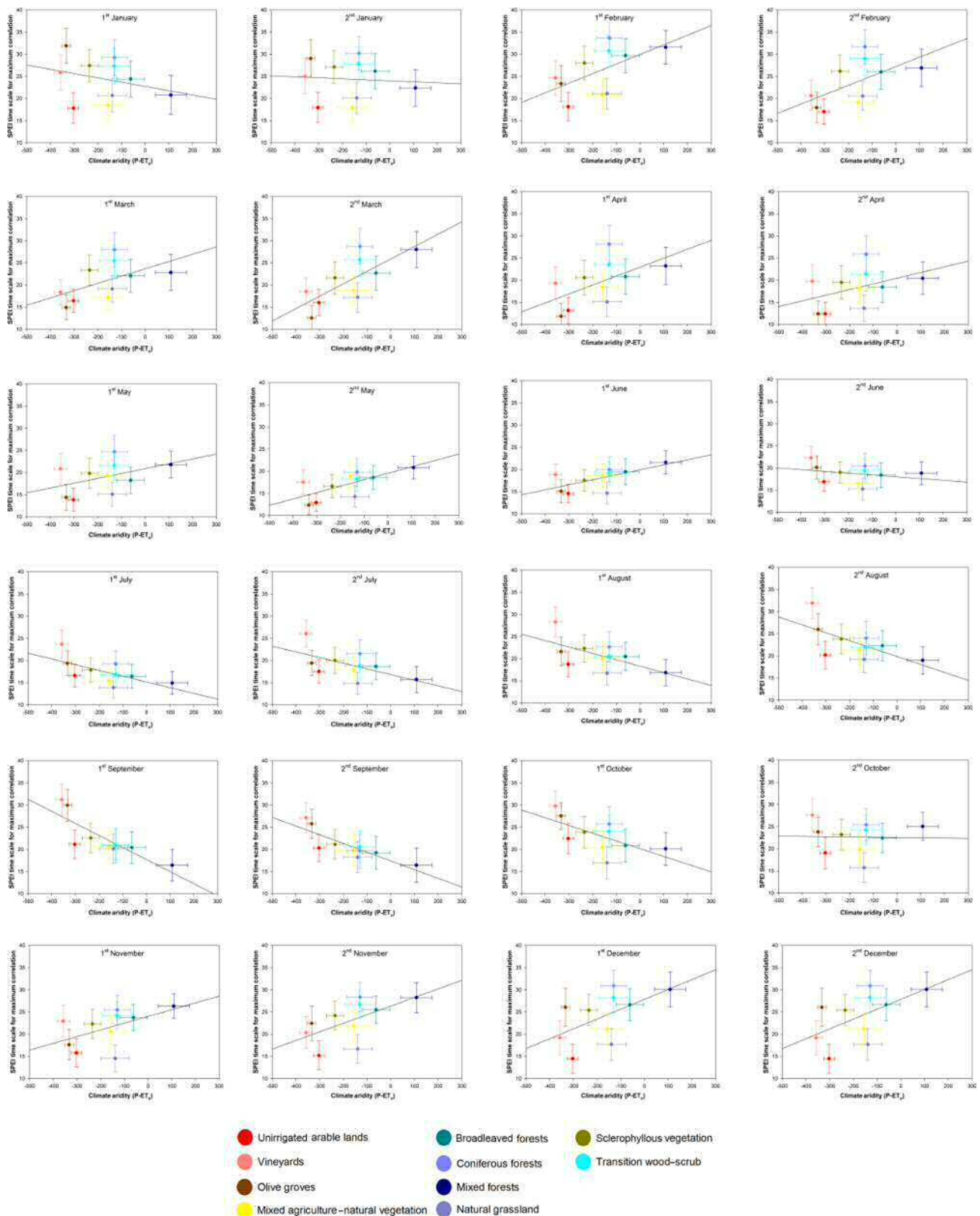


Figure 13. Scatterplots showing the relationship between the mean annual aridity and the SPEI timescale at which the maximum correlation is found between the sNDVI and SPEI for the different land cover types. Vertical and horizontal bars represent one-fourth the standard deviation around the mean values.

Table 1. Percentage of the total surface area according to the different significance categories of Pearson's r correlations between the sNDVI and SPEI.

	Negative ($p < 0.05$)	Negative ($p > 0.05$)	Positive ($p > 0.05$)	Positive ($p < 0.05$)
1 Jan	0.3	9.8	41.3	48.6
2 Jan	0.4	8.7	40.2	50.7
1 Feb	0.3	7.5	39.9	52.3
2 Feb	0.1	7.5	39.0	53.4
1 Mar	0.2	8.9	41.6	49.4
2 Mar	0.2	11.3	38.2	50.3
1 Apr	0.0	7.6	34.9	57.5
2 Apr	0.0	3.4	27.0	69.7
1 May	0.0	1.6	19.0	79.4
2 May	0.0	0.9	14.2	84.9
1 Jun	0.0	1.2	10.8	88.0
2 Jun	0.0	0.5	7.4	92.0
1 Jul	0.0	0.3	5.3	94.4
2 Jul	0.0	0.1	4.5	95.4
1 Aug	0.0	0.1	5.9	94.1
2 Aug	0.0	0.2	10.6	89.2
1 Sep	0.0	0.6	14.0	85.4
2 Sep	0.0	0.4	16.9	82.6
1 Oct	0.0	1.5	24.5	74.0
2 Oct	0.0	1.9	31.1	67.0
1 Nov	0.0	4.5	35.6	59.8
2 Nov	0.0	4.8	41.8	53.4
1 Dec	0.0	4.4	38.9	56.7
2 Dec	0.2	5.9	43.1	50.8

response of the NDVI to drought is similar during summer months, even with the different land cover types and environmental conditions.

4.3 The importance of drought timescales

A relevant finding of this study is that the response of the NDVI is highly dependent on the timescale at which drought is quantified. Numerous studies indicated that the accumulation of precipitation deficits during different time periods is essential to determine the influence of drought on the NDVI (e.g. Malo and Nicholson, 1990; Liu and Kogan, 1996; Lotsch et al., 2003; Ji and Peters, 2003; Wang et al., 2003). This is simply because soil moisture is impacted largely by precipitation and the atmospheric evaporative demand over previous cumulative periods (Scaini et al., 2015). Moreover, the different morphological, physiological, and phenological strategies would also explain the varying response of vegetation types to different drought timescales. This finding is confirmed in previous works using NDVI and different timescales of a drought index (e.g. Ji and Peters, 2003; Vicente-Serrano, 2007), but also using other variables like tree-ring growth (e.g. Pasho et al., 2011; Arzac et al., 2016; Vicente-Serrano et al., 2014a). This study confirms this finding, given that there is a high

spatial diversity in the SPEI timescale at which vegetation has its maximum correlation with the NDVI. These spatial variations, combined with strong seasonal differences, are mainly controlled by the dominant land cover types and aridity conditions. In their global assessment, Vicente-Serrano et al. (2013) found gradients in the response of the world biomes to drought, which are driven mainly by the timescale at which the biome responds to drought in a gradient of aridity. Again, the response to these different timescales implies not only different vulnerabilities of vegetation to water deficits, but also various strategies from plants to cope with drought. In Spain, we showed that the NDVI responds mostly to the SPEI at timescales of around 20 semi-monthly periods (10 months), but with some few seasonal differences (i.e. shorter timescales in spring and early autumn than in late summer and autumn). Herein, it is also noteworthy to indicate that there are differences in this response, as a function of land cover types. Overall, during the periods of highest vegetation activity, the herbaceous land covers (e.g. unirrigated arable lands and grasslands) respond to shorter SPEI timescales than other forest types. This pattern can be seen in the context that herbaceous covers are more dependent on the weather conditions recorded during short periods. These vegetation types could not reach deep soil levels, which are driven by climatic conditions during longer periods (Changnon and Easterling, 1989; Berg et al., 2017). In contrast, the tree root systems would access these deeper levels, having the capacity to buffer the effect of short-term droughts, albeit with more vulnerability to long droughts that ultimately would affect deep soil moisture levels. This pattern has been recently observed in southeastern Spain when comparing herbaceous crops and vineyards (Contreras and Hunink, 2015). Recently, Okin et al. (2018) linked the different responses to drought timescales between scrubs and chaparral herbaceous vegetation in California to soil water depletion at different levels.

Albeit with these general patterns, we also found some relevant seasonal patterns. For example, irrigated lands responded to long SPEI timescales (> 15 months) during summer months, whilst they responded to shorter timescales (< 7 months) during spring and autumn. This behaviour can be linked to water management in these areas. Specifically, during spring months, these areas do not receive irrigation and accordingly vegetation activity is determined by water stored in the soil. Conversely, summer irrigation depends on the water stored in the dense net of reservoirs existing in Spain; some of them have a multiannual capacity. Water availability in the reservoirs usually depends on the climate conditions recorded during long periods (1 or 2 years) (López-Moreno et al., 2004; Lorenzo-Lacruz et al., 2010), which determine water availability for irrigation. This explains why vegetation activity in irrigated lands depends on long timescales of drought. Similarly, vineyards and olive groves respond to long SPEI timescales during summer. These cultivations are highly resistant to drought stress

(Quiroga and Iglesias, 2009). However, these adapted cultivations can be sensitive to severe droughts under extreme summer dryness. In comparison to other natural vegetation, mixed forests show a response to shorter SPEI timescales. This could be explained by the low resistance of these forest species to water deficits (e.g. the different fir species located in humid mountain areas; Camarero et al., 2011, 2018).

Here, we also showed that climate aridity can partially explain the response of the NDVI to the different SPEI timescales. In Spain, the range of the mean aridity recorded by the mean land cover types is much lower than that observed at the global scale for the world biomes (Vicente-Serrano et al., 2013). This might explain why there are no clear patterns in the response of the land cover types to the aridity gradients and the SPEI timescales at which the maximum correlation between the NDVI and SPEI is found. Nevertheless, we found some seasonal differences between the cold and warm seasons. In summer, the NDVI responds to longer SPEI timescales, as opposed to the most humid forests that respond to shorter timescales. This stresses that – in addition to aridity – the degree of vulnerability to different duration water deficits, which are well-quantified using the drought timescales, may contribute to explaining the spatial distribution of the main land cover types across Spain given different biophysical conditions, but also the different strategies of vegetation types to cope with water stress (Chaves et al., 2003; McDowell et al., 2008), which are strongly variable in complex Mediterranean ecosystems.

5 Conclusions

The main conclusions of this study are as follows.

- Vegetation activity over large parts of Spain is closely related to the interannual variability of drought.
- The response of vegetation activity to drought is more pronounced during the warm season, which is attributed to the phenology of vegetation under different land cover types.
- There are clear seasonal differences in the response of the NDVI to drought.
- Natural grasslands and sclerophyllous vegetation show an earlier response to drought.
- There is a control in the response of the NDVI to drought severity by the climatic aridity, which is partially controlled by the land cover.
- The response of the NDVI is highly dependent on the timescale at which drought is quantified although there are differences in this response, as a function of land cover types.

Data availability. The drought index dataset is available at <http://monitordesequia.csic.es> (Begueria et al., 2019). The NDVI data are available upon request.

Supplement. The supplement related to this article is available online at: <https://doi.org/10.5194/nhess-19-1189-2019-supplement>.

Author contributions. SMVS designed the research; SMVS performed research. CAM, MTB, NMH, and MPG worked on data generation. MG, SB, FDC, MPG and IN assisted with data processing and figure creation. SMVS and AEK drafted the paper and all the authors contributed to the writing.

Competing interests. The authors declare that they have no conflict of interest.

Special issue statement. This article is part of the special issue “Hydroclimatic extremes and impacts at catchment to regional scales”. It is not associated with a conference.

Financial support. This research has been supported by the Spanish Commission of Science and Technology and FEDER (grant no. PCIN-2015-220), the Spanish Commission of Science and Technology and FEDER (grant no. CGL2014-52135-C03-01), the Spanish Commission of Science and Technology and FEDER (grant no. CGL2017-83866-C3-3-R), the Spanish Commission of Science and Technology and FEDER (grant no. CGL2017-82216-R), WaterWorks 2014 (grant no. 690462, IMDROFLOOD), the JPI Climate (grant no. 690462, INDECIS), and WaterWorks 2015 (FORWARD grant).

Review statement. This paper was edited by Chris Reason and reviewed by two anonymous referees.

References

- Abrams, M. D., Schultz, J. C., and Kleiner, K. W.: Ecophysiological responses in mesic versus xeric hardwood species to an early-season drought in central Pennsylvania, *Forest Sci.*, 36, 970–981, 1990.
- Allen, C. D., Macalady, A. K., Chenchouni, H., Bachelet, D., McDowell, N., Vennetier, M., Kitzberger, T., Rigling, A., Breshears, D. D., Hogg, E. H., T., Gonzalez, P., Fensham, R., Zhang, Z., Castro, J., Demidova, N., Lim, J.-H., Allard, G., Running, S. W., Semerci, A., and Cobb, N.: A global overview of drought and heat-induced tree mortality reveals emerging climate change risks for forests, *Forest Ecol. Manag.*, 259, 660–684, <https://doi.org/10.1016/j.foreco.2009.09.001>, 2010.
- Allen, C. D., Breshears, D. D., and McDowell, N. G.: On underestimation of global vulnerability to tree mortality and forest die-

- off from hotter drought in the Anthropocene, *Ecosphere*, 6, 1–5, <https://doi.org/10.1890/ES15-00203.1>, 2015.
- Allen, R. G., Pereira, L. S., Raes, D., and Smith, M.: Crop Evapotranspiration Guidel, Comput. Crop Water Requir., Add FAO, Rome, 1998.
- Anyamba, A. and Tucker, C. J.: Analysis of Sahelian vegetation dynamics using NOAA-AVHRR NDVI data from 1981–2003, *J. Arid Environ.*, 63, 596–614, <https://doi.org/10.1016/j.jaridenv.2005.03.007>, 2005.
- Arzac, A., García-Cervigón, A. I., Vicente-Serrano, S. M., Loidi, J., and Olano, J. M.: Phenological shifts in climatic response of secondary growth allow *Juniperus sabina* L. to cope with altitudinal and temporal climate variability, *Agr. Forest Meteorol.*, 217, 35–45, <https://doi.org/10.1016/j.agrformet.2015.11.011>, 2016.
- Asseng, S., Ewert, F., Martre, P., Rötter, R. P., Lobell, D. B., Cammarano, D., Kimball, B. A., Ottman, M. J., Wall, G. W., White, J. W., Reynolds, M. P., Alderman, P. D., Prasad, P. V. V., Aggarwal, P. K., Anothai, J., Basso, B., Biernath, C., Challinor, A. J., De Sanctis, G., Doltra, J., Fereres, E., Garcia-Vila, M., Gayler, S., Hoogenboom, G., Hunt, L. A., Izaurrealde, R. C., Jabloun, M., Jones, C. D., Kersebaum, K. C., Koehler, A.-K., Müller, C., Naresh Kumar, S., Nendel, C., O’leary, G., Olesen, J. E., Palosuo, T., Priesack, E., Eyshi Rezaei, E., Ruane, A. C., Semenov, M. A., Shcherbak, I., Stöckle, C., Stratonovitch, P., Streck, T., Supit, I., Tao, F., Thorburn, P. J., Waha, K., Wang, E., Wallach, D., Wolf, J., Zhao, Z., and Zhu, Y.: Rising temperatures reduce global wheat production, *Nat. Clim. Change*, 5, 143–147, <https://doi.org/10.1038/nclimate2470>, 2015.
- Austin, R. B., Cantero-Martínez, C., Arrúe, J. L., Playán, E., and Cano-Marcellán, P.: Yield-rainfall relationships in cereal cropping systems in the Ebro river valley of Spain, *Eur. J. Agron.*, 8, 239–248, [https://doi.org/10.1016/S1161-0301\(97\)00063-4](https://doi.org/10.1016/S1161-0301(97)00063-4), 1998.
- Bachmair, S., Kohn, I., and Stahl, K.: Exploring the link between drought indicators and impacts, *Nat. Hazards Earth Syst. Sci.*, 15, 1381–1397, <https://doi.org/10.5194/nhess-15-1381-2015>, 2015.
- Bachmair, S., Tanguy, M., Hannaford, J., and Stahl, K.: How well do meteorological indicators represent agricultural and forest drought across Europe?, *Environ. Res. Lett.*, 13, 034042, <https://doi.org/10.1088/1748-9326/aaafda>, 2018.
- Bailing, M., Zhiyong, L., Cunzhu, L., Lixin, W., Chengzhen, J., Fuxiang, B., and Chao, J.: Temporal and spatial heterogeneity of drought impact on vegetation growth on the Inner Mongolian Plateau, *Rangel. J.*, 40, 113–128, <https://doi.org/10.1071/RJ16097>, 2018.
- Baldocchi, D. D., Xu, L., and Kiang, N.: How plant functional-type, weather, seasonal drought, and soil physical properties alter water and energy fluxes of an oak-grass savanna and an annual grassland, *Agr. Forest Meteorol.*, 123, 13–39, <https://doi.org/10.1016/j.agrformet.2003.11.006>, 2004.
- Barbosa, H. A., Huete, A. R., and Baethgen, W. E.: A 20-year study of NDVI variability over the Northeast Region of Brazil, *J. Arid Environ.*, 67, 288–307, <https://doi.org/10.1016/j.jaridenv.2006.02.022>, 2006.
- Barker, L. J., Hannaford, J., Chiverton, A., and Svensson, C.: From meteorological to hydrological drought using standardised indicators, *Hydrol. Earth Syst. Sci.*, 20, 2483–2505, <https://doi.org/10.5194/hess-20-2483-2016>, 2016.
- Beguieria, S., Latorre, B., Reig, F., and Vicente-Serrano, S. M.: Drought Indices dataset for Spain, available at: <http://monitordesequia.csic.es>, last access: 29 May 2019.
- Berg, A., Sheffield, J., and Milly, P. C. D.: Divergent surface and total soil moisture projections under global warming, *Geophys. Res. Lett.*, 44, 236–244, <https://doi.org/10.1002/2016GL071921>, 2017.
- Bhuiyan, C., Singh, R. P., and Kogan, F. N.: Monitoring drought dynamics in the Aravalli region (India) using different indices based on ground and remote sensing data, *Int. J. Appl. Earth Obs. Geoinf.*, 8, 289–302, <https://doi.org/10.1016/j.jag.2006.03.002>, 2006.
- Breshears, D. D., Cobb, N. S., Rich, P. M., Price, K. P., Allen, C. D., Balice, R. G., Romme, W. H., Kastens, J. H., Floyd, M. L., Belnap, J., Anderson, J. J., Myers, O. B., and Meyer, C. W.: Regional vegetation die-off in response to global-change-type drought, *P. Natl. Acad. Sci. USA*, 102, 15144–15148, <https://doi.org/10.1073/pnas.0505734102>, 2005.
- Camarero, J. J., Bigler, C., Linares, J. C., and Gil-Pelegrín, E.: Synergistic effects of past historical logging and drought on the decline of Pyrenean silver fir forests, *Forest Ecol. Manag.*, 262, 759–769, <https://doi.org/10.1016/j.foreco.2011.05.009>, 2011.
- Camarero, J. J., Gazol, A., Sangüesa-Barreda, G., Oliva, J., and Vicente-Serrano, S. M.: To die or not to die: Early warnings of tree dieback in response to a severe drought, *J. Ecol.*, 103, 44–57, <https://doi.org/10.1111/1365-2745.12295>, 2015.
- Camarero, J. J., Gazol, A., Sangüesa-Barreda, G., Cantero, A., Sánchez-Salguero, R., Sánchez-Miranda, A., Granda, E., Serramalguer, X., and Ibáñez, R.: Forest growth responses to drought at short- and long-term scales in Spain: Squeezing the stress memory from tree rings, *Front. Ecol. Evol.*, 6, <https://doi.org/10.3389/fevo.2018.00009>, 2018.
- Carlson, T. N. and Ripley, D. A.: On the relation between NDVI, fractional vegetation cover, and leaf area index, *Remote Sens. Environ.*, 62, 241–252, [https://doi.org/10.1016/S0034-4257\(97\)00104-1](https://doi.org/10.1016/S0034-4257(97)00104-1), 1997.
- Carnicer, J., Coll, M., Ninyerola, M., Pons, X., Sánchez, G., and Peñuelas, J.: Widespread crown condition decline, food web disruption, and amplified tree mortality with increased climate change-type drought, *P. Natl. Acad. Sci. USA*, 108, 1474–1478, <https://doi.org/10.1073/pnas.1010070108>, 2011.
- Castro-Díez, P., Villar-Salvador, P., Pérez-Rontomé, C., Maestro-Martínez, M., and Monserrat-Martí, G.: Leaf morphology and leaf chemical composition in three *Quercus* (Fagaceae) species along a rainfall gradient in NE Spain, *Trees-Struct. Funct.*, 11, 127–134, <https://doi.org/10.1007/s004680050068>, 1997.
- Changnon, S. A. and Easterling, W. E.: Measuring Drought Impacts: The Illinois Case, *J. Am. Water Resour. Assoc.*, 25, 27–42, <https://doi.org/10.1111/j.1752-1688.1989.tb05663.x>, 1989.
- Chaves, M. M., Maroco, J. P., and Pereira, J. S.: Understanding plant responses to drought – From genes to the whole plant, *Funct. Plant Biol.*, 30, 239–264, <https://doi.org/10.1071/FP02076>, 2003.
- Ciais, P., Reichstein, M., Viovy, N., Granier, A., Ogee, J., Allard, V., Aubinet, M., Buchmann, N., Bernhofer, C., Carrara, A., Chevallier, F., De Noblet, N., Friend, A. D., Friedlingstein, P., Grünwald, T., Heinesch, B., Keronen, P., Knohl, A., Krinner, G., Loustau, D., Manca, G., Matteucci, G., Miglietta, F., Ourcival, J. M., Papale, D., Pilegaard, K., Rambal, S., Seufert,

- G., Soussana, J. F., Sanz, M. J., Schulze, E. D., Vesala, T., and Valentini, R.: Europe-wide reduction in primary productivity caused by the heat and drought in 2003, *Nature*, 437, 529–533, <https://doi.org/10.1038/nature03972>, 2005.
- Contreras, S. and Hunink, J. E.: Drought effects on rainfed agriculture using standardized indices: A case study in SE Spain, in *Drought: Research and Science-Policy Interfacing – Proceedings of the International Conference on Drought: Research and Science-Policy Interfacing*, 65–70, 2015.
- Dardel, C., Kergoat, L., Hiernaux, P., Mougin, E., Grippa, M., and Tucker, C. J.: Re-greening Sahel: 30 years of remote sensing data and field observations (Mali, Niger), *Remote Sens. Environ.*, 140, 350–364, <https://doi.org/10.1016/j.rse.2013.09.011>, 2014.
- De Keersmaecker, W., Lhermitte, S., Hill, M. J., Tits, L., Coppin, P., and Somers, B.: Assessment of regional vegetation response to climate anomalies: A case study for Australia using GIMMS NDVI time series between 1982 and 2006, *Remote Sens.*, 9, <https://doi.org/10.3390/rs9010034>, 2017.
- del Barrio, G., Puigdefabregas, J., Sanjuan, M. E., Stellmes, M., and Ruiz, A.: Assessment and monitoring of land condition in the Iberian Peninsula, 1989–2000, *Remote Sens. Environ.*, 114, 1817–1832, <https://doi.org/10.1016/j.rse.2010.03.009>, 2010.
- FAO: Food and Agricultural Organization, Food and Agriculture data, available from: <http://www.fao.org>, last access: 1 October 2018.
- Fischer, E. M., Seneviratne, S. I., Vidale, P. L., Lüthi, D., and Schär, C.: Soil moisture-atmosphere interactions during the 2003 European summer heat wave, *J. Clim.*, 20, 5081–5099, <https://doi.org/10.1175/JCLI4288.1>, 2007.
- Gallardo, M. and Martínez-Vega, J.: Three decades of land-use changes in the region of Madrid and how they relate to territorial planning, *Eur. Plan. Stud.*, 24, 1016–1033, <https://doi.org/10.1080/09654313.2016.1139059>, 2016.
- García, M., Litago, J., Palacios-Orueta, A., Pinzón, J. E., and Ustin Susan, L.: Short-term propagation of rainfall perturbations on terrestrial ecosystems in central California, *Appl. Veg. Sci.*, 13, 146–162, <https://doi.org/10.1111/j.1654-109X.2009.01057.x>, 2010.
- García-Haro, F. J., Campos-Taberner, M., Sabater, N., Belda, F., Moreno, A., Gilabert, M. A., Martínez, B., Pérez-Hoyos, A., and Meliá, J.: Vegetation vulnerability to drought in Spain, *Vulnerabilidad de la vegetación a la sequía en España*, *Rev. Teledetec.*, 42, 29–37, <https://doi.org/10.4995/raet.2014.2283>, 2014.
- Gazol, A., Camarero, J. J., Anderegg, W. R. L., and Vicente-Serrano, S. M.: Impacts of droughts on the growth resilience of Northern Hemisphere forests, *Glob. Ecol. Biogeogr.*, 26, 166–176, <https://doi.org/10.1111/geb.12526>, 2017.
- Gazol, A., Camarero, J. J., Vicente-Serrano, S. M., Sánchez-Salguero, R., Gutiérrez, E., de Luis, M., Sangüesa-Barreda, G., Novak, K., Rozas, V., Tíscar, P. A., Linares, J. C., Martín-Hernández, N., Martínez del Castillo, E., Ribas, M., García-González, I., Silla, F., Camisón, A., Génova, M., Olano, J. M., Longares, L. A., Hevia, A., Tomás-Burguera, M., and Galván, J. D.: Forest resilience to drought varies across biomes, *Glob. Change Biol.*, 24, 2143–2158, <https://doi.org/10.1111/gcb.14082>, 2018.
- Gessner, U., Naeimi, V., Klein, I., Kuenzer, C., Klein, D., and Dech, S.: The relationship between precipitation anomalies and satellite-derived vegetation activity in Central Asia, *Glob. Planet. Change*, 110, 74–87, <https://doi.org/10.1016/j.gloplacha.2012.09.007>, 2013.
- González-Alonso, F. and Casanova, J. L.: Application of NOAA-AVHRR images for the validation and risk assessment of natural disasters in Spain, in *Remote Sensing '96*, Balkema, Rotterdam, 227–233, 1997.
- González-Hidalgo, J. C., Vicente-Serrano, S. M., Peña-Angulo, D., Salinas, C., Tomas-Burguera, M., and Beguería, S.: High-resolution spatio-temporal analyses of drought episodes in the western Mediterranean basin (Spanish mainland, Iberian Peninsula), *Acta Geophys.*, 66, 381–392, <https://doi.org/10.1007/s11600-018-0138-x>, 2018.
- Gouveia, C. M., Bastos, A., Trigo, R. M., and Dacamara, C. C.: Drought impacts on vegetation in the pre- and post-fire events over Iberian Peninsula, *Nat. Hazards Earth Syst. Sci.*, 12, 3123–3137, <https://doi.org/10.5194/nhess-12-3123-2012>, 2012.
- Gouveia, C. M., Páscoa, P., Russo, A., and Trigo, R. M.: Land degradation trend assessment over Iberia during 1982–2012, *Evaluación de la tendencia a la degradación del suelo en Iberia durante 1982–2012*, *Cuad. Investig. Geogr.*, 42, 89–112, <https://doi.org/10.18172/cig.2808>, 2016.
- Gouveia, C. M., Trigo, R. M., Beguería, S., and Vicente-Serrano, S. M.: Drought impacts on vegetation activity in the Mediterranean region: An assessment using remote sensing data and multi-scale drought indicators, *Glob. Planet. Change*, 151, 15–27, <https://doi.org/10.1016/j.gloplacha.2016.06.011>, 2017.
- Grissino-Mayer, H. D. and Fritts, H. C.: The International Tree-Ring Data Bank: An enhanced global database serving the global scientific community, *Holocene*, 7, 235–238, <https://doi.org/10.1177/095968369700700212>, 1997.
- Gu, Y., Brown, J. F., Verdin, J. P., and Wardlow, B.: A five-year analysis of MODIS NDVI and NDWI for grassland drought assessment over the central Great Plains of the United States, *Geophys. Res. Lett.*, 34, L06407, <https://doi.org/10.1029/2006GL029127>, 2007.
- Herrmann, S. M., Anyamba, A., and Tucker, C. J.: Recent trends in vegetation dynamics in the African Sahel and their relationship to climate, *Glob. Environ. Change*, 15, 394–404, <https://doi.org/10.1016/j.gloenvcha.2005.08.004>, 2005.
- Herrmann, S. M., Didan, K., Barreto-Munoz, A., and Crimmins, M. A.: Divergent responses of vegetation cover in Southwestern US ecosystems to dry and wet years at different elevations, *Environ. Res. Lett.*, 11, <https://doi.org/10.1088/1748-9326/11/12/124005>, 2016.
- Hill, J., Stellmes, M., Udelhoven, T., Röder, A., and Sommer, S.: Mediterranean desertification and land degradation, Mapping related land use change syndromes based on satellite observations, *Glob. Planet. Change*, 64, 146–157, <https://doi.org/10.1016/j.gloplacha.2008.10.005>, 2008.
- Hirschi, M., Seneviratne, S. I., Alexandrov, V., Boberg, F., Boroneant, C., Christensen, O. B., Formayer, H., Orlowsky, B., and Stepanek, P.: Observational evidence for soil-moisture impact on hot extremes in southeastern Europe, *Nat. Geosci.*, 4, 17–21, <https://doi.org/10.1038/ngeo1032>, 2011.
- Huete, A., Didan, K., Miura, T., Rodriguez, E. P., Gao, X., and Ferreira, L. G.: Overview of the radiometric and biophysical performance of the MODIS vegetation indices, *Remote Sens. Environ.*, 83, 195–213, [https://doi.org/10.1016/S0034-4257\(02\)00096-2](https://doi.org/10.1016/S0034-4257(02)00096-2), 2002.

- Huxman, T. E., Smith, M. D., Fay, P. A., Knapp, A. K., Shaw, M. R., Lolk, M. E., Smith, S. D., Tissue, D. T., Zak, J. C., Weltzin, J. F., Pockman, W. T., Sala, O. E., Haddad, B. M., Harte, J., Koch, G. W., Schwinning, S., Small, E. E., and Williams, D. G.: Convergence across biomes to a common rain-use efficiency, *Nature*, 429, 651–654, <https://doi.org/10.1038/nature02561>, 2004.
- Iglesias, E., Garrido, A., and Gómez-Ramos, A.: Evaluation of drought management in irrigated areas, *Agr. Econ.*, 29, 211–229, [https://doi.org/10.1016/S0169-5150\(03\)00084-7](https://doi.org/10.1016/S0169-5150(03)00084-7), 2003.
- Ivits, E., Horion, S., Fensholt, R., and Cherlet, M.: Drought footprint on European ecosystems between 1999 and 2010 assessed by remotely sensed vegetation phenology and productivity, *Glob. Change Biol.*, 20, 581–593, <https://doi.org/10.1111/gcb.12393>, 2014.
- Jenkins, J. C., Chojnacky, D. C., Heath, L. S., and Birdsey, R. A.: National-scale biomass estimators for United States tree species, *Forest Sci.*, 49, 12–35, 2003.
- Ji, L. and Peters, A. J.: Assessing vegetation response to drought in the northern Great Plains using vegetation and drought indices, *Remote Sens. Environ.*, 87, 85–98, [https://doi.org/10.1016/S0034-4257\(03\)00174-3](https://doi.org/10.1016/S0034-4257(03)00174-3), 2003.
- Julien, Y., Sobrino, J. A., Mattar, C., Ruescas, A. B., Jiménez-Muñoz, J. C., Soria, G., Hidalgo, V., Atitar, M., Franch, B., and Cuenca, J.: Temporal analysis of normalized difference vegetation index (NDVI) and land surface temperature (LST) parameters to detect changes in the Iberian land cover between 1981 and 2001, *Int. J. Remote Sens.*, 32, 2057–2068, <https://doi.org/10.1080/01431161003762363>, 2011.
- Knipling, E. B.: Physical and physiological basis for the reflectance of visible and near-infrared radiation from vegetation, *Remote Sens. Environ.*, 1, 155–159, [https://doi.org/10.1016/S0034-4257\(70\)80021-9](https://doi.org/10.1016/S0034-4257(70)80021-9), 1970.
- Kogan, F. N.: Global Drought Watch from Space, *B. Am. Meteorol. Soc.*, 78, 621–636, 1997.
- Lasanta, T. and Vicente-Serrano, S. M.: Complex land cover change processes in semiarid Mediterranean regions: An approach using Landsat images in northeast Spain, *Remote Sens. Environ.*, 124, 1–14, <https://doi.org/10.1016/j.rse.2012.04.023>, 2012.
- Lasanta, T., Arnáez, J., Pascual, N., Ruiz-Flaño, P., Errea, M. P., and Lana-Renault, N.: Space–time process and drivers of land abandonment in Europe, *Catena*, 149, 810–823, <https://doi.org/10.1016/j.catena.2016.02.024>, 2017.
- Lecina, S., Isidoro, D., Playán, E., and Aragüés, R.: Irrigation modernization and water conservation in Spain: The case of Riegos del Alto Aragón, *Agr. Water Manage.*, 97, 1663–1675, <https://doi.org/10.1016/j.agwat.2010.05.023>, 2010.
- Liu, N., Harper, R. J., Dell, B., Liu, S., and Yu, Z.: Vegetation dynamics and rainfall sensitivity for different vegetation types of the Australian continent in the dry period 2002–2010, *Ecophysiology*, 10, e1811, <https://doi.org/10.1002/eco.1811>, 2017.
- Liu, W. T. and Kogan, F. N.: Monitoring regional drought using the vegetation condition index, *Int. J. Remote Sens.*, 17, 2761–2782, <https://doi.org/10.1080/01431169608949106>, 1996.
- Lloret, F., Lobo, A., Estevan, H., Maisongrande, P., Vayreda, J., and Terradas, J.: Woody plant richness and NDVI response to drought events in Catalanian (northeastern Spain) forests, *Ecology*, 88, 2270–2279, <https://doi.org/10.1890/06-1195.1>, 2007.
- Lobell, D. B., Hammer, G. L., Chenu, K., Zheng, B., Mclean, G., and Chapman, S. C.: The shifting influence of drought and heat stress for crops in northeast Australia, *Glob. Change Biol.*, 21, 4115–4127, <https://doi.org/10.1111/gcb.13022>, 2015.
- López-Moreno, J. I., Beguería, S., and García-Ruiz, J. M.: The management of a large Mediterranean reservoir: Storage regimens of the Yesa Reservoir, Upper Aragon River basin, Central Spanish Pyrenees, *Environ. Manag.*, 34, 508–515, <https://doi.org/10.1007/s00267-003-0249-1>, 2004.
- López-Moreno, J. I., Vicente-Serrano, S. M., Zabalza, J., Beguería, S., Lorenzo-Lacruz, J., Azorin-Molina, C., and Morán-Tejeda, E.: Hydrological response to climate variability at different time scales: A study in the Ebro basin, *J. Hydrol.*, 477, 175–188, <https://doi.org/10.1016/j.jhydrol.2012.11.028>, 2013.
- Lorenzo-Lacruz, J., Vicente-Serrano, S. M., López-Moreno, J. I., Beguería, S., García-Ruiz, J. M., and Cuadrat, J. M.: The impact of droughts and water management on various hydrological systems in the headwaters of the Tagus River (central Spain), *J. Hydrol.*, 386, <https://doi.org/10.1016/j.jhydrol.2010.01.001>, 2010.
- Lorenzo-Lacruz, J., Morán-Tejeda, E., Vicente-Serrano, S. M., and López-Moreno, J. I.: Streamflow droughts in the Iberian Peninsula between 1945 and 2005: spatial and temporal patterns, *Hydrol. Earth Syst. Sci.*, 17, 119–134, <https://doi.org/10.5194/hess-17-119-2013>, 2013.
- Lotsch, A., Friedl, M. A., Anderson, B. T., and Tucker, C. J.: Coupled vegetation–precipitation variability observed from satellite and climate records, *Geophys. Res. Lett.*, 30, 1774, <https://doi.org/10.1029/2003GL017506>, 2003.
- Ma, X., Huete, A., Moran, S., Ponce-Campos, G., and Eamus, D.: Abrupt shifts in phenology and vegetation productivity under climate extremes, *J. Geophys. Res.-Biogeo.*, 120, 2036–2052, <https://doi.org/10.1002/2015JG003144>, 2015.
- Malo, A. R. and Nicholson, S. E.: A study of rainfall and vegetation dynamics in the African Sahel using normalized difference vegetation index, *J. Arid Environ.*, 19, 1–24, 1990.
- Martínez-Fernández, J. and Ceballos, A.: Temporal Stability of Soil Moisture in a Large-Field Experiment in Spain, *Soil Sci. Soc. Am. J.*, 67, 1647–1656, 2003.
- McDowell, N., Pockman, W. T., Allen, C. D., Breshears, D. D., Cobb, N., Kolb, T., Plaut, J., Sperry, J., West, A., Williams, D. G., and Yezzer, E. A.: Mechanisms of plant survival and mortality during drought: Why do some plants survive while others succumb to drought?, *New Phytol.*, 178, 719–739, <https://doi.org/10.1111/j.1469-8137.2008.02436.x>, 2008.
- McKee, T. B., Doesken, N. J., and Kleist, J.: The relationship of drought frequency and duration to time scales, *Eighth Conf. Appl. Climatol.*, *Am. Meteorol. Soc.*, 179–184, 1993.
- Milich, L. and Weiss, E.: Characterization of the sahel: Implications of correctly calculating interannual coefficients of variation (CoVs) from GAC NDVI values, *Int. J. Remote Sens.*, 18, 3749–3759, <https://doi.org/10.1080/014311697216603>, 1997.
- Molina, A. J. and del Campo, A. D.: The effects of experimental thinning on throughfall and stemflow: A contribution towards hydrology-oriented silviculture in Aleppo pine plantations, *Forest Ecol. Manag.*, 269, 206–213, <https://doi.org/10.1016/j.foreco.2011.12.037>, 2012.
- Mu, Q., Zhao, M., Kimball, J. S., McDowell, N. G., and Running, S. W.: A remotely sensed global terrestrial drought severity index, *B. Am. Meteorol. Soc.*, 94, 83–98, <https://doi.org/10.1175/BAMS-D-11-00213.1>, 2013.

- Mühlbauer, S., Costa, A. C., and Caetano, M.: A spatiotemporal analysis of droughts and the influence of North Atlantic Oscillation in the Iberian Peninsula based on MODIS imagery, *Theor. Appl. Climatol.*, 124, 703–721, <https://doi.org/10.1007/s00704-015-1451-9>, 2016.
- Mukherjee, S., Mishra, A., and Trenberth, K. E.: Climate Change and Drought: a Perspective on Drought Indices, *Curr. Clim. Change Reports*, 4, 145–163, <https://doi.org/10.1007/s40641-018-0098-x>, 2018.
- Myneni, R. B., Hall, F. G., Sellers, P. J., and Marshak, A. L.: Interpretation of spectral vegetation indexes, *IEEE T. Geosci. Remote*, 33, 481–486, <https://doi.org/10.1109/36.377948>, 1995.
- Newberry, T. L.: Effect of climatic variability on $\delta^{13}\text{C}$ and tree-ring growth in piñon pine (*Pinus edulis*), *Trees-Struct. Funct.*, 24, 551–559, <https://doi.org/10.1007/s00468-010-0426-9>, 2010.
- Nicholson, S. E., Davenport, M. L., and Malo, A. R.: A comparison of the vegetation response to rainfall in the Sahel and East Africa, using normalized difference vegetation index from NOAA AVHRR, *Climate Change*, 17, 209–241, <https://doi.org/10.1007/BF00138369>, 1990.
- Okin, G. S., Dong, C., Willis, K. S., Gillespie, T. W., and MacDonald, G. M.: The Impact of Drought on Native Southern California Vegetation: Remote Sensing Analysis Using MODIS-Derived Time Series, *J. Geophys. Res.-Biogeophys.*, 123, 1927–1939, <https://doi.org/10.1029/2018JG004485>, 2018.
- Olsen, J. L., Ceccato, P., Proud, S. R., Fensholt, R., Grippa, M., Mougín, B., Ardö, J., and Sandholt, I.: Relation between seasonally detrended shortwave infrared reflectance data and land surface moisture in semi-arid Sahel, *Remote Sens.*, 5, 2898–2927, <https://doi.org/10.3390/rs5062898>, 2013.
- Ortigosa, L. M., Garcia-Ruiz, J. M., and Gil-Pelegrin, E.: Land reclamation by reforestation in the Central Pyrenees, *Mt. Res.-Dev.*, 10, 281–288, <https://doi.org/10.2307/3673607>, 1990.
- Palazón, A., Aragonés, L., and López, I.: Evaluation of coastal management: Study case in the province of Alicante, Spain, *Sci. Total Environ.*, 572, 1184–1194, <https://doi.org/10.1016/j.scitotenv.2016.08.032>, 2016.
- Páscoa, P., Gouveia, C. M., Russo, A., and Trigo, R. M.: The role of drought on wheat yield interannual variability in the Iberian Peninsula from 1929 to 2012, *Int. J. Biometeorol.*, 61, 439–451, <https://doi.org/10.1007/s00484-016-1224-x>, 2017.
- Pasho, E., Camarero, J. J., de Luis, M., and Vicente-Serrano, S. M.: Impacts of drought at different time scales on forest growth across a wide climatic gradient in north-eastern Spain, *Agr. Forest Meteorol.*, 151, 1800–1811, <https://doi.org/10.1016/j.agrformet.2011.07.018>, 2011.
- Pausas, J. G.: Changes in fire and climate in the eastern Iberian Peninsula (Mediterranean Basin), *Climate Change*, 63, 337–350, <https://doi.org/10.1023/B:CLIM.0000018508.94901.9c>, 2004.
- Pausas, J. G. and Fernández-Muñoz, S.: Fire regime changes in the Western Mediterranean Basin: From fuel-limited to drought-driven fire regime, *Climate Change*, 110, 215–226, <https://doi.org/10.1007/s10584-011-0060-6>, 2012.
- Peco, B., Ortega, M., and Levassor, C.: Similarity between seed bank and vegetation in Mediterranean grassland: A predictive model, *J. Veg. Sci.*, 9, 815–828, <https://doi.org/10.2307/3237047>, 1998.
- Peña-Gallardo, M., Vicente-Serrano, S. M., Camarero, J. J., Gazol, A., Sánchez-Salguero, R., Domínguez-Castro, F., El Kenawy, A., Beguería-Portugés, S., Gutiérrez, E., de Luis, M., Sangüesa-Barreda, G., Novak, K., Rozas, V., Tiscar, P. A., Linares, J. C., del Castillo, E., Ribas Matamoros, M., García-González, I., Silla, F., Camisón, Á., Génova, M., Olano, J. M., Longares, L. A., Hevia, A., and Galván, J. D.: Drought Sensitiveness on Forest Growth in Peninsular Spain and the Balearic Islands, *Forests*, 9, 2018a.
- Peña-Gallardo, M., SM, V.-S., Domínguez-Castro, F., Quiring, S., Svoboda, M., Beguería, S., and Hannaford, J.: Effectiveness of drought indices in identifying impacts on major crops across the USA, *Clim. Res.*, 75, 221–240, 2018b.
- Pinzon, J. E. and Tucker, C. J.: A non-stationary 1981–2012 AVHRR NDVI time series, *Remote Sens.*, 6, 6929–6960, <https://doi.org/10.3390/rs6086929>, 2014.
- Quiring, S. M. and Ganesh, S.: Evaluating the utility of the Vegetation Condition Index (VCI) for monitoring meteorological drought in Texas, *Agr. Forest Meteorol.*, 150, 330–339, <https://doi.org/10.1016/j.agrformet.2009.11.015>, 2010.
- Quiroga, S. and Iglesias, A.: A comparison of the climate risks of cereal, citrus, grapevine and olive production in Spain, *Agr. Syst.*, 101, 91–100, <https://doi.org/10.1016/j.agry.2009.03.006>, 2009.
- Reichstein, M., Ciais, P., Papale, D., Valentini, R., Running, S., Viovy, N., Cramer, W., Granier, A., Ogee, J., Allard, V., Aubinet, M., Bernhofer, C., Buchmann, N., Carrara, A., Grünwald, T., Heimann, M., Heinesch, B., Knohl, A., Kutsch, W., Loustau, D., Manca, G., Matteucci, G., Miglietta, F., Ourcival, J. M., Pilegaard, K., Pumpanen, J., Rambal, S., Schaphoff, S., Seufert, G., Soussana, J.-F., Sanz, M.-J., Vesala, T., and Zhao, M.: Reduction of ecosystem productivity and respiration during the European summer 2003 climate anomaly: A joint flux tower, remote sensing and modelling analysis, *Glob. Change Biol.*, 13, 634–651, <https://doi.org/10.1111/j.1365-2486.2006.01224.x>, 2007.
- Restaino, C. M., Peterson, D. L., and Littell, J.: Increased water deficit decreases Douglas fir growth throughout western US forests, *P. Natl. Acad. Sci. USA*, 113, 9557–9562, <https://doi.org/10.1073/pnas.1602384113>, 2016.
- Rhee, J., Im, J., and Carbone, G. J.: Monitoring agricultural drought for arid and humid regions using multi-sensor remote sensing data, *Remote Sens. Environ.*, 114, 2875–2887, <https://doi.org/10.1016/j.rse.2010.07.005>, 2010.
- Russi, L., Cocks, P. S., and Roberts, E. H.: Seed bank dynamics in a Mediterranean grassland, *J. Appl. Ecol.*, 29, 763–771, <https://doi.org/10.2307/2404486>, 1992.
- Scaini, A., Sánchez, N., Vicente-Serrano, S. M., and Martínez-Fernández, J.: SMOS-derived soil moisture anomalies and drought indices: A comparative analysis using in situ measurements, *Hydrol. Process.*, 29, 373–383, <https://doi.org/10.1002/hyp.10150>, 2015.
- Schultz, P. A. and Halpert, M. S.: Global analysis of the relationships among a vegetation index, precipitation and land surface temperature, *Int. J. Remote Sens.*, 16, 2755–2777, <https://doi.org/10.1080/01431169508954590>, 1995.
- Serra, P., Pons, X., and Saurí, D.: Land-cover and land-use change in a Mediterranean landscape: A spatial analysis of driving forces integrating biophysical and human factors, *Appl. Geogr.*, 28, 189–209, <https://doi.org/10.1016/j.apgeog.2008.02.001>, 2008.
- Slayback, D. A., Pinzon, J. E., Los, S. O., and Tucker, C. J.: Northern hemisphere photosynthetic trends 1982–99, *Glob. Change Biol.*, 9, 1–15, <https://doi.org/10.1046/j.1365-2486.2003.00507.x>, 2003.

- Sona, N. T., Chen, C. F., Chen, C. R., Chang, L. Y., and Minh, V. Q.: Monitoring agricultural drought in the lower mekong basin using MODIS NDVI and land surface temperature data, *Int. J. Appl. Earth Obs. Geoinf.*, 18, 417–427, <https://doi.org/10.1016/j.jag.2012.03.014>, 2012.
- Stagge, J. H., Kohn, I., Tallaksen, L. M., and Stahl, K.: Modeling drought impact occurrence based on meteorological drought indices in Europe, *J. Hydrol.*, 530, 37–50, <https://doi.org/10.1016/j.jhydrol.2015.09.039>, 2015.
- Stellmes, M., Röder, A., Udelhoven, T., and Hill, J.: Mapping syndromes of land change in Spain with remote sensing time series, demographic and climatic data, *Land Use Policy*, 30, 685–702, <https://doi.org/10.1016/j.landusepol.2012.05.007>, 2013.
- Tucker, C. J.: Red and photographic infrared linear combinations for monitoring vegetation, *Remote Sens. Environ.*, 8, 127–150, [https://doi.org/10.1016/0034-4257\(79\)90013-0](https://doi.org/10.1016/0034-4257(79)90013-0), 1979.
- Tucker, C. J., Pinzon, J. E., Brown, M. E., Slayback, D. A., Pak, E. W., Mahoney, R., Vermote, E. F., and El Saleous, N.: An extended AVHRR 8-km NDVI dataset compatible with MODIS and SPOT vegetation NDVI data, *Int. J. Remote Sens.*, 26, 4485–4498, <https://doi.org/10.1080/01431160500168686>, 2005.
- Udelhoven, T., Stellmes, M., del Barrio, G., and Hill, J.: Assessment of rainfall and NDVI anomalies in Spain (1989–1999) using distributed lag models, *Int. J. Remote Sens.*, 30, 1961–1976, <https://doi.org/10.1080/01431160802546829>, 2009.
- Vicente-Serrano, S. M.: Spatial and temporal analysis of droughts in the Iberian Peninsula (1910–2000), *Hydrol. Sci. J.*, 51, 83–97, <https://doi.org/10.1623/hysj.51.1.83>, 2006.
- Vicente-Serrano, S. M.: Evaluating the impact of drought using remote sensing in a Mediterranean, Semi-arid Region, *Nat. Hazards*, 40, 173–208, <https://doi.org/10.1007/s11069-006-0009-7>, 2007.
- Vicente-Serrano, S. M. and Beguería, S.: Comment on “Candidate distributions for climatological drought indices (SPI and SPEI)” by James H. Stagge et al., *Int. J. Climatol.*, 36, 2120–2131, <https://doi.org/10.1002/joc.4474>, 2016.
- Vicente-Serrano, S. M., Cuadrat-Prats, J. M., and Romo, A.: Aridity influence on vegetation patterns in the middle Ebro Valley (Spain): Evaluation by means of AVHRR images and climate interpolation techniques, *J. Arid Environ.*, 66, 353–375, <https://doi.org/10.1016/j.jaridenv.2005.10.021>, 2006.
- Vicente-Serrano, S. M., Beguería, S., and López-Moreno, J. I.: A multiscalar drought index sensitive to global warming: The standardized precipitation evapotranspiration index, *J. Clim.*, 23, 1696–1718, <https://doi.org/10.1175/2009JCLI2909.1>, 2010.
- Vicente-Serrano, S. M., Beguería, S., and López-Moreno, J. I.: Comment on Characteristics and trends in various forms of the Palmer Drought Severity Index (PDSI) during 1900–2008 by Aiguo Dai, *J. Geophys. Res.-Atmos.*, 116, D19112, <https://doi.org/10.1029/2010JD015541>, 2011.
- Vicente-Serrano, S. M., Beguería, S., Lorenzo-Lacruz, J., Camarero, J. J., López-Moreno, J. I., Azorin-Molina, C., Revuelto, J., Morán-Tejeda, E., and Sanchez-Lorenzo, A.: Performance of drought indices for ecological, agricultural, and hydrological applications, *Earth Interact.*, 16, <https://doi.org/10.1175/2012EI000434.1>, 2012.
- Vicente-Serrano, S. M., Gouveia, C., Camarero, J. J., Beguería, S., Trigo, R., López-Moreno, J. I., Azorin-Molina, C., Pasho, E., Lorenzo-Lacruz, J., Revuelto, J., Morán-Tejeda, E., and Sanchez-Lorenzo, A.: Response of vegetation to drought time-scales across global land biomes, *P. Natl. Acad. Sci. USA*, 110, 52–57, <https://doi.org/10.1073/pnas.1207068110>, 2013.
- Vicente-Serrano, S. M., Camarero, J. J., and Azorin-Molina, C.: Diverse responses of forest growth to drought time-scales in the Northern Hemisphere, *Glob. Ecol. Biogeogr.*, 23, 1019–1030, <https://doi.org/10.1111/geb.12183>, 2014a.
- Vicente-Serrano, S. M., Lopez-Moreno, J.-I., Beguería, S., Lorenzo-Lacruz, J., Sanchez-Lorenzo, A., García-Ruiz, J. M., Azorin-Molina, C., Morán-Tejeda, E., Revuelto, J., Trigo, R., Coelho, F., and Espejo, F.: Evidence of increasing drought severity caused by temperature rise in southern Europe, *Environ. Res. Lett.*, 9, 044001, <https://doi.org/10.1088/1748-9326/9/4/044001>, 2014b.
- Vicente-Serrano, S. M., Azorin-Molina, C., Sanchez-Lorenzo, A., Revuelto, J., López-Moreno, J. I., González-Hidalgo, J. C., Moran-Tejeda, E., and Espejo, F.: Reference evapotranspiration variability and trends in Spain, 1961–2011, *Glob. Planet. Change*, 121, 26–40, <https://doi.org/10.1016/j.gloplacha.2014.06.005>, 2014c.
- Vicente-Serrano, S. M., Azorin-Molina, C., Sanchez-Lorenzo, A., Revuelto, J., Morán-Tejeda, E., López-Moreno, J. I., and Espejo, F.: Sensitivity of reference evapotranspiration to changes in meteorological parameters in Spain (1961–2011), *Water Resour. Res.*, 50, 8458–8480, <https://doi.org/10.1002/2014WR015427>, 2014d.
- Vicente-Serrano, S. M., Cabello, D., Tomás-Burguera, M., Martín-Hernández, N., Beguería, S., Azorin-Molina, C., and Kenawy, A. E.: Drought variability and land degradation in semiarid regions: Assessment using remote sensing data and drought indices (1982–2011), *Remote Sens.*, 7, 4391–4423, <https://doi.org/10.3390/rs70404391>, 2015.
- Vicente-Serrano, S. M., Tomas-Burguera, M., Beguería, S., Reig, F., Latorre, B., Peña-Gallardo, M., Luna, M. Y., Morata, A., and González-Hidalgo, J. C.: A High Resolution Dataset of Drought Indices for Spain, *Data*, 2, <https://doi.org/10.3390/data2030022>, 2017.
- Vicente-Serrano, S. M., Martín-Hernández, N., Reig, F., Azorin-Molina, C., Zabalza, J., Beguería, S., Domínguez-Castro, F., El Kenawy, A., Peña-Gallardo, M., Noguera, I., and García, M.: Vegetation greening in Spain detected from long term data (1981–2015), *Int. J. Remote Sens.*, in review, 2018.
- Wan, Z., Wang, P., and Li, X.: Using MODIS Land Surface Temperature and Normalized Difference Vegetation Index products for monitoring drought in the southern Great Plains, USA, *Int. J. Remote Sens.*, 25, 61–72, <https://doi.org/10.1080/0143116031000115328>, 2004.
- Wang, J., Rich, P. M., and Price, K. P.: Temporal responses of NDVI to precipitation and temperature in the central Great Plains, USA, *Int. J. Remote Sens.*, 24, 2345–2364, <https://doi.org/10.1080/01431160210154812>, 2003.
- Xulu, S., Peerbhay, K., Gebreslasie, M., and Ismail, R.: Drought influence on forest plantations in Zululand, South Africa, using MODIS time series and climate data, *Forests*, 9, <https://doi.org/10.3390/f9090528>, 2018.
- Yang, S., Meng, D., Li, X., and Wu, X.: Multi-scale responses of vegetation changes relative to the SPEI meteorological drought index in North China in 2001–

- 2014, *Shengtai Xuebao, Acta Ecol. Sin.*, 38, 1028–1039, <https://doi.org/10.5846/stxb201611242398>, 2018.
- Zhang, L., Xiao, J., Zhou, Y., Zheng, Y., Li, J., and Xiao, H.: Drought events and their effects on vegetation productivity in China, *Ecosphere*, 7, e01591, <https://doi.org/10.1002/ecs2.1591>, 2016.
- Zhang, Q., Kong, D., Singh, V. P., and Shi, P.: Response of vegetation to different time-scales drought across China: Spatiotemporal patterns, causes and implications, *Glob. Planet. Change*, 152, 1–11, <https://doi.org/10.1016/j.gloplacha.2017.02.008>, 2017.
- Zhao, M. and Running, S. W.: Drought-induced reduction in global terrestrial net primary production from 2000 through 2009, *Science*, 329, 940–943, <https://doi.org/10.1126/science.1192666>, 2010.
- Zhao, M., Geruo, A., Velicogna, I., and Kimball, J. S.: Satellite observations of regional drought severity in the continental United States using GRACE-based terrestrial water storage changes, *J. Clim.*, 30, 6297–6308, <https://doi.org/10.1175/JCLI-D-16-0458.1>, 2017.
- Zhao, X., Wei, H., Liang, S., Zhou, T., He, B., Tang, B., and Wu, D.: Responses of natural vegetation to different stages of extreme drought during 2009–2010 in Southwestern China, *Remote Sens.*, 7, 14039–14054, <https://doi.org/10.3390/rs71014039>, 2015.

Supplement of Nat. Hazards Earth Syst. Sci., 19, 1189–1213, 2019
<https://doi.org/10.5194/nhess-19-1189-2019-supplement>
© Author(s) 2019. This work is distributed under
the Creative Commons Attribution 4.0 License.



Supplement of

A high-resolution spatial assessment of the impacts of drought variability on vegetation activity in Spain from 1981 to 2015

Sergio M. Vicente-Serrano et al.

Correspondence to: Sergio M. Vicente-Serrano (svicen@ipe.csic.es)

The copyright of individual parts of the supplement might differ from the CC BY 4.0 License.

	Negative (p < 0.05)	Negative (p > 0.05)	Positive (p > 0.05)	Positive (p < 0.05)
1st Jan	0.1	7.9	47.1	44.9
2nd Jan	0.5	7.8	43.6	48.2
1st Feb	0.2	7.3	43.2	49.3
2sd Feb	0.0	6.1	45.2	48.6
1st Mar	0.0	9.5	48.2	42.2
2sd Mar	0.3	13.0	44.0	42.7
1st Apr	0.0	8.6	35.5	55.9
2sd Apr	0.0	4.7	25.3	69.9
1st May	0.0	1.0	13.7	85.3
2sd May	0.0	0.3	7.2	92.5
1st Jun	0.0	0.1	2.4	97.5
2sd Jun	0.0	0.0	1.3	98.7
1st Jul	0.0	0.0	1.8	98.2
2sd Jul	0.0	0.0	2.3	97.7
1st Aug	0.0	0.0	3.5	96.4
2sd Aug	0.0	0.1	5.6	94.2
1st Sep	0.0	0.2	9.7	90.1
2sd Sep	0.0	0.2	12.7	87.1
1st Oct	0.0	0.5	22.0	77.5
2sd Oct	0.0	1.1	35.9	63.1
1st Nov	0.0	3.1	42.7	54.2
2sd Nov	0.0	3.5	48.5	47.9
1st Dec	0.0	1.9	40.6	57.5
2sd Dec	0.0	4.1	45.8	50.1

Supplementary Table 1: Percentage of the total surface area in Spain showing positive or negative, significant or non-significant Pearson's r correlations between the sNDVI and the SPEI. Non-irrigated arable lands.

	Negative (p < 0.05)	Negative (p > 0.05)	Positive (p > 0.05)	Positive (p < 0.05)
1st Jan	0.0	4.0	32.5	63.5
2nd Jan	0.2	5.1	28.0	66.7
1st Feb	0.3	4.4	27.1	68.2
2sd Feb	0.1	2.8	26.1	71.0
1st Mar	0.0	3.3	31.7	65.0
2sd Mar	0.0	4.4	32.8	62.8
1st Apr	0.0	3.5	30.7	65.8
2sd Apr	0.0	3.0	26.3	70.7
1st May	0.0	2.6	24.7	72.7
2sd May	0.0	1.6	16.9	81.5
1st Jun	0.0	1.0	14.4	84.7
2sd Jun	0.0	0.3	11.0	88.7
1st Jul	0.0	0.3	12.0	87.6
2sd Jul	0.0	0.1	9.8	90.1
1st Aug	0.0	0.2	11.6	88.2
2sd Aug	0.0	0.7	17.2	82.1
1st Sep	0.0	1.1	22.1	76.7
2sd Sep	0.0	0.5	20.8	78.7
1st Oct	0.0	0.8	25.8	73.4
2sd Oct	0.0	2.3	35.5	62.2
1st Nov	0.0	1.8	37.0	61.2
2sd Nov	0.0	2.0	40.6	57.3
1st Dec	0.0	1.1	30.6	68.3
2sd Dec	0.0	2.2	32.3	65.4

Supplementary Table 2: Percentage of the total surface area in Spain showing positive or negative, significant or non-significant Pearson's r correlations between the sNDVI and the SPEI. Irrigated lands

	Negative (p < 0.05)	Negative (p > 0.05)	Positive (p > 0.05)	Positive (p < 0.05)
1st Jan	0.0	1.6	32.4	66.1
2nd Jan	0.0	1.2	29.3	69.4
1st Feb	0.0	1.1	35.4	63.5
2sd Feb	0.0	0.9	37.0	62.1
1st Mar	0.0	3.8	44.8	51.4
2sd Mar	0.0	6.3	41.2	52.4
1st Apr	0.0	1.0	33.1	65.9
2sd Apr	0.0	0.2	14.1	85.7
1st May	0.0	0.1	9.0	90.9
2sd May	0.0	0.1	4.4	95.5
1st Jun	0.0	0.1	5.3	94.6
2sd Jun	0.0	0.0	1.7	98.3
1st Jul	0.0	0.0	0.9	99.1
2sd Jul	0.0	0.0	0.6	99.4
1st Aug	0.0	0.0	0.8	99.2
2sd Aug	0.0	0.0	1.9	98.1
1st Sep	0.0	0.0	4.1	95.9
2sd Sep	0.0	0.0	2.7	97.3
1st Oct	0.0	0.1	5.0	94.9
2sd Oct	0.0	0.2	11.3	88.5
1st Nov	0.0	0.2	22.7	77.1
2sd Nov	0.0	0.4	40.3	59.4
1st Dec	0.0	0.5	40.1	59.3
2sd Dec	0.0	1.8	45.3	52.9

Supplementary Table 3: Percentage of the total surface area in Spain showing positive or negative, significant or non-significant Pearson's r correlations between the sNDVI and the SPEI. Vineyards

	Negative (p < 0.05)	Negative (p > 0.05)	Positive (p > 0.05)	Positive (p < 0.05)
1st Jan	0.0	2.9	43.1	54.0
2nd Jan	0.0	1.6	36.4	61.9
1st Feb	0.0	1.5	31.7	66.8
2sd Feb	0.0	0.6	24.2	75.2
1st Mar	0.0	1.5	28.0	70.5
2sd Mar	0.0	1.5	23.0	75.5
1st Apr	0.0	0.6	11.9	87.5
2sd Apr	0.0	0.2	5.7	94.2
1st May	0.0	0.1	4.6	95.3
2sd May	0.0	0.0	1.2	98.8
1st Jun	0.0	0.0	0.9	99.1
2sd Jun	0.0	0.0	1.7	98.3
1st Jul	0.0	0.0	2.7	97.3
2sd Jul	0.0	0.0	2.6	97.4
1st Aug	0.0	0.0	4.7	95.2
2sd Aug	0.0	0.1	10.9	89.1
1st Sep	0.0	0.1	20.2	79.7
2sd Sep	0.0	0.0	12.6	87.4
1st Oct	0.0	0.0	4.5	95.5
2sd Oct	0.0	0.1	6.8	93.1
1st Nov	0.0	0.2	16.4	83.4
2sd Nov	0.0	0.5	31.2	68.3
1st Dec	0.0	0.5	23.4	76.1
2sd Dec	0.0	1.8	39.6	58.6

Supplementary Table 4: Percentage of the total surface area in Spain showing positive or negative, significant or non-significant Pearson's r correlations between the sNDVI and the SPEI. Olive groves.

	Negative (p < 0.05)	Negative (p > 0.05)	Positive (p > 0.05)	Positive (p < 0.05)
1st Jan	0.0	7.7	39.1	53.1
2nd Jan	0.0	5.7	39.7	54.6
1st Feb	0.0	5.6	39.0	55.3
2nd Feb	0.0	6.6	37.4	55.9
1st Mar	0.0	6.9	38.7	54.4
2nd Mar	0.1	12.3	34.4	53.1
1st Apr	0.0	9.6	34.1	56.3
2nd Apr	0.0	4.0	28.9	67.0
1st May	0.0	0.9	20.5	78.5
2nd May	0.0	0.8	15.8	83.4
1st Jun	0.0	1.6	15.1	83.3
2nd Jun	0.0	0.6	9.5	89.9
1st Jul	0.0	0.1	5.4	94.5
2nd Jul	0.0	0.0	4.2	95.8
1st Aug	0.0	0.0	5.4	94.6
2nd Aug	0.0	0.1	8.8	91.1
1st Sep	0.0	0.6	9.4	89.9
2nd Sep	0.0	0.4	15.6	83.9
1st Oct	0.0	1.0	26.4	72.5
2nd Oct	0.0	1.3	32.1	66.6
1st Nov	0.0	4.5	37.6	57.9
2nd Nov	0.0	4.9	42.2	52.9
1st Dec	0.0	4.1	41.0	54.9
2nd Dec	0.0	4.1	39.9	56.0

Supplementary Table 5: Percentage of the total surface area in Spain showing positive or negative, significant or non-significant Pearson's r correlations between the sNDVI and the SPEI. Mixed agriculture/natural vegetation

	Negative (p < 0.05)	Negative (p > 0.05)	Positive (p > 0.05)	Positive (p < 0.05)
1st Jan	0.2	15.9	45.5	38.4
2nd Jan	0.2	12.3	49.5	38.0
1st Feb	0.2	11.3	47.5	41.0
2sd Feb	0.1	13.2	44.3	42.3
1st Mar	0.1	13.6	46.7	39.7
2sd Mar	0.2	17.9	41.8	40.1
1st Apr	0.0	12.6	45.3	42.0
2sd Apr	0.0	5.8	42.5	51.7
1st May	0.0	3.3	33.1	63.5
2sd May	0.0	2.6	29.1	68.3
1st Jun	0.0	4.7	25.2	70.2
2sd Jun	0.0	1.9	18.9	79.2
1st Jul	0.0	1.0	13.5	85.5
2sd Jul	0.0	0.2	11.5	88.4
1st Aug	0.0	0.1	14.1	85.8
2sd Aug	0.0	0.4	21.0	78.6
1st Sep	0.0	1.6	20.9	77.5
2sd Sep	0.0	1.7	28.9	69.5
1st Oct	0.0	4.4	37.2	58.3
2sd Oct	0.0	2.9	39.2	57.9
1st Nov	0.0	7.0	43.6	49.4
2sd Nov	0.0	8.1	47.7	44.2
1st Dec	0.0	9.0	46.0	45.0
2sd Dec	0.1	8.8	51.0	40.1

Supplementary Table 6: Percentage of the total surface area in Spain showing positive or negative, significant or non-significant Pearson's r correlations between the sNDVI and the SPEI. Broad-leaved forests

	Negative (p < 0.05)	Negative (p > 0.05)	Positive (p > 0.05)	Positive (p < 0.05)
1st Jan	0.4	15.9	46.0	37.7
2nd Jan	0.6	15.1	47.0	37.3
1st Feb	0.3	11.3	45.2	43.3
2sd Feb	0.2	12.1	45.5	42.2
1st Mar	0.3	14.2	51.1	34.5
2sd Mar	0.2	14.0	48.4	37.3
1st Apr	0.0	10.2	48.7	41.1
2sd Apr	0.0	4.8	42.2	53.0
1st May	0.0	2.9	32.7	64.4
2sd May	0.0	1.4	27.2	71.4
1st Jun	0.0	1.5	19.9	78.6
2sd Jun	0.0	0.8	13.6	85.6
1st Jul	0.0	0.3	9.6	90.0
2sd Jul	0.0	0.1	7.2	92.7
1st Aug	0.0	0.1	8.2	91.7
2sd Aug	0.0	0.5	20.3	79.2
1st Sep	0.0	1.6	26.4	72.0
2sd Sep	0.0	0.9	31.3	67.8
1st Oct	0.0	3.7	37.9	58.3
2sd Oct	0.0	5.6	42.8	51.7
1st Nov	0.1	10.8	47.3	41.8
2sd Nov	0.1	9.5	51.2	39.2
1st Dec	0.1	9.5	48.0	42.3
2sd Dec	0.3	10.8	49.2	39.8

Supplementary Table 7: Percentage of the total surface area in Spain showing positive or negative, significant or non-significant Pearson's r correlations between the sNDVI and the SPEI. Coniferous forests

	Negative (p < 0.05)	Negative (p > 0.05)	Positive (p > 0.05)	Positive (p < 0.05)
1st Jan	0.9	19.6	53.6	25.9
2nd Jan	1.8	18.4	55.6	24.2
1st Feb	1.5	17.2	55.5	25.8
2sd Feb	0.1	17.8	59.8	22.2
1st Mar	0.1	16.4	62.9	20.7
2sd Mar	0.8	20.8	60.1	18.3
1st Apr	0.0	12.7	62.7	24.6
2sd Apr	0.0	5.4	50.4	44.2
1st May	0.0	3.5	39.4	57.0
2sd May	0.0	1.7	31.3	66.9
1st Jun	0.0	2.8	26.0	71.2
2sd Jun	0.0	1.9	20.5	77.6
1st Jul	0.0	0.4	14.4	85.1
2sd Jul	0.0	0.0	9.7	90.2
1st Aug	0.0	0.1	10.6	89.2
2sd Aug	0.0	0.8	21.5	77.6
1st Sep	0.0	0.9	24.8	74.3
2sd Sep	0.0	0.9	27.4	71.7
1st Oct	0.0	4.1	47.2	48.6
2sd Oct	0.0	6.0	52.8	41.2
1st Nov	0.1	13.4	47.3	39.1
2sd Nov	0.1	12.4	57.6	29.9
1st Dec	0.1	11.9	64.8	23.2
2sd Dec	0.2	13.4	61.4	25.0

Supplementary Table 8: Percentage of the total surface area in Spain showing positive or negative, significant or non-significant Pearson's r correlations between the sNDVI and the SPEI. Mixed forests

	Negative (p < 0.05)	Negative (p > 0.05)	Positive (p > 0.05)	Positive (p < 0.05)
1st Jan	1.7	16.2	34.3	47.8
2nd Jan	2.0	13.1	33.2	51.7
1st Feb	1.2	11.5	33.4	54.0
2sd Feb	1.0	11.8	29.5	57.7
1st Mar	1.4	12.2	27.6	58.8
2sd Mar	0.5	13.3	26.5	59.7
1st Apr	0.0	9.1	25.7	65.2
2sd Apr	0.0	2.7	23.2	74.1
1st May	0.0	2.2	16.5	81.3
2sd May	0.0	1.8	13.7	84.4
1st Jun	0.0	2.5	10.7	86.7
2sd Jun	0.0	1.8	7.8	90.4
1st Jul	0.1	1.4	6.5	92.0
2sd Jul	0.0	0.8	6.0	93.1
1st Aug	0.0	0.1	6.8	93.1
2sd Aug	0.0	0.2	10.8	88.9
1st Sep	0.0	0.2	12.4	87.3
2sd Sep	0.0	0.2	13.7	86.0
1st Oct	0.0	1.4	18.9	79.7
2sd Oct	0.0	1.7	22.4	75.9
1st Nov	0.0	6.5	26.7	66.8
2sd Nov	0.2	6.7	32.0	61.1
1st Dec	0.3	7.6	28.7	63.4
2sd Dec	1.3	10.8	36.2	51.8

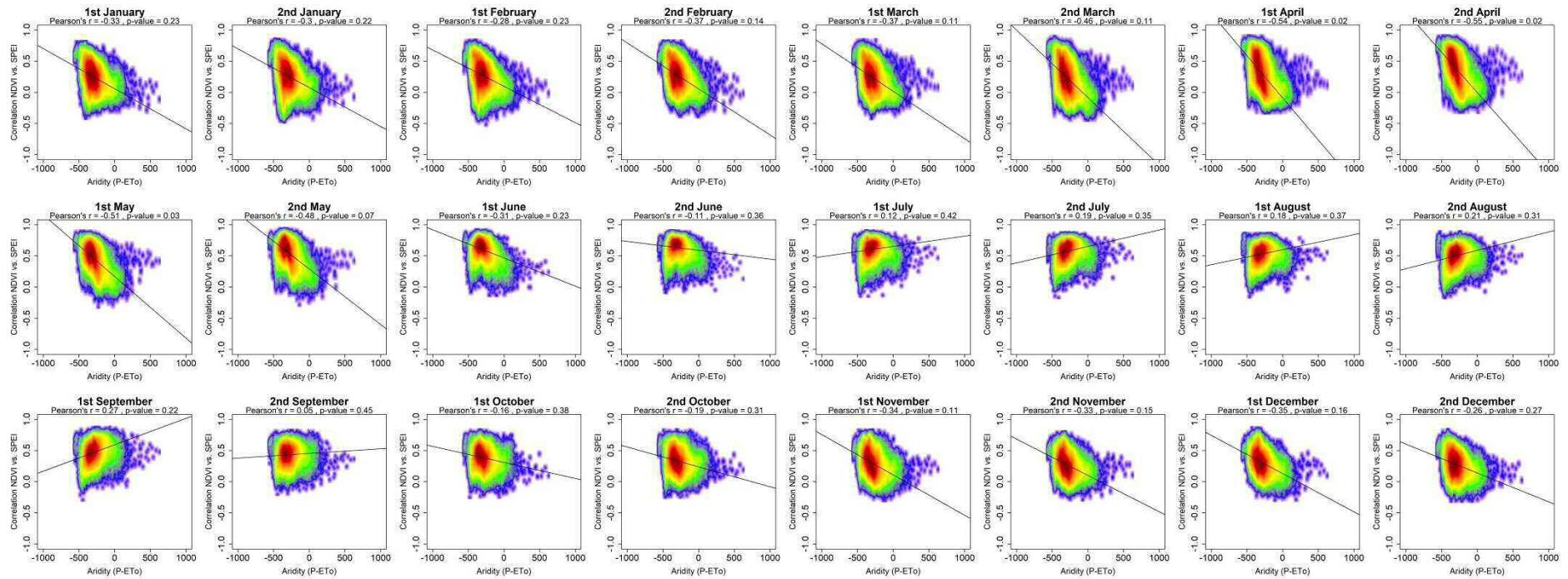
Supplementary Table 9: Percentage of the total surface area in Spain showing positive or negative, significant or non-significant Pearson's r correlations between the sNDVI and the SPEI. Natural grassland

	Negative (p < 0.05)	Negative (p > 0.05)	Positive (p > 0.05)	Positive (p < 0.05)
1st Jan	0.1	7.8	37.4	54.7
2nd Jan	0.1	6.2	36.9	56.8
1st Feb	0.1	4.3	35.6	60.0
2sd Feb	0.0	4.0	33.1	62.9
1st Mar	0.1	5.0	37.8	57.2
2sd Mar	0.1	5.7	34.2	60.0
1st Apr	0.0	5.0	29.8	65.1
2sd Apr	0.0	1.8	21.5	76.7
1st May	0.0	1.1	15.1	83.8
2sd May	0.0	0.4	9.4	90.2
1st Jun	0.0	0.1	4.0	95.9
2sd Jun	0.0	0.0	1.8	98.1
1st Jul	0.0	0.0	1.2	98.8
2sd Jul	0.0	0.0	1.2	98.8
1st Aug	0.0	0.0	2.2	97.8
2sd Aug	0.0	0.1	5.7	94.2
1st Sep	0.0	0.2	8.8	91.1
2sd Sep	0.0	0.2	10.7	89.2
1st Oct	0.0	0.6	15.8	83.6
2sd Oct	0.0	0.9	21.4	77.8
1st Nov	0.0	3.1	28.6	68.3
2sd Nov	0.0	3.2	33.7	63.2
1st Dec	0.0	2.8	31.5	65.8
2sd Dec	0.0	4.7	37.4	57.8

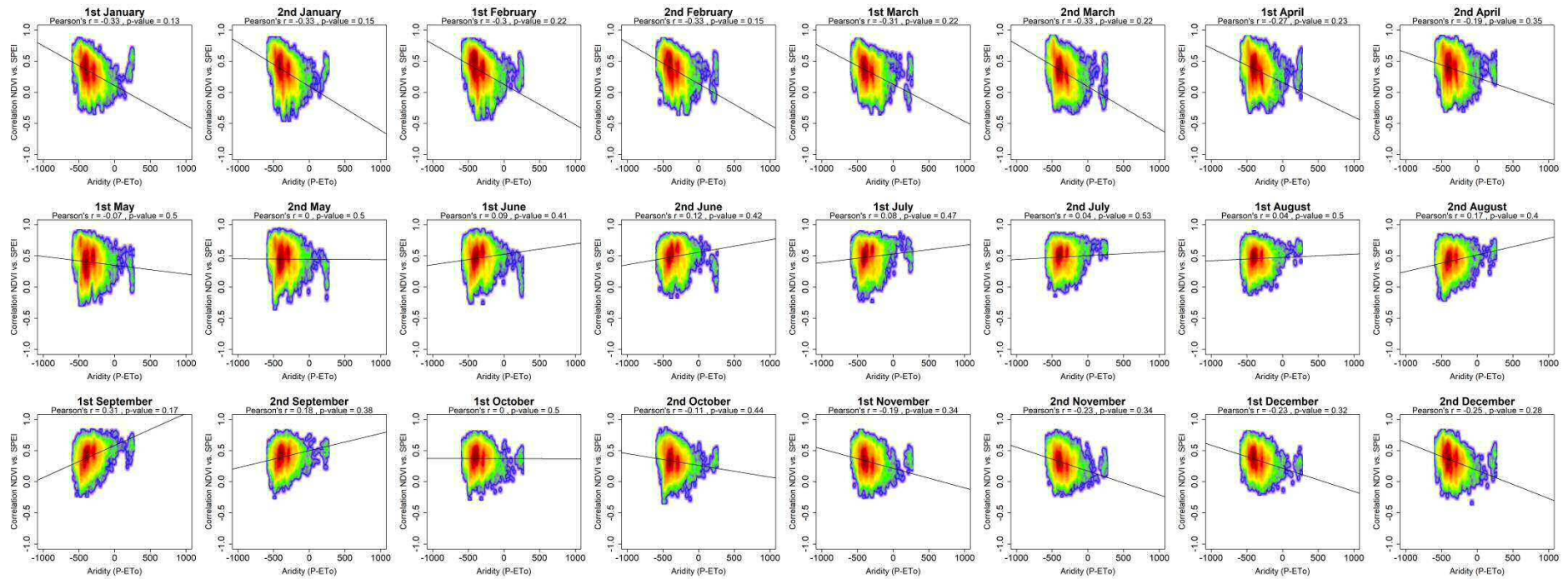
Supplementary Table 10: Percentage of the total surface area in Spain showing positive or negative, significant or non-significant Pearson's r correlations between the sNDVI and the SPEI. Sclerophyllous vegetation

	Negative (p < 0.05)	Negative (p > 0.05)	Positive (p > 0.05)	Positive (p < 0.05)
1st Jan	0.1	11.7	44.0	44.1
2nd Jan	0.2	9.9	44.1	45.9
1st Feb	0.1	6.8	43.4	49.6
2nd Feb	0.1	6.5	42.6	50.8
1st Mar	0.1	8.1	45.0	46.9
2nd Mar	0.2	10.1	42.9	46.8
1st Apr	0.0	7.7	40.2	52.1
2nd Apr	0.0	2.9	30.3	66.8
1st May	0.0	1.9	23.1	75.0
2nd May	0.0	0.9	17.4	81.7
1st Jun	0.0	0.8	11.7	87.5
2nd Jun	0.0	0.5	7.3	92.2
1st Jul	0.0	0.1	3.7	96.2
2nd Jul	0.0	0.0	2.6	97.3
1st Aug	0.0	0.0	3.9	96.1
2nd Aug	0.0	0.1	8.9	91.0
1st Sep	0.0	0.3	13.4	86.3
2nd Sep	0.0	0.2	18.9	80.9
1st Oct	0.0	1.5	28.5	70.0
2nd Oct	0.0	2.5	33.0	64.5
1st Nov	0.0	5.3	37.1	57.6
2nd Nov	0.0	4.7	43.3	52.0
1st Dec	0.0	4.5	42.8	52.7
2nd Dec	0.1	7.0	46.8	46.1

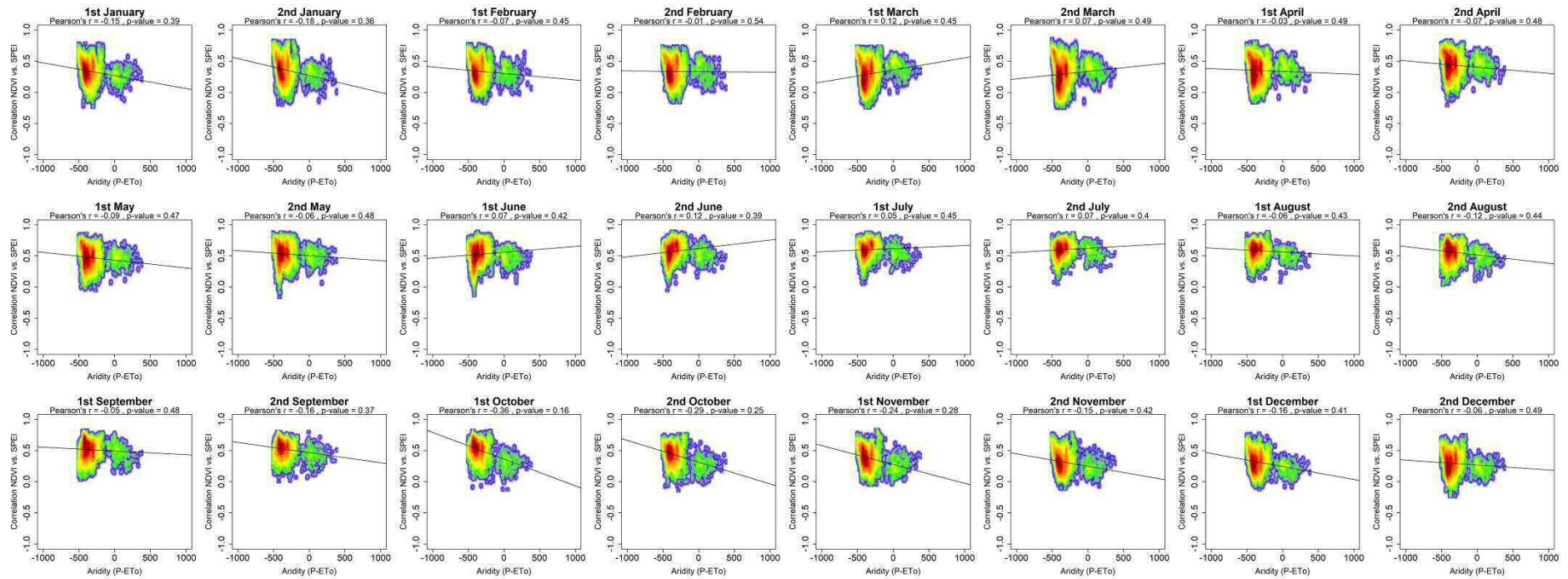
Supplementary Table 11: Percentage of the total surface area in Spain showing positive or negative, significant or non-significant Pearson's r correlations between the sNDVI and the SPEI. Transition wood-scrub.



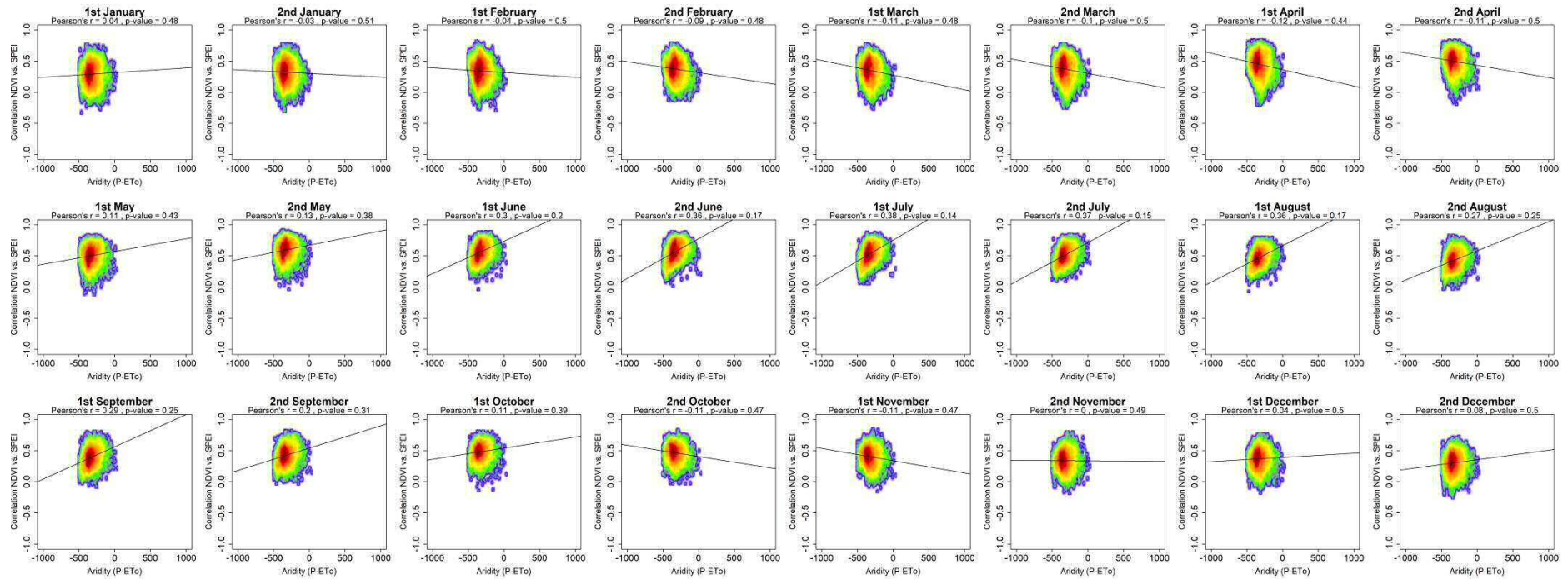
Supplementary Figure 1: Relationship between the average aridity (P-ETo) and the maximum correlations obtained between NDVI and the SPEI during the 24 semi-monthly periods of the year. Non Irrigated arable lands. Given the high number of points the signification of correlation was obtained by means of 1000 random samples of 30 cases from which correlations and p-values were obtained. The final signification was assessed by means of the average of the obtained p-values.



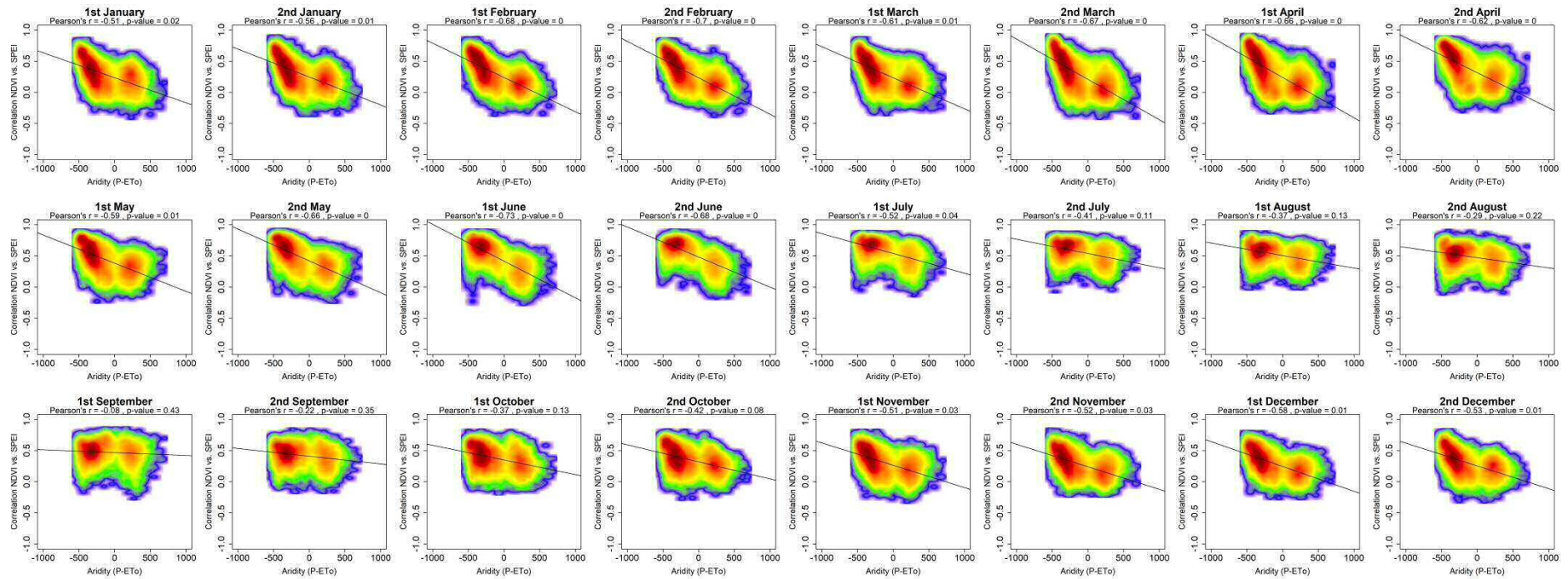
Supplementary Figure 2: Relationship between the average aridity (P-ETo) and the maximum correlations obtained between NDVI and the SPEI during the 24 semi-monthly periods of the year. Irrigated lands. Given the high number of points the signification of correlation was obtained by means of 1000 random samples of 30 cases from which correlations and p-values were obtained. The final signification was assessed by means of the average of the obtained p-values.



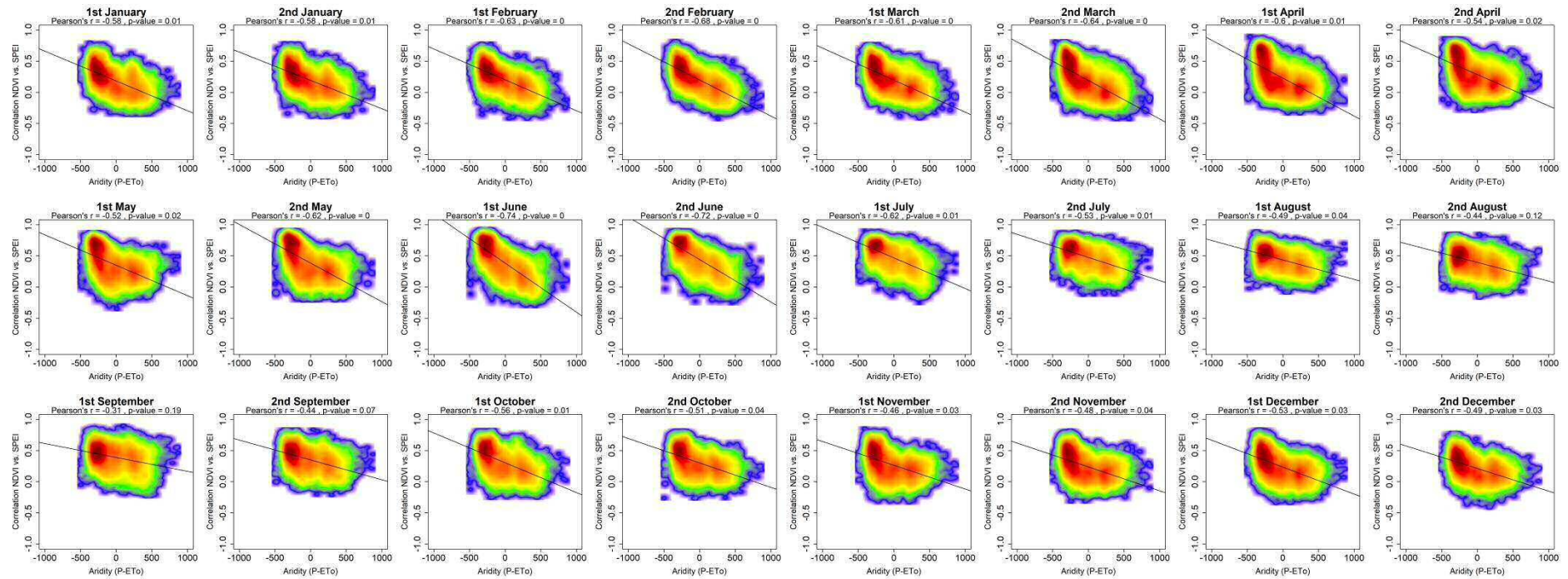
Supplementary Figure 3: Relationship between the average aridity (P-ETo) and the maximum correlations obtained between NDVI and the SPEI during the 24 semi-monthly periods of the year. Vineyards. Given the high number of points the signification of correlation was obtained by means of 1000 random samples of 30 cases from which correlations and p-values were obtained. The final signification was assessed by means of the average of the obtained p-values.



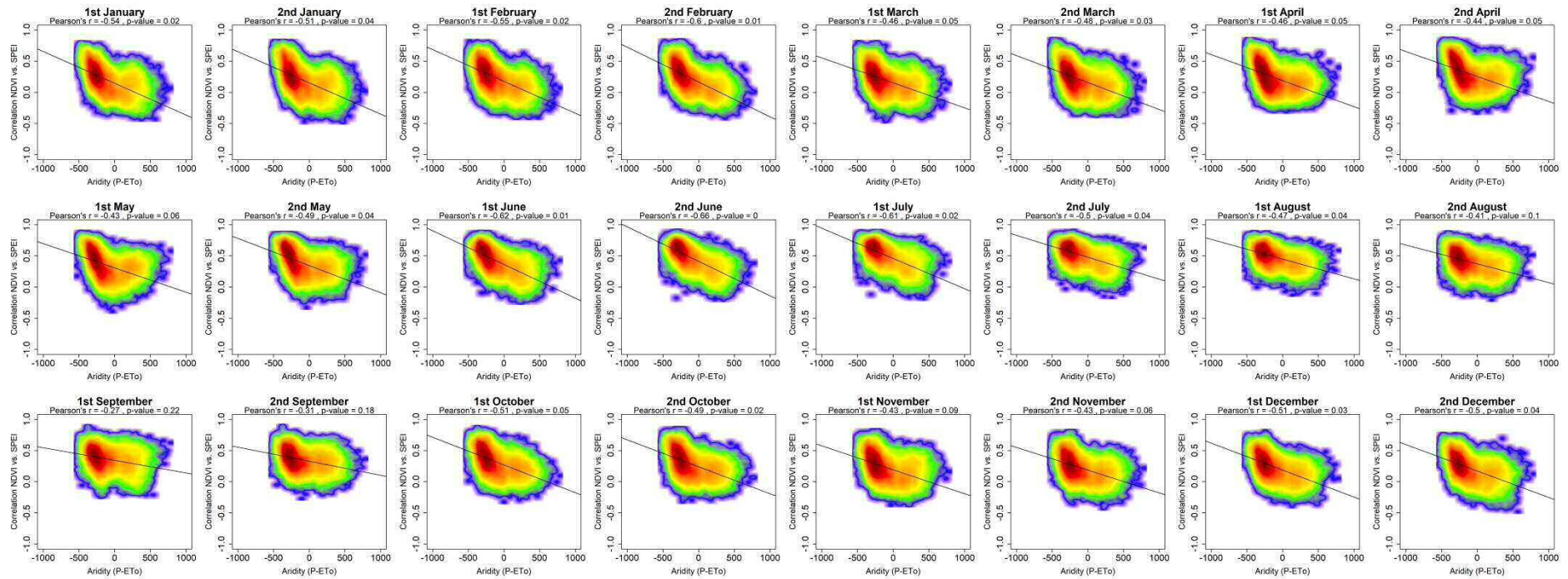
Supplementary Figure 4: Relationship between the average aridity (P-ETo) and the maximum correlations obtained between NDVI and the SPEI during the 24 semi-monthly periods of the year. Olive groves. Given the high number of points the significance of correlation was obtained by means of 1000 random samples of 30 cases from which correlations and p-values were obtained. The final signification was assessed by means of the average of the obtained p-values.



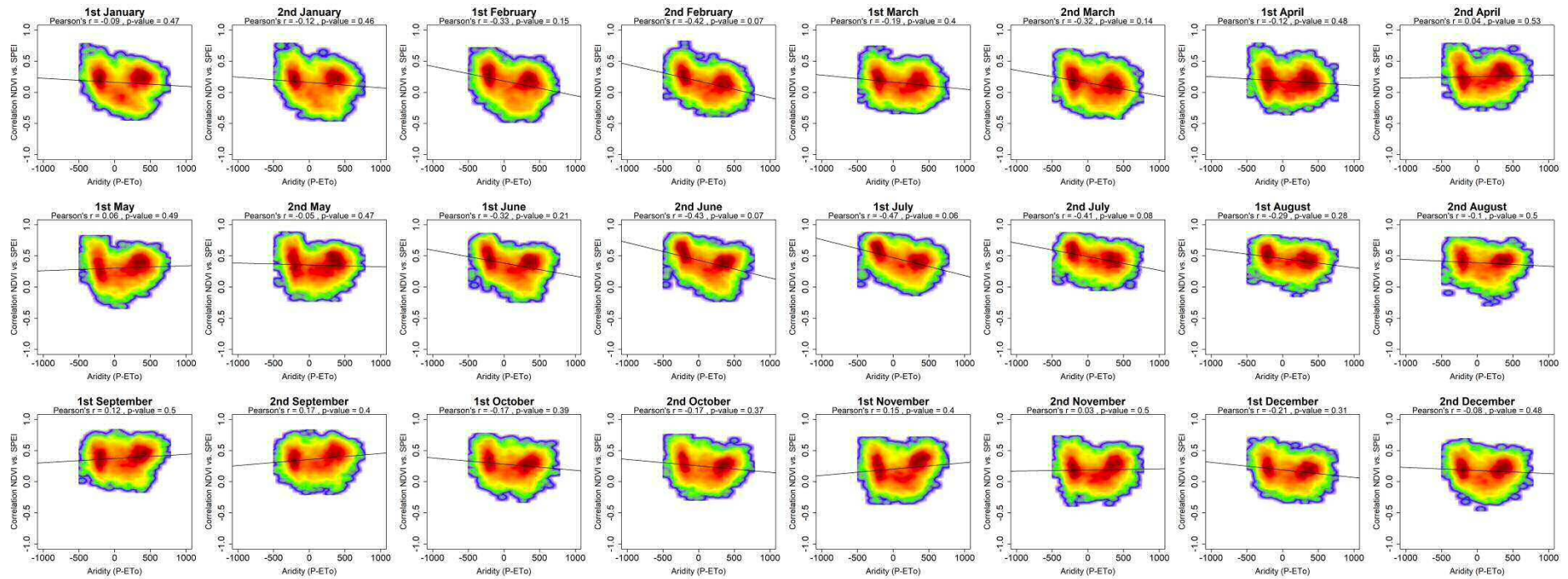
Supplementary Figure 5: Relationship between the average aridity (P-ETo) and the maximum correlations obtained between NDVI and the SPEI during the 24 semi-monthly periods of the year. Mixed agriculture/natural vegetation. Given the high number of points the signification of correlation was obtained by means of 1000 random samples of 30 cases from which correlations and p-values were obtained. The final signification was assessed by means of the average of the obtained p-values.



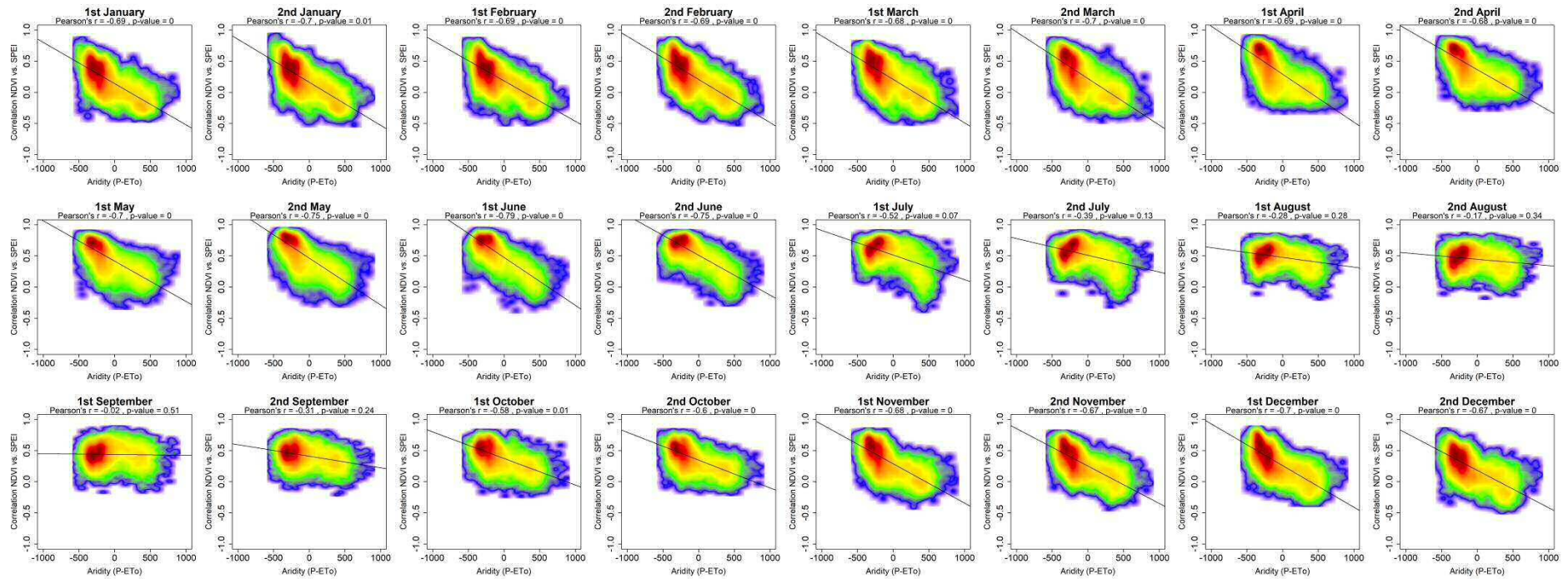
Supplementary Figure 6: Relationship between the average aridity (P-ETo) and the maximum correlations obtained between NDVI and the SPEI during the 24 semi-monthly periods of the year. Broad-leaved forests. Given the high number of points the signification of correlation was obtained by means of 1000 random samples of 30 cases from which correlations and p-values were obtained. The final signification was assessed by means of the average of the obtained p-values.



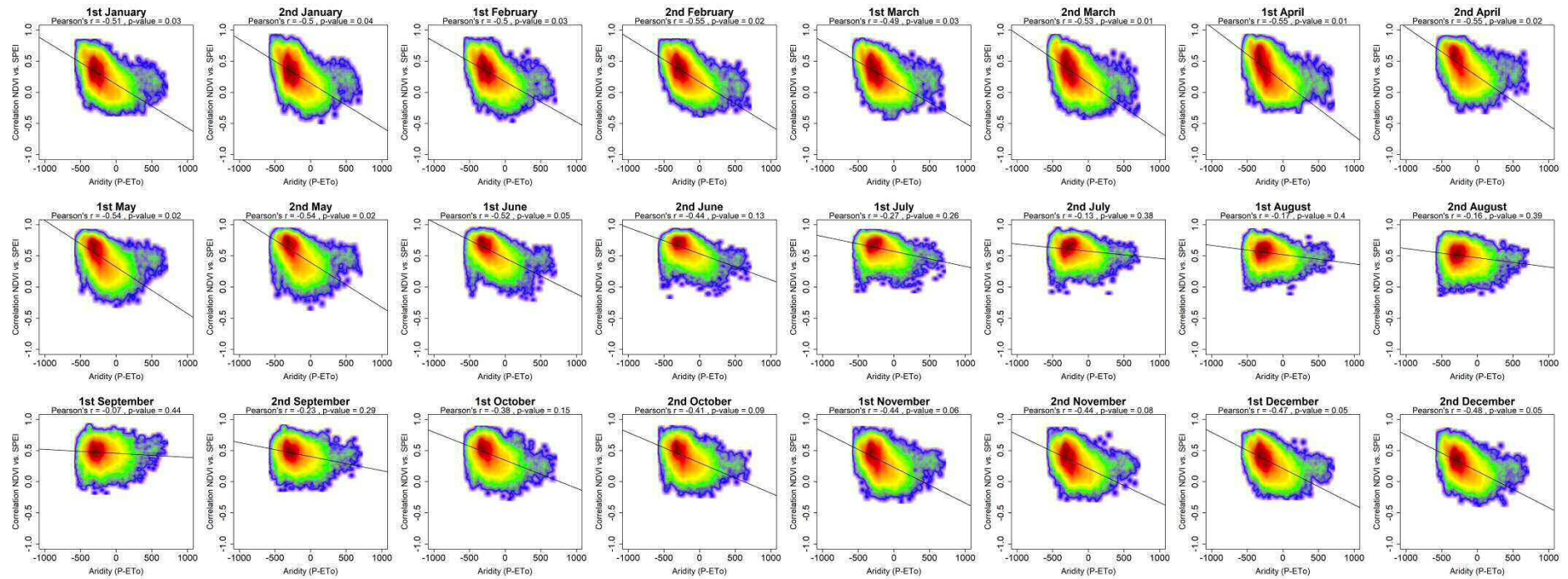
Supplementary Figure 7: Relationship between the average aridity (P-ETo) and the maximum correlations obtained between NDVI and the SPEI during the 24 semi-monthly periods of the year. Coniferous forests. Given the high number of points the significance of correlation was obtained by means of 1000 random samples of 30 cases from which correlations and p-values were obtained. The final signification was assessed by means of the average of the obtained p-values.



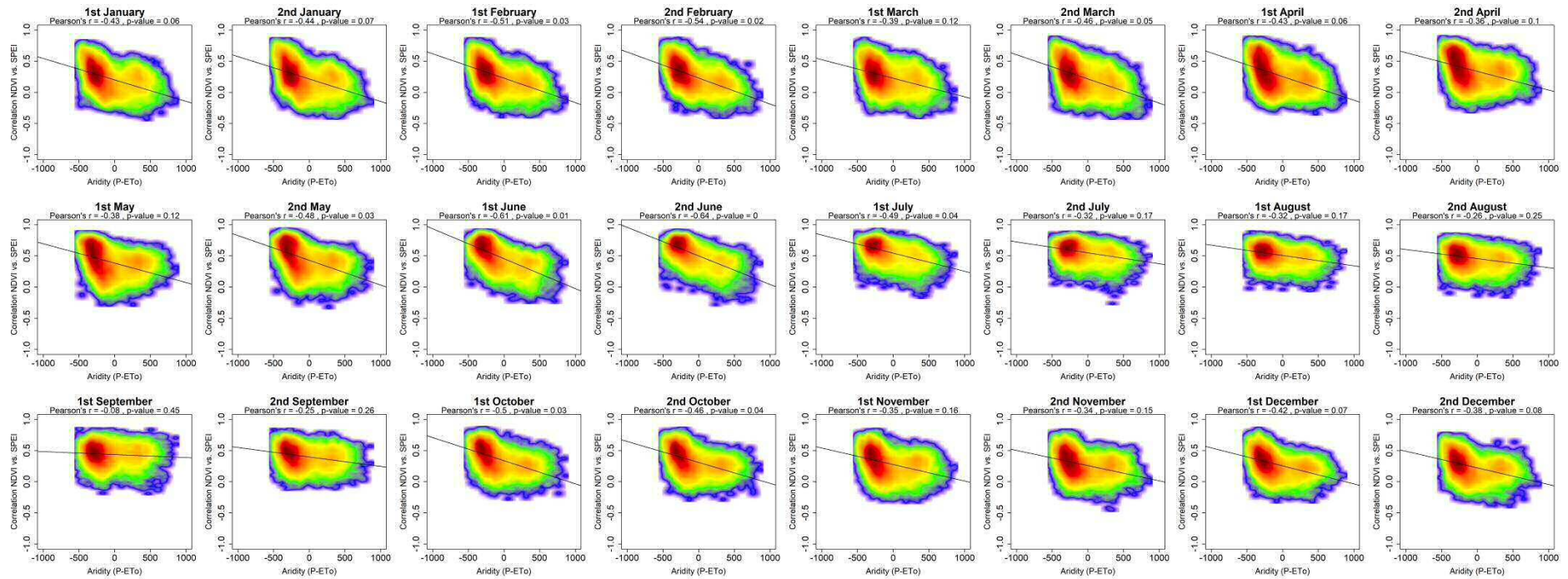
Supplementary Figure 8: Relationship between the average aridity (P-ETo) and the maximum correlations obtained between NDVI and the SPEI during the 24 semi-monthly periods of the year. Mixed forests. Given the high number of points the signification of correlation was obtained by means of 1000 random samples of 30 cases from which correlations and p-values were obtained. The final signification was assessed by means of the average of the obtained p-values.



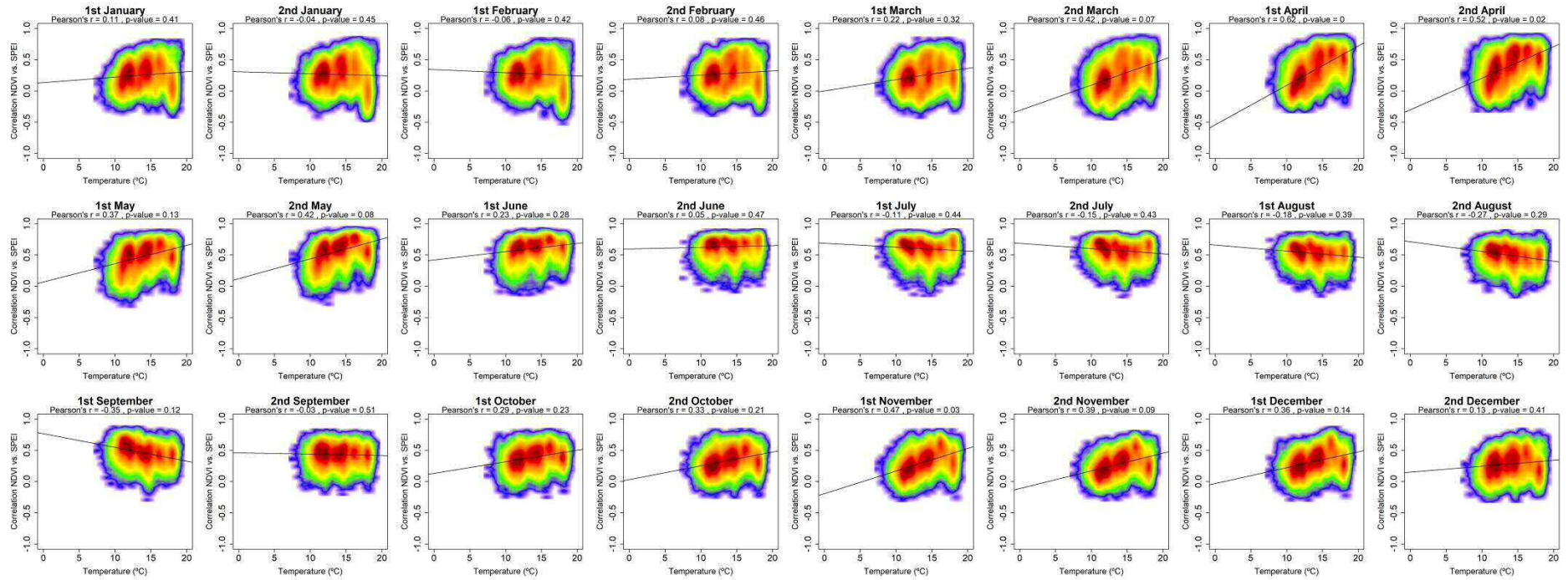
Supplementary Figure 9: Relationship between the average aridity (P-ETo) and the maximum correlations obtained between NDVI and the SPEI during the 24 semi-monthly periods of the year. Natural grasslands. Given the high number of points the significance of correlation was obtained by means of 1000 random samples of 30 cases from which correlations and p-values were obtained. The final significance was assessed by means of the average of the obtained p-values.



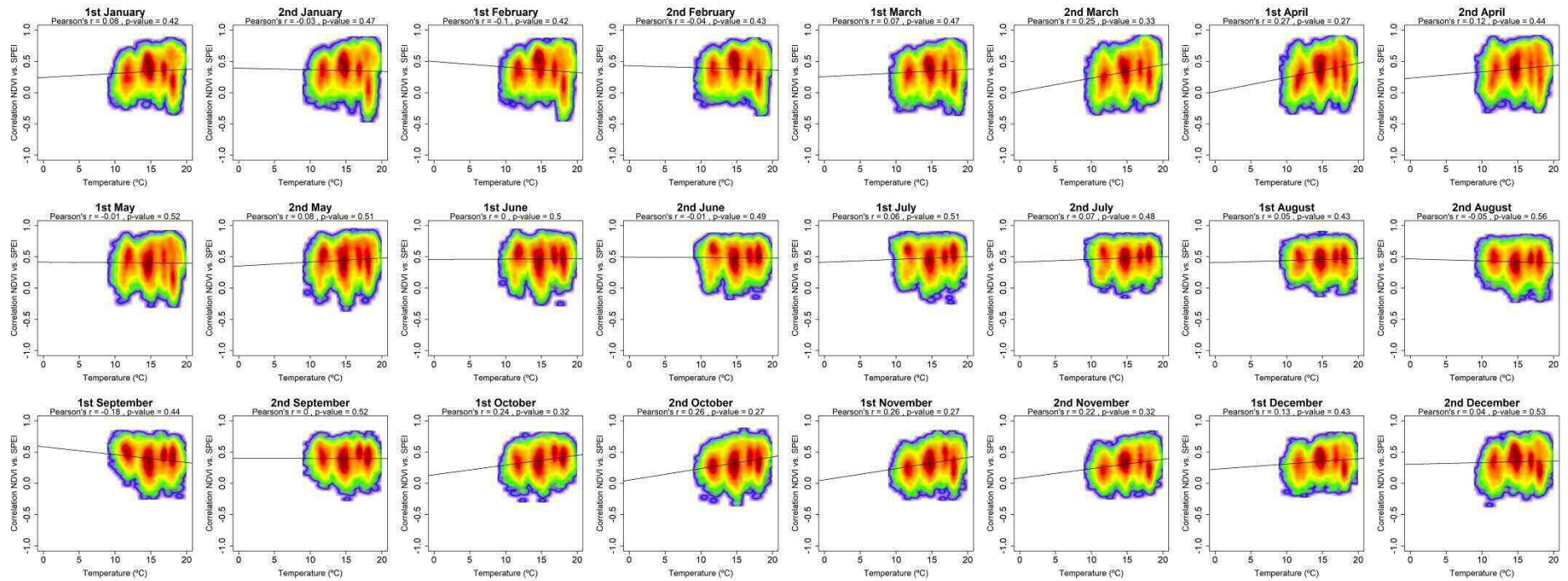
Supplementary Figure 10: Relationship between the average aridity (P-ETo) and the maximum correlations obtained between NDVI and the SPEI during the 24 semi-monthly periods of the year. Sclerophyllous vegetation. Given the high number of points the significance of correlation was obtained by means of 1000 random samples of 30 cases from which correlations and p-values were obtained. The final significance was assessed by means of the average of the obtained p-values.



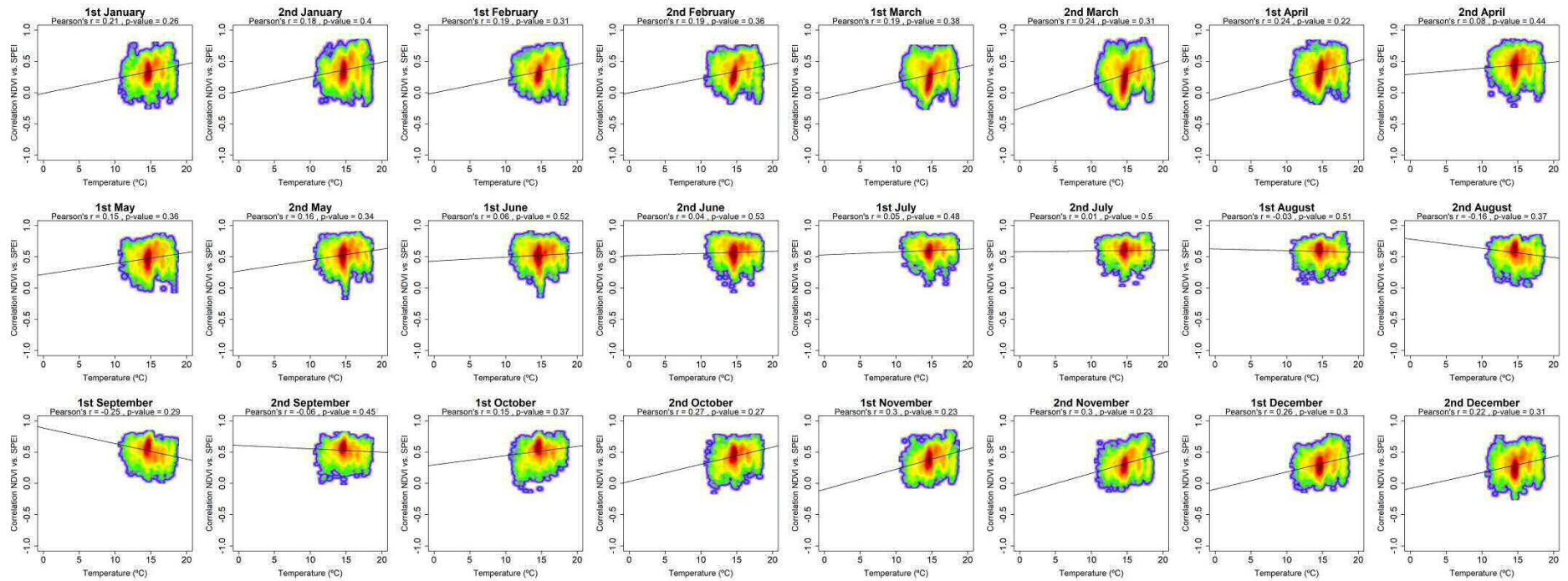
Supplementary Figure 11: Relationship between the average aridity (P-ETo) and the maximum correlations obtained between NDVI and the SPEI during the 24 semi-monthly periods of the year. Transition wood-scrub. Given the high number of points the significance of correlation was obtained by means of 1000 random samples of 30 cases from which correlations and p-values were obtained. The final significance was assessed by means of the average of the obtained p-values.



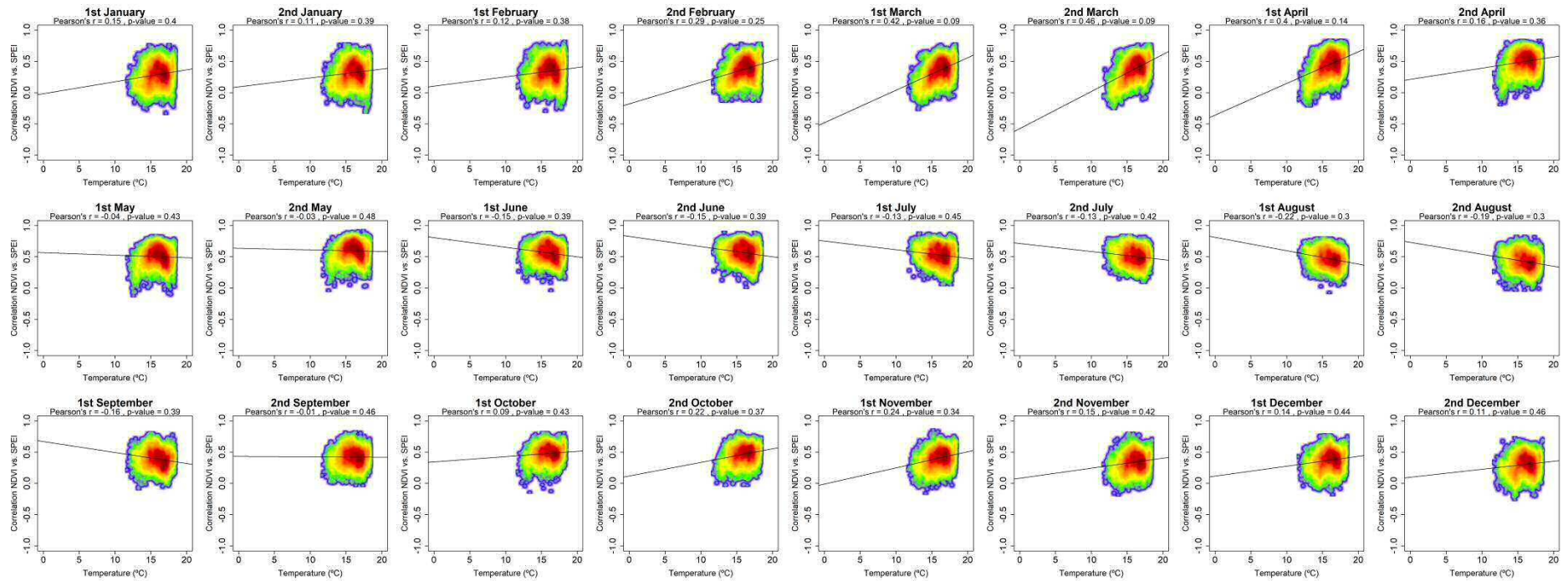
Supplementary Figure 12: Relationship between the average temperature and the maximum correlations obtained between NDVI and the SPEI during the 24 semi-monthly periods of the year. Non Irrigated arable lands. Given the high number of points the signification of correlation was obtained by means of 1000 random samples of 30 cases from which correlations and p-values were obtained. The final signification was assessed by means of the average of the obtained p-values.



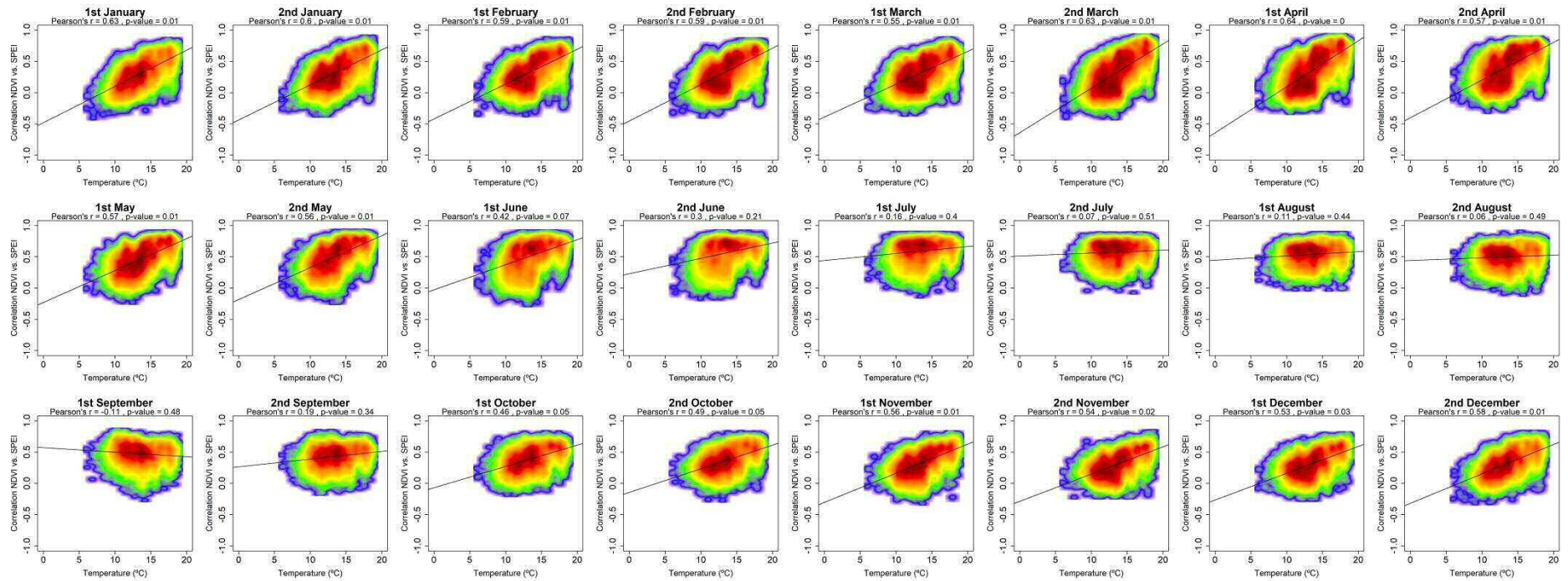
Supplementary Figure 13: Relationship between the average temperature and the maximum correlations obtained between NDVI and the SPEI during the 24 semi-monthly periods of the year. Irrigated lands. Given the high number of points the signification of correlation was obtained by means of 1000 random samples of 30 cases from which correlations and p-values were obtained. The final signification was assessed by means of the average of the obtained p-values.



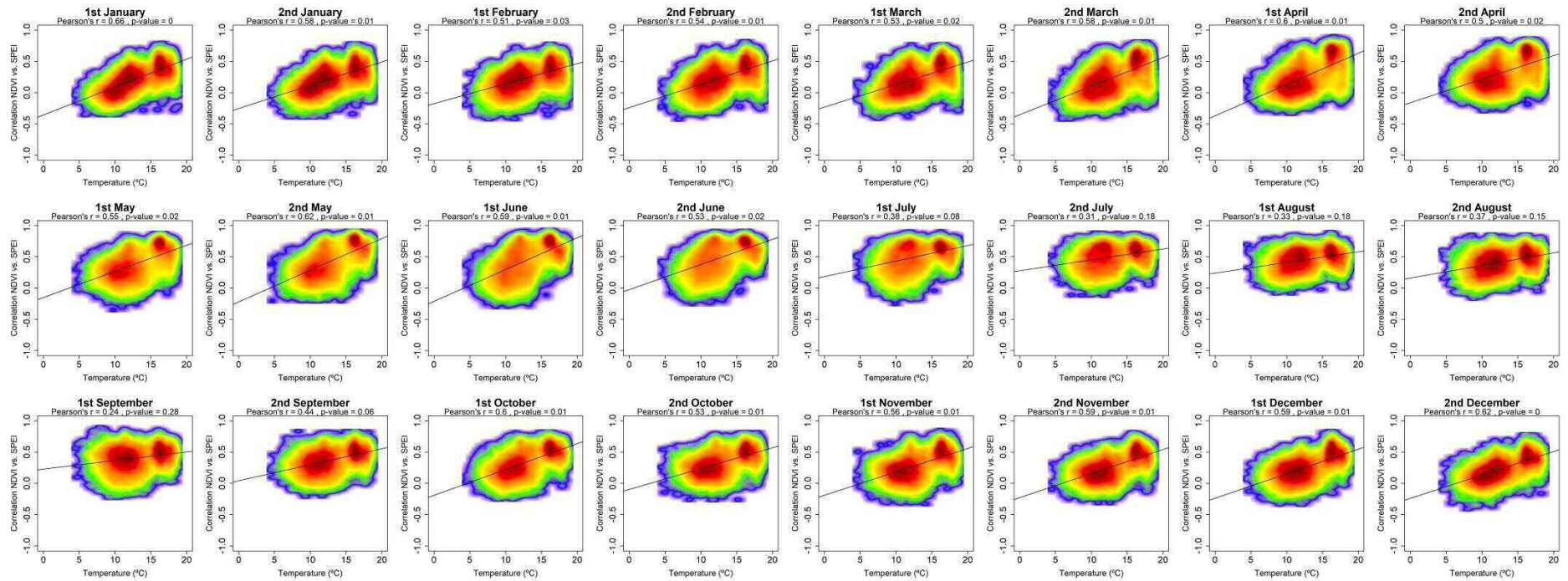
Supplementary Figure 14: Relationship between the average temperature and the maximum correlations obtained between NDVI and the SPEI during the 24 semi-monthly periods of the year. Vineyards. Given the high number of points the significance of correlation was obtained by means of 1000 random samples of 30 cases from which correlations and p-values were obtained. The final significance was assessed by means of the average of the obtained p-values.



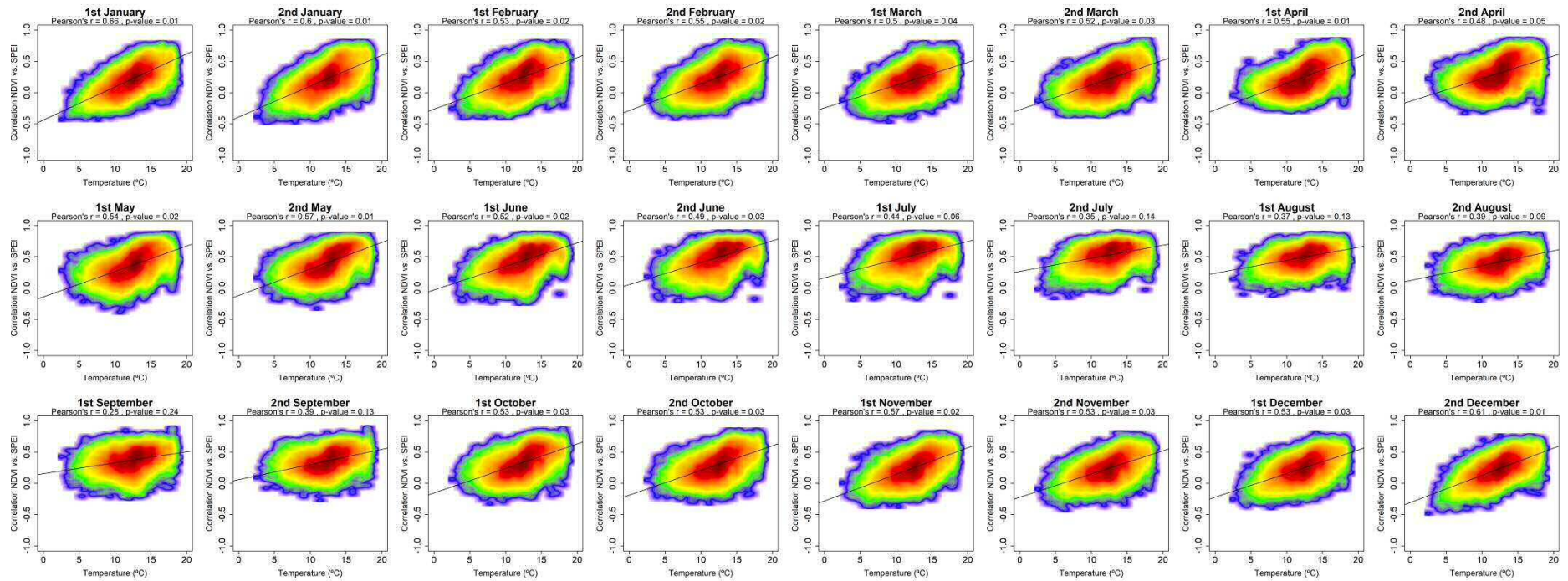
Supplementary Figure 15: Relationship between the average temperature and the maximum correlations obtained between NDVI and the SPEI during the 24 semi-monthly periods of the year. Olive groves. Given the high number of points the significance of correlation was obtained by means of 1000 random samples of 30 cases from which correlations and p-values were obtained. The final signification was assessed by means of the average of the obtained p-values.



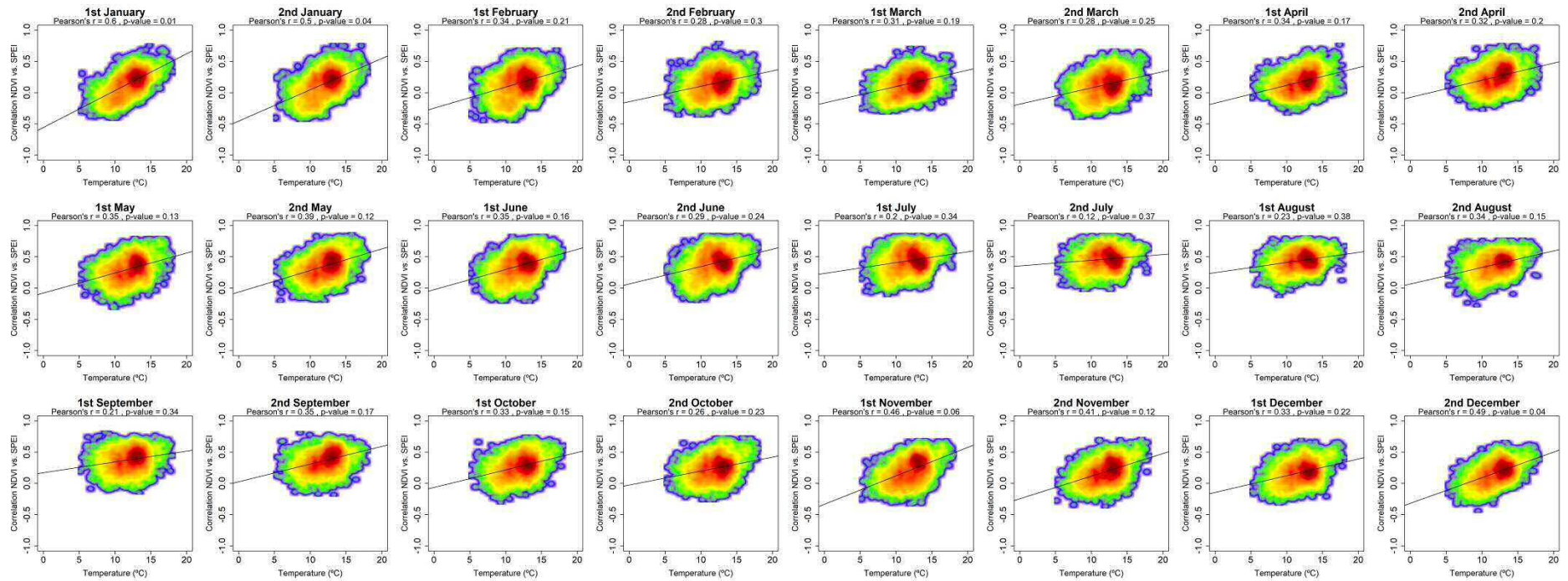
Supplementary Figure 16: Relationship between the average temperature and the maximum correlations obtained between NDVI and the SPEI during the 24 semi-monthly periods of the year. Mixed agriculture/natural vegetation. Given the high number of points the signification of correlation was obtained by means of 1000 random samples of 30 cases from which correlations and p-values were obtained. The final signification was assessed by means of the average of the obtained p-values.



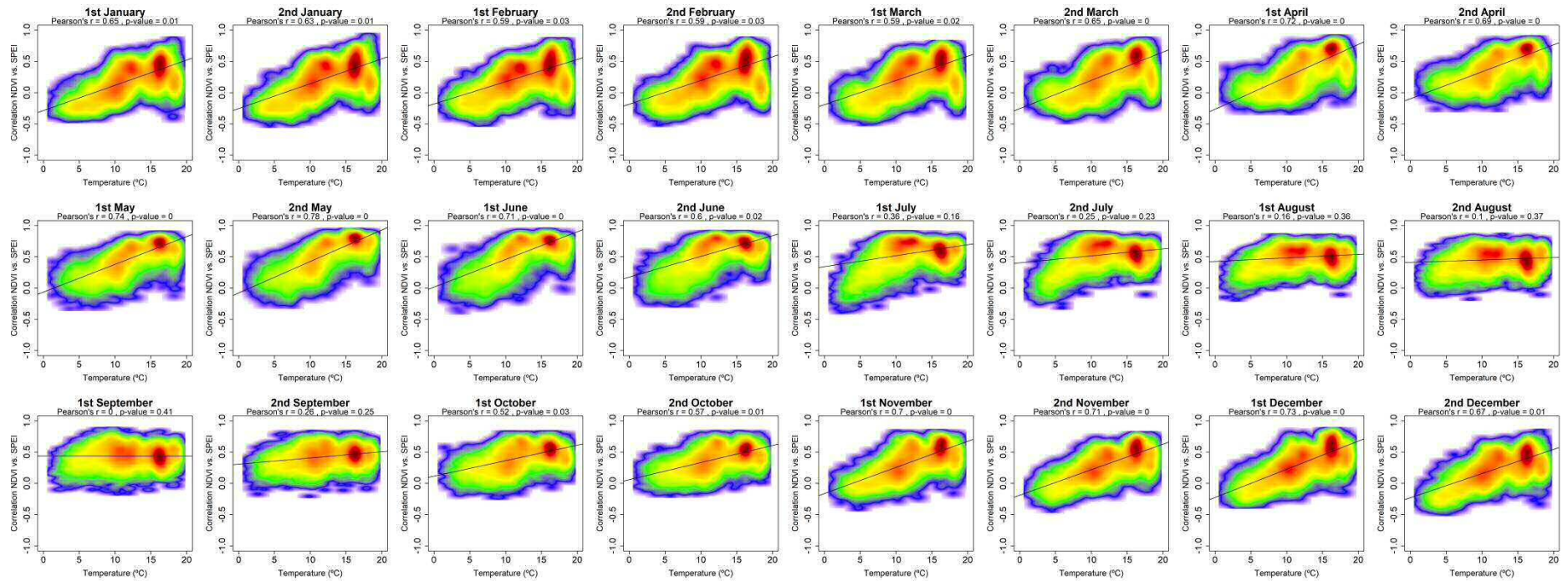
Supplementary Figure 17: Relationship between the average temperature and the maximum correlations obtained between NDVI and the SPEI during the 24 semi-monthly periods of the year. Broad-leaved forests. Given the high number of points the signification of correlation was obtained by means of 1000 random samples of 30 cases from which correlations and p-values were obtained. The final signification was assessed by means of the average of the obtained p-values.



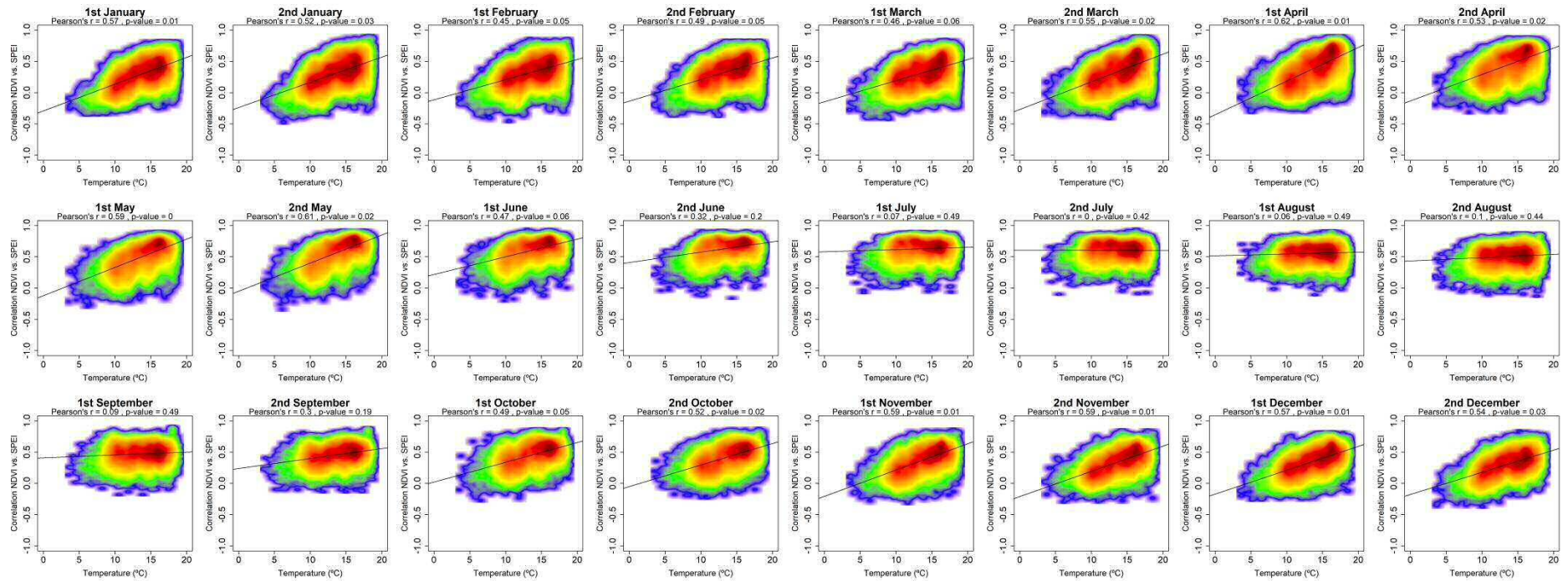
Supplementary Figure 18: Relationship between the average temperature and the maximum correlations obtained between NDVI and the SPEI during the 24 semi-monthly periods of the year. Coniferous forests. Given the high number of points the significance of correlation was obtained by means of 1000 random samples of 30 cases from which correlations and p-values were obtained. The final significance was assessed by means of the average of the obtained p-values.



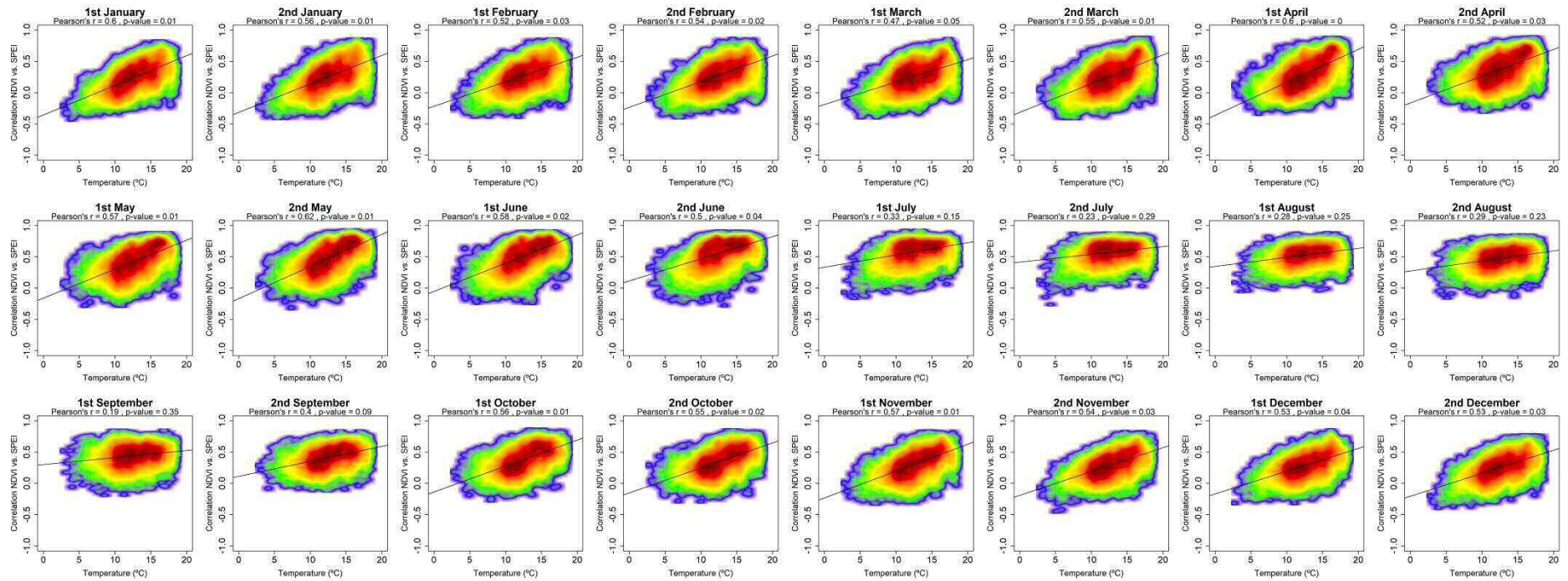
Supplementary Figure 19: Relationship between the average temperature and the maximum correlations obtained between NDVI and the SPEI during the 24 semi-monthly periods of the year. Mixed forests. Given the high number of points the signification of correlation was obtained by means of 1000 random samples of 30 cases from which correlations and p-values were obtained. The final signification was assessed by means of the average of the obtained p-values.



Supplementary Figure 20: Relationship between the average temperature and the maximum correlations obtained between NDVI and the SPEI during the 24 semi-monthly periods of the year. Natural grasslands. Given the high number of points the significance of correlation was obtained by means of 1000 random samples of 30 cases from which correlations and p-values were obtained. The final significance was assessed by means of the average of the obtained p-values.



Supplementary Figure 21: Relationship between the average temperature and the maximum correlations obtained between NDVI and the SPEI during the 24 semi-monthly periods of the year. Sclerophyllous vegetation. Given the high number of points the signification of correlation was obtained by means of 1000 random samples of 30 cases from which correlations and p-values were obtained. The final signification was assessed by means of the average of the obtained p-values.



Supplementary Figure 22: Relationship between the average temperature and the maximum correlations obtained between NDVI and the SPEI during the 24 semi-monthly periods of the year. Transition wood-scrub. Given the high number of points the signification of correlation was obtained by means of 1000 random samples of 30 cases from which correlations and p-values were obtained. The final signification was assessed by means of the average of the obtained p-values.

The impact of drought on the productivity of two rainfed crops in Spain



The impact of drought on the productivity of two rainfed crops in Spain

Marina Peña-Gallardo^{1,*}, Sergio Martín Vicente-Serrano¹, Fernando Domínguez-Castro¹, and Santiago Beguería²

¹Instituto Pirenaico de Ecología, Consejo Superior de Investigaciones Científicas (IPE-CSIC), Zaragoza, Spain

²Estación Experimental de Aula Dei, Consejo Superior de Investigaciones Científicas (EEAD-CSIC), Zaragoza, Spain

* *Invited contribution by Marina Peña-Gallardo, recipient of the EGU Natural Hazards Outstanding Student Poster and PICO Award 2018.*

Correspondence: Marina Peña-Gallardo (marinapgallardo@ipe.csic.es)

Received: 1 January 2019 – Discussion started: 9 January 2019

Accepted: 9 May 2019 – Published: 19 June 2019

Abstract. Drought events are of great importance in most Mediterranean climate regions because of the diverse and costly impacts they have in various economic sectors and on the environment. The effects of this natural hazard on rainfed crops are particularly evident. In this study the impacts of drought on two representative rainfed crops in Spain (wheat and barley) were assessed. As the agriculture sector is vulnerable to climate, it is especially important to identify the most appropriate tools for monitoring the impact of the weather on crops, and particularly the impact of drought. Drought indices are the most effective tool for that purpose. Various drought indices have been used to assess the influence of drought on crop yields in Spain, including the Standardized Precipitation Evapotranspiration Index (SPEI), the Standardized Precipitation Index (SPI), the Palmer drought indices (Palmer Drought Severity Index, PDSI; Palmer Z Index, Z Index; Palmer Hydrological Drought Index, PHDI; Palmer Modified Drought Index, PMDI), and the Standardized Palmer Drought Index (SPDI). Two sets of crop yield data at different spatial scales and temporal periods were used in the analysis. The results showed that drought indices calculated at different timescales (SPI, SPEI) most closely correlated with crop yield. The results also suggested that different patterns of yield response to drought occurred depending on the region, period of the year, and the drought timescale. The differing responses across the country were related to season and the magnitude of various climate variables.

1 Introduction

The Mediterranean region is one of the major areas in Europe likely to be subject to the potential impacts of climate change. Many semiarid regions of southwestern Europe are expected to undergo a critical decline in water availability as a consequence of reduced precipitation and an increase in interannual and intra-annual rainfall variability (IPCC, 2014, EEA, 2017). It is also expected that future changes in the precipitation regime, along with a rise in temperature, will inevitably bring more extreme and severe weather events (Giorgi and Lionello, 2008; Webber et al., 2018; Wigley, 2009) that will impact ecosystems and economic sectors (Asseng et al., 2014; Tack et al., 2015). It has been suggested that precipitation and temperature changes in the western Mediterranean region will lead to more severe and longer drought events in coming decades (Alcamo et al., 2007; Dai, 2011; Forzieri et al., 2016; Giorgi and Lionello, 2008; Spinoni et al., 2018; Vicente-Serrano et al., 2014). This is significant because agriculture plays a key role in food supply; in 2017 it accounted for 2.59 % of GDP in Spain, 1.92 % in Italy, and 3.53 % in Greece (World Bank, 2017).

The agriculture sector is highly vulnerable to drought, as it depends directly on water availability (Hanjra and Qureshi, 2010; Meng et al., 2016; Tsakiris and Tigkas, 2007). Although each crop differs in its resilience to water stress (Liu et al., 2016; Lobell et al., 2011), droughts can cause crop failure if the weather conditions are adverse during the most sensitive stage of crop growth (Lobell and Field, 2007). The adverse impacts of drought have been highlighted in recent severe events, including in 2003 when the agricultural

and forestry losses from drought in France, Italy, Germany, Spain, Portugal, and Austria were approximately EUR 13 billion (Fink et al., 2004; García-Herrera et al., 2010). The most recent drought, which mostly affected north–central Europe, caused European farmers to claim agricultural aid because of the low production that resulted (European Commission, 2018).

For these reasons the vulnerability of agricultural production to extreme events and the quantification of drought impacts on crop yields have become a focus of interest. In recent years diverse studies in the Mediterranean region have assessed these issues from multiple perspectives. For example, Capa-Morocho et al. (2016) investigated the link between seasonal climate forecasts and crop models in Spain, Loukas and Vasiliades (2004) used a probabilistic approach to evaluate the spatiotemporal characteristics of drought in an agricultural plain region in Greece, and Moore and Lobell (2014) estimated the impacts of climate projections on various crop types across Europe.

Droughts are difficult to measure and quantify (Vicente-Serrano et al., 2016), and consequently a wide range of drought indices have been developed to provide tools for quantifying the effects of drought across different sectors (Zargar et al., 2011). In this respect, drought indices are the most widely used method for monitoring drought impacts on agriculture; examples of their use available in the scientific literature include that in Europe (Hernandez-Barrera et al., 2016; Potopová et al., 2016a; Sepulcre-Canto et al., 2012; Vergni and Todisco, 2011), America (McEvoy et al., 2012; Quiring and Papakryiakou, 2003), and Asia (Ebrahimpour et al., 2015; Wang et al., 2016a). However, there is no general consensus on the most suitable indices for this purpose (Esfahanian et al., 2017). Despite the existing literature, very few studies (Peña-Gallardo et al., 2018a; Tian et al., 2018) have compared drought indices to identify their appropriateness for monitoring drought impacts on agriculture and for various crop types.

Among Mediterranean countries, agriculture in Spain is particularly sensitive to climate because of the low average precipitation level and its marked interannual variability (Vicente-Serrano, 2006). Spain has been subject to multiple episodes of drought (Domínguez-Castro et al., 2012), with those in the last century being amongst the most severe to have occurred in Europe (González-Hidalgo et al., 2018; Vicente-Serrano, 2006). In 2017 the agricultural and livestock losses caused by drought were estimated to be at least EUR 3600 million (UPA, 2017), highlighting the need to establish appropriate tools for monitoring drought impacts on crops. Recent studies such as that conducted by Ribeiro et al. (2019) in the Iberian Peninsula stressed the risk of this region of suffering from yield losses in the context of climate change. For that purpose, these authors analyzed the exposure of cereal rainfed crops to drought conditions using remote sensing information and performing a multi-scalar drought index.

Information on crop production is commonly limited in terms of spatial or temporal availability. Recent studies in Spain have analyzed the impact of climate on various crops since the early 21st century at national or provincial scales (Cantelaube et al., 2004; Hernandez-Barrera et al., 2016; Páscoa et al., 2016; Ribeiro et al., 2019), but few have used yield data at finer resolution (García-León et al., 2019). In this study we compared different drought indices using two datasets at different spatial scales: provincial information provided by the national statistical services and a regional dataset specifically developed for the study. The objectives of this study were (1) to determine the most appropriate and functional drought index among four Palmer-related drought indices (Palmer Drought Severity Index, PDSI; Palmer Hydrological Drought Index, PHDI; Palmer Z Index, Z Index; Palmer Modified Drought Index, PMDI) and the Standardized Precipitation Evapotranspiration Index (SPEI), the Standardized Precipitation Index (SPI), and the Standardized Palmer Drought Index (SPDI); (2) to identify the temporal response of two main herbaceous rainfed crops (wheat and barley) to drought; and (3) to determine whether there were common spatial patterns, by comparing the two datasets at different spatial scales.

2 Methods and datasets

2.1 Crop yield data

The statistical analysis was conducted using an annual dataset of crop yields for peninsular Spain and the Balearic Islands at two spatial scales for the two main herbaceous rainfed crops (barley and wheat). We obtained provincial annual yield data from the National Agricultural Statistics Annularies published by the Spanish Ministry of Agriculture, Fishing and Environment (MAPA), available at <https://www.mapa.gob.es/es/estadistica/temas/publicaciones/anuario-de-estadistica/default.aspx> (last access: March 2018); these include agricultural statistics since the early 20th century. We used data from 1962 to 2014 to match climate data that were available for this period. The Gipuzkoa and Vizcaya provinces were not used in the analysis at the province scale as wheat has not been cultivated there since 1973 and 1989, respectively. We used crop production data collected by the Encuesta sobre Superficies y Rendimientos de Cultivos (ESYRCE; Survey on surface and crop yields), an agrarian yield survey that has been undertaken by the MAPA since 1990. This survey records information about crop production at parcel scale every year from a sample of parcels. Yield observations were aggregated to the main spatial unit defined for agricultural districts by the MAPA (Fig. 1). As not all territories were included in this survey until 1993, we only considered the period 1993–2015. Data on barley production are limited in the ESYRCE database, and the agricultural districts considered

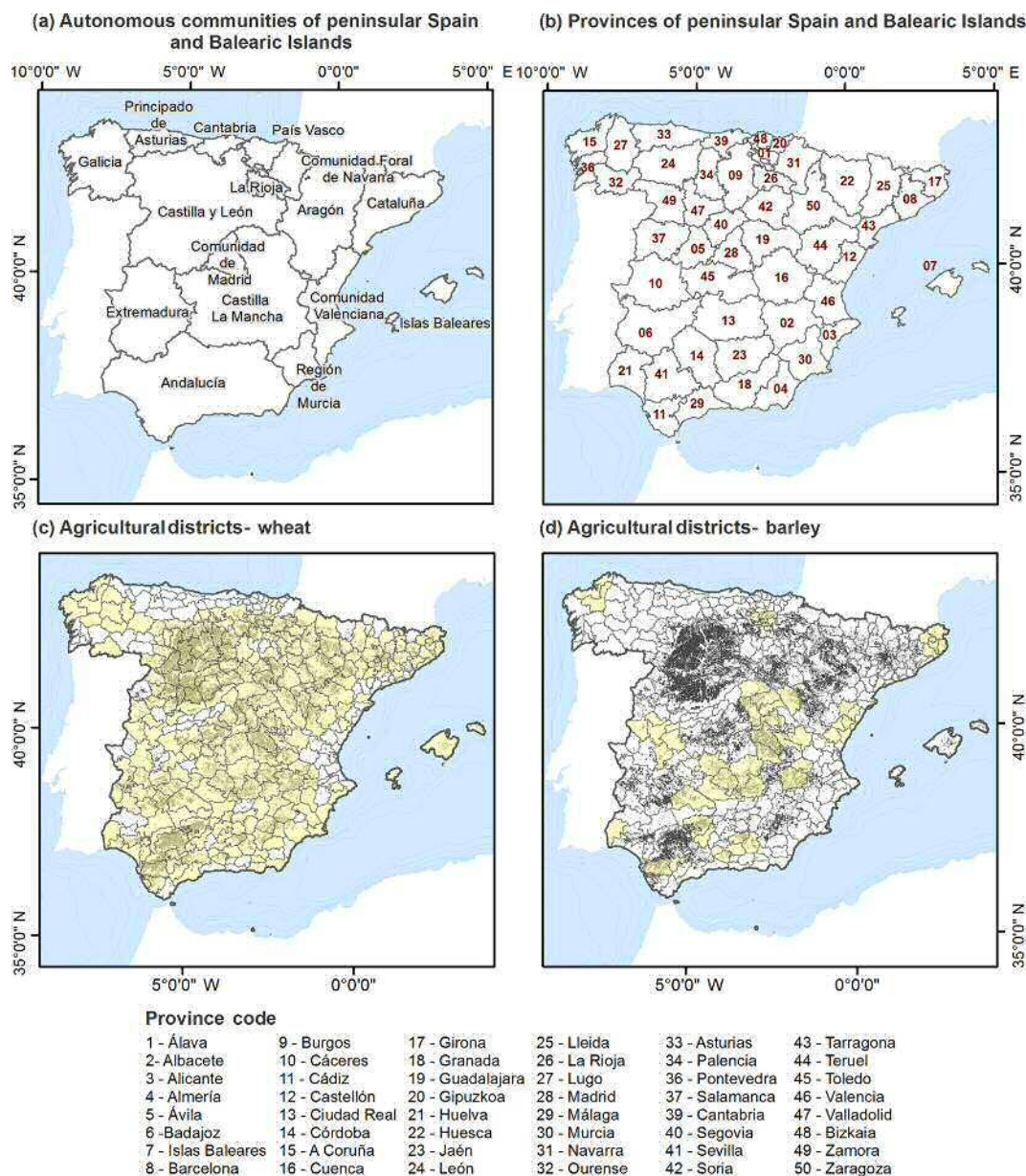


Figure 1. Location of Spanish autonomous communities (a) and provinces (b) and the distribution of agricultural districts with data available (yellow) for wheat (c) and barley (d) yields for the period 1993–2015. Areas where rainfed cereal crops are cultivated (Corine Land Cover 2006) are shown in grey.

in this study did not correspond to all the areas where this crop is cultivated.

For both datasets the unit of measure was the harvested production per unit of harvested area (kg ha^{-1}); it did not include any measure of production related to the area of the crop planted in each province or region. To consider the total area covered by the crops we used the defined rainfed crop delimited area for Spain, derived from the Corine Land Cover 2000 database (<http://centrodedescargas.cnig.es/CentroDescargas/catalogo.do?Serie=MPPIF>, last access: March 2018).

The spatial resolution of yield data can influence the interpretation of drought impacts on agriculture. Figure 2 shows a comparison of crop yields for the common period of available information in both datasets (1993–2014). Overall, the average production was greater at the agricultural district scale than at the provincial scale. Tables S1 and S2 (in the Supplement) summarize the relationships between the datasets for each province for the available common period, based on Pearson’s correlations coefficients for wheat and barley yields, respectively. It was surprising that both datasets showed very different temporal variability in crop

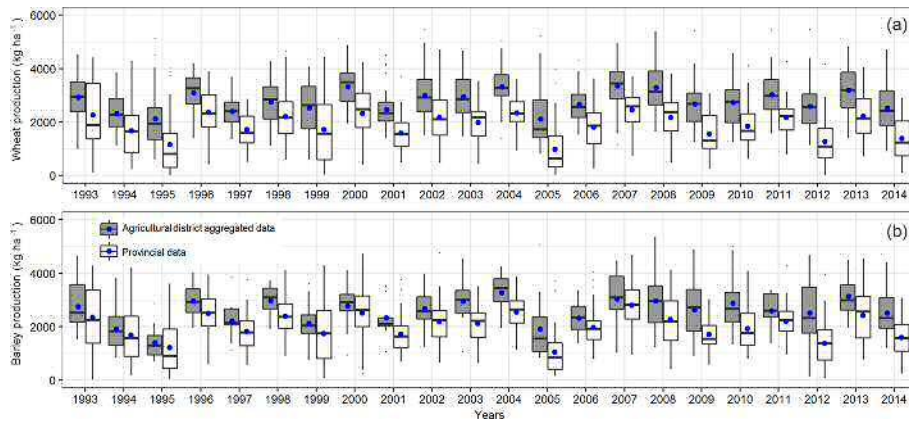


Figure 2. Temporal series of wheat (a) and barley (b) yields for the provincial data and the aggregated agricultural district data at the province scale for the common period 1993–2014. The solid black line shows the median, and the blue dot shows the mean.

yields in the analyzed provinces. Wheat yields showed good agreement and highly significant correlations between both datasets in provinces including Ávila ($r = 0.77$), Barcelona ($r = 0.69$), Burgos ($r = 0.82$), Cuenca ($r = 0.86$), Guadalajara ($r = 0.87$), León ($r = 0.69$), Palencia ($r = 0.73$), Salamanca ($r = 0.87$), Segovia ($r = 0.94$), Teruel ($r = 0.83$), Valladolid ($r = 0.92$), and Zamora ($r = 0.75$), while in other provinces including Castellón, Málaga, Murcia, and Navarra the correlations were nonsignificant or negative. Thus, the national statistics for these districts were unreliable. For barley yields the available regional data were more limited, but similar relationships with good agreement and more highly significant correlations were found among the datasets for the provinces where wheat was also cultivated, including Cáceres ($r = 0.48$), Cuenca ($r = 0.88$), Granada ($r = 0.51$), Guadalajara ($r = 0.86$), La Rioja ($r = 0.76$), and Tarragona ($r = 0.88$); however, for Sevilla the correlation was negative and significant ($r = -0.35$).

Mechanization and innovation in agriculture have increased in the last century, resulting in a trend of increased yields (Lobell and Field, 2007), which is also evident in data for Spain. To remove bias introduced by non-climate factors, and to enable comparison of yields between the two crop types, the original series were transformed to standardized yield residuals series (SYRS) using the following quadratic polynomial equation:

$$\text{SYRS} = \frac{y_d - \mu}{\sigma},$$

where y_d denotes the residuals of the de-trended yield obtained by fitting a linear regression model, μ is the mean of the de-trended series, and σ is the standard deviation of the de-trended yield.

This methodology has been applied in other similar studies (Chen et al., 2016; Tian et al., 2018). First announced as SYRS by Potopová et al. (2015), the full procedure of the following methodology is described by Lobell and Asner (2003)

and Lobell et al. (2011). In Fig. S1 (Supplement) an example of the positive trend (more evident in the provincial data due to the length of available data) and the temporal evolution of SYRS is illustrated for both type of crops and spatial scale.

2.2 Climate data

We used a weekly gridded dataset of meteorological variables (precipitation, maximum and minimum temperature, relative humidity, and sunshine duration) at 1.1 km resolution for peninsular Spain and the Balearic Islands for the period 1962–2015. The grids were generated from a daily meteorological dataset provided by the Spanish National Meteorological Agency (AEMET), following quality control and homogenization of the data. Further details on the method and the gridding procedure are provided by Vicente-Serrano et al. (2017). Reference evapotranspiration (ET_o) was calculated using the FAO-56 Penman–Monteith equation (Allen et al., 1998). Weekly data were aggregated at the monthly scale for calculation of the various drought indices.

2.3 Methods

2.3.1 Drought indices

Palmer drought indices

Palmer (1965) developed the Palmer Drought Severity Index (PDSI). Variations of this index include the Palmer Hydrological Drought Index (PHDI), the Palmer Moisture Anomaly Index (Z Index), and the Palmer Modified Drought Index (PMDI). Computation of the Palmer indices is mainly based on estimation of the ratio between the surface moisture and the atmospheric demand. Subsequent studies have revealed that spatial comparison among regions is problematic (Alley, 1984; Doesken and Garen, 1991; Heim, 2002). In this context we followed the variation introduced by Wells et al. (2004); this enables spatial comparison when deter-

mining a suitable regional coefficient, developing the self-calibrated Palmer indices. Palmer indices are also referred to as uni-scalar indices, which can only be calculated at fixed and unknown timescales (Guttman, 1998; Vicente-Serrano et al., 2010); this is a limitation of these indices.

Standardized Precipitation Index (SPI)

The Standardized Precipitation Index (SPI) was introduced by McKee et al. (1993) and provided a new approach to the quantification of drought at multiple timescales. The index is based on the conversion of precipitation series to a standard normal variable, with a mean equal to 0 and variance equal to 1, by adjusting an incomplete gamma distribution. The SPI is a meteorological index used worldwide and is especially recommended by the World Meteorological Organization (WMO, 2012) for drought monitoring and early warning.

Standardized Precipitation Evapotranspiration Index (SPEI)

Vicente-Serrano et al. (2010) proposed the Standardized Precipitation Evapotranspiration Index (SPEI) as a drought index that takes into consideration the effect of atmospheric evaporative demand on drought severity. It provides monthly climate balances (precipitation minus reference evapotranspiration), and the values are transformed to normal standardized units using a three-parameter log-logistic distribution. Following the concept of the SPI, the SPEI enables comparison of drought characteristics at various timescales among regions, independently of their climatic conditions. The SPEI has been widely used in drought-related studies, including to investigate the impacts of drought on various crops worldwide (Chen et al., 2016; Kuhnert et al., 2016; Peña-Gallardo et al., 2018b; Potopová et al., 2016b; Vicente-Serrano et al., 2012).

Standardized Precipitation Drought Index (SPDI)

The Standardized Precipitation Drought Index (SPDI) was developed by Ma et al. (2014) and relies on the concept of timescales. It is considered to be a combined version of the PDSI and the SPEI because the SPDI accumulates the internal water balance anomalies (D) obtained in the PDSI scheme at various timescales, and the values are later transformed into z units following a standard normal distribution. For this purpose a log-logistic distribution has been used because this has been shown to be effective at the global scale (Vicente-Serrano et al., 2015).

The SPEI, SPI, and SPDI are referred to here as multi-scalar indices and the Palmer drought indices as uni-scalar indices. Thus, the multi-scalar indices were computed at scales of 1, 12, 18, and 24 months and along with the Palmer drought indices series were de-trended by adjusting a linear regression model to enable accurate comparisons with de-

trended crop yield information. Following the same procedure used for the yield series, the residual of each monthly series was summed to the average value for the period.

2.3.2 Correlation between drought indices and crop yields

The relationship between the drought indices and the SYRS for both datasets was assessed by calculating polynomial correlation coefficients (c) (Baten and Frame, 1959). We used a second-order polynomial regression model, given the common nonlinear relationship between drought indices and crop production (Páscoa et al., 2016; Zipper et al., 2016). Hereafter, the references made to correlations refer to results obtained using the polynomial approach. The months of August and September were excluded from the analysis because they correspond to the post-harvest period, and we were considering only the period from sowing to harvest.

As the month of the year when the greatest correlation between the drought index and the crop yield was not known beforehand, all 10 monthly series for each index were correlated with the annual yield, and the highest correlation value was used. In the case of the multi-scalar indices, for each monthly series and timescale we obtained 10 correlations (one for each of the 10 months and the 14 timescales considered in the analysis). Thus, 140 correlations were obtained for each crop and spatial unit considered in the analysis (only correlations significant at $p < 0.05$ were considered). In addition, we used the timescale (in the case of multi-scalar drought indices) and the month in which the strongest correlation was found.

A t test was performed to assess the significance of the differences in the polynomial regression correlation coefficients obtained from the drought–yield relationships, to determine whether there were significant similarities or differences among the indices.

2.4 Identification of spatial patterns for crop yield response to drought

A principal component analysis (PCA) was performed to identify general patterns in the effect of drought on crop yields, in relation to seasonality of the effects. PCA is a mathematical technique that enables the dimensionality of a large range of variables to be reduced, by fitting linear combinations of variables. We conducted a T-mode analysis, and used the varimax method to rotate the components to obtain more spatially robust patterns (Richman, 1986). The monthly series of the monthly maximum correlation values found from the yield–drought relationship were the variables (one data point per month), and the provinces and agricultural districts were the cases. We selected two principal components (PCs) that in combination explained $> 60\%$ of the variance (individually the other components explained $< 5\%$ of the variance) and aggregated each province or agricultural district

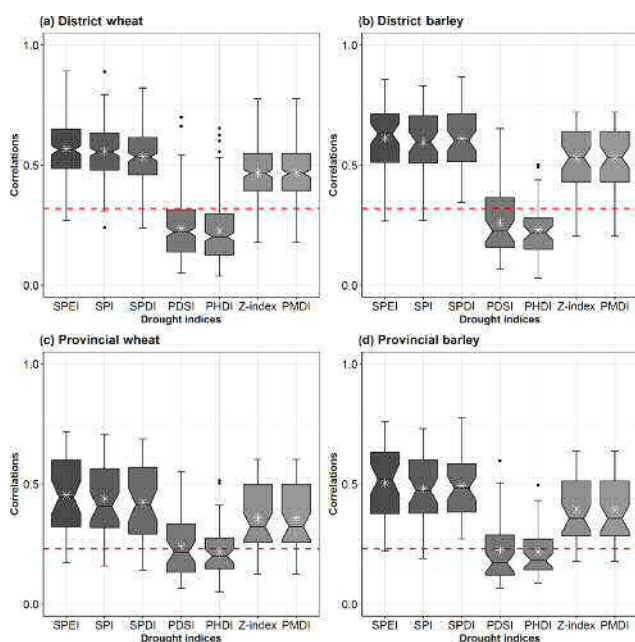


Figure 3. Box plots showing the strongest correlation coefficients found between drought indices and wheat and barley yields at the agricultural district (a and b) and provincial (c and d) scales, for all districts and provinces analyzed. The solid black line shows the median, the white asterisk shows the mean, and the dashed red lines show the $p < 0.05$ significance level.

according to the maximum loading rule (i.e., assigning each spatial unit to the PC for which the highest loading value was found). The loadings were expressed in the original correlation magnitudes using the matrix of component weights.

3 Results

3.1 Relationship of drought indices to crop yields

Figure 3 shows the strongest correlation found between the crop yield for each dataset and the monthly drought indices. The correlations differed substantially between the two groups of indices. Independently of the crop type, month of the year, or the drought timescale considered, the correlation coefficients for the multi-scalar indices were much higher than those for the uni-scalar indices. In both cases weaker correlations were found for the wheat crops compared with the barley crops. The PDSI, PHDI, and PMDI correlations were nonsignificant ($p < 0.05$), but the correlations for the Z Index and the multi-scalar indices were significant for most provinces and agricultural districts. The correlation values for the three multi-scalar drought indices were similar. At district scale the average values were $c = 0.57$ and $c = 0.6$ for wheat and barley, respectively, and $c = 0.41$ and $c = 0.48$ at the provincial scale. Thus, the datasets showed a stronger correlation for the drought indices at district scale than at the

provincial scale. In addition, more variability was found in the provincial data than in the regional data, associated with the length of the available records.

The spatial distribution of the maximum correlation coefficients between the drought indices and the crop yields is shown in Figs. 4 and 5, for the province and district scales, respectively. The wheat and barley yield–drought correlations showed a similar spatial pattern among indices at the province scale. Stronger correlations ($c \geq 0.7$) were found for the SPEI and SPI for the provinces of Castilla y León (Valladolid, Zamora, Segovia, and Soria), Aragón (Zaragoza and Teruel), Castilla La Mancha (Guadalajara, Albacete, and Toledo), and Valencia (particularly the cereal agricultural districts). The weakest correlations were found for the southern (Andalusian) provinces. For the Palmer drought indices, the PMDI and Z Index showed similar spatial patterns to the multi-scalar indices (especially in the central and northern provinces), but the correlations were weaker ($c = 0.25$ – 0.6). For most provinces the weakest correlations were found for the PDSI and PHDI ($c = 0.1$ – 0.25) for both crops, with no clear spatial difference in the correlations.

The spatial distribution of correlations between wheat yields and the drought indices at the agricultural district scale showed clearer patterns than those for the province level. Thus, the response of drought indices at district scale is similar to the response observed at provincial scale, showing stronger correlations for the multi-scalar indices and weaker correlations for the Palmer indices, especially the PDSI and PHDI. The distribution of correlations among the multi-scalar indices was very similar. The most correlated agricultural districts ($c \geq 0.8$) were in Castilla y León, especially Valladolid, Segovia, north of Ávila, and northeast of Salamanca. Similar correlations were found for areas of northeast Spain. There was a gradient in correlations from north to south, with the exception of some districts in northwestern Málaga, where wheat is extensively cultivated. In addition, in some districts of Galicia, where expansion of the planted wheat area has not been large, there was a strong relationship between drought indices and crop yields. The results for barley suggest a similar spatial relationship for the various drought indices. The highest coefficients were found for the multi-scalar indices, followed by the Z Index and the PMDI, with districts north of Cáceres, north of Galicia, and in Guadalajara showing correlations on the order of $c = 0.8$, while the correlations were weaker ($c = 0.25$ – 0.4) in districts in the south of Córdoba and Jaén.

3.2 Relationship of drought indices to crop yields: temporal responses

Table 1 summarizes the timescales at which the strongest correlations were found for each of the three multi-scalar indices. Strongest correlations were found for short timescales (1–3 months) for both datasets and both crops, in general with little difference between the indices. For wheat,

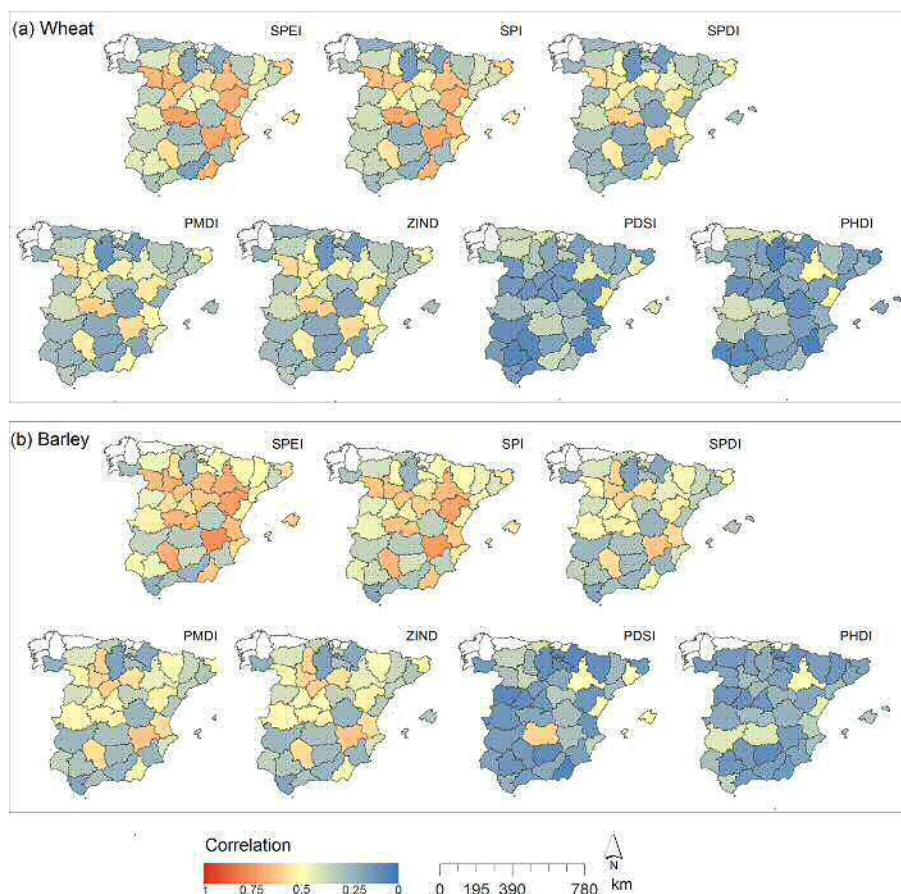


Figure 4. Spatial distribution of the highest correlation coefficients between the drought indices and the wheat (a) and barley (b) yields at the provincial scale, independently of the timescale.

for 52.6% of the agricultural districts the yield was most strongly correlated with all three drought indices at a timescale of 1–3 months; this was also the case for 49.6% of provinces. In agricultural districts where wheat is cultivated the strongest correlations were predominantly at the 1-month scale (20.37%), especially for the SPDI, while for most of the provinces this occurred at the 3-month scale, particularly for the SPEI and SPI (23.26%). For barley, 57.4% of the districts and 58.7% of provinces where this crop was grown, the strongest correlations were predominantly at 1- to 3-month timescales. Among the various indices for districts, the SPI showed the strongest correlation at the 1-month scale, while for provinces the SPEI showed the strongest correlation at the 3-month scale (33.33%).

The multi-scalar drought indices showed similar results. Among these, the SPEI was the index most strongly correlated with yield in the highest percentage of provinces and districts (Table 2). For wheat crops the SPEI was the most strongly correlated index with yield in ~37% of the agricultural districts and ~58% of the provinces; these correlations were found predominantly at the 3-month timescale. For this crop the SPDI was most strongly correlated with

yield in a similar proportion of districts (~33%), primarily at the 1-month scale, but only ~14% at the province scale. In general, most of the maximum correlations corresponded to short timescales.

Figure 6 shows the spatial distribution of the most strongly correlated drought indices. For most of the provinces the SPEI was the index most strongly correlated with crop yield. For the agricultural districts there was substantial spatial variability and, along with the provincial results, no well-defined spatial pattern that distinguished specific areas for which one index was most effective at monitoring drought. For barley the SPDI showed the best correlation with yield among districts (~44%), while in provinces the SPEI was best correlated (~69%). No clear spatial patterns were evident. The similarities in the magnitude of the correlations between multi-scalar drought indices and crop yields were statistically significant. A *t* test (Fig. S2) was used to determine whether there were significant differences in the magnitude of correlations obtained using the various multi-scalar drought indices. This showed significant differences between the SPEI and the SPDI in ~30% of agricultural districts where wheat was grown; these were districts that showed

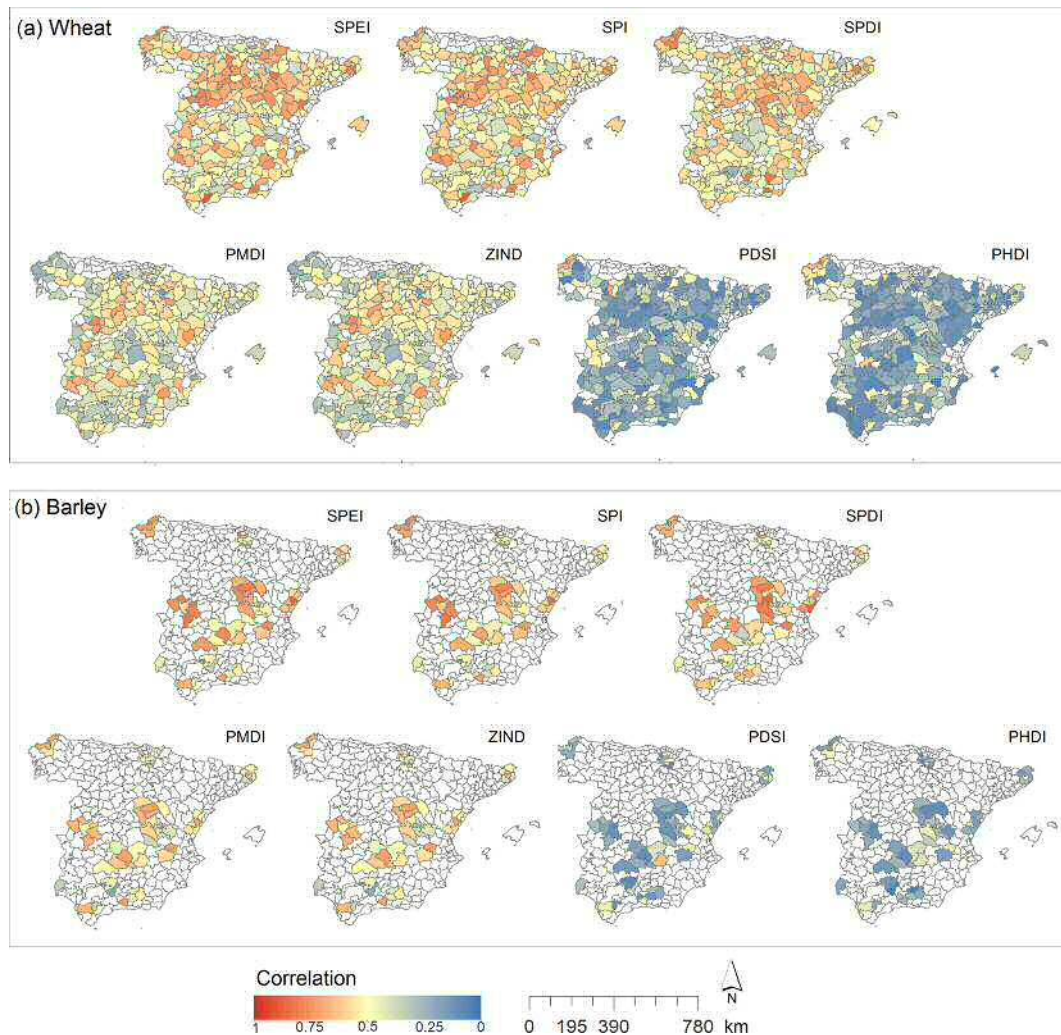


Figure 5. Spatial distribution of the highest correlation coefficients between the drought indices and the wheat (a) and barley (b) yields at the agricultural district scale, independently of the timescale.

a weaker correlation of yield with drought indices. The results suggest that, for districts with strong correlations between drought indices and crop yields, the two indexes were equally useful. A lower proportion of districts where barley is planted showed that statistical differences among indices exist. In contrast, for provinces no significant differences were found. Overall, this suggests the appropriateness of using any of these multi-scalar indices indistinctly.

3.3 Spatial patterns of drought index correlations at the monthly scale

Regionalization of the crop yield response to drought based on monthly correlations with the drought indices was undertaken in relation to the most correlated drought index in each region, independently of the month in which this maximum correlation occurred. Thus, in this analysis the results obtained using the various multi-scalar drought indices were

merged. General spatial patterns in the effect of drought conditions on yield were identified using a T-mode PCA. Figures 7 and 8 show the results for the provincial and regional datasets, respectively. We selected two components that explained more than the 60% of the variance in each case. This classification reinforced the north–south pattern of correlations previously found for both datasets. Figure 9 shows the timescales for which the maximum monthly correlations were found for the provinces and agricultural districts for each of the defined components, using a maximum loading rule.

3.3.1 Wheat

Agricultural district scale

At the district scale the PCA for wheat (Fig. 7a) showed more defined spatial patterns than the PCA did at the provincial

Table 1. Percentage of analyzed agricultural districts (a) and provinces (b) where wheat and barley are cultivated, for which the maximum correlations per timescale were found using the multi-scalar indices.

Timescale		1	2	3	4	5	6	7	8	9	10	11	12	18	24
(a) Agricultural district data															
Wheat	SPI	18.38	15.38	13.68	9.83	4.27	7.26	2.56	5.13	1.28	3.42	6.41	2.14	5.98	4.27
	SPEI	16.67	14.96	17.09	9.83	6.41	3.42	5.13	4.7	3.42	2.56	3.85	4.27	5.13	2.56
	SPDI	26.07	21.79	13.68	5.13	3.42	2.99	2.56	2.56	2.14	5.13	1.71	3.85	3.42	5.56
Averaged %		20.37	17.38	14.82	8.26	4.70	4.56	3.42	4.13	2.28	3.70	3.99	3.42	4.84	4.13
Barley	SPI	29.63	14.81	14.81	12.96	0	3.7	3.7	1.85	3.7	1.85	1.85	3.7	3.7	3.7
	SPEI	24.07	12.96	22.22	9.26	1.85	3.7	5.56	3.7	3.7	1.85	0	5.56	1.85	
	SPDI	24.07	14.81	14.81	7.41	7.41	3.7	11.11	1.85	0	3.7	0	0	3.7	7.41
Averaged %		25.92	14.19	17.28	9.88	3.09	3.70	6.79	2.47	2.47	2.47	0.62	3.09	3.08	4.94
(b) Provincial data															
Wheat	SPI	6.98	13.95	23.26	6.98	2.33	6.98	6.98	6.98	6.98	2.33	4.65	4.65	4.65	2.33
	SPEI	9.3	11.63	23.26	11.63	9.3	0	6.98	6.98	2.33	2.33	4.65	4.65	4.65	2.33
	SPDI	13.95	32.56	13.95	2.33	2.33	4.65	4.65	6.98	0	2.33	6.98	2.33	0	6.98
Averaged %		10.08	19.38	20.16	6.98	4.65	3.88	6.20	6.98	3.10	2.33	5.43	3.88	3.10	3.88
Barley	SPI	7.14	19.05	30.95	9.52	4.76	7.14	0	2.38	2.38	0	0	11.9	0	4.76
	SPEI	11.9	11.9	33.33	7.14	4.76	4.76	7.14	4.76	7.14	0	0	2.38	2.38	2.38
	SPDI	9.52	38.1	14.29	4.76	4.76	7.14	0	0	7.14	0	2.38	4.76	2.38	4.76
Averaged %		9.52	23.02	26.19	7.14	4.76	6.35	2.38	2.38	5.55	0.00	0.79	6.35	1.59	3.97

Table 2. Percentage of analyzed agricultural districts and provinces where wheat and barley are cultivated, for which the maximum correlations with the multi-scalar indices were found. Information in parentheses shows the timescale at which the provinces and agricultural districts correlate most and the percentage of the provinces and district.

		SPEI	SPDI	SPI
Agricultural districts	Wheat	36.75 (3, 7.26)	33.33 (1, 7.69)	29.91 (2, 4.70)
	Barley	35.19 (3, 11.11)	44.44 (1, 12.96)	20.37 (1, 11.11)
Provinces	Wheat	58.14 (3, 18.60)	13.95 (24, 4.65)	27.9 (3, 4.65)
	Barley	69.04 (3, 16.66)	9.52 (1, 7.14)	21.42 (5, 24, 4.76)

scale. The first component (PC1) explained 43.36 % of the variance and was characterized by stronger correlations ($c = 0.7-0.9$) in districts mainly located on the north and central plateau; these were stronger than those recorded for the same locations at the provincial scale. Weaker correlations ($c = 0.15-0.5$) were dispersed, although these were found predominantly in the south and northwest. The scores for PC1 showed particular sensitivity to drought during spring, although strong correlations were also found during autumn. The second component (PC2) explained 18.63 % of the variance, and the loading coefficients also showed a clear spatial pattern, with the agricultural districts north of Sevilla and east of Castilla La Mancha having the highest values. The weakest correlations were found for the districts of Andalucía, Extremadura, and Aragón. Lower scores in PC2 characterized the interannual response to drought relative to

PC1. These districts in PC2 also showed a stronger response during spring but not autumn, as was found for PC1. The distribution of PCs according to the maximum loading rule enabled identification of a north-south component in the sensitivity of wheat yields to the drought index. The timescales at which wheat yields in agricultural districts responded most during spring varied from shorter timescales (3 months) in districts in PC1 to longer timescales (5 to 6 months) for those in PC2 (Fig. 9e, f), which also showed greater variability in most months relative to districts from PC1. Greater variability for wheat at the district scale was observed relative to that at the provincial scale. Due to the major number of observations considered, the response to drought in Spain when considering district scale shows more heterogeneity than at provincial scale.

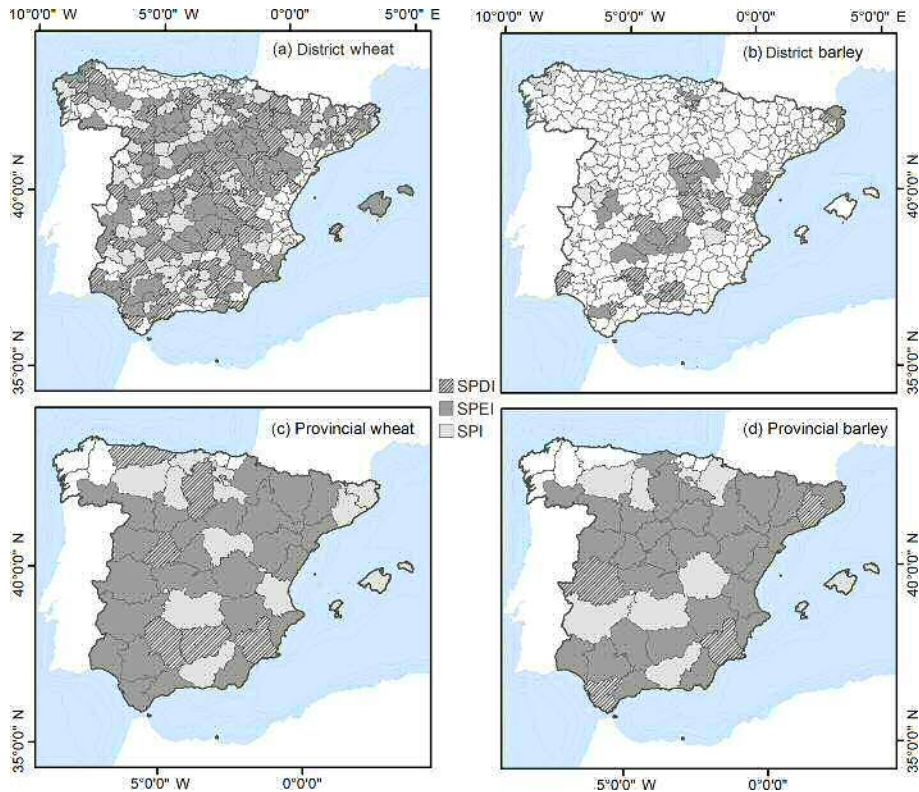


Figure 6. Spatial distribution of the drought indices with the strongest correlations with wheat (**a, c**) and barley (**b, d**) at the province (**c, d**) and agricultural district (**a, b**) scales.

Provincial scale

The results for wheat at the provincial scale (Fig. 7b) showed that the first (PC1) and second (PC2) components explained 51.7 % and 20.8 % of the variance, respectively. The loadings of the first component were higher for the central plateau and the east of Spain. These represent provinces in the Castilla y León and Castilla y La Mancha districts and the provinces of Castellón, Valencia, Alicante, Cantabria, and Huelva, and Sevilla and Almería in Andalucía. In these provinces there was a strong correlation between drought indices and crop yields, especially during spring, with particularly strong correlations in May. In contrast, during winter the correlations were weaker, especially in February. PC2 showed greater spatial heterogeneity, with strong correlations in the east (Zaragoza and Tarragona provinces) and south (Cádiz, Córdoba, Málaga, Granada, and Jaén provinces) of Spain. For this component the temporal response to drought was not as strong as that for PC1, but the maximum correlation was also found during May. The distribution of the maximum loadings showed a dispersed pattern, with PC1 grouping provinces in the central plateau and east of Spain and PC2 grouping those in southern and some northeastern provinces. The averaged temporal response to drought during spring is set at medium timescales (4–7 months). In particular, in May most of the

provinces correlated at 5 months (Fig. 9a, b), indicating the importance of climatic conditions during winter and spring to the crop yields obtained. This was also evident for the longer timescales at which most of the provinces correlated during the winter months (11–18 months). It is noteworthy that there was great variability in the temporal response of provinces in PC1 in October, February, March, and April.

3.3.2 Barley

Agricultural district scale

For barley crops (Fig. 8a) both components showed strong correlations ($c = 0.6–0.9$) in most of the agricultural districts. In general, the districts showing the strongest correlations in PC1 and PC2 were those located in Castilla La Mancha and north of Cáceres and Córdoba. Scores for PC1 for barley crops were similar to those for PC1 for wheat during spring and autumn, but the results for PC2 suggest that there was little interannual sensitivity to drought. Most of the correlations for spring indicate that barley responded to drought conditions at the 3–4-month scale, mainly in those districts associated with PC1. Barley yields in districts associated with PC2 were more affected by drought conditions in May at 7–9-month timescales (Fig. 9g, h).

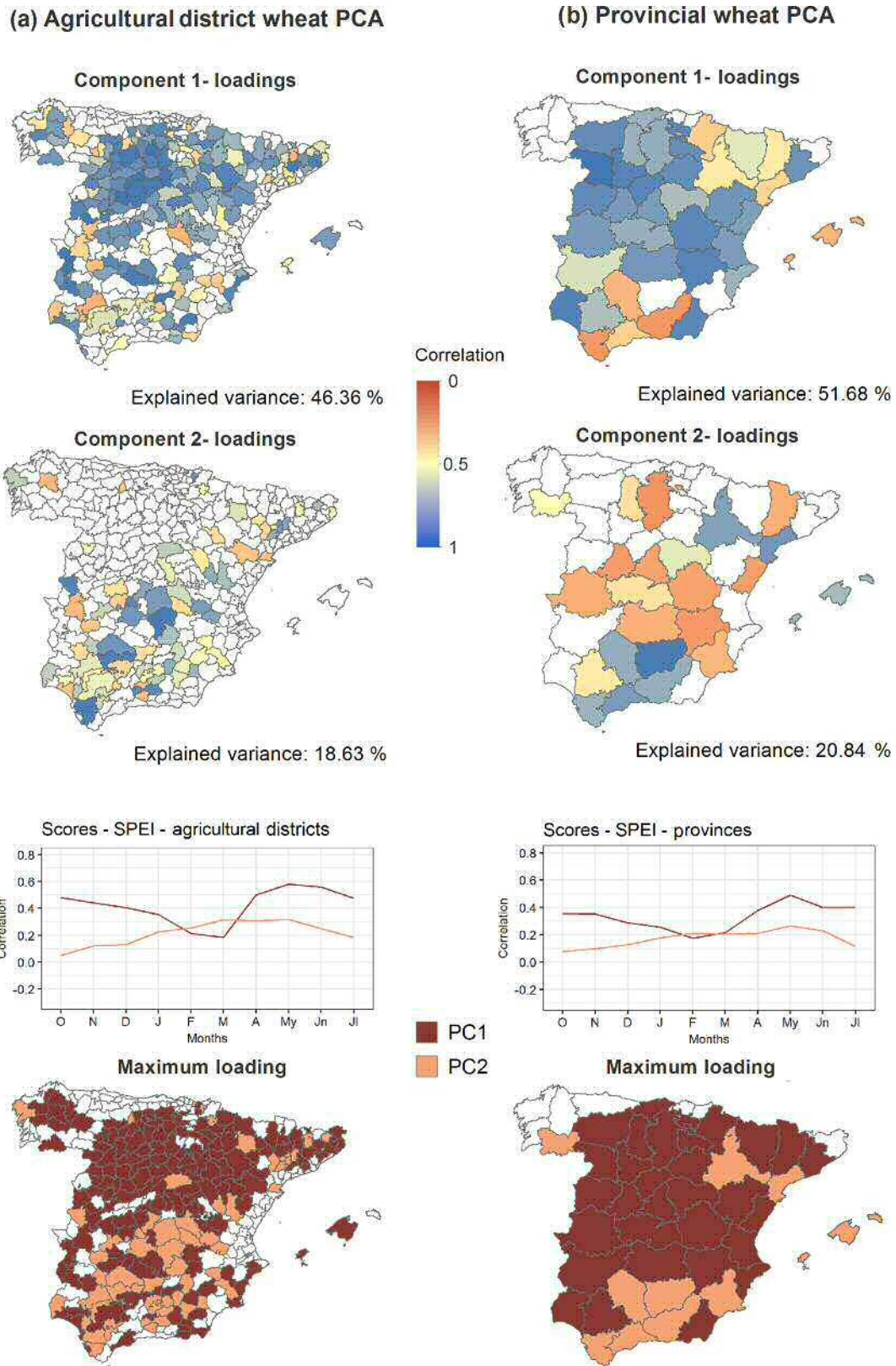


Figure 7. PC loadings, PC scores, timescales, and maximum loading rules from the PCA for monthly maximum correlation coefficients between the SPEI and wheat yields at the agricultural district (a) and provincial (b) scales, independently of the timescale. The PC loadings and maximum loadings were significant at $p < 0.05$.

(a) Agricultural district barley PCA

(b) Provincial barley PCA

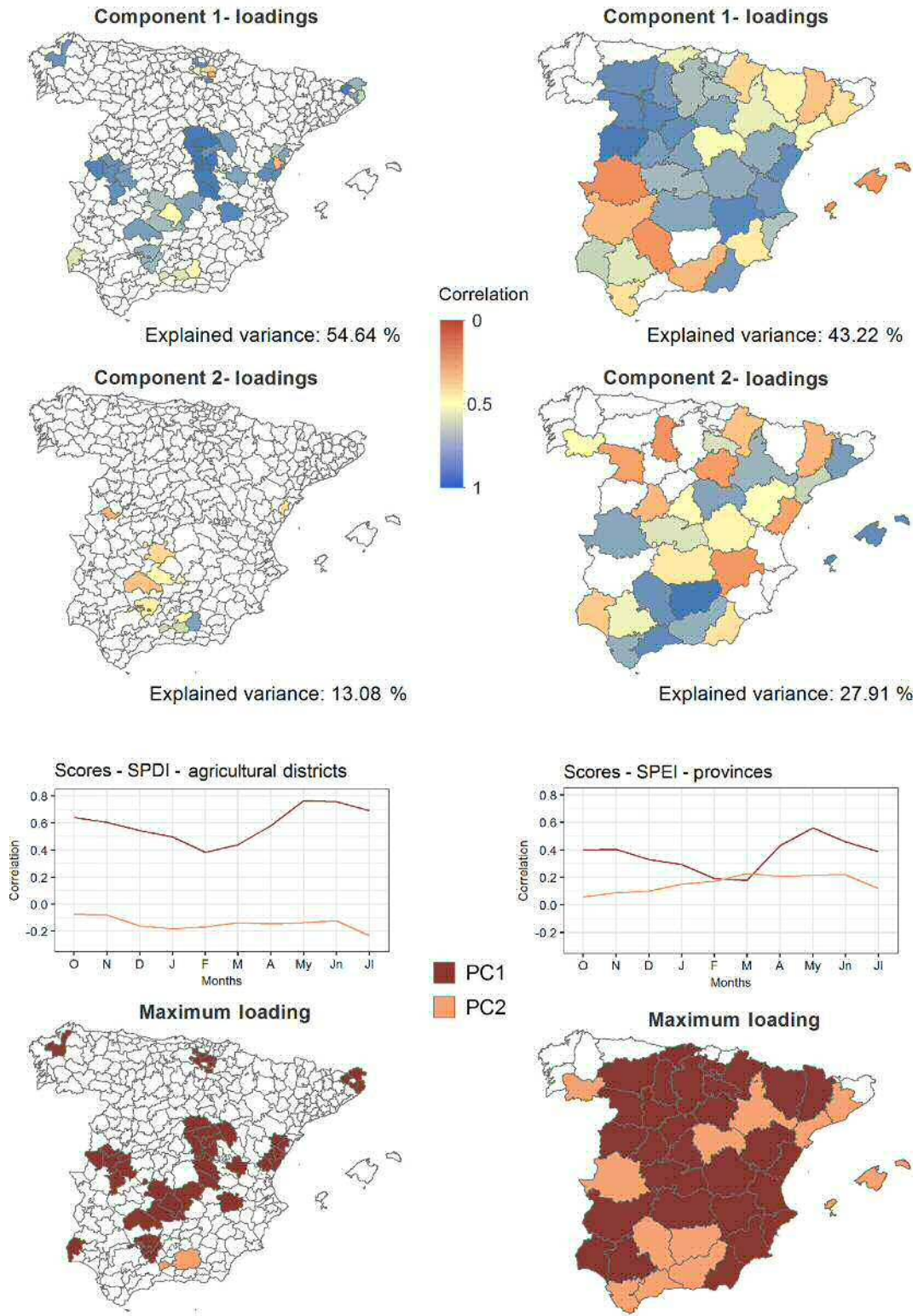


Figure 8. PC loadings, PC scores, timescales, and maximum loading rules from the PCA for monthly maximum correlation coefficients between the SPEI and barley yields at the agricultural district scale (a) and the SPDI and barley yields at the provincial scale (b), independently of the timescale. The PC loadings and maximum loadings were significant at $p < 0.05$.

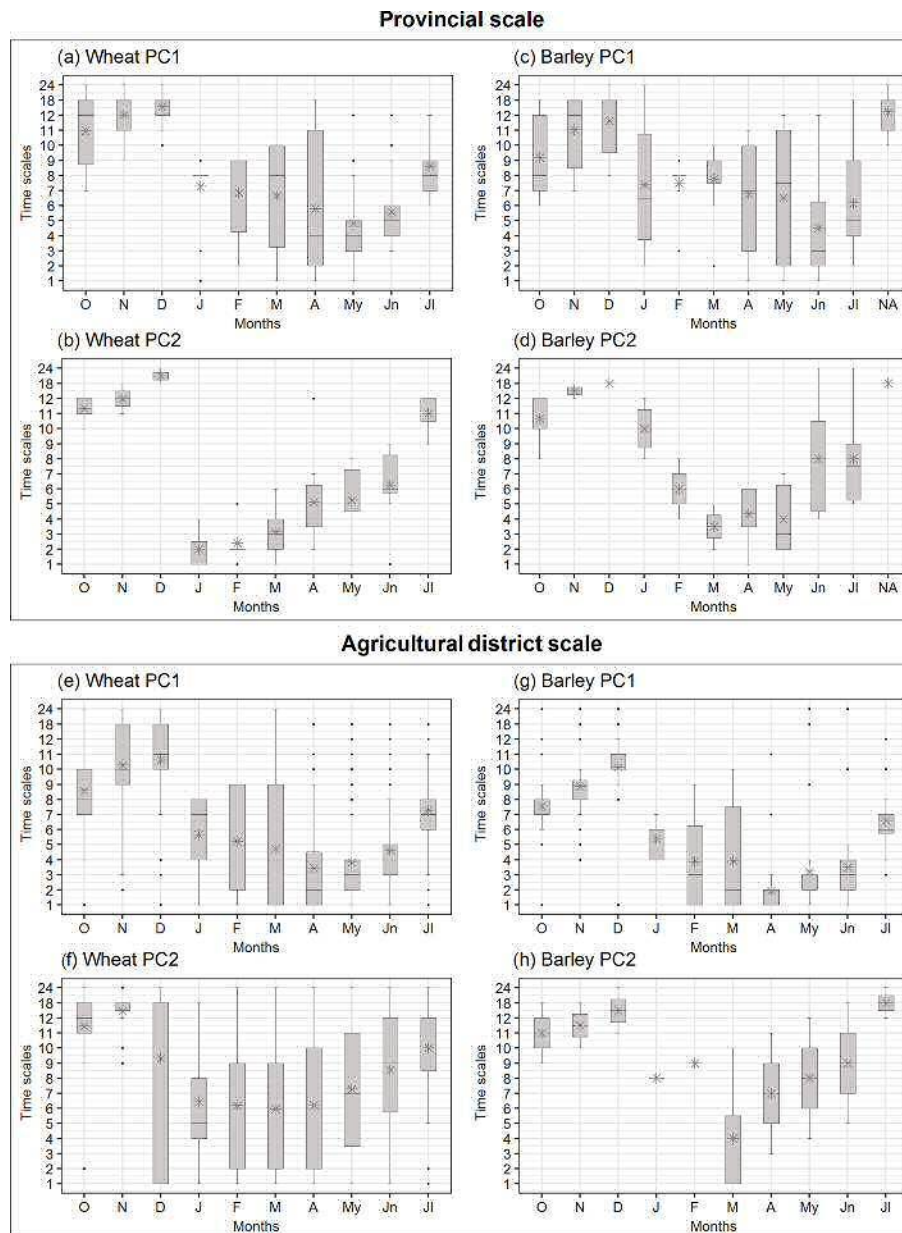


Figure 9. Box plots showing the timescale at which significant monthly correlations were found in the provinces (a–d) and agricultural districts (e–h) for wheat and barley for each of the components defined in the PCA.

Provincial scale

For barley at the provincial scale (Fig. 8b) we found more variability in the magnitude of correlations. For PC1 (explaining 43.22% of the variance) strong correlations ($r = 0.7–0.9$) were found for the north and central provinces of Castilla y León, the central provinces of Castilla y la Mancha, and Madrid, Teruel, Valencia, and Castellón. The provinces associated with PC2 (explaining 27.91% of the variance) were more dispersed than those in PC1, and those showing strong correlations included Zaragoza and Guadalajara

in the north, Barcelona and Balearic Islands in the north-east and east, Cáceres in the west, and Cádiz, Córdoba, Málaga, Granada, and Jaén in the south. Provinces showing weaker correlations in PC1 were spread in the north-east (e.g., Navarra, Zaragoza, and Lleida) and west of Spain (e.g., Cáceres and Badajoz). Component scores for PC1 were higher than for PC2, although for wheat crops both showed maximum scores during spring (March) and minimum scores in autumn and winter. More provinces in May were correlated with drought indices at medium drought timescales (4–8 months). During spring, provinces in PC1 showed corre-

lations at longer timescales (7–8 months), while provinces in PC2 showed responses at shorter timescales (3–4 months) (Fig. 9c, d).

3.3.3 General climatological characteristics for the PCA components

Figures S3–S12 show the distribution of climatic characteristics including precipitation, atmospheric evaporative demand (AED), maximum and minimum temperature, and the hydroclimatic balance (precipitation minus AED) at the district scale for the two PCA components. For those districts where wheat was cultivated, no major differences in AED values were found among the components. However, minor differences were observed in precipitation among districts belonging to different PCA components. Those in PC2 had on average less precipitation than those in PC1, especially during autumn, but the difference was not substantial. Greater differences were observed for temperature, with PC1 mainly characterized by districts that had higher maximum temperatures in autumn and spring, and with higher minimum temperatures than the districts in PC2. These results highlight the important role of temperature in the different responses of crop yield to drought and demonstrate that, contrary to what may have been expected, temperature and not precipitation was the main factor constraining crop growth. Thus, changes in extreme temperature levels may influence future crop yields. Districts in PC2 where the barley yield correlated with drought indices were characterized by lower levels of precipitation and higher maximum and minimum temperatures than districts represented by PC1 and by higher AED, especially from April to July. Extremes of temperature also seemed to be the major factor determining barley crop yield.

4 Discussion

In this study we investigated the impacts of drought on two rainfed crops in Spain, as measured by a variety of drought indices. We used two datasets of annual crop yields, one from agricultural statistics at the provincial scale spanning the period 1962–2013 and the other a new database at the agricultural district scale from the available parcel data from the national survey covering the period 1993–2015. To identify the best indicator of the impact of drought on yields and their sensitivity to climate, we evaluated the performance of seven drought indices. The selection of drought indices was based on those commonly used to monitoring droughts worldwide, including the Standardized Precipitation Evapotranspiration Index (SPEI), the Standardized Precipitation Index (SPI), the Palmer drought indices (PDSI, Z Index, PHDI, and PMDI), and the Standardized Palmer Drought Index (SPDI).

Independently of the type of crop and the temporal scale considered, our results showed that drought indices calculated at different timescales (the SPEI, the SPI, and the SPDI)

had greater capacity to reflect the impacts of climate on crop yields, relative to uni-scalar drought indices. The better performance of these multi-scalar drought indices was mainly because of their flexibility in reflecting the negative impacts of drought over a range of regions with very different characteristics (Vicente-Serrano et al., 2011). This issue is especially relevant in agriculture, as vegetation components do not respond equally to water deficit. The sensitivity and vulnerability of each type of crop to drought and the characteristics of the specific region influence the variability evident in the response to droughts (Contreras and Hunink, 2015). Nonetheless, the results of the assessment of the performance of the Palmer drought indices demonstrated that correlations varied markedly among them, showing some exceptions that may affect their usefulness for monitoring purposes. Overall, our results showed that the PHDI had the weakest relationship to crop yields, followed by the PDSI and the PMDI. The better performance of the PDSI over the PHDI was expected, as the latter was primarily developed for hydrological purposes. Likewise, our results confirmed a better performance of the PMDI (a modified version of the PDSI) over the original PDSI for both crops. Our results are consistent with those of previous studies assessing agricultural drought impacts on crop yields at the global (Vicente-Serrano et al., 2012) and regional (Peña-Gallardo et al., 2018b) scales. The Z Index was the best uni-scalar index among the set analyzed in our study. This index measures short-term moisture conditions, which is a major factor in crop stress (Quiring and Papakryiakou, 2003). Thus, the Z Index was more closely correlated with crop yield than any of the other Palmer indices, indicating its usefulness relative to other Palmer drought indices (Karl, 1986).

Although our findings point to poorer performance of the Palmer drought indices relative to the multi-scalar drought indices, they remain among the most widely accepted indices. Numerous studies have used the Palmer indices in assessments of the use of drought indices for monitoring agricultural drought in various regions worldwide and have reported the superiority of the Z Index (Mavromatis, 2007; Quiring and Papakryiakou, 2003; Sun et al., 2012; Tunalıoğlu and Durdu, 2012; our results confirm its usefulness among the Palmer drought indices).

Nevertheless, it is important to stress that the usefulness of Palmer drought indices is less than drought indices that can be computed at different timescales (Vicente-Serrano et al., 2012). We demonstrated that the three multi-scalar drought indices in our study (SPEI, SPI, and SPDI) were able to detect drought at different timescales, enabling past weather conditions to be related to present conditions in regions characterized by diverse climatic conditions. This is consistent with previous comparative studies in various regions that reported multi-scalar drought indices were effective for monitoring drought impacts on agricultural lands (Blanc, 2012; Kim et al., 2012; Potopová, 2011; Potopová et al., 2016a; Tian et al., 2018; Zhu et al., 2016; Zipper et al., 2016). Al-

though previous studies reported differences among some of the above three indices (e.g., the SPDI and the SPEI; Ghabaei Sough et al., 2018), others have reported similarities in their performance in assessing agricultural drought impacts (Labudová et al., 2016; Peña-Gallardo et al., 2018a). The similar magnitudes of their correlations suggest a similar ability to characterize the impact of drought on crop yields. However, minor differences among these indices suggested the SPEI performed best. First, for both crops slightly stronger correlations were observed with the SPEI, although the SPDI was superior in relation to barley yields at the agricultural district scale. In general, the SPEI was found to be the most suitable drought index in the majority of agricultural districts and provinces, in accordance to Ribeiro et al. (2018) who also found it suitable in Spain for relating drought conditions and yields variability. This suggests that inclusion of AED in the drought index calculation, as occurs in the SPEI, provides greater capacity to predict drought impacts on crop yields compared with the use of precipitation only. Variation in the maximum and minimum temperatures has been found to be the major factor differentiating agricultural districts and provinces with greater sensitivity to drought. Previous studies have stressed the risks associated with an increase in global temperatures, particularly maximum temperatures, and the possible effects on crop yields (Lobell and Field, 2007; Moore and Lobell, 2014). Thus, a $\sim 5.4\%$ reduction in grain yields resulting from an increase in average temperature is expected to occur under the current global warming scenario (Asseng et al., 2014; Zhao et al., 2017).

The temporal and spatial effects of drought on yields seem to be very complex, given the observed variability in Spain. In this respect, significant yield effects of drought were found in both datasets. Nevertheless, at the agricultural district scale there was a more evident spatial effect of drought on agricultural yields. This is a key finding for spatial-scale analyses, although the lack of long time series datasets on regional yields is a common constraint.

Drought effects on barley and wheat were similar in space and time, although their sensitivity to drought differed, as shown by differences in the magnitude of the correlations with the drought indices, with wheat yields showing stronger correlations than barley yields. This can be explained by the different physiological characteristics of the two crops, as barley is less dependent on water availability at germination and the grain filling stage than wheat (Mamnouie et al., 2006). Although the transpiration coefficient for barley is higher, this crop is not as subject as wheat to water stress under drought conditions (Fischer et al., 1998). Our results indicate that the temporal responses of barley and wheat to drought conditions were very similar, despite the fact that in Spain barley is typically cultivated later than wheat and in soils with poor moisture retention. Therefore, the phenological characteristics of each type of crop determine how drought affects yields. The results showed that temperature had a more important role than precipitation, suggesting that

extreme variations in average temperature conditions during the most sensitive growth stages may have a negative impact on crops.

Overall, crop yields in Spain tend to respond to short drought timescales (1–3 months). However, the sensitivity of crops to drought is greater during spring at medium (4–6 months) timescales. These results are in line with previous studies conducted in the Iberian Peninsula with a similar database at provincial scale that also point to shorter timescales, mostly during spring months (1–6 months) (Ribeiro et al., 2018). This highlights that moisture conditions during winter (the period corresponding to planting and the first growth stages of tillering and stem elongation) are crucial for the successful development of the plants (Çakir, 2004; Moorhead et al., 2015; Wang et al., 2016a, b).

We found a stronger response of crops to climatic conditions in provinces and agricultural districts in the central plateau and an unexpectedly weaker response in southwestern districts. This reflects the inconsistencies reported for the Iberian Peninsula by Páscoa et al. (2016), who argued that spatial differences can be explained mainly by the differing productivities in the various districts; we noted this for the mainly agrarian areas of peninsular Spain (Castilla y León and Castilla La Mancha) and the characteristically heterogeneity of this territory. In the southwestern agricultural areas, where the precipitation rates are lower and temperatures higher, the correlations of yield with drought were weaker. In addition, conclusions achieved by Gouveia et al. (2016) in the same region supported the statement of the strong control of drought on plants activity, especially in semiarid areas. Even though our findings from crop yields suggest the contrary due to the predominance of cereal croplands in north-central regions of Spain, this can be attributed to episodes of abnormal extreme temperatures, such as the very low temperatures in early spring or warmer than usual temperatures in winter. These would affect the expected low evapotranspiration rates during the cold season (Fontana et al., 2015; Kolář et al., 2014). A recent study by Hernandez-Barrera et al. (2016) demonstrated that during autumn and spring, precipitation deficit is the most influential climate factor affecting wheat growth, while an increase in the diurnal temperature range causes a reduction in wheat yield. We found no major differences in precipitation among districts belonging to any of the two defined components but found other differences including in the average maximum and minimum temperatures. These findings highlight the complexity in choosing a useful drought index that encompasses the specificities of each crop, including its sensitivity to moisture and environmental conditions throughout the entire growth cycle, and its seasonality. This underscores the importance of testing and comparing the appropriateness of different drought indices to ensure accurate identification of the multi-temporal impacts of drought on natural systems.

5 Conclusions

The main findings of this study are summarized below.

1. Assessment of the efficacy of drought indices for monitoring the effect of climate on agricultural yields demonstrated the better performance of multi-scalar indices. The ability to calculate these indices at various timescales enabled drought impacts to be more precisely defined than with the use of indices lacking this characteristic. The multi-scalar drought indices assessed also had fewer computational and data requirements (particularly the SPEI and the SPI), which is a significant consideration when performing analyses based on scarce climate data.
2. From a quantitative evaluation of the relationship of drought indices to crop yields we determined that both of the multi-scalar drought indices tested were useful for the assessment of agricultural drought in Spain. However, the SPEI had slightly better correlations and is the most highly recommended for the purpose.
3. The spatial definition of yield responses to drought was clearer at the district scale, where the finer spatial resolution enabled better definition of the patterns of responses because the climatic variability of each region was better captured at this scale.
4. Barley and wheat yields were more vulnerable to drought during spring, both at short (1–3 months) and medium (4–6 months) timescales. Moisture conditions during late autumn and winter also had an impact on the crop yields.
5. The strongest relationships between drought indices and crop yields were found for the northern and central agricultural districts. The relationships for the southern districts were weaker because of the difficulty of characterizing drought impacts over the diverse and complex territory involved.
6. The climatic and agricultural conditions in Spain are very diverse. The large spatial diversity and the complexity of droughts highlight the need to establish accurate and effective indices to monitor the variable evolution of drought in vulnerable agriculture areas. Climate change is likely to lead to yield losses because of increased drought stress on crops, so in this context effective monitoring tools are of utmost importance. The authors consider that further analysis complementing this study may help to unravel the climate mechanisms that influence the spatiotemporal responses of yields to climate in Spain.

Data availability. Crop yield data are publicly available and can be accessed for free upon request from the Spanish Ministry of Agri-

culture, Fisheries and Food. Climatic information used to create the gridded datasets was provided privately by the Spanish Meteorological Agency (AEMET). It can be accessed by users upon request to the agency.

Supplement. The supplement related to this article is available online at: <https://doi.org/10.5194/nhess-19-1215-2019-supplement>.

Author contributions. SMVS and SBP designed the research. MPG performed the formal analysis and drafted the paper. SMVS, SB, and FDC contributed to writing the review and editing the paper.

Competing interests. The authors declare that they have no conflict of interest.

Special issue statement. This article is part of the special issue “Hydroclimatic extremes and impacts at catchment to regional scales”. It is not associated with a conference.

Acknowledgements. Authors thank the three anonymous reviewers for their constructive comments in the review of this paper and the anonymous judges that evaluated this study during the OSPP-EGU 2018.

Financial support. This research has been supported by the European Geosciences Union (OSPP Award 2018 grant), the Spanish Commission of Science and Technology and FEDER (grant nos. PCIN-2015-220 and CGL2014-52135-C03-01), the Water Works 2014 and European Commission (IMDROFLOOD grant), the JPI Climate, funded by FORMAS (SE), DLR (DE), BMWFW (AT), IFD (DK), MINECO (ES), and ANR (FR), with co-funding by the European Union (INDECIS, ERA4CS, and ERA-NET grants, grant no. 690462), and the Spanish Ministry of Economy and Competitiveness (grant no. FPI2015 – BES-2015-072022).

Review statement. This paper was edited by Chris Reason and reviewed by three anonymous referees.

References

- Alcamo, J., Flörke, M., and Märker, M.: Future long-term changes in global water resources driven by socio-economic and climatic changes, *Hydrol. Sci. J.*, 52, 247–275, <https://doi.org/10.1623/hysj.52.2.247>, 2007.
- Allen, R. G., Pereira, L. S., Raes, D., and Smith, M.: No Title, *Crop Evapotranspiration Guidel, Comput. Crop Water Requir.*, ISBN 92-5-104219-5, 1998.
- Alley, W. M.: The Palmer Drought Severity Index: Limitations and Assumptions, *J. Clim. Appl. Mete-*

- orol., 23, 1100–1109, [https://doi.org/10.1175/1520-0450\(1984\)023<1100:TPDSIL>2.0.CO;2](https://doi.org/10.1175/1520-0450(1984)023<1100:TPDSIL>2.0.CO;2), 1984.
- Asseng, S., Foster, I., and Turner, N. C.: The impact of temperature variability on wheat yields, *Glob. Chang. Biol.*, 17, 997–1012, <https://doi.org/10.1111/j.1365-2486.2010.02262.x>, 2011.
- Asseng, S., Ewert, F., Martre, P., Rötter, R. P., Lobell, D. B., Cammarano, D., Kimball, B. A., Ottman, M. J., Wall, G. W., White, J. W., Reynolds, M. P., Alderman, P. D., Prasad, P. V. V., Aggarwal, P. K., Anothai, J., Basso, B., Biernath, C., Challinor, A. J., De Sanctis, G., Doltra, J., Fereres, E., Garcia-Vila, M., Gayler, S., Hoogenboom, G., Hunt, L. A., Izaurrealde, R. C., Jabloun, M., Jones, C. D., Kersebaum, K. C., Koehler, A.-K., Müller, C., Naresh Kumar, S., Nendel, C., O’Leary, G., Olesen, J. E., Palosuo, T., Priesack, E., Eysbi Rezaei, E., Ruane, A. C., Semenov, M. A., Shcherbak, I., Stöckle, C., Stratonovitch, P., Streck, T., Supit, I., Tao, F., Thorburn, P. J., Waha, K., Wang, E., Wallach, D., Wolf, J., Zhao, Z., and Zhu, Y.: Rising temperatures reduce global wheat production, *Nat. Clim. Change*, 5, 143–147, <https://doi.org/10.1038/nclimate2470>, 2014.
- Blanc, E.: The Impact of Climate Change on Crop Yields in Sub-Saharan Africa, *Am. J. Clim. Change*, 1, 1–13, <https://doi.org/10.4236/ajcc.2012.11001>, 2012.
- Çakir, R.: Effect of water stress at different development stages on vegetative and reproductive growth of corn, *F. Crop. Res.*, 89, 1–16, <https://doi.org/10.1016/j.fcr.2004.01.005>, 2004.
- Cantelaube, P., Terres, J., and Doblas-Reyes, F.: Influence of climate variability on European agriculture-analysis of winter wheat production, *Clim. Res.*, 27, 135–144, <https://doi.org/10.3354/cr027135>, 2004.
- Capa-Morocho, M., Ines, A. V. M., Baethgen, W. E., Rodríguez-Fonseca, B., Han, E., and Ruiz-Ramos, M.: Crop yield outlooks in the Iberian Peninsula: Connecting seasonal climate forecasts with crop simulation models, *Agric. Syst.*, 149, 75–87, <https://doi.org/10.1016/J.AGSY.2016.08.008>, 2016.
- Chen, T., Xia, G., Liu, T., Chen, W., Chi, D., Chen, T., Xia, G., Liu, T., Chen, W., and Chi, D.: Assessment of Drought Impact on Main Cereal Crops Using a Standardized Precipitation Evapotranspiration Index in Liaoning Province, China, *Sustainability*, 8, 1069, <https://doi.org/10.3390/su8101069>, 2016.
- Contreras, S. and Hunink, J. E.: Drought effects on rainfed agriculture using standardized indices: A case study in SE Spain, in *Drought: Research and Science-Policy Interfacing*, 2015.
- Dai, A.: Drought under global warming: a review, *Wiley Interdiscip. Rev. Clim. Change*, 2, 45–65, <https://doi.org/10.1002/wcc.81>, 2011.
- Doesken, N. J. and Garen, D.: Drought Monitoring in the Western United States using a Surface Water Supply Index, Preprints, Seventh Conference on Applied Climatology, Salt Lake City, UT, American Meteorological Society, 266–269, 1991.
- Domínguez-Castro, F., Ribera, P., García-Herrera, R., Vaquero, J. M., Barriendos, M., Cuadrat, J. M., and Moreno, J. M.: Assessing extreme droughts in Spain during 1750–1850 from rogation ceremonies, *Clim. Past*, 8, 705–722, <https://doi.org/10.5194/cp-8-705-2012>, 2012.
- Ebrahimpour, M., Rahimi, J., Nikkhab, A., and Bazrafshan, J.: Monitoring Agricultural Drought Using the Standardized Effective Precipitation Index, *J. Irrig. Drain. Eng.*, 141, 04014044, [https://doi.org/10.1061/\(ASCE\)IR.1943-4774.0000771](https://doi.org/10.1061/(ASCE)IR.1943-4774.0000771), 2015.
- Esfahanian, E., Nejadhashemi, A. P., Abouali, M., Adhikari, U., Zhang, Z., Daneshvar, F., and Herman, M. R.: Development and evaluation of a comprehensive drought index, *J. Environ. Manage.*, 185, 31–43, <https://doi.org/10.1016/j.jenvman.2016.10.050>, 2017.
- European Commission, Agriculture and Rural Development: Commission offers further support to European farmers dealing with droughts, available at: https://ec.europa.eu/info/news/commission-offers-further-support-european-farmers-dealing-droughts-2018-aug-02_0_en, last access: 26 October 2018.
- European Environment Agency (EEA): Climate change, impacts and vulnerability in Europe 2016, An indicator-based report, Luxembourg, 424 pp., 2017.
- Fink, A. H., Brücher, T., Krüger, A., Leckebusch, G. C., Pinto, J. G., and Ulbrich, U.: The 2003 European summer heatwaves and drought – synoptic diagnosis and impacts, 59, 209–216, <https://doi.org/10.1256/wea.73.04>, 2004.
- Fischer, R. A., Rees, D., Sayre, K. D., Lu, Z.-M., Condon, A. G., and Saavedra, A. L.: Wheat Yield Progress Associated with Higher Stomatal Conductance and Photosynthetic Rate, and Cooler Canopies, *Crop. Sci.*, 38, 1467, <https://doi.org/10.2135/cropsci1998.0011183X003800060011x>, 1998.
- Fontana, G., Toreti, A., Ceglar, A., and De Sanctis, G.: Early heat waves over Italy and their impacts on durum wheat yields, *Nat. Hazards Earth Syst. Sci.*, 15, 1631–1637, <https://doi.org/10.5194/nhess-15-1631-2015>, 2015.
- Forzieri, G., Feyen, L., Russo, S., Vousdoukas, M., Alfieri, L., Outten, S., Migliavacca, M., Bianchi, A., Rojas, R., and Cid, A.: Multi-hazard assessment in Europe under climate change, *Clim. Change*, 137, 105–119, <https://doi.org/10.1007/s10584-016-1661-x>, 2016.
- García-Herrera, R., Díaz, J., Trigo, R. M., Luterbacher, J., and Fischer, E. M.: A Review of the European Summer Heat Wave of 2003, *Crit. Rev. Environ. Sci. Technol.*, 40, 267–306, <https://doi.org/10.1080/10643380802238137>, 2010.
- García-León, D., Contreras, S., and Hunink, J.: Comparison of meteorological and satellite-based drought indices as yield predictors of Spanish cereals, *Agr. Water Manage.*, 213, 388–396, <https://doi.org/10.1016/J.AGWAT.2018.10.030>, 2019.
- Ghabaei Sough, M., Zare Abyaneh, H., and Mosaedi, A.: Assessing a Multivariate Approach Based on Scalogram Analysis for Agricultural Drought Monitoring, *Water Resour. Manag.*, 32, 3423–3440, <https://doi.org/10.1007/s11269-018-1999-0>, 2018.
- Giorgi, F. and Lionello, P.: Climate change projections for the Mediterranean region, *Glob. Planet. Change*, 63, 90–104, <https://doi.org/10.1016/j.gloplacha.2007.09.005>, 2008.
- Gouveia, C. M., Trigo, R. M., Beguería, S., and Vicente-Serrano, S. M.: Drought impacts on vegetation activity in the Mediterranean region: An assessment using remote sensing data and multi-scale drought indicators, *Glob. Planet. Change*, 151, 15–27, <https://doi.org/10.1016/j.gloplacha.2016.06.011>, 2016.
- Guttman, N. B.: Comparing the Palmer Drought Index and The Standardized Precipitation Index, *J. Am. Water Resour. Assoc.*, 34, 113–121, <https://doi.org/10.1111/j.1752-1688.1998.tb05964.x>, 1998.

- Hanjra, M. A. and Qureshi, M. E.: Global water crisis and future food security in an era of climate change, *Food Policy*, 35, 365–377, <https://doi.org/10.1016/J.FOODPOL.2010.05.006>, 2010.
- Heim, R. R.: A Review of Twentieth-Century Drought Indices Used in the United States, *B. Am. Meteorol. Soc.*, 83, 1149–1165, [https://doi.org/10.1175/1520-0477\(2002\)083<1149:AROTDI>2.3.CO;2](https://doi.org/10.1175/1520-0477(2002)083<1149:AROTDI>2.3.CO;2), 2002.
- Hernandez-Barrera, S., Rodriguez-Puebla, C., and Challinor, A. J.: Effects of diurnal temperature range and drought on wheat yield in Spain, *Theor. Appl. Climatol.*, 129, 503–519, <https://doi.org/10.1007/s00704-016-1779-9>, 2016.
- IPCC 2014: Climate Change 2014: Mitigation of Climate Change, Contribution of Working Group III to the Fifth Assessment Report of the Intergovernmental Panel on Climate Change, edited by: Edenhofer, O., Pichs-Madruga, R., Sokona, Y., Farahani, E., Kadner, S., Seyboth, K., Adler, A., Baum, I., Brunner, S., Eickemeier, P., Kriemann, B., Savolainen, J., Schlömer, S., von Stechow, C., Zwickel, T., and Minx, J. C., Cambridge University Press, Cambridge, United Kingdom and New York, NY, 1454 pp., USA.
- Karl, T. R.: The Sensitivity of the Palmer Drought Severity Index and Palmer's Z-Index to their Calibration Coefficients Including Potential Evapotranspiration, *J. Clim. Appl. Meteorol.*, 25, 77–86, [https://doi.org/10.1175/1520-0450\(1986\)025<0077:TSOTPD>2.0.CO;2](https://doi.org/10.1175/1520-0450(1986)025<0077:TSOTPD>2.0.CO;2), 1986.
- Kim, B.-S., Sung, J.-H., Kang, H.-S., and Cho, C.-H.: Assessment of Drought Severity over South Korea using Standardized Precipitation Evapo-transpiration Index (SPEI), *J. Korea Water Resour. Assoc.*, 45, 887–900, <https://doi.org/10.3741/JKWRA.2012.45.9.887>, 2012.
- Kolář, P., Trnka, M., Brázdil, R., and Hlavinka, P.: Influence of climatic factors on the low yields of spring barley and winter wheat in Southern Moravia (Czech Republic) during the 1961–2007 period, *Theor. Appl. Climatol.*, 117, 707–721, <https://doi.org/10.1007/s00704-013-1037-3>, 2014.
- Kuhnert, M., Yeluripati, J., Smith, P., Hoffmann, H., van Oijen, M., Constantin, J., Coucheney, E., Dechow, R., Eckersten, H., Gaiser, T., Grosz, B., Haas, E., Kersebaum, K.-C., Kiese, R., Klatt, S., Lewan, E., Nendel, C., Raynal, H., Sosa, C., Specka, X., Teixeira, E., Wang, E., Weihermüller, L., Zhao, G., Zhao, Z., Ogle, S., and Ewert, F.: Impact analysis of climate data aggregation at different spatial scales on simulated net primary productivity for croplands, *Eur. J. Agron.*, 88, 41–52, <https://doi.org/10.1016/j.eja.2016.06.005>, 2016.
- Labudová, L., Labuda, M., and Takáč, J.: Comparison of SPI and SPEI applicability for drought impact assessment on crop production in the Danubian Lowland and the East Slovakian Lowland, *Theor. Appl. Climatol.*, 1–16, <https://doi.org/10.1007/s00704-016-1870-2>, 2016.
- Liu, B., Asseng, S., Müller, C., Ewert, F., Elliott, J., Lobell, D. B., Martre, P., Ruane, A. C., Wallach, D., Jones, J. W., Rosenzweig, C., Aggarwal, P. K., Alderman, P. D., Anothai, J., Basso, B., Biersnath, C., Cammarano, D., Challinor, A., Deryng, D., Sanctis, G. D., Doltra, J., Fereres, E., Folberth, C., Garcia-Vila, M., Gayler, S., Hoogenboom, G., Hunt, L. A., Izaurralde, R. C., Jabloun, M., Jones, C. D., Kersebaum, K. C., Kimball, B. A., Koehler, A.-K., Kumar, S. N., Nendel, C., O'Leary, G. J., Olesen, J. E., Ottman, M. J., Palosuo, T., Prasad, P. V. V., Priesack, E., Pugh, T. A. M., Reynolds, M., Rezaei, E. E., Rötter, R. P., Schmid, E., Semenov, M. A., Shcherbak, I., Stehfest, E., Stöckle, C. O., Stratonovitch, P., Streck, T., Supit, I., Tao, F., Thorburn, P., Waha, K., Wall, G. W., Wang, E., White, J. W., Wolf, J., Zhao, Z., and Zhu, Y.: Similar estimates of temperature impacts on global wheat yield by three independent methods, *Nat. Clim. Change*, 6, 1130–1136, <https://doi.org/10.1038/nclimate3115>, 2016.
- Lobell, D. B. and Asner, G. P.: Climate and management contributions to recent trends in U.S. agricultural yields, *Science*, 80, 1032, <https://doi.org/10.1126/science.1078475>, 2003.
- Lobell, D. B. and Field, C. B.: Global scale climate-crop yield relationships and the impacts of recent warming, *Environ. Res. Lett.*, 2, 014002, <https://doi.org/10.1088/1748-9326/2/1/014002>, 2007.
- Lobell, D. B., Schlenker, W., and Costa-Roberts, J.: Climate Trends and Global Crop Production Since 1980, *Science*, 333, 6042, 616–620, 2011.
- Loukas, A. and Vasiliades, L.: Probabilistic analysis of drought spatiotemporal characteristics in Thessaly region, Greece, *Nat. Hazards Earth Syst. Sci.*, 4, 719–731, <https://doi.org/10.5194/nhess-4-719-2004>, 2004.
- Ma, M., Ren, L., Yuan, F., Jiang, S., Liu, Y., Kong, H., and Gong, L.: A new standardized Palmer drought index for hydro-meteorological use, *Hydrol. Process.*, 28, 5645–5661, <https://doi.org/10.1002/hyp.10063>, 2014.
- Mamnouie, E., Ghazvini, R. F., Esfahany, M., and Nakhoda, B.: The Effects of Water Deficit on Crop Yield and the Physiological Characteristics of Barley (*Hordeum vulgare* L.) Varieties, available at: <http://jast.modares.ac.ir/article-23-5420-en.pdf> (last access: 24 November 2018), 2006.
- Mavromatis, T.: Drought index evaluation for assessing future wheat production in Greece, *Int. J. Climatol.*, 27, 911–924, <https://doi.org/10.1002/joc.1444>, 2007.
- McEvoy, D. J., Huntington, J. L., Abatzoglou, J. T., Edwards, L. M., McEvoy, D. J., Huntington, J. L., Abatzoglou, J. T., and Edwards, L. M.: An Evaluation of Multiscalar Drought Indices in Nevada and Eastern California, *Earth Interact.*, 16, 1–18, <https://doi.org/10.1175/2012EI000447.1>, 2012.
- McKee, T. B., Doesken, N. J., and Kleist, J.: The relationship of drought frequency and duration to time scales, Eighth Conf. Appl. Climatol., 17–22 available at: http://www.droughtmanagement.info/literature/AMS_Relationship_Drought_Frequency_Duration_Time_Scales_1993.pdf (last access: 30 May 2018), 1993.
- Meng, Q., Chen, X., Lobell, D. B., Cui, Z., Zhang, Y., Yang, H., and Zhang, F.: Growing sensitivity of maize to water scarcity under climate change, *Sci. Rep.*, 6, 19605, <https://doi.org/10.1038/srep19605>, 2016.
- Moore, F. C. and Lobell, D. B.: Adaptation potential of European agriculture in response to climate change, *Nat. Clim. Change*, 4, 610–614, <https://doi.org/10.1038/nclimate2228>, 2014.
- Moorhead, J. E., Gowda, P. H., Singh, V. P., Porter, D. O., Marek, T. H., Howell, T. A., and Stewart, B. A.: Identifying and Evaluating a Suitable Index for Agricultural Drought Monitoring in the Texas High Plains, *JAWRA J. Am. Water Resour. Assoc.*, 51, 807–820, <https://doi.org/10.1111/jawr.12275>, 2015.
- Palmer, W. C.: Meteorological Drought, Research Paper, U.S. Dep. Commer. Weather Bur. Washington, DC, Research P., 45, p. 58., 1965.
- Páscoa, P., Gouveia, C. M., Russo, A., and Trigo, R. M.: The role of drought on wheat yield interannual variability in the Iberian

- Peninsula from 1929 to 2012, *Int. J. Biometeorol.*, 61, 1–13, <https://doi.org/10.1007/s00484-016-1224-x>, 2016.
- Peña-Gallardo, M., Vicente-Serrano, S., Domínguez-Castro, F., Quiring, S., Svoboda, M., Beguería, S., and Hannaford, J.: Effectiveness of drought indices in identifying impacts on major crops across the USA, *Clim. Res.*, 75, 221–240, <https://doi.org/10.3354/cr01519>, 2018a.
- Peña-Gallardo, M., Quiring, S., Svoboda, M., Hannaford, J., Tomas-Burguera, M., Martín-Hernández, N., Domínguez-Castro, F. and El Kenawy, A.: Response of crop yield to different time-scales of drought in the United States: Spatio-temporal patterns and climatic and environmental drivers, *Agr. Forest Meteorol.*, 264, 40–55, <https://doi.org/10.1016/j.agrformet.2018.09.019>, 2018b.
- Potopová, V.: Evolution of drought severity and its impact on corn in the Republic of Moldova, *Theor. Appl. Climatol.*, 105, 469–483, <https://doi.org/10.1007/s00704-011-0403-2>, 2011.
- Potopová, V., Štěpánek, P., Možný, M., Türkott, L., and Soukup, J.: Performance of the standardised precipitation evapotranspiration index at various lags for agricultural drought risk assessment in the Czech Republic, *Agr. Forest Meteorol.*, 202, 26–38, <https://doi.org/10.1016/J.AGRFORMET.2014.11.022>, 2015.
- Potopová, V., Štěpánek, P., Farda, A., Türkott, L., Zahradníček, P., and Soukup, J.: Drought stress impact on vegetable crop yields in the Elbe River lowland between 1961 and 2014, *Cuad. Investig. Geográfica*, 42, 127, <https://doi.org/10.18172/cig.2924>, 2016a.
- Potopová, V., Boroneanț, C., Boincean, B., and Soukup, J.: Impact of agricultural drought on main crop yields in the Republic of Moldova, *Int. J. Climatol.*, 36, 2063–2082, <https://doi.org/10.1002/joc.4481>, 2016b.
- Quiring, S. M. and Papakryiakou, T. N.: An evaluation of agricultural drought indices for the Canadian prairies, *Agr. Forest Meteorol.*, 118, 49–62, [https://doi.org/10.1016/S0168-1923\(03\)00072-8](https://doi.org/10.1016/S0168-1923(03)00072-8), 2003.
- Ribeiro, A. F. S., Russo, A., Gouveia, C. M., and Páscoa, P.: Modelling drought-related yield losses in Iberia using remote sensing and multiscale indices, *Theor. Appl. Climatol.*, 136, 203–220, <https://doi.org/10.1007/s00704-018-2478-5>, 2019.
- Richman, M. B.: Rotation of principal components, *J. Climatol.*, 6, 293–335, <https://doi.org/10.1002/joc.3370060305>, 1986.
- Sepulcre-Canto, G., Horion, S., Singleton, A., Carrao, H., and Vogt, J.: Development of a Combined Drought Indicator to detect agricultural drought in Europe, *Nat. Hazards Earth Syst. Sci.*, 12, 3519–3531, <https://doi.org/10.5194/nhess-12-3519-2012>, 2012.
- Spinoni, J., Vogt, J. V., Naumann, G., Barbosa, P., and Dosio, A.: Will drought events become more frequent and severe in Europe?, *Int. J. Climatol.*, 38, 1718–1736, <https://doi.org/10.1002/joc.5291>, 2018.
- Sun, L., Mitchell, S. W., and Davidson, A.: Multiple drought indices for agricultural drought risk assessment on the Canadian prairies, *Int. J. Climatol.*, 32, 1628–1639, <https://doi.org/10.1002/joc.2385>, 2012.
- Tack, J., Barkley, A., and Nalley, L. L.: Effect of warming temperatures on US wheat yields., *P. Natl. Acad. Sci. USA*, 112, 6931–6936, <https://doi.org/10.1073/pnas.1415181112>, 2015.
- Tian, L., Yuan, S., and Quiring, S. M.: Evaluation of six indices for monitoring agricultural drought in the south-central United States, *Agr. Forest Meteorol.*, 249, 107–119, <https://doi.org/10.1016/J.AGRFORMET.2017.11.024>, 2018.
- Tsakiris, G. and Tigkas, D.: Drought Risk in Agriculture in Mediterranean Regions. Case Study: Eastern Crete, in *Methods and Tools for Drought Analysis and Management*, Springer Netherlands, Dordrecht, 399–414, 2007.
- Tunalıoğlu, R. and Durdu, Ö. F.: Assessment of future olive crop yield by a comparative evaluation of drought indices: a case study in western Turkey, *Theor. Appl. Climatol.*, 108, 397–410, <https://doi.org/10.1007/s00704-011-0535-4>, 2012.
- UPA, Unión de Pequeños Agricultores y Ganaderos: La sequía y sus efectos sobre la agricultura y la ganadería, available at: <https://www.upa.es/upa/uControlador/index.php?nodo=1021&hn=2232> (last access: 25 October 2018), 2017.
- Vergni, L. and Todisco, F.: Spatio-temporal variability of precipitation, temperature and agricultural drought indices in Central Italy, *Agr. Forest Meteorol.*, 151, 301–313, <https://doi.org/10.1016/j.agrformet.2010.11.005>, 2011.
- Vicente-Serrano, S. M.: Spatial and temporal analysis of droughts in the Iberian Peninsula (1910–2000), *Hydrol. Sci. J.*, 51, 83–97, <https://doi.org/10.1623/hysj.51.1.83>, 2006.
- Vicente-Serrano, S. M., Beguería, S., and López-Moreno, J. I.: A Multiscalar Drought Index Sensitive to Global Warming: The Standardized Precipitation Evapotranspiration Index, *J. Climate*, 23, 1696–1718, <https://doi.org/10.1175/2009JCLI2909.1>, 2010.
- Vicente-Serrano, S. M., Beguería, S., and López-Moreno, J. I.: Comment on “Characteristics and trends in various forms of the Palmer Drought Severity Index (PDSI) during 1900–2008” by Aiguo Dai, *J. Geophys. Res.*, 116, D19112, <https://doi.org/10.1029/2011JD016410>, 2011.
- Vicente-Serrano, S. M., Beguería, S., Lorenzo-Lacruz, J., Camarero, J. J., López-Moreno, J. I., Azorin-Molina, C., Revuelto, J., Morán-Tejada, E., Sanchez-Lorenzo, A., Vicente-Serrano, S. M., Beguería, S., Lorenzo-Lacruz, J., Camarero, J. J., López-Moreno, J. I., Azorin-Molina, C., Revuelto, J., Morán-Tejada, E., and Sanchez-Lorenzo, A.: Performance of Drought Indices for Ecological, Agricultural, and Hydrological Applications, 16, 1–27, <https://doi.org/10.1175/2012EI000434.1>, 2012.
- Vicente-Serrano, S. M., Lopez-Moreno, J.-I., Beguería, S., Lorenzo-Lacruz, J., Sanchez-Lorenzo, A., García-Ruiz, J. M., Azorin-Molina, C., Morán-Tejada, E., Revuelto, J., Trigo, R., Coelho, F., and Espejo, F.: Evidence of increasing drought severity caused by temperature rise in southern Europe, *Environ. Res. Lett.*, 9, 44001–44009, <https://doi.org/10.1088/1748-9326/9/4/044001>, 2014.
- Vicente-Serrano, S. M., Van der Schrier, G., Beguería, S., Azorin-Molina, C., and Lopez-Moreno, J.-I.: Contribution of precipitation and reference evapotranspiration to drought indices under different climates, *J. Hydrol.*, 526, 42–54, <https://doi.org/10.1016/j.jhydrol.2014.11.025>, 2015.
- Vicente-Serrano, S. M., Camarero, J. J., Olano, J. M., Martín-Hernández, N., Peña-Gallardo, M., Tomás-Burguera, M., Gazol, A., Azorin-Molina, C., Bhuyan, U., and El Kenawy, A.: Diverse relationships between forest growth and the Normalized Difference Vegetation Index at a global scale, *Remote Sens. Environ.*, 187, 14–29, <https://doi.org/10.1016/j.rse.2016.10.001>, 2016.
- Vicente-Serrano, S. M., Tomas-Burguera, M., Beguería, S., Reig, F., Latorre, B., Peña-Gallardo, M., Luna, M. Y., Morata, A., and González-Hidalgo, J. C.: A High Resolution Dataset of Drought Indices for Spain, *Data*, 2, 22, <https://doi.org/10.3390/data2030022>, 2017.

- Wang, H., Vicente-serrano, S. M., Tao, F., Zhang, X., Wang, P., Zhang, C., Chen, Y., Zhu, D., and Kenawy, A. El: Monitoring winter wheat drought threat in Northern China using multiple climate-based drought indices and soil moisture during 2000–2013, *Agr. Forest Meteorol.*, 228, 1–12, <https://doi.org/10.1016/j.agrformet.2016.06.004>, 2016a.
- Wang, Q., Wu, J., Li, X., Zhou, H., Yang, J., Geng, G., An, X., Liu, L., and Tang, Z.: A comprehensively quantitative method of evaluating the impact of drought on crop yield using daily multi-scale SPEI and crop growth process model, *Int. J. Biometeorol.*, 1–15, <https://doi.org/10.1007/s00484-016-1246-4>, 2016b.
- Webber, H., Ewert, F., Olesen, J. E., Müller, C., Fronzek, S., Ruane, A. C., Bourgault, M., Martre, P., Ababaei, B., Bindi, M., Ferrise, R., Finger, R., Fodor, N., Gabaldón-Leal, C., Gaiser, T., Jabloun, M., Kersebaum, K.-C., Lizaso, J. I., Lorite, I. J., Manceau, L., Moriondo, M., Nendel, C., Rodríguez, A., Ruiz-Ramos, M., Semenov, M. A., Siebert, S., Stella, T., Stratonovitch, P., Trombi, G., and Wallach, D.: Diverging importance of drought stress for maize and winter wheat in Europe, *Nat. Commun.*, 9, 4249, <https://doi.org/10.1038/s41467-018-06525-2>, 2018.
- Wells, N., Goddard, S., Hayes, M. J., Wells, N., Goddard, S., and Hayes, M. J.: A Self-Calibrating Palmer Drought Severity Index, *J. Climate*, 17, 2335–2351, [https://doi.org/10.1175/1520-0442\(2004\)017<2335:ASPDSI>2.0.CO;2](https://doi.org/10.1175/1520-0442(2004)017<2335:ASPDSI>2.0.CO;2), 2004.
- Wigley, T. M. L.: The effect of changing climate on the frequency of absolute extreme events, *Clim. Change*, 97, 67–76, <https://doi.org/10.1007/s10584-009-9654-7>, 2009.
- WMO: Standardized Precipitation Index User Guide, 24 pp., 2012.
- World Bank: World Bank Data, Agriculture, forestry, and fishing, value added (% of GDP) Data, available at: <https://data.worldbank.org/indicator/nv.agr.totl.zs> (last access: 25 October 2018), 2017.
- Zargar, A., Sadiq, R., Naser, B., and Khan, F. I.: A review of drought indices, *Environ. Rev.*, 19, 333–349, <https://doi.org/10.1139/a11-013>, 2011.
- Zhao, C., Liu, B., Piao, S., Wang, X., Lobell, D. B., Huang, Y., Huang, M., Yao, Y., Bassu, S., Ciaia, P., Durand, J.-L., Elliott, J., Ewert, F., Janssens, I. A., Li, T., Lin, E., Liu, Q., Martre, P., Müller, C., Peng, S., Peñuelas, J., Ruane, A. C., Wallach, D., Wang, T., Wu, D., Liu, Z., Zhu, Y., Zhu, Z., and Asseng, S.: Temperature increase reduces global yields of major crops in four independent estimates., *P. Natl. Acad. Sci. USA*, 114, 9326–9331, <https://doi.org/10.1073/pnas.1701762114>, 2017.
- Zhu, Y., Wang, W., Singh, V. P., and Liu, Y.: Combined use of meteorological drought indices at multi-time scales for improving hydrological drought detection, *Sci. Total Environ.*, 571, 1058–1068, <https://doi.org/10.1016/J.SCITOTENV.2016.07.096>, 2016.
- Zipper, S. C., Qiu, J., and Kucharik, C. J.: Drought effects on US maize and soybean production: spatiotemporal patterns and historical changes, *Environ. Res. Lett.*, 11, 094021, <https://doi.org/10.1088/1748-9326/11/9/094021>, 2016.

Supplement of Nat. Hazards Earth Syst. Sci., 19, 1215–1234, 2019
<https://doi.org/10.5194/nhess-19-1215-2019-supplement>
© Author(s) 2019. This work is distributed under
the Creative Commons Attribution 4.0 License.



Supplement of

The impact of drought on the productivity of two rainfed crops in Spain

Marina Peña et al.

Correspondence to: Marina Peña-Gallardo (marinapgallardo@ipe.csic.es)

The copyright of individual parts of the supplement might differ from the CC BY 4.0 License.

Supplementary Table 1. Relationship between provincial and agricultural district data, aggregated at the provincial scale, for wheat cultivation for the common period 1993–2014.

Codes	Provinces	r	Codes	Provinces	r
1	Álava	0.16	23	Jaén	0.38*
2	Albacete	0.41*	24	León	0.69*
3	Alicante	0.1	25	Lleida	0.52*
4	Almería	0.47*	26	La Rioja	0.35*
5	Ávila	0.77*	28	Madrid	0.81*
6	Badajoz	0.49*	29	Málaga	0.11
7	Islas Baleares	-0.22	30	Murcia	0.13
8	Barcelona	0.69*	31	Navarra	-0.25
9	Burgos	0.82*	32	Ourense	0.37*
10	Cáceres	0.34*	33	Asturias	-0.16
11	Cádiz	0.32*	34	Palencia	0.73*
12	Castellón	-0.19	37	Salamanca	0.87*
13	Ciudad Real	0.43*	40	Segovia	0.94*
14	Córdoba	0.46*	41	Sevilla	0.25
15	A Coruña	0.1	42	Soria	0.89*
16	Cuenca	0.86*	43	Tarragona	0.54*
17	Girona	0.1	44	Teruel	0.83*
18	Granada	0.3	45	Toledo	0.48*
19	Guadalajara	0.87*	46	Valencia	0.2
21	Huelva	0.29	47	Valladolid	0.92*

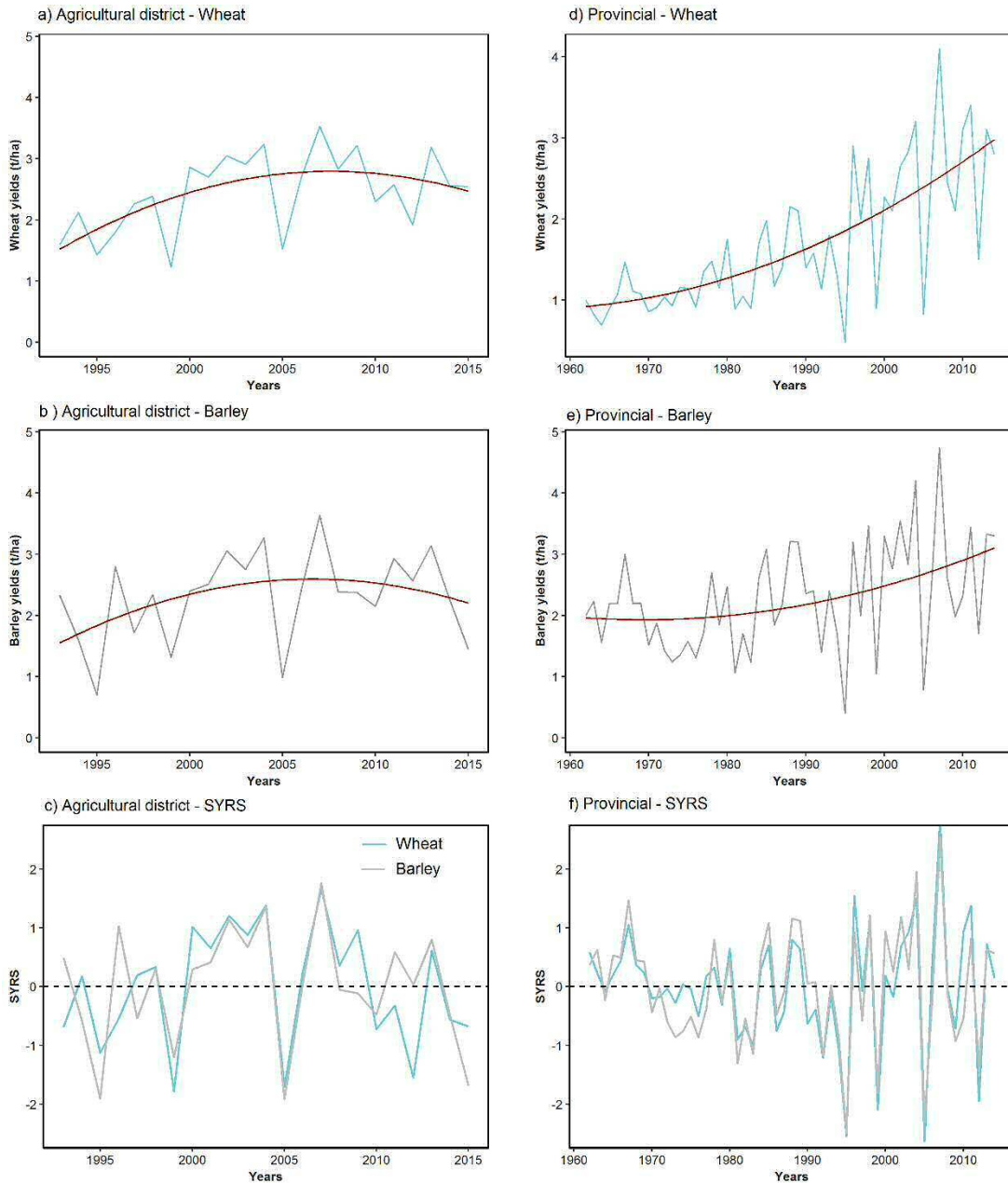
22	Huesca	0.4*	49	Zamora	0.75*
			50	Zaragoza	0.51*

(*) correlations are significant at $p < 0.05$

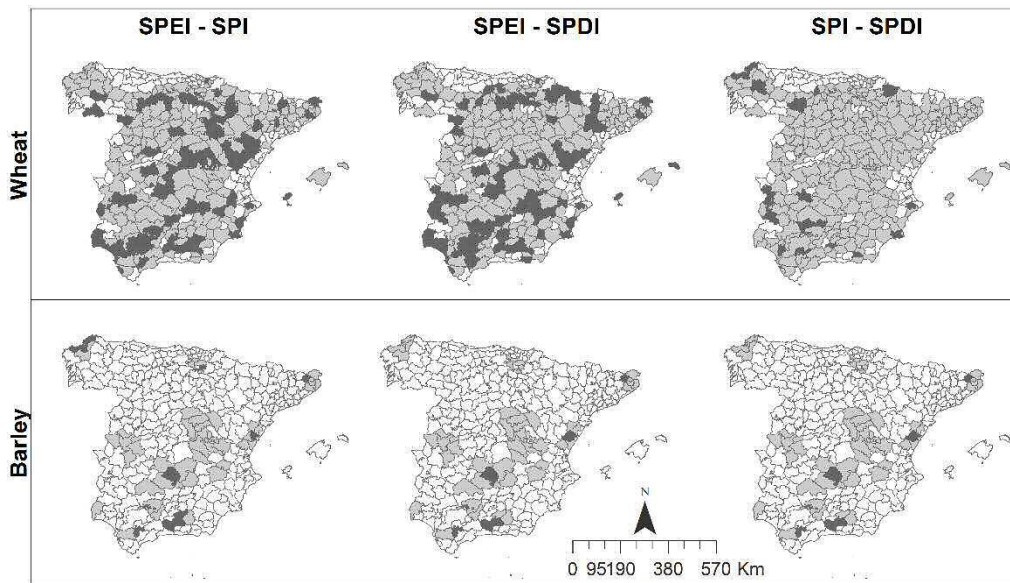
Supplementary Table 2. Relationship between provincial and agricultural district data, aggregated at provincial scale, for barley cultivation for the common period 1993–2014.

Code s	Provinces	r
1	Álava	0.11
2	Albacete	0.2
10	Cáceres	0.48*
11	Cádiz	0.32*
12	Castellón	-0.14
13	Ciudad Real	0.28
14	Córdoba	0.54*
15	A Coruña	-0.09
16	Cuenca	0.88*
17	Girona	0.08
18	Granada	0.51*
19	Guadalajar a	0.86*
22	Huelva	0.57*
26	La Rioja	0.76*
31	Navarra	0.01
41	Sevilla	- 0.35*
43	Tarragona	0.88*

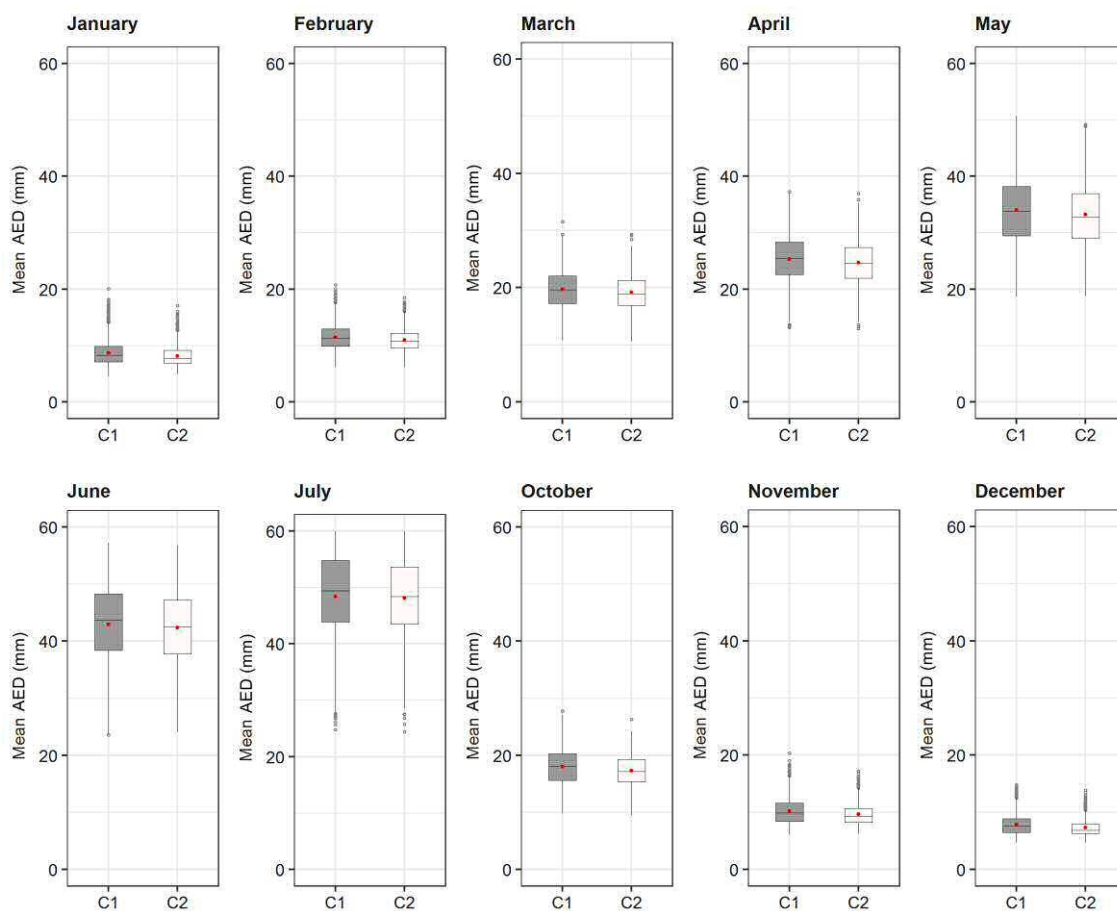
(*) correlations are significant at $p < 0.05$



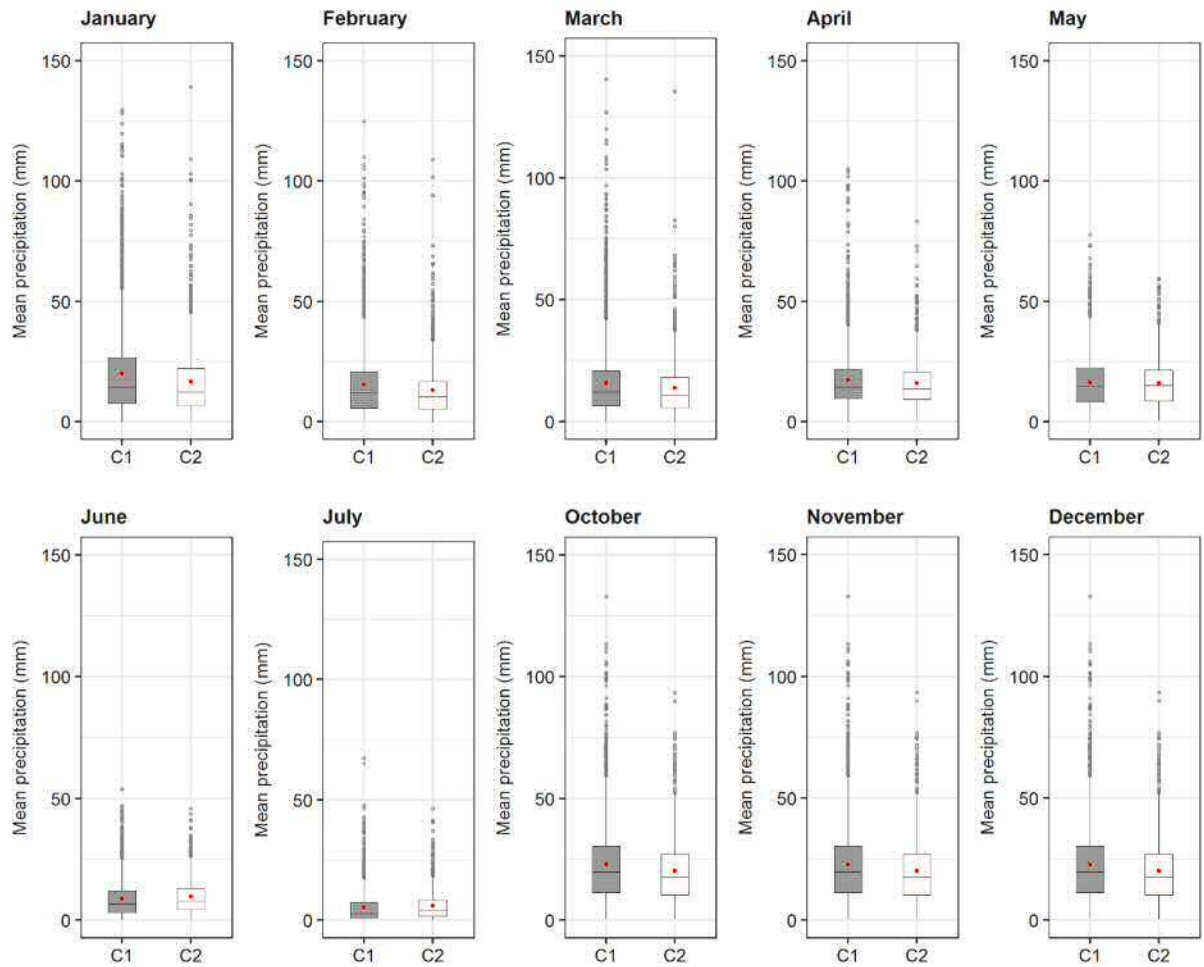
Supplementary Fig. 1. Example of temporal trends of provincial and agricultural district yields of wheat (a, d) and barley (b, e) in the province of Cáceres and the district Navalmoral de la Mata (Cáceres) and the temporal evolution of the SYRS at both scales (c, f) for the available period of time in each case. Red line represents the fitting of a quadratic function. Dashed black line represents the threshold 0-value.



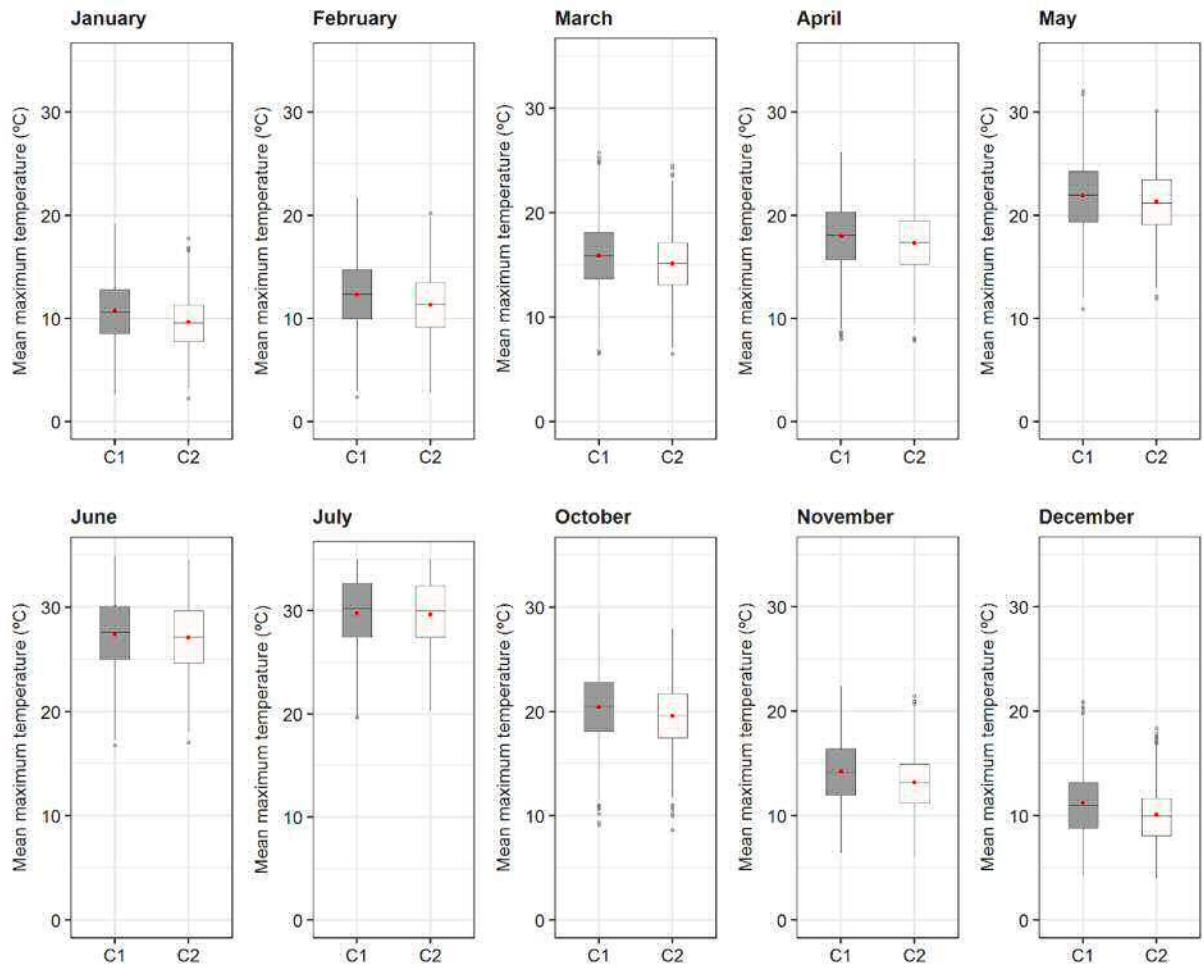
Supplementary Fig. 2. Spatial distribution of regions where significant differences (dark grey) and non significant differences (light grey) were found in the t-tests.



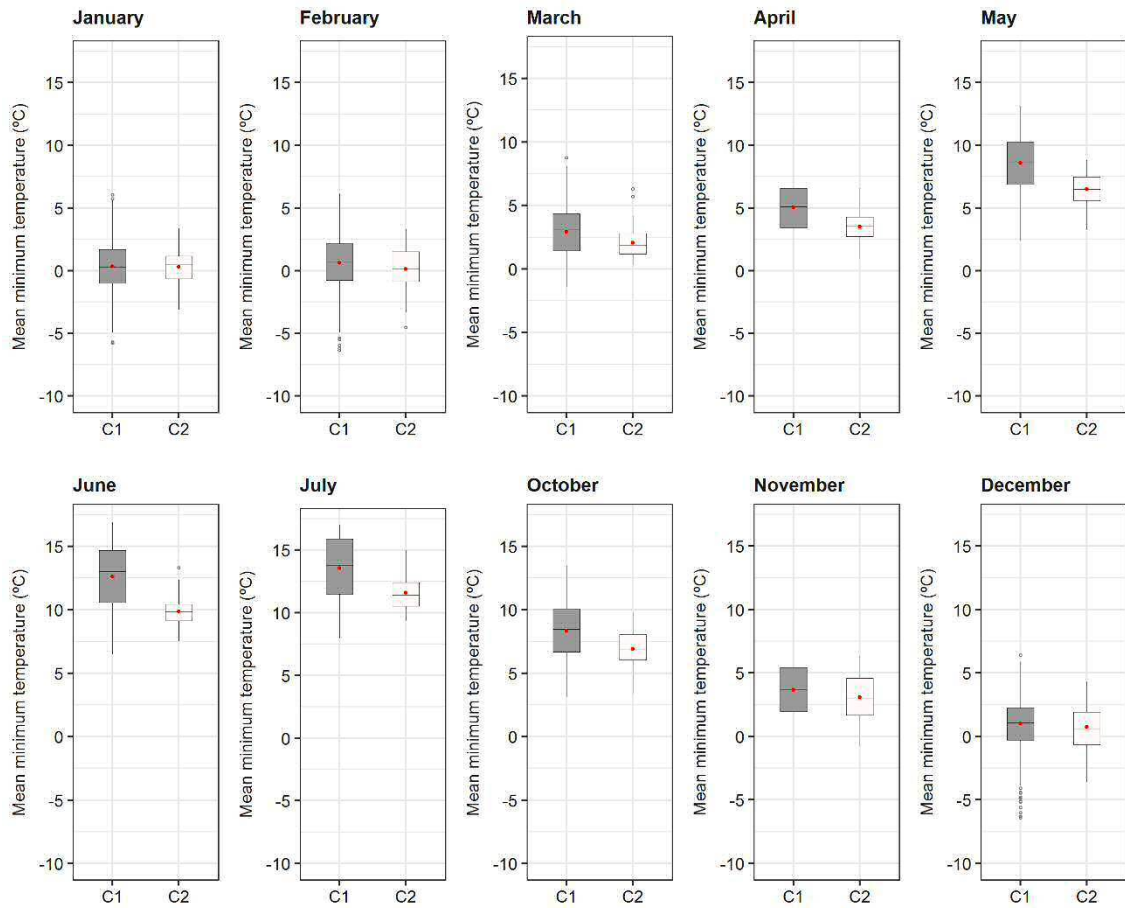
Supplementary Fig. 3. Monthly mean AED conditions in the agricultural districts where wheat was cultivated, classified into principal components (C1 and C2) for the period 1993–2015. The red dot shows the mean, and the black line shows the median.



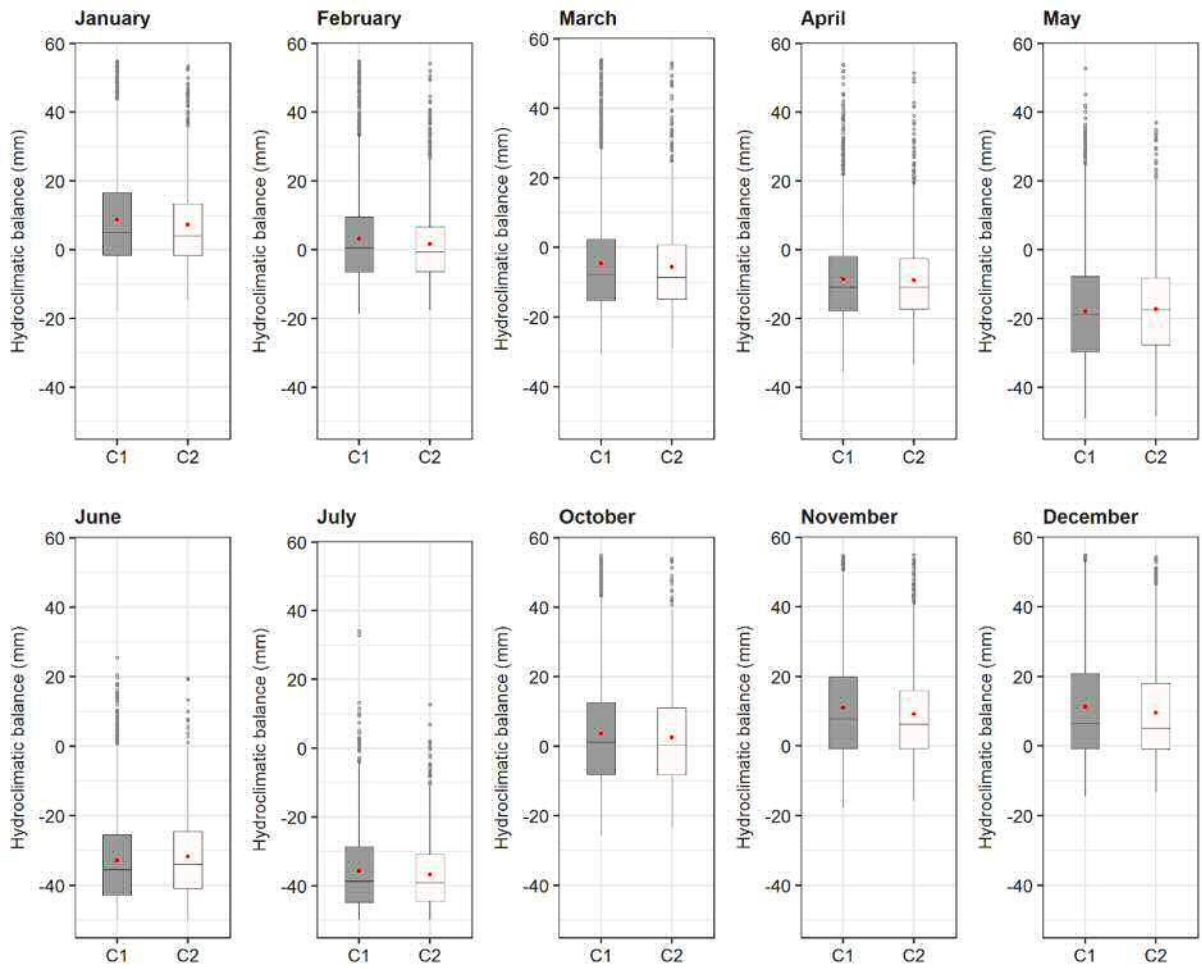
Supplementary Fig. 4. As for Supplementary Fig. 3, but for the monthly mean precipitation.



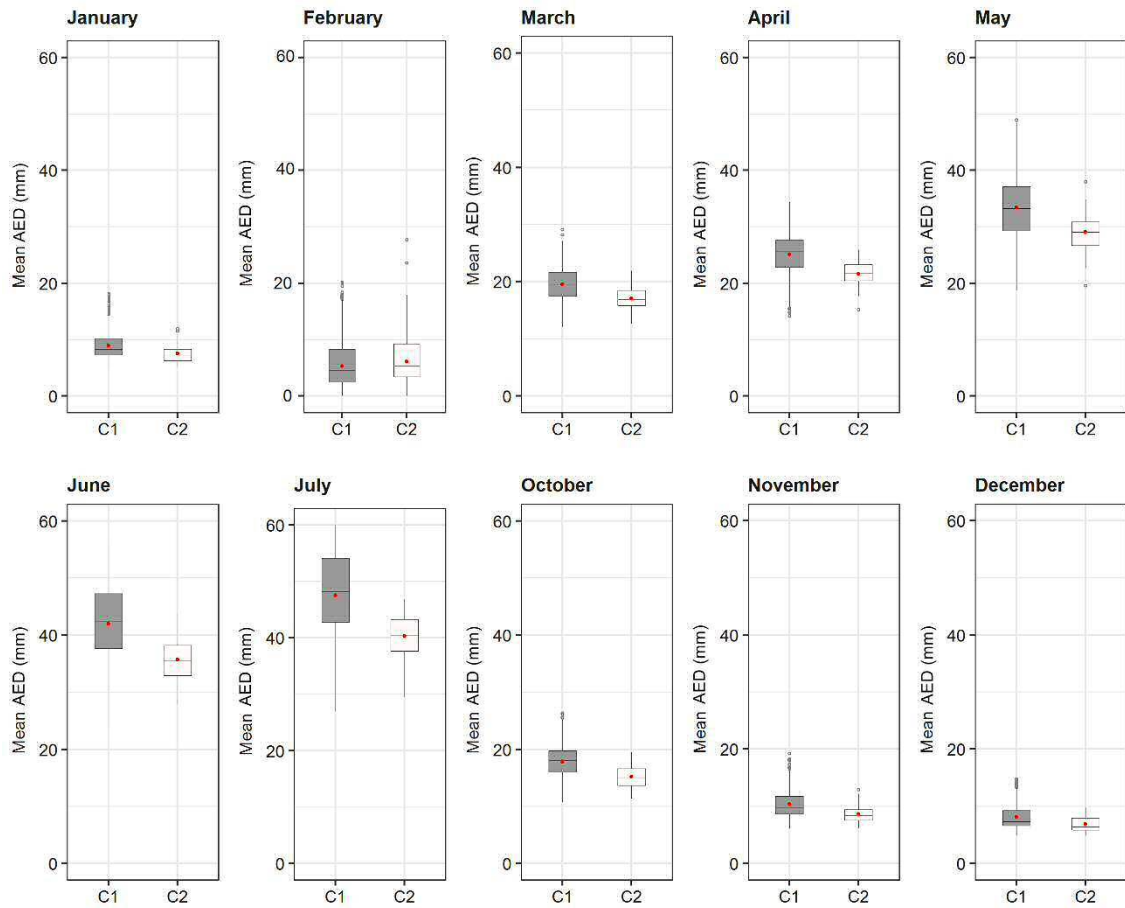
Supplementary Fig. 5. As for Supplementary Fig. 3, but for the monthly mean maximum temperature.



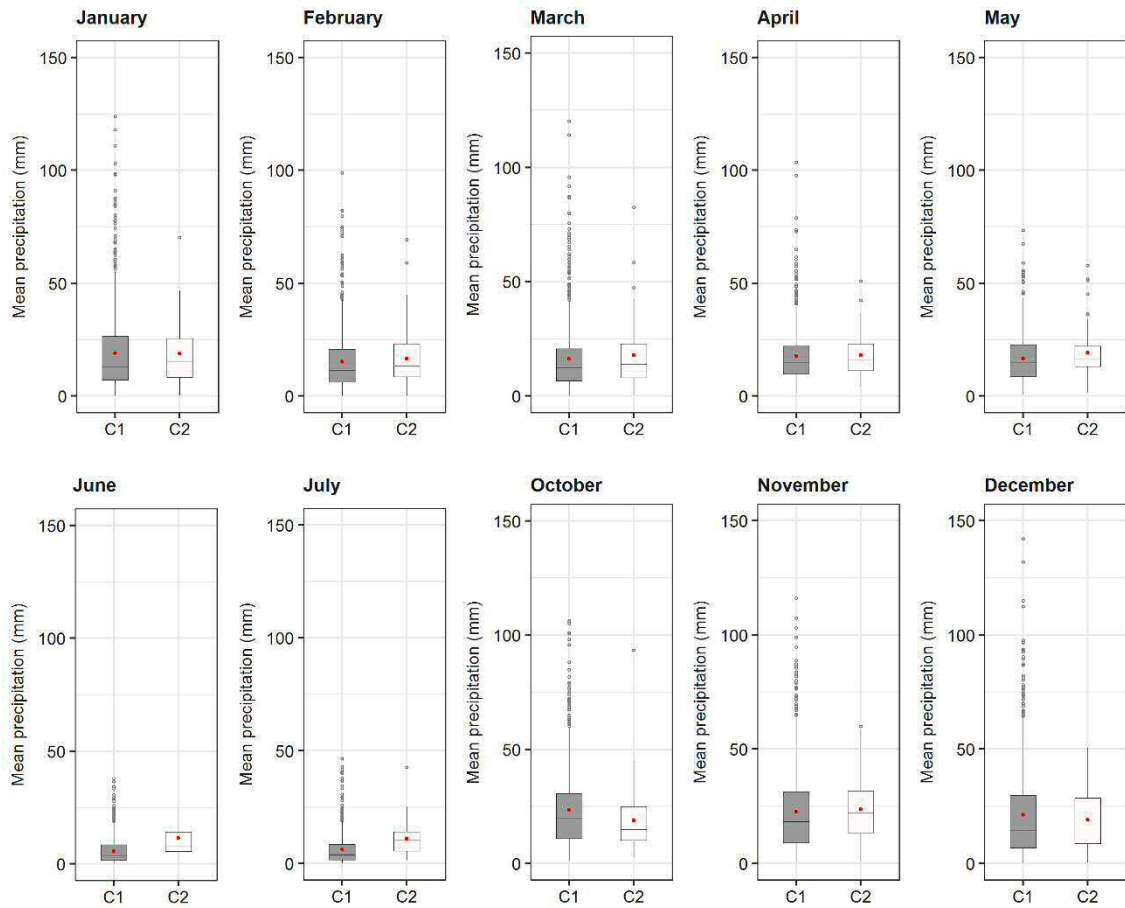
Supplementary Fig. 6. As for Supplementary Fig. 3, but for the monthly mean minimum temperature.



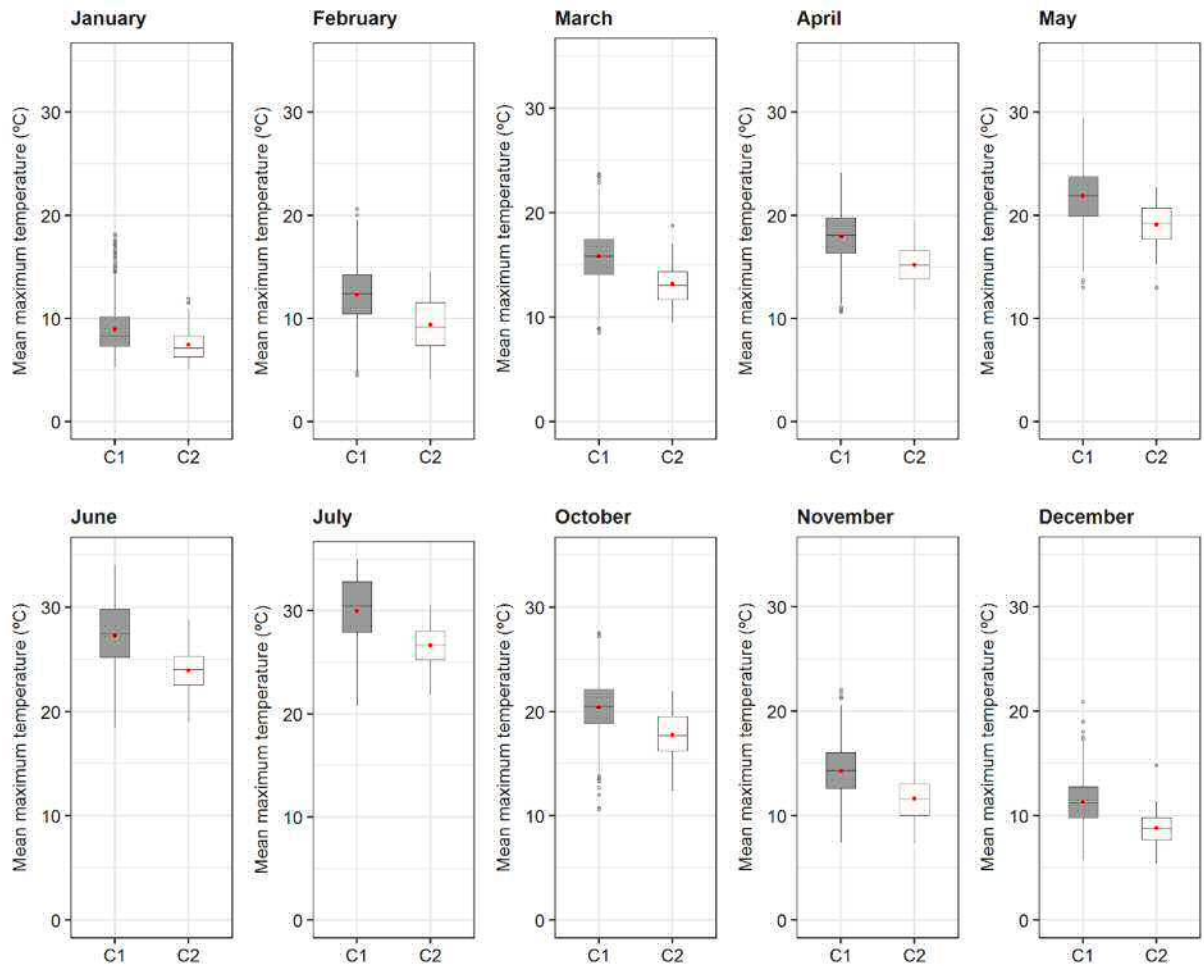
Supplementary Fig. 7. As for Supplementary Fig. 3, but for the monthly mean hydroclimatic balance.



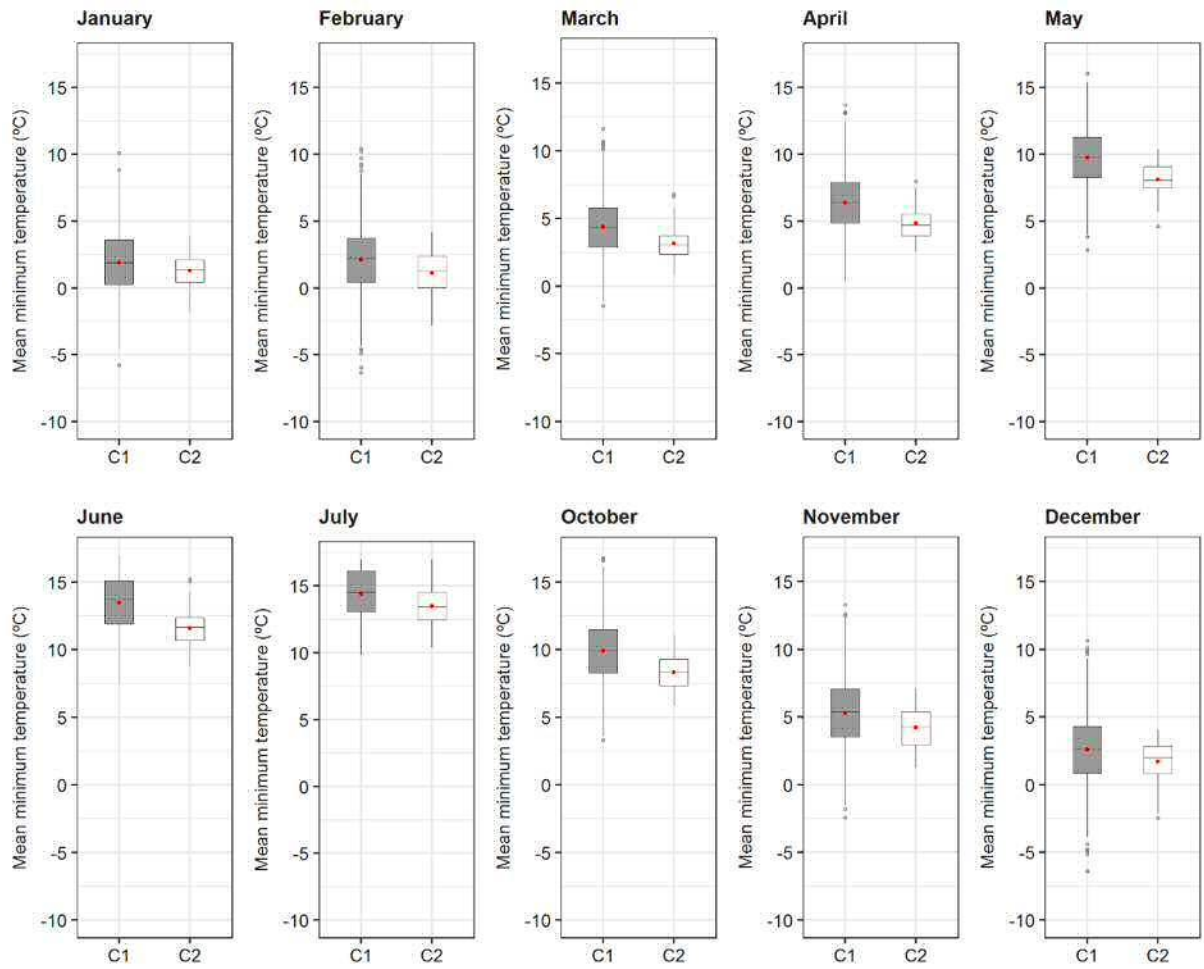
Supplementary Fig. 8. Monthly mean AED conditions in the agricultural districts where barley was cultivated, classified into principal components (C1 and C2) for the period 1993–2015. The red dot show the mean, and black line shows the median.



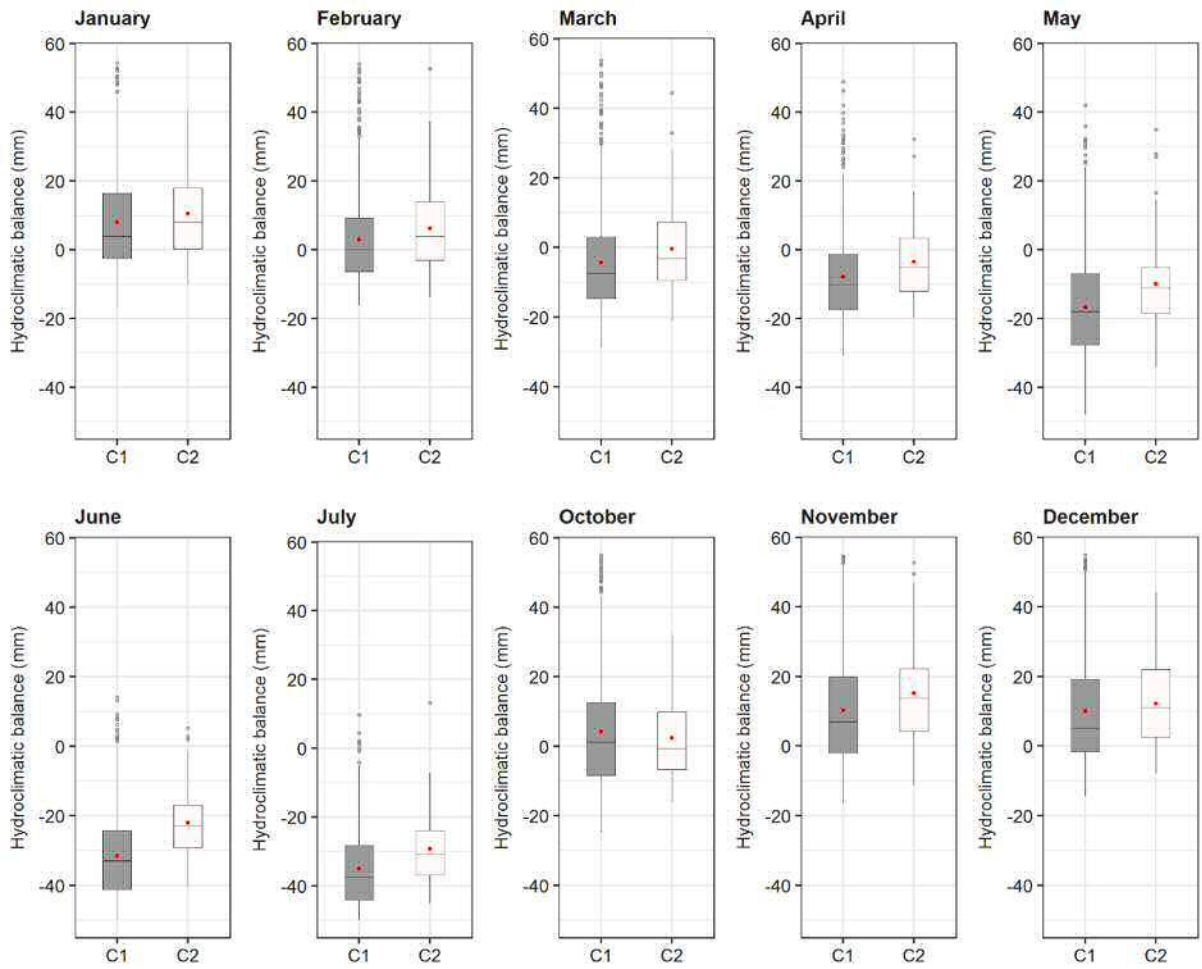
Supplementary Fig. 9. As for Supplementary Fig. 8, but for the monthly mean precipitation.



Supplementary Fig. 10. As for Supplementary Fig. 8, but for the monthly mean maximum temperature.



Supplementary Fig. 11. As for Supplementary Fig. 8, but for the monthly mean minimum temperature.



Supplementary Fig. 12. As for Supplementary Fig. 8, but for the monthly mean hydroclimatic balance.